technische universität dortmund

fakultät für chemie und chemische biologie

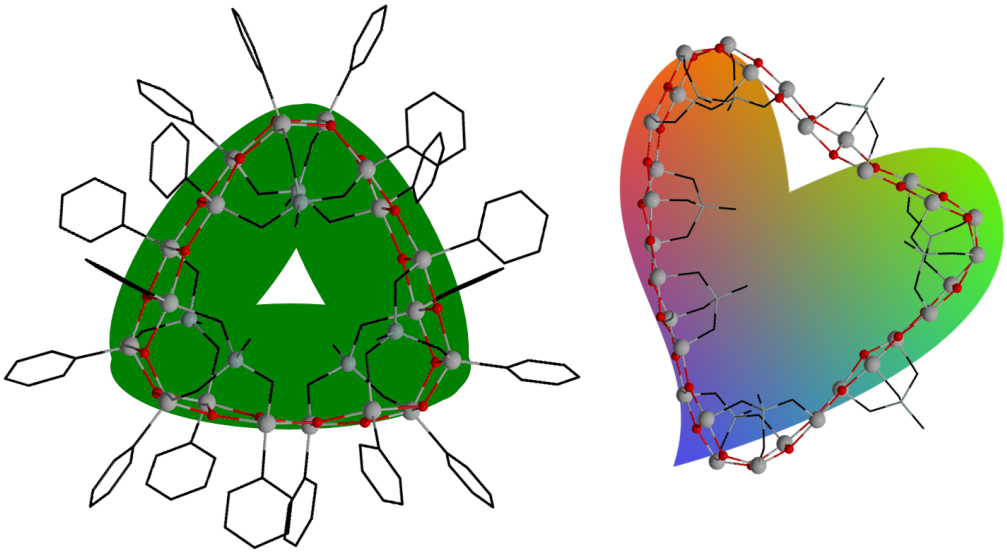

Thesis presented for obtaining the degree of

DOKTOR DER NATURWISSENSCHAFTEN

(Doctor rer. nat.)

Tripod-shaped Organotin Compounds: Complexation Studies towards Lewis Bases and Chalcogenido Clusters of Unprecedented Nuclearity

Dipl.-Ing. Jihed Ayari

First Reviewer: **Prof. Dr. Klaus Jurkschat**

Second Reviewer: **Privatdozent Dr. Uwe Zachwieja**

ACKNOWLEDGMENT

The present work was carried out from July 2014 until September 2018 at the Institute of Inorganic Chemistry of the Technische Universität Dortmund

under the supervision of

PROF. DR. KLAUS JURKSCHAT

whom I pay my greatest gratitude and thanks for the interesting topic, for his skilful guidance and encouragement throughout the course of this research, for his human relationship and moral support. You are always my source of admiration.

My sincere thanks and regards go also to

PRIVATDOZENT DR. UWE ZACHWIEJA

for writing the second review report.

My sincere thanks are also extended to all the scientific co-workers of the research group of Prof. Dr. K. JURKSCHAT for their moral and technical support during my entire journey of research.

In particular, I would like to thank:

Dr. HAZEM ELNASR, Dr. MICHAEL LUTTER, and Dr. CHRISTIAN R. GÖB

for performing the X-ray diffraction analyses.

Prof. Dr. WOLF HILLER

for NMR spectroscopic measurements and help concerning the interpretation of data.

Mrs. SYLVIA MARZIAN and Ms. LAURA SCHNEIDER

for ESI Mass spectrometry measurements.

I also appreciate the technical staff for their day-to-day services.

I express my heartful gratitude for my husband Yassine for his presence, his emotional and moral support that helped me to continue the path under all circumstances. He always stood by my side and still, for that a big THANK YOU!

My profound thanks goes to my Mom Habiba and Dad Mokhtar who believed in me unconditionally and still along my life. They are the source of my continuous optimism, even in the darkest moments. I affectional thank my beloved sister Nidhal and my brother Mohamed, for their encouragement, love and care all along my life, my cheerful niece Fatima Zahraa for her sweet smiley face, that spread happiness and hope, wherever she goes.

My Dearest “Tata Mounira” peace upon her soul, to whom I dedicate this work. I deeply thank my father-in-law Jalel for his support and encouragements. My sweet thoughts go to my dear grandfathers, my dearest grandmother Halima, peace upon their souls, and to my beloved grandmother Baya.

Finally, I would like to thank all my family’s members and friends who encourage me, even with a smile, throughout this journey.

"Die Gelehrten sind die Erben der Propheten. Die Propheten haben keinen Dinar oder Dirham geerbt, sondern sie haben das Wissen geerbt, und wer immer es nimmt, hat reichlich Glück erhalten", sagte der Prophet Mohammed, Gott segne ihn und schenke ihm Frieden.

Dinar, Dirham: alte Goldwährung in der arabischen Welt.

Contents

List of Figures

Table of Schemes

List of Charts

List of Tables

List of Abbreviations

General Abbreviations			
R	Organic group	c	Concentration
Ar	Aryl	M	Molarity
Ph	Phenyl	mL	Milliliter
Me	Methyl	t	Time
Et	Ethyl	min	Minutes
t-Bu	*tert*-Butyl	T	Temperature
Cy	Cyclohexyl	*i*	Ipso-position in aromatic ring
X	Halide	*o*	Ortho-position in aromatic ring
THF	Tetrahydrofuran	*m*	Meta-position in aromatic ring
DMSO	Dimethyl sulfoxide	*p*	Para-position in aromatic ring
Molar equiv	Molar equivalent	Calcd	Calculated
Spectrometry and Spectroscopy Parameters			
MS	Mass spectrometry	MHz	Megaherz
ESI	Electrospray Ionization	s	Singulett
m/z	Mass per charge	d	Dublett
NMR	Nuclear magnetic resonance	t	Triplett
ppm	Parts per million	m	Multiplett
δ	Chemical shift in ppm	dd	doublet of doublet
J	Coupling constant	IR	Infrarot
Hz	Hertz		
X-Ray Diffractometer Analysis			
a, b, c	Unit cell dimensions	Z	Number of molecules in the unit cell
Å	Angström	σ	Standard deviation
α, β, γ	Unit cell angles	μ	Absorption coefficient
°	Degree	F(000)	number of electrons in the unit cell
V	Volume of the unit cell	Dc	Density

1. General Introduction

1.1 Host-Guest Approach in Supramolecular Chemistry

Supramolecular chemistry, as cited by Jean-Marie Lehn in 2002, is "the chemistry involving two or more molecules held together by non-covalent interactions".[1] As a matter of fact, host-guest chemistry is a class of supramolecular chemistry. A simplified graphic illustrating this statement is presented in Chart 1.[2] It shows the different components forming a host-guest complex. The host is either an organic molecule containing receptor sites the binding capacity of which is based on hydrogen bonding (as for instance amide, pyrrole, hydroxyl groups in enzymes),[2] or it is composed of Lewis-acidic metal centers.[3] The guests can be neutral molecules, anions or cations.[4,5] These two components form together the host-guest complex which is held together via forces such as coulomb attraction, hydrogen bonds, $\pi - \pi$ stacking, dipole-dipole, and Van der Waals interactions.[6] It is important to note that the first fundamental proposal of the concept of host-guest chemistry was presented by Emil Fischer 1894 as "Lock and Key", in which the Lock is the host and the Key is the guest.[6] Some examples of characteristic host-guest complexes are shown in Figure 1.[2,6]

Chart 1. Host-guest concept in chemistry.[2]

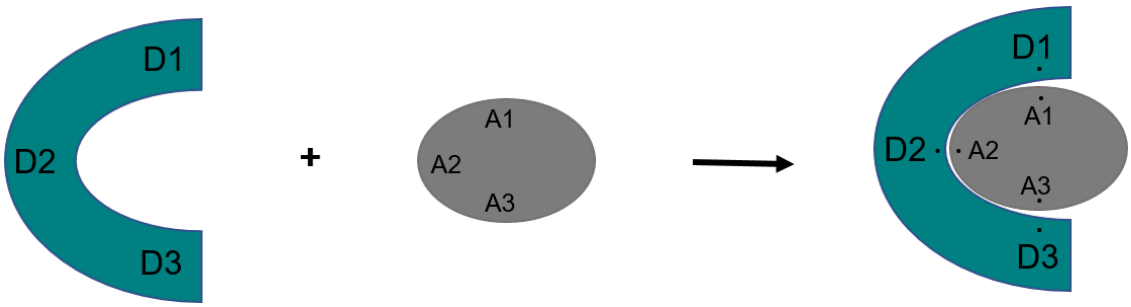

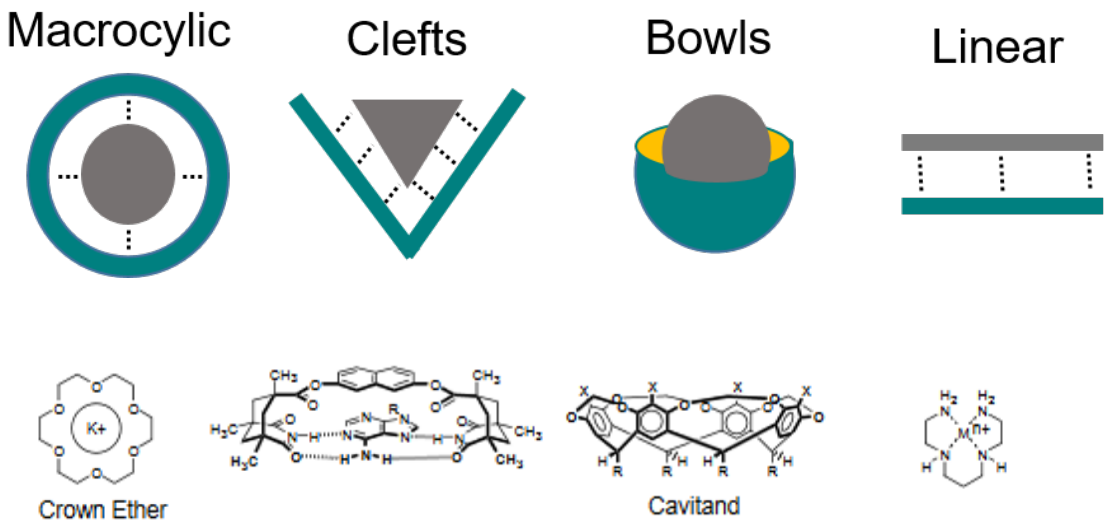

Figure 1. Examples of the most known characteristic host-guest complexes.[2,6]

The global interest in this branch of chemistry is demonstrated by a major increase in research activities in the last decades, and it is rather progressing till now. This is due to the potential supramolecular chemistry has for biological applications and catalytic processes such as "pollutant sequestration, biomedical and environmental monitoring, anion-exchange and anion-transport".[7]

1.2 Organotin Compounds in Host-Guest Chemistry

In connection with what is mentioned above, one field of the host-guest chemistry is the design of complexes oriented toward the recognition of anions and Lewis bases, in a general perspective. The first anion receptors were recognised in the early 1950s and 1960s.[3] In fact this affiliate of research found a huge amount of difficulties back in time, giving the critical technicity degree when managing anion with diver characteristics and large radii. Although, in the near past decades, this field showed important development as the appearance of different geometrical receptor molecules with higher affinity and selectivity. It exhibit interesting abilities in biological processes such as ions-sensing, small molecules activation as well as chemical catalysis.[3] These type of receptors present as a Lewis acid binding sites metal centres. Most of these are from the group 12, 13 and 14 elements such as boron, aluminium, tin, indium, silicon, tin and mercury...[8,9] This leads us to the question: what is the utility of organotin compounds as Lewis-bases receptors? First of all, back to the fundamentals; the reason is that tin as a metal centre shows considerable Lewis acidity. As the matter of fact, this character is the most important to bind Lewis-bases in a stable frame with high affinity aspects. It has to be underlined that the Lewis acidity can be tremendously increased by variation of the substituents bound to the tin

atom. Furthermore, cooperative effects can be expected when linking several tin atoms by organic spacers, giving so-called multidentate or multicentric Lewis acids. The latter concept was in part developed by Jurkschat and co-workers in the last twenty years. A sum-up of the most interesting multicentric organotin-containing precursors for binding of anions and neutral Lewis bases is presented in Scheme 1, in addition to some crystal structures of multidentate organostannate complexes (Figure 2).[3,8–12]

Scheme 1. Multicentric organotin-containing compounds as anion, Lewis base as well as ditopic receptors.[3,8–12]

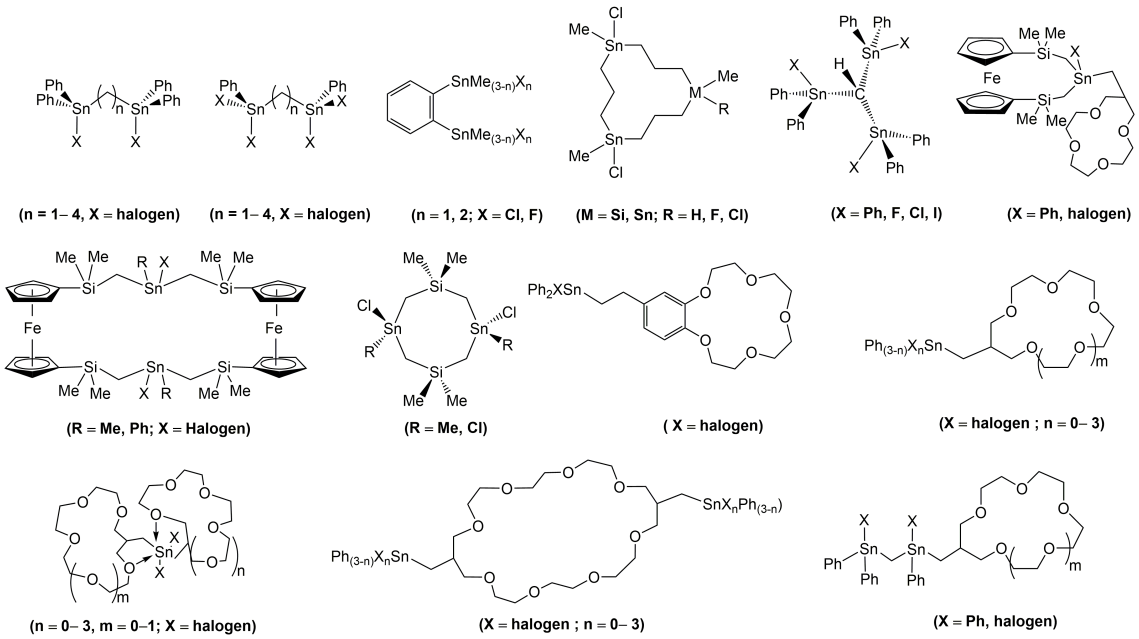

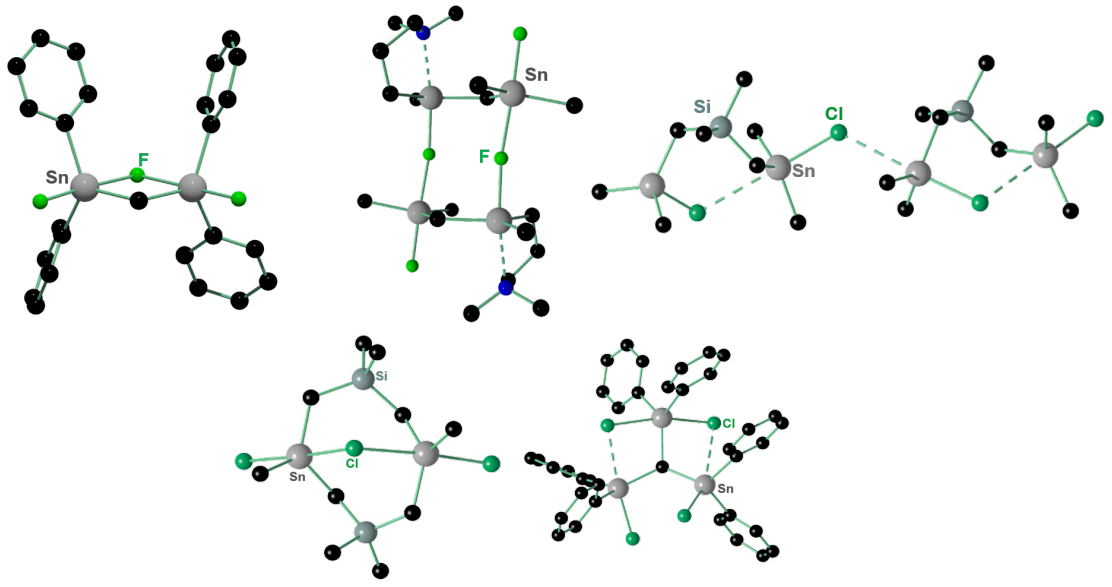

Figure 2. Examples of multidentate organostannate complexes.[3,8–12]

Another characteristic feature of organotin compounds, also related to supramolecular chemistry, is their ability for building chalcogeno-clusters that hold potential to integrate small guest molecules.[13] Especially organotin oxoclusters exhibit a high catalytic activity for transesterification reactions, acylation of alcohols,[14] and for polymerisation processes.[13] Going back to history, an early study of the cluster chemistry of organotin compounds started in 1921. *Lambourne* reported the synthesis of the first organotin oxocluster of the types $[RSn(O)O_2CR]_n$, n = 3, 6 and $[(R'Sn(O)O_2CR)_2R'Sn(O_2CR)_3]_2$; R, R' = aryl, alkyl. This was the result of the condensation reactions of alkylstannoic with carboxylic acids. However, there has been no evidence of further investigation on the structure of those clusters in the solid state or in solution.[13] It is worth mentioning that the complexity of working with such compounds in terms of isolation and identification[13,14] explains the long period of time between the first report in 1921 and the complete characterization of the compounds in 1985, when *R. R. Holmes* et al. recognized the first drum structure with the formula $[PhSn(O)O_2CC_6H_{11}]_6$.[15] This was the first launch of a novel class of tin compounds, and after that was the appearance of the ladder type structure, known as an open drum.[16,17] Scheme 2 gives an overview about synthesis methods for tetraorganodistannoxanes, the backbones of the ladder-like organotin oxoclusters. As the matter of fact, Jurkschat, Dakternieks and co-workers contributed enormously to the identification of a variety of organotin oxoclusters, exhibiting ladder-like structures in their skeletons. Actually, they reported three types of assemblies of this class of compounds (Scheme 2. b)[14] : (i) an A-type double ladder structure such as $\{[R(Cl)Sn(CH_2)_3Sn(Cl)R]O\}_4$, (Z = CH_2, X = Cl, R = CH_2SiMe_3),[18] (ii) a dimeric B-type ladder structure such as $\{[(Me_3Si)_2CH(F)Sn(CH_2)_3Sn(F)CH(SiMe_3)_2]O\}_2$, and (iii) a C-type monomer ring structure such as $[(Me_3Si)_2CH(Cl)Sn(CH_2)_3Sn(Cl)CH(SiMe_3)_2]O$.[19] Finally, some representative crystal structures of organotin oxoclusters synthesized in our research group are presented in Figure 3.[18,20–23]

Scheme 2 a). Syntheses methods for obtaining ladder-like tetraorganodistannoxanes.

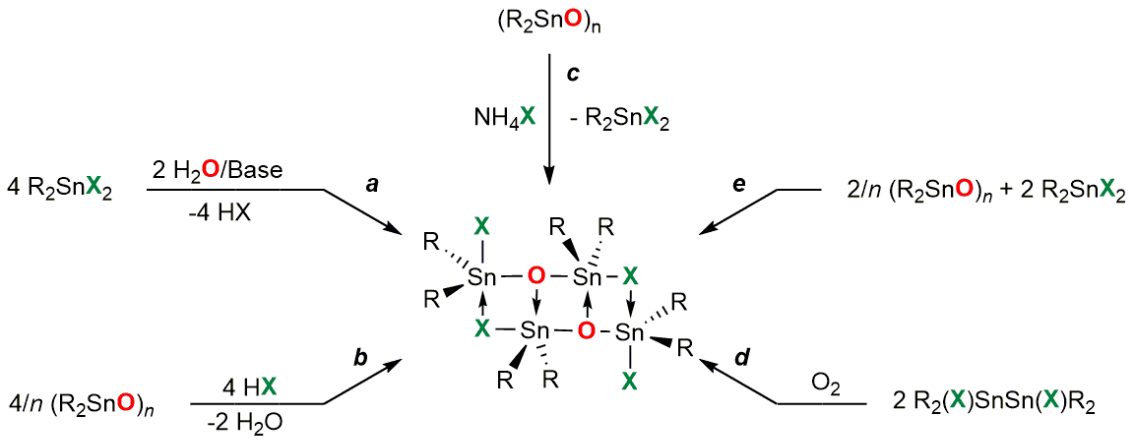

R, R' = Alkyl, Aryl; X = Halogen, OH, OC(O)R', OR', OSiR'$_3$, NR'$_2$, NCO, NCS,

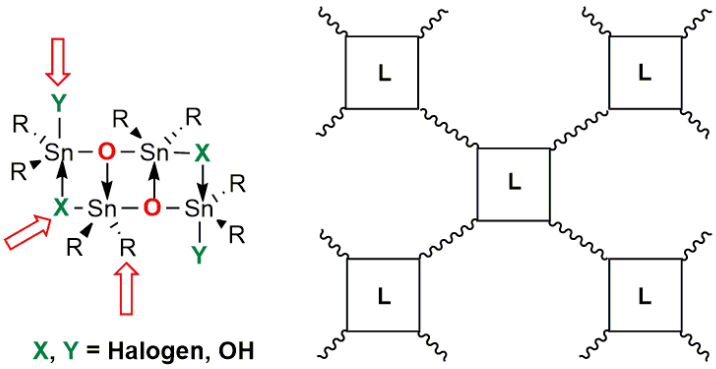

X, Y = Halogen, OH

L refers to "Ladder"

Scheme 2 b). Different A, B and C-types of ladder-type structures.[14,18,19]

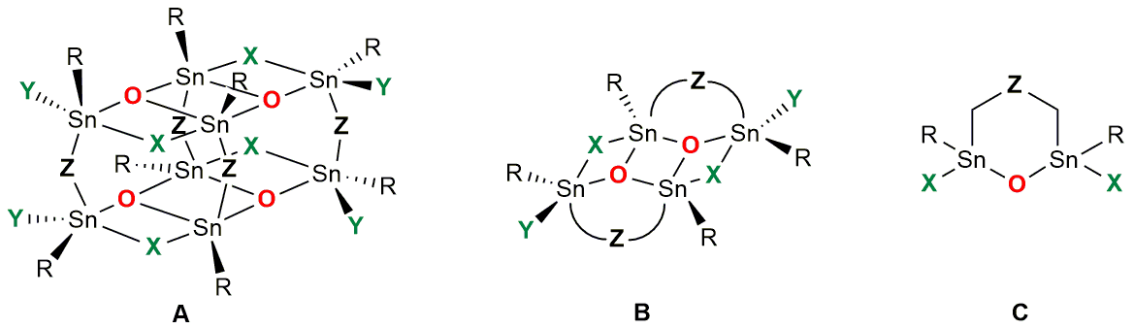

A **B** **C**

X, Y = Halogen, OH; R = Alkyl, Aryl; Z = $(CH_2)_n$

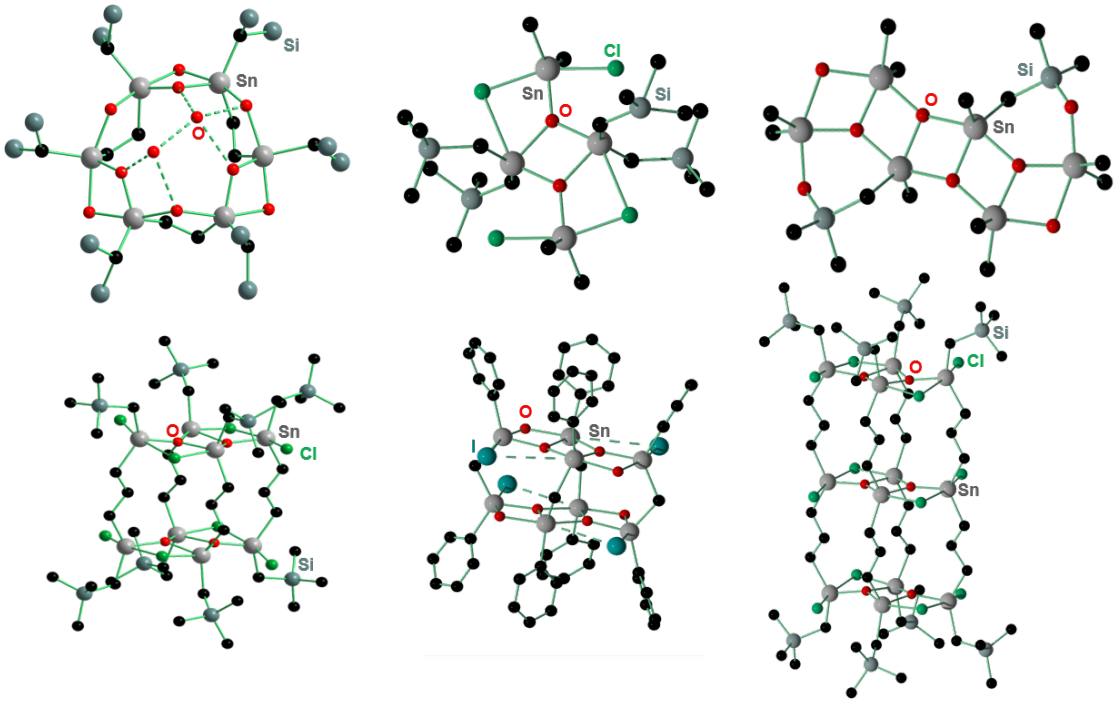

Figure 3. Examples for tetraorganodistannoxanes showing double- and triple-ladder structures, respectively.[18,20–23]

The main objective of this thesis project was to synthesize tripodal tris(organostannylmethyl)silanes of the type $MeSi(CH_2SnR_{(3-n)}X_n)_3$ (n = 0– 3; X = I, F, Cl, Br; R = Ph, CH_2SiMe_3) and study their complexation behaviour towards anions and neutral Lewis bases. Furthermore, the potential of selected examples for the formation of well-defined molecular organotin chalcogeno clusters will be evaluated. Among these, the unprecedented 18- and 30-nuclear molecular diorganotin oxides $[MeSi(CH_2SnPhO)_3]_6$ and $[MeSi(CH_2SnCH_2SiMe_3O)_3]_{10}$, respectively, first examples of organotin chalcogenides with adamantane-type structures containing both organosilicon and organotin moieties, a tetraorganodistannoxane double ladder based on a silicon-containing spacer-bridged ditin compound are reported.

2. Synthesis of $MeSi(CH_2SnR_{(3-n)}X_n)_3$ (n = 0– 3; X = I, F, Cl, Br; R = Ph, CH_2SiMe_3), its Characterization, and its Complexation Behaviour toward Lewis-Bases

2.1 Syntheses and characterization of $MeSi(CH_2SnR_{(3-n)}X_n)_3$ (n = 0– 3; X = I, F, Cl, Br; R = Ph, CH_2SiMe_3)

Scheme 3 shows the syntheses of the compounds **2**–**12**.

Scheme 3. Syntheses of the organotin derivatives $MeSi(CH_2SnR_{(3-n)}X_n)_3$, (n = 0– 3; X = I, F, Cl, Br; R = Ph, CH_2SiMe_3).

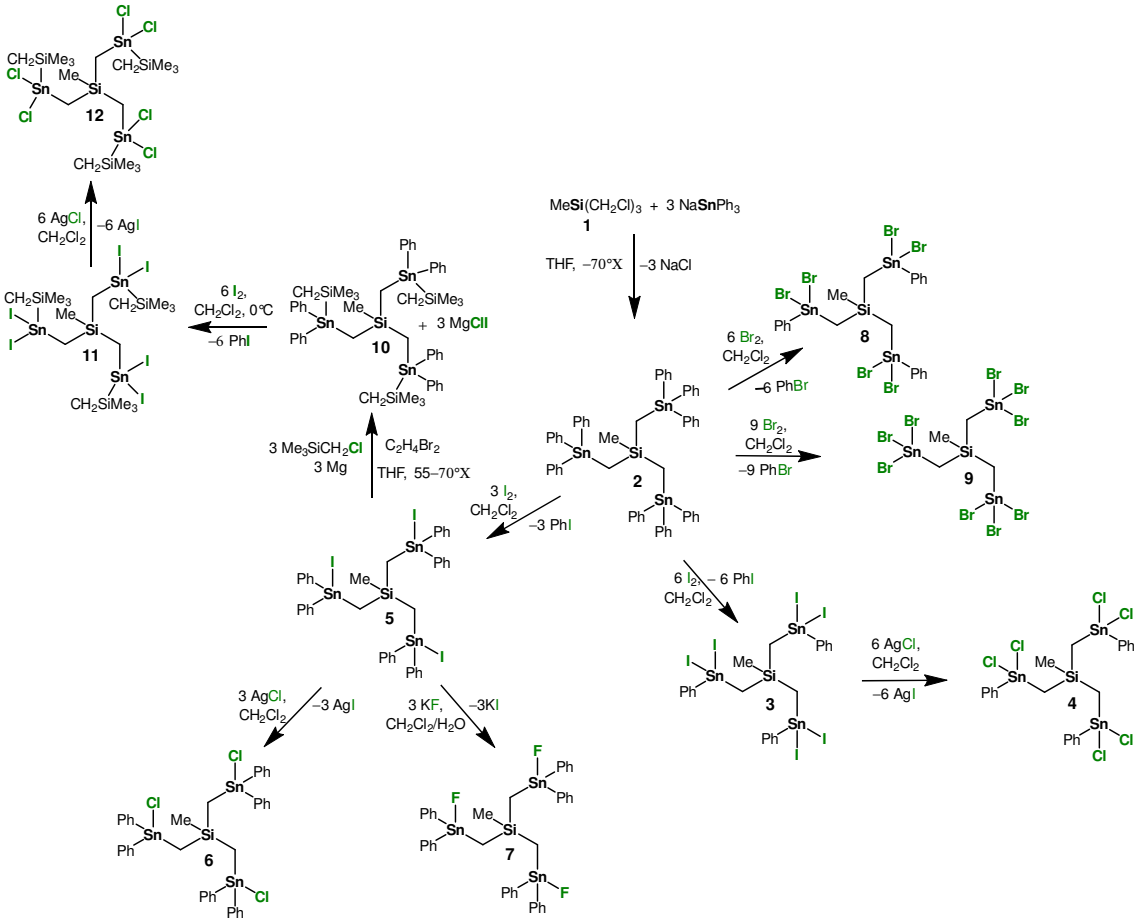

The reaction of tris(chlormethyl)methylsilane $MeSi(CH_2Cl)_3$, **1**,[24] with sodiumtriphenylstannide, $NaSnPh_3$, in THF affords tris(tri-phenylstannylmethyl)methylsilane $MeSi(CH_2SnPh_3)_3$, **2**, as a white solid material in very good yield (Scheme 3).

Compound **2** is recrystallized from hot iso-hexan to give single crystals suitable for X-ray diffraction analysis. It crystallizes in the monoclinic space group $P2_1/c$. Figure 4 shows the molecular structure and selected interatomic distances and angles are given in Table 1.

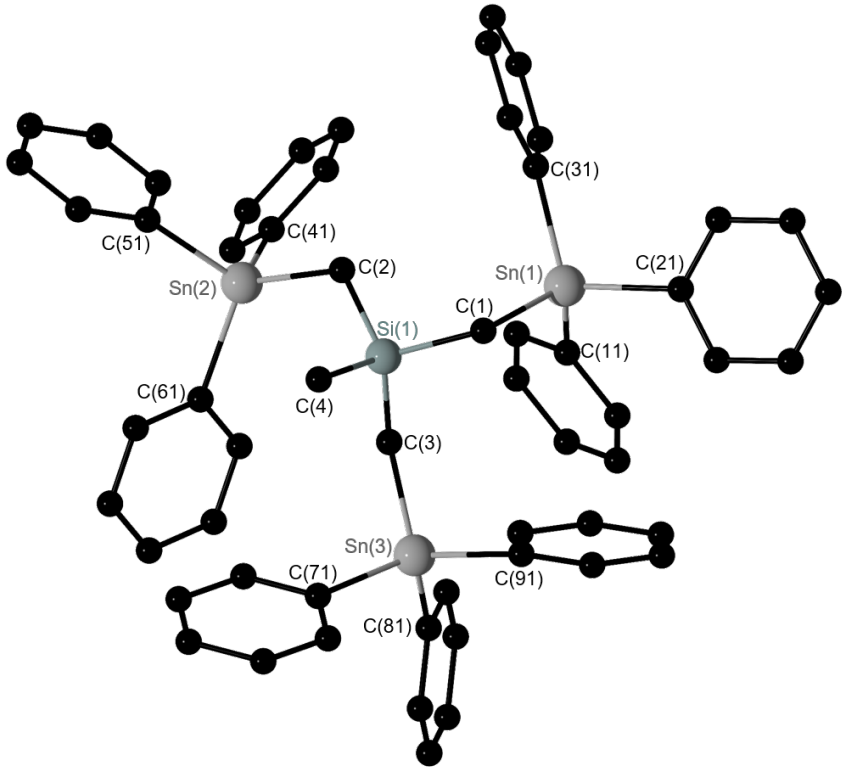

Figure 4. General view (POV-Ray) of a molecule of **2** showing 30 % probability displacement ellipsoids and the crystallographic numbering scheme. There are disorders of the phenyl ring C(11) to C(16) and the phenyl ring C(51) to C(56) with a ratio of 60:40 and 55:45, respectively. Only the C_i carbon atoms of the phenyl substituents are shown for clarity. Selected interatomic distances and angles are given in Table 1.

The environments at Sn(1), Sn(2) and Sn(3) are distorted tetrahedral with angles varying between 105.13(9)° (C3–Sn3–C81) and 118.66(10)° (C2–Sn2–C61). The Sn–C distances varying from 2.120(7) Å (Sn2–C51) and 2.1687(9) Å (Sn2–C61) are typical for tetraorganotin compounds.[9,12,23,25] Nevertheless, the most interesting aspect to mention is the tripod geometry of this novel compound **2**. The Si(1)–C(1)–Sn(1), Si(1)–C(2)–Sn(2), and Si(1)–C(3)–Sn(3) interatomic angles of 117.40(14)°, 120.29(15)°, and 120.52(14)°, respectively are very near. As well, the interatomic distances Si(1)–C(1) 1.867(3) Å, Si(1)–C(2) 1.871(3) Å, Si(1)–C(3) 1.866(3) Å, and Si(1)–C(4) 1.860(3) Å are almost equal as

expected. The same holds for the Sn(1)–C(1) 2.154(3) Å, Sn(2)–C(2) 2.147(3) Å, and Sn(3)–C(3) 2.132(3) Å distances. The environment at the silicon atom is distorted tetrahedral with almost equal angles varying between 107.96(17)° (C4–Si1–C2) and 110.52(14)° (C3–Si1–C2) and are comparable to the three angles (Si1–C1–Sn1), (Si1–C2–Sn2), and (Si1–C3–Sn3).

A ^{119}Sn NMR spectrum (Figure 5) of a solution of compound **2** in $CDCl_3$ shows one singlet resonance at -89 ppm ($^1J(^{119}Sn-^{13}C)$ = 492 Hz), which is comparable to those reported for the tetraorganotin compounds $(Ph_3Sn)_2CH_2$ (δ –79 ppm),[26] $(Ph_3SnCH_2)_2SnPh_2$ (^{ter}Sn δ –79 ppm),[25] and the structurally alike compound $(Ph_3Sn)_3CH$ (δ –78 ppm).[12] However, a comparison with the silicon methylene-bridged organotin compound *cyclo*-$Me_2Sn(CH_2SiMe_2CH_2)_2SnMe_2$ (δ 16 ppm)[9] shows that compound **2** is low-frequency shifted. This can be explained as a result of the different substituent patterns and the ring structure of the latter compound.

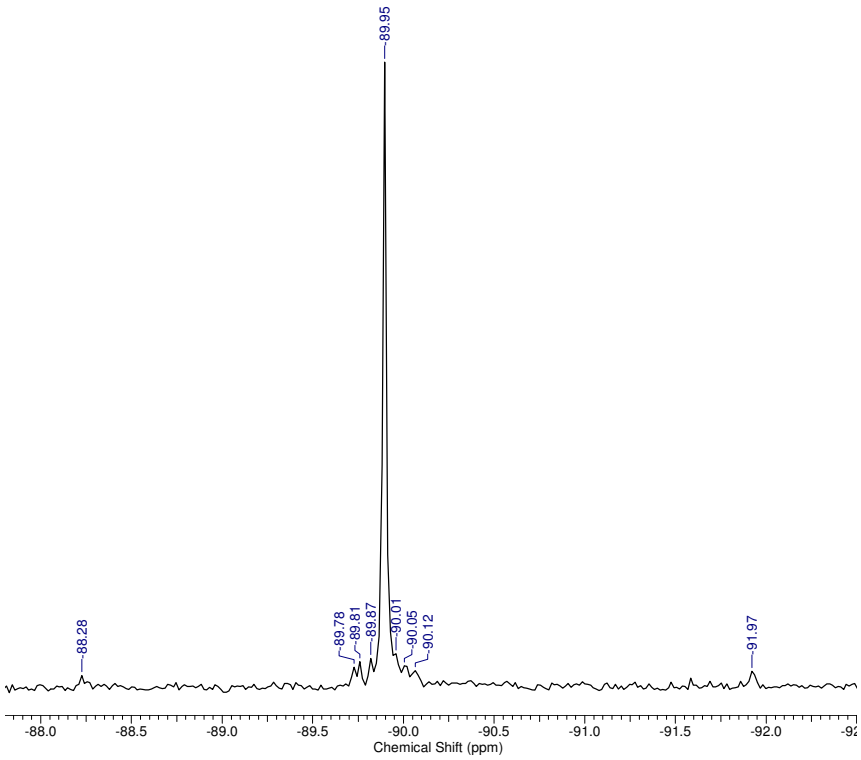

Figure 5. ^{119}Sn NMR spectrum (149.26 MHz, $CDCl_3$) of compound **2**.

A ^{29}Si NMR spectrum shows a singlet resonance at δ 8.75 ppm ($^2J(^{29}Si-^{117/119}Sn)$ = 21 Hz). It is slightly different with that reported for the analogous compound *cyclo*-$Me_2Sn(CH_2SiMe_2CH_2)_2SnMe_2$ at δ 5.01 ppm ($^2J(^{29}Si-^{117/119}Sn)$ = 50 Hz).[9] This difference is the result of slightly different substituent patterns in both compounds. In the ^{1}H NMR spectrum a singlet resonance corresponding to the SiCH_3 protons at δ –0.19 ppm and another chemical shift are assigned to the (SiCH_2Sn) protons at δ 0.33 ppm

($^2J(^1H-^{117/119}Sn)$ = 78 Hz). This coupling constant value is close to that reported for the corresponding protons in *cyclo*-$Me_2Sn(CH_2SiMe_2CH_2)_2SnMe_2$ ($^2J(^1H-^{117/119}Sn)$ = 69 Hz).[9]

In a ^{13}C NMR spectrum the chemical shift at δ 3.9 ppm ($^3J(^{13}C-^{117/119}Sn)$ = 12 Hz, $^1J(^{13}C-^{29}Si)$ = 51 Hz) is assigned to the ($SiCH_3$) carbon atom. This chemical shift is close to that reported for the corresponding carbon atom in *cyclo*-$Me_2Sn(CH_2SiMe_2CH_2)_2SnMe_2$ at δ 3.6 ppm ($^3J(^{13}C-^{117/119}Sn)$ = 20 Hz).[9] In addition to that, we find the singlet resonance referring to the ($SiCH_2Sn$) carbon atom at δ –1.7 ppm ($^1J(^{13}C-^{117/119}Sn)$ = 262/274 Hz, $^1J(^{13}C-^{29}Si)$ = 48 Hz). These values are comparable to those measured for the corresponding carbon atom in *cyclo*-$Me_2Sn(CH_2SiMe_2CH_2)_2SnMe_2$ at δ –2.5 ppm ($^1J(^{13}C-^{117/119}Sn)$ = 229/240 Hz, $^1J(^{13}C-^{29}Si)$ = 24 Hz).[9] In the aromatic part, the chemical shifts corresponding to the carbon atoms C_m at δ 128.4 ppm ($^3J(^{13}C-^{117/119}Sn)$ = 49 Hz), C_p at δ 128.7 ppm ($^4J(^{13}C-^{117/119}Sn)$ = 10 Hz), C_o at δ 136.9 ppm ($^2J(^{13}C-^{117/119}Sn)$ = 37 Hz), and C_i at δ 139.6 ppm ($^1J(^{13}C-^{117/119}Sn)$ = 460/492 Hz), are very close to those reported for the corresponding carbon atoms in $(SnPh_3)_3CH$, respectively, at δ 128.1 ppm ($^3J(^{13}C-^{117/119}Sn)$ = 51 Hz), δ 128.5 ppm ($^4J(^{13}C-^{117/119}Sn)$ = 11 Hz), δ 137.2 ppm ($^2J(^{13}C-^{117/119}Sn)$ = 38 Hz), and δ 140.2 ppm ($^1J(^{13}C-^{117/119}Sn)$ = 486/511 Hz).[12] All these data are evidence that the tin atoms in compound **2** are four-coordinated with distorted tetrahedral geometries, as observed in the solid state. An electrospray ionization mass spectrum (ESI MS positive mode) shows mass clusters centred at m/z 119.1 (100, Sn^+) and 383.0097 $C_{18}H_{15}SnO_2^+$ (50, [M – $C_{40}H_{43}SiSn_2$ + 2 H_2O]), respectively (See Supporting Information, Chapter 2, Figures S4- S10).

The treatment of compound **2** with six molar equiv of elemental iodine in CH_2Cl_2 produces the iodine-substituted tris(diiodidophenylstannylmethyl)methylsilane $MeSi(CH_2SnPhI_2)_3$, **3**, in quantitative yield. The latter, once reacted with six molar equiv of silver chloride in CH_2Cl_2, gives the organotin dichloride derivative tris(dichloridophenylstannylmethyl)methylsilane $MeSi(CH_2SnPhCl_2)_3$, **4**, in good yield (Scheme 3).

Compound **4** is a white solid, as to compound **3** is a yellowish oil. Both compounds show good solubility in common organic solvents such as CH_2Cl_2, $CHCl_3$, and CH_3CN. A ^{119}Sn NMR spectrum of the diiodido-substituted organotin derivative **3** in $CDCl_3$ (Figure 6) shows a singlet resonance at δ –228 ppm which is high-frequency shifted with respect to the ^{119}Sn chemical shifts reported for $(Ph_2I_2Sn)_3CH$ (δ –262 ppm[12]) and low-frequency shifted in comparison to that reported for $(Ph_2I_2Sn)_2CH_2$ (δ –24 ppm[21]). The ^{119}Sn chemical shift of compound **3** is close to that reported for the similar substituted compound

Ph_2SnI_2 (δ –245 ppm).[27] A ^{29}Si NMR spectrum displays a singlet resonance at δ 8.87 ppm ($^2J(^{29}Si-^{117/119}Sn)$ = 36 Hz).

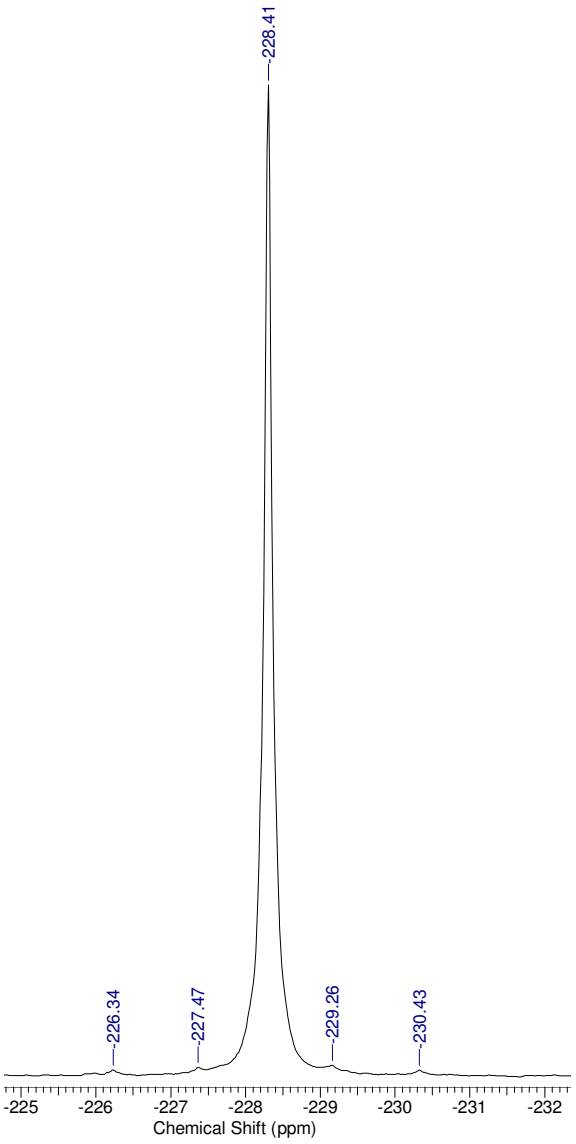

Figure 6. ^{119}Sn NMR spectrum (149.26 MHz, $CDCl_3$) of compound **3**.

Moreover, in the ^{1}H NMR spectrum a singlet resonance assigned to the SiCH_3 protons at δ 0.53 ppm is observed in addition to the singlet resonance corresponding to the (SiCH_2Sn) protons at δ 1.71 ppm ($^2J(^1H-^{117/119}Sn)$ = 84 Hz). The latter resonance is considerably low-frequency shifted as compared to that reported for the corresponding methylene protons in $(Ph_2I_2Sn)_2CH_2$ at δ 2.77 ppm ($^2J(^1H-^{117/119}Sn)$ = 65 Hz).[21] A ^{13}C NMR spectrum shows one singlet resonance assigned to the SiCH_3 carbon atom at δ 3.2 ppm ($^3J(^{13}C-^{117/119}Sn)$ = 20 Hz, $^1J(^{13}C-^{29}Si)$ = 40 Hz). Furthermore, a singlet resonance is observed at δ 11.9 ppm ($^1J(^{13}C-^{117/119}Sn)$ = 259/272 Hz, $^1J(^{13}C-^{29}Si)$ = 50 Hz) referring to the SiCH_2Sn carbon atom. This ^{13}C NMR chemical shift is very

close to that reported for the corresponding carbon atom in $(Ph_2I_2Sn)_2CH_2$ δ 12.1 ppm ($^1J(^{13}C-^{117/119}Sn)$ = 269/280 Hz).[21] In the aromatic part, the chemical shifts corresponding respectively to the carbon atoms C_m at δ 129.1 ppm ($^3J(^{13}C-^{117/119}Sn)$ = 77 Hz), C_p at δ 130.9 ppm ($^4J(^{13}C-^{117/119}Sn)$ = 21 Hz), C_o at δ 134.1 ppm ($^2J(^{13}C-^{117/119}Sn)$ = 60 Hz), and C_i at δ 136.6 ppm ($^1J(^{13}C-^{117/119}Sn)$ = 603 Hz), are very close to those reported for the corresponding carbon atoms in $(SnPh_3)_3CH$, respectively, at δ 129.0 ppm ($^3J(^{13}C-^{117/119}Sn)$ = 88 Hz), δ 131.4 ppm ($^4J(^{13}C-^{117/119}Sn)$ = 19 Hz), δ 135.1 ppm ($^2J(^{13}C-^{117/119}Sn)$ = 66 Hz), and δ 136.6 ppm (no $^1J(^{13}C-^{117/119}Sn)$ indicated).[12] Also, after an investigation with 2D NMR COESY, HSQC, and HMBC (See Supporting Information, Chapter 2, Figures S12- S21) compound **3** shows a perfect match with the previous 1D NMR study. A ^{119}Sn NMR spectrum of the organotin dichloride-substituted derivative **4** in C_6D_6 (Figure 7) presents a singlet resonance at δ 41 ppm ($^2J(^{117/119}Sn-^{29}Si)$ = 48 Hz), which is high-frequency shifted with respect to the ^{119}Sn chemical shifts of the similar compounds $(Ph_2Cl_2Sn)CH_2$ (δ 32 ppm)[12] and $(PhCl_2SnCH_2)_2SnCl_2$ (δ –55.8 and δ –101.3 ppm) in CD_3CN.[25] This difference is due to the polarity of the solvent in which the measurement was done.

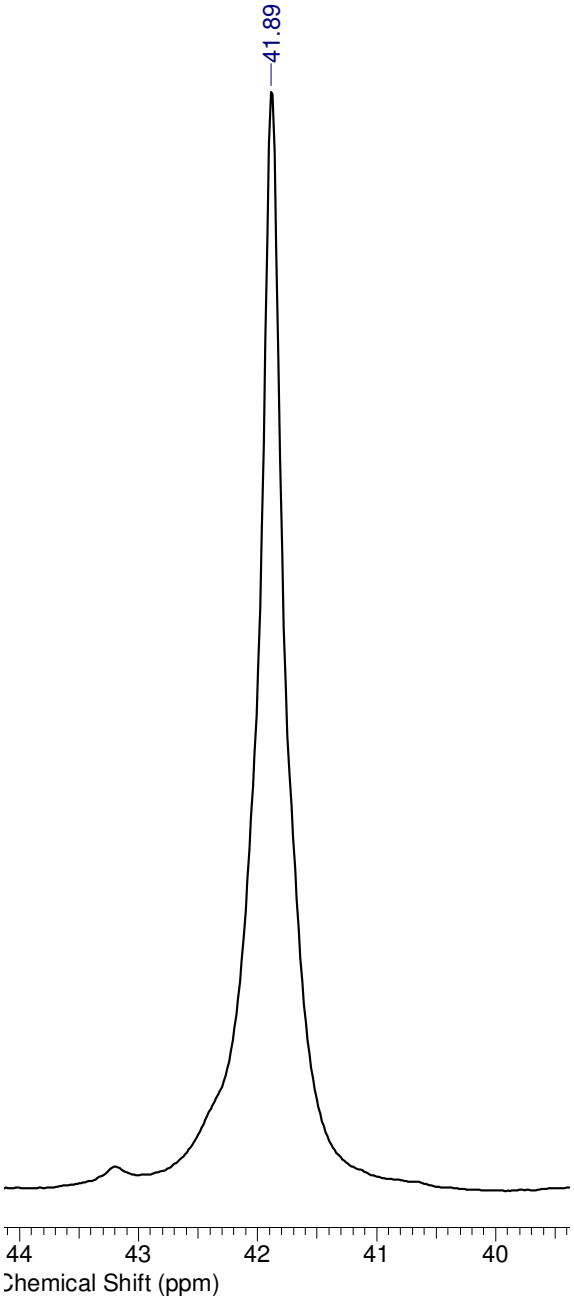

Figure 7. ^{119}Sn NMR spectrum (149.26 MHz, C_6D_6) of compound **4**.

A ^{29}Si NMR spectrum shows a singlet resonance at δ 7.5 ppm ($^1J(^{29}Si-^{119/117}Sn)$ = 48 Hz). This signal is slightly high-field shifted from the ^{29}Si chemical shift in *cyclo*-$Cl_2Sn(CH_2SiMe_2CH_2)_2SnCl_2$ at 4.1 ppm.[9] The difference is due to the different substitution pattern of the silicon atoms in the two compounds.

A ^1H NMR spectrum of compound **4** displays a singlet resonance assigned to the $SiCH_3$ protons at 0.69 ppm which is comparable to that reported for the corresponding protons in *cyclo*-$Cl_2Sn(CH_2SiMe_2CH_2)_2SnCl_2$ at δ 0.35 ppm.[9] Furthermore, the singlet resonance corresponding to the $SiCH_2Sn$ protons is found at δ 1.50 ppm ($^2J(^1H-^{117/119}Sn)$

= 88 Hz). This resonance is shifted to high frequency as compared to that reported for the corresponding protons in *cyclo*-$Cl_2Sn(CH_2SiMe_2CH_2)_2SnCl_2$ at δ 1.02 ppm ($^2J(^1H-^{117/119}Sn)$ = 49/52 Hz).[9] In a ^{13}C NMR spectrum, one singlet resonance at δ 3.5 ppm ($^3J(^{13}C-^{117/119}Sn)$ = 22 Hz, $^1J(^{13}C-^{29}Si)$ = 35 Hz) is observed referring to the Si*C*H_3 carbon atom. The singlet resonance at δ 11.2 ppm ($^1J(^{13}C-^{117/119}Sn)$ = 361/376 Hz, $^1J(^{13}C-^{29}Si)$ = 47 Hz) is assigned to the Si*C*H_2Sn carbon atom. The latter ^{13}C NMR shift is close to those reported for the corresponding carbon atom in *cyclo*-$Cl_2Sn(CH_2SiMe_2CH_2)_2SnCl_2$ at δ 13.4 ppm ($^1J(^{13}C-^{117/119}Sn)$ = 293/306 Hz, $^1J(^{13}C-^{29}Si)$ = 44 Hz).[9] However, this shift is low-frequency shifted compared to that reported for the Sn*C*H_2Sn carbon in $(PhCl_2SnCH_2)_2SnCl_2$ at δ 34.5 ppm ($^1J(^{13}C-^{117/119}Sn)$ = 606 Hz).[25] In the aromatic part, the chemical shifts corresponding to the carbon atoms C_m at δ 129.4 ppm ($^3J(^{13}C-^{117/119}Sn)$ = 85 Hz), C_p at δ 131.4 ppm ($^4J(^{13}C-^{117/119}Sn)$ = 17 Hz), C_o at δ 134.3 ppm ($^2J(^{13}C-^{117/119}Sn)$ = 65 Hz), and C_i at δ 139.7 ppm ($^1J(^{13}C-^{117/119}Sn)$ = 742/773 Hz), are very close to those reported for the corresponding carbon atoms in $(PhCl_2SnCH_2)_2SnCl_2$, respectively, at δ 129.6 ppm ($^3J(^{13}C-^{117/119}Sn)$ =101 Hz), δ 131.4 ppm ($^4J(^{13}C-^{117/119}Sn)$ = 20 Hz), δ 135.3 ppm ($^2J(^{13}C-^{117/119}Sn)$ = 67 Hz), and δ 143 ppm.[25] (See Supporting Information, Chapter 2, Figures S34- S37). All these information confirm that the tin atoms in compounds **3** and **4** are four-coordinated in solution. As well, the electrospray ionization mass spectrum (positive mode) shows for 3 mass clusters centred at m/z 392.1, 721.0 corresponding to $I_2SnH_3O^+$ (30, $[M - C_{22}H_{24}I_4SiSn_2 + H^+ + H_2O]^+$) and $C_{16}H_{19}ISiSn_3^+$ (15, $[M - C_6H_5I_5]^+$), respectively, and in the negative mode mass clusters centred at m/z 127.3 I^- (8, $[M - C_{22}H_{24}I_5SiSn_3]^-$), 381.0 I_3^- (100, $[M - C_{22}H_{24}I_3SiSn_3]^-$), 1450.3017 ($C_{22}H_{25}I_6OSiSn_3 \cdot 1.00\,[M+OH-]^- + C_{22}H_{24}I_6ClSiSn_3 \cdot 0.10\,[M + Cl-]^-$), and 1560.1988 $C_{22}H_{24}I_7OSiSn_3^-$ ($[M + I]^-$) (See Supporting Information, Chapter 2, Figures S22- S32).

A spectrum of **4**, in the positive mode, revealed clusters at m/z 738.7, 766.8694, and 776.8050 fitting to $C_{16}H_{21}Cl_4SiSn_3^+$ (25, $[M - Ph - 2\,Cl^- + H^+]^+$), $C_{21}H_{24}Cl_3SiSn_3^+$ (100, $[M - Me - 3\,Cl^- + H^+]^+$), and $C_{16}H_{22}Cl_5SiSn_3^+$, respectively (See Supporting Information, Chapter 2, Figures S38- S41).

The reaction of compound **2** with three molar equiv of elemental iodine in CH_2Cl_2 gives the iodine-substituted tris(iodidophenylstannylmethyl)methylsilane $MeSi(CH_2SnPh_2I)_3$, **5**, in quantitative yield as a slightly yellow oil. The corresponding organotin chloride $MeSi(CH_2SnPh_2Cl)_3$, **6** is obtained as a colourless crystalline material through the reaction of **5** with an excess of AgCl in CH_2Cl_2. Compound **6** crystallizes in the orthorhombic space *Pna*2_1. Compound **5**, once reacted with excess of KF in biphasic mixture CH_2Cl_2/H_2O for 3 days, gives the tris(fluoridodiphenylstannylmethyl)methylsilane $MeSi(CH_2SnPh_2F)_3$, **7**, as a white insoluble solid in very good yield. Further purification is realized by a re-

peated wash with acetone, water, and methanol. As to compound **5** and **6**, they show good solubility in $CHCl_3$, CH_2Cl_2, CH_3CN, and acetone (Scheme 3).

The ^{119}Sn NMR spectra of the iodido-substituted derivative **5** and the chlorido-substituted derivative **6** in $CDCl_3$ exhibit both one intense resonance, respectively, at δ –67 ppm and δ 24 ppm (Figure 8). These shifts are very similar to those reported for $(IPh_2Sn)_2CH_2$ (δ –68 ppm)[26] $(IPh_2Sn_2CH_2)_2SiMe_2$ (δ –65 ppm),[28] $(Ph_2ISn)_3CH$ (δ –70 ppm),[12] $(ClPh_2Sn)_2CH_2$ (δ 20 ppm),[26] $(Ph_2ClSnCH_2)_2SnClPh$ (^{ter}Sn δ 20 ppm), $(Ph_2ClSnCH_2SnClPh_2)_2CH_2$ (^{ter}Sn δ 17 ppm).[25] However, when we compare the ^{119}Sn chemical shift of **5** to that corresponding in $\{(CH_2)_3NMe_2\}PhISnCH_2SnPh_3$ (δ –92 ppm),[29] we found it high-frequency shifted, as for $fc(SiMe_2CH_2SnIPhCH_2SiMe_2)_2fc$ (δ –13 ppm),[11] is low-frequency shifted. As for compound **6**, the ^{119}Sn NMR shift is low-frequency shifted in comparison with that reported for $(ClMe_2Sn_2CH_2)_2SiMe_2$ (δ 163 ppm), *cyclo*-$(Me(Cl)Sn(CH_2SiMe_2CH_2)_2Sn(Cl)Me$ (δ 174 ppm),[9] and $fc(SiMe_2CH_2SnClPhCH_2SiMe_2)_2fc$ (δ 95 ppm).[11] Nevertheless, this chemical shift is high-frequency shifted, as in approach with that reported for $(Ph_2ClSn)_3CH$ (δ –9 ppm).[12] This dissimilarity of the chemical shifts mentioned above is explained by the variety of the substituent patterns about the tin atoms in these different compounds. All these information are evidences for the four coordination geometry of the tin atoms in **5** and **6** (Figures 5, 6).

The ^{29}Si NMR spectra of 5 and 6 display both a singlet resonance, respectively, at 8.97 ppm ($^2J(^{29}Si-^{117/119}Sn)$ = 28 Hz) and 8.61 ppm ($^2J(^{29}Si-^{117/119}Sn)$ = 30 Hz) (See Supporting Information, Chapter 2, Figures S45, S56). These shifts are close to those reported for $(IPh_2Sn_2CH_2)_2SiMe_2$ (δ 6.7 ppm) ($^2J(^{29}Si-^{117/119}Sn)$ = 27 Hz), and $(ClPh_2Sn_2CH_2)_2SiMe_2$ (δ 6.1 ppm) ($^2J(^{29}Si-^{117/119}Sn)$ = 29 Hz).[28] The ^1H NMR spectra of the organotin compounds **5** and **6** show for both, as expected, two singlet resonances, at 0.15 ppm and 0.35 ppm, respectively, referring to the $SiCH_3$ protons, and two singlet resonances at 0.99 ppm ($^2J(^1H-^{117/119}Sn)$ = 80 Hz) and 0.96 ppm ($^2J(^1H-^{117/119}Sn)$ = 79 Hz), respectively, referring to the $SiCH_2Sn$ protons (See Supporting Information, Chapter 2, Figures S43, S54). These shifts are very similar to those corresponding to the $SiCH_3$ protons in $(IPh_2Sn_2CH_2)_2SiMe_2$ (δ 0.21 ppm)[28] and $(ClMe_2Sn_2CH_2)_2SiMe_2$ (δ 0.18 ppm).[9] In addition to that, the shifts corresponding to the $SiCH_2Sn$ protons in **5** and **6** are very close to those reported for $(IPh_2Sn_2CH_2)_2SiMe_2$ (δ 1.03 ppm) ($^2J(^1H-^{117/119}Sn)$ = 78/81 Hz) and $(ClPh_2Sn_2CH_2)_2SiMe_2$ (δ 0.79 ppm) ($^2J(^1H-^{117/119}Sn)$ = 77/80 Hz).[28] However, these latter signals are low-frequency shifted, in comparison with those for compounds $(IPh_2Sn)_2CH_2$ (δ 1.87 ppm) and $(ClPh_2Sn)_2CH_2$ (δ 1.54 ppm).[26]

In the ^{13}C NMR spectra of **5** and **6**, (See Supporting Information, Chapter 2, Figures S44, S55) the chemical shifts referring to the $SiCH_3$ carbons are, respec-

tively, 3.76 ppm ($^3J(^{13}C-^{117/119}Sn)$ = 15 Hz) and 3.6 ppm ($^3J(^{13}C-^{117/119}Sn)$ = 15 Hz, $^1J(^{13}C-^{29}Si)$ = 40 Hz). These are close to those reported for the corresponding carbons in $(IPh_2Sn_2CH_2)_2SiMe_2$) (δ 2.5 ppm) ($^3J(^{13}C-^{117/119}Sn)$ = 16 Hz, $^1J(^{13}C-^{29}Si)$ = 53 Hz)[28] and in *cyclo*-(Me(Cl)Sn($CH_2SiMe_2CH_2$)$_2$Sn(Cl)Me (δ 3.57 ppm) ($^3J(^{13}C-^{117/119}Sn)$ = 26 Hz).[9]

The chemical shifts assigned to the Si*C*H_2Sn carbon atoms of **5** and **6** are, respectively, 4.14 ppm ($^3J(^{13}C-^{117/119}Sn)$ = 23 Hz, $^1J(^{13}C-^{29}Si)$ = 48 Hz, $^1J(^{13}C-^{117/119}Sn)$ = 253/264 Hz) and 4.13 ppm ($^3J(^{13}C-^{117/119}Sn)$ = 21 Hz, $^1J(^{13}C-^{29}Si)$ = 48 Hz, $^1J(^{13}C-^{117/119}Sn)$ = 285/296 Hz). These latter chemical shifts are close to those reported for the corresponding carbon atoms in fc($SiMe_2CH_2SnIPhCH_2SiMe_2$)$_2$fc ($\delta$ 4.32 ppm) ($^1J(^{13}C-^{117/119}Sn)$ =250 Hz) and fc($SiMe_2CH_2SnIPhCH_2SiMe_2$)$_2$fc ($\delta$ 4.8 ppm) ($^1J(^{13}C-^{117/119}Sn)$ = 266/279 Hz).[11] However, these shifts are high-field shifted comparing to those reported for the corresponding carbon atoms in $(IPh_2Sn_2CH_2)_2SiMe_2$ (δ 3.5 ppm) ($^3J(^{13}C-^{117/119}Sn)$ = 27 Hz, $^1J(^{13}C-^{29}Si)$ = 47 Hz, $^1J(^{13}C-^{117/119}Sn)$ = 253/267 Hz) and $(ClPh_2Sn_2CH_2)_2SiMe_2$ (δ 3.1 ppm) ($^1J(^{13}C-^{117/119}Sn)$ = 314/318 Hz).[28] In the aromatic part, the chemical shifts corresponding to the carbon atoms in **5** and **6** are C_m (**5**: δ 128.8 ppm, $^3J(^{13}C-^{117/119}Sn)$ = 60 Hz; **6**: δ 128.9 ppm, $^3J(^{13}C-^{117/119}Sn)$ = 63 Hz), C_p (**5**: δ 129.9 ppm, $^4J(^{13}C-^{117/119}Sn)$ = 14 Hz; **6**: δ 130.1 ppm, $^4J(^{13}C-^{117/119}Sn)$ = 12 Hz), C_o (**5**: δ 135.8ppm, $^2J(^{13}C-^{117/119}Sn)$ = 60 Hz; **6**: δ 135.5 ppm, $^2J(^{13}C-^{117/119}Sn)$ = 61 Hz), and C_i (**5**: δ 137.6 ppm,) $^1J(^{13}C-^{117/119}Sn)$ = 520/544 Hz; **6**: δ 139.2 ppm, $^1J(^{13}C-^{117/119}Sn)$ = 564/589 Hz). These values are very close to those reported for the corresponding carbon atoms in $(IPh_2Sn_2CH_2)_2SiMe_2$, respectively, C_m (δ 128.8 ppm, $^3J(^{13}C-^{117/119}Sn)$ = 60 Hz), C_p (δ 129.9) ($^4J(^{13}C-^{117/119}Sn)$ = 13 Hz), C_o (δ 135.7) ($^2J(^{13}C-^{117/119}Sn)$ = 49 Hz), and C_i (δ 137.8) ($^1J(^{13}C-^{117/119}Sn)$ = 540 514/Hz) and $(ClPh_2Sn_2CH_2)_2SiMe_2$ C_m (δ 128.9) ($^3J(^{13}C-^{117/119}Sn)$ = 61 Hz), C_p (δ 130.1) ($^4J(^{13}C-^{117/119}Sn)$ = 13 Hz), C_o (δ 135.5) ($^2J(^{13}C-^{117/119}Sn)$ = 51 Hz), and C_i (δ 139.4). For the latter, no coupling constant is reported.[28] Furthermore, the ESI mass spectrum (positive mode) of **5** shows mass clusters centred at m/z 919.2 $C_{39}H_{44}NaSiSn_3^+$ (100, $[M - Me - 3I^- + 4H^+ + Na^+]^+$), and 969.2 $C_{12}H_{23}I_3O_2SiSn_3^+$ (100, $[M - 5Ph^- + 6H^+ + Na^+ + 2MeOH]^+$), and in negative mode one mass cluster at m/z negative mode 127.3 I^- (100, $[M - C_{40}H_{33}I_2SiSn_3^+]^-$) (See Supporting Information, Chapter 2, Figures S47- S52). As for **6** the ESI MS spectrum exhibits in negative mode two mass clusters centred at m/z 1044.86 and 1136.79 fitting to $[C_{40}H_{39}Cl_4SiSn_3]^-$ and $[C_{40}H_{39}Cl_3ISiSn_3]^-$, respectively (See Supporting Information, Chapter 2, Figures S58- S63).

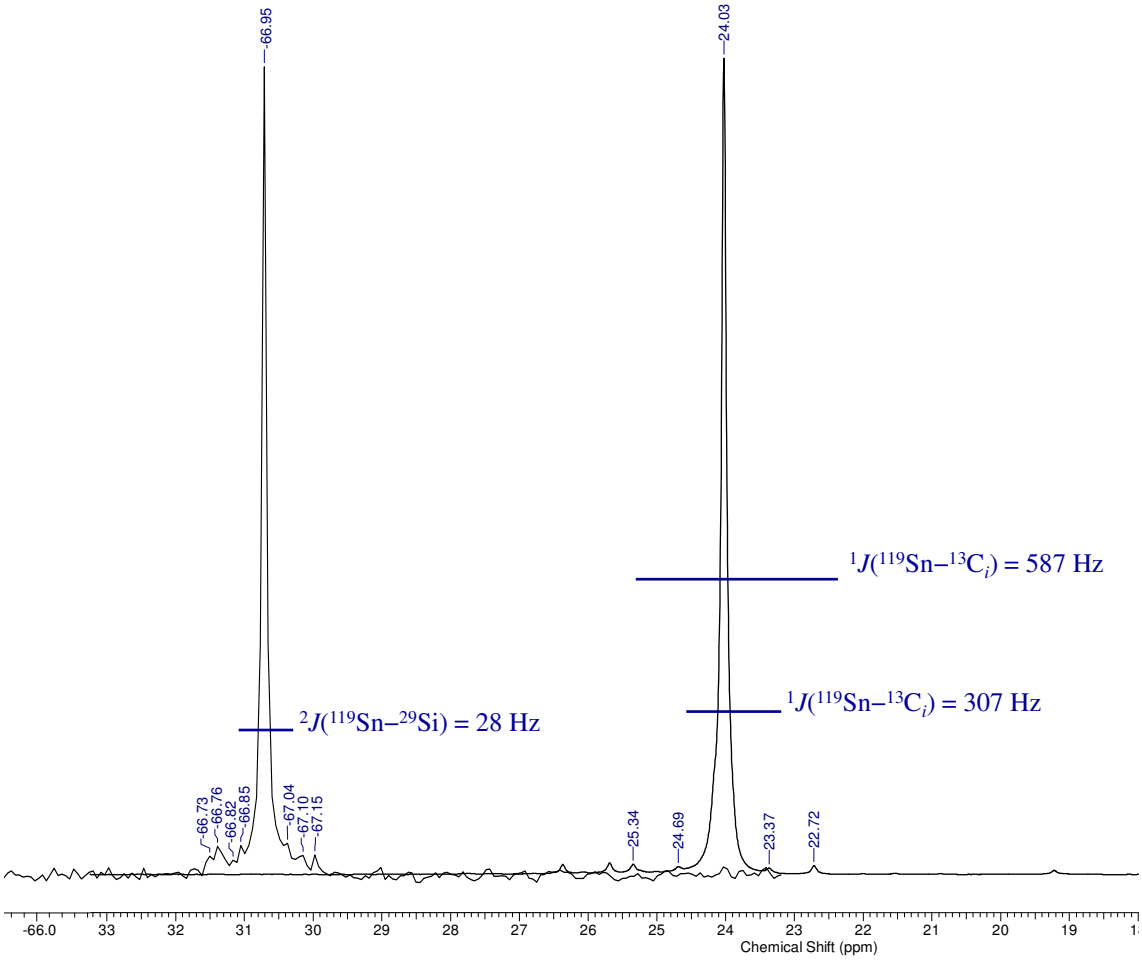

Figure 8. ^{119}Sn NMR spectra of compound **5** (149.26 MHz, $CDCl_3$) (left) and **6** (223.85 MHz, $CDCl_3$) (right).

Figure 9 shows the molecular structure in the solid state of compound **6**. Table 1 contains selected interatomic distances and angles. Compound **6** crystallizes in the orthorhombic space group *Pna*21. The Si–C and Sn–C distances are as expected and vary between 1.8541(52) (Si1–C3) and 1.8675(56) Å (Si1–C2), and 2.1214(48) (Sn2–C3) and 2.1258(48) Å (Sn1–C2), respectively. The Si(1) atom shows a slightly distorted tetrahedral environment with C–Si–C angles varying between 109.184(222)° (C3–Si1–C4), and 110.911(27)° (C1–Si1–C4). The Si–C–Sn angles are rather similar and vary between 116.764(245)° (Si1–C3–Sn2) and 117.522(254)° (Si1–C2–Sn1).

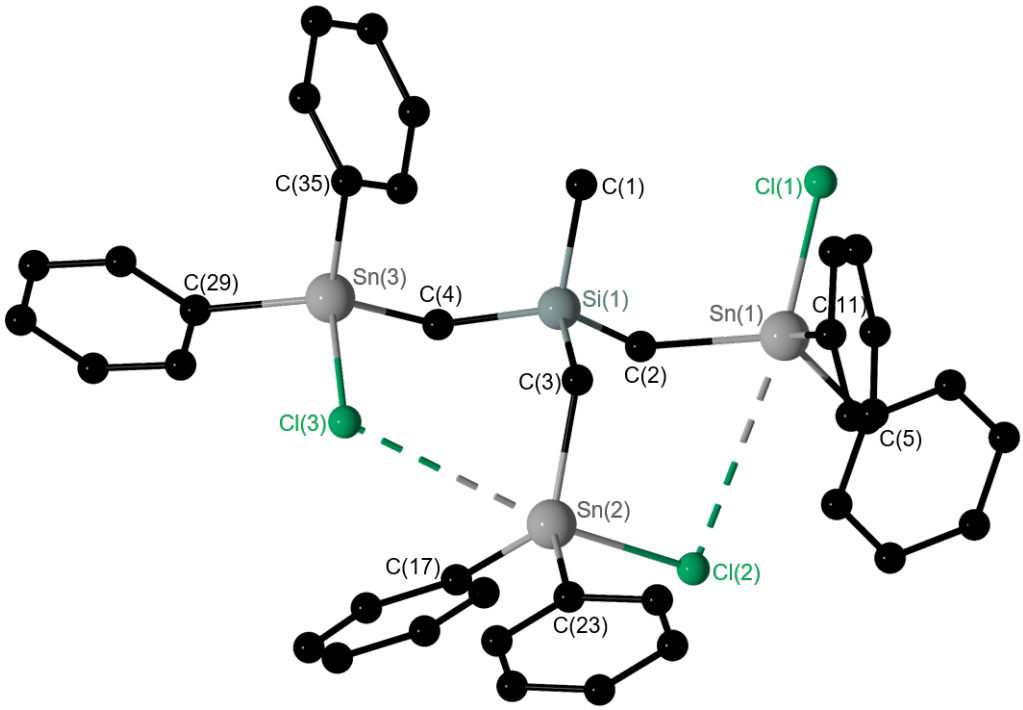

Figure 9. General view (POV-Ray) of a molecule of **6** showing 30 % probability displacement ellipsoids and the crystallographic numbering scheme.

Both compounds **2** and **6** show tripod geometry. An essential difference between the structures of both compounds is the environment about the tin atoms. In compound **6**, the Sn(1) and Sn(2) atoms are [4+1]-coordinated and exhibit a distorted trigonal bipyramidal environment. The C(2), C(5), C(11) (at Sn1) and the C(3), C(17), C(23) (at Sn2) atoms occupy the equatorial, and the Cl(1), Cl(2) (at Sn 1) and Cl(2), Cl(3) (at Sn2) atoms occupy the axial positions. The geometrical goodness $\Delta\Sigma(\theta)$[22] for Sn(1) is 39.2° and for Sn(2) 56.2°. The Sn–Cl distances of 3.8027(17) Å (Sn1–Cl2) and 3.4956(17) Å (Sn2–Cl3) are shorter than the sum of the van der Waals radii, here after referred to as vdW, of tin and chlorine atoms (3.92 Å).[30] The latter distances are comparable to those reported for the chlorido-substituted organotin compounds $(Ph_2ClSn)_3CH$ [3.4639(19) and 3.3125(19) Å][12] and $Me_3SiCH_2(Cl_2)Sn\ (CH_2)_3Sn(Cl_2)CH_2SiMe_3$ [3.319(5) and 3.510(5) Å].[31] The third tin atom Sn(3), has a tetrahedral environment. The other Sn–Cl distances are ranging between 2.3831(17) Å and 2.4067(17) Å. These latter are nearly equal to those reported in the tetra-coordinated triorganotin chloride $[PhC(CH_3)_2CH_2]_3SnCl$ [2.395(4) Å] and $(Ph_2ClSn)_3CH$ [2.4059(19) and 2.4205(19) Å].[12]

As mentioned earlier the triorganotin fluoride compound **7** is an insoluble polymer, which is characteristic to such fluorido-substituted compounds.[28] Therefore, there were attempts of solubilization via functionalization of such compounds via the use of intramolecularly coordinating built-in moieties, as for example $\{Me_2N(CH_2)_3\}$.[29] In our case, the identity

of **7** is established via elemental analysis, which fits exactly with the proposed molecule of $C_{40}H_{39}F_3SiSn_3$ with one molecule of H_2O and one molecule of HF. The ESI mass spectra (negative mode) of **7** shows two mass clusters centred at m/z 255.2263 $SnH_2F_7^-$ [80, $(SnF_6^{2-} + HF^+H^+)]^-$ and 978.9520 $C_{40}H_{39}F_4SiSn_3^-$ [40, $(M + F-)]^-$ (See Supporting Information, Chapter 2, Figures S65- S70). The complexation behaviour of compound **7** towards fluoride anion will be discussed subsequently.

Treatment of compound **2** with six and nine molar equiv of elemental bromine at −55 °C in CH_2Cl_2 gave the tris(dibromidophenylstannylmethyl)methylsilane $MeSi(CH_2SnPhBr_2)_3$, **8**, and the tris(tribromidophenylstannylmethyl)methylsilane $MeSi(CH_2SnBr_3)_3$, **9**, respectively. Compounds **8** and **9** were isolated in good (**8**) and excellent (**9**) yields as oily yellow respectively brown crystalline materials. Both compounds show very good solubility in CH_2Cl_2, $CHCl_3$, and CH_3CN (Scheme 3).

The nonabromido-substituted compound **9** crystallizes in the orthorhombic space group *P*na2_1. Figure 10 shows its molecular structure. Table 1 contains selected interatomic distances and angles. The interatomic Si–C distances ranging between 1.869(16) Å (Si1–C2) and 1.886(16) Å (Si1–C3) are rather similar, as are the Sn–C distances vary between 2.099(14) Å (Sn3–C3) and 2.124(15) Å (Sn1–C1). As expected, the silicon atom has a slightly distorted tetrahedral environment with C–Si–C angles varying between 107.7(8)° (C2–Si1–C1) and 111.8(7)° (C2–Si1–C4). The Si(1)–C(1)–Sn(1) 117.3(8)°, Si(1)–C(2)–Sn(2) 118.1(8)°, and Si(1)–C(3)–Sn(3) (118.8(8)°) are also rather similar and comparable with the corresponding angles in compound **6**. The environments about the tin atoms are distorted tetrahedral, with angles varying between 103.47(8)° (Br4–Sn2–Br5) and 117.5(4)° (C2–Sn2–Br6). The Sn–Br bond distances vary between 2.438(2) (Sn3–Br7) and 2.480(2) Å (Sn1–Br3). These distances are slightly shorter than that reported in Bromo(1,4,7,10,13,16-hexaoxacyclononadec-18-methyl)diphenylstannane Sn(1)–Br(1) 2.5846(4) Å.[32] A closer inspection of the supramolecular structure of **9** (Figure 11) reveals intermolecular interactions between Br(3)···Sn(2) and Br(9)···Sn(1) of 3.987 Å and 4.007 Å, respectively, both being shorter than the sum of the vdW radii of the atoms involved (4.12 Å).[30] Remarkably, there are also secondary intermolecular interactions between Br(2)···Br(5) (3.605 Å), Br(5)···Br(9) (3.686 Å), and Br(6)···Br(7) (3.608 Å). All these distances are slightly shorter than twice the van der Waals radius of bromine (3.70 Å).[30]

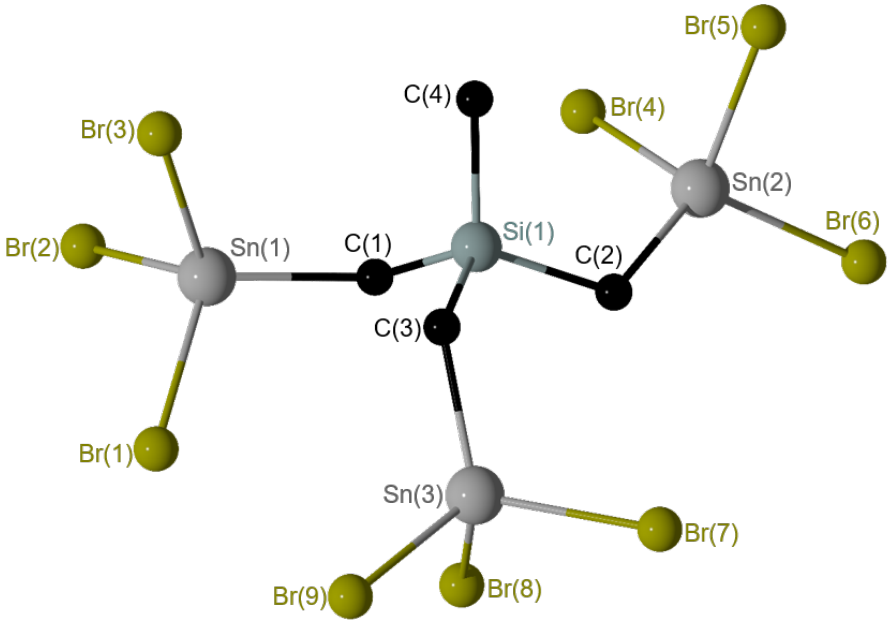

Figure 10. General view (POV-Ray) of a molecule of **9** showing crystallographic numbering scheme.

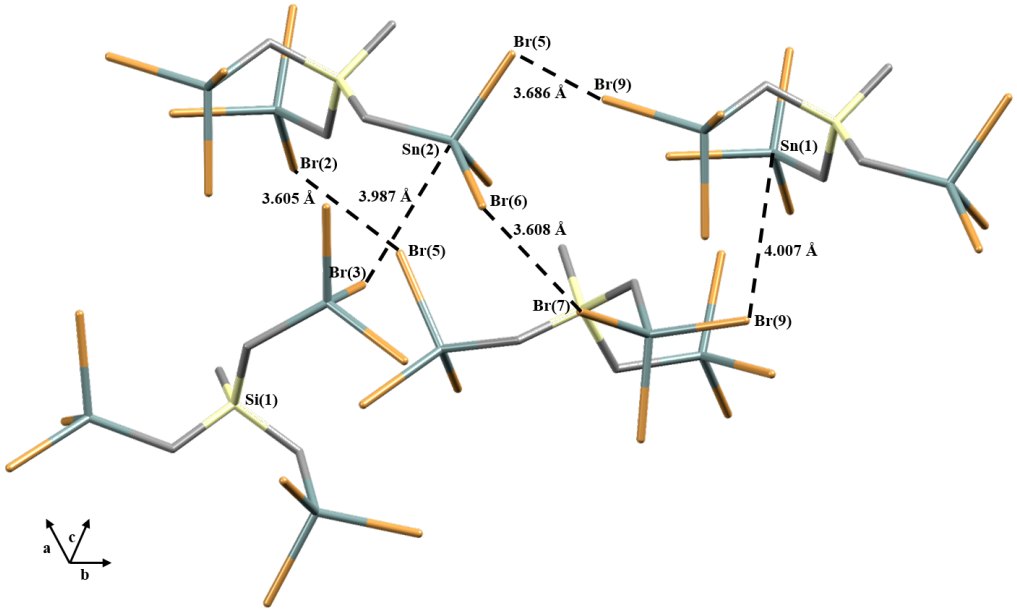

Figure 11. Polymeric chain of **9** established through Br···Sn and Br···Br intermolecular interactions (shown with broken lines).

^{119}Sn NMR spectra show for both **8** and **9** singlet resonances at δ –16 ppm (**8**) and δ –210 ppm (**9**) indicating tetracoordination of the corresponding tin atoms (Figure 12). The signal of **8** is slightly high-frequency shifted in comparison with that reported for the similar

compound $(Br_2PhSn)_2CH_2$ (δ –33 ppm), and low-frequency shifted when compared to that corresponding to $(BrPh_2Sn)_2CH_2$ (δ –0.03).[26] The ^{119}Sn NMR chemical shift of **9** is slightly low-frequency shifted to that reported for $MeSnBr_3$ (δ –165 ppm) and $EtSnBr_3$ (δ –141 ppm).[27] The differences are due to the variance of the environment about the tin atoms in each compound. Furthermore, the ^{1}H NMR chemical shifts of the methylene protons in the bromine-substituted compounds **8** and **9** (See Supporting Information, Chapter 2, Figures S71, S84), respectively, at δ 1.57 ppm ($^2J(^1H-^{117/119}Sn)$ = 88 Hz) and δ 1.10 ppm ($^2J(^1H-^{117/119}Sn)$ = 120/126 Hz) are low-frequency shifted in comparison to those assigned to the corresponding protons in bromo(1,4,7,10,13,16-hexaoxacyclononadec-18-methyl)diphenylstannane δ 1.69 ppm ($^2J(^1H-^{117/119}Sn)$ = 68/83 Hz),[32] $(Br_2PhSn)_2CH_2$ (δ 2.33 ppm), and $(BrPh_2Sn)_2CH_2$ (δ 1.68 ppm).[26] In addition to that, in the ^{13}C NMR spectra (See Supporting Information, Chapter 2, Figures S72, S85), the shifts corresponding to the $SiCH_2Sn$ carbon atoms in **8** and **9**, respectively, at δ 11.85 ppm ($^1J(^{13}C-^{117/119}Sn)$ = 318/333 Hz) and δ 18.62 ppm ($^1J(^{13}C-^{117/119}Sn)$ = 420 Hz) are very close to those reported for $(Br_2PhSn)_2CH_2$ (δ 16.26 ppm) ($^1J(^{13}C-^{117/119}Sn)$ = 359 Hz)[26] and bromo(1,4,7,10,13,16-hexaoxacyclononadec-18-methyl)diphenylstannane (δ 18.9 ppm) ($^1J(^{13}C-^{117/119}Sn)$ = 503/527 Hz).[32] The ^{29}Si NMR spectra of **8** and **9** (See Supporting Information, Chapter 2, Figures S73, S86), as well, display both a singlet resonance, respectively, at 7.52 ppm ($^2J(^{29}Si-^{117/119}Sn)$ = 44 Hz) and 6.09 ppm ($^2J(^{29}Si-^{117/119}Sn)$ = 45 Hz). An ESI mass spectrum (positive mode) of **8** shows one mass cluster centred at m/z 721.0 that is assigned to $C_{12}H_{20}Br_2NSiSn_3^+$ (100, $[M - 4Br^- - 2Ph + CH_3CN + H^+]^+$). An ESI mass of **9** shows two mass clusters centred at m/z 356.3 (100, $[PhSnBr_2H + H^+])^+$ and 725.5 ($C_4H_{11}Br_5NOSn_2$, 50,$[M - MeSiC_2H_4SnBr_4 + MeOH + CH_3CN + H^+])^+$. In the negative mode, for **8** a tin-containing mass cluster centred at m/z 944.7 ($C_3H_{13}Br_6O_2SiSn_3^-$,30,$[M - Me + 3Ph + H_2O + OH^-]^-$) and for **9** a mass cluster centred at m/z 358.8 ($SnBr_3^-$,100,$[M - MeC_3H_6SiSn_2Br_6])^-$ were observed (See Supporting Information, Chapter 2, Figures S75- S82, S88- S93).

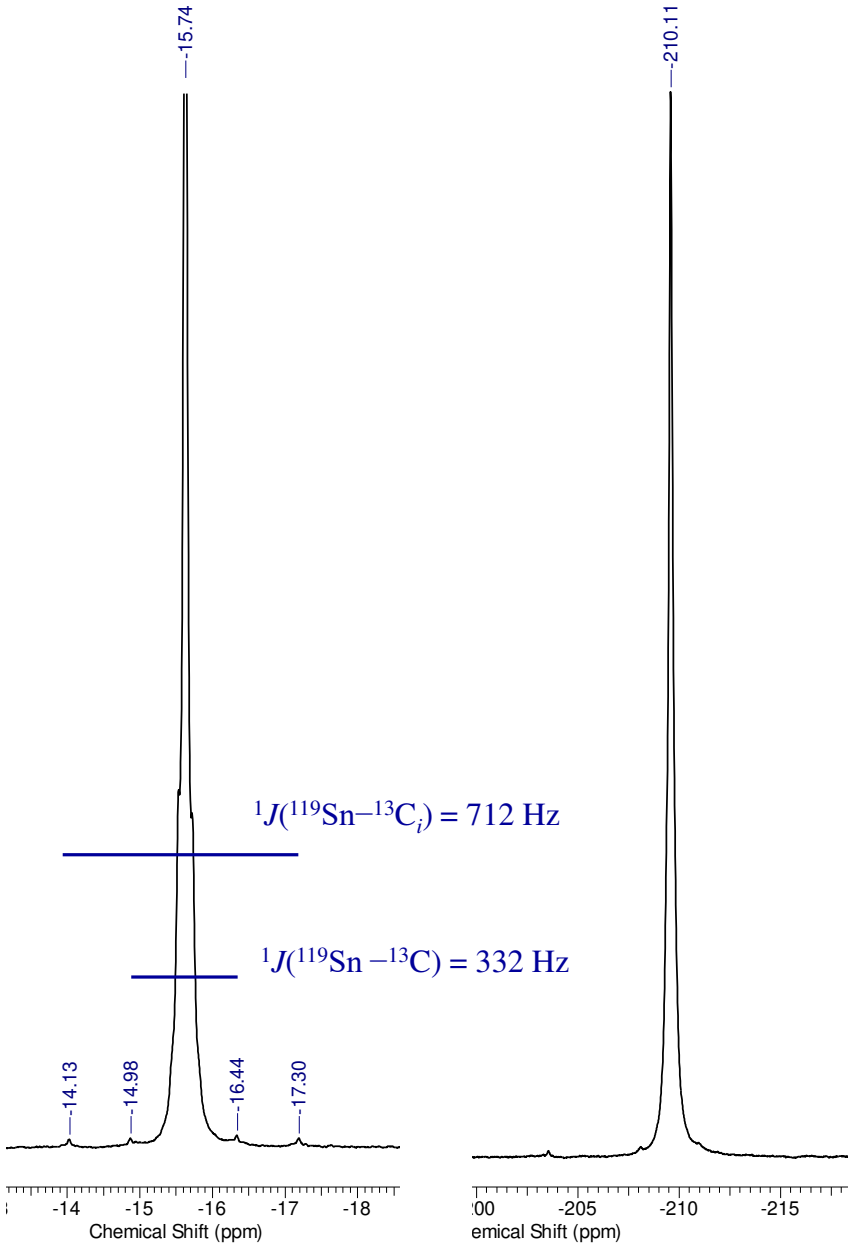

Figure 12. ^{119}Sn NMR spectra of compound **8** (223.85 MHz, C_6D_6) (left) and **9** (149.26 MHz, $CDCl_3$) (right).

The reaction of the monoiodido-substituted organotin compound **3** with three molar equiv of trimethylsilylmethylmagnesium chloride in THF gives the tetraorganotin derivative tris[diphenyl(trimethylsilylmethyl)stannylmethyl)methylsilane $MeSi[CH_2Sn(CH_2SiMe_3)Ph_2]_3$, **10**. The latter was isolated in good yield as a slightly yellow oily substance. Further purification was achieved by several washings with *iso*-hexane. Furthermore, the treatment of **10** with six molar equiv of elemental iodine in CH_2Cl_2 provides the diiodine-substituted tris(diiodido(trimethylsilylmethyl)stannylmethyl)methylsilane $MeSi[CH_2Sn(CH_2SiMe_3)I_2]_3$, **11**. The latter, once reacted with six mo-

lar equiv of silver chloride in CH_2Cl_2, gives the organotin dichloride derivative tris[dichlorido(trimethylsilylmethyl)stannylmethyl]methylsilane $MeSi[CH_2Sn(CH_2SiMe_3)Cl_2]_3$, **12**. Compounds **11** and **12** are obtained in very good yields, respectively, as yellow-orange and colourless solids. Compounds **10**– **12** show very good solubility in common organic solvents such as CH_2Cl_2, $CHCl_3$, and THF (Scheme 3).

The ^{119}Sn NMR spectra of compounds **10**– **12** exhibit each one singlet resonance. These tin atoms are tetra-coordinated as it is evidenced by their tin chemical shifts at δ –49 ppm (**10**), δ –190 ppm (**11**), and δ 131 ppm (**12**) (Figure 14), respectively, being similar to those reported for $fc(SiMe_2CH_2SnPh_2CH_2SiMe_2)_2fc$ (δ –51 ppm),[11] $[Me_2N(CH_2)_3Ph_2SnCH_2)_2SiMe_2$ (δ –60 ppm),[28] $(I_2PhSnCH_2)_2SiMe_2$ (δ –219 ppm),[28] *cyclo*-$Cl_2Sn(CH_2SiMe_2CH_2)_2SnCl_2$ (δ 139 ppm).[9] The chemical shifts of the CH_2SiMe_3 silicon atoms in the organotin compounds **10** (δ 2.68 ppm), **11** (δ 3.81 ppm), and **12** (δ 2.7 ppm) are low-frequency shifted in comparison to those reported for the corresponding silicon atoms in $(Ph_3SnCH_2)_2SiMe_2$ (δ 6.2 ppm), $(I_2PhSnCH_2)_2SiMe_2$ (δ 6.8 ppm),[28] and *cyclo*-$Cl_2Sn(CH_2SiMe_2CH_2)_2SnCl_2$ (δ 4.1 ppm).[9] The ^1H NMR spectra of the organotin compounds **10**–**12** (See Supporting Information, Chapter 2, Figures S95, S103, S111) show that the signals of the $SiCH_2Sn$ protons in **10** (δ 0.1 ppm, $^2J(^1H-^{117/119}Sn)$ = 72/74 Hz) (see as an example Figure 13), **11** (δ 1.72 ppm, $^2J(^1H-^{117/119}Sn)$ = 74 Hz), and **12** (δ 1.2 ppm, $^2J(^1H-^{117/119}Sn)$ = 76 Hz), respectively, are low-frequency shifted in comparison to that reported for $(Ph_3SnCH_2)_2SiMe_2$ (δ 0.46ppm $^2J(^1H-^{117/119}Sn)$ = 75/77 Hz), and close to those reported for $(I_2PhSnCH_2)_2SiMe_2$ (δ 1.55 ppm, $^2J(^1H-^{117/119}Sn)$ = 87/90 Hz), and $(Cl_2PhSnCH_2)_2SiMe_2$ (δ 1.22 ppm, $^2J(^1H-^{117/119}Sn)$ = 89/92 Hz).[28] Furthermore, the ^{13}C NMR chemical shifts corresponding to the CH_2SiMe_3 carbon atoms in the organotin compounds **10** (δ –3.33 ppm, $^1J(^{13}C-^{117/119}Sn)$ = 255/267 Hz), **11** (δ 14.74 ppm, $^1J(^{13}C-^{117/119}Sn)$ = 251/263 Hz), and **12** (δ 14.09 ppm, $^1J(^{13}C-^{117/119}Sn)$ = 328/342 Hz), respectively (See Supporting Information, Chapter 2, Figures S96, S104-S105, S112- S113), are close to that reported for $(Ph_3SnCH_2)_2SiMe_2$ (δ –3.2 ppm, $^1J(^{13}C-^{117/119}Sn)$ = 265/277 Hz), and high-frequency shifted in comparison to those reported for $(I_2PhSnCH_2)_2SiMe_2$ (δ 12.6 ppm, $^1J(^{13}C-^{117/119}Sn)$ = 260/271 Hz),[28] and *cyclo*-$Cl_2Sn(CH_2SiMe_2CH_2)_2SnCl_2$ (δ 13.4 ppm, $^1J(^{13}C-^{117/119}Sn)$ = 293/306 Hz).[9] The ESI mass spectra (positive mode) of the organotin compounds **10**, **11**, and **12**, respectively, show mass clusters centred at m/z 1129.3 (**10**, $C_{43}H_{69}Cl_2O_2Si_3Sn_3^+$), 824.9353 $C_4H_{12}I_3SiSn_3^+$ (100, $[M-(CH_2SiMe_3I)_3+H^+]^+$), and 778.929 $C_8H_{29}Cl_5O_4Si_2Sn_3^+$ (100, $[M-Cl^- -2\,CH_2SiMe_3+4\,H_2O+H^+])^+$ (See Supporting Information, Chapter 2, Figures S99- S101, S108- S109, S116- S117).

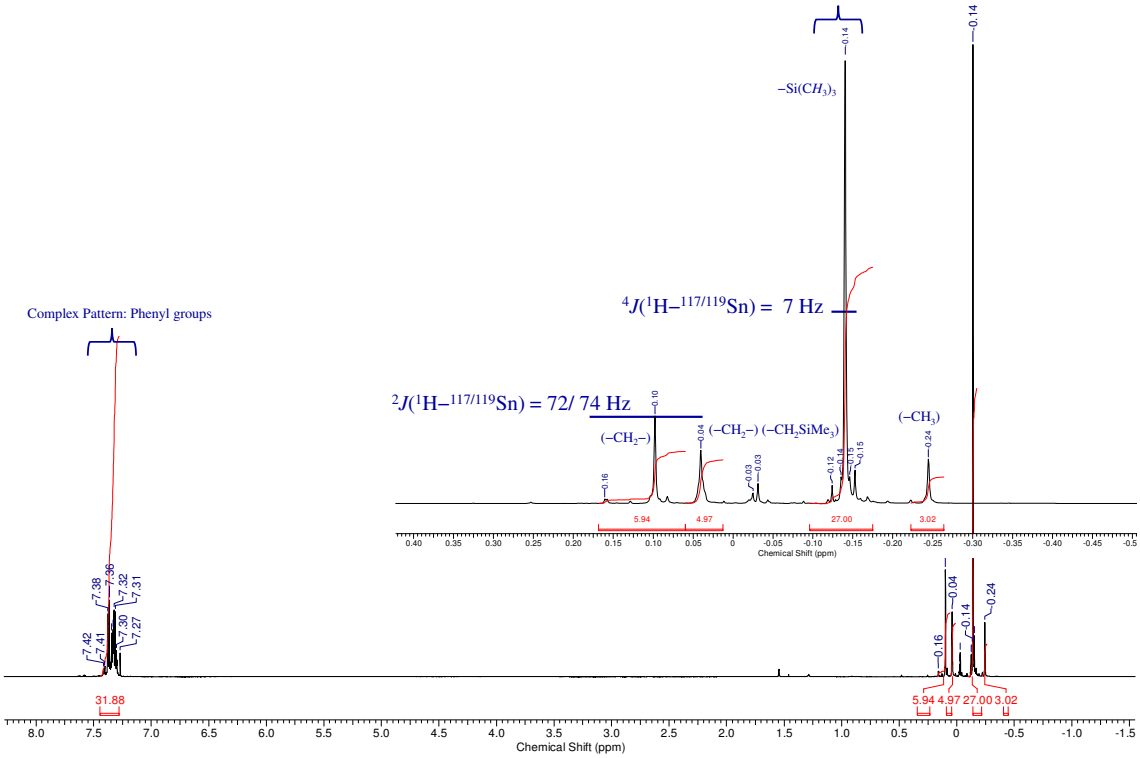

Figure 13. ^1H NMR spectrum (600.29 MHz, $CDCl_3$) of compound **10**.

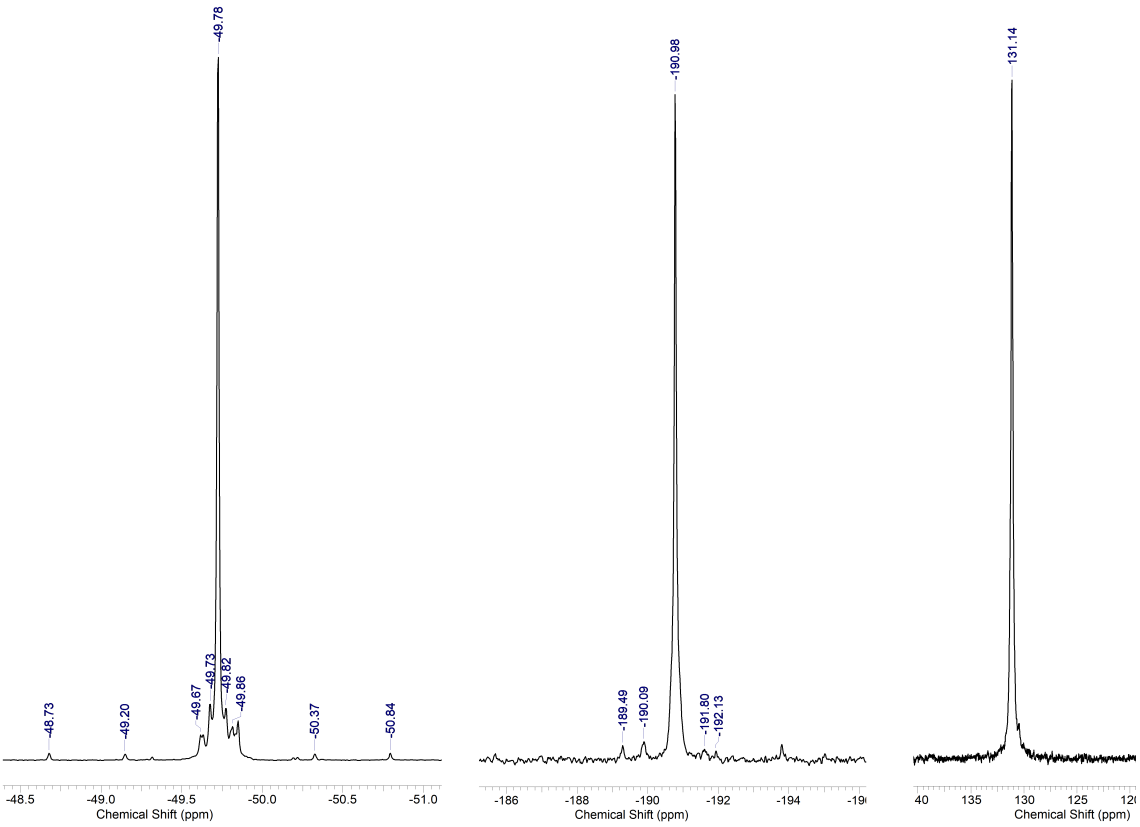

Figure 14. ^{119}Sn NMR spectra (223.85 MHz, $CDCl_3$) of **10**, **11** (149.26 MHz, $CDCl_3$) and **12** (149.26 MHz, C_6D_6) (from left to right).

Finally, it's worth noting that the three tin atoms in each of the silicon-bridged organotin compounds **2**– **12** are equivalent on the ^1H, ^{13}C, and ^{119}Sn NMR time scale. The tin atoms are all tetracoordinated, as evidenced by their ^{119}Sn NMR chemical shifts. From the data at hand it is evident that the structures in solution of the organotin compounds **2**– **12** are rather similar to the structures in the solid state as established by single crystal X-ray diffraction analyses. It is worth mentioning that the $^1J(^{13}C-^{117/119}Sn)$ and $^2J(^1H-^{117/119}Sn)$ coupling constants for the methylene protons and carbon atoms, respectively, increase with the Lewis acidity of the tin atoms. Thus, the nonabromido-substituted monoorganotin compound **9** shows the biggest values with $^2J(^1H-^{117/119}Sn)$ = 120/126 Hz and $^1J(^{13}C-^{117/119}Sn)$ = 414/430 Hz.

Table 1. Selected interatomic distances /Å and angles /° in compounds **2**, **6**, and **9**.

	2	**6**	**9**
		X(1) = Cl(1)	X(1) = Br(2)
		X(2) = Cl(2)	X(2) = Br(5)
		X(3) = Cl(3)	X(3) = Br(7)
Si(1)–C(1)	1.867(3)	1.8599(68)	1.877(16)
Si(1)–C(2)	1.871(3)	1.8675(56)	1.869(16)
Si(1)–C(3)	1.866(3)	1.8541(52)	1.886(16)
Si(1)–C(4)	1.860(3)	1.8648(49)	1.853(15)
Sn(1)–C(1)	2.154(3)		
Sn(1)–C(2)	2.147(3)		
Sn(1)–C(3)	2.132(3)		
Sn(1)–X(1)		2.3831(17)	2.449(2)
Sn(2)–X(2)		2.3985(15)	2.446(2)
Sn(3)–X(3)		2.4067(17)	2.438(2)
Si(1)–C(1)–Sn(1)	117.40(14)		117.3(8)
Si(1)–C(2)–Sn(2)	120.29(15)		118.1(8)
Si(1)–C(3)–Sn(3)	120.52(14)		118.8(8)
Si(1)–C(2)–Sn(1)		117.522(254)	
Si(1)–C(3)–Sn(2)		116.764(245)	
Si(1)–C(4)–Sn(3)		116.808(246)	
C(2)–Sn(2)–C(61)	118.66(10)		
C(3)–Sn(3)–C(81)	105.13(9)		
C(2)–Sn(1)–Cl(1)		102.999(156)	
C(5)–Sn(1)–Cl(1)		102.866(167)	
Br(5)–Sn(2)–Br(4)			103.47(8)
C(2)–Sn(2)–Br(6)			117.5(4)

2.2 Reactivity of halogen-substituted derivatives $MeSi(CH_2SnR_{(3-n)}X_n)_3$ (n = 1– 3; X = I, F, Cl, Br; R = Ph, CH_2SiMe_3) towards anions and neutral Lewis-Bases

The complexation behaviour of the silicon-bridged organotin compounds of **4**– **7**, **9**, and **12** with Cl^-, CH_3COO^-, F^-, Br^-, and HMPA are studied in solution by ^{119}Sn, ^{19}F, ^{31}P, ^{13}C, ^1H NMR spectroscopy and ESI mass spectrometry (**4**– **9**, **12**). The study in solid state is exclusive for **4**– **7**, **9**, and **12**.

2.2.1 Complexation behaviour of 4 and 12 towards chloride anions and HMPA, respectively

The ability of the hexachlorido-derivatives **4** and **12** to complex chloride anions (as imidazolium chloride, $C_{11}H_{21}N_2Cl$) in solution is studied. A ^{119}Sn NMR spectrum (CH_2Cl_2/C_6D_6) at ambient temperature of a solution of **4** in dichloromethane to which one molar equiv of $C_{11}H_{21}N_2Cl$ had been added (Scheme 4) shows an unresolved broad resonances, which cannot be defined. It indicates chloride exchange being fast on the ^{119}Sn NMR scale.

Scheme 4. Reaction of **4** with one molar equiv of $C_{11}H_{21}N_2Cl$.

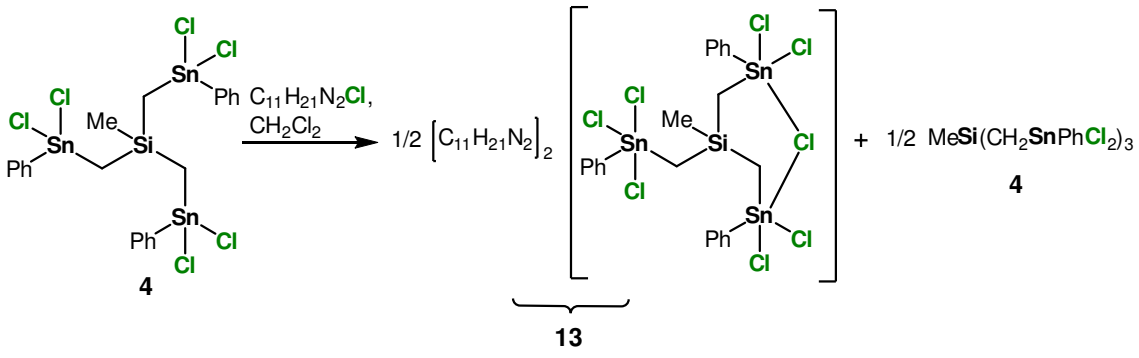

From this reaction mixture a crystalline material was isolated and re-crystallized from dichloromethane/ toluene giving the imidazolium salt of the diorganochloridostannate complex $(C_{11}H_{21}N_2)_2[MeSi(CH_2SnPhCl_2)_3 \cdot 2Cl]$, **13** (Scheme 4). Figure 15 shows its molecular structure and the figure caption contains selected interatomic distances and angles.

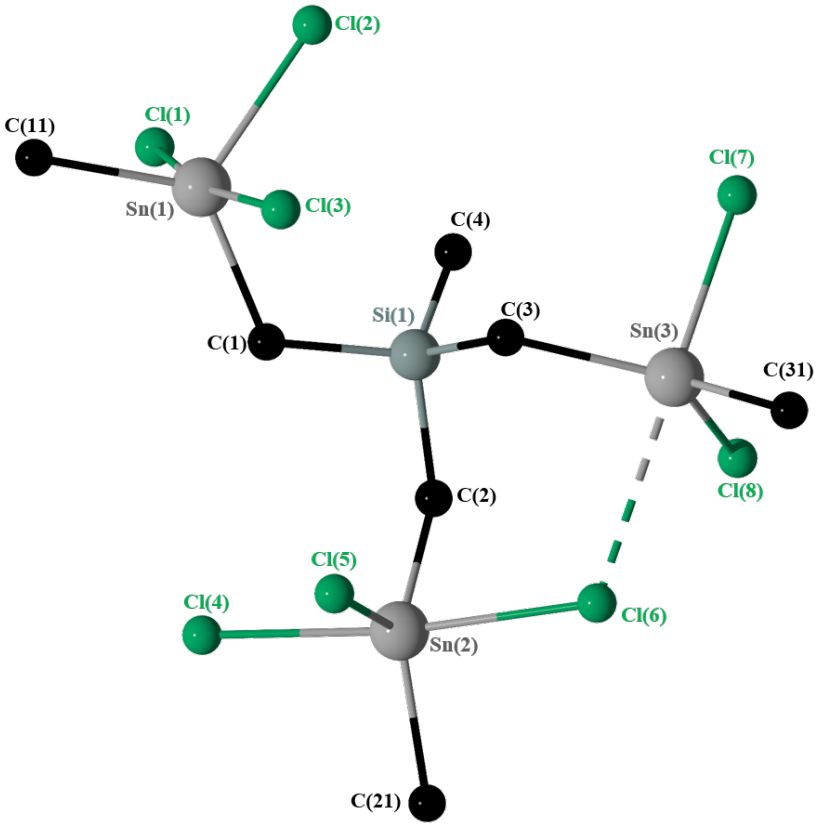

Figure 15. General view (POV–Ray) of a molecule of **13** showing crystallographic numbering scheme. Only the C_i of the phenyl substituents are shown, Hydrogen atoms and the $N_2C_{11}H_{21}^+$ cations are omitted. Selected interatomic distances (Å): Sn(1)–C(1) 2.113(6), Sn(1)–C(11) 2.161(6), Sn(1)–Cl(1) 2.554(2), Sn(1)–Cl(2) 2.3798(18), Sn(1)–Cl(3) 2.554(2), Sn(2)–C(2) 2.099(6), Sn(2)–C(21) 2.142(7), Sn(2)–Cl(4) 2.505(2), Sn(2)–Cl(5) 2.3738(18), Sn(2)–Cl(6) 2.6515(19), Sn(3)–C(3) 2.113(6), Sn(3)–C(31) 2.115(8), Sn(3)–Cl(6) 2.9217(18), Sn(3)–Cl(7) 2.426(2), Sn(3)–Cl(8) 2.3487(18). Selected interatomic angles (°): Cl(1)–Sn(1)–Cl(3) 169.68(6), C(1)–Sn(1)–C(11) 125.4(2), C(1)–Sn(1)–Cl(2) 120.81(18), C(11)–Sn(1)–Cl(2) 113.74(18), Cl(4)–Sn(2)–Cl(6) 170.51(6), C(2)–Sn(2)–C(21) 127.9(3), C(2)–Sn(2)–Cl(5) 119.11(18), C(21)–Sn(2)–Cl(5) 112.8(2), Cl(6)–Sn(3)–Cl(7) 172.56(7), C(3)–Sn(3)–C(31) 126.4(3), C(3)–Sn(3)–Cl(8) 120.58(19), C(31)–Sn(3)–Cl(8) 109.0(2).

Compound **13** crystallizes, as its toluene solvate **13**·2C_7H_8, in the monoclinic space group $P21/n$ with four molecules in the unit cell. The Sn(1), Sn(2), and Sn(3) centers are each pentacoordinated and show distorted trigonal bipyramidal environments with Cl(1) and Cl(3) (at Sn1), Cl(4) and Cl(6) (at Sn2), and Cl(6) and Cl(7) (at Sn3) occupying the axial, and C(1), C(11) and Cl2 (at Sn1), C(2), C(21) and Cl(5) (at Sn2), and C(3), C(31) and Cl(8) (at Sn3) occupying the equatorial positions. As it is evident from the geometric

goodness $\delta\Sigma(\theta)$[22] = 91.5° for Sn1, 81.1° for Sn2, and 66.5° for Sn3, the distortion from the ideal trigonal bipyramid is low for Sn(1) and Sn(2). However, the Sn(3) center can be seen as [4+1] coordinated with Cl(6) approaching Sn(3) vial the tetrahedral face defined by C(3), C(31) and Cl(8) at a distance of 2.9217(18) Å which, however, is shorter than the sum of the van der Waals radii of the tin (2.17 Å) and chlorine (1.75 Å) atoms.[30] As result of this intramolecular Cl(6)→Sn(3) interaction, the Sn(2)–Cl(6) distance is lengthened to 2.6515(19) Å. These values (formally) indicate an unsymmetrical chelation of the chloride anion Cl(6) by the Lewis acidic tin centers Sn(2) and Sn(3). The distances resemble those reported for the tetraphenylphosphonium organochloridostannate complex $(Ph_4P)[HC(SnClPh_2)_3{\cdot}Cl]$ (2.9397(14) and 2.6307(14) Å).[12]

A ^{119}Sn NMR spectrum (poor signal-to-noise ratio as result of low solubility of **13** at low temperature) of a CD_2Cl_2 solution of **13** at −80 °C showed two broad signals at δ –49 and δ –151 ppm, respectively. These two resonances are low-frequency shifted in comparison to the parent compound **4** (δ 41 ppm). This is evidence of the formation of a chloridostannate complex **13** $(C_{11}H_{21}N_2)_2[MeSi(CH_2SnPhCl_2)_3 \cdot 2Cl]$ (Scheme 4) chelating two chloride anions in a bidentate manner. However, in another ^{119}Sn NMR Spectrum in CD_3CN at −30 °C, only one broad signal is shown at δ –153 ppm (See Supporting Information, Chapter 2, Figures S119, S120). This difference is due to the kinetic lability of such compounds. It is worth noting that despite that the reaction was with one molar equiv of chloride anion, **4** reacts additionally with another chloride anion to form a bidentate specie, this is approachable to the complexation behaviour of methylene-bridged organotin compounds such as $(ClPh_2Sn)_2(CH_2)_3$ and $(FPh_2Sn)_2(CH_2)_3$.[3] This is related to the geometry of each compound and its Lewis-acidity. This kind of bidentate complexation is explained also that there are two substituted chloride on each tin atom, which encourage the formation of the 1: 2 adduct. As for the monosubstituted halido-orgatin compounds, they, generally, chelate the halide anions in a monodentate manner.[3] To conclude for complex **13**, each tin atom interacts with three chlorine atoms and cannot be involved in additional intramolecular interaction with a fourth Cl^-, they are all satisfied.

A ^{119}Sn NMR spectrum at ambient temperature of a solution of **4** in acetonitrile, to which two molar equiv of $C_{11}H_{21}N_2Cl$ had been added, shows a single resonance at δ –160 ppm, $W_{1/2}$ = 255 Hz (Scheme 5).

Scheme 5. Reaction of **4** with two molar equiv $C_{11}H_{21}N_2Cl$.

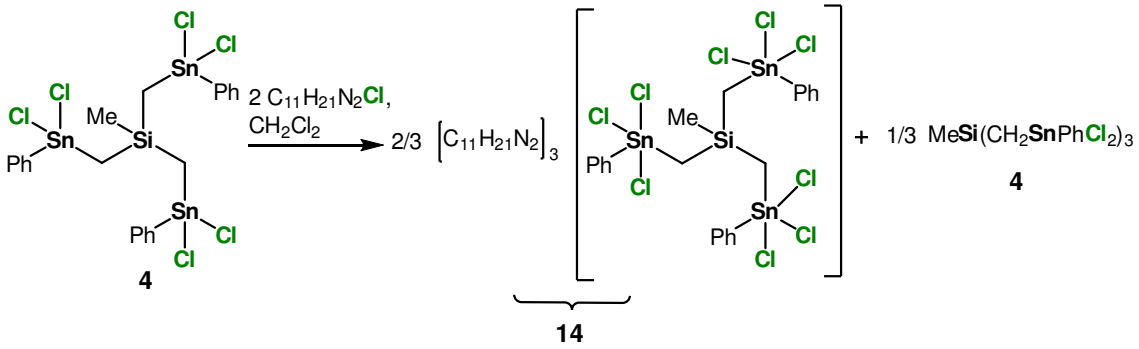

It is low-frequency shifted in comparison to the parent compound **4** (δ 41 ppm) and proves formation of organochloridostannate species. All tin atoms involved in the equilibrium shown in Scheme 5 are equivalent on the ^{119}Sn NMR time scale. Even at −80 °C no de-coalescence of the ^{119}Sn NMR signal was observed. From this reaction mixture, the imidazolium organochloridostannate $(C_{11}H_{21}N_2)_3[MeSi(CH_2SnPhCl_2)_3 \cdot 3\,Cl]$, **14** was isolated as colourless crystalline material. From an acetonitrile/dichloromethane solution, **14** crystallized in the orthorhombic space group *P*na2$_1$ with four molecules in the unit cell. Figure 16 shows the molecular structure and Table 2 contains selected interatomic distances and angles.

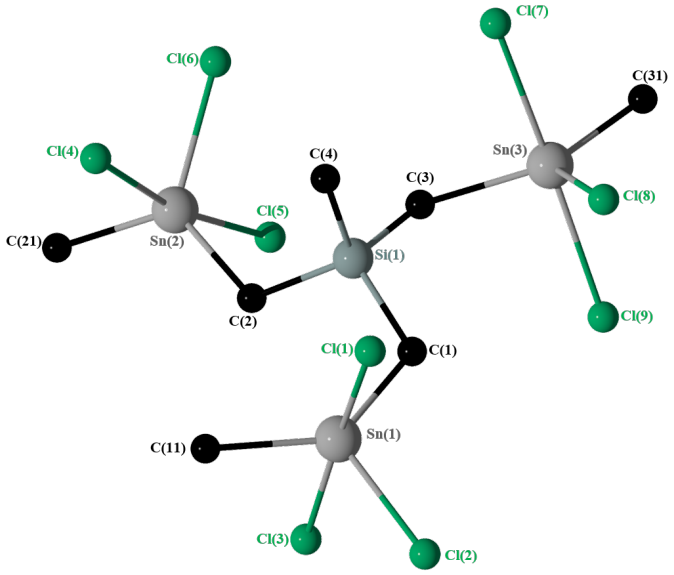

Figure 16. General view (POV-Ray) of a molecule of **14** showing crystallographic numbering scheme. Only the C_i of the phenyl substituents are shown, Hydrogen atoms and the $N_2C_{11}H_{21}^+$ cations are omitted.

The binding mode of **14** show that each tin is substituted with three chlorine atoms, in which the tin atoms are all pentacoordinated with distorted trigonal bipyramidal environments. The geometrical goodnesses $\Delta\Sigma(\theta)$[22] of Sn(1), Sn(2), and Sn(3) are 89.4°, 88.6°, and 89.1°, respectively, with Cl(2), C(1), C(11) (at Sn1), Cl(6), C(2), C(21) (at Sn2), and Cl(8), C(3), C(31) (at Sn3) occupying the equatorial, and Cl(1), Cl(3) (at Sn1), Cl(4), Cl(5) (at Sn2), and Cl(7), Cl(9) (at Sn3) occupying the axial positions. There are no intramolecular bridges, as it is the case for similar organochloridostannates.[3,9,12] The Sn–Cl distances vary between 2.368(5) Å (Sn3–Sn8) and 2.587(4) Å (Sn2–Sn5). These are shorter than the corresponding Sn–Cl distances in almost all related organochloridostannate compounds, taking as examples $(PPh_4)_2$[*cyclo*-$Cl_2Sn(CH_2SiMe_2CH_2)_2SnCl_2 \cdot 3\,Cl$][9] and $(PPh_4)_2[HC(SnCl_2Ph)_3 \cdot 2\,Cl]$.[12]

Table 2. Selected interatomic distances /Å and angles /° in compounds **13**, **14**, and **25**.

	13	**14**	**25**
	X(1) = Cl(6)		X(1) = Cl(7)
		X(2) = Cl(5)	
	X(3) = Cl(6)	X(3) = Cl(8)	X(3) = Cl(7)
Sn(1)–X(1)	2.6515(19)		2.7199(12)
Sn(2)–X(2)		2.587(4)	
Sn(3)–X(3)	2.9218(19)	2.368(5)	2.8367(13)
Cl(1)–Sn(1)–Cl(3)	169.68(6)	174.69(18)	
Cl(4)–Sn(2)–Cl(6)	170.51(6)	86.17(16)	
Cl(7)–Sn(3)–Cl(8)	92.72(7)	86.0(2)	
C(31)–Sn(3)–C(3)	126.4(3)	127.1(6)	131.8(3)
Cl(1)–Sn(1)–Cl(2)			90.20(5)
Cl(3)–Sn(2)–Cl(4)			88.26(5)
Cl(5)–Sn(3)–Cl(6)			91.77(6)

A ^{119}Sn NMR spectrum is comparable to that of the crude mixture with a single resonance at δ –175 ppm. As well, the ^1H and ^{13}C NMR spectra of a crystal sample of **14** support the formation of $(C_{11}H_{21}N_2)_3$ [$MeSi(CH_2SnPhCl_2)_3 \cdot 3\,Cl$] (Scheme 5). The ^1H NMR spectrum shows the Si*C*H_3 single resonance at δ 0.58 ppm, displaced to slightly lower frequency in comparison to that of **4** (δ 0.65 ppm). As to the Si*C*H_2Sn resonance appears at δ 1.42 ppm, shifting to higher frequency in comparison with the methylene group of 4 (δ 1.18 ppm). As to the resonances referring to the *t*-Bu groups (δ 1.65 ppm, 54H) and the C*H* groups (δ 7.64 ppm 6H, δ 8.63 ppm 3H) of the imidazolium cation, correspond to three cations of $C_{11}H_{21}N_2^+$. In the ^{13}C NMR spectrum, the resonances corresponding to

Si*C*H_3 at δ 3.67 ppm and Si*C*H_2Sn at δ 27.49 ppm displace to higher frequencies in comparison with those of **4**, respectively, at δ 3.51 and 11.25 ppm. An ESI-MS spectrum of **14** in the positive mode show three mass clusters centered at m/z 721.0, 739.0, and 1504.3 assigned to $[M - 3(C_{11}H_{21}N_2)^+ - 6Cl^- - Ph + H_2O]^+$, $[M - 3(C_{11}H_{21}N_2)^+ - 5Cl^- + H^+]^+$, and $[M - Cl^- - N^- + H^+ + H_2O]^+$, respectively (See Supporting Information, Chapter 2, Figures S121- S130).

Despite that the formation of complex **14** is resulted from the reaction of **4** with two molar equiv of chloride anion, even though, the third tin atom chelate an additional Cl^-. This result is interestingly surprising, giving the affirmation saying that dichlorido-substituted organotin compounds attempt to complex chloride anion in a bidentate manner and the third tin atom do not involve in the complexation process.[3] In our case, this result is in analogy with the previous bidentate specie **13**, result of the reaction of **4** with one equiv molar chloride anion.

In fact, upon the addition of a third molar equiv of imidazolium chloride to a solution of **13** in acetonitrile, a ^{119}Sn NMR spectrum shows a single resonance at δ –178 ppm (See Supporting Information, Chapter 2, Figure S132), which proves the formation of **14** in solution. No crystalline material was isolated from this reaction mixture. This finding confirms that all three tin atoms are satisfied via interactions with a maximum of three chlorine atoms on each one.

When we compare the complexation behaviour of the phenyl-substituted compound **4** towards chloride anions, to that of the corresponding trimethylsilylmethyl-substituted derivative **12**, we find an interesting result.

A ^{119}Sn spectrum of a solution of **12** in CD_3CN at ambient temperature, to which one molar equiv of $C_{11}H_{21}N_2Cl$ had been added, shows a broad resonance at δ –11 ppm, $W_{1/2}$ = 528 Hz (See Supporting Information, Chapter 2, Figure S231) shifted to lower frequency in comparison to the parent compound **12** (δ 131 ppm). No crystalline material is isolated from this reaction mixture. However, a ^{119}Sn spectrum of a solution of **12** in acetonitrile reacting with two molar equiv of $C_{11}H_{21}N_2Cl$, shows a broad resonance displaced to a much lower frequency at δ –48 ppm. At –40 °C, the ^{119}Sn spectrum exhibits two broad resonances at δ –122 and -76 ppm, respectively, with integration of 1: 2. (See Supporting Information, Chapter 2, Figures S229, S230) This finding is interpreted in terms of the formation of the organochloridostannate complex $(C_{11}H_{21}N_2)_2[MeSi(CH_2SnCH_2SiMe_3Cl_2)_3 \cdot 2Cl]$ (**25**, Scheme 6).

Scheme 6. Reaction of **12** with one molar equiv $C_{11}H_{21}N_2Cl$.

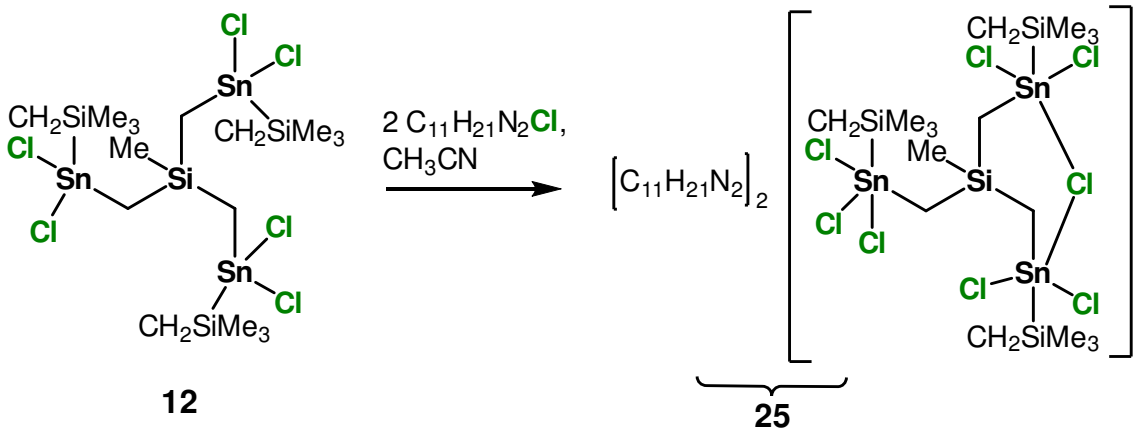

Colourless single crystals suitable for X-ray diffraction study were obtained from a solution of CH_2Cl_2/CH_3CN. Complex **25** crystallizes in the triclinic space group *P*–1. Figure 17 shows its molecular structure and Table 2 contains selected interatomic distances and angles. The Sn(1) and Sn(3) centers are intramolecularly bridged via Cl(7) in a slightly non-symmetrical fashion (Sn1–Cl7) 2.7199(12) Å and (Sn3–Cl7) 2.8367(13) Å. These Sn– distances are comparable to those of 2.7717(8) and 2.8451(8) Å in $(PPh_4)[Me_2Si(CH_2SnClMe_2)_2 \cdot Cl]$.[9] There is a formation of a six membered (Si–C–Sn–Cl–Sn–C) ring via this Sn–Cl–Sn bridge. The Sn(2) centre binds the second chloride anion. All tin atoms are pentacoordinated and exhibit distorted-trigonal bipyramidal environments with geometrical goodness[22] $\Delta\Sigma(\theta)$ = 78.8° (Sn1), 90.1° (Sn2), and 72.9° (Sn3). The equatorial positions are occupied by Cl(2), C(1), C(11) at Sn(1), Cl(3), C(2), C(21) at Sn(2), and Cl(5), C(3), C(31) at Sn(3). The axial positions are occupied by Cl(3), Cl(7) at Sn(1), Cl(4), Cl(8) at Sn(2), and Cl(6), Cl(7) at Sn(3).

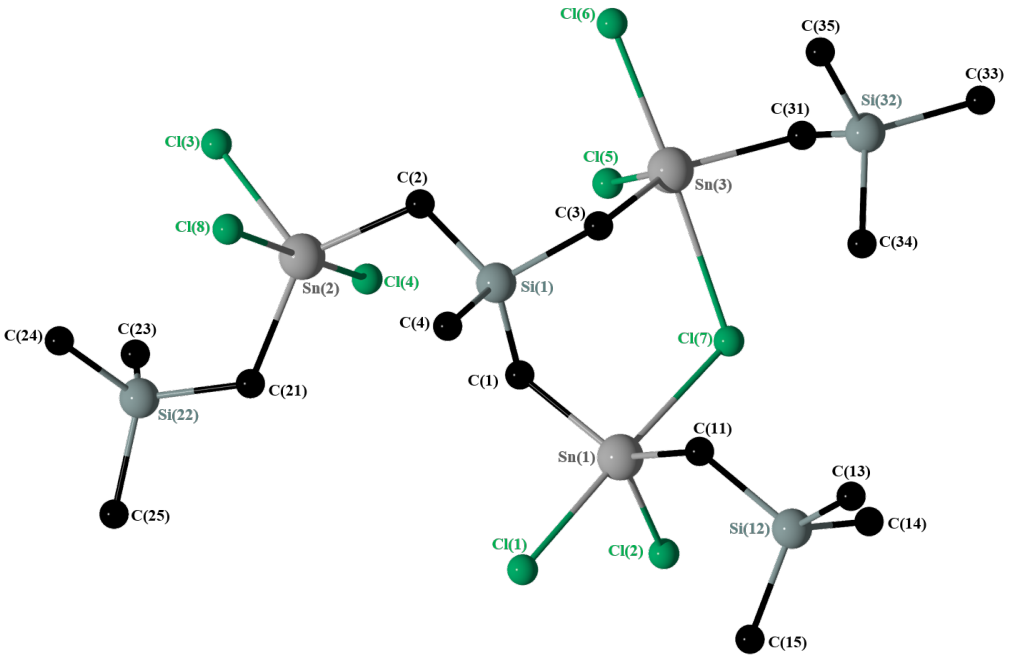

Figure 17. General view (POV-Ray) of a molecule of **25** showing crystallographic numbering scheme. Hydrogen atoms and the $N_2C_{11}H_{21}^+$ cations are omitted for clarity.

A ^{1}H NMR spectrum of a solution of **25** in CD_3CN shows that the $Si(CH_3)_3$ resonances at δ 0.08–0.14 ppm, displaced to slightly lower frequency in comparison to that of **12** (δ 0.06–0.40 ppm), same for the methyl group $SiCH_3$ single resonance which appear at δ 0.47 ppm shifting to a slightly lower frequency comparing to the corresponding methyl group of **12** (δ 0.59 ppm). As to the CH_2SiMe_3 and $SiCH_2Sn$ resonances appear, respectively at δ 0.92 and 1.28 ppm, shifting the first to slightly lower frequency and the second to higher frequency in comparison with the corresponding methylene groups of **12** (δ 0.97 and 1.20 ppm). As to the resonances referring to the *t*-Bu groups (δ 1.6 ppm, 36H) and the C*H* groups (δ 7.56 ppm 4H, δ 8.44 ppm 2H) of the imidazolium cation, correspond to two cations of $C_{11}H_{21}N_2^+$. A ^{29}Si NMR spectrum show two resonances at δ 1.82 and 3.92 ppm corresponding, respectively, to $Si(CH_3)_3$ and $Si(CH_3)$. These two shift to lower frequencies comparing to the corresponding silicon atoms in the parent compound **12** (δ 2.7 and 7.29 ppm). An ESI-MS mass spectrum of complex **25** in the negative mode show one mass cluster centered at m/z 1127.4, assigned to $[M - (C_{11}H_{21}N_2)^+ - 2Cl^- - 3H^+]^-$ and in the positive mode one mass cluster centered at m/z 771.1, corresponding to $[M - 2(C_{11}H_{21}N_2)^+ - 7Cl^- - CH_2SiMe_3 + 2H_2O + CH_3CN]^+$ (See Supporting Information, Chapter 2, Figures S227- S228, S233- S236).

Upon addition of a third molar equiv of $C_{11}H_{21}N_2Cl$ to the reaction mixture discussed above, a ^{119}Sn NMR spectrum in CD_3CN at ambient temperature shows a broad signal at δ –77 ppm, $W_{1/2}$ = 509 Hz (See Supporting Information, Chapter 2, Figure S232), which

is low-frequency shifted in comparison to the hexachlorido-derivative **12**. But this value is comparable to that of **25**. A crystalline material was isolated from this reaction mixture, showing the same molecular structure of the organotinchloridostannate **25**. Giving this finding, we conclude that compound **12** behaves analogously to the addition of two or three molar equiv of chloride anions, chelating one in a bidentate manner, while the second one is complexed to one tin center. The tin centers appear to be satisfied and do not react with a third molar equiv of Cl^-. This behaviour is in contrast to that of compound **14**. This is probably due to a lower Lewis-acidity of the hexachlorido-derivative **12** in comparison with that of **4**. The latter is able binds three chloride anions even upon addition of only two molar equiv of the chloride anion.

A ^{119}Sn NMR Spectrum of a solution of **4** in CD_2Cl_2 to which one molar equiv of NO_3PPh_4[33] had been added shows a broad resonance at δ –84 ppm (See Supporting Information, Chapter 2, Figure S136), which is low-frequency shifted when comparing with the parent compound **4** (δ 41 ppm). This finding is interpreted in terms of the formation of the 1: 1 adduct $(PPh_4)[MeSi(CH_2SnPhCl_2)_3 \cdot NO_3]$ (**15**, Scheme 7).

Scheme 7. Reaction of **4** with one molar equiv NO_3PPh_4.

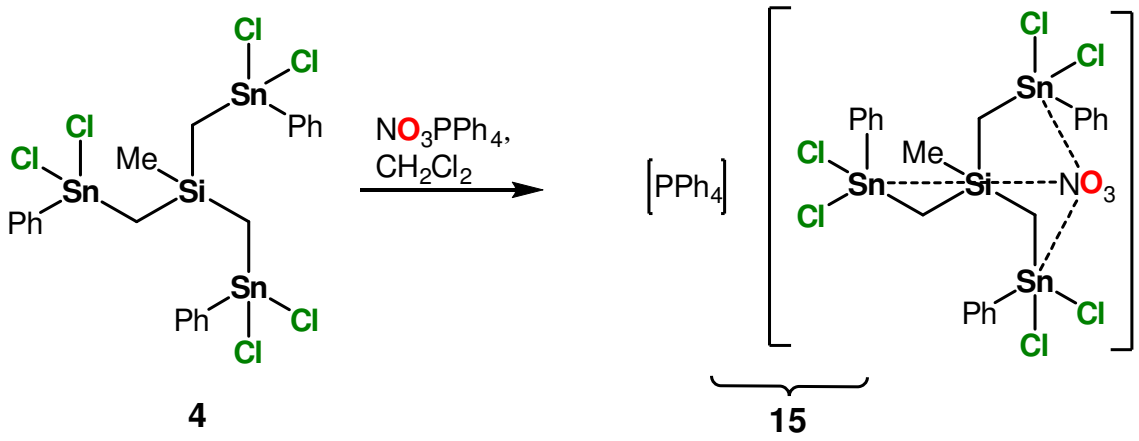

Compound **15** was isolated from the reaction mixture as amorphous solid material, the elemental analysis of which matches perfectly with the Anal. Calcd (%) for $C_{46}H_{44}Cl_6NO_3PSiSn_3$: C 42.94, H 3.45, N 1.09, with a (%) of C 43.0, H 3.75, N 0.6. The identity of **15** gets support by ^1H, ^{13}C and ^{31}P NMR spectroscopy and ESI-MS spectrometry. (See Supporting Information, Chapter 2, Figures S133-S143). A ^1H NMR spectrum exhibits a singlet resonance for the the $SiCH_2Sn$ protons at δ 1.56 ppm with $^2J(^1H-^{117/119}Sn)$ = 102 Hz. It is shifted to higher frequency in comparison with the methylene protons of 4 (δ 1.18 ppm, $^2J(^1H-^{117/119}Sn)$ = 84 Hz). As to the complex pattern referring to the phenyl groups of one PPh_4^+ cation (20H) combined with those of the novel complex (15H) appears at δ 7.30–8.03 ppm. A ^{13}C NMR spectrum, displays the resonance

corresponding to $SiCH_3$ at δ 2.22 ppm which is slightly lower frequency shifted and that of $SiCH_2Sn$ at δ 18.33 ppm, which is displaced to higher frequencies in comparison with those of **4**, respectively, at δ 3.51 and 11.25 ppm. As well, in the aromatic part, there are the signal resonances referring to C_m (δ 128.5 ppm), C_p (δ 130.08 ppm), C_o (δ 135.1 ppm), and C_i (δ 143.7 ppm) of the phenyl groups of complex 15. These latter, except for C_i, are all slightly lower frequency shifted in comparison with the corresponding ^{13}C shifts in the parent compound 4 (δ C_m 130.1, C_p 132.1, C_o 134.9 ppm). The resonance for C_i is high frequency shifted (4 δ C_i 139.7 ppm). In addition to those of C_m (δ 130.7 ppm), C_p (δ 117.7 ppm), C_o (δ 134.2 ppm), and C_i (δ 135.7 ppm) of the PPh_4^+ counter cation. An ESI-MS mass spectrum of complex **15** in the negative mode shows mass clusters centred at m/z 62.7, 1125.3, and 1152.3, which correspond, respectively, to $[NO_3]^-$, $\{[(MeSi(CH_2SnCl_2Ph)_3 \cdot NO_3]^- + HPPh_2 + H_2O\}^-$, and $[(C_{22}H_{25}Cl_3SiSn_3)_3^+ + 3\,OH^- + NO_3^- + 2\,H_2O + 3\,CH_3CN + MeOH]^-$.

A ^{119}Sn NMR spectrum at room temperature of a solution of **4** in $CDCl_3$ to which three molar equiv of HMPA had been added (See Supporting Information, Chapter 2, Figure S147) shows an rather broad signal at δ –187 ppm ($W_{1/2}$ = 809 Hz), indicative for a fast exchange process on the ^{119}Sn NMR time scale. resonance similar chemical shift was observed for the complex $[(Ph_2SnCH_2)_2SnClPh \cdot 2\,HMPA]$ (δ –186 ppm).[25] It is low frequency-shifted comparing to that of the parent compound **4** (δ 41 ppm). A ^{31}P NMR spectrum of the crude reaction mixture at ambient temperature shows a single resonance at δ 24.3 ppm with no $^{117/119}Sn$ satellites. The NMR data proof the formation of a HMPA complex of **4** that is kinetically labile on the corresponding NMR time scales at room temperature.

From the reaction mixture, the complex $MeSi(CH_2SnPhCl_2 \cdot HMPA)_3$, **16**, (Scheme 8) was isolated as colourless crystalline material that shows good solubility in dichloromethane, diethyl ether and acetonitrile. Single crystals of **16** suitable for X-ray diffraction analysis were obtained from its CH_2Cl_2/CH_3CN solution.

Scheme 8. Reaction of **4** with three molar equiv HMPA (1) and six molar equiv HMPA (2).

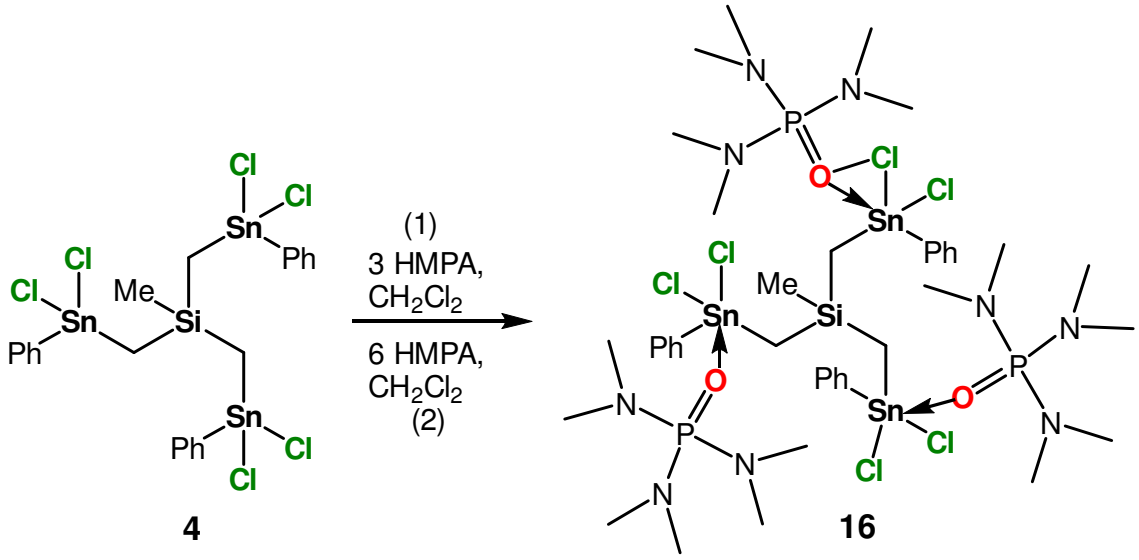

Compound **16** crystallizes in the trigonal space group R_{3c} with 6 molecules in the unit cell. Figure 18 shows its molecular structure and Table 3 contains selected interatomic distances and angles. Compound **16** shows a propeller-type structure. Both enantiomers with clockwise and anti-clockwise orientation are present. The three tin atoms are crystallographically equivalent. They are penta-coordinated and exhibit a distorted trigonal bipyramidal environment with the axial positions being occupied by O(1) and Cl(1) and the equatorial positions by Cl(2), C(2) and C(3). The distortion is best reflected in the O(1)–Sn(1)–Cl(1) angle of 173.75(6)°, which deviates from the ideal angle of 180°. The geometrical goodness $\Delta\Sigma(\theta)$[22] is 81.5°. The Sn(1)–O(1) distance is 2.214(2) Å is similar to that of the corresponding distances in $[o-C_6H_4(SnClMe_2)_2 \cdot HMPA]$[8] and $[(Ph_2ClSnCH_2)_2 \cdot HMPA]$.[34]

The Sn(1)–Cl(1) and Sn(1)–Cl(2) distances are 2.3862(8) and 2.4861(8) Å, respectively. They are shorter than the corresponding distances in the HMPA complex mentioned above.[8] Another interesting aspect is the bowl-alike molecular structure of **16**, in which the "bottom" is the methylsilyl head characterising this novel backbone, in addition to that all Phenyl- and HMPA groups are oriented to the c- axis, in trans-position in regards to the chlorine atoms. (Figure 19) This is probably due to the innovative tripod geometry of the novel silicon bridged organotin precursors. As it is reported in literature,[25] the complexation behaviour of halido di- or tricentric organotin compounds towards HMPA molecules, show these latter as non-bridging donors. This is approved, also by the chelation manner described for compound **16**.

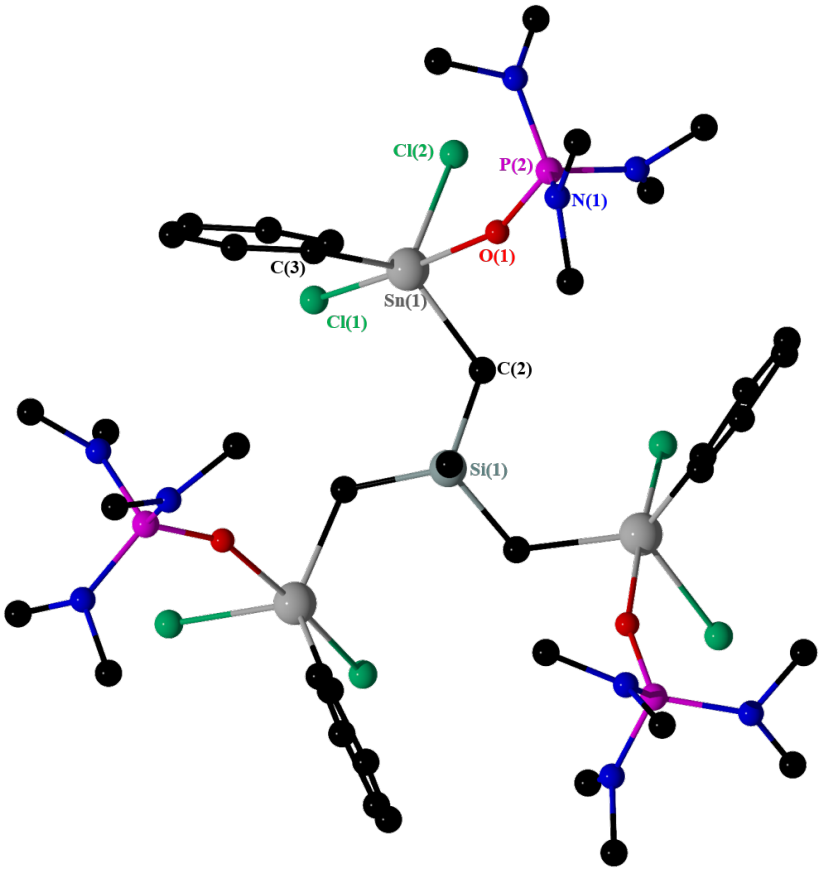

Figure 18. General view (POV-Ray) of a molecule of **16** showing crystallographic numbering scheme for Sn(1). Hydrogen atoms are omitted for clarity.

At −80 °C, a ^{119}Sn NMR spectrum of a solution of single crystalline sample of **4** in CD_2Cl_2 exhibits four major signals at δ –213.4, -214.7, -216.6, and -217.8 ppm, respectively, with a total integral of 74 %. In addition, there are low intense broad resonances centered at δ –190 (integral 5.4 %) and δ –253 ppm (partially structured, integral 10.8 %) (See Supporting Information, Chapter 2, Figure S149). These chemical shifts are are low-frequency shifted compared with similar compounds; [*o*−$C_6H_4(SnClMe_2)_2$·HMPA] (δ –98.9 ppm),[8] [$(Ph_2SnCH_2)_2$SnClPh·HMPA] (δ –162.9 ppm), but comparable to that for the complex [$(Ph_2SnCH_2)_2$SnClPh·2 HMPA] (δ –186 ppm).[25] A ^{31}P NMR spectrum of the same sample at −80 °C displays a major resonance at δ 23.53 ppm with an unresolved $^2J(^{31}P-^{117/119}Sn)$ coupling of 181 Hz resembling the chemical shifts reported for the neutral complexes [*o*−$C_6H_4(SnClMe_2)_2$·HMPA] (δ 24.5 ppm, $^2J(^{31}P-^{117/119}Sn)$ = 135 Hz),[8] [$(Ph_2SnCH_2)_2$SnClPh·HMPA] (δ 25.6 ppm, $^2J(^{31}P-^{117/119}Sn)$ = 147 Hz), and [$(Ph_2SnCH_2)_2$SnClPh·2 HMPA] (δ 24.1 ppm, $^2J(^{31}P-^{117/119}Sn)$ = 148 Hz).[25] Besides, there are three minor intense resonances (total integral 8.75 % of the major resonance) at δ 23.81, 24.74, and 25.2 ppm, for which no assignment is made. This case is the same for the

similar compounds mentioned above.[8,25] The identity of **16** is further supported by ^{1}H, ^{13}C, and ^{31}P NMR spectra as well as by ESI-MS mass spectrometry. A ^{1}H NMR spectrum shows a singlet resonance for the $Si(CH_3)$ protons at δ 0.58 ppm, displaced to slightly lower frequency in comparison to that of **4** (δ 0.65 ppm). The $SiCH_2Sn$ methylene protons show a single resonance at δ 1.53 ppm ($^{2}J(^{1}H-^{117/119}Sn)$ = 117 Hz) in comparison with the parent compound **4** (δ 1.18 ppm, $^{2}J(^{1}H-^{117/119}Sn)$ = 84 Hz).

The resonance at δ 2.55 ppm, ($^{3}J(^{1}H-^{31}P)$ = 137 Hz, 54H) refers to the $(-N(CH_3)_2)_3$ protons of three molecules of HMPA. In a ^{13}C NMR spectrum, the resonances corresponding to $SiCH_3$ at δ 4 ppm and that of $SiCH_2Sn$ at δ 18.33 ppm $^{1}J(^{13}C-^{117/119}Sn)$ = 519 Hz, are displaced to higher frequencies in comparison with those of 4, respectively, at δ 3.51 and 11.25 ppm, $^{1}J(^{13}C-^{117/119}Sn)$ = 361/376 Hz. As well, in the aromatic part, there are the signal resonances referring to C_m (δ 128.4 ppm), C_p (δ 129.8 ppm), C_o (δ 135.06 ppm), and C_i (δ 145.3 ppm, $^{1}J(^{13}C-^{117/119}Sn)$ = 921/955 Hz) of the phenyl groups of complex **16**. These latter, except for C_i, are all slightly lower frequency shifted in comparison with the corresponding carbon shifts in the parent compound 4 (δ C_m 130.1, C_p 132.1, C_o 134.9 ppm). The signal for C_i is high frequency shifted with a bigger coupling constant in comparison to **4** (C_i δ 139.7 ppm, $^{1}J(^{13}C-^{117/119}Sn)$ = 742/773 Hz) (See Supporting Information, Chapter 2, Figures S144- 149).

In fact, the formation of the 1:3 complex $[MeSi(CH_2SnCl_2Ph)_3 \cdot 3\,HMPA]$ is proved by the observation of one methyl and one methylene groups in the ^{1}H and ^{13}C NMR spectra, evidence that the three tin centres are all equivalent, so each tin atom is in interaction with one molecule of HMPA. It is worth noting to underline that the structural change in **16** imposed on the three tin centres, upon coordination with 3 molecules of HMPT, is affecting extremely both NMR shifts and coupling constants.

An ESI-MS mass spectrum of complex 16 in the negative mode shows a mass cluster centred at m/z 810.7 assigned to $[C_{18}H_{23}Cl_4NO_2P_2SiSn_3]^-$. In the positive mode, two mass clusters are shown centered at m/z 180.1 which correspond to [POH(NMe2)3]+ and 740.8 assigned to $[C_{12}H_{42}Cl_3N_6O_4P_2Sn_2]^+$. The IR spectrum shows P=O absorption band at $\nu_{P=O}$ = 1121.9 cm^{-1} (See Supporting Information, Chapter 2, Figures S150- S157).

Upon addition of 3 more molar equiv of HMPA to the reaction mixture, compound **4** behaves analogously as complex **16** towards HMPA molecules (Scheme 8). A crystalline material is isolated, which displays the same molecular structure as **16**. We can conclude that there are no formation of 1:6 adduct $[MeSi(CH_2SnCl_2Ph)_3 \cdot 6\,HMPA]$. This is can be explained with the deficiency of Lewis-acidity of **4**.

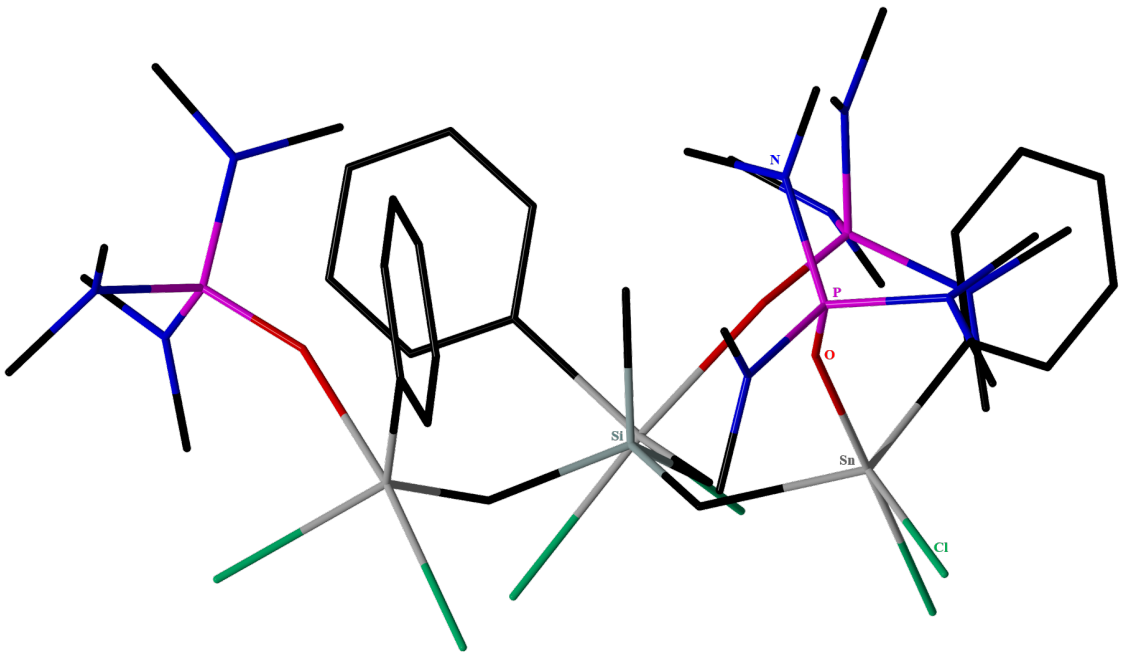

Figure 19. A POV-Ray image in sticks of a molecule of **16** showing bowl-alike molecular structure. Hydrogen atoms are omitted for clarity.

2.2.2 Complexation behaviour of 6 towards HMPA molecules and chloride anions

The complexation behaviour of the trichlorido silicon-bridged triorganotin compound **6** towards HMPA molecules and Chloride anions was also investigated.

A ^{119}Sn NMR spectrum ($CDCl_3$) at ambient temperature of a solution of **6** with a slightly excess (four molar equiv) of HMPA in CH_2Cl_2 exhibits an extremely broad signal at δ –81 ppm ($W_{1/2}$ = 1675 Hz) due to an exchange process being fast on the NMR time scale (See Supporting Information, Chapter 2, Figure S168). This resonance is very low-frequency shifted as compared to that of the parent compound **6** at δ 24 ppm and proofs the formation of a novel neutral HMPA-containing complex. A ^{31}P NMR spectrum of the crude mixture at ambient temperature shows a signal resonance at δ 24.64 ppm with no $^{117/119}Sn$ satellites due also to the kinetic lability of such compounds. The ^{1}H NMR spectrum is also an evidence of the formation of a novel complex. The $Si(CH_3)$ resonance at δ 0.23 ppm is displaced to slightly lower frequency in comparison to that of **6** (δ 0.35 ppm). The same holds for the methylene proton $SiCH_2Sn$ single resonance which appears at δ 0.86 ppm ($^{2}J(^{1}H-^{117/119}Sn)$ = 92 Hz) as compared to that of the parent compound **6** (δ 0.96 ppm, $^{2}J(^{1}H-^{117/119}Sn)$ = 79 Hz). The resonance referring to the $(-N(CH_3)_2)_3$ protons (δ 2.46 ppm, $^{2}J(^{1}H-^{1}H)$ = 9 Hz, $^{3}J(^{1}H-^{31}P)$ = 135 Hz, 72H) corresponds to four molecules of HMPA. In a ^{13}C NMR spectrum, the resonance corresponding to $SiCH_3$ at

δ 3.44 ppm is slightly low-frequency shifted as to that of $SiCH_2Sn$ at δ 9.05 ppm. It is displaced to higher frequencies in comparison with that of **6**, respectively, at δ 3.60, and 4.13 ppm (See Supporting Information, Chapter 2, Figures S164- 166).

A crystalline material was isolated from a solution of CH_2Cl_2/ CH_3CN, suitable for X-Ray diffraction study. A close inspection of this crystalline material revealed the presence of two different types of crystals which could be separated manually. They proved to be the complexes [MeSi(CH2SnPh2)2Cl3$CH_2SnPh_2(HMPA)_2$], **18**, and the HMPA solvate $[MeSi\{CH_2SnClPh_2(HMPA)_3\}_3]\cdot$HMPA, **19** (Scheme 9). Figures 20 (**18**) and 21 (**19**) show the molecular structures and Table 3 contains selected interatomic distances and angles.

Scheme 9. Reaction of **6** with four molar equiv HMPA: formation of **18** and **19**.

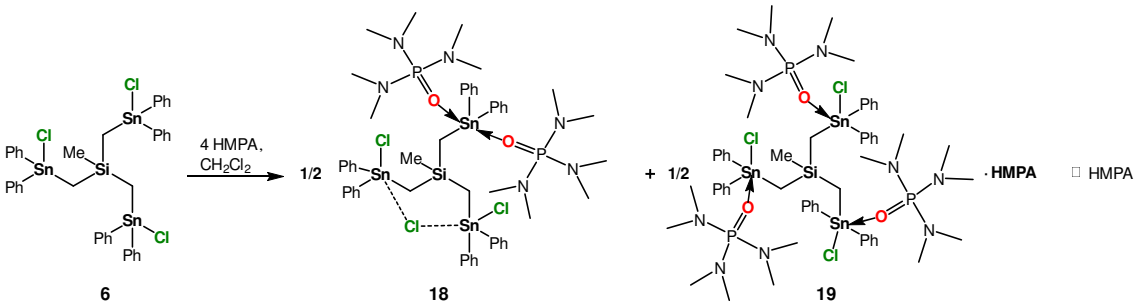

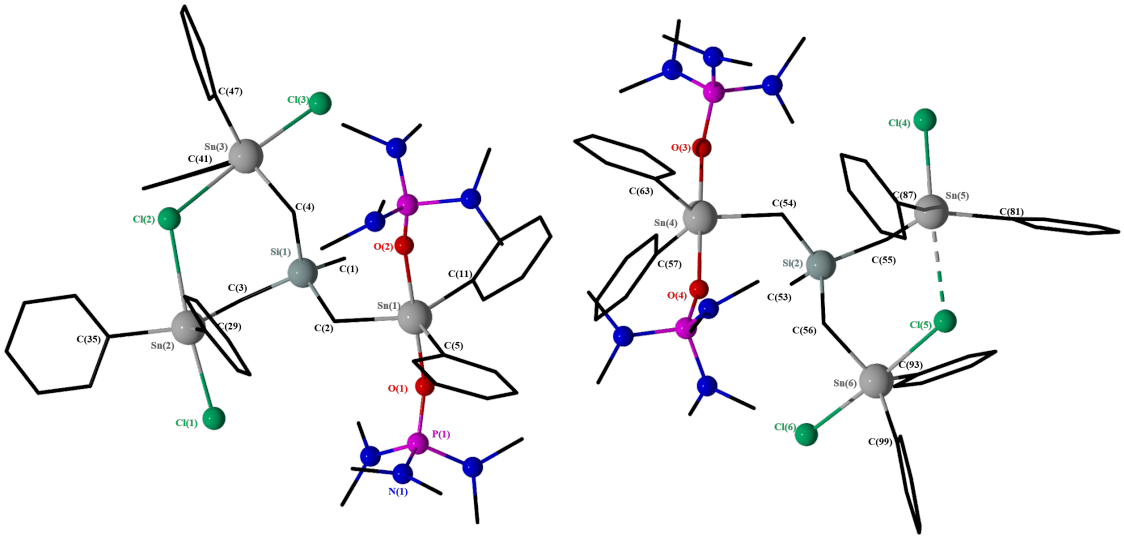

Figure 20. General view (POV-Ray) of a molecule of **18** showing the two molecules in one-unit cell with the crystallographic numbering scheme. Hydrogen atoms are omitted for clarity and carbon atoms are shown as sticks.

Complex **18** crystallizes in the triclinic space group *P*–1 with two independent molecules in the unit cell presenting two enantiomers. The geometric parameters of both molecules resemble each other and only the structure of the molecule containing Sn(1)–Sn(3) is discussed in detail. Complex **18** is the product of autoionization. Two HMPA molecules kick out a chloride anion at Sn(1) and stabilizes a tin cation by two O→Sn interactions at distances of 2.198(6) Å (Sn1–O1) and 2.240(7) Å (Sn1–O2). The Sn(2) and Sn(3) atoms complex the chloride anion unsymmetrically at Sn(2)–Cl(2) and Sn(3)–Cl(2) distances of 2.880(2) and 2.814(3) Å, respectively. These bond distances are similar to those of the corresponding distances reported for $[o\text{-}C_6H_4(SnClMe_2)_2 \cdot HMPA]$[8] and $[(Ph_2ClSnCH_2)_2 \cdot HMPA]$.[34] Crystallographically, there are six non-equivalent tin atoms; all of these are pentacoordinated, displaying distorted trigonal bipyramidal geometries with geometrical goodnesses $\Delta\Sigma(\theta)$[22] of 90.9° (Sn1), 76.2° (Sn2), 76.7° (Sn3), 88.0° (Sn4), 68.2° (Sn5), and 82.8° (Sn6). In which, respectively, the axial positions are occupied by O(1) and O(2) at(at Sn1), Cl(1) and Cl(2) (at Sn2), Cl(2) and Cl(3) (at Sn3), O(3) and O(4) (at Sn4), Cl(4) and Cl(5) (at Sn5), and Cl(5) and Cl(6) (at Sn6). The equatorial positions are occupied by C2, C5, C11 (at Sn1), C3, C29, C35 (at Sn2), C4, C41, C47 (at Sn3), C54, C57, C63 (at Sn4), C55, C81, C87 (at Sn5), and C56, C93, C99 (at Sn6). Sn(5) shows the strongest deviation from the ideal trigonal bipyramidal geometry and can be seen as [4+1] coordinated with the Cl(5) atom intramolecularly approaching Sn(5) at a Sn(5)–Cl(5) distance of 2.9073(24) Å. This latter is shorter than 3.92 Å (sum of the vdW radii of Cl and Sn atoms).[33]

Complex **19** crystallizes in the monoclinic space group $P2_1/n$. All Sn atoms are pentacoordinated and show distorted trigonal bipyramidal environments. The geometrical goodness $\Delta\Sigma(\theta)$[22] are equal to 81.9° (Sn1), 79.4° (Sn2), 79.3° (Sn3). The axial positions are occupied by Cl(1), O(1) (at Sn1), Cl(2), O(2) (at Sn2), and Cl(3), O(3) (at Sn3). The equatorial positions are occupied by C(2), C(5), C(11) (at Sn1), C(3), C(23), C(29) (at Sn2), and C(4), C(41), C(47) (at Sn3). The distortion is best reflected in the angles of 131.9(2)° (C2–Sn1–C52), 133 4(2)° (C3–Sn2–C23), and 129.7(2)° (C4–Sn3–C41), which deviate from the ideal angle of 120°.

There are no intramolecular Sn–Cl–Sn bridges. The Sn–Cl distances are very similar and vary between (Sn1–Cl1) 2.5018(17) Å and (Sn2–Cl2) 2.521(2) Å. The Sn–O distances are between 2.301(11) Å (Sn1–O1) and 2.339(5) Å (Sn3–O3). All these values are comparable to the corresponding distances in $[o\text{-}C_6H_4(SnClMe_2)_2 \cdot HMPA]$[8] and $[(Ph_2ClSnCH_2)_2 \cdot HMPA]$.[34]

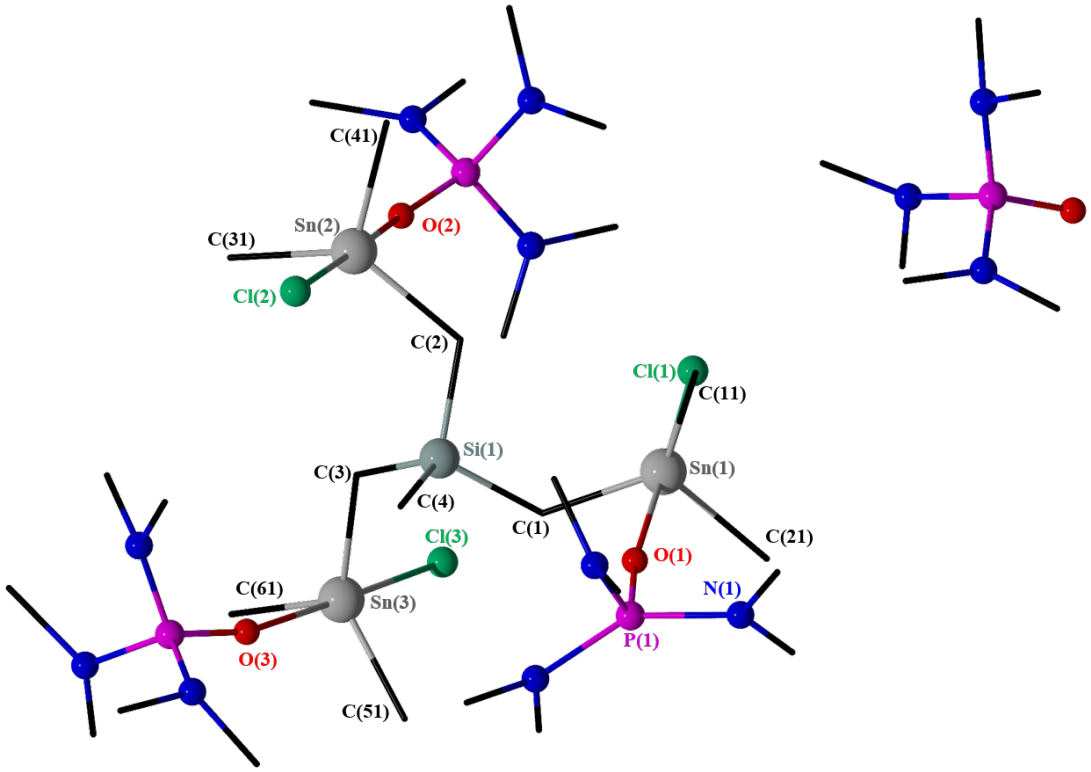

Figure 21. General view (POV-Ray) of a molecule of **19** showing the crystallographic numbering scheme. There is a free HMPA solvent molecule in the unit cell. Hydrogen atoms are omitted for clarity and carbon atoms are presented in sticks. Only C_i carbons of the phenyl groups are shown.

Table 3. Selected interatomic distances /Å and angles /° in compounds **16**, **18**, and **19**.

	16	18	19
Sn(1)–Cl(1)	2.3862(8)		2.5018(17)
Sn(1)–Cl(2)	2.4861 (8)		
Sn(1)–O(1)	2.214(2)	2.198(6)	2.301(11)
Sn(1)–O(2)		2.240(7)	
Sn(3)–O(3)			2.339(5)
Sn(4)–O(4)		2.245(6)	
Sn(2)–Cl(2)		2.880(2)	2.521(2)
Sn(3)–Cl(2)		2.814(3)	
Sn(5)–Cl(5)		2.9072(24)	
Sn(6)–Cl(5)		2.717(2)	
O(1)–Sn(1)–Cl(1)	173.75(6)		173.7(3)
Cl(1)–Sn(1)–C(2)			92.8(19)
Cl(2)–Sn(1)–C(2)	111.21(9)		
Cl(2)–Sn(1)–C(3)	117.11(8)		93.0(2)
C(2)–Sn(1)–C(3)	130.96(12)		
O(1)–Sn(1)–Cl(2)	84.51(6)		
O(1)–Sn(1)–O(2)		178.1(3)	
O(1)–Sn(1)–C(2)		88.8(3)	85.1(5)
C(2)–Sn(1)–C(5)			131.9(2)
Cl(1)–Sn(2)–C(3)		91.2(2)	
C(3)–Sn(2)–C(23)			133.4(2)
Cl(3)–Sn(3)–C(4)			92.42(19)
O(4)–Sn(4)–C(63)		91.5(3)	
C(55)–Sn(5)–C(87)		120.3(3)	

At −80 °C, the ^{119}Sn NMR spectrum in CD_2Cl_2 of the solid crystalline material from which the single crystal of **18** was taken from (the homogeneity of which was, however, not established by X-ray powder diffraction measurement) exhibits 6 signals referring each to non-equivalent tin atoms corresponding to more than one species in solution (compounds **18** + **19**) or more with integration ratio from left to right of [1:3:1:1:2], at δ –104 (1.3) , -133 (3.5) ppm, -170 (broad signal, $W_{1/2}$ = 920 Hz, 1.4), -185 (broad signal, $W_{1/2}$ = 950 Hz, 1.2), -197 (t, $^2J(^{31}P-^{117/119}Sn)$ = 313 Hz, 1.9), corresponding to two tin atoms in coordination each with two HMPA molecules (Figure 22). This latter is close to the corresponding resonances in $[(Ph_2SnCH_2)_2SnClPh\cdot HMPA]$ (δ –162.9 ppm), and

$[(Ph_2SnCH_2)_2SnClPh\cdot 2\,HMPA]$ (δ –186 ppm).[25] There is also a very low intensity doublet signal at -254 ppm, for which no assignment is made.

The ^{31}P NMR Spectrum of this same crystals sample at −80° (Figure 23) displays 2 broad signals with ratio of 4:3, respectively at δ 23.2 and 23.62 ppm. Whereas, no Sn satellites were defined due to exchange processes being fast even at low temperature. ^{31}P NMR spectrum need to be measured at even lower temperature for better interpretation of the complexation behaviour in solution. These latter resonances are very close to the corresponding phosphorus atoms in the resembling complexes $[o-C_6H_4(SnClMe_2)_2\cdot HMPA]$ (δ 24.5 ppm),[8] $[(Ph_2SnCH_2)_2SnClPh\cdot HMPA]$ (δ 25.6 ppm), and $[(Ph_2SnCH_2)_2SnClPh\cdot 2\,HMPA]$ (δ 24.1 ppm). There are also three low-intensity signals at δ 22.7, 24.1 and 24.3 ppm like the case of **16**, for which no assignments are made.

An ESI mass spectrum in the negative mode taken from a crystalline sample shows a mass cluster centred at m/z 1291.1, which is assigned to $[(MeSi(CH_2SnCl_3Ph_2)_3\cdot HMPA + PClOH^- - (NMe_2)_3]^-$ and 1046.1 referring to $[(MeSi(CH_2SnCl_3Ph_2)(CH_2SnClPh_2)(CH_2SnO_2Ph_2)]_2^-$ (See Supporting Information, Chapter 2, Figures S167, S169- S172). To distinguish between these two compounds in solution, we need ^{119}Sn and ^{31}P NMR measurements at even lower temperature. Within the time frame of this PhD, further investigation in solution could not be performed.

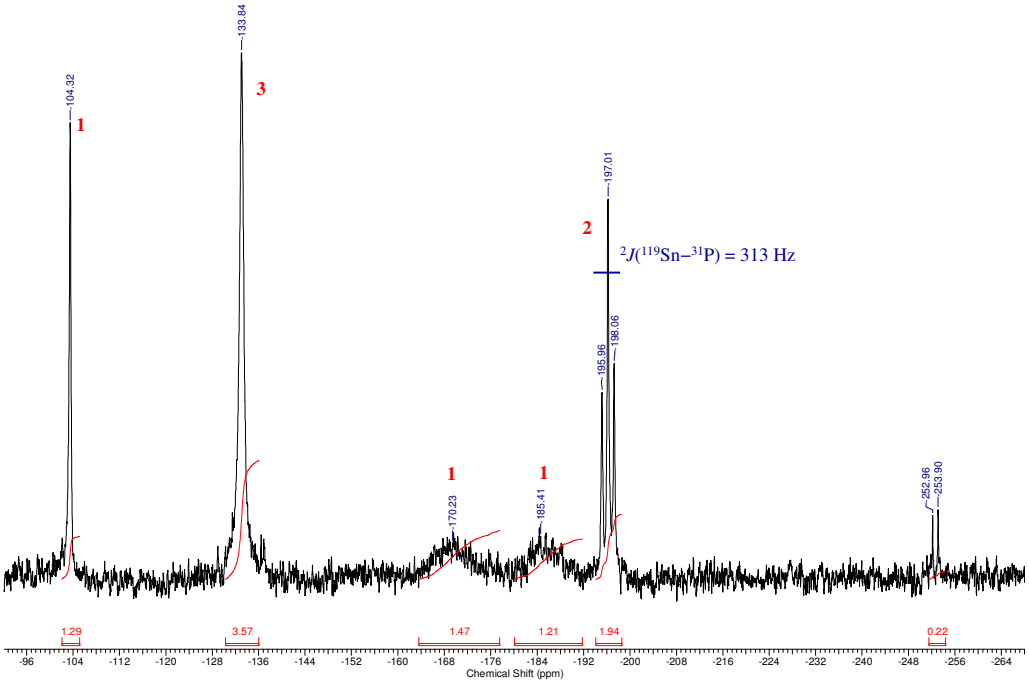

Figure 22. ^{119}Sn NMR spectrum of a crystals sample at –80 °C (149.26 MHz, $CDCl_3$) of complexes **18** and **19**.

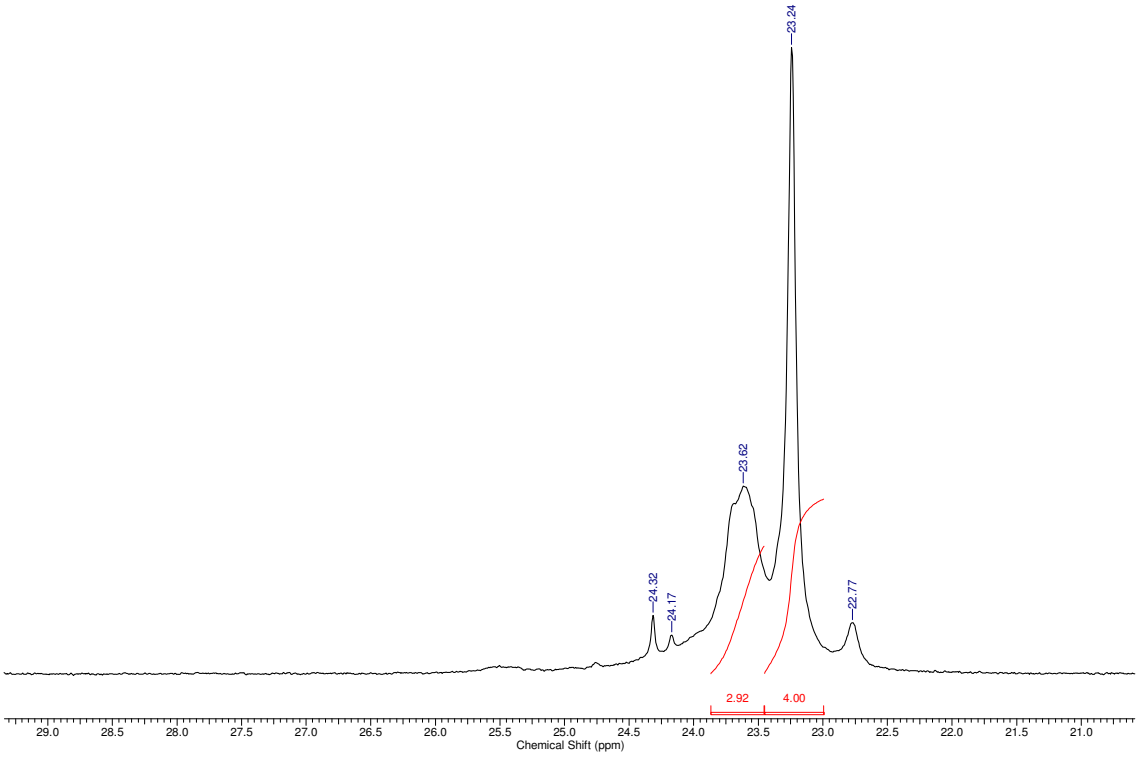

Figure 23. ^{31}P NMR spectrum of a crystals sample at −80 °C (162.02 MHz, CD_2Cl_2) of compound **18** + **19**.

We want to investigate the complexation behaviour of **6**, when we change the type of Lewis-base, will that be affecting its chelating manner? Therefore, we study the complexation reaction of this latter toward chloride anions.

A ^{119}Sn NMR Spectrum of a solution containing **6** and one molar equiv of $[PPh_4]Cl$ in CD_2Cl_2 shows a broad resonance at δ –77 ppm, $W_{1/2}$ = 980 Hz (See Supporting Information, Chapter 2, Figure S178), which is very low-frequency shifted when comparing with the parent compound **6** (δ 24 ppm).

At −80 °C, there are two broad signals at δ –52 ppm (integral 2) and δ –87 ppm (integral 1), respectively. These two resonances are very low frequency shifted in comparison to the parent compound **6** (δ 24 ppm). This is evidence of the formation of the 1:1 chloridostannate complex $(PPh_4)[MeSi(CH_2SnPh_2Cl)_3 \cdot Cl]$, **20** (Scheme 10) in which two tin centres chelate one chloride anion in a bidentate manner (Table 4).

Scheme 10. Reaction of **6** with one molar equiv PPh_4Cl.

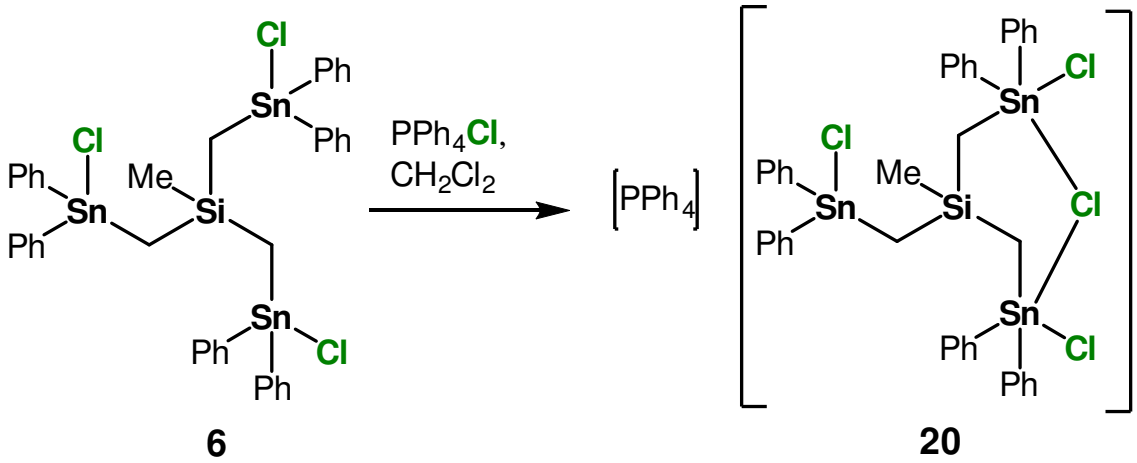

6 **20**

This view is also supported by ^{1}H, ^{13}C and ^{29}Si NMR spectroscopy and ESI-MS spectrometry. A ^{1}H NMR spectrum exhibits the $SiCH_2Sn$ resonance appearing at δ 0.92 ppm with $^{2}J(^{1}H-^{117/119}Sn)$ = 98 Hz, and that referring to the $SiCH_3$ resonance at δ 0.3 ppm, shifting both to lower frequency in comparison to the corresponding proton resonances of **6** (δ 0.36, 0.96 ppm, $^{2}J(^{1}H-^{117/119}Sn)$ = 84 Hz). As to the complex pattern referring to the phenyl groups of one PPh_4^+ cation (20H) combined with those of the novel complex (30H) appears at δ 7.24-8.01 ppm. A ^{13}C NMR spectrum, displays the resonance corresponding to $SiCH_3$ at δ 2.96 ppm which is slightly lower frequency shifted and that of $SiCH_2Sn$ at δ 12.05 ppm, which is displaced to higher frequencies in comparison with those of **6**, respectively, at δ 3.6 and 4.13 ppm. As well, in the aromatic part, there are the resonances referring to C_m (δ 127.9 ppm), C_p (δ 128.6 ppm), these two are slightly lower frequency shifted in comparison with the corresponding carbon shifts in the parent compound 6 (δ C_m 128.9, C_p 130.1). As for the resonances of C_o (δ 136.56 ppm) and C_i (δ 143.7 ppm) are high-frequency shifted regarding that of the parent compound **6** (C_o 135.5, C_i 139.2 ppm). In addition to those of C_p (δ 117.2 ppm), C_m (δ 130.6 ppm), C_o (δ 134.1 ppm), and C_i (δ 135.7 ppm) of the PPh_4^+ counter cation. An ESI-MS mass spectrum of complex **20** in the negative mode show a mass cluster centred at m/z 1026.7902 which corresponds to $[M - PPh_4^+ - Cl^- + OH-]^-$ (See Supporting Information, Chapter2, Figures S175-S181).

A ^{119}Sn NMR spectrum at ambient temperature in CD_2Cl_2 the previous reaction mixture to which a second molar equivalent of $[PPh_4]Cl$ had been added, shows an extremely broad signal at δ –109 ppm ($W_{1/2}$ = 957 Hz). This resonance is low-frequency shifted with respect to the parent compound **6** (δ 24 ppm) and the chloridostannate complex **20** (δ –77 ppm) (Table 4).

Table 4. Selected NMR data measured in $CDCl_3$ and CD_2Cl_2 solutions for the chloride complexes.

	δ $^{13}C(CH_2)$	$^{1}H(CH_2)$	$^{119}Sn(RT)$	$^{119}Sn(-80\,°C)$ CD_2Cl_2
20	12.05	0.92	-77	-52, -87
21	14.21	0.97	-109	—

Scheme 11. Reaction of **6** with two molar equiv PPh_4Cl.

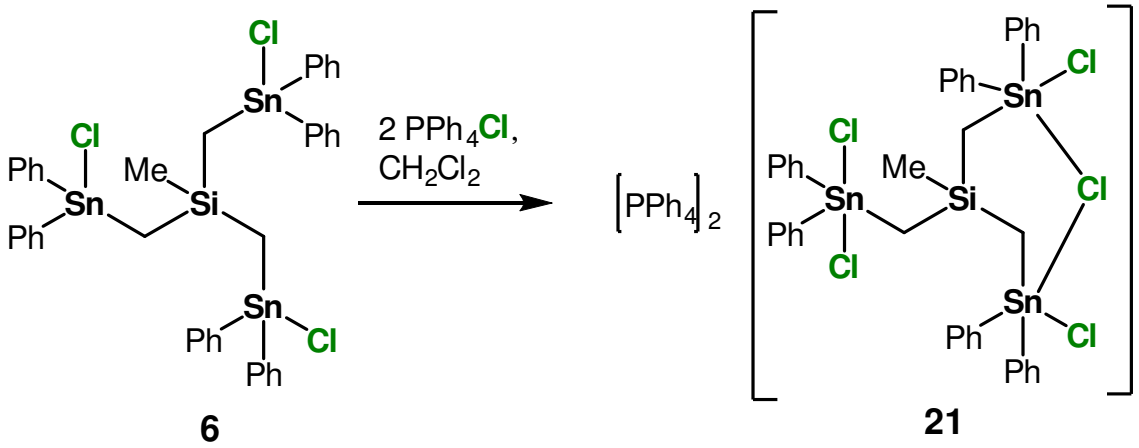

6 **21**

This finding is interpreted with caution to the formation of the chloridostannate complex $(PPh_4)_2[MeSi(CH_2SnPh_2Cl)_3 \cdot 2Cl]$, 21 (Scheme 11). In addition, there are three low intense signals at –252, –134, and –89 ppm, for which no assignment is made. Further experimental support for the formation of **21** stems from the 13C, and ^{29}Si NMR spectroscopy and ESI-MS spectrometry. A ^{13}C NMR spectrum displays a resonance corresponding to $SiCH_3$ at δ 3.62 ppm and that of $SiCH_2Sn$ at δ 14.21 ppm, which are both displaced to higher frequencies in comparison with those of **20**, respectively, at δ 2.96 and 12.05 ppm, and **6** at δ 3.6 and 4.13 ppm. A ^{29}Si NMR spectrum shows a resonance signal at δ 5.53 ppm, shifting to lower frequency regarding to that of **6** (δ 8.61 ppm). An ESI-MS mass spectrum of complex 21 in the positive mode shows two mass clusters centred at m/z 339.2 and 919.2 which correspond to $[PPh_4]^+$ and $[M - 2PPh_4^+ - 2Cl- - CH_3 + H^+]^+$, respectively. No tin-containing mass cluster is observed in an ESI-MS spectrum in the negative mode (See Supporting Information, Chapter 2, Figures S183- S190).

2.2.3 Complexation behaviour of 7 towards fluoride anions

The triorganofluorido tin compound **7** appears to be almost insoluble in all organic solvents. However, upon addition of one molar equiv of $NEt_4F \cdot 2\,H_2O$ in CH_3CN, the solution becomes clear. A ^{119}Sn NMR Spectrum in CD3CN at ambient temperature shows a very broad resonance at δ –188 ppm ($W_{1/2}$ = 2276 Hz). A ^{19}F NMR spectrum of the same solution displays four unresolved resonances between δ –161 and -82 ppm. Even at –80 °C, there are still unresolved broad signals appearing in both ^{119}Sn and ^{19}F NMR spectra (See Supporting Information, Chapter 2, Figures S192, 193). This can be explained due to the inter- and/or intramolecular exchange of the bridging and terminal fluorine atoms in a fluoridostannate complex, which still remains rapid on the NMR time scale even at low temperature. An ESI MS(negative mode) shows a mass cluster centred at m/z 979.2 which corresponds to the fluoridostannate anion $[MeSi(CH_2SnFPh_2)_3 \cdot F]^-$. It proves the formation of the 1:1 adduct in solution (See Supporting Information Figures S.202, S203).

Single crystals of fluoridostannate complex $(NEt_4)_2[\{MeSi(CH_2SnFPh_2)_3\}_2 \cdot 2F]$ **22** (Scheme 12) were isolated from the reaction mixture by slow evaporation of a dichloromethane/diethyl ether solution at room temperature. Complex **22** crystallizes in monoclinic space group $P2_1/n$. This crystalline material is poorly soluble in organic solvents which prevents detailed NMR spectroscopic studies in solution. Figure 24 shows the molecular structure of **22**. Table 5 contains selected interatomic distances and angles.

Scheme 12. Reaction of **7** with one molar equiv $NEt_4F \cdot 2\,H_2O$.

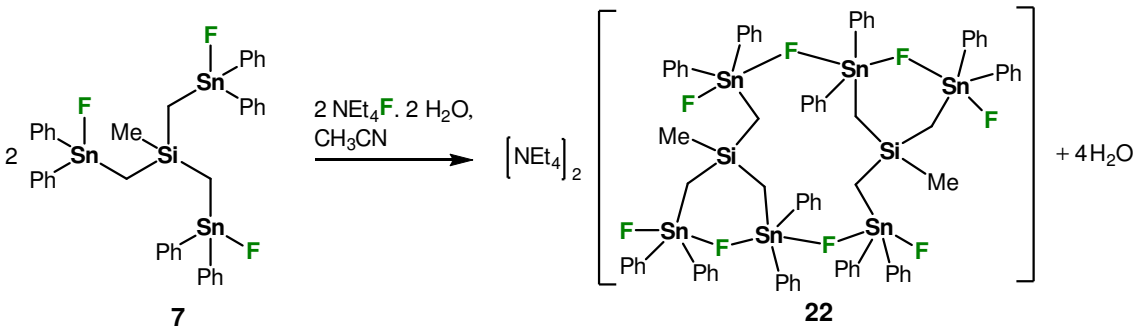

7 **22**

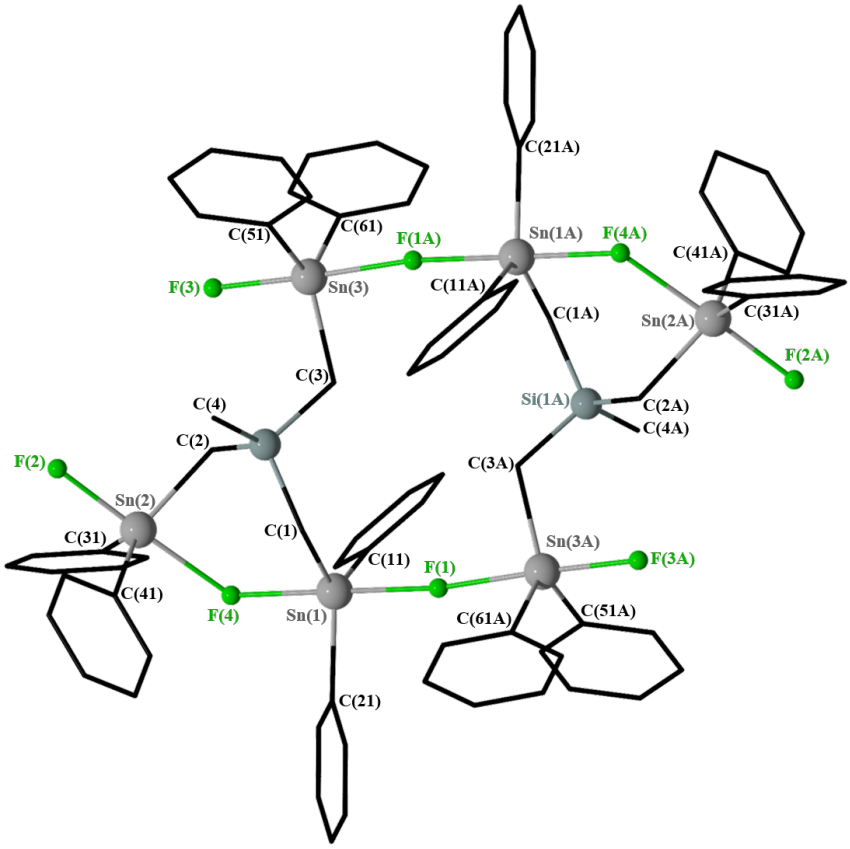

Figure 24. General view (POV-Ray) of a molecule of **22** showing the crystallographic numbering scheme. Counter cations NEt_4^+ and hydrogen atoms are omitted for clarity. Carbon atoms are presented in sticks.

Compound **22** is a centrosymmetric head-to-tail dimer that is realized via unsymmetrical Sn(1)–F(1)–Sn(3A) bridges at Sn–F distances of 2.166(4) and 2.226(4) Å. These distances are comparable to those reported for the organofluorido stannate complexes $NEt_4[CH_2(SnXPh_2)_2{\cdot}F]$ (X = F, Br, I), ranging between 2.204(2) and 2.274(5) Å,[35] and for $[o-C_6H_4(SnClMe_2)_2{\cdot}F][K{\cdot}C_{20}H_{24}O_6]$ 2.204(2) and 2.274(5) Å.[8]

The Sn(2)–F(2) (2.032(4) Å) and Sn(3)–F(3) (2.032(4) Å) distances involving terminal fluorine atoms are shorter than the Sn(1)–F(4) (2.172(4) Å) and Sn(2)–F(4) (2.258(4) Å) distances involving bridging fluorine atoms. This is similar as reported for $[(Ph_2FSnCH_2)_2SnFPh{\cdot}F][C_{12}H_{24}O{\cdot}K]$, with Sn–F distances ranging between 2.02(4) and 2.342(4) Å.[25]

The dimer is composed of two six-membred rings (Sn1–F4–Sn2–C2–Si1–C1) and (Sn1A–F4A–Sn2A–C2A–Si1A–C1A) and one 12-membred ring (Sn1–C1–Si1–C3–Sn3–F1A–Sn1A–C1A–Si1A–C3A–Sn3A–F1). There is a central cavity with a volume of 104 $Å^3$, holding potential for the inclusion of small guest molecules. However, so far attempts at obtaining host-guest complexes based on **22** failed. All tin atoms are pentacoordinated and

exhibit distorted trigonal-bipyramidal geometries [geometrical goodness $\Delta\Sigma(\theta)$[22] 90.1° (Sn1), 79.8° (Sn2), 81.8° (Sn3)]. The axial positions are occupied by F1, F4 (at Sn1), F2, F4 (at Sn2), F1A, F3 (at Sn3). The equatorial positions are occupied by C1, C11, C21 (at Sn1), C2, C31, C41 (at Sn2), C3, C51, C61 (at Sn3). To conclude, the molecular structure of **22** in solid stay, is evidence of the formation of 1:1 anionic adduct, as a dimer structure.

A ^{119}Sn NMR spectrum at room temperature of a solution of **7** in CH_3CN to which two mole equiv. of $NEt_4F\cdot 2H_2O$ had been added exhibits three very broad resonances at δ –220 ppm ($W_{1/2}$ = 530 Hz) (integration: 1), -213 ppm ($W_{1/2}$ = 430 Hz) (integration: 1), and -205 ppm ($W_{1/2}$ = 440 Hz) (integration: 1) (See Supporting Information; Chapter 2, Figure S195). The corresponding ^{19}F spectrum (Figure 25) displays four intense resonances at δ –162, -158, -142, and -129 ppm, with integral ratio of 1:1:1:1. Both the number of signals and the coupling patterns are evidences of the formation of the 1:1 fluoride adduct 22 in solution. In the ^{119}Sn NMR spectrum, there are two terminal Sn^1 at δ –220 ppm and -213 and one bridging Sn^2 at δ –205 ppm. With caution, we assign the two latter resonances, with the lower-shifted frequencies to the terminal fluorine atoms F^1 and F^4, in which, respectively, $^1J(^{19}F^1 - ^{117/119}Sn_1)$ = 1939/2018 Hz, with a satellite-to-signal-to-satellite ratio of approximately [10:80:10], and $^1J(^{19}F^4 - ^{117/119}Sn_1)$ = 2010 Hz with a satellite-to-signal-to-satellite ratio of approximately [6:88:6]. The signal at δ –142 ppm refers to the bridging fluorine atoms F^2, with $^1J(^{19}F^2 - ^{117/119}Sn)$ = 1930 Hz, with a satellite-to-signal-to-satellite ratio of approximately [8:84:8], and that at δ –129 ppm refers to the bridging fluorine atoms F^3. This latter is too broad to enable observation of $^1J(^{19}F - ^{117/119}Sn)$ (Figures 25, 26). These NMR resonance shifts and their coupling constants are comparable to those reported for $[(Ph_2F^aSn_2CH_2)_2Sn_1F^bPh\cdot F^b][Bu_4N]^+$ at δ –101 ppm [$^1J(^{19}F^b - ^{117/119}Sn_1)$ = 1174/1224, $^1J(^{19}F^b - ^{117/119}Sn^2)$ = 573 Hz] and -182 ppm [$^1J(^{19}F^b - ^{117/119}Sn^1)$ = 2163 Hz] and in $[(Ph_2F^aSn_2CH_2Sn_1F^bPh)_2CH_2\cdot 2F^c][Bu_4N]^+]^+$ at δ –122 ppm [$^1J(^{19}F^b - ^{117/119}Sn)$ = 1171 Hz], -145 ppm [$^1J(^{19}F^c - ^{117/119}Sn_1)$ = 1826 Hz], and -151 ppm [$^1J(^{19}F^a - ^{117/119}Sn_2)$ = 1906 Hz]. The F^a and F^b are assigned to the terminal and bridging fluorine atoms respectively, and F^c are the chelated fluorine atoms.[28]

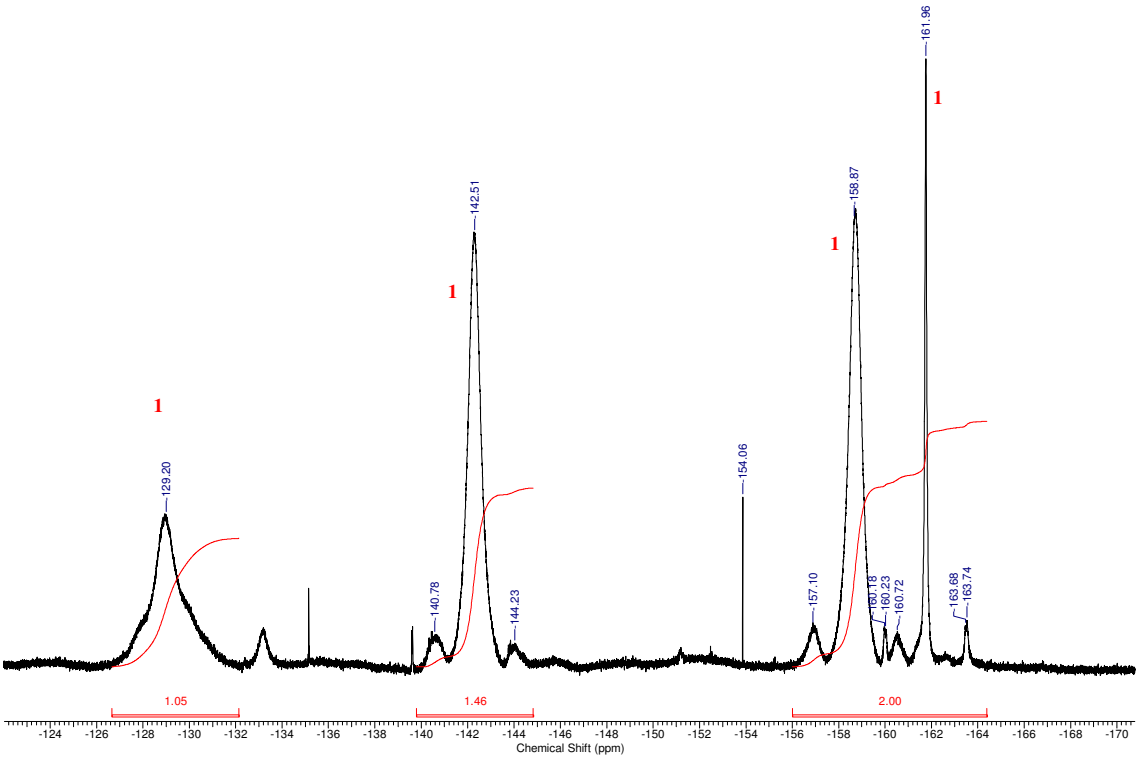

Figure 25. ^{19}F NMR spectrum (564.84 MHz, CD_3CN) at ambient temperature of the mixture containing **7** and two molar equiv of $NEt_4F \cdot 2\,H_2O$.

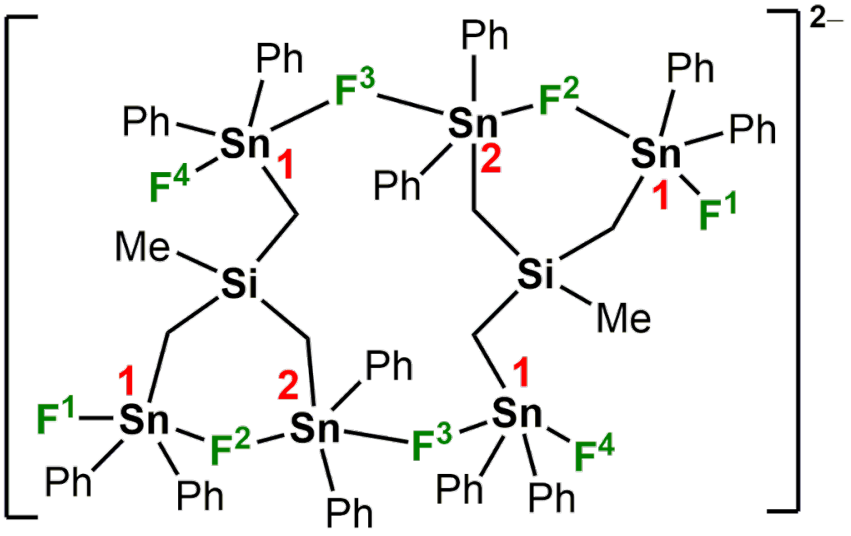

Figure 26. The dianionic fluoridostannate **22**, presenting the different terminal and bridging tin and fluorine atoms.

An ESI-MS spectrum (negative mode) of a crystals sample reveals a 20 % mass cluster centred at m/z 979.2, fitting perfectly to the species $[MeSi(CH_2SnFPh_2)_3 \cdot F]^-$ (See Supporting Information, Chapter 2, Figures S202, S203).

Addition of a third mole equivalent of $NEt_4F \cdot 2H_2O$ to **7** in CH_3CN presents also a clear solution. A ^{19}F NMR spectrum of this solution at ambient temperature in CD_3CN is evidence of the formation of two different species in solution (Figure 27), one with major intensity (94 %) presented with three broad signals of integral ratio 2:2:1, respectively, at δ –158 ppm [$^nJ(^{19}F-^{117/119}Sn)$ = 2013 Hz] with a satellite-to-signal-to-satellite ratio of approximately [8:84:8], -142 ppm [$^nJ(^{19}F-^{117/119}Sn)$ = 1899 Hz] with a satellite-to-signal-to-satellite ratio of approximately [9:82:9], and -129 ppm [$^nJ(^{19}F-^{117/119}Sn)$ = 1153 Hz] satellite-to-signal-to-satellite ratio of approximately [16:68:16]. The second species is present in low intensity (6 %), with four resonances of integral ratio 3:1:2:2, respectively, at δ –162 ppm [$^nJ(^{19}F-^{117/119}Sn)$ = 1942/2029 Hz] with a satellite-to-signal-to-satellite ratio of approximately [8:84:8], -154 ppm [$^nJ(^{19}F-^{117/119}Sn)$ = 1506/1585 Hz] with a satellite-to-signal-to-satellite ratio of approximately [8:84:8], -140 ppm [$^nJ(^{19}F-^{117/119}Sn)$ = 2334/2373 Hz] satellite-to-signal-to-satellite ratio of approximately [8:84:8], and -127 ppm [$^nJ(^{19}F-^{117/119}Sn)$ = 2182/2214 Hz, $^nJ(^{19}F-^{19}F)$ = 116 Hz], satellite-to-signal-to-satellite ratio of approximately [8:84:8].

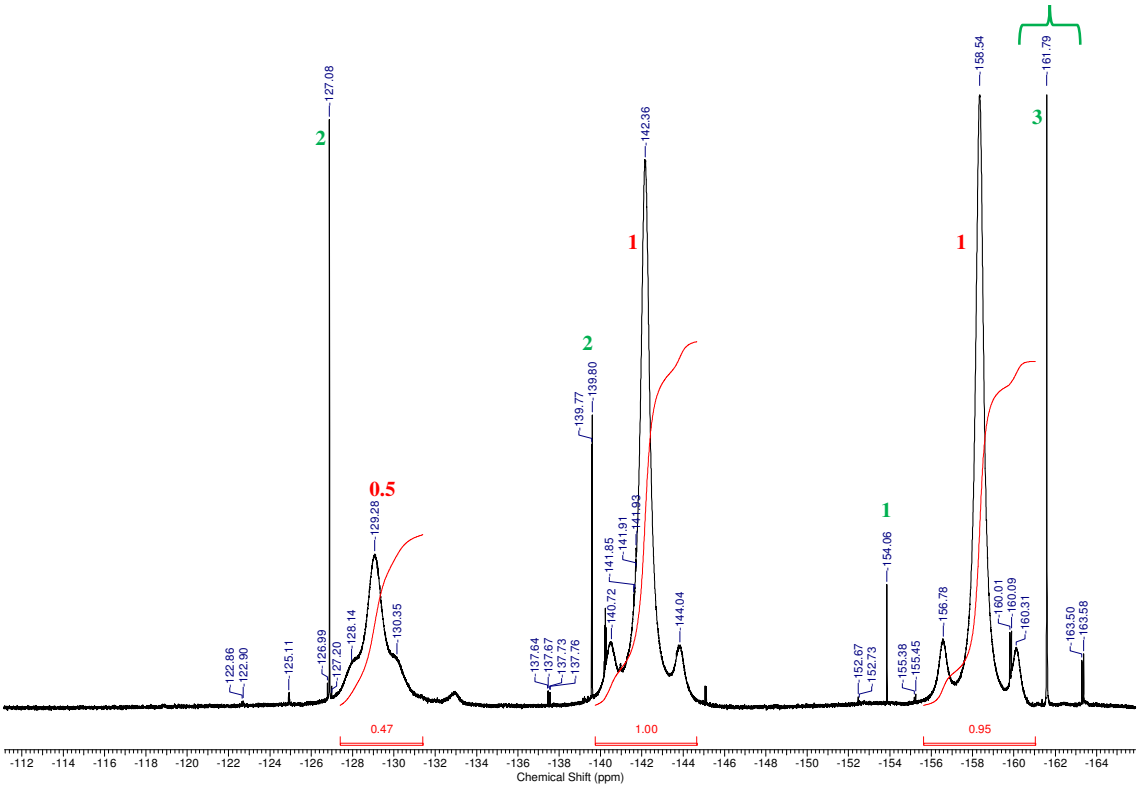

Figure 27. ^{19}F NMR spectrum (564.84 MHz, CD_3CN) at ambient temperature of a mixture containing **7** and three molar equiv of $NET_4F \cdot 2H_2O$ (Integration ratios of the major intensities resonances are written in red and that of the minor intensities with green).

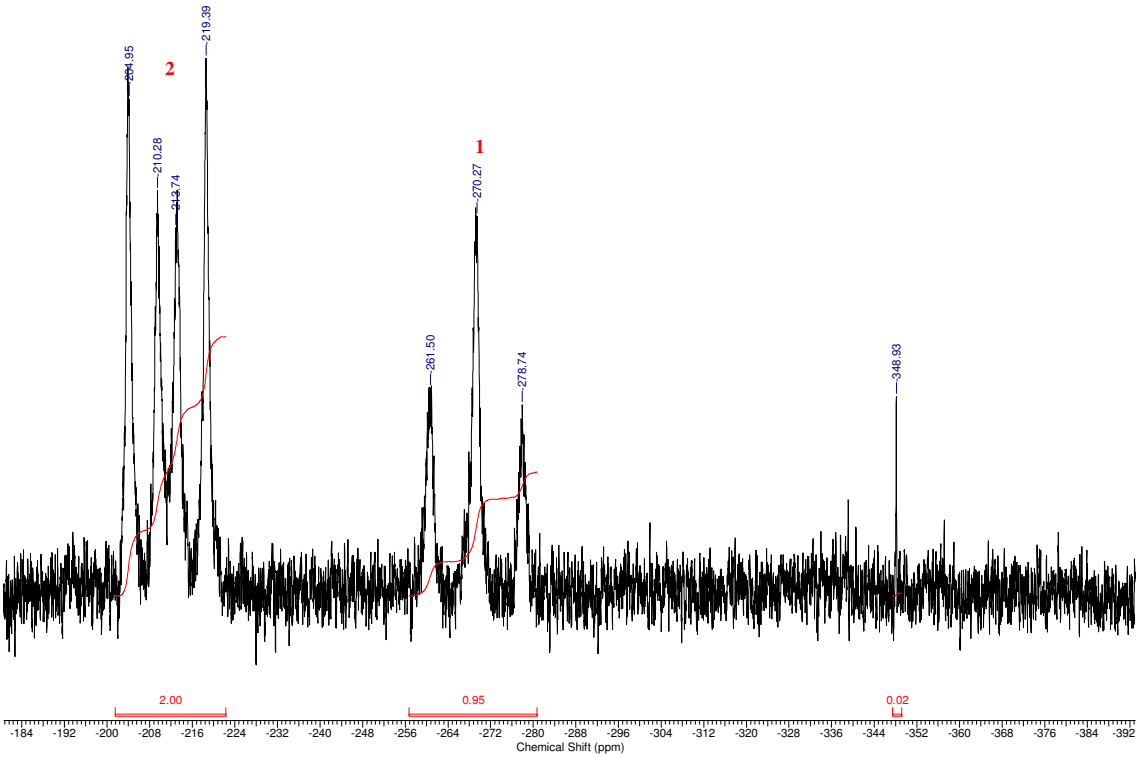

Figure 28. ^{119}Sn NMR spectrum (223.85 MHz, CD_3CN) at ambient temperature of compound **7** to which three molar equiv of $NEt_4F \cdot 2\,H_2O$ had been added.

The ^{119}Sn NMR of this crude mixture at ambient temperature in CD_3CN exhibits two signal resonances with integration ratio of 2:1, corresponding respectively, to one doublet of doublets at δ –211 ppm and one triplet at δ –270 ppm ($W_{1/2}$ = 1983 Hz). (Figure 28) Most likely the lower-frequency shifted resonance corresponds to terminal tin atoms as to the other is corresponding to bridging tin atoms, this statement is known in literature.[25,28] The rather broad signals in both the ^{19}F and ^{119}Sn NMR spectra might be the result of exchange between bridging and terminal fluorine atoms. Single crystals suitable for X-ray diffraction study were isolated. These show the same molecular structure as **22** and similar structure, as the crude mixture in solution (See Supporting Information, Chapter 2, Figures S200, S201). An ESI-MS spectrum (negative mode) of a crystal sample reveals a low intensity mass cluster centered at m/z 979.2, fitting perfectly to the monomer anionic specie $[MeSi(CH_2SnFPh_2)_3 \cdot F]^-$ (See Supporting Information, Chapter 2, Figures S202, S203).

Finally, we can conclude, that the fluoridostannate **22** does not behave analogously in solution and solid state, giving that two different species are present in solution. No one is referring to the molecular structure found in solid state. However, the dianionic dimeric form proposed by the molecular structure of **22** seems to be the most stable one. Even upon addition of two respectively three molar equiv of F^-, crystals of **22** are isolated. There

is always a formation of 1:1 anionic adduct in the solid state. Poor solubility precluded detailed NMR spectroscopic studies at variable temperature.

2.2.4 Complexation behaviour of 5 towards acetate anions

A ^{119}Sn NMR spectrum of the iodido-substituted triorganotin compound **5** in C_6D_6 to which three molar equiv of $AgO(O)CCH_3$ had been added shows six broad signals at δ –218, -204, -171, -167, -91, and -44 ppm, respectively (See Supporting Information, Chapter 2, Figure S158). This indicates a fast exchange process. The acetate triorganostannate complex **17** $\{MeSi[CH_2Sn(OCOCH_3)Ph_2]_3\}_2$ was isolated from the corresponding solution in diethyl ether/CH_2Cl_2 as single-crystalline material suitable for X-ray diffraction analysis (Scheme 13, Figure 29).

Scheme 13. Reaction of **5** with three molar equiv $AgO(O)CCH_3$.

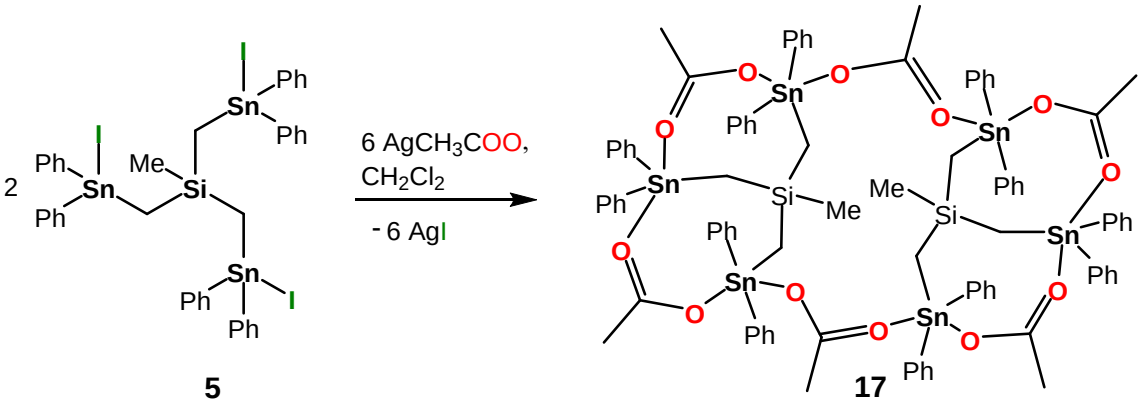

A ^{119}Sn NMR spectrum of **17** in $CDCl_3$ (Figure 30) shows three single resonances at δ –91(2 *Sn1'*), –90 (2 *Sn1*), these two resonances are too broad to enable observation of $^4J(^{119}Sn-^{117}Sn)$ and –40 ppm ($^4J(^{119}Sn_2-^{117/119}Sn_1/Sn_1') = 220$ Hz, 2 *Sn2*), which are low respectively high frequency-shifted as compared to the parent compound **5** (δ –67 ppm). Most likely, the signal at –40 ppm corresponds to the two Sn2 atoms while the signals at δ –91 and –90 ppm belong to the Sn1 and Sn1' atoms (Figure 31). These NMR shifts are high frequency-shifted in comparison to the corresponding resonances in $HC[Sn(OAc)Ph_2]_3$ (δ –206 ppm)[12] and $H_2C[Sn_2(OAc)_3]_2$ (δ –540 ppm).[26] An IR spectrum shows an absorption stretch bands corresponding to the C=O group at $\nu_{C=O}$ = 1539 cm^{-1}, and C–O groups at ν_{C-O} = 1428, 1018 cm^{-1} (Figure 32).

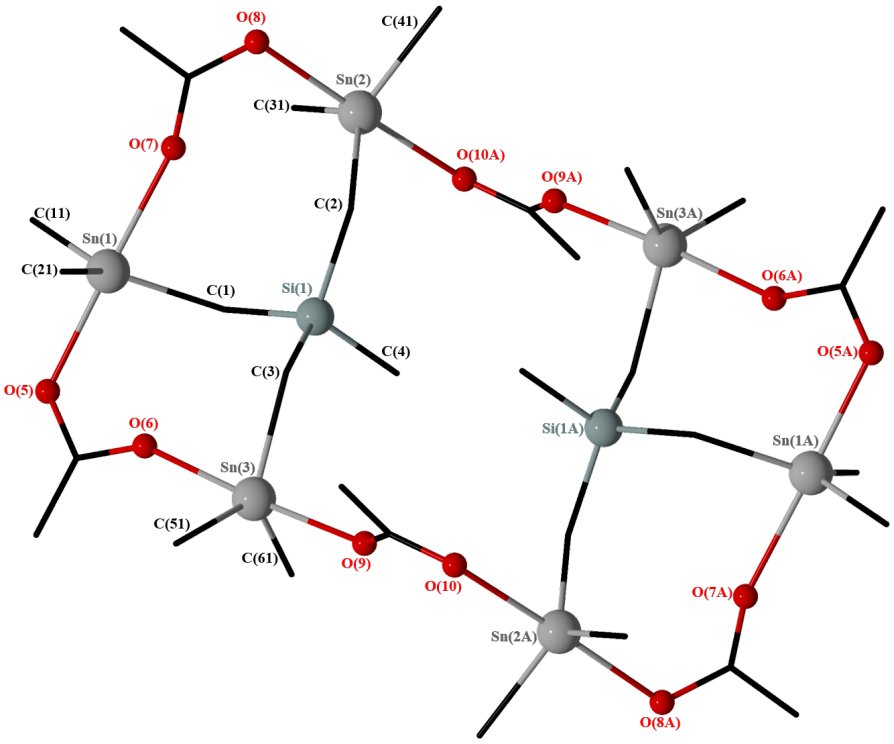

Figure 29. General view (POV-Ray) of a molecule of **17** showing the crystallographic numbering scheme. Hydrogen atoms are omitted for clarity. Carbon atoms are presented in sticks, only C_i of the phenyl groups are shown.

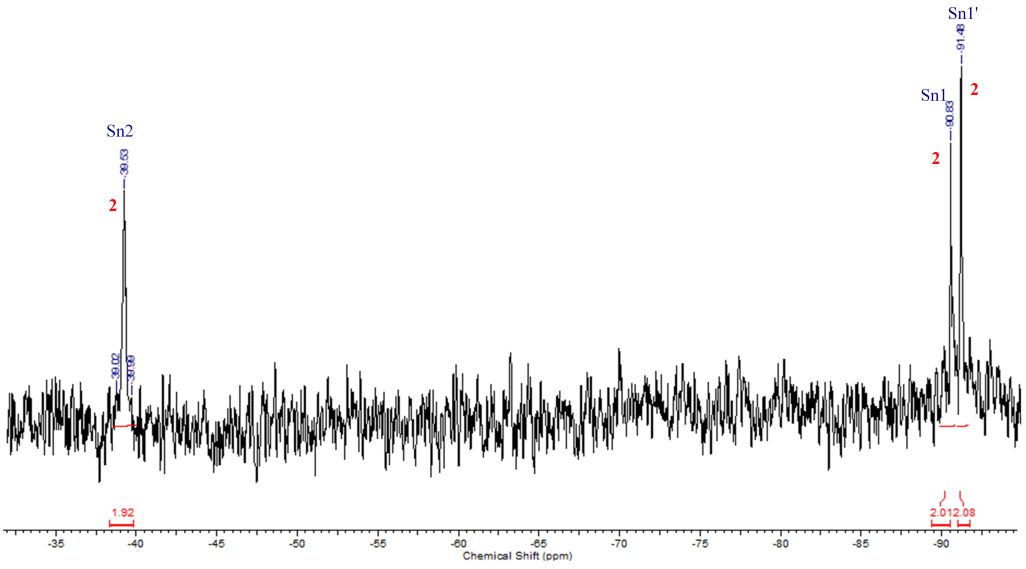

Figure 30. ^{119}Sn NMR spectrum of crystals sample of **17** at room temperature (400.25 MHz, $CDCl_3$).

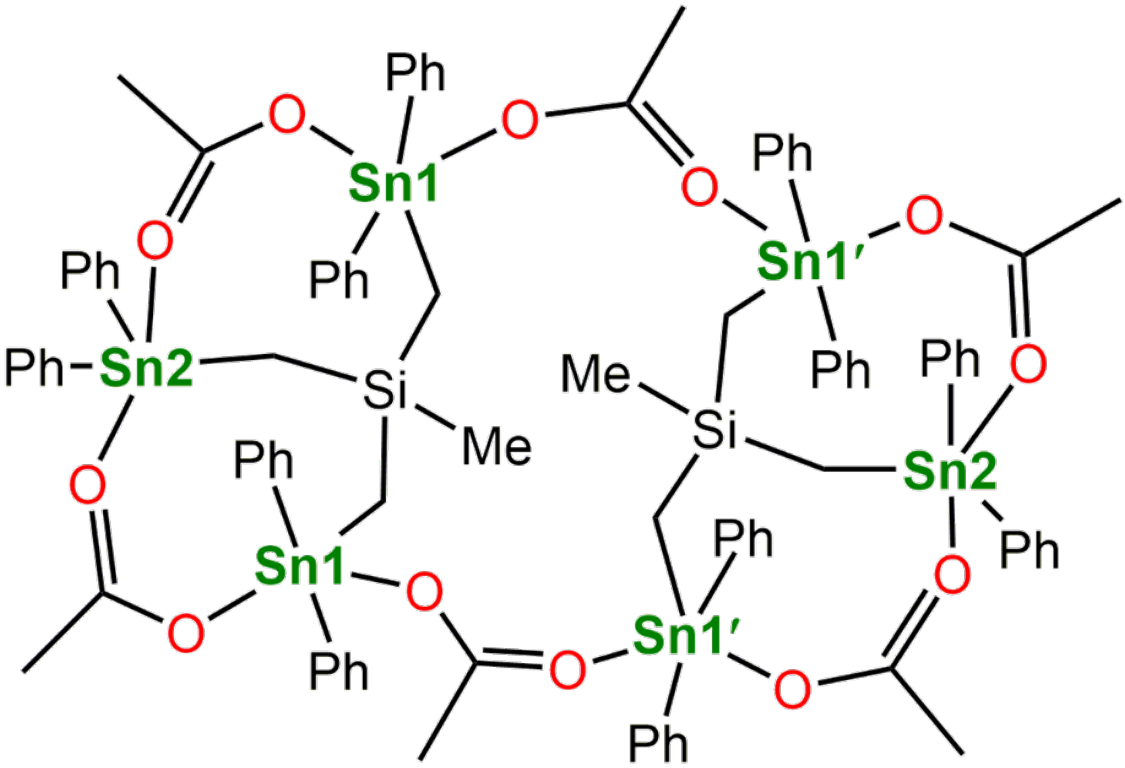

Figure 31. The acetate triorganostannate **17**, presenting the different tin atoms Sn1, Sn1'and Sn2 atoms of the eight- and 16-membred rings in the skeleton.

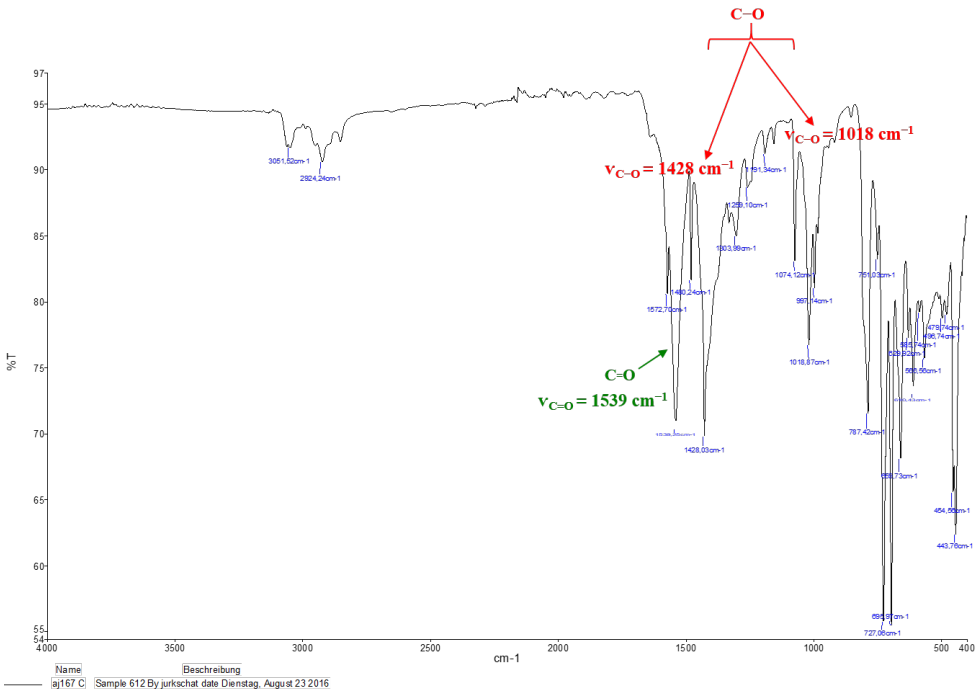

Figure 32. IR spectrum of acetate complex **17**, in which the C=O absorption stretch and the C–O stretching bands.

An ESI-MS mass spectrum of complex **17** in the positive mode shows a mass cluster centred at m/z 1640.4 corresponding to $C_{47}H_{60}Cl_2O_{10}Si_2Sn_6^+$ [M – 2 $COCH_3$ – 7 Ph + H_2O + CH_2Cl_2 + H^+]$^+$ (See Supporting Information Figure S.161, 162). No assignments could be made, referring most likely to one or more hydrolysis products, appear in the ^{119}Sn, ^{1}H, and ^{13}C NMR spectra. Therefore, further investigation in solution were not performed.

The triorganotin acetate **17** crystalizes in triclinic space group *P*–1. This crystalline material shows low solubility in non-polar organic solvents. It is more soluble in polar organic solvents such as acetonitrile, ethanol, ethyl acetat...

The molecular structure is presented in Figure 29, selected interatomic distances and bond angles are listed in Table 5. Compound **17** presents a centrosymmetric head to tail dimer via (Sn–O–C–O–Sn) bridges, composed of four eight-membered rings (Sn–O–C–O–Sn–C–Si–C) and one central sixteen-membered ring (Sn–O–C–O–Sn–C–Si–C–Sn–O–C–O–Sn–C–Si–C), showing a similar molecular structure as the organofluorido stannate **22**.

The two neighbour acetate anions located in the eight-membered rings coordinate the tin atom Sn(1) unsymmetrically at Sn(1)–O(5) and Sn(1)–O(7) distances of 2.212(17) and 2.299(15) Å, respectively. As to acetate moieties adjacent to both eight- and eighteen-membered rings, they coordinate tin atoms in almost perfect isobidentate manner at Sn(2)–O(8), Sn(2)–O(10A), Sn(3)–O(6), and Sn(3)–O(9) distances of 2.276(15), 2.286(14), 2.239(14), and 2.218(15) Å, respectively. These distances are similar to the corresponding distances in the organotin acetate $HC[Sn(OAc)Ph_2]_3$ ranging between 2.235(2) and 2.246(2) Å,[12] and those in the diorganotin carboxylate derivative $[\{Me_2Sn(O_2CMe)\}_2O]_2$, ranging between 2.24(1) and 2.38(2) Å.[36]

Like the organofluorido stannate **22**, the organotin acetate **17** contains as well a central cavity. However, no host molecules were detected after several trials. A calculation of the radii of a simulated guest for **17** is realized via calculation of the average of distances between a simulated centroid of the 208 atoms and the 12 atoms situated in the cavity plan: H(4A) 1.419 Å, H(4A') 1.419 Å, H(2A) 2.695 Å, H(2A') 2.695 Å, H(3B) 2.310 Å, H(3B') 2.310 Å, O(9) 3.492 Å, O(9A) 3.492 Å, Sn(2) 4.925 Å, Sn(2A) 4.925 Å, Sn(3) 3.940 Å, Sn(3A) 3.940 Å; with substraction of the vdW radius of each atom: H (1.06 Å), O (1.42 Å), and Sn (2.16 Å).[5] The average of the distances with $n = 12$ is: $\frac{1}{n}\sum_{i=1}^{n} X_i$. The radius found equal to 1.6435 Å (Figure 33).

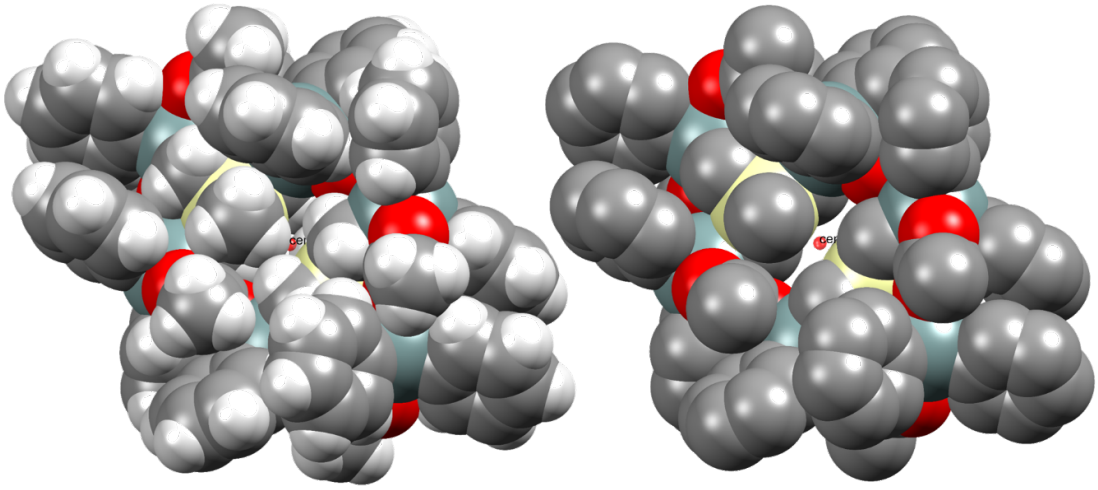

Figure 33. POV Ray images of **17** in space fill mode (left with protons, right: without protons): simulation of a centroid of the 208 atoms of one molecule of **17** as an imaginary guest.

All tin atoms are pentacoordinated, exhibiting distorted trigonal-bipyramidal geometries with geometrical goodnesses $\Delta\Sigma(\theta)$[22] of 87.2° (Sn1), 90.3° (Sn2), and 85.2° (Sn3). The axial positions are occupied by O(5), O(7) (at Sn1), O(8), O(10A) (at Sn2), O(6), O(9) (at Sn3). The equatorial positions are occupied by C(1), C(11), C(21) (at Sn1), C(2), C(31), C(41) (at Sn2), C(3), C(51), C(61) (at Sn3). To conclude, the molecular structure of **17** in the solid state reveals the formation of the organotin acetate $[MeSi\{CH_2SnOC(O)CH_3Ph_2\}_3]_2$. Formally, this can be interpreted as the product of a ring opening dimerization of a hypothetical $MeSi\{CH_2SnOC(O)CH_3Ph_2\}_3$ showing adamantine-type structure. Consequently, we deduce that triorganotin carboxylates attempt to build coordination polymers, in which the carboxylate anions coordinate the tin centres either in unisobidentate or isobidentate manner.[36,37]

Table 5. Selected interatomic distances /Å and angles /°C in compounds **17** and **22**.

	17	**22**
Sn(1)–O(5)	2.212(17)	
Sn(1)–O(7)	2.299(15)	
Sn(2)–O(8)	2.276(15)	
Sn(2)–O(10A)	2.286(14)	
Sn(3)–O(6)	2.239(14)	
Sn(3)–O(9)	2.218(15)	
Sn(1)–F(1)		2.166(4)
Sn(1)–F(4)		2.172(4)
Sn(2)–F(2)		2.032(4)
Sn(2)–F(4)		2.258(4)
Sn(3)–F(1A)		2.226(4)
Sn(3)–F(3)		2.043(4)
O(5)–Sn(1)–O(7)	178.7(5)	
O(5)–Sn(1)–C(1)	94.5(8)	
O(8)–Sn(2)–O(10A)	177.9(6)	
C(31)–Sn(2)–C(2)	124.6(8)	
O(6)–Sn(3)–O(9)	176.5(6)	
O(9)–Sn(3)–C(3)	95.9(8)	
F(1)–Sn(1)–F(4)		178.9(14)
F(1)–Sn(1)–C(21)		90.32(16)
C(11)–Sn(1)–C(21)		120.8(18)
F(2)–Sn(2)–F(4)		177.34(18)
F(2)–Sn(2)–C(2)		94.9(3)
C(2)–Sn(2)–C(31)		114.9(3)
F(3)–Sn(3)–F(1A)		177.69(14)
F(1A)–Sn(3)–C(3)		86.7(2)
C(3)–Sn(3)–C(51)		124.2(2)

2.2.5 Complexation behaviour of 9 towards bromide anions

The ability of the nonabromido-substituted organotinderivative 9 to chelate bromide anions is studied. Thus, a ^{119}Sn NMR spectrum of compound **9** in CD_2Cl_2 at room temperature, to which one molar equiv of tetraphenylphosphonium bromide, $[PPh_4]Br$, had been added shows a broad signal at δ –353 ppm, $W_{1/2}$ = 780 Hz without $^{119/117}$Sn NMR satellites indicating an exchange process that is fast on the NMR scale (See Supporting Information,

Chapter 2, Figure S210). This resonance is very low-frequency shifted in comparison to the parent compound **9** (δ –210 ppm) and proves the formation of a new organobromido stannate complex. The complex $[PPh_4][MeSi(CH_2SnBr_3)_3 \cdot Br]$, **23**, (Scheme 14) was isolated as single-crystalline material from a mixture of diethyl ether/ dichloromethane.

Scheme 14. Reaction of **9** with one molar equiv PPh_4Br.

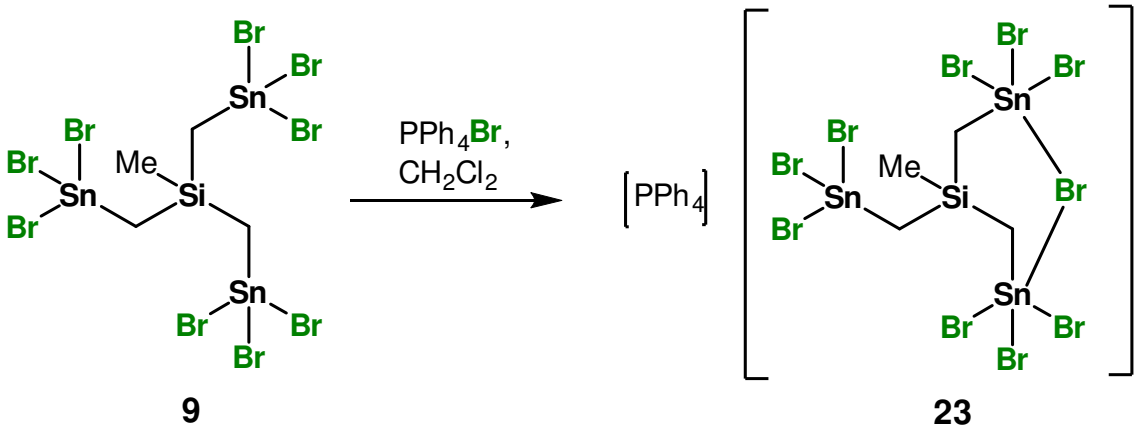

9 **23**

Compound **23** crystallizes as its dichloromethane solvate, **23**$\cdot 0.5\,CH_2Cl_2$, in the monoclinic space group *P*–1. Figure 34 shows its molecular structure. Table 6 contains selected interatomic distances and angles.

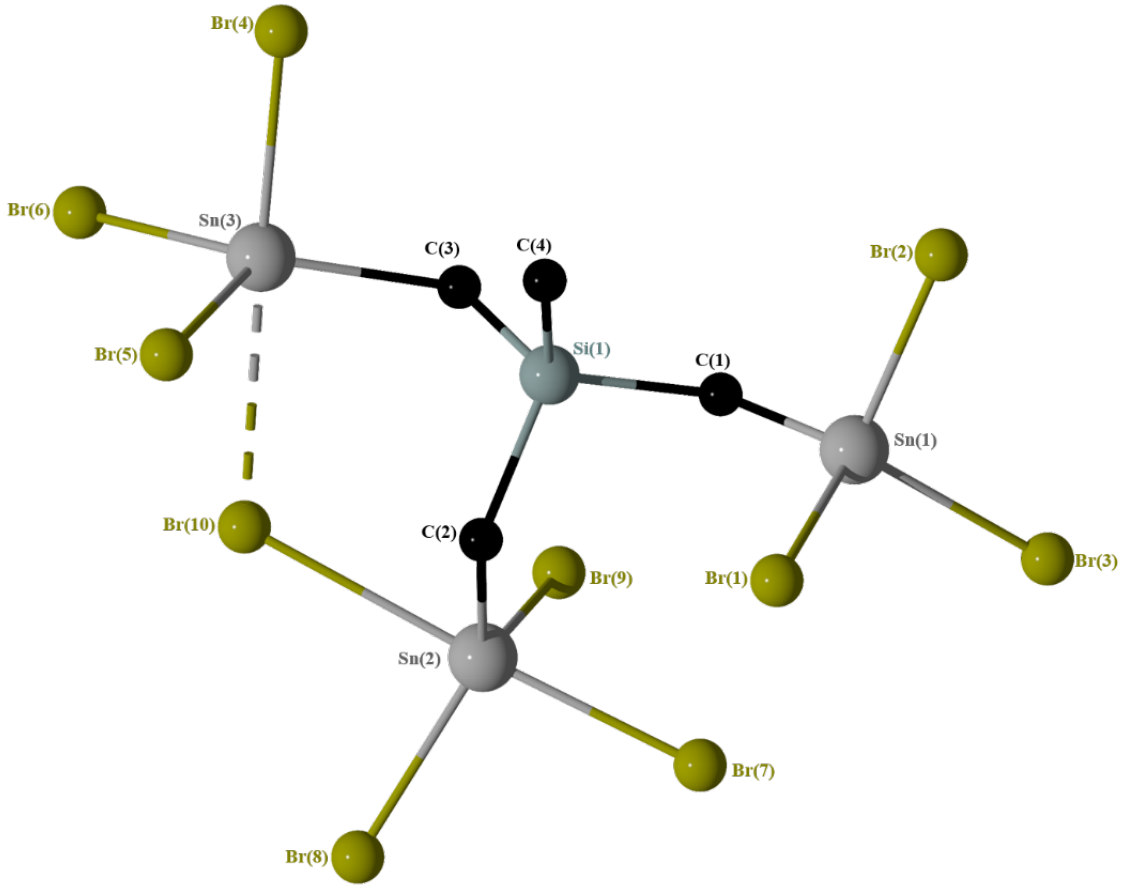

Figure 34. General view (POV-Ray) of a molecule of **23**·0.5 CH_2Cl_2 showing crystallographic numbering scheme. Hydrogen atoms, the PPh_4^+ cation and the CH_2Cl_2 solvate molecule are omitted for clarity.

The molecular structure of **23**·0.5 CH_2Cl_2 shows that Sn(2) and Sn(3)chelate the bromide anion Br(10) unsymmetrically at Sn(2)–Br(10) and Sn(3)–Br(10) distances of 2.8756(3) and 3.0349(9) Å, respectively, forming a six-membered ring (Si–C–Sn–Br–Sn–C). The Sn(1) centre is [4+1]-coordinated and exhibits a distorted trigonal-bipyramidal environment, with angles varying between 103.44(3)° (Br2–Sn1–Br3) and 118.30(17)° (C1–Sn1–Br1). The Br(7) atom approaches the Sn(1) via the face defined by Br(1), Br(3), C(1) at a Sn(1)–Br(7) distance of 4.0690(10) Å. Sn(1)–Br distances vary between 2.4507(8) Å (Sn1–Br3) and 2.4610(8) Å (Sn1–Br2). As for Sn(2) and Sn(3), Sn-Br distances vary between 2.5335(9) Å (Sn3–Br4) and 2.5713(8) Å (Sn2–Br7).

The Sn(2) and Sn(3) atoms are pentacoordinated, exhibiting distorted trigonal bipyramidal environments, with geometrical goodness $\Delta\Sigma(\theta)$[22] equal to 72.5° with C(2), Br(8), and Br(9) occupying the equatorial positions and Br(7) and Br(10) occupying the axial positions at Sn(2) and a $\Delta\Sigma(\theta)$[22] equal to 64.6° with C(3), Br(5), and Br(6) occupying the equatorial positions and Br(4) and Br(10) occupying the axial positions at Sn(3). These dis-

tortions are explained by Br(7)–Sn(2)–Br(10) and Br(4)–Sn(3)–Br(6) angles, respectively of 178.31(3)° and 177.74(3)°, deviating from the ideal angle of 180°.

We further investigate the behaviour of **23** in solution. A ^{119}Sn NMR spectrum in CD_2Cl_2 at −80 °C shows an unresolved broad signal. This is very common for such compounds given their kinetic lability even at low temperature. The ^{1}H and ^{13}C NMR spectra of the same sample support the formation of the bromidostannate complex **23**. The ^{1}H NMR spectrum shows the $SiCH_3$ single resonance at δ 0.71 ppm, displaced to slightly lower frequency in comparison to that of **9** (δ 0.76 ppm). As to the $SiCH_2Sn$ resonance appears at δ 2.31 ppm, shifting to higher frequency in comparison with the methylene protons of **9** (δ 1.96 ppm). In a ^{13}C NMR spectrum, the resonances corresponding to $SiCH_3$ at δ 1.87 ppm are slightly lower-frequency shifted comparing to **9** (δ 2.21 ppm) and $SiCH_2Sn$ at δ 27.56 ppm displace to higher frequencies in comparison with that of **9** at δ 11.25 ppm (Table 7).

An ESI-MS spectrum of 23 in the positive mode shows one mass cluster centred at m/z 339.3 assigned to the cation $[PPh_4]^+$ and in the negative mode a mass cluster centred at 1242.1 corresponding to $[M - PPh_4^+]^-$: $[MeSi(CH_2SnBr_3)_3{\cdot}Br]^-$ (See Supporting Information, Chapter 2, Figures S207- S214).

We witness the formation of the 1:1 anionic adduct **23** in a bidentate manner, when the nonabromido derivative **9** in which are three halogen substituents on each tin atoms, reacts with one equiv molar of bromide. However, there is formation of the 1:2 anionic adduct **13**, resulting from the reaction of the dihalogenido-substituted compound **4** with one equiv molar of chloride. This difference of the complexation behaviour between **4** and **9** can be explained, that the third tin atom in **9**, not involved in the complexation, is satisfied by interaction with three bromine atoms. This is not the case in compound **4**. As it was already mentioned before, the chelation behaviour is related always to the geometry of each compound and its Lewis-acidity.[3]

A ^{119}Sn NMR spectrum at ambient temperature of a solution of **9** in CD_2Cl_2, to which two molar equiv of NEt_4Br had been added, shows a very broad resonance at δ –424 ppm, $W_{1/2}$ = 34 408 Hz, (see Supporting Information Figure S.219) very low-frequency shifted in comparison to the parent compound **9** (δ –210 ppm). This proves the formation of a novel organobromidostannate complex. A colourless crystalline material is isolated from a diethyl-ether/dichloromethane solution suitable for X-ray diffraction study. Figure 35 shows the molecular structure of the complex **24** $(NEt_4)_2[MeSi(CH_2SnBr_3)_{3\cdot 2}Br]$, confirming the formation of a 1:2 adduct (Scheme 15).

Scheme 15. Reaction of **9** with two molar equiv NEt_4Br.

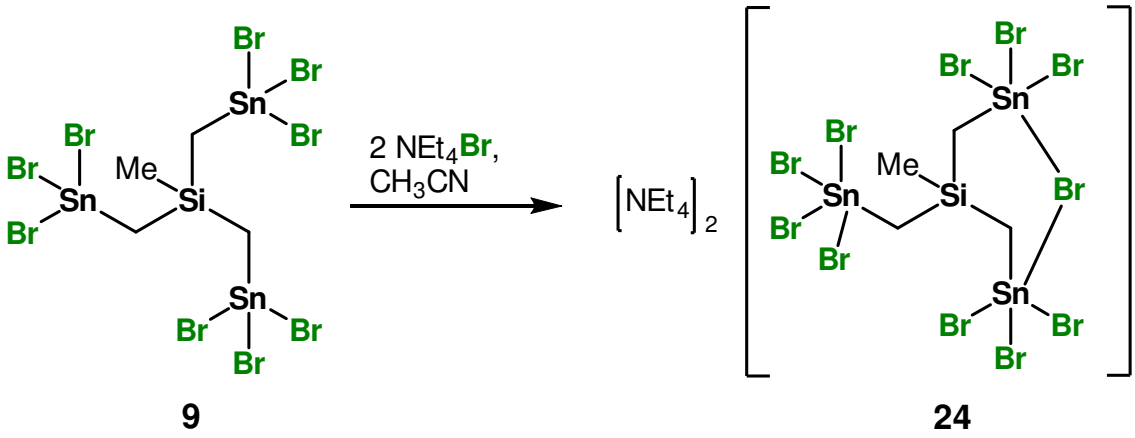

9 **24**

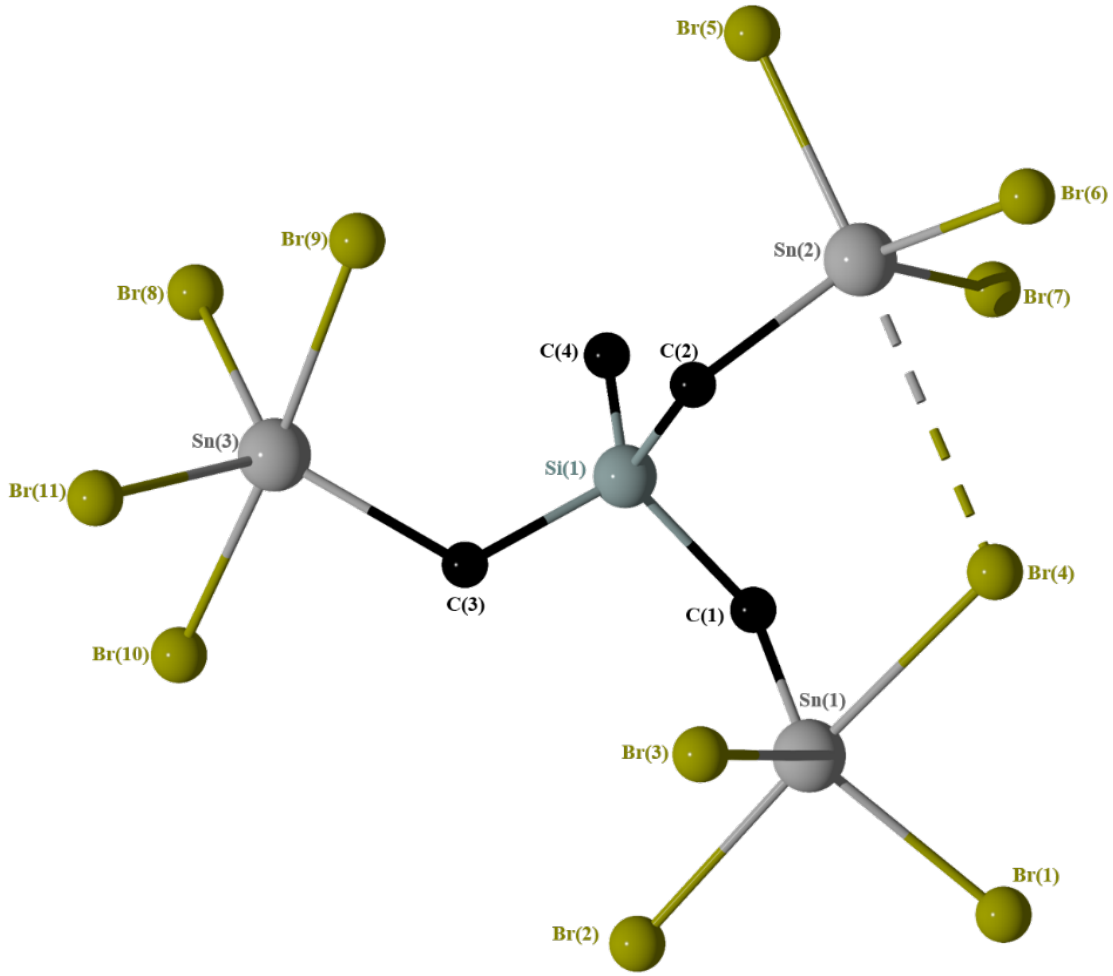

Figure 35. General view (POV-Ray) of a molecule of **24** showing crystallographic numbering scheme. Hydrogen atoms and NEt_4^+ cations are omitted for clarity.

Complex **24** crystallizes in the orthorhombic space group *P*ba2, from an acetonitrile/ dichloromethane solution. Figure 35 shows its molecular structure and Table 6 contains selected interatomic distances and angles. The Sn(1) and Sn(2) centres are intramolecularly non-symmetrically bridged via Br(4), at Sn1–Br4 and Sn2–Br4 distances of 2.735(5) and 3.439(3) Å, respectively. There is a formation of a six membered cycle (Si–C–Sn-Br–Sn–C) via this Sn–Br–Sn bridge. The third tin centre Sn(3) chelates the second bromide anion. Sn(3)–Br distances vary between 2.485(2) Å (Sn3–Br11) and 2.660 Å (Sn3–Br9). All tin atoms are pentacoordinated and exhibit distorted-trigonal bipyramidal environments with geometrical goodness[22] $\Delta\Sigma(\theta)$ = 83.3° (Sn1), 44.6° (Sn2), and 88.8° (Sn3). The equatorial positions are occupied by C(1), Br(1), Br(3) at Sn(1), C(2), Br(6), Br(7) at Sn(2), and C(3), Br(8), Br(11) at Sn(3). The axial positions are occupied by Br(2), Br(4) at Sn(1), Br(4), Br(5) at Sn(2), and Br(9), Br(10) at Sn(3).

The 1:2 anionic adduct **24** exhibits an approachable complexation behaviour as the organochlorido stannate **13**. However, this latter resulted from the reaction of **4** with only one molar equiv of chloride anion. This is due maybe to the high Lewis acidity of the nonabromido derivative **9**, and that all tin atoms are satisfied with four coordinated bromine atoms. This has a significant connection with the complexation behaviour of complex **14**, in which the hexachlorido derivative **4** reacts with only two molar equiv of chloride anions, though every tin atom chelate one additional third chloride anion.

Table 6. Selected interatomic distances /Å and angles /°C in compounds **23**·0.5CH_2Cl_2 and **24**.

	23	**24**
Sn(1)–Br(2)	2.4610(8)	2.622(3)
Sn(1)–Br(3)	2.4507(8)	2.486(2)
Sn(1)–Br(7)	4.0690(10)	
Sn(2)–Br(10)	2.8756(8)	
Sn(3)–Br(10)	3.0349(9)	
Sn(1)–Br(4)		2.735(5)
Sn(2)–Br(4)		3.439(3)
Sn(3)–Br(9)		2.660(2)
Sn(3)–Br(11)		2.485(2)
Br(2)–Sn(1)–Br(3)	103.44(3)	
Br(1)–Sn(1)–C(1)	118.30(17)	
Br(7)–Sn(2)–Br(10)	177.74(3)	
Br(7)–Sn(2)–C(2)	94.96(17)	
C(2)–Sn(2)–Br(9)	121.33(17)	
Br(4)–Sn(3)–Br(10)	178.31(3)	
C(3)–Sn(3)–Br(4)	97.77(16)	
C(3)–Sn(3)–Br(5)	128.77(16)	
Br(5)–Sn(3)–Br(6)	106.52(3)	
Br(2)–Sn(1)–Br(4)		176.19(10)
Br(2)–Sn(1)–C(1)		95.3(5)
C(1)–Sn(1)–Br(3)		121.2(4)
Br(4)–Sn(2)–Br(5)		175.70(10)
C(2)–Sn(2)–Br(5)		103.0(5)
Br(6)–Sn(2)–Br(7)		105.83(10)
Br(9)–Sn(3)–Br(10)		175.31(8)
C(3)–Sn(3)–Br(10)		92.5(6)
C(3)–Sn(3)–Br(8)		135.0(5)

A ^{119}Sn NMR spectrum at −80 °C shows an unresolved broad signal which cannot be defined which prevents a detailed NMR spectroscopic studies in solution even at low temperature due to fast exchange processes undergoing. As to the ^{1}H and ^{13}C NMR spectra of the same sample support the formation of **24**. The ^{1}H NMR spectrum displays a single resonance for the $SiCH_3$ protons at δ 0.81 ppm and for the $SiCH_2Sn$ resonance at

δ 2.39 ppm. These are shifted to higher frequencies in comparison with the corresponding resonances in **9** (δ 0.76, 1.96 ppm). The resonances referring to the CH_2 protons (δ 3.15 ppm, 16H) and the CH_3 protons (δ 1.21 ppm, 24H) indicate the presence of two NEt_4^+ cations. In a ^{13}C NMR spectrum, the resonances corresponding to $SiCH_3$ at δ –3.41 ppm and $SiCH_2Sn$ at δ 15.22 ppm shifting to lower frequencies in comparison with the corresponding resonances of **9**, respectively, at δ 2.21 and 18.94 ppm. As to the resonances referring to the NEt_4^+ cations, the CH_3 carbon signal appears at δ 7.83 ppm and the CH_2 carbon signal at δ 53.19 ppm (Table 7).

An ESI-MS spectrum of 24 in the positive mode shows one mass cluster centred at m/z 130.3 assigned to the cation $[NEt_4]^+$ and in the negative mode a mass cluster centred at 1240.1 and 1534.2 corresponding, respectively, to $[M - Br^- - 2NEt_4^+]^-$: $[MeSi(CH_2SnBr_3)_3 \cdot Br]^-$ and $[M - NEt_4^+ + 2CH_3CN]^-$: $\{[MeSi(CH_2SnBr_3)_3 \cdot 2Br]^{2-}\} \cdot NEt_4^+ + 2CH_3CN$ (See Supporting Information, Chapter 2, Figures S216- S225).

In fact, upon the addition of a third molar equiv of $[PPh_4]Br$ in CD_2Cl_2, a ^{119}Sn NMR spectrum shows a very broad single resonance at δ –511 ppm, $W_{1/2}$ = 2438 Hz (See Supporting Information, Chapter 2, Figure S220). It is shifted to lower frequency comparing to that of the nonabromido derivative **9** (δ –210 ppm), and the two organobromidostannates complexes **23** (δ –353 ppm) and **24** (δ –424 ppm). This finding can be considered, with caution, as prove for the formation of a new complex in solution. However, no crystalline material was isolated from this reaction mixture. Therefore, there is no confirmation that each tin atom is satisfied via interactions with a maximum of four bromide atoms. No further investigation in solution is realized giving the difficulties of ^{119}Sn NMR measurements of such kinetically label compounds even at low temperatures.

Table 7. Selected NMR data measured in CD_2Cl_2 and CD_3CN solutions of the bromide complexes.

	δ $^{13}C(CH_2)$	δ $^{1}H(CH_2)$	δ ^{119}Sn(RT)	δ ^{119}Sn(–80 °C)
23	27.04	2.31	–353	–
24	15.22 (CD_3CN)	2.39 (CD_3CN)	–424	–

2.3 Conclusion

The novel spacer-bridged tritin compounds $MeSi\{CH_2SnXnR_{(3-n)}\}_3$ (X = Cl, Br, F; n = 1– 3) exhibits a chelation ability towards both neutral and charged Lewis bases, in a

bidentate rather than a tridentate manner. This finding come to defend the affirmation saying that spacer-bridged tri- and tetranuclear organotin compounds attempt to chelate Lewis bases in a bidentate manner, not as expected in a tridentate or tetradentate one.[3] In fact, the tin atoms, not involved in the complexation process are satisfied due to additional intramolecular interactions giving the specificity of each compound's geometry or a luck of Lewis-acidity. Secondly, we underline the characteristic of these tripod organtin derivatives to build organostannate complexes having cavities in their skeletons. This refers to the possibility of such compounds for hosting guest molecules. This theme will be more interpreted in the coming chapters. However, in a similar context, the next chapter will focuss on the study of the chelation ability of a novel tetranuclear organotin compound $R'Sn(CH_2SnR_{(3-n)}X_n)_3$, (n = 0 - 2; X = I, Cl; R = Ph, R'= R, X) towards Lewis bases taking as example chloride anions.

2.4 Experimental Section

- **Synthesis of tris(chloromethyl)methylsilane $MeSi(CH_2Cl)_3$ (1)**[24]

A 2.5 M solution of *n*-butyllithium in hexane (40.14 mL, 100.35 mmol,) was added dropwise at −70 °C within a period of 5 h to a magnetically stirred mixture consisting of trichloromethylsilane (5.00 g, 33.45 mmol), and bromochloromethane (19.47 g, 150.52 mmol) in THF (200 mL). The *n*-butyllithium solution was added via a special horizontally elongated side neck of the three-necked flask, which itself was immersed in the cooling bath to ensure precooling of the *n*-butyllithium solution before making contact with the reaction mixture. After completion of the addition, the mixture was stirred at −78 °C for another 5 h and then, the reaction mixture was warmed to room temperature overnight. The solvent was removed under reduced pressure. The residue thus obtained was extracted with diethyl ether (400 mL) and washed with distilled water (3 × 100 mL) in order to remove the remaining salts. The organic phase was dried over $MgSO_4$ and filtrated. The solvent of the filtrate and excess of $BrCH_2Cl$ were removed under reduced pressure. The residue was purified by distillation (65 °C, 12 mbar) to give **1** as a colourless liquid (4.61 g, 24.09 mmol, 72 % yield).[24] ^{1}H NMR (C_6D_6, 400.25, 298 K): δ 0.06 ppm (s, 3 H, $SiCH_3$), 2.60 ppm (s, 6 H, $SiCH_2Cl$), ^{13}C NMR (C_6D_6, 100.64, 298 K): δ –8.53 ppm ($SiCH_3$), 25.60 ppm ($SiCH_2Cl$). ^{29}Si NMR (C_6D_6, 79.52, 298 K): δ 1.6 ppm ($SiCH_3$).

- **Synthesis of tris(triphenylstannylmethyl)methylsilane $MeSi(CH_2SnPh_3)_3$ (2)**

To a solution of $SnPh_3Cl$ (10 g, 25.94 mmol,) in THF (250 mL) were added metallic sodium (1.43 g, 62.26 mmol) and a catalytic amount of naphthalene. The mixture was stirred at room temperature for 3 days, during which its colour changed to deep black. Further activation to accelerate the process was realized by sonification with ultrasound

(45 min). After the solution had been separated from non-reacted sodium, 1 (1.65 g, 8.62 mmol,) was added dropwise at −70 °C under magnetic stirring. Overnight, the reaction mixture was warmed to room temperature and the solvent was evaporated in vacuo. The residue obtained was extracted with 300 mL diethyl ether followed by washing with 150 mL distilled water in order to remove the sodium chloride. The organic phase was dried over anhydrous $MgSO_4$ and filtrated. The solvent was removed from the filtrate under reduced pressure, giving **2** as amorphous white solid (9.59 g, 8.54 mmol, 98 % yield). Further purification was achieved by recrystallization from hot *iso*-hexane to give transparent needles with a mp of 132 °C.

^{1}H NMR ($CDCl_3$, 400.25, 298 K): δ –0.19 ppm (s, 3H, SiCH_3), 0.33 ppm (s, 6H, $^2J(^1H-^{117/119}Sn)$ = 78 Hz, SiCH_2Sn), 7.30-7.44 ppm (complex pattern, 45H, Ph). $^{13}C\{^1H\}$ NMR ($CDCl_3$, 150.94, 298 K): δ –1.7 ppm ($^3J(^{13}C-^{117/119}Sn)$ = 20 Hz, $^1J(^{13}C-^{29}Si)$ = 48 Hz, $^1J(^{13}C-^{117/119}Sn)$ = 262/274 Hz, SiCH_2Sn), 3.9 ppm ($^3J(^{13}C-^{117/119}Sn)$ = 12 Hz, $^1J(^{13}C-^{29}Si)$ = 51 Hz, SiCH_3), 128.4 ppm ($^3J(^{13}C-^{117/119}Sn)$ = 49 Hz, C_m), 128.7 ppm ($^4J(^{13}C-^{117/119}Sn)$ = 10 Hz, C_p), 136.9 ppm ($^2J(^{13}C-^{117/119}Sn)$ = 37 Hz, C_o), 139.6 ppm ($^1J(^{13}C-^{117/119}Sn)$ = 460/492 Hz, C_i). ^{29}Si NMR ($CDCl_3$, 79.52, 298 K): δ 8.7 ppm ($^2J(^{29}Si-^{117/119}Sn)$ = 21 Hz, *Si*CH_2Sn). ^{119}Sn NMR ($CDCl_3$, 149.26, 298 K): δ –89 ppm (*Sn*Ph_3). Anal. Calcd (%) for $C_{58}H_{54}SiSn_3$: C 61.36, H 4.79. Found: C 61.3, H 4.8. Electrospray MS: m/z (%) positive mode 119.1 (100, Sn+), 383.0097 $C_{18}H_{15}SnO_2^+$ (50, [M – $C_{40}H_{43}SiSn_2$ + 2 H_2O]).

- **Synthesis of tris(diiodidophenylstannylmethyl)methylsilane $MeSi(CH_2SnPhI_2)_3$ (3)**

Over a period of 10h, elemental iodine (8.39 g, 33.06 mmol, 6 equiv) was added in small portions at 0 °C to a stirred solution of **2** (6.36 g, 5.60 mmol, 1 equiv). The stirring was continued and the reaction mixture was warmed to room temperature overnight. Dichloromethane and iodobenzene were removed in vacuo (10^{-3} mmHg) to afford **3** as a yellow oil in 99 % yield (7.95 g, 5.54 mmol).

^{1}H NMR ($CDCl_3$, 400.25, 298 K): δ 0.53 ppm (s, 3H, SiCH_3), 1.71 ppm (s, 6H, $^2J(^1H-^{117/119}Sn)$ = 84 Hz, SiCH_2Sn), 7.43-7.73 ppm (complex pattern, 15H, Ph). $^{13}C\{^1H\}$ NMR ($CDCl_3$, 150.94, 298 K): δ 3.23 ppm ($^3J(^{13}C-^{117/119}Sn)$ = 20 Hz, $^1J(^{13}C-^{29}Si)$ = 40 Hz, SiCH_3), 11.9 ppm ($^3J(^{13}C-^{117/119}Sn)$ = 20 Hz, $^1J(^{13}C-^{29}Si)$ = 50 Hz, $^1J(^{13}C-^{117/119}Sn)$ = 259/272 Hz, SiCH_2Sn), 129.2 ppm ($^3J(^{13}C-^{117/119}Sn)$ = 78 Hz, C_m), 131.1 ppm ($^4J(^{13}C-^{117/119}Sn)$ = 16 Hz, C_p), 134.1 ppm ($^2J(^{13}C-^{117/119}Sn)$ = 59 Hz, C_o), 136.5 ppm ($^1J(^{13}C-^{117/119}Sn)$ = 580/601 Hz, C_i). ^{29}Si NMR ($CDCl_3$, 119.26, 298 K): δ 8.8 ppm ($^2J(^{29}Si-^{117/119}Sn)$ = 36 Hz, *Si*CH_2Sn). ^{119}Sn NMR (C_6D_6, 149.26, 298 K): δ –228 ppm (*Sn*I_2Ph). Anal. Calcd (%) for $C_{22}H_{24}I_6SiSn_3$: C 18.43, H 1.69. Found: C 18.8, H 1.9. Electrospray MS: m/z (%) positive mode 392.1 $I_2SnH_3O^+$ (30, [M –

$C_{22}H_{24}I_4SiSn_2 + H^+ + H_2O]^+$), 721.0 $C_{16}H_{19}ISiSn_3^+$ (15, $[M - C_6H_5I_5]^+$), m/z (%) negative mode 127.3 I^- (8, $[M - C_{22}H_{24}I_5SiSn_3]^-$), 381.0 I_3^- (100, $[M - C_{22}H_{24}I_3SiSn_3]^-$), 1450.3017 ($C_{22}H_{25}I_6OSiSn_3 * 1.00\,[M + OH-]^- + C_{22}H_{24}I_6ClSiSn_3 * 0.10\,[M + Cl-]^-$), 1560.1988 $C_{22}H_{24}I_7OSiSn_3^-$ ($[M + I]^-$).

- **Synthesis of tris(dichloridophenylstannylmethyl)methylsilane $MeSi(CH_2SnPhCl_2)_3$ (4)**

To a solution of **3** (1.17g, 0.813 mmol) in CH_2Cl_2 (150 mL) was added excess of silver chloride (1.05g, 7.32 mmol). The resulting mixture was stirred at room temperature in the dark for 14 days. The formed AgI and the non-reacted AgCl was removed by filtration. The CH_2Cl_2 of the filtrate was evaporated in vacuo (10^{-3} mmHg) to afford an oily transparent substance in 98 % yield (0.707 g, 789 µmol).

^{1}H NMR (C_6D_6, 400.25, 298 K): δ 0.65 ppm (s, 3H, $SiCH_3$), 1.18 ppm (s, 6H, $^2J(^1H-^{117/119}Sn)$ = 84 Hz, $SiCH_2Sn$), 7.07-7.50 ppm (complex pattern, 15H, Ph). $^{13}C\{^1H\}$ NMR (C_6D_6, 100.64, 298 K): δ 3.5 ppm ($^3J(^{13}C-^{117/119}Sn)$ = 22 Hz, $^1J(^{13}C-^{29}Si)$ = 40 Hz, $SiCH_3$), 11.2 ppm ($^3J(^{13}C-^{117/119}Sn)$ = 25 Hz, $^1J(^{13}C-^{29}Si)$ = 47 Hz, $^1J(^{13}C-^{117/119}Sn)$ = 361/376, $SiCH_2Sn$), 130.1 ppm ($^3J(^{13}C-^{117/119}Sn)$ = 87 Hz, C_m), 132.1 ppm ($^4J(^{13}C-^{117/119}Sn)$ = 16 Hz, C_p), 134.9 ppm ($^2J(^{13}C-^{117/119}Sn)$ = 66 Hz, C_o), 139.7 ppm ($^1J(^{13}C-^{117/119}Sn)$ = 742/773 Hz, C_i). ^{29}Si NMR (C_6D_6, 79.52, 298 K): δ 7.4 ppm ($^2J(^{29}Si-^{117/119}Sn)$ = 49 Hz, $SiCH_2Sn$). ^{119}Sn NMR (C6D6, 149.26, 298 K): δ 41 ppm ($SnPhCl_2$). Anal. Calcd (%) for $C_{22}H_{24}Cl_6SiSn_3$: C 29.85, H 2.73. Found: C 29.5, H 2.9. Electrospray MS: m/z (%) positive mode 738.7 $C_{16}H_{21}Cl_4SiSn_3^+$ (25, M – Ph – 2 Cl^- + H^+]$^+$), 766.8694 $C_{21}H_{24}Cl_3SiSn_3^+$ (100, [M – Me – 3 Cl^- + H^+]$^+$), 776.8050 $C_{16}H_{22}Cl_5SiSn_3^+$.

- **Synthesis of tris(iodidodiphenylstannylmethyl)methylsilane $MeSi(CH_2SnPh_2I)_3$ (5)**

Over a period of 3 h, elemental iodine (0.341 g, 1.34 mmol, 2.88 equiv) was added in small portions at 0 °C to a stirred solution of **2** (0.529 g, 465.97 µmol, 1 equiv) in dichloromethane. The stirring was continued and the reaction mixture was warmed to room temperature overnight. Dichloromethane and iodobenzene were removed in vacuo (10^{-3} mmHg) to afford a slightly yellow oil in 95 % yield (0.502 g, 391.18 µmol). Further purification was realized by repeatedly wash with *iso*-hexane.

^{1}H NMR ($CDCl_3$, 400.25, 298 K): δ 0.15 ppm (s, 3H, $SiCH_3$), 0.99 ppm (s, 6H, $^2J(^1H-^{117/119}Sn)$ = 80 Hz, $SiCH_2Sn$), 7.35-7.67 ppm (complex pattern, 15H, Ph). $^{13}C\{^1H\}$ NMR ($CDCl_3$, 150.94, 298 K): δ 3.76 ppm ($^3J(^{13}C-^{117/119}Sn)$ = 15 Hz, $SiCH_3$), 4.14 ppm ($^3J(^{13}C-^{117/119}Sn)$ = 23 Hz, $^1J(^{13}C-^{29}Si)$ = 48 Hz, $^1J(^{13}C-^{117/119}Sn)$ = 253, 264 Hz, $SiCH_2Sn$), 128.8 ppm ($^3J(^{13}C-^{117/119}Sn)$ = 60 Hz, C_m), 129.9 ppm ($^4J(^{13}C-^{117/119}Sn)$ =

14 Hz, C_p), 135.8 ppm ($^2J(^{13}C-^{117/119}Sn)$ = 50 Hz, C_o), 137.6 ppm ($^1J(^{13}C-^{117/119}Sn)$ = 520/544 Hz, C_i). ^{29}Si NMR ($CDCl_3$, 119.26, 298 K): δ 8.97 ppm ($^2J(^{29}Si-^{117/119}Sn)$ = 28 Hz, *Si*CH2Sn). ^{119}Sn NMR ($CDCl_3$, 223.85, 298 K): δ –67 ppm (*Sn*IPh_2). Anal. Calcd (%) for $C_{40}H_{33}I_3SiSn_3$: C 37.4, H 3.06. Found: C 38.3, H 3.4. Electrospray MS: m/z (%) positive mode 919.2 $C_{39}H_{44}NaSiSn_3^+$ (100, $[M - Me - 3I^- + 4H^+ + Na^+]^+$), 969.2 $C_{12}H_{23}I_3O_2SiSn_3^+$ (100, $[M - 5Ph^- + 6H^+ + Na^+ + 2MeOH]^+$), m/z (%) negative mode 127.3 I^- (100, $[M - C_{40}H_{33}I_2SiSn_3^+]^-$).

- **Synthesis of tris(chloridodiphenylstannylmethyl)methylsilane $MeSi(CH_2SnPh_2Cl)_3$ (6)**

To a solution of **5** (4.93 g, 3.84 mmol) in CH_2Cl_2 (150 mL) was added excess of silver chloride (2.48 g, 17.28 mmol). The resulting mixture was stirred at room temperature in the dark for 14 days. The fored AgI and the non-reacted AgCl was removed by filtration. The CH_2Cl_2 of the filtrate was evaporated in vacuo (10^{-3} mmHg) to afford amorphous white solid (3.80 g, 3.76 mmol, 97 % yield). Further purification was achieved by recrystallization from CH_2Cl_2/diethyl ether to give transparent needles.

^1H NMR ($CDCl_3$, 600.29, 298 K): δ 0.35 ppm (s, 3H, SiCH_3), 0.96 ppm (s, 6H, $^2J(^1H-^{117/119}Sn)$ = 79 Hz, SiCH_2Sn), 7.45-7.78 ppm (complex pattern, 30H, Ph). $^{13}C\{^1H\}$ NMR ($CDCl_3$, 150.94, 298 K): δ 3.6 ppm ($^3J(^{13}C-^{117/119}Sn)$ = 15 Hz, $^1J(^{13}C-^{29}Si)$ = 40 Hz, Si*C*H_3), 4.13 ppm ($^3J(^{13}C-^{117/119}Sn)$ = 21 Hz, $^1J(^{13}C-^{29}Si)$ = 48 Hz, $^1J(^{13}C-^{117/119}Sn)$ = 285/296, Si*C*H_2Sn), 128.94 ppm ($^3J(^{13}C-^{117/119}Sn)$ = 63 Hz, C_m), 130.14 ppm ($^4J(^{13}C-^{117/119}Sn)$ = 12 Hz, C_p), 135.51 ppm ($^2J(^{13}C-^{117/119}Sn)$ = 60 Hz, C_o), 139.21 ppm ($^1J(^{13}C-^{117/119}Sn)$ = 564/589 Hz, C_i). ^{29}Si NMR ($CDCl_3$, 79.52, 298 K): δ 8.61 ppm ($^2J(^{29}Si-^{117/119}Sn)$ = 30 Hz, *Si*CH_2Sn). ^{119}Sn NMR (C_6D_6, 149.26, 298 K): δ 24 ppm (*Sn*Ph_2Cl). Anal. Calcd (%) for $C_{40}H_{39}Cl_3SiSn_3$: C 47.55, H 3.89. Found: C 47.2, H 3.9. Electrospray MS: m/z (%) positive mode 957.2 $C_{33}H_{38}NaSiSn_3^+$ (100, $[M - Me - Ph + H_2O + H^+]^+$), m/z (%) negative mode 1044.8610 $[C_{40}H_{39}Cl_4SiSn_3]^-$ (100, $[M + Cl-]^-$), 1136.7966 $[C_{40}H_{39}Cl_3ISiSn_3]^-$ (100, $[M + I-]^-$).

- **Synthesis of tris(fluoridodiphenylstannylmethyl)methylsilane $MeSi(CH_2SnPh_2F)_3$ (7)**

A solution of **3** (376 mg, 0.292 mmol) in CH_2Cl_2 (25 mL) was mixed with excess of KF (153mg, 2.63 mmol) in water (20 mL). The biphasic mixture was stirred at room temperature for 3 days. The organic phase was then separated, dried over $MgSO_4$, and filtered. Removing the solvent in vacuo afforded a white solid (270 mg, 0.28 mmol, 95 % yield). Further purification was achieved by several wash with water, methanol, acetone... to give an amorphous white solid. Anal. Calcd (%) for $C_{40}H_{39}F_3SiSn_3$: C 50, H 4.09. Found: C 47.6, H 4.1 calculated for ($C_{40}H_{39}F_3SiSn_3^+ H_2O$ + HF). Electrospray MS: m/z (%) nega-

tive mode 255.2263 $SnH_2F_7^-$ [80, $(SnF_{62}^- + HF^+H^+)]^-$ and 978.9520 $C_{40}H_{39}F_4SiSn_3^-$ [40, $(M + F-)]^-$.

- **Synthesis of tris(dibromidodiphenylstannylmethyl)methylsilane $MeSi(CH_2SnPhBr_2)_3$ (8)**

To a cooled solution (−55 °C) of **2** (479 mg, 0.421 mmol) in CH_2Cl_2 (30 mL) was added dropwise a solution of bromine (403.89 mg, 2.53 mmol) in CH_2Cl_2 (15 mL). After the addition was completed, the mixture was stirred and warmed to room temperature overnight. From the orange-red solution obtained, the solvent and the PhBr formed were removed in vacuo (10^{-3} mmHg) to afford a light-yellow oil (480 mg, 416 mmol, 98 %).

^{1}H NMR ($CDCl_3$, 400.25, 298 K): δ 0.65 ppm (s, 3H, SiCH_3), 1.57 ppm (s, 6H, $^2J(^1H-^{117/119}Sn)$ = 88 Hz, SiCH_2Sn), 7.50-7.75 ppm (complex pattern, 15H, Ph). $^{13}C\{^1H\}$ NMR ($CDCl_3$, 100.64, 298 K): δ 3.26 ppm ($^3J(^{13}C-^{117/119}Sn)$ = 22 Hz, SiCH_3), 11.85 ppm ($^3J(^{13}C-^{117/119}Sn)$ = 29 Hz, $^1J(^{13}C-^{29}Si)$ = 47 Hz, $^1J(^{13}C-^{117/119}Sn)$ = 318/333, SiCH_2Sn), 129.53 ppm ($^3J(^{13}C-^{117/119}Sn)$ = 86 Hz, C_m), 131.57 ppm ($^4J(^{13}C-^{117/119}Sn)$ = 20 Hz, C_p), 134.28 ppm ($^2J(^{13}C-^{117/119}Sn)$ = 63 Hz, C_o), 138.87 ppm. ^{29}Si NMR (C6D6, 119.26, 298 K): δ 7.52 ppm ($^2J(^{29}Si-^{117/119}Sn)$ = 44 Hz, *Si*CH_2Sn). ^{119}Sn NMR (C6D6, 223.85, 298 K): δ –16 ppm (*Sn*$PhBr_2$). Anal. Calcd (%) for $C_{22}H_{24}Br_6SiSn_3$: C 22.94, H 2.1. Found: C 23.9, H 2.4 calculated for ($C_{22}H_{24}Br_6SiSn_3 + CH_3CN + H_2O$). Electrospray MS: m/z (%) positive mode 721.0 $C_{12}H_{20}Br_2NSiSn_3^+$ (100, $[M - 4Br^- - 2Ph + CH_3CN + H^+]^+$), m/z (%) negative mode 79.5 (100, $Br-)^-$, 944.7 $C_3H_{13}Br_6O_2SiSn_3^-$ (30, $[M - Me - 3Ph + H_2O + OH-]^-$).

- **Synthesis of tris(tribromidodiphenylstannylmethyl)methylsilane $MeSi(CH_2SnBr_3)_3$ (9)**

To a cooled solution (−55 °C) of **2** (491 mg, 0.432 mmol) in CH_2Cl_2 (30 mL) was added dropwise a solution of bromine (1.01 g, 3.98 mmol) in CH_2Cl_2 (40 mL). After the addition was completed, the mixture was stirred and warmed to room temperature overnight. From the red solution obtained, the solvent and the PhBr formed were removed in vacuo (10^{-3} mmHg) to afford an orange-brown solid (684 mg, 0.432 mmol, 99 %). Further purification was achieved by recrystallization from CH_2Cl_2/diethyl ether to give orange needles.

^{1}H NMR ($CDCl_3$, 400.25, 298 K): δ 0.76 ppm (s, 3H, SiCH_3), 1.96 ppm (s, 6H, $^2J(^1H-^{117/119}Sn)$ = 120/126 Hz, SiCH_2Sn). $^{13}C\{^1H\}$ NMR ($CDCl_3$, 100.64, 298 K): δ 2.21 ppm ($^3J(^{13}C-^{117/119}Sn)$ = 26 Hz, $^1J(^{13}C-^{29}Si)$ = 57 Hz, SiCH_3), 18.94 ppm ($^3J(^{13}C-^{117/119}Sn)$ = 37 Hz, $^1J(^{13}C-^{29}Si)$ = 77 Hz, $^1J(^{13}C-^{117/119}Sn)$ = 414/430, SiCH_2Sn). ^{29}Si NMR ($CDCl_3$, 79.52, 298 K): δ 6.09 ppm ($^2J(^{29}Si-^{117/119}Sn)$ = 45 Hz, *Si*CH_2Sn). ^{119}Sn NMR ($CDCl_3$, 149.26, 298 K): δ –210 ppm (*Sn*Br_3). Anal. Calcd (%) for $C_4H_9Br_9SiSn_3$: C 4.14, H 0.78. Found: C 4.6, H 0.9. Electrospray MS: m/z (%) positive

mode 356.3 $PhSnBr_2H_2^+$ (100, $[PhSnBr_2H + H^+])^+$, 725.5 $C_4H_{11}Br_5NOSn_2^+$ (50, $[M - MeSiC_2H_4SnBr_4 + MeOH + CH_3CN + H^+])^+$, m/z (%) negative mode 358.8 $SnBr_3^-$ (100, $[M - MeC_3H_6SiSn_2Br_6])^-$.

- **Synthesis of tris[diphenyl(trimethylsilylmethyl)stannylmethyl)methylsilane $MeSi[CH_2Sn(CH_2SiMe_3)Ph_2]_3$ (10)**

A solution of $MeSi(CH_2SnPh_2I)_3$, **5** (4.77g, 3.56 mmol, 0.9 equiv) in THF (120 mL) was added dropwise to a solution of Me_3SiCH_2MgCl, prepared from Me_3SiCH_2Cl (1.46 g, 11.87 mmol, 3 equiv) and magnesium (0.307 g, 12.66 mmol, 3.2 equiv) in THF (40 mL), for a period of 1 h. After the addition had been completed, the reaction mixture was heated to reflux overnight and then cooled to room temperature. THF was distilled off under reduced pressure; then cold water (50 mL) was added, and the mixture was extracted three times with 100 mL diethyl ether. The combined organic phases were dried over $MgSO_4$ and the solvents removed under reduced pressure, giving **10** as a slightly yellow oil (4.341 g, 3.73 mmol, 94 %). Further purification was achieved by several wash with *iso*-hexane.

^{1}H NMR ($CDCl_3$, 600.29, 298 K): δ –0.24 ppm (s, 3H, $SiCH_3$), –0.15–0.12 ppm (s, 27H, $Si(CH_3)_3$), 0.04 ppm (s, 6H, CH_2SiMe_3), 0.10 ppm (s, 6H, $^2J(^1H-^{117/119}Sn)$ = 72/74 Hz, $SiCH_2Sn$), 7.30-7.41 ppm (complex pattern, 30H, Ph). $^{13}C\{^1H\}$ NMR ($CDCl_3$, 100.46, 298 K): δ –3.33 ppm ($^1J(^{13}C-^{117/119}Sn)$ = 255/267 Hz, CH_2SiMe_3), -0.06 ppm ($^3J(^{13}C-^{117/119}Sn)$ = 21 Hz, $^1J(^{13}C-^{117/119}Sn)$ = 248/266 Hz, $SiCH_2Sn$), 1.53 ppm ($^3J(^{13}C-^{117/119}Sn)$ = 14 Hz, $^1J(^{13}C-^{29}Si)$ = 51 Hz , Si(CH3)3), 3.85 ppm ($^3J(^{13}C-^{117/119}Sn)$ = 12 Hz, $SiCH_3$), 128.1 ppm (C_m), 128.4 ppm (C_p), 136.7 ppm ($^2J(^{13}C-^{117/119}Sn)$ = 38 Hz, C_o), 141.4 ppm ($^1J(^{13}C-^{117/119}Sn)$ = 452/477 Hz, C_i). ^{29}Si NMR ($CDCl_3$, 79.52, 298 K): δ 7.84 ppm ($^2J(^{29}Si-^{117/119}Sn)$ = 26 Hz, $SiCH_3$), 2.68 ppm ($^1J(^{29}Si-^{13}C)$ = 51 Hz, CH_2SiMe_3). ^{119}Sn NMR ($CDCl_3$, 223.85, 298 K): δ –49 ppm ($SnCH_2SiMe_3Ph_2$). Anal. Calcd (%) for $C_{52}H_{72}Si_4Sn_3$: C 53.58, H 6.23. Found: C 54.2, H 6.2. Electrospray MS: m/z (%) positive mode 1129.3 (10, $C_{43}H_{69}Cl_2O_2Si_3Sn_3^+$).

- **Synthesis of tris[diiodido(trimethylsilylmethyl)stannylmethyl)methylsilane $MeSi[CH_2Sn(CH_2SiMe_3)I_2]_3$ (11)**

Over a period of 3h, elemental iodine (0.769 g, 3.03 mmol, 6 equiv) was added in small portions at 0 °C to a stirred solution of **10** (0.589 g, 505.31 µmol, 1 equiv). The stirring was continued and the reaction mixture was warmed to room temperature overnight. Dichloromethane and iodobenzene were removed in vacuo (10^{-3} mmHg) to afford a yellow solid in 99 % yield (0.732 g, 500.25 µmol).

^{1}H NMR ($CDCl_3$, 400.25, 298 K): δ 0.16-0.23 ppm (s, 27H, $Si(CH_3)_3$), 0.67 ppm (s, 3H, $SiCH_3$), 1.45 ppm (s, 6H, $^2J(^1H-^{117/119}Sn)$ = 88/92 Hz, CH_2SiMe_3), 1.72 ppm (s, 6H, $^2J(^1H-^{117/119}Sn)$ = 74 Hz, $SiCH_2Sn$). $^{13}C\{^1H\}$ NMR ($CDCl_3$, 150.94, 298 K):

δ 0.74-1.74 ppm ($^3J(^{13}C-^{117/119}Sn)$ = 26 Hz, $^1J(^{13}C-^{29}Si)$ = 52 Hz, $Si(CH_3)_3$), 3.13 ppm ($^3J(^{13}C-^{117/119}Sn)$ = 18 Hz, $SiCH_3$), 12.60 ppm ($^1J(^{13}C-^{117/119}Sn)$ = 242/254 Hz, $^1J(^{13}C-^{29}Si)$ = 49 Hz, ($^3J(^{13}C-^{117/119}Sn)$ = 24 Hz, $SiCH_2Sn$), 14.74 ppm ($^1J(^{13}C-^{29}Si)$ = 43 Hz, $^1J(^{13}C-^{117/119}Sn)$ = 251/264 Hz, CH_2SiMe_3). ^{29}Si NMR ($CDCl_3$, 79.52, 298 K): δ 3.81 ppm ($^2J(^{29}Si-^{117/119}Sn)$ = 39 Hz, $^1J(^{29}Si-^{13}C)$ = 53 Hz, CH_2SiMe_3), 9.52 ppm ($^2J(^{29}Si-^{117/119}Sn)$ = 44 Hz, *Si*Me). ^{119}Sn NMR ($CDCl_3$, 149.26, 298 K): δ –190 ppm ($SnCH_2SiMe_3I_2$). Anal. Calcd (%) for $C_{16}H_{42}I_6Si_4Sn_3$: C 13.12, H 2.89. Found: C 13.1, H 2.9. Electrospray MS: m/z (%) positive mode 824.9353 $C_4H_{12}I_3SiSn_3^+$ (100, $[M-(CH_2SiMe_3I)_3+H^+]^+$).

- **Synthesis of tris[dichlorido(trimethylsilylmethyl)stannylmethyl)methylsilane $MeSi[CH_2Sn(CH_2SiMe_3)Cl_2]_3$ (12)**

To a solution of **11** (1.59 g, 13.6 mmol, 1 equiv). in CH_2Cl_2 (150 mL) was added excess of silver chloride (13.64 g, 95.2 mmol, 7 equiv). The resulting mixture was stirred at room temperature in the dark for 14 days. The formed AgI and the non-reacted AgCl was removed by filtration. The CH_2Cl_2 of the filtrate was evaporated in vacuo (10^{-3} mmHg) to afford a white solid in 98 % yield (12.2 g, 13.328 mmol, 1 equiv).

^1H NMR ($CDCl_3$, 400.25, 298 K): δ 0.06-0.40 (s, 27H, $SiMe_3$), 0.59 (s, 3H, SiMe), 0.97 (s, 6H, $^2J(^1H-^{117/119}Sn)$ = 95/100 Hz, CH_2SiMe_3), 1.2 (s, 6H, $^2J(^1H-^{117/119}Sn)$ = 75 Hz, $SiCH_2Sn$). $^{13}C\{^1H\}$ NMR ($CDCl_3$, 100.46, 298 K): δ 1.03 ($^3J(^{13}C-^{117/119}Sn)$ = 33 Hz, $^1J(^{13}C-^{29}Si)$ = 54 Hz, $SiMe_3$), 1.5 ($^3J(^{13}C-^{117/119}Sn)$ = 20 Hz, $SiCH_3$), 2.98 ($^3J(^{13}C-^{117/119}Sn)$ = 20 Hz, $^1J(^{13}C-^{29}Si)$ = 54 Hz, $SiCH_2Sn$), 14.09 ($^3J(^{13}C-^{117/119}Sn)$ = 35 Hz, $^1J(^{13}C-^{117/119}Sn)$ = 328/342 Hz, CH_2SiMe_3). ^{29}Si NMR ($CDCl_3$, 79.52, 298 K): δ 7.29 ($^2J(^{29}Si-^{117/119}Sn)$ = 54 Hz, *Si*Me), 2.7 ($^2J(^{29}Si-^{117/119}Sn)$ = 41 Hz, CH_2SiMe_3). ^{119}Sn NMR (C_6D_6, 149.26, 298 K): δ 131 ($SnCH_2SiMe_3Cl_2$). Anal. Calcd (%) for $C_{16}H_{42}Cl_6Si_4Sn_3$: C 20.99, H 4.62. Found: C 22.4, H 4.7 calculated for ($C_{16}H_{42}Cl_6Si_4Sn_3 + CH_3CN + H_2O$). Electrospray MS: m/z (%) positive mode 778.929 $C_8H_{29}Cl_5O_4Si_2Sn_3^+$ (100, $[M - Cl^- - 2\,CH_2SiMe_3 + 4\,H_2O + H^+])^+$.

Complexation Studies

- **Synthesis of $(C_{11}H_{21}N_2)_2[MeSi(CH_2SnPhCl_2)_3 \cdot 2\,Cl]$ (13)**

Imidazolium chloride (16.16 mg, 0.074 mmol) is added to a solution of **4** (66 mg, 0.074 mmol) in 15 mL CH_2Cl_2 and the mixture is stirred at room temperature overnight. The solvent is evacuated to afford a white solid. Re-crystallization from dichloromethane/toluene give 35 mg (42 %) of pure **13** as colourless crystals of mp 250 °C. ^{119}Sn NMR (CD_3CN, 149.26): at –30 °C δ –153. ^{119}Sn NMR (CD_2Cl_2, 149.26): at –80 °C δ –49(1.7), –151(1.3). Given a loss of material, no further investigations of the structure of **13** in solid state or in solution are realized.

- **Synthesis of $(C_{11}H_{21}N_2)_3[MeSi(CH_2SnPhCl_2)_3 \cdot 3\,Cl]$ (14)**

Imidazolium chloride (55.33 mg, 0.255 mmol) is added to a solution of **4** (113 mg, 0.127 mmol) in 20 mL CH_2Cl_2 and the mixture is stirred at room temperature overnight. The solvent is evacuated to afford a white solid. Re-crystallization from acetonitrile/dichloromethane give 80 mg (47 %) of pure **14** as colourless crystals of mp 273 °C.

^{1}H NMR (CD_3CN, 600.29, 298 K): δ 0.58 (s, 3H, SiMe), 1.42 (s, 6H, $^2J(^1H-^{117/119}Sn)$ = 152 Hz, SiCH_2Sn), 1.65 (s, 54H, *t*-Bu), 7.36-8.17 ppm (complex pattern, 15H, Ph), 7.64 (d, 6H, C*H*), 8.63 (t, 3H, C*H*). $^{13}C\{^1H\}$ NMR (CD_3CN, 150.49, 298 K): δ 3.67 ($^3J(^{13}C-^{117/119}Sn)$ = 19 Hz, Si*C*H$_3$), 27.49 ($^3J(^{13}C-^{117/119}Sn)$ = 40 Hz, Si*C*H$_2$Sn), 121.27 (CH, $C_{11}H_{21}N_2^+$), 132.91 (CH, $C_{11}H_{21}N_2^+$), 128.91 ppm ($^3J(^{13}C-^{117/119}Sn)$ = 98 Hz, C_m), 130.05 ppm ($^4J(^{13}C-^{117/119}Sn)$ = 18 Hz, C_p), 136.51 ppm ($^2J(^{13}C-^{117/119}Sn)$ = 64 Hz, C_o), 150.59 ppm ($^1J(^{13}C-^{117/119}Sn)$ = 985 Hz, C_i). ^{29}Si NMR (CD_3CN, 119.26, 298 K): δ 2.73 ($^2J(^{29}Si-^{117/119}Sn)$ = 38 Hz, *Si*Me). ^{119}Sn NMR ($CDCl_3$, 149.26, 298 K): δ –160, $W_{1/2}$ = 255 Hz (crude mixture), ^{119}Sn NMR ($CDCl_3$, 149.26, 298 K): δ –175 (crystals sample) (SnCl). Anal. Calcd (%) for $C_{55}H_{87}Cl_9N_6SiSn_3$: C 43.02, H 5.71. N 5.47 Found: C 42.7, H 5.7, N 5.6. Electrospray MS: m/z (%) positive mode 721.0 $[M - 3(C_{11}H_{21}N_2)^+ - 6Cl^- - Ph + H_2O]^+$, 739.0 $[M - 3(C_{11}H_{21}N_2)^+ - 5Cl^- + H^+]^+$, 1504.3 $[M - Cl^- - N^- + H^+ + H_2O]^+$.

- **Reaction of 4 with three equiv molar $(C_{11}H_{21}N_2Cl)$**

Imidazolium chloride (61.7 mg, 0.284 mmol) is added to a solution of **4** (84 mg, 0.094 mmol) in 20 mL CH_2Cl_2 and the mixture is stirred at room temperature overnight. The solvent is evacuated to afford an oily transparent substance. ^{119}Sn NMR (CD_3CN, 149.26, 298 K): δ –178 (*Sn*Cl). No crystalline material is isolated. No further investigations are done.

- **Synthesis of $(PPh_4)[MeSi(CH_2SnCH_2SiMe_3Cl_2)_3 \cdot NO_3]$ (15)**

Tetraphenylphosphoinium nitrate is synthesized according to literature[33] and characterized via IR spectroscopy (See Supporting Information S.142). To a solution of NO_3PPh_4 (67.55 mg, 0.168 mmol) is added solution of **4** (149 mg, 0.168 mmol) in 25 mL CH_2Cl_2. The mixture is stirred at room temperature overnight. The solvent is evacuated to afford a colourless oily substance. No crystalline material is isolated.

^{1}H NMR ($CDCl_3$, 400.25, 298 K): δ 0.65 (s, 3H, SiMe), 1.56 (s, 6H, $^2J(^1H-^{117/119}Sn)$ = 102 Hz, SiCH_2Sn), 1.65 (s, 54H, *t*-Bu), 7.30– 8.03 ppm (complex pattern, 20 H + 15 H, **4** + PPh_4^+). $^{13}C\{^1H\}$ NMR ($CDCl_3$, 100.64, 298 K): δ 2.22 ($^3J(^{13}C-^{117/119}Sn)$ = 31 Hz, Si*C*H$_3$), 18.33 ($^3J(^{13}C-^{117/119}Sn)$ = 21 Hz, Si*C*H$_2$Sn), (130.7, C_m (PPh_4^+)), (117.7, C_p (PPh_4^+)), (134.2, C_o (PPh_4^+)), and (135.7, C_i (PPh_4^+)), 128.5 ppm ($^3J(^{13}C-^{117/119}Sn)$ =

89 Hz, C_m), 130.08 ppm ($^4J(^{13}C-^{117/119}Sn)$ = 20 Hz, C_p), 135.1 ppm ($^2J(^{13}C-^{117/119}Sn)$ = 68 Hz, C_o), 143.7ppm. ^{31}P NMR ($CDCl_3$, 162.02, 298 K): δ 23.18 PPh_4^+. ^{119}Sn NMR ($CDCl_3$, 400.25, 298 K): δ –84 (crude mixture). Anal. Calcd (%) for $C_{46}H_{44}Cl_6NO_3PSiSn_3$: C 42.94, H 3.45, N 1.09. Found (%) of C 43.0, H 3.75, N 0.6. Electrospray MS: m/z (%) negative mode 62.7 $[NO_3]^-$, 1125.3 $\{[(MeSi(CH_2SnCl_2Ph)_3 \cdot NO_3]^- + HPPh_2 + H_2O\}^-$, 1152.3 $[(C_{22}H_{25}Cl_3SiSn_3)_3^+ + 3\,OH^- + NO_3^- + 2\,H_2O + 3\,CH_3CN + MeOH]^-$.

- **Synthesis of $[MeSi(CH_2SnCl_2Ph)_3 \cdot 3\,HMPA]$ (16)**

A solution of HMPA (59.51 mg, 0.332 mmol) is added to a solution of **4** (98.00 mg, 0.110 mmol) in 5 mL CH_2Cl_2 and the mixture is stirred at room temperature overnight. The solvent is removed in vacuo, and the oily residue is dissolved in 25 mL of a mixture acetonitrile/dichloromethane. Slow evaporation of the solvents affords 126 mg (80 %) of pure 16 as colourless crystals of mp 205 °C.

^1H NMR ($CDCl_3$, 600.29, 298 K): δ 0.58 (s, 3H, SiMe), 1.53 (s, 6H, $^2J(^1H-^{117/119}Sn)$ = 117 Hz, $SiCH_2Sn$), 2.55 (d, 54H, $^3J(^1H-^{31}P)$ = 137 Hz, $N(CH_3)_2$), 7.38– 8.03 ppm (complex pattern, 15H, Ph). ^{13}C $\{^1H\}$ NMR ($CDCl_3$, 150.49, 298 K): δ 4 ($SiCH_3$), 18.33 ($^1J(^{13}C-^{117/119}Sn)$ = 519 Hz, $SiCH_2Sn$), 36.7 ($N(CH_3)_2$), 128.4 ($^3J(^{13}C-^{117/119}Sn)$ = 95 Hz, C_m), 129.8 (C_p), 135.06 ($^2J(^{13}C-^{117/119}Sn)$ = 69 Hz, C_o), 145.3 ppm ($^1J(^{13}C-^{117/119}Sn)$ = 912/964 Hz, C_i). ^{31}P $\{^1H\}$ NMR (CD_2Cl_2, 162.02, 193 K): δ 23.5 ($^2J(^{31}P-^{117/119}Sn)$ = 181 Hz, PO→Sn), 23.8 (8 %, no assignment), 24.7 (8 %, no assignment), 25.2 (8 %, no assignment). ^{119}Sn NMR ($CDCl_3$, 400, 298 K): δ –187 (crude mixture, $W_{1/2}$ = 809 Hz), ^{119}Sn NMR (CD_2Cl_2, 149.26, 193 K): δ –216 (crystals sample) (m, 74 %, SnCl), -253 (5 %, no assignment), -252 (5 %, no assignment), -190 (5 %, no assignment). IR (KBr) $\nu_{P=O}$ = 1121.9 cm^{-1}. Electrospray MS: m/z (%) positive mode 180.1 $[POH(NMe_2)_3]^+$, 740.8 $[C_{12}H_{42}Cl_3N_6O_4P_2Sn_2]^+$, negative mode, 810.7 $[C_{18}H_{23}Cl_4NO_2SiSn_3]^-$. Anal. Calcd (%) for $C_{40}H_{78}Cl_6N_9O_3P_3SiSn_3$: C 33.76, H 5.53, N 8.86. Found: C 33.6, H 5.5, N 8.8.

- **Synthesis of $\{MeSi[CH_2Sn(OCOCH_3)Ph_2]_3\}_2$ (17)**

Three molar equivalents of silver acetate (60.42 mg, 0.361 mmol) were added to a solution of **5** (155 mg, 0.120 mmol) in 40 mL CH_2Cl_2 and the mixture is stirred at room temperature in the dark for seven days. The AgI formed is removed by filtration. Re-crystallization from dichloromethane/diethyl-ether gives 39 mg (30 %) of pure **17** as colourless crystals of mp 210 °C.

^{29}Si NMR ($CDCl_3$, 119.26, 298 K): δ –21.9 ($^2J(^{29}Si-^{117/119}Sn)$ = 36 Hz, *Si*Me). ^{119}Sn NMR ($CDCl_3$, 400, 298 K): (crude mixture) δ –218 (10 %), –204 ($W_{1/2}$ = 682 Hz, 46 %), –171 (7 %), –167 (6 %), –91/–90 (19 %), and –44 (10 %). ^{119}Sn NMR ($CDCl_3$, 400.25,

193 K): (crystals sample) δ –91 (2*Sn*1'), –90 (2 *Sn*1), –40 ($^4J(^{119}Sn_2 - ^{117/119}Sn_1/Sn_1$') = 220 Hz, 2*Sn*2). IR (KBr) $\nu_{C=O}$ = 1539 cm^{-1}, ν_{C-O} = 1428, 1018 cm^{-1}. Electrospray MS: m/z (%) positive mode 1640.4 $C_{47}H_{60}Cl_2O_{10}Si_2Sn_6^+$ [M – 2 $COCH_3$ – 7 Ph + H_2O + CH_2Cl_2 + H^+]$^+$. Anal. Calcd (%) for $C_{92}H_{96}O_{12}N_2Si_2Sn_6$ + 3 H_2O + C_6H_{14}: C 51.1, H 5.08. Found: C 51.1, H 5.2.

- **Reaction of 6 with four equiv molar HMPA: formation of {[$MeSi(CH_2SnCl_2Ph_2)_2(CH_2SnPh_2)\cdot 2$ HMPA][$MeSi(CH_2SnCl_2Ph_2)(CH_2SnPh_2Cl)(CH_2SnPh_2)\cdot 2$ HMPA]} (18) and [$MeSi(CH_2SnClPh_2)_3\cdot 3$ HMPA]+HMPA (19)**

A solution of HMPA (82.76 mg, 0.461 mmol) is added to a solution of **4** (117 mg, 0.115 mmol) in 10 mL CH_2Cl_2 and the mixture is stirred at room temperature overnight. The solvent is removed in vacuo, and the oily residue is dissolved in 25 mL of a mixture acetonitrile/dichloromethane. Slow evaporation of the solvents affords 100 mg (56 %) of a crystalline material of **18** and **19**. Due to difficulties in the separation of these two compounds, there is no intensive study in solution of each compound separately.

^{1}H NMR ($CDCl_3$, 600.29, 298 K): (crude mixture) δ 0.23 (s, 3H, SiMe), δ 0.86 (s, 6H, $^2J(^1H - ^{117/119}Sn)$ = 92 Hz, $SiCH_2Sn$), 2.46 (d, 72H, $^2J(^1H - ^1H)$ = 9 Hz, $^3J(^1H - ^{31}P)$ = 135 Hz, $N(CH_3)_2$), 7.31-8.03 (complex pattern, 30H, Ph). ^{13}C {^{1}H} NMR ($CDCl_3$, 150.49, 298 K): (crude mixture) δ 3.44 ($SiCH_3$), 9.05 ($SiCH_2Sn$), 36.2 ($N(CH_3)_2$), 127.9 ($^3J(^{13}C - ^{117/119}Sn)$ = 66 Hz, C_m), 128.8 (C_p), 135.7 ($^2J(^{13}C - ^{117/119}Sn)$ = 52 Hz, C_o), 142.9 ppm (C_i). ^{31}P {^{1}H} NMR ($CDCl_3$, 243, 298 K): δ 24 (crude mixture). ^{31}P {^{1}H} NMR (CD_2Cl_2, 162.02, 193 K (-80 °C)): (crystals sample) δ 23.28 (s, 48 %), 23.62 (broad signal, 39 %), 22.7 (5 %), 24.1 (3 %), 24.3 (4 %). ^{119}Sn NMR ($CDCl_3$, 223.58, 298 K): δ –81 (crude mixture) (broad signal, $W_{1/2}$ = 1675 Hz), ^{119}Sn NMR (CD_2Cl_2, 149.26, 193 K (–80 °C)): (crystals sample) δ –104 (s, 1.2), -133 (s, 3.5), -170 (broad signal, $W_{1/2}$ = 920 Hz, 1.4), -185 (broad signal, $W_{1/2}$ = 950 Hz, 1.2), -197 (t, $^2J(^{31}P - ^{117/119}Sn)$ = 313 Hz, 1.9). To distinguish between these two compounds in solution, we need more probably a much lower temperature ^{119}Sn and ^{31}P NMR measurements. Within the time frame of this PhD, further investigation in solution could not be performed.

Electrospray MS: m/z (%) negative mode 1291.1 [($MeSi(CH_2SnCl_3Ph_2)_3\cdot$HMPA + $PClOH^-$ – $(NMe_2)_3$]$^-$, 1046.1 [($MeSi(CH_2SnCl_3Ph_2)(CH_2SnClPh_2)(CH_2SnO_2Ph_2)]_2^-$. Anal. Calcd (%) for $C_{52}H_{77}Cl_3N_6O_2P_3SiSn_3$ (**18**): C 45.56, H 5.66, N 6.13. Found: C 46.1, H 5.6, N 5.8. Anal. Calcd (%) for C64H111Cl3N12O4P4SiSn3 (**19**): C 44.48, H 6.48, N 9.73, found C 44.4, H 6.4, N 9.2.

- **Reaction of 6 with one equiv molar PPh_4Cl: [PPh_4][$MeSi(CH_2SnPh_2Cl)_3\cdot Cl$] (20)**

Tetraphenylphosphonium chloride (33.02 mg, 0.088 mmol) is added to a solution of **6** (89 mg, 0.088 mmol) in 20 mL CH_2Cl_2 and the mixture is stirred at room temperature overnight. The solvent is evacuated to afford $(PPh_4)[MeSi(CH_2SnPh_2Cl)_3{\cdot}Cl]$, 20 (119 mg, 97 %) as an amorphous white substance. No crystalline material is isolated.

^1H NMR ($CDCl_3$, 400.25, 298 K): δ 0.3 (s, 3H, SiMe), 0.92 (s, 6H, $^2J(^1H-^{117/119}Sn)$ = 98 Hz, SiCH2Sn), 7.24- 8.01 (complex pattern, 20H (PPh_4) + 30H (**20**), Ph). $^{13}C\{^1H\}$ NMR ($CDCl_3$, 100.64, 298 K): δ 2.96 ($^3J(^{13}C-^{117/119}Sn)$ = 21 Hz, Si*C*H_3), 12.05 (Si*C*H_2Sn), 127.9 ($^3J(^{13}C-^{117/119}Sn)$ = 62 Hz, C_m), 128.6 ($^4J(^{13}C-^{117/119}Sn)$ = 12 Hz, C_p), 136.56 ($^2J(^{13}C-^{117/119}Sn)$ = 49 Hz, C_o), 143.7 ppm (C_i), 117.2 (C_p, PPh_4), 130.6 (C_m, PPh_4), 134.1 (Co, PPh_4), 135.7 (C_i, PPh_4). ^{29}Si NMR ($CDCl_3$, 119.26, 298 K): δ 5.72 ($^2J(^{29}Si-^{117/119}Sn)$ = 36 Hz, *Si*Me). ^{119}Sn NMR ($CDCl_3$, 149.26, 298 K): δ –77 (crude mixture, $W_{1/2}$ = 980 Hz), ^{119}Sn NMR (CD_2Cl_2, 223.85, 193 K (-80 °C)): δ –87 (1*Sn*), –52 (2*Sn*). Electrospray MS: m/z (%) negative mode 1026.7902 [M – PPh_4^+ – Cl^- + OH–]$^-$. Anal. Calcd (%) for $C_{63}H_{59}Cl_4PSiSn_3$: C 55.50, H 4.29. Found: C 54.5, H 4.3.

- **Reaction of 6 with two equiv molar PPh_4Cl: $(PPh_4)_2[MeSi(CH_2SnPh_2Cl)_3 \cdot 2Cl]$ (21)**

Tetraphenylphosphonium chloride (54.17 mg, 0.144 mmol) is added to a solution of **6** (73 mg, 0.072 mmol) in 25 mL CH_2Cl_2 and the mixture is stirred at room temperature overnight. The solvent is evacuated to afford $(PPh_4)_2[MeSi(CH_2SnPh_2Cl)_3{\cdot}2Cl]$, 21 (124 mg, 98 %) as an amorphous white substance. No crystalline material is isolated.

^1H NMR (CD_2Cl_2, 400.25, 298 K): δ 0.31 (s, 3H, SiMe), 0.97 (s, 6H, $^2J(^1H-^{117/119}Sn)$ = 100 Hz, SiC*H*2Sn), 7.24– 8.15 (complex pattern, 40H (PPh_4) + 30H (**21**), Ph). $^{13}C\{^1H\}$ NMR (CD_2Cl_2, 100.64, 298 K): δ 3.62 ($^3J(^{13}C-^{117/119}Sn)$ = 25 Hz, Si*C*H_3), 14.21 ($^3J(^{13}C-^{117/119}Sn)$ = 23 Hz, Si*C*H_2Sn), 128.2 ($^3J(^{13}C-^{117/119}Sn)$ = 64 Hz, C_m), 128.8 ($^4J(^{13}C-^{117/119}Sn)$ = 15 Hz, C_p), 137.1 ($^2J(^{13}C-^{117/119}Sn)$ = 48 Hz, C_o), 145.9 ppm (C_i), 117.9 (C_p, PPh4), 131.1 (C_m, PPh_4), 134.8 (C_o, PPh_4), 136.2 (C_i, PPh_4). ^{29}Si NMR (CD_2Cl_2, 79.52, 298 K): δ 5.53 ($^2J(^{29}Si-^{117/119}Sn)$ = 37 Hz, *Si*Me). ^{119}Sn NMR (CD_2Cl_2, 149.26, 298 K): δ –109 (crude mixture, $W_{1/2}$ = 957 Hz, 88 %), –89 (1.2 %), –134 (4.4 %), –252 (6.8 %). No further investigation in solution is made given the ignorance of the aspect of **21** in solid state. Electrospray MS: m/z (%) positive mode 339.2 $[PPh_4]^+$, 919.2 [M – 2PPh_4^+ – 2Cl^- – CH_3 + H^+]$^+$. Anal. Calcd (%) for $C_{88}H_{79}Cl_5P_2SiSn_3$: C 60.05, H 4.52. Found: 59.6, H 4.6.

- **Synthesis of $(NEt_4)_2[MeSi(CH2SnFPh2)3_2 \cdot 2F]$ (22)**

Tetraethylammonium fluoride (10.99 mg, 0.059 mmol) is added to a solution of 7 (57 mg, 0.059 mmol) in 10 mL CH_3CN and the mixture is stirred at room temperature

overnight. The solvent is evacuated to afford a white solid. Re-crystallization from acetonitrile/dichloromethane give 60 mg (89 %) of pure **22** as colourless crystals of mp 240 °C.

^{19}F NMR (CD_3CN, 564.84, 298 K): (crude mixture) δ –81 (20 %), –129 (12 %), –142 (22 %), –159 (15 %), –161 (25 %). ^{119}Sn NMR (CD_3CN, 223.85, 298 K): δ –188 (crude mixture, $W_{1/2}$ = 957 Hz). Given the low solubility of the crystals of 22, at −40 °C and −80 °C, there are no reliable ^{19}F or ^{119}Sn NMR spectra. Electrospray MS: m/z (%) negative mode 979.2 $[MeSi(CH_2SnFPh_2)_3{\cdot}F]^-$. Anal. Calcd (%) for $C_{96}H_{118}F_8N_2Si_2Sn_6 + H_2O$: C 51.5, H 5.4, N 1.25. Found: C 51.3, H 5.4, N 1.2.

- **Reaction of 7 with two equiv molar of ($NEt_4.2H_2O$)**

Tetraethylammonium fluoride (26.22 mg, 0.141 mmol) is added to a solution of **7** (68 mg, 0.070 mmol) in 20 mL CH_2Cl_2 and the mixture is stirred at room temperature overnight. The solvent is evacuated to afford a white solid. Re-crystallization from acetonitrile/dichloromethane give 70 mg (92 %), the same crystalline material as **22** (mp 240 °C)

^{19}F NMR (CD_3CN, 564.84, 298 K): (crude mixture) δ –162 ($^1J(^{19}F^1 - ^{117/119}Sn^1)$ = 1939/2018 Hz, $1F^1$), –158 ($^1J(^{19}F^4 - ^{117/119}Sn^1)$ = 2010 Hz, $1F^4$), -142 ($^1J(^{19}F^2 - ^{117/119}Sn)$ = 1930 Hz, $1F^2$), -129 ($1F^3$). ^{119}Sn NMR (CD_3CN, 223.85, 298 K): (crude mixture) δ –220 ($1Sn^1$), –213 ($1Sn^1$), –205 ($1Sn^2$) . Given the low solubility of the crystals of **22** at −40 °C and −80 °C, there are no reliable ^{19}F or ^{119}Sn NMR spectra. Electrospray MS: m/z (%) negative mode 979.2 $\{20, [MeSi(CH_2SnFPh_2)_3 \cdot F]^-\}$. Anal. Calcd (%) for $C_{96}H_{118}F_8N_2Si_2Sn_6 + H_2O + 2CH_3CN$: C 51.7, H 5.5, N 2.4. Found: C 51.6, H 5.8, 2.3.

- **Reaction of 7 with three equiv molar of ($NEt_4.2H_2O$)**

Tetraethylammonium fluoride (35.86 mg, 0.193 mmol) is added to a solution of **7** (62 mg, 0.064 mmol) in 25 mL CH_2Cl_2 and the mixture is stirred at room temperature overnight. The solvent is evacuated to afford a white solid. Re-crystallization from acetonitrile/dichloromethane give 60 mg (87 %), the same crystalline material as **22** (mp 240 °C).

^{19}F NMR (CD3CN, 564.84, 298 K): (crude mixture) major specie (94 %): δ –158 ($^nJ(^{19}F - ^{117/119}Sn)$ = 2013 Hz, $2F$), –142 ($^nJ(^{19}F - ^{117/119}Sn)$ = 1899 Hz , 2F), –129 ($^nJ(^{19}F - ^{117/119}Sn)$ = 1153 Hz, $1F$), minor specie (6 %): δ –162 ($^nJ(^{19}F - ^{117/119}Sn)$ = 1942/2029 Hz, $3F$), -154 ($^nJ(^{19}F - ^{117/119}Sn)$ = 1506/1585 Hz, $1F$), -140 ($^nJ(^{19}F - ^{117/119}Sn)$ = 2334/2373 Hz, $2F$), -127 ($^nJ(^{19}F - ^{117/119}Sn)$ = 2182/2214 Hz,$^nJ(^{19}F - ^{19}F)$ = 116 Hz, $2F$) . ^{29}Si NMR (CD_3CN, 119.26, 298 K): δ 6.17 ($^2J(^{29}Si - ^{117/119}Sn)$ = 35 Hz, SiMe). ^{119}Sn NMR (CD_3CN, 223.85, 298 K): (crude mixture) δ –270 (t, $W_{1/2}$ = 1983 Hz, $1Sn$), –211 (dd, $2Sn$) . A crystals sample shows the same behaviour in solution via ^{19}F and ^{119}Sn NMR spectra. Electrospray

MS: m/z (%) negative mode 978.2 $[MeSi(CH_2SnFPh_2)_3 \cdot F]^-$. Anal. Calcd (%) for $C_{96}H_{118}F_8N_2Si_2Sn_6 + 2H_2O + 2CH_3CN$: C 51.3, H 5.5, N 2.4. Found: C 51.1, H 6.9, N 2.2.

- **Synthesis of $(PPh_4)[MeSi(CH_2SnBr_3)_3 \cdot Br]$ (23)**

Tetraphenylphosphonium bromide (32.16 mg, 0.077 mmol) is added to a solution of **9** (89 mg, 0.077 mmol) in 15 mL CH_2Cl_2 and the mixture is stirred at room temperature overnight. The solvent is evacuated to afford a white solid. Re-crystallization from dichloromethane/diethyl-ether give 100 mg (82 %) of pure **23** as colourless crystals of mp 250 °C.

^{1}H NMR (CD_2Cl_2, 400.25, 298 K): δ 0.71 (s, 3H, SiMe, 2.31 (s, 6H, $^2J(^1H-^{117/119}Sn)$ = 129/135 Hz, SiCH_2Sn), 7.58–7.95 ppm (20H, PPh_4^+). $^{13}C\{^1H\}$ NMR (CD_2Cl_2, 100.64, 298 K): δ 1.87 (SiCH_3), 27.56 ($^3J(^{13}C-^{117/119}Sn)$ = 38 Hz, SiCH_2Sn), 118.0 (C_p, PPh_4), 131.2 (C_m, PPh_4), 134.9 (C_o, PPh4), 136.3 (C_i, PPh_4). ^{29}Si NMR (CD_2Cl_2, 119.26, 298 K): δ 4.22 ($^2J(^{29}Si-^{117/119}Sn)$ = 43 Hz, SiMe). ^{119}Sn NMR (CD_2Cl_2, 223.85, 298 K): (crude mixture) δ –353 ($W_{1/2}$ = 780 Hz). Electrospray MS: m/z (%) negative mode 1242.1 [M – PPh_4^+]$^-$: $[MeSi(CH_2SnBr_3)_3 \cdot Br]^-$, m/z (%) positive mode 339.3 $[PPh_4]^+$. Anal. Calcd (%) for $C_{28}H_{31}Br_{10}PSiSn_3 + CH_3CN$: C 22.2, H 2.11 Found: of C 22.1, H 2.2.

- **Synthesis of $(NEt_4)_2[MeSi(CH_2SnBr_3)_3 \cdot 2Br]$ (24)**

Tetraethylammonium bromide (41.29 mg, 0.196 mmol) is added to a solution of **9** (114 mg, 0.098 mmol) in 20 mL acetonitrile and the mixture is stirred at room temperature overnight. The solvent is evacuated to afford a white solid. Re-crystallization from acetonitrile/dichloromethane give 150.6 mg (97 %) of pure **24** as colourless crystals of mp 283 °C.

^{1}H NMR (CD_3CN, 400.25, 298 K): δ 0.81 (s, 3H, SiMe), 1.21 (t, CH_3, 24H, $2NEt_4^+$), 2.39 (s, 6H, $^2J(^1H-^{117/119}Sn)$ = 141 Hz, SiCH_2Sn), 3.15 (q, CH_2, 16H, $2NEt_4^+$). $^{13}C\{^1H\}$ NMR (CD_3CN, 150.94, 298 K): δ –3.41 (SiCH_3), 7.83 (CH_3, NEt_4^+), 15.22 (SiCH_2Sn), 53.19 (*C*H2, NEt4+). ^{29}Si NMR (CD_2Cl_2, 119.26, 298 K): δ 5.16 ($^2J(^{29}Si-^{117/119}Sn)$ = 50 Hz, *Si*Me). ^{119}Sn NMR (CD_2Cl_2, 223.85, 298 K): (crude mixture) δ –424 ($W_{1/2}$ = 34 408 Hz). Anal. Calcd (%) for $C_{20}H_{49}Br_{11}N_2SiSn_3$: C 15.2, H 3.12, N 1.77. Found: C 15.2, H 3.4, N 1.9. Electrospray MS: m/z (%) negative mode 1240.1 [M – Br^- – $2NEt_4^+$]$^-$: $[MeSi(CH_2SnBr_3)_3 \cdot Br]^-$, 1534.2 [M – NEt_4^+ + $2CH_3CN$]$^-$: $\{[MeSi(CH_2SnBr_3)_3 \cdot 2Br]^{2-}\} \cdot NEt_4^+ + 2CH_3CN$, m/z (%) positive mode 130.3 $[NEt_4]^+$.

- **Reaction of 9 with three equiv molar (PPh_4Br)**

Tetraphenylphosphonium bromide (74.79 mg, 0.178 mmol) is added to a solution of **9** (69 mg, 0.059 mmol) in 15 mL CH_2Cl_2 and the mixture is stirred at room temperature

overnight. The solvent is evacuated to afford a yellow oily substance. ^{119}Sn NMR (CD_2Cl_2, 223.85, 298 K): (crude mixture) δ –511 ($W_{1/2}$ = 2438 Hz, *Sn*Br). No crystalline material is isolated. No further investigations are done given the high kinetic lability of such compounds even at low temperature.

- **Reaction of 12 with one equiv molar of ($C_{11}H_{21}N_2Cl$)**

Imidazolium chloride (10.18 mg, 0.046 mmol) is added to a solution of **12** (43 mg, 0.046 mmol) in 15 mL CH_3CN and the mixture is stirred at room temperature overnight. The solvent is evacuated to afford an oily transparent substance. ^{119}Sn NMR (CD_3CN, 149.26, 298 K): δ –11, $W_{1/2}$ = 528 Hz, (*Sn*Cl). No crystalline material is isolated. No further investigations are done given the luck of solubility.

- **Synthesis of $(C_{11}H_{21}N_2)_2[MeSi(CH_2SnCH_2SiMe_3Cl_2)_3 \cdot 2Cl]$ (25)**

Imidazolium chloride (22.25 mg, 0.102 mmol) is added to a solution of **12** (47 mg, 0.051 mmol) in 15 mL CH_3CN and the mixture is stirred at room temperature overnight. The solvent is evacuated to afford a white solid. Re-crystallization from acetonitrile/dichloromethane give 50 mg (72 %) of pure **25** as colourless crystals of mp 281 °C.

^{1}H NMR (CD_3CN, 400.25, 298 K): δ 0.08-0.14 (s, 27H, $SiMe_3$), 0.47 (s, 3H, SiMe), 0.92 (s, 6H, $^2J(^1H-^{117/119}Sn)$ = 110 Hz, CH_2SiMe_3), 1.28 (s, 6H, $SiCH_2Sn$), 1.60 (s, 36H, *t*-Bu), 7.56 (d, 4H, CH), 8.44 (t, 2H, CH). ^{29}Si NMR (CD_3CN, 119.26, 298 K): δ 1.82 (CH_2SiMe_3), 3.92 ($^2J(^{29}Si-^{117/119}Sn)$ = 56 Hz, SiMe). ^{119}Sn NMR (CD_3CN, 400.25): at 25 °C, δ –48, at –40 °C -122, -76 (SnCl). Anal. Calcd (%) for $C_{40}H_{93}Cl_8N_4Si_4Sn_3$: C 34.76, H 6.78, N 4.05 Found: C 34.6, H 6.5, N 3.6. Electrospray MS: m/z (%) negative mode1127.4 $[M - (C_{11}H_{21}N_2)^+ - 2Cl^- - 3H^+]^-$, m/z (%) positive mode 771.1 $[M - 2(C_{11}H_{21}N_2)^{+-} 7Cl^- - CH_2SiMe_3 + 2H_2O + CH_3CN]^+$.

- **Reaction of 12 with three equiv molar ($C_{11}H_{21}N_2Cl$)**

Imidazolium chloride (62.5 mg, 0.288 mmol) is added to a solution of **12** (88 mg, 0.096 mmol) in 20 mL CH_3CN and the mixture is stirred at room temperature overnight. The solvent is evacuated to afford a white solid. Re-crystallization from acetonitrile/dichloromethane give 100 mg (77 %) of the same crystalline material as **25** (mp 282 °C). ^{119}Sn NMR (CD_3CN, 149.26, 298 K): crude mixture δ –77 (SnCl).

3. The Spacer-Bridged Tetrastannanes R'Sn($CH_2SnR_{(3-n)}X_n$)$_3$, (n = 0– 2; X = I, Cl; R = Ph, R'= R, X), Syntheses, Structures and Complexation Studies

3.1 Introduction

The synthesis and complexation behaviour of the spacer bridged tetratin compounds R'Sn($CH_2SnR_{(3-n)}X_n$)$_3$, (n = 0– 2; X = I, Cl; R = Ph, R' = R, X), having a similar structure as the previous tripod silicon bridged organotin MeSi($CH_2SnR_{(3-n)}X_n$)$_3$, (n = 0– 3; X = I, F, Cl, Br; R = Ph, CH2SiMe3) is under investigation. We want to define the chelation characteristics of these novel backbones and compare its complexation ability with the previous mentioned compounds. Scheme 16 shows the syntheses of the compounds **1**– **5**. The numbering of compounds in this chaper is independent from the previous chapter.

Scheme 16. Syntheses of the tris(organostannylmethyl)stannane derivatives R'Sn($CH_2SnR_{(3-n)}X_n$)$_3$, (n = 0– 2; X = I, Cl; R = Ph, R' = R, X).

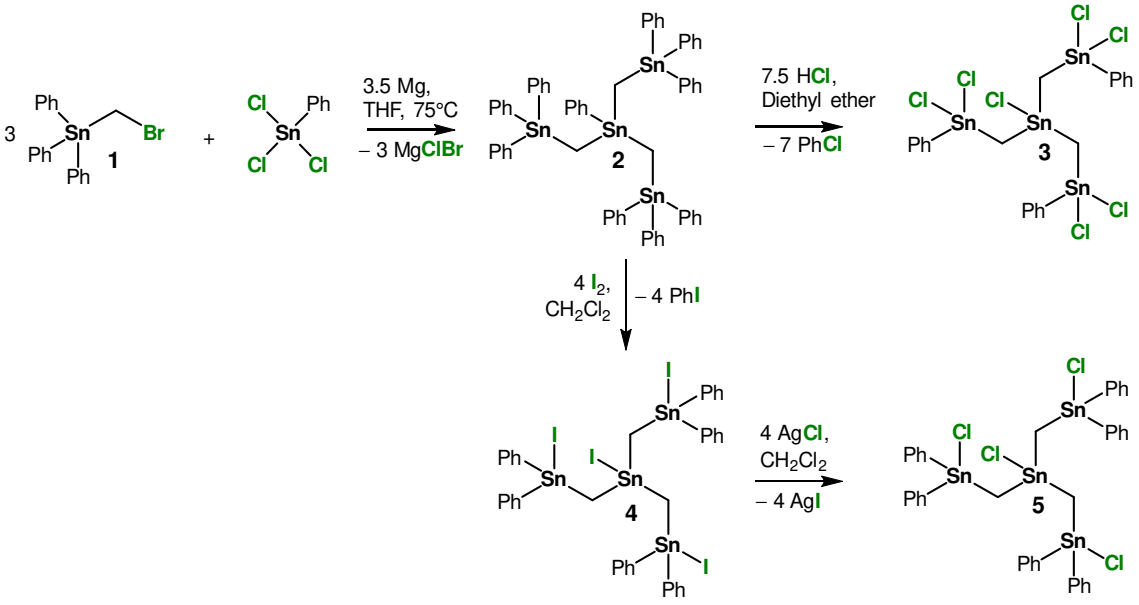

3.2 Syntheses and characterization of R'Sn($CH_2SnR_{(3-n)}X_n)_3$, (n = 0– 2; X = I, Cl; R = Ph, R'= R, X)

The reaction of one molar equiv of $SnPhCl_3$ in THF with three molar equiv of the Grignard reagent Ph_3SnCH_2MgBr, **1**,[38] under reflux overnight at 75 °C gives the tris(triphenylstannylmethyl)phenylstannane $PhSn(CH_2SnPh_3)_3$, **2**, as a white solid material in a very good yield.

Single crystals of compound **2** suitable for X-ray diffraction analysis are obtained by slow evaporation from a CH_2Cl_2/*iso*-hexane at room temperature. It crystallizes in the triclinic space group $P-1$. Figure 36 shows the molecular structure and selected interatomic distances and bond angles are listed in Table 8. The Sn(1), Sn(2), Sn(3) and Sn(4) are four-coordinated and show distorted tetrahedral geometries with angles varying between 102.4(3)° (C81–Sn4–C91) and 115.5(3)° (C3–Sn4–C81'). The Sn–C distances vary from 1.984(9) Å (Sn4–C91') and 2.330(6) Å (Sn4–C91). It is worth mentioning that the tripod geometry characteristic of **2** is comparable to that of silicon bridged organotin compound $MeSi(CH_2SnPh_3)_3$. In fact, the Sn(1)–C(1)–Sn(2), Sn(1)–C(2)–Sn(3), and Sn(1)–C(3)–Sn(4) angles of 116.9(2)°, 121.2(3)°, and 118.1(3)°, respectively, presenting the three "arms" of the tripod are similar. The environment at the "head" tin atom Sn(1) is distorted tetrahedral with almost equal angles varying between 107.14(19)° (C3–Sn1–C4) and 112.6(2)° (C1–Sn1–C3).

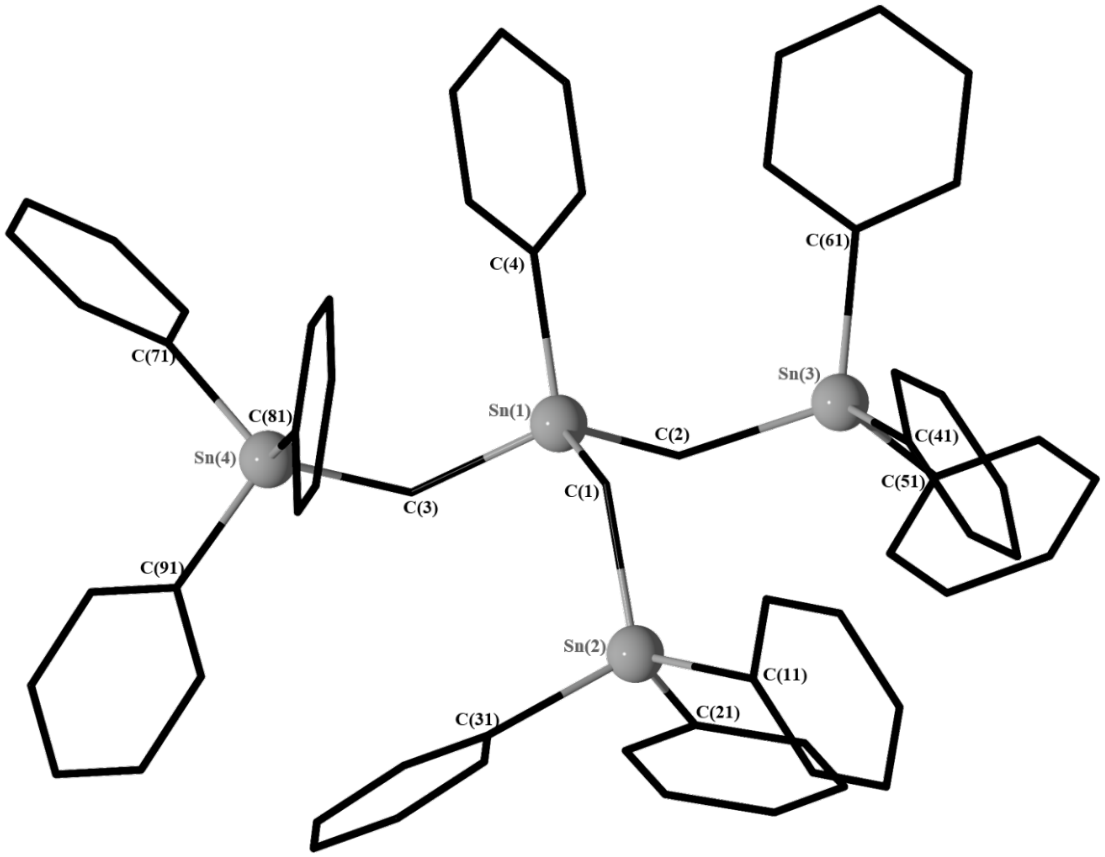

Figure 36. General view (POV-Ray) of a molecule of **2** showing the crystallographic numbering scheme. There are disorders of the phenyl rings C(31) to C(36) and C(31') to C(36') with a ratio of 51:49, C(81) to C(86) and C(81') to C(86') with a ratio of 50:50, and C(91) to C(96) and C(91') to C(96') with a ratio of 55:45, respectively.

A ^{119}Sn NMR spectrum (Figure 37) of a solution of compound 2 in CDCl3 shows two singlet resonances with 3: 1 ratio, respectively at δ –78 ppm ($^4J(^{119}Sn-^{117}Sn)$ = 44 Hz, $^2J(^{119}Sn-^{117/119}Sn)$ = 245/257 Hz, $^1J(^{119}Sn-^{13}C_i)$ = 504 Hz), corresponding to the three equivalent (^{ter}Sn) atoms; Sn(2), Sn(3), and Sn(4) (Figure 33), and at δ –34 ppm, corresponding to the head tin atom Sn(1) (^{gem}Sn). This latter shift resonance is comparable to those reported for the alkyl-substituted organotin compounds $Me_3Sn(C_6H_5)$ (δ 32.3 ppm) and $Me_3Sn(t\text{-}Bu)$ (δ 32.3 ppm).[27] As to the lower-frequency shifted resonance is very close to the corresponding resonances in $(Ph_3Sn)_2CH_2$ (δ –79 ppm),[26] $(Ph_3SnCH_2)_2SnPh_2$ (^{ter}Sn δ –79 ppm),[25] and the structurally alike compounds $(Ph_3Sn)_3CH$ (δ –78 ppm)[12] and the novel silicon-bridged organotin compound $MeSi(CH_2SnPh_3)_3$ at -89 ppm.

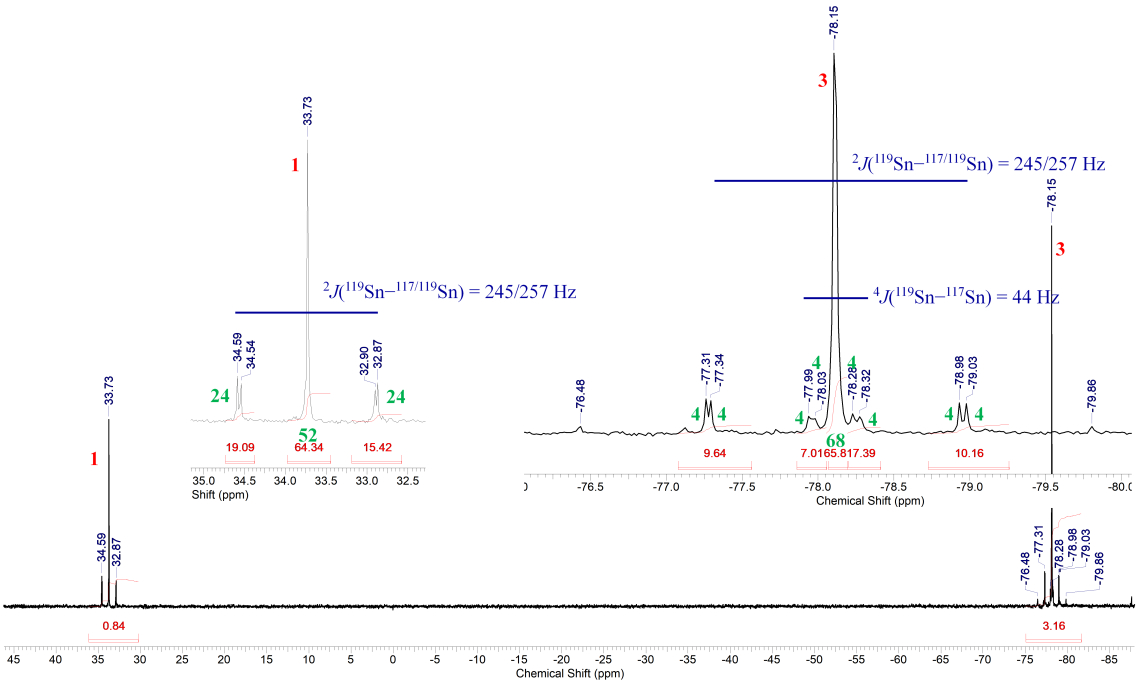

Figure 37. ^{119}Sn NMR spectrum (149.26 MHz, $CDCl_3$) of compound **2**.

A ^{1}H NMR spectrum of a solution of **2** in C_6D_6 shows a singlet resonance corresponding to the SnCH2 protons at δ 0.43 ppm ($^2J(^1H–^{117/119}Sn)$ = 61 Hz) , this single resonance is close to that reported of the corresponding ($SiCH_2Sn$) protons in $MeSi(CH_2SnPh_3)_3$ at δ 0.33 ppm ($^2J(^1H–^{117/119}Sn)$ = 78 Hz), with a smaller coupling constant. A complex pattern appears at δ 6.97- 7.63 ppm (50H) which belongs to the phenyl protons. In a ^{13}C NMR spectrum of **2** in $CDCl_3$, the singlet resonance referring to the ($SiCH_2Sn$) carbon is shown at δ 1.35 ppm ($^1J(^{13}C–^{117/119}Sn)$ = 275 Hz). This value is higher-frequency shifted comparing to that of $MeSi(CH_2SnPh_3)_3$ at δ –1.7 ppm.

In the aromatic part, the chemical shift corresponding to the carbon atoms C_m is shown at δ 128.9 ppm ($^3J(^{13}C_m–^{117/119}Sn_1)$ = 61 Hz, $^5J(^{13}C_m–^{117/119}Sn_2)$ = 18 Hz), with Sn1 is the "head" Sn atom and Sn2 corresponds to the three other tin atoms. The singlet resonances of C_p, C_o, and C_i appear respectively at δ 130.21 ppm ($^4J(^{13}C_p–^{117/119}Sn)$ = 14 Hz), δ 135.9 ppm ($^2J(^{13}C_o–^{117/119}Sn)$ = 50 Hz), and 137.0 ppm, the coupling constant $^1J(^{13}C_i–^{117/119}Sn)$ are not detected. All these data evidence that the tin atoms in compound **2** are four-coordinated with distorted tetrahedral geometries, as observed in the solid state. An ESI MS spectrum in the positive mode shows mass clusters centred at m/z 923.1 $C_{44}H_{40}Sn_3^+$ (60, $[M – (CH_2SnPh_3]^+$) and 1310.5 (10, $[M + \frac{1}{2}H_2O + H_2O]^+$), respectively (See Supporting Information, Chapter 3 Figures S1- S7).

The treatment of compound **2** with seven molar equiv of a solution of HCL in diethyl ether produces tris(dichloridophenylstannylmethyl)chloridostannane $ClSn(CH_2SnPhCl_2)_3$, **3**, in

70 % yield (Scheme 5). Compound **3** is a yellowish oil, showing good solubility in common organic solvents such as CH_2Cl_2, $CHCl_3$, and CH_3CN.

A ^{119}Sn NMR spectrum (Figure 38) of the organotin dichloride-substituted derivative **3** in C_6D_6 exhibits two singlet resonances, with a ratio of 3:1, respectively, at δ 26 ppm (^{ter}Sn) and δ 54 ppm (^{gem}Sn). These resonance shifts are close to that reported in the dichloride-substituted derivative in the previous chapter MeSi($CH_2SnPhCl_2)_3$ at δ 41 ppm, also are near to the corresponding resonance in ($Ph_2Cl_2Sn)CH_2$ (δ 32 ppm).[12] There are additional unresolved resonance signals at δ 25 ppm (25 %) and -29 ppm (9 %) indicating the presence of by-products (See Supporting Information, Chapter 3, Figure S9). Attempts at purifying compound **3** by re-crystallization failed. A further purification is not possible, given the instability of such compounds toward column chromatography. Therefore, this mixture is used in the next reactions without further purification.

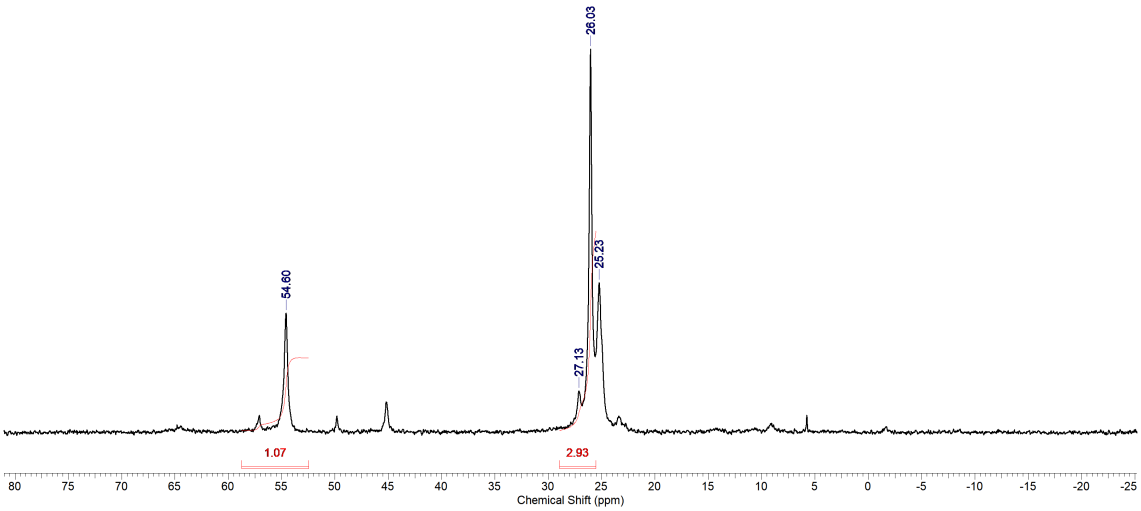

Figure 38. ^{119}Sn NMR spectrum (111.92 MHz, $CDCl_3$) of compound **3**.

A ^{1}H NMR spectrum of compound **3** displays a singlet resonance assigned to the CH_2 protons at 2.11 ppm ($^2J(^1H-^{117/119}Sn)$ = 72 Hz) which is higher-frequency shifted as compared to that reported in MeSi($CH_2SnPhCl_2)_3$ at δ 1.50 ppm ($^2J(^1H-^{117/119}Sn)$ = 88 Hz) and in the *cyclo*-$Cl_2Sn(CH_2SiMe_2CH_2)_2SnCl_2$ at 1.02 ppm ($^2J(^1H-^{117/119}Sn)$ = 49/52 Hz).[9] As to the complex pattern of the phenyl groups appears at δ 7.42–7.86 ppm (See Supporting Information, Chapter 3, Figure S8).

The reaction of compound **2** with four molar equiv of elemental iodine at 0 °C in CH_2Cl_2 gives the iodine-substituted tris(iodidophenylstannylmethyl)iodidostannane $ISn(CH_2SnPh_2I)_3$, **4**, in quantitative yield as a slightly yellow oil. The corresponding organotin chloride $ClSn(CH_2SnPh_2Cl)_3$, **5** is obtained as a colourless oily substance through the reaction of **4** with four molar equiv of AgCl in CH_2Cl_2. Compounds **4** and **5** show good solubility in common organic solvents such as CH_2Cl_2, $CHCl_3$, and CH_3CN. (Scheme 16)

Single crystals of compound **4** suitable for X-ray diffraction analysis are obtained by slow evaporation from its CH_2Cl_2/*iso*-hexane solution at room temperature. It crystallizes in the triclinic space group $P-1$. Figure 39 shows the molecular structure and selected interatomic distances and angles are listed in Table 8. The molecular structure of **4** preserves as well the tripod geometry, characteristic of the novel backbones. The Sn(2), Sn(3) and Sn(4) centres are four-coordinated and show distorted tetrahedral geometries with angles varying between 102.55(12)° (C41–Sn3–I3) and 115.27(17)° (C51–Sn3–C2). However, Sn(1) exhibits a [4+1] coordination via an intramolecular I→Sn interaction at a Sn(1)–I(2) distance of 3.9496(4) Å that is shorter than the sum of vdW radii of tin (2.17 Å) and iodine (1.98 Å).[31] The environment at Sn(1) is a distorted trigonal bipyramid with a geometrical goodness[22] equal to $\Delta\Sigma(\theta)$= 31.1°. The equatorial positions are occupied by C(1), C(2), and C(3) and the axial positions are occupied by I(1) and I(2). This distortion is explained by I(1)–Sn(1)–C(1), I(1)–Sn(1)–C(2), and I(1)–Sn(1)–C(3) angles, respectively equal to 105.55(11)°, 102.0(25)°, and 104.11(13)° deviating from the ideal angle of 90°. The Sn–I distances are nearly equal varying between 2.7046(4) Å (Sn4–I4) and 2.7229(4) Å (Sn1-I1).

A ^{119}Sn NMR spectrum of the iodido-substituted derivative **4** (Figure 40) displays two singlet resonances, with a ratio of 3:1, respectively, at δ –66 ppm (^{ter}Sn) ($^4J(^{119}Sn-^{117}Sn)$ = 54 Hz, $^2J(^{119}Sn-^{117/119}Sn)$ = 319 Hz, $^1J(^{119}Sn-^{13}C_i)$ = 553 Hz), and δ 42 ppm (^{gem}Sn) ($^2J(^{119}Sn-^{117/119}Sn)$ = 319 Hz). The resonance shift corresponding to the three ^{ter}Sn is close to that reported for the structurally alike iodine-derivative MeSi(CH_2SnIPh_2)$_3$ (δ –67 ppm), as well as very similar to those reported for (IPh_2Sn)$_2CH_2$ (δ –68 ppm)[26] ($IPh_2Sn_2CH_2$)$_2SiMe_2$ (δ –65 ppm),[28] (Ph_2ISn)$_3CH$ (δ –70 ppm).[12]

A ^{1}H NMR spectrum of a solution of **4** in C_6D_6 shows a singlet resonance corresponding to the $SnCH_2$ protons at δ 1.52 ppm ($^2J(^1H-^{117/119}Sn)$ = 61 Hz) , this single resonance is slightly higher frequency-shifted as compared to that reported for the corresponding ($SiCH_2Sn$) protons in MeSi(CH_2SnIPh_2)$_3$ at δ 0.99 ppm ($^2J(^1H-^{117/119}Sn)$ = 80 Hz) but with a smaller coupling constant. Also this shift resonance is close to those corresponding in ($IPh_2Sn_2CH_2$)$_2SiMe_2$ (δ 1.03 ppm) and (IPh_2Sn)$_2CH_2$ (δ 1.87 ppm). A complex pattern is shown for the phenyl protons at δ 7.39-7.68 ppm (30H).

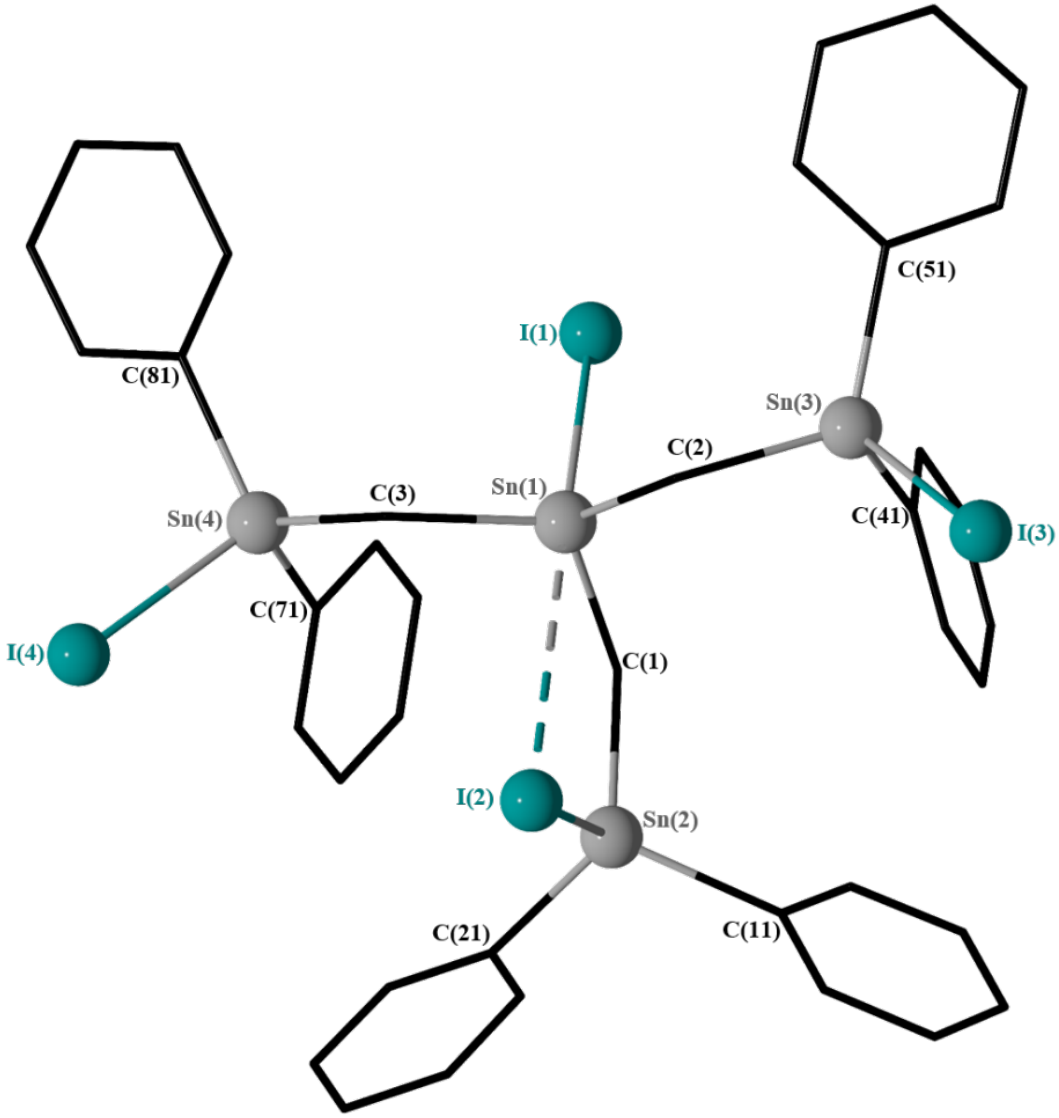

Figure 39. General view (POV-Ray) of a molecule of **4** showing the crystallographic numbering scheme.

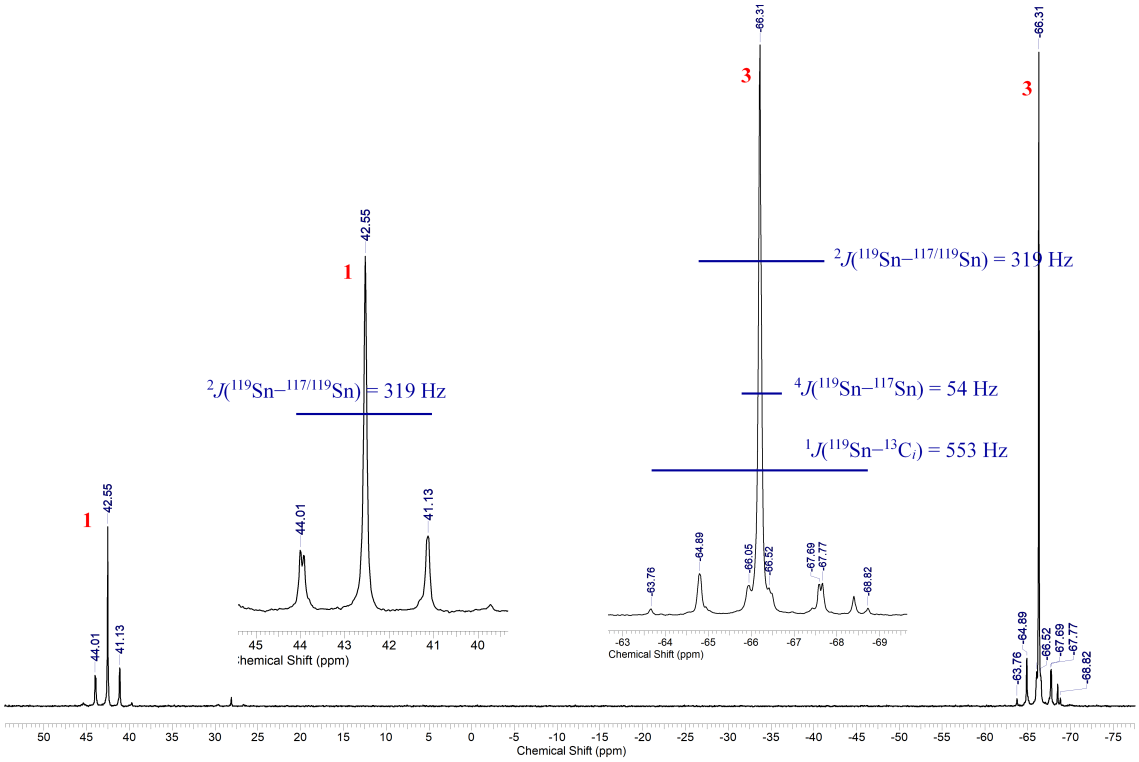

Figure 40. ^{119}Sn NMR spectrum (111.92 MHz, $CDCl_3$) of compound **4**.

In a ^{13}C NMR spectrum of 4 in $CDCl_3$, the singlet resonance referring to the ($SiCH_2Sn$) carbon atom is shown at δ 1.29 ppm [($^1J(^{13}C–^{117/119}Sn)$ = 264/277 Hz]. This value is lower-frequency shifted comparing to the corresponding reported for $MeSi(CH_2SnIPh_2)_3$ at 4.14 ppm ($^1J(^{13}C–^{117/119}Sn)$ = 253/264 Hz) and for $(IPh_2Sn_2CH_2)_2SiMe_2$ (δ 3.5 ppm) ($^1J(^{13}C–^{117/119}Sn)$ = 253/267 Hz). In the aromatic part, the chemical shifts corresponding to the carbon atoms C_m is shown at δ 128.9 ppm ($^3J(^{13}C_m–^{117/119}Sn_1)$ = 60 Hz. The singlet resonances of C_p, C_o, and C_i appear respectively at δ 130.2 ppm ($^4J(^{13}C_p–^{117/119}Sn)$ = 12 Hz), δ 135.9 ppm ($^2J(^{13}C_o–^{117/119}Sn)$ = 52Hz), and 137.0 ppm ($^1J(^{13}C_i–^{117/119}Sn_1)$ = 543/566 Hz, $^4J(^{13}C_i–^{117/119}Sn_2)$ = 10 Hz), with Sn1 being ^{gem}Sn and Sn2 being ^{ter}Sn. All these data prove that the tin atoms in compound **4** are four-coordinated with distorted tetrahedral geometries, as observed in the solid state. An ESI MS spectrum in the positive mode shows mass clusters centred at m/z 1169.0 $C_{21}H_{31}I_3O_2Sn_4^+$ (100, [M – I^- – 3 Ph^- + 3 H_2O + 4 H^+]$^+$) and 1250.9 $C_{27}H_{37}I_3O_2Sn_4^+$ (50, [M – Ph^- – I^- + 2 H_2O + 3 H^+]$^+$), respectively (See Supporting Information, Chapter 3, Figure S10- S15).

A ^{119}Sn NMR spectrum of the chlorido-substituted derivative tris(dichloridophenylstannylmethyl)chloridostannane $ClSn(CH_2SnClPh_2)_3$, **5**, in $CDCl_3$ exhibits two singlet resonances, with an integral ratio of 3:1, respectively, at δ 17 ppm (^{ter}Sn) and δ 151 ppm (^{gem}Sn). The chemical shift corresponding to the ^{ter}Sn is close to that reported for the dichloride-substituted derivative $MeSi(CH_2SnClPh_2)_3$ at δ 24 ppm

as well to those corresponding to $(ClPh_2Sn)_2CH_2$ (δ 20 ppm),[26] $(Ph_2ClSnCH_2)_2SnClPh$ (^{ter}Sn δ 20 ppm), $(Ph_2ClSnCH_2SnClPh_2)_2CH_2$ (^{ter}Sn δ 17 ppm). There are three additional unresolved resonance signals having 3 % total integral at δ –90, 38, 174 ppm. Most likely, they are referring to hydrolysis products. No further purification is realized, given the instability of such compounds toward column chromatography. Also, attempts for recrystallization of **5** failed. Therefore, this mixture is used without further purification for the subsequent reactions discussed below.

A ^{1}H NMR spectrum of compound 5 shows a singlet resonance assigned to the CH_2 protons at 1.3 ppm ($^2J(^1H-^{117/119}Sn)$ = 72 Hz) which is higher-frequency shifted in regards to that reported in $MeSi(CH_2SnClPh_2)_3$ at δ 0.96 ppm ($^2J(^1H-^{117/119}Sn)$ = 79 Hz) and those corresponding in $(ClMe_2Sn_2CH_2)_2SiMe_2$ (δ 0.18 ppm), $(ClPh_2Sn_2CH_2)_2SiMe_2$ (δ 0.79 ppm) ($^2J(^1H-^{117/119}Sn)$ = 77/80 Hz).[28] However, this shift is lower-frequency shifted, in comparison with that in compound $(ClPh_2Sn)_2CH_2$ (δ 1.54 ppm).[26] As to the complex pattern of the phenyl protons appear as complex pattern at δ 7.44-7.75 ppm with an integration of 30H (See Supporting Information, Chapter 3, Figures S.17, S18).

Table 8. Selected interatomic distances /Å and angles /°C in compounds **2** and **4**.

	2	**4**
Sn(2)–Br(10)	2.8756(8)	
Sn(3)–Br(10)	3.0349(9)	
Sn(1)–Br(4)		2.735(5)
Sn(2)–Br(4)		3.439(3)
Sn(3)–Br(9)		2.660(2)
Sn(3)–Br(11)		2.485(2)
Br(2)–Sn(1)–Br(3)	103.44(3)	
Br(1)–Sn(1)–C(1)	118.30(17)	
Br(7)–Sn(2)–Br(10)	177.74(3)	
Br(7)–Sn(2)–C(2)	94.96(17)	
C(2)–Sn(2)–Br(9)	121.33(17)	
Br(4)–Sn(3)–Br(10)	178.31(3)	
C(3)–Sn(3)–Br(4)	97.77(16)	
C(3)–Sn(3)–Br(5)	128.77(16)	
Br(5)–Sn(3)–Br(6)	106.52(3)	
Br(2)–Sn(1)–Br(4)		176.19(10)
Br(2)–Sn(1)–C(1)		95.3(5)
C(1)–Sn(1)–Br(3)		121.2(4)
Br(4)–Sn(2)–Br(5)		175.70(10)
C(2)–Sn(2)–Br(5)		103.0(5)
Br(6)–Sn(2)–Br(7)		105.83(10)
Br(9)–Sn(3)–Br(10)		175.31(8)
C(3)–Sn(3)–Br(10)		92.5(6)
C(3)–Sn(3)–Br(8)		135.0(5)

3.3 Attempts for the complexation of chloride anions via $ClSn(CH_2SnPhCl_2)_3$, 3

A ^{119}Sn NMR spectrum ($CDCl_3$) at ambient temperature of a solution of **3** in dichloromethane to which one molar equiv of [PPh_4]Cl had been added shows four resonance signals at δ –117 ppm (integral 24 %), -75 ppm (15 %), -32 ppm (36 %), to which no assignments are made, in addition to the signal resonances corresponding to the starting material at δ –28 and -54 ppm with an integration of 23 % (Figure 41).

From this reaction mixture, by addition of some iso-hexane, the organostannate complexes $(PPh_4)[CH_2(SnCl_2Ph)_2 \cdot Cl]$, **6**, and $(PPh_4)_2[Cl_2Sn(CH_2SnCl_2Ph)_2 \cdot 2Cl]$, **7**, were isolated as crystalline materials suitable for X-ray diffraction analysis. Apparently, under the given experimental conditions, compound **3** underwent a sort of fragmentation into smaller molecules (Scheme 17). Figures 42 and 43 show the molecular structures of these new complexes **6** and **7**. No further investigations in solution are made given the difficulties to characterize separately the two produced species. However, An ESI-MS mass spectrum of complexes **6** in the negative mode shows one mass cluster centered at m/z 582.8 assigned to $[CH_2(SnCl_2Ph)_2 \cdot Cl]^-$, [100, M – $(PPh_4)^+]^-$ and in the positive mode one mass cluster centred at m/z 339.1, corresponding to $[(PPh_4)^+]^+$ (See Supporting Information, Chapter 3, Figures S20- S23).

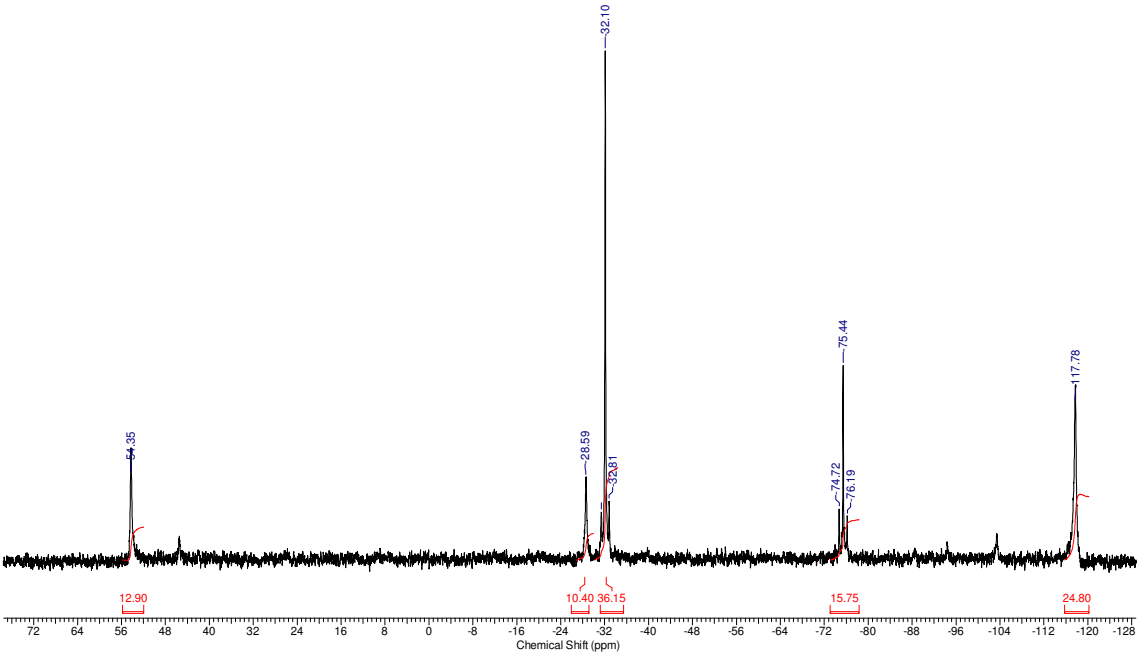

Figure 41. ^{119}Sn NMR spectrum of crude mixture of the reaction of formation of **6** and **7** at ambient temperature (149.26 MHz, $CDCl_3$).

Scheme 17. Products of the complexation attempt of the dichloride-substituted compound **3**.

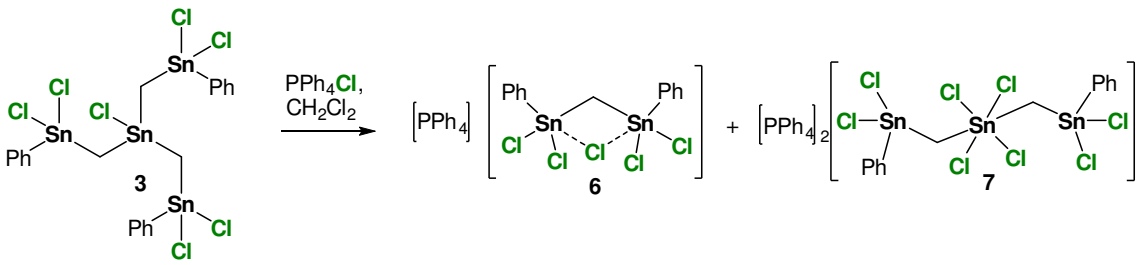

The organochlorido stannate **6** crystallizes in the triclinic space group $P-1$. Figure 42 shows its molecular structure and the figure caption contains selected interatomic distances and angles. The intermolecular binding mode of **6** shows, interestingly, a tetranuclear dimer presenting a ladder-like structure via three Sn_2Cl_2 moieties. This dimer is formed via unsymmetrical bridges (Sn1–Cl1A–Sn1A) and (Sn2–Cl1A–Sn1), in which Sn(1)–Cl(1A), Sn(1A)–Cl(1A), and Sn(2)–Cl(1A) are, respectively, distant of 3.126, 2.5450(10), and 3.763 Å. All three distances are shorter than the sum of the van der Waals radii[31] of tin (2.17 Å) and Cl (1.75 Å), and render all Sn atoms hexacoordinated exhibitng a distorted octahedral all-trans SnC2Cl4 environments with angles, respectively, at Sn(1) and Sn(2) of (C7–Sn1–C11) 155.46(15)°, (Cl1A–Sn1–Cl2) 175.685(35)°, (Cl1–Sn1–Cl5) 173.32(3)°, (C1–Sn2–Cl7) 144.16(15)°, (Cl3–Sn2–Cl5) 175.74(4)°, and (Cl1A–Sn2–Cl4) 160.165(36)°. These values are comparable to the corresponding angles in $(PPh_4)_2[HC(SnCl_2Ph)_3 \cdot 2Cl]$.[12]

There is a chelation of Cl(5) by Sn(1) and Sn(2), via an unsymmetrical intramolecular Sn–Cl–Sn bridge, with Sn(1)–Cl(5) and Sn(2)–Cl(5) distances of 2.6441(10) and 2.7750(10) Å, respectively. Therefore, there is formation of a centrosymmetric doubly intramolecularly and intermolecularly chlorido-bridged organostannate anion.

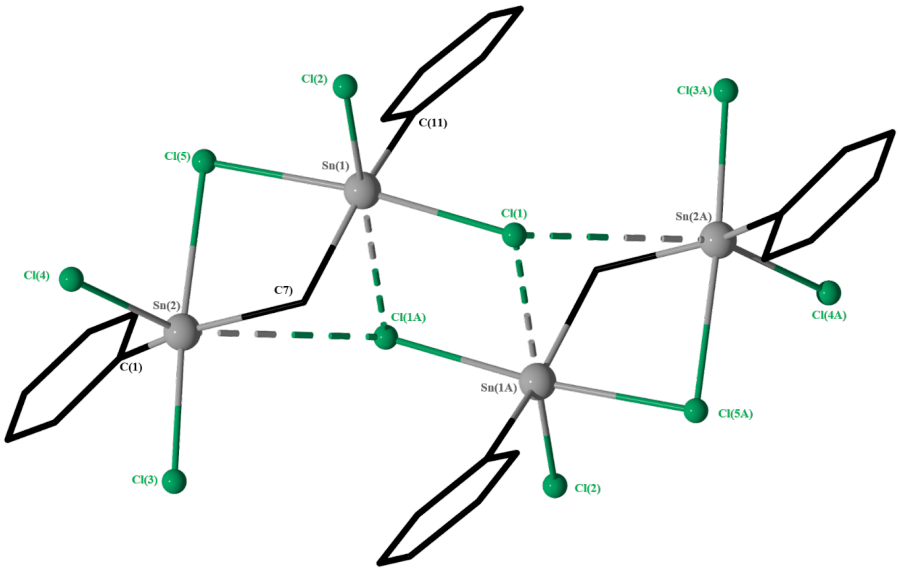

Figure 42. General view (POV-Ray) of a molecule of **6** showing crystallographic numbering scheme and the intermolecular interaction. Hydrogen atoms and the PPh_4^+ cations are omitted. Selected interatomic distances (Å): Sn(1)–Cl(1A) 3.126, Sn(1A)–Cl(1A) 2.5450(10), Sn(2)–Cl(1A) 3.763, Sn(1)–Cl(5) 2.6441(10), Sn(2)–Cl(5) 2.7750(10). Selected interatomic angles (°): C(7)–Sn(1)–C(11) 155.46(15), Cl(1A)–Sn(1)–Cl(2) 175.685(35), Cl(1)–Sn(1)–Cl(5) 173.32(3), C(1)–Sn(2)–Cl(7) 144.16(15), Cl(3)–Sn(2)–Cl(5) 175.74(4), Cl(1A)–Sn(2)–Cl(4) 160.165(36).

Complex **7** crystallizes in the triclinic space group $P-1$. Figure 43 shows its molecular structure and the figure caption contains selected interatomic distances and angles. The molecular structure of 7 shows an overall perfect symmetry with intramolecular symmetrical chloride interactions by Sn(2), in which the Sn(2)–Cl(3) (2.564(11) Å) and Sn(2)–Cl(4) (2.5609(12) Å) distances are almost equal. The Sn(1)–Cl(1) and Sn(1)–Cl(2) distances of 2.3968(13) and 2.4119(12) Å, respectively, are almost equal.

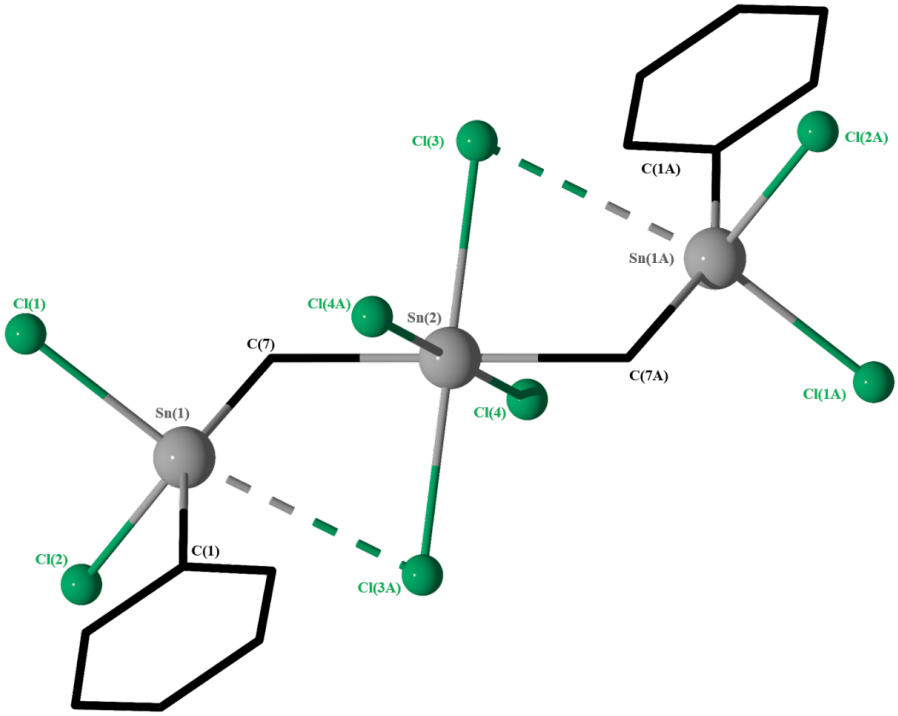

Figure 43. General view (POV-Ray) of a molecule of **7** showing the crystallographic numbering scheme. Hydrogen atoms and the PPh_4^+ cations are omitted. Selected interatomic distances (Å): Sn(1)–Cl(1) 2.3968(13), Sn(1)–Cl(2) 2.4119(12), Sn(1)–Cl(3A) 3.109, Sn(2)–Cl(3) 2.564(11), Sn(2)–Cl(4) 2.5609(12). Selected interatomic angles (°): Cl(2)–Sn(1)–Cl(1) 97.98(5), Cl(1)–Sn(1)–C(7) 102.26(14), C(1)–Sn(1)–C(7) 152.03(17), C(7)–Sn(1)–Cl(2) 97.41(13), C(7)–Sn(2)–C(7A) 180.00(18), Cl(3)–Sn(2)–Cl(3A) 180.0, Cl(4)–Sn(2)–Cl(4A) 180.0.

The Sn(2) center is hexacoordinated by four chlorine (Cl3, Cl3A, Cl4, Cl4A) and two carbon atoms (C7, C7A) and shows a octahedral all-trans SnC_2Cl_4 environment with C(7)–Sn(2)–C(7A), Cl(3)–Sn(2)–Cl(3A), and Cl(4)–Sn(2)–Cl(4A) angles of 180.0°.

Sn(1) and Sn(1A) display distorted tetrahedral environments, with angles varying between 97.98(5)° (Cl2–Sn1–Cl1) and 102.26(14)° (Cl1–Sn1–C7). This distortion from the theoretic geometry is due to the Cl(3) and Cl(3A) atoms intramolecularly and symmetrically approaching Sn(1) and Sn(1A) at distance of 3.109 Å. These bond distances are shorter

than the sum of the van der Waals radii[31] of tin (2.17 Å) and Cl (1.75 Å), and render the corresponding atoms [4+1]-coordinated. The geometrical goodness $\Delta\Sigma(\theta)$[22] at Sn(1) and Sn(1A) is equal to 49.3°, with C(1), Cl(2), and C(7) occupying the equatorial positions and Cl(1) and Cl(3A) occupying the axial positions.

A ^{119}Sn NMR spectrum ($CDCl_3$) at ambient temperature of compound **3** to which had been added four molar equiv of PPh_4Cl, displays as well four resonances at δ –250 ppm (16 %), -179 ppm (23 %), -141 ppm (40 %), and -59 ppm (19 %), to which no assignment is made (See Supporting Information, Chapter 3, Figure S26). Further investigation in solution could not be done given the difficulties to characterize complex **8** separately in presence of other fragmentation products. Complex $(PPh_4)_2[CH_2(SnCl_2Ph)_2 \cdot 2Cl]$, **8**, (Scheme 18) was isolated as single crystalline material suitable for X-ray diffraction studies, from a solution of diethyl-ether/dichloromethane. Figure 44 shows the molecular structure of complex **8** and the figure caption contains selected interatomic distances and angles. However, given the lack of material no further investigations of **8** in solution were performed.

Scheme 18. Complex **8** as a product of the complexation attempt of the dichloride-substituted compound **3**.

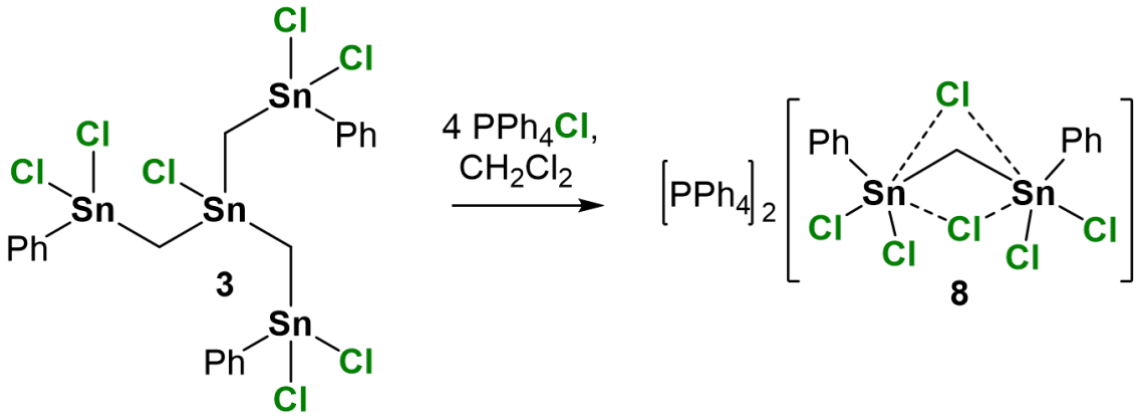

The organochloridostannate complex **8** crystallizes, as its water solvate $\mathbf{8} \cdot 0.5H_2O$, in the monoclinic space group $P2_1/n$ with two independent molecules in the unit cell. The geometric parameters of both molecules resemble each other and only the structure of the molecule containing Sn(1)- Sn(2) is discussed in detail. Figure 44 shows its molecular structure and the figure caption contains selected interatomic distances and angles. It consists of a centrosymmetric doubly intramolecular chloride bridges, in which each tin is substituted with four chlorine atoms, via chelation of Cl(5) and Cl(6) by Sn(1) and Sn(2), with bond distances of, respectively 2.9897(12) Å (Sn1–Cl5), 2.7940(11) Å (Sn1–Cl6), 2.8286(11) Å (Sn2–Cl5), and 2.7255(11) Å (Sn2–Cl6).

Sn(1) and Sn(2) centers are hexa-coordinated, exhibiting distorted octahedral all-trans SnC_2Cl_4 environments with C(1)–Sn(1)–C(11), C(1)–Sn(2)–C(21), Cl(1)–Sn(1)–Cl(6), Cl(2)–Sn(1)–Cl(5), Cl(4)–Sn(2)–Cl(6), and Cl(3)–Sn(2)–Cl(5), angles of 158.44(13)°, 163.26(13)°, 171.83(5)°, 169.483(42)°, 176.118(39)°, 168.94(4)°, respectively. The Sn–Cl distances involving the non-bridging Cl atoms vary between 2.4129(39) Å (Sn1–Cl2) and 2.4874(12) Å (Sn2–Cl4). There is an intermolecular interaction between a half molecule of water and one anion of 8 at Cl(10)···H(1)O(1L) and Cl(11)···H(2)O(1L) distant, respectively, of 2.680 and 2.791 Å.

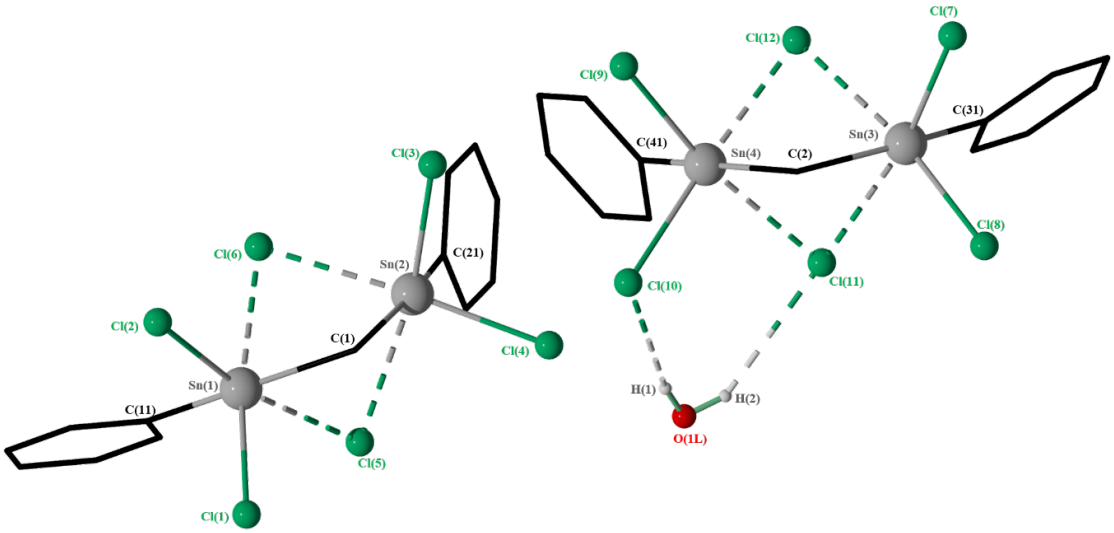

Figure 44. General view (POV-Ray) of a molecule of $\mathbf{8}\cdot 0.5\,H_2O$ showing crystallographic numbering scheme. Hydrogen atoms and the PPh_4^+ cations are omitted. Selected interatomic distances (Å): Sn(1)–Cl(2) 2.4129(39), Sn(1)–Cl(5) 2.9897(12), Sn(1)–Cl(6) 2.7940(11), Sn(2)–Cl(4) 2.4874(12), Sn(2)–Cl(5) 2.8286(11), Sn(2)–Cl(6) 2.7255(11), Cl(10)–H(1)O(1L) 2.680, Cl(11)–H(2)O(1L) 2.791. Selected interatomic angles (°): C(1)–Sn(1)–C(11) 158.44(13), Cl(1)–Sn(1)–Cl(6) 171.83(5), Cl(2)–Sn(1)–Cl(5) 169.483(42), C(1)–Sn(2)–C(21) 163.26(13), Cl(4)–Sn(2)–Cl(6) 176.118(39), and Cl(3)–Sn(2)–Cl(5) 168.94(4).

A ^{119}Sn NMR spectrum of a solution of compound **3** in $CDCl_3$ to which had been added one molar equiv of pyridinium chloride shows five resonances at δ –95 ppm (7.5 %), -28 ppm (29.4 %), -5 ppm (37 %), 46 ppm (6 %), and 56 ppm (20 %) to which no assignment is made (See Supporting Information, Chapter 3, Figure S29). From this reaction mixture, after addition of some diethyl ether, the organostannate complex $(C_5H_6N)_2[CH_2(SnCl_2Ph)_2\cdot 2Cl]$, **9**, (Figure 45) was obtained as a colourless crystalline material suitable for X-Ray diffraction analysis. Apparently, chloride anion caused Sn–C bond cleavage and phenyl group migration under the given experimental conditions (Scheme 19). However, we succeeded to have a ^{119}Sn NMR spectrum of **9** in $CDCl_3$,

showing a broad resonance signal at δ –30 ppm, $W_{1/2}$ = 200 Hz. An ESI-MS mass spectrum of complex 9 in the positive mode shows one mass cluster centered at m/z 841.1 assigned to $C_{25}H_{33}Cl_6N_3OSn_2^+$, [60, M + CH_3CN + H_2O + H^+]$^+$. (See Supporting Information, Chapter 3, Figures S30, S31)

Scheme 19. Reaction of compound **3** with one molar equiv pyridinium chloride giving organochloridostannate complex **9** as the only isolated material.

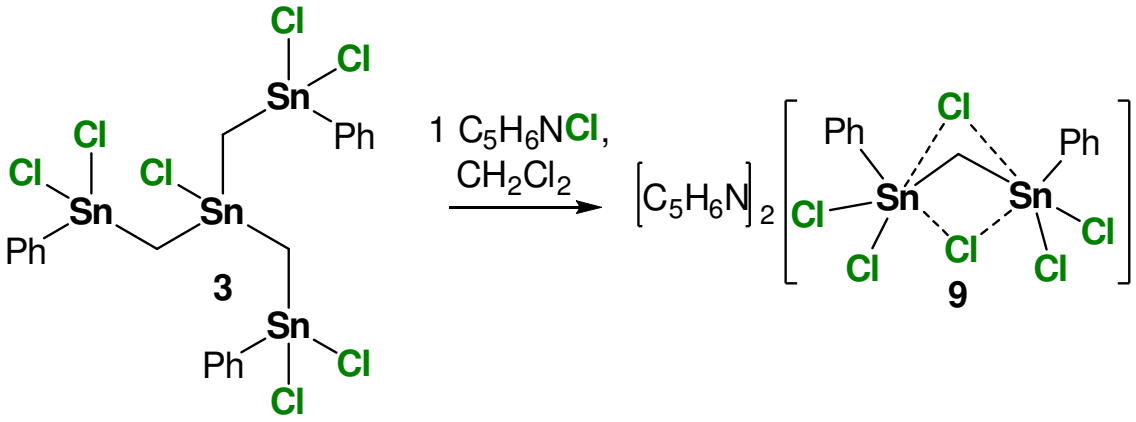

The organochloridostannate complex **9** crystallizes in the monoclinic space group $P2_1/n$. Figure 37 shows its molecular structure and the figure caption contains selected interatomic distances and angles. The structure of **9** resembles that of **8**·0.5 H_2O with the difference that the two pyridinium cations are involved in hydrogen bridges with the chlorine atoms of the stannate anion at H(21)–Cl(4), H(21)–Cl(6), and H(31)–Cl(6) distances of 2.782, 2.440, and 2.437 Å, respectively. The Sn(1)–Cl(5), Sn(2)–Cl(5), Sn(1)–Cl(6), and Sn(2)–Cl(6) distances are 2.9106(13), 2.6835(12), 3.3223(14), and 2.7304(11) Å, respectively. Sn(1) and Sn(2) centers are hexa-coordinated, exhibiting distorted octahedral all-trans SnC_2Cl_4 environments with C(1)–Sn(1)–C(7), C(7)–Sn(2)–C(11), Cl(1)–Sn(1)–Cl(6), Cl(2)–Sn(1)–Cl(5), Cl(4)–Sn(2)–Cl(5), and Cl(3)–Sn(2)–Cl(6), angles of 148.1(2), 170.12(16), 160.31(4), 171.03(4), 171.394(39), and 173.88(4)°.

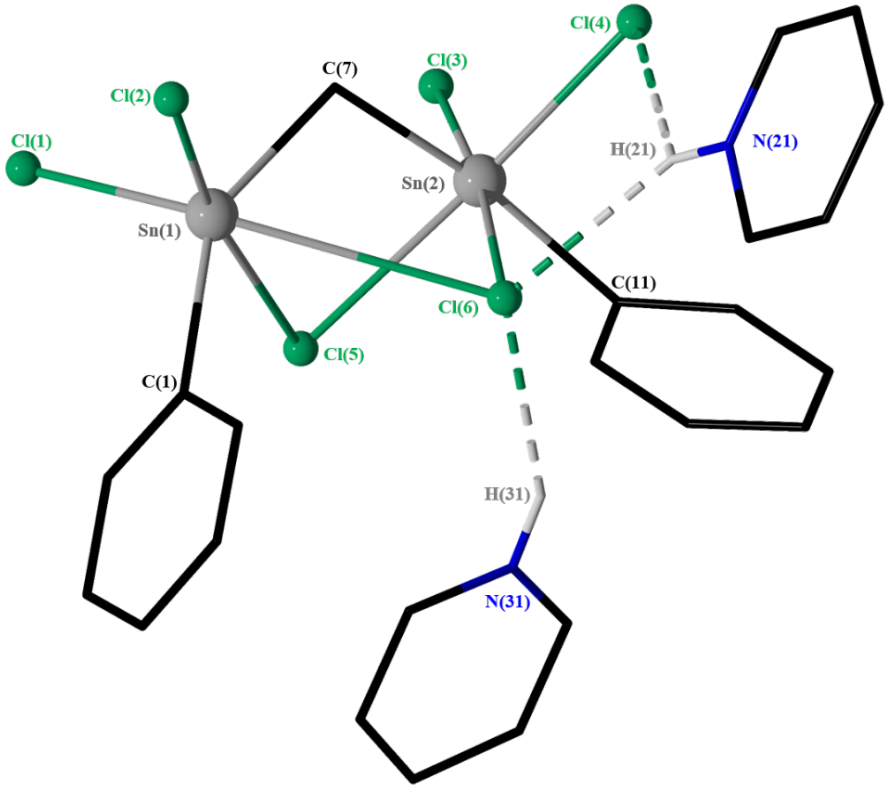

Figure 45. General view (POV-Ray) of a molecule of **9** showing crystallographic numbering scheme and NH···Cl intramolecular interactions with the pyridinium cations. Selected interatomic distances (Å): Sn(1)–Cl(5) 2.9106(13), Sn(2)–Cl(5) 2.6835(12), Sn(1)–Cl(6) 3.3223(14), Sn(2)–Cl(6) 2.7304(11), N(21)H(21)–Cl(4) 2.782, N(21)H(21)–Cl(6) 2.440, and N(31)H(31)–Cl(6) 2.437. Selected interatomic angles (°): C(1)–Sn(1)–C(7) 148.1(2), Cl(1)–Sn(1)–Cl(6) 160.31(4), Cl(2)–Sn(1)–Cl(5) 171.03(4), C(7)–Sn(2)–C(11) 170.12(16), Cl(4)–Sn(2)–Cl(5) 171.394(39), and Cl(3)–Sn(2)–Cl(6) 173.88(4).

3.4 Conclusion

Despite the similarity between MeSi($CH_2SnR_{(3-n)}X_n$)$_3$, (n = 0– 3; X = I, F, Cl, Br; R = Ph, CH_2SiMe_3) and R'Sn($CH_2SnR_{(3-n)}X_n$)$_3$, (n = 0– 2; X = I, Cl; R = Ph, R' = R, X), the latter compounds show unexpected reactivity towards chloride anions. The chloride anions induce Sn–C bond cleavage and phenyl group migration. Di- and trinuclear organochloridostannate complexes were isolated, but no tetranuclear such complexes. Further studies are needed to get deeper inside into this type of reactivity. Within the time frame of this PhD, further studies could not be performed.

3.5 Experimental section

- **Synthesis of $PhSn(CH_2SnPh_3)_3$ (2)**

A solution of $SnPhCl_3$ (1.04 g, 3.44 mmol, 0.9 equiv) in THF (50 mL) was added dropwise to a solution of Ph_3SnCH_2MgBr (**1**),[38] prepared from Ph_3SnCH_2Br (5.09 g, 11.46 mmol, 3 equiv) and magnesium (0.324 g, 13.37 mmol, 3.5 equiv) in THF (40 mL), for a period of 1h. After the addition had been completed, the reaction mixture was heated to reflux overnight and then cooled to room temperature. THF was distilled off under reduced pressure; then cold water (50 mL) was added, and the mixture was extracted three times with 100 mL diethyl ether. The combined organic phases were dried over MgSO4 and the solvents removed under reduced pressure, giving **2** as a white solid (4.8 g, 3.72 mmol, 97 %). Further purification was achieved by recrystallization from CH_2Cl_2/ *iso*-hexane to give transparent needles with a mp of 152 °C.

^{1}H NMR (C_6D_6, 400.25, 298 K): δ 0.43 ppm (s, 6H, $^2J(^1H-^{117/119}Sn)$ = 61 Hz, $Sn_1CH_2Sn_2$), 6.97- 7.63 ppm (complex pattern, 50H, Ph). $^{13}C\{^1H\}$ NMR ($CDCl_3$, 100.64, 298 K): δ 1.35 ppm ($^1J(^{13}C-^{117/119}Sn)$ = 275 Hz, CH_2Sn), 128.9 ppm ($^3J(^{13}C_m-^{117/119}Sn_1)$ = 61 Hz, $^5J(^{13}C_m-^{117/119}Sn_2)$ = 18 Hz, C_m), 130.2 ppm ($^4J(^{13}C_p-^{117/119}Sn)$ = 14 Hz, C_p), 135.9 ppm ($^2J(^{13}C_o-^{117/119}Sn)$ = 50 Hz, Co), 137.0 ppm (Ci). ^{119}Sn NMR ($CDCl_3$, 149.26, 298 K): δ –73 ppm (3Sn, $^4J(^{119}Sn-^{117}Sn)$ = 44 Hz, $^2J(^{119}Sn-^{117/119}Sn)$ = 245/257 Hz, $^1J(^{119}Sn-^{13}C_i)$ = 504 Hz, Sn2), -34 ppm (1Sn, $^2J(^{119}Sn-^{117/119}Sn)$ = 245/257 Hz, Sn1). Anal. Calcd (%) for $C_{63}H_{56}Sn_4$: C 58.75, H 4.38. Found: C 58.4, H 4.4. Electrospray MS: m/z (%) positive mode 923.1 $C_{44}H_{40}Sn_3^+$ (60, $[M-(CH_2SnPh_3]^+$), 1310.5 (10, $[M+\frac{1}{2}H_2O+H_2O]^+$).

- **Synthesis of $ClSn(CH_2SnPhCl_2)_3$ (3)**

To a solution of **2** (0.831 g, 0.645 mmol, 1 equiv) in CH_2Cl_2 (40 mL) was added excess of HCl solution in diethyl ether (2 M) (0.176 g, 4.84 mmol, 7.5 equiv). The resulting mixture was stirred at 0 °C overnight. Solvents were evaporated in vacuo (10^{-3} mmHg) to afford a yellowish oily substance in 60 % yield (0.385 g, 386 µmol). No purification by column chromatography could be realized given the instability of such compounds. No crystalline material was isolated.

^{1}H NMR ($CDCl_3$, 400.25, 298 K): δ 2.11 ppm (s, 6H, $^2J(^1H-^{117/119}Sn)$ = 72 Hz, $Sn_1CH_2Sn_2$), 7.42- 7.86 ppm (complex pattern, 15H, Ph). ^{119}Sn NMR ($CDCl_3$, 111.92, 298 K): δ 26 ppm (3Sn, Sn2), 54 ppm (1Sn, Sn1).

- **Synthesis of $ISn(CH_2SnPh_2I)_3$ (4)**

Over a period of 5h, elemental iodine (3.67 g, 14.47 mmol, 3.9 equiv) was added in small portions at 0 °C to a stirred solution of **2** (4.78 g, 3.71 mmol, 1 equiv) in dichloromethane. The stirring was continued and the reaction mixture was warmed to room temperature overnight. Dichloromethane and iodobenzene were removed in vacuo (10^{-3} mmHg) to afford a slightly yellow oil in 95 % yield (5.24 g, 3.52 mmol). Further purification was realized by recrystallization from dichloromethane/ *iso*-hexane to give slightly yellow needles with a mp of 175 °C.

^{1}H NMR ($CDCl_3$, 300.13, 298 K): δ 1.52 ppm (s, 6H, $^2J(^1H-^{117/119}Sn)$ = 61 Hz, $Sn_1CH_2Sn_2$), 7.39- 7.68 ppm (complex pattern, 30H, Ph). $^{13}C\{^1H\}$ NMR ($CDCl_3$, 75.47, 298 K): δ 1.29 ppm ($^1J(^{13}C-^{117/119}Sn)$ = 264/277 Hz, CH2Sn), 128.9 ppm ($^3J(^{13}C_m-^{117/119}Sn_1)$ = 60 Hz, C_m), 130.2 ppm ($^4J(^{13}C_p-^{117/119}Sn)$ = 12 Hz, C_p), 135.9 ppm ($^2J(^{13}C_o-^{117/119}Sn)$ = 52 Hz, C_o), 137.0 ppm ($^1J(^{13}C_i-^{117/119}Sn_1)$ = 543/566 Hz, $^4J(^{13}C_i-^{117/119}Sn_2)$ = 10 Hz, C_i). ^{119}Sn NMR ($CDCl_3$, 149.26, 298 K): δ –66 ppm (3Sn, $^4J(^{119}Sn-^{117}Sn)$ = 54 Hz, $^2J(^{119}Sn-^{117/119}Sn)$ = 319 Hz, $^1J(^{119}Sn-^{13}C_i)$ = 553 Hz, Sn2), 42 ppm (1Sn, $^2J(^{119}Sn-^{117/119}Sn)$ = 319 Hz, Sn1). Anal. Calcd (%) for $C_{39}H_{36}I_4Sn_4$: C 31.5, H 2.44. Found: C 31.4, H 2.5. Electrospray MS: m/z (%) positive mode 1169.0 $C_{21}H_{31}I_3O_2Sn_4^+$ (100, $[M - I^- - 3Ph^- + 3H_2O + 4H^+]^+$), 1250.9 $C_{27}H_{37}I_3O_2Sn_4^+$ (50, $[M - Ph^- - I^- + 2H_2O + 3H^+]^+$).

- **Synthesis of $ClSn(CH_2SnPh_2Cl)_3$ (5)**

To a solution of **4** (0.416 g, 0.280 mmol) in CH_2Cl_2 (40 mL) was added excess of silver chloride (0.16 g, 1.12 mmol). The resulting mixture was stirred at room temperature in the dark for 14 days. The formed AgI and the non-reacted AgCl was removed by filtration. The CH_2Cl_2 of the filtrate was evaporated in vacuo (10^{-3} mmHg) to afford a yellowish oily substance in 70 % yield (0.219 g, 0.195 mmol). No purification by column chromatography could be realized given the instability of such compounds. No crystalline material was isolated.

^{1}H NMR ($CDCl_3$, 300.13, 298 K): δ 1.3 ppm (s, 6H, $^2J(^1H-^{117/119}Sn)$ = 72 Hz, $Sn_1CH_2Sn_2$), 7.44- 7.75 ppm (complex pattern, 30H, Ph). ^{119}Sn NMR ($CDCl_3$, 111.92, 298 K): δ 17 ppm (3Sn, Sn2), 151 ppm (1Sn, Sn1).

Complexation studies

- **Formation of $(PPh_4)[CH_2(SnCl_2Ph)_2 \cdot Cl]$ (6), and $(PPh_4)_2[Cl_2Sn(CH_2SnCl_2Ph)_2 \cdot 2Cl]$ (7)**

Tetraphenylphosphonium chloride (21.44 mg, 0.057 mmol) is added to a solution of 3 (57 mg, 0.057 mmol) in 20 mL CH_2Cl_2 and the mixture is stirred at room temperature overnight. The solvent is evacuated to afford a white solid. Re-crystallization from

dichloromethane/ *iso*-hexane give two types of colourless crystals 6 and 7 as fragmentation products.

^{119}Sn NMR ($CDCl_3$, 149.26, 298 K): (crude mixture) δ 117 ppm (24 %), -75 ppm (15 %), -32 ppm (36 %), and the starting material 3: δ –28 and -54 ppm (23 %). Electrospray MS for 6: m/z (%) negative mode 582.8 $[CH_2(SnCl_2Ph)_2 \cdot Cl]^-$ (100,[M – $(PPh_4)^+]^-$), m/z (%) positive mode 339.1 (100, PPh_4^+). Anal. Calcd (%) for **6**: $C_{37}H_{34}Cl_5PSn_2$ + 2 H_2O: C 46.28, H 3.99. Found: C 46.2, H 3.7. Anal. Calcd (%) for **7**: $C_{62}H_{55}Cl_8P_2Sn_3$ + H_2O + CH_2Cl_2: C 47.15, H 3.71. Found: C 47.3, H 3.6. No further investigations could be realized within the time frame of this PhD, given the luck of material and the difficulties to separate.

- **Formation of $(PPh_4)_2[CH_2(SnCl_2Ph)_2 \cdot 2Cl]$ (8)**

Tetraphenylphosphonium chloride (58.69 mg, 0.156 mmol) is added to a solution of **3** (39 mg, 0.039 mmol) in 20 mL CH_2Cl_2 and the mixture is stirred at room temperature overnight. The solvent is evacuated to afford a white solid. Re-crystallization from dichloromethane/ diethyl-ether give colourless crystals **8** as fragmentation product.

^{119}Sn NMR ($CDCl_3$, 149.26, 298 K): (crude mixture) δ –250 ppm (16 %), -179 ppm (23 %), -141 ppm (40 %), and -59 ppm (19 %). Anal. Calcd (%) for: $C_{61}H_{55}Cl_6P_2Sn_2$ + 2 H_2O: C 54.8, H 4.4. Found: C 54.8, H 4.1. No further investigations could be realized within the time frame of this PhD, given the luck of material and the difficulties to separate different fragmentation products.

- **Formation of $(C_5H_6N)_2[CH_2(SnCl_2Ph)_2 \cdot 2Cl]$ (9)**

Pyridinium chloride (7.42 mg, 0.064 mmol) is added to a solution of **3** (64 mg, 0.064 mmol) in 20 mL CH_2Cl_2 and the mixture is stirred at room temperature overnight. The solvent is evacuated to afford a white solid. Re-crystallization from dichloromethane/ diethyl-ether give colourless crystals 9 as fragmentation product.

^{119}Sn NMR ($CDCl_3$, 149.26, 298 K): (crude mixture) δ –95 ppm (7.5 %), -28 ppm (29.4 %), -5 ppm (37 %), 46 ppm (6 %), and 56 ppm (20 %). ^{119}Sn NMR ($CDCl_3$, 149.26, 298 K): δ –30 ppm ($W_{1/2}$ = 200 Hz). Electrospray MS: m/z (%) positive mode 841.1 $C_{25}H_{33}Cl_6N_3OSn_2^+$ [60, M + CH_3CN + H_2O + $H^+]^+$. Anal. Calcd (%) for: $C_{23}H_{27}Cl_6N_2Sn_2$ + H_2O: C 34.55, H 3.66. N 3.5 Found: C 34.5, H 3.9, N 3.8. No further investigations could be realized within the time frame of this PhD.

4. $MeSi(CH_2SnR_{(3-n)}X_n)_3$ (n = 0– 3; X = I, Cl, Br; R = Ph , CH_2SiMe_3) as Precursors for Unprecedented Diorganotin Oxo Clusters and Adamantane-like Structures

4.1 Introduction

Over the last decade, we witnessed the global growing interest for the studying of macrocycles containing transition-metal group elements versus a luck of such supramolecular architectures either as macrocycles or coordination polymers presenting in their skeletons main[39]group elements, especially Tin (II) and Tin (IV) compounds. So far such macrocycles and extended network structures have been reported only for a limited number, and most of them are triorganotin derivatives. This is explained by the requirement of a subtle balance of electronic and steric effects of the organic groups attached to the tin and ligand moieties.[40]

It is common knowledge that the complete replacement of the electronegative substituents X in diorganotin compounds of type R_2SnX_2 (X = halogen, alkoxide, carboxylate) with oxide dianion gives the corresponding diorganotin oxides $(R_2SnO)_n$. Depending on the identity of the organic substituents R, these oxides can either be polymeric (type **I**, n = ∞),[41] trimeric (type **II**, n = 3)[23,42,43] or even dimeric (type **III**, n = 3) (Chart 2).[39,44] Sterically less demanding organic substituents such as *n*-alkyl or phenyl give polymers which, as a result of intermolecular O→Sn interactions making the tin atoms five-or even six-coordinate, are almost insoluble in common organic solvents. Increasing the steric bulk of the organic substituents enables the formation of six- or even four-membered rings in which the tin atoms are four-coordinate. The same principle holds for the formation of the molecular diorganotin oxides of types **IIa** (in which two parallel six-membered Sn_3O_3 rings are linked to each other by three organic spacers),[43] **IV** (adamantane-type structure),[19] and **V** (the only chrystallographically characterized diorganotin oxide containing an eight-membered Sn_4O_4 ring).[19] More recently, intramolecular N→Sn or P = O →Sn coordination proved to be alternatives to steric bulk for the stabilization of type **III** diorganotin oxides. (Chart 2).[44,45]

Herein, we report that even diorganotin compounds containing sterically less-crowded substituents (Ph, Me_3SiCH_2) but having a particular tripod architechture compounds $MeSi(CH_2SnR_{(3-n)}X_n)_3$ give a new serie of ladder-containing oxo clusters, among which

cyclic polynuclear molecular diorganotin oxides of unprecedented large sizes in which the tin atoms adopt the coordination number five. These are the two first and longest simple ladder- containing macrocycles with 18 and 30 Tin centers, linked to each other through planar Sn_2-O_2 rings and assembled without linking bridges, as it is known in literature for such polymeric structures.[46] There is also formation of first S- and Se-containing adamantane-type structures, in which both organosilicon and organotin moieties are present. The numbering of compounds in this Chapter follows consecutively the numbering in chapter 2.

Chart 2. Different types of diorganotin oxides.[45]

$(R_2SnO)_n$

I: R = Me, Et, *n*-Bu, Ph...; n = ∞

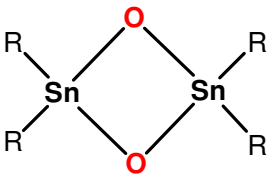

III: R = R' = $CH(SiMe_3)_2$,
R = {2,6-P(O)(O *i*-Pr)$_2$}$_2$-4-*t*-BuC_6H_2, R' = Et,
R = 2,6-$(Me_2NCH_2)_2C_6H_3$, R' = *n*-Bu;

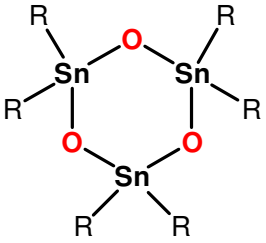

II: R = *t*-Bu,Me_3SiCH_2,$CEtMe_2$,
$CSiMe_3$/Me,2,6-Me_2-C_6H_3,
2,6-Et_2-C_6H_3,2,4,6-$(CF_3)_3$-C_6H_2,
2,4,6-*i*-Pr-C_6H_2;

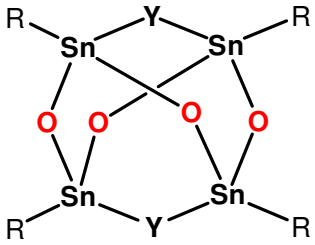

IV: R = $CH(SiMe_3)_2$; Y = CMe_2, $(CH_2)_2$

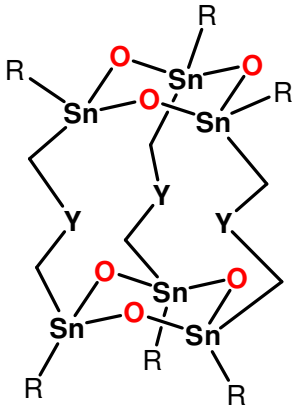

IIa: Y = $C_6H_4(SiMe_2CH_2)_2$-1,4;
R = $CH(SiMe_3)_2$

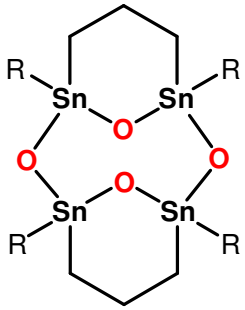

V: R = $CH(SiMe_3)_2$

$[MeSi(CH_2SnRO)_3]_n$

VI: R = Ph, n = 6; R = CH_2SiMe_3, n = 10,
(this work)

4.2 New ladder-type containing diorganotin oxo-clusters

A ^{119}Sn NMR of the crude mixture resulting from a reaction of the organotin hexachlorido derivative MeSi($CH_2SnPhCl_2$)$_3$, **4**, with one molar equiv di-tert-butyltin oxide (t-Bu_2SnO)$_3$ in $CDCl_3$, shows resonances from δ –331 ppm to -54 ppm, with six major signals at δ –230 (5 %), -201 (6 %), -192 (6 %), -117 (4 %), -100.6 (7 %), and 54 ppm (44 %). The latter signal refers to the by-product t-$BuSnCl_2$. There are also minor signals appearing from δ –331 to –100.3, with integrations varying between 0.3-1.2 %. (See Supporting Information Chapter 4, Figure S7) After several washings with *iso*-hexane of the white residue resulting from the reaction mixture after the solvent had been evaporated in vacuo, and recrystallization from dichloromethane/*iso*-hexane gives compound **26**, [(MeSi(CH_2)$_3$)Sn(μ_3-O)$_3$(Ph)Sn(Cl)(Ph)Sn(μ_2-OH)(Ph)Sn(t–Bu)$_2$]$_2$, (Scheme 20) as colourless crystals suitable for X-Ray diffraction study.

Scheme 20. Synthesis of the octanuclear ladder-like oxocluster **26**.

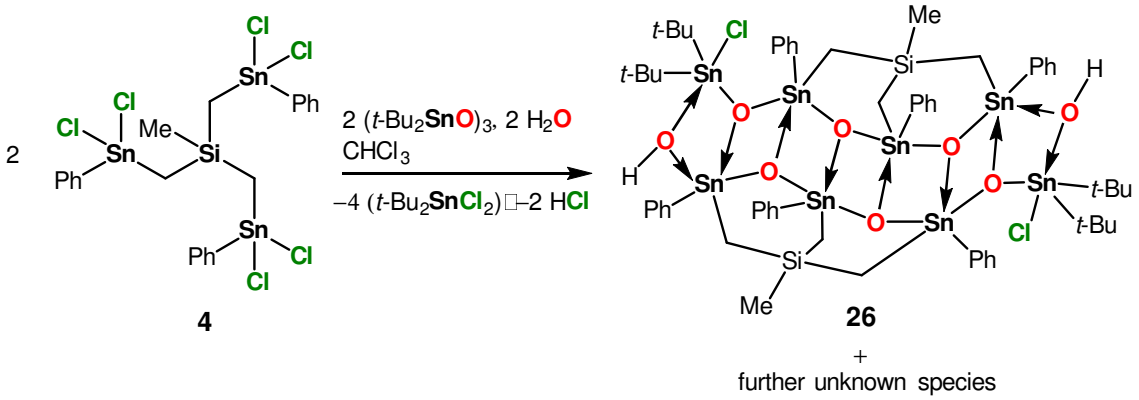

The molecular structure of **26** is shown in Figure 46, selected interatomic distances and angles are listed in the figure caption. It shows a centrosymmetric dimer containing four crystallographically independent tin atoms (Sn1, Sn2, Sn3 and Sn4), (Figures 46, 49). The ladder-like structure consists of four 6-membered-rings (Si–C–Sn–O–Sn–C) and seven 4-membered Sn_2O_2-rings.

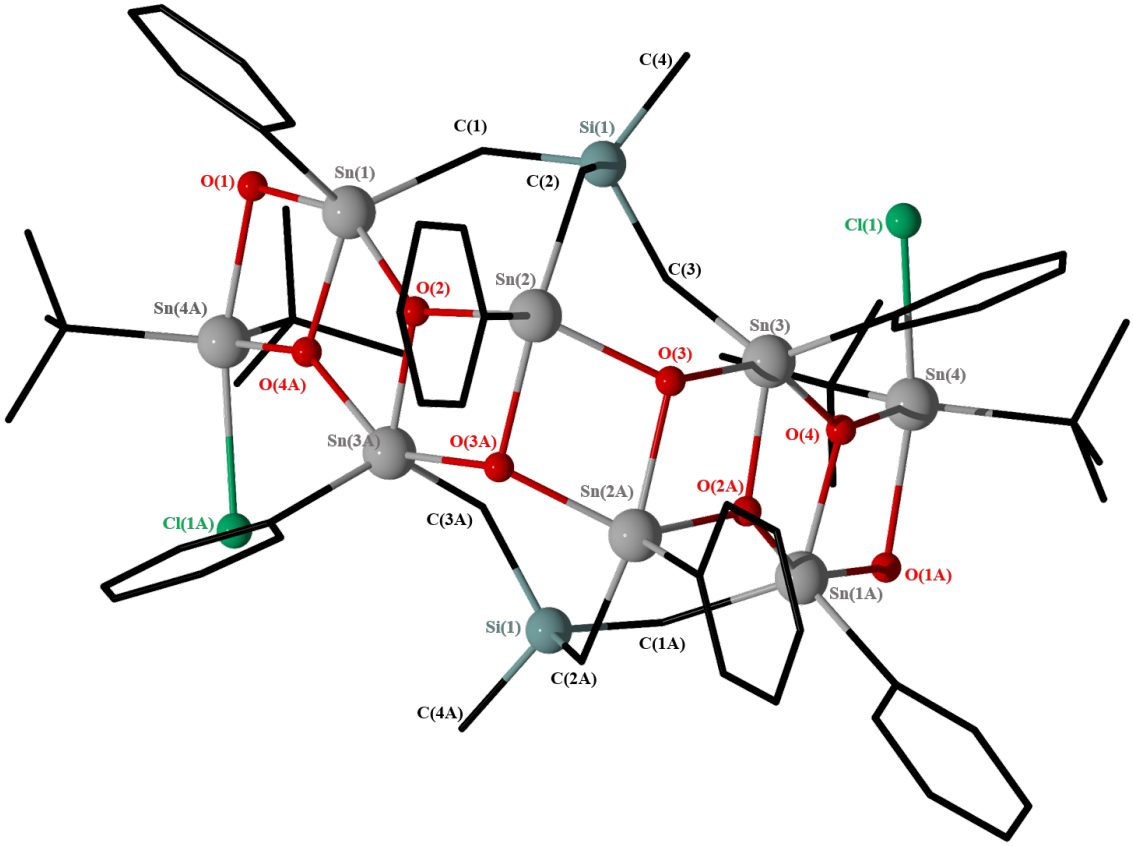

Figure 46. POV-Ray image of the molecular structure of $[(MeSi(CH_2)_3)Sn(\mu_3\text{-}O)_3(Ph)Sn(Cl)(Ph)Sn(\mu_2\text{-}OH)(Ph)Sn(t\text{-}Bu)_2]_2$, **26**. The proton at the oxygen atom O1 was not found on the electron density map. Selected interatomic distances (Å): Sn(1)–O(1) 2.140(4), Sn(4A)–O(1) 2.220(5), Sn(2)–O(2) 2.078(4), Sn(3A)–O(2) 2.036(5), Si(1)–C(1) 1.879(7), Si(1)–C(2) 1.858(7), Si(1)–C(3) 1.855(7), C(1)–Sn(1) 2.126(7), C(2)–Sn(2) 2.154(7), C(3)–Sn(3) 2.121(7). Selected interatomic angles (°): O(4A)–Sn(1)–O(2) 75.02(17), O(4A)–Sn(1)–C(11) 121.9(2), O(2)–Sn(1)–C(11) 98.0(2), O(4A)–Sn(1)–C(1) 117.9(2), O(2)–Sn(1)–C(1) 97.8(2), C(11)–Sn(1)–C(1) 120.2(3), O(3)–Sn(2)–O(3A) 76.20(19), O(3)–Sn(2)–C(21) 116.1(2), O(3A)–Sn(2)–C(21) 95.8(2), O(3)–Sn(2)–C(2) 94.2(2), O(3A)–Sn(2)–C(2) 150.4(2), O(21)–Sn(2)–C(2) 113.5(3), O(2)–Sn(3A)–C(3A) 117.1(3), O(2)–Sn(3A)–C(31A) 112.0(2), C(3A)–Sn(3A)–C(31A) 130.9(3), O(2)–Sn(3A)–O(3A) 74.63(18), C(3A)–Sn(3A)–O(3A) 95.6(2), C(31A)–Sn(3A)–O(3A) 96.8(2), O(4A)–Sn(4A)–C(45A) 114.2(2), O(4A)–Sn(4A)–C(41A) 121.7(2), C(45A)–Sn(4A)–C(41A) 123.2(3), O(4A)–Sn(4A)–O(1) 73.69(17), C(45A)–Sn(4A)–O(1) 92.4(2), C(41A)–Sn(4A)–O(1) 94.0(2), Si(1)–C(1)–Sn(1) 120.1(3), Si(1)–C(2)–Sn(2) 113.5(3), Si(1)–C(3)–Sn(3) 121.2(4).

Both the endo-cyclic and exo-cyclic tin atoms exhibit a distorted trigonal bipyramidal environment with the equatorial positions being occupied by two carbon atoms and one

oxygen atom [C(1), C(11), O(4A) for Sn(1)], [C(2), C(21), O(3A) for Sn(2)], [C(3A), C(31A), O(2) for Sn(3A)], and [C(41A), C(45A), O(4A) for Sn(4A)] (Figure 47).

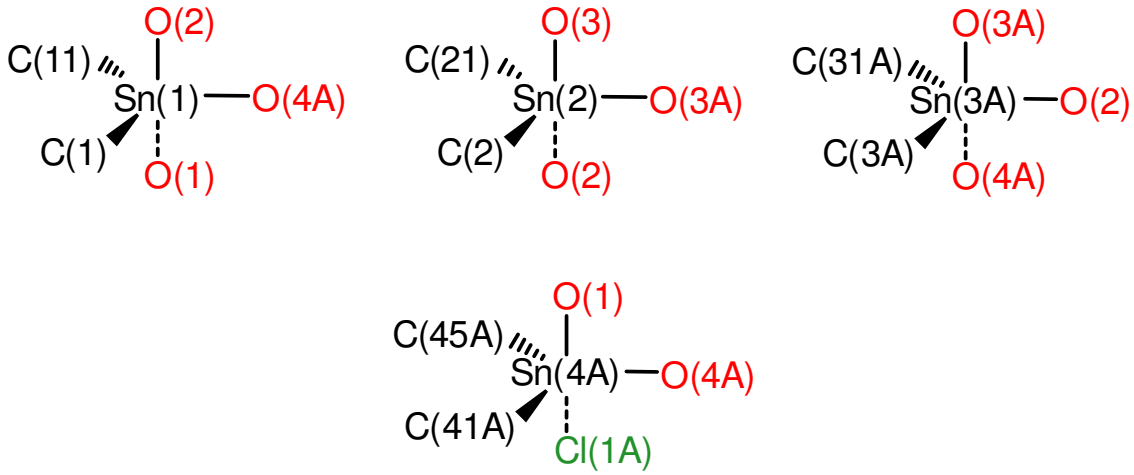

Figure 47. Configuration of the trigonal bipyramidal endo-tin atoms Sn(1), Sn(2) and Sn(3A) and the exo-cyclic tin atom Sn(4A) of compound **26**.

For the endocyclic tin atoms, the axial positions are occupied by two oxygen atoms [O(2), μ_2-O(1) for Sn(1)], [O(3), O(2) for Sn(2)], [O(3A),O(4A) for Sn(3A)]. For the exocyclic tin atom Sn(4A), the axial positions are occupied by μ_2–O(1) and Cl(1A) (Figure 47). The geometrical goodnesses[22] are $\Delta\Sigma(\theta) = 89.2°$ for Sn(1) , 73.2° for Sn(2), 92.6° for Sn(3A), and 80.1° for Sn(4A). Notably, $\Delta\Sigma(\theta)$ of Sn3A is higher than 90°, this is probably due to the distortion of the angles ($C_3A-Sn_3A-C_{31}A$) 130.9(3)° and ($C_{31}A-Sn_3A-O_4A$) 100.9(2)° from the ideal geometry, respectively, 120 and 90°.

The Sn–O interatomic distances range between 2.036(5) and 2.220(5) Å. The $Sn_{endo}-\mu_2-O-Sn_{exo}$ bridges are unsymmetrical with Sn(1)–O(1) 2.140(4) Å and Sn(4 A)–O(1) 2.220(5) Å. This data is typical for such ladder-like compounds.[20,22,23] The Si(1)–C(1)–Sn(1), Si(1)–C(2)–Sn(2) and Si(1)–C(3)–Sn(3) angles are 120.1(3), 113.5(3), and 121.2(4)°. As the matter of fact, we observe in compound **26** the $Sn_4O_2X_2Y_2$-structural motif, (X, Y = OH, Cl), characteristic for tetraorganodistannoxanes.[23,47,48] This motif is presented as $Sn_4O_6OH_2Cl_2$, exhibiting an unymmetrical combination, in which the hydroxy groups are located in the bridging positions and the chlorine atoms are bonded to the exocyclic tin atoms. This can be due to a competition between the different donor strength of OH and Cl. It is well-known that OH has a higher bridging capacity than Cl. To conclude, the ladder-like compound **26** presenting the structural motif [$Ph_3(MeSi(CH_2)_3)Sn(\mu_3\text{-}O)_3SnClSn(\mu_2\text{-}OH)Sn(t\text{–}Bu)_2$], resembles [$t\text{–}Bu_2(\mu_2\text{-}OH)Sn(\mu_3\text{-}O)SnCl(CH_2Si(Me)_3)_2$], [$t\text{–}Bu_2(\mu_2\text{-}OH)Sn(\mu_3\text{-}O)SnPh(CH_2(Me)_2SiO)Sn - t\text{–}Bu_2(\mu_3 - O)$][22] and related compounds. Comparing to the first example we extended the silicon methylene-bridged

tin arms to have four more Sn–O bridges and concerning the second example, we have one more Sn_2O_2 ring due to the third silicon methylene-bridged tin arm missing in this later. Compound **26** is the first octanuclear simple ladder-like organotin tin oxo cluster. In fact, referring to the Cambridge Structural Data Base, only a maximum of hexanuclear simple ladder-like tin oxo clusters having different features such as open-drum structures were reported until now.[16, 17, 49]

The identity of compound **26** is retained in solution. The compound is kinetically inert on the ^{1}H, ^{13}C, ^{29}Si and ^{119}Sn NMR time scales. Thus, a ^{1}H NMR spectrum (C_6D_6 solution, Figure 48) shows two resonances referring to four *t*-Bu_2 groups at δ 1.07 ($^{3}J(^{1}H-^{117/119}Sn)$ 116 Hz; integral 18) and 1.63 ($^{3}J(^{1}H-^{117/119}Sn)$ 116 Hz; integral 18) ppm. The resonance signal of the $SiCH_3$ protons appears at δ 0.78 ppm (integral 6). The $SiCH_2$ protons, with integration each of 2H, appear as equally intense AX-type resonances at δ –0.075 ($^{2}J(^{1}H-^{117/119}Sn)$ = 81 Hz, $^{2}J(^{1}H-^{1}H)$ = 13 Hz), 0.215 ($^{2}J(^{1}H-^{117/119}Sn)$ = 68 Hz, $^{2}J(^{1}H-^{1}H)$ = 13 Hz), 0.52 ($^{2}J(^{1}H-^{117/119}Sn)$ = 80 Hz, $^{2}J(^{1}H-^{1}H)$ = 13 Hz), 0.805 ($^{2}J(^{1}H-^{117/119}Sn)$ not measured, $^{2}J(^{1}H-^{1}H)$ = 13 Hz), 2.17 ppm ($^{2}J(^{1}H-^{117/119}Sn)$ = 126 Hz, $^{2}J(^{1}H-^{1}H)$ = 13 Hz), 2.37 ($^{2}J(^{1}H-^{117/119}Sn)$ = 106 Hz, $^{2}J(^{1}H-^{1}H)$ = 13 Hz). The complex pattern referring to the phenyl protons appears at δ 6.98-8.27 ppm with integration of 30H (See Supporting Information Chapter 4, Figures S1-S3). In a ^{13}C NMR spectrum (C_6D_6 solution, see Supporting Information Chapter 4, Figures S4- S6), the resonances corresponding to $SiCH_3$ at δ 5.5 ppm ($^{1}J(^{13}C-^{29}Si)$ = 74 Hz, $^{3}J(^{13}C-^{117/119}Sn)$ = 53 Hz) and those of $SiCH_2Sn$ at δ 7.6, 11.4, 18.1, 41.4, 42.0 ppm with coupling constants, respectively, equal to $^{1}J(^{13}C-^{117/119}Sn)$ = 464, 517, 503, 568, and 576. The resonances corresponding to the *t*-Bu groups appear at 30.5 ($C(CH_3)_3$), 31.02($C(CH_3)_3$), and 31.6 ($C(CH_3)_3$), 31.9 ($C(CH_3)_3$) ppm. In the aromatic part, there are three signal resonances referring to each carbon of the phenyl groups, indicating that there are three non-equivalent tin atoms coordinated to the phenyl groups; C_m (δ 128.7, 128.8, 128.9 ppm), C_p (δ 130.2, 130.26, 130.47 ppm, $^{4}J(^{13}C-^{117/119}Sn)$ = 14 Hz), C_o (δ 136.2, 136.7, 137.1 ppm, 2J(13C-117/119Sn) = 59 Hz), and C_i (δ 143.9, 144.61, 144.67 ppm, $^{1}J(^{13}C-^{117/119}Sn)$ = 759/805 Hz).

A ^{119}Sn NMR spectrum of a solution in $CDCl_3$ of a crystalline sample of **26** (Figure 49) shows four resonances with equal ratio; 1:1:1:1 at δ –195 (Sn3A) ($^{2}J(^{119}Sn_3A-^{117/119}Sn_{exo})$ = 298 Hz, $^{2}J(^{119}Sn_3A-^{117}Sn_{endo})$ = 180 Hz, $^{2}J(^{119}Sn_3A-^{29}Si)$ = 62 Hz), -208 (Sn2) ($^{2}J(^{119}Sn_2-^{117/119}Sn_{endo})$ = 243 Hz, $^{2}J(^{119}Sn_2-^{117}Sn_{endo})$ = 90 Hz) and two very close resonances at δ –228 ppm (Sn1) ($^{2}J(^{119}Sn_1-^{117/119}Sn_{exo})$ = 285 Hz, $^{2}J(^{119}Sn_2-^{117/119}Sn_{endo})$ = 209 Hz, $^{2}J(^{119}Sn_1-^{117}Sn_{endo})$ = 99 Hz) and -230 ppm (Sn4A). Sn1, Sn2 and Sn3A are endocyclic tin atoms whereas Sn4A is exocyclic. These four signal resonances correspond to four non-equivalent tin atoms, which matches perfectly with the molecular structure

found in the solid state. The chemical shifts indicate that all tin atoms are pentacoordinated.[22,23,47] This underlines the stability of 26 in solution, which is rather rare for such organotin oxo clusters.[22,50] An ESI-MS spectrum (positive mode) of 26 shows one intense mass cluster centred at m/z 2012.7485 corresponding to the cation $[C_{60}H_{87}Cl_2O_8Si_2Sn_8]^+$ ($[M + H]^+$), which confirms that the cluster remains intact in solution even under harsh ESI-MS conditions. Finally, an IR spectrum shows an absorption band at ν 2924-2849 cm^{-1} corresponding to OH groups (See Supporting Information Chapter 4, Figures S11–S14). However, referring to the crystallographic study, the protons at the oxygen atom O(1) and O(1A) were not found in the electron density map. The presence of hydroxy groups in such position is rather typical for similar compounds.[22,23]

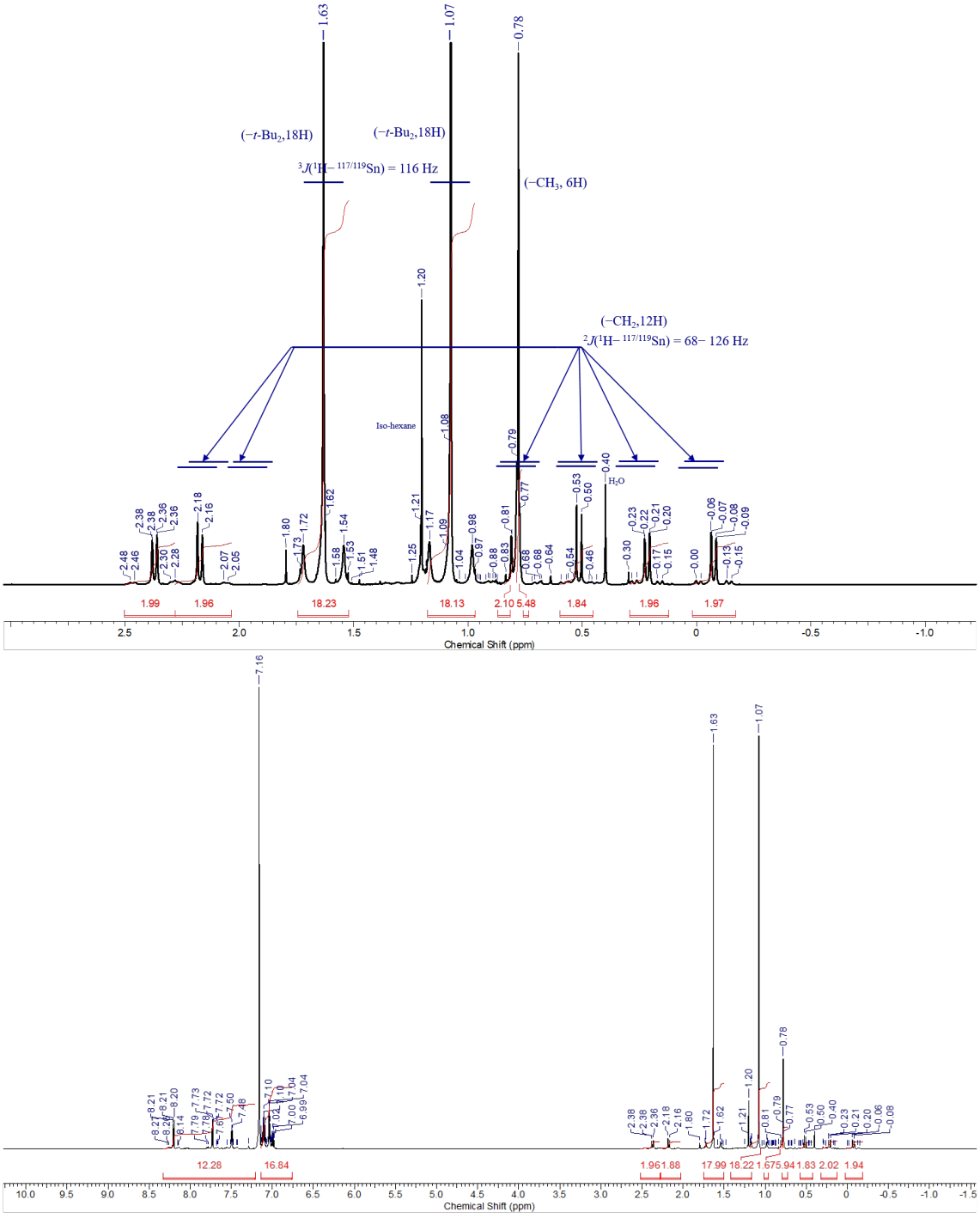

Figure 48. ^{1}H NMR spectrum (600.29 MHz, C_6D_6) of crystals sample of **26**: hole spectrum and aliphatic part are shown.

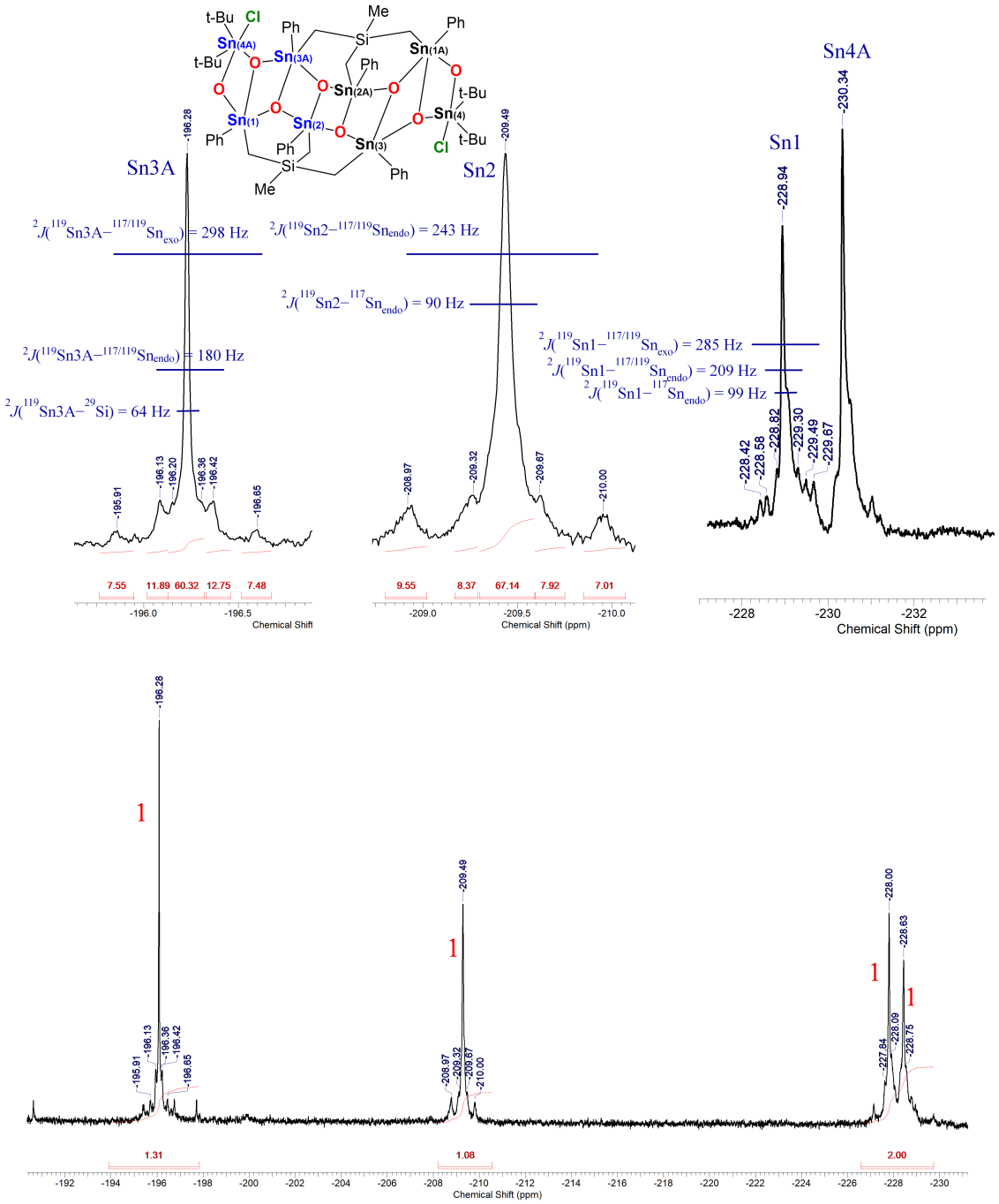

Figure 49. ^{119}Sn NMR spectrum (223.85 MHz, $CDCl_3$) of crystals sample of **26**.

The reaction of the hexachlorido-derivative MeSi($CH_2SnCH_2SiMe_3Cl_2)_3$, **12**, with one molar equiv di-tert-butyltin oxide $(t\text{-}Bu_2SnO)_3$ in $CHCl_3$ give a white solid material which is soluble in CH_2Cl_2 and CH_3Cl··A ^{119}Sn NMR spectrum in C_6D_6 of this material shows signals from δ –242 ppm to -29 ppm, with major signals at δ –82 ppm (25.2 %) and -29 ppm (22 %), referring, respectively to the remaining reagent cyclo-$(t\text{-}Bu_2SnO)_3$, and $(t\text{-}Bu_2SnOHCl)_2$ as by-products. The other resonances appear at -242 (5.8 %), -228 (12 %), -222 (9 %), -146 (6.5 %), -139 (6 %),

and -124 (13.3 %) ppm (See Supporting Information, Chapter 4, Figure S18). After several washings of this white residue resulting from the reaction mixture, with *iso*-hexane, recrystallization from dichloromethane/*iso*-hexane gives compound 27, $\{[MeSi(CH_2)_3]SnCl(CH_2SiMe_3)(\mu_3\text{-}O)SnCl(CH_2SiMe_3)Sn(\mu_3\text{-}O)(Cl)_2(CH_2SiMe_3)Sn(t\text{-}Bu)_2\}$, (Scheme 21) as colourless single crystals suitable for X-ray diffraction study.

Scheme 21. Synthesis of the tetranuclear ladder-like diorganotin oxocluster **27**.

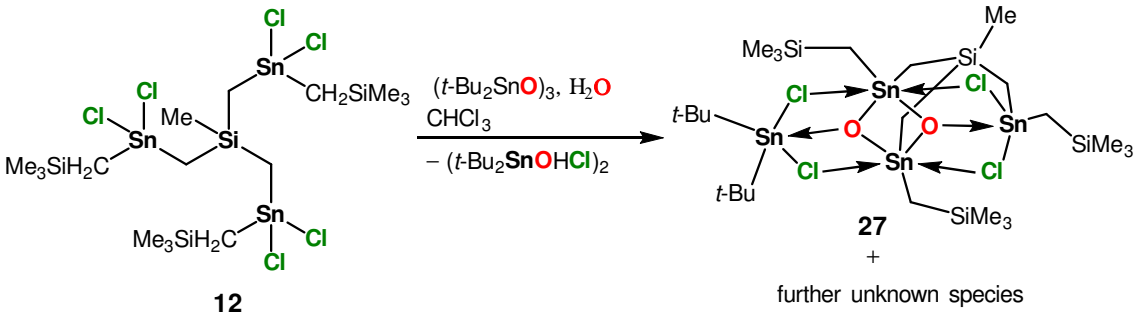

Figure 50 shows the molecular structure of **27** and the figure caption contains selected interatomic distances and angles. It shows a typical planar $Sn_4Cl_4O_2$ layer with a central Sn_2O_2 ring characteristics of a ladder-like structure. This is due to O→Sn and Cl→Sn intramolecular coordination. This structure is very similar to that of $\{[(R(Cl)Sn(CH_2)_3Sn(Cl)(CH_2)_2SiMe_2]O_2\}_2$, R = CH_2SiMe_3,[20] only this latter is a double ladder dimer interconnected with four trimethylene chains. As to compound **27** is a simple ladder monomeric structure, which, can be considered, with caution as a modified adamantane-type structure $[MeSi(CH_2SnCH_2SiMe_3)_3OCl_2]$ in coordination with a μ_3-oxygen atom, that can be issued from the reagent *t*-Bu_2SnO or from H_2O present under the experiment conditions and a *t*-Bu_2SnCl_2 molecule resulting from the reaction between compound **12** and the reagent *t*-Bu_2SnO (Scheme 22). Different perspectives of this adamantine-like structure are shown in Figure 51. Consequently, compound **27** contains four crystallographically independent tin atoms (Sn1, Sn2, Sn3 and Sn4) (Figure 50). This is also the case for the similar compound mentioned above.[20]

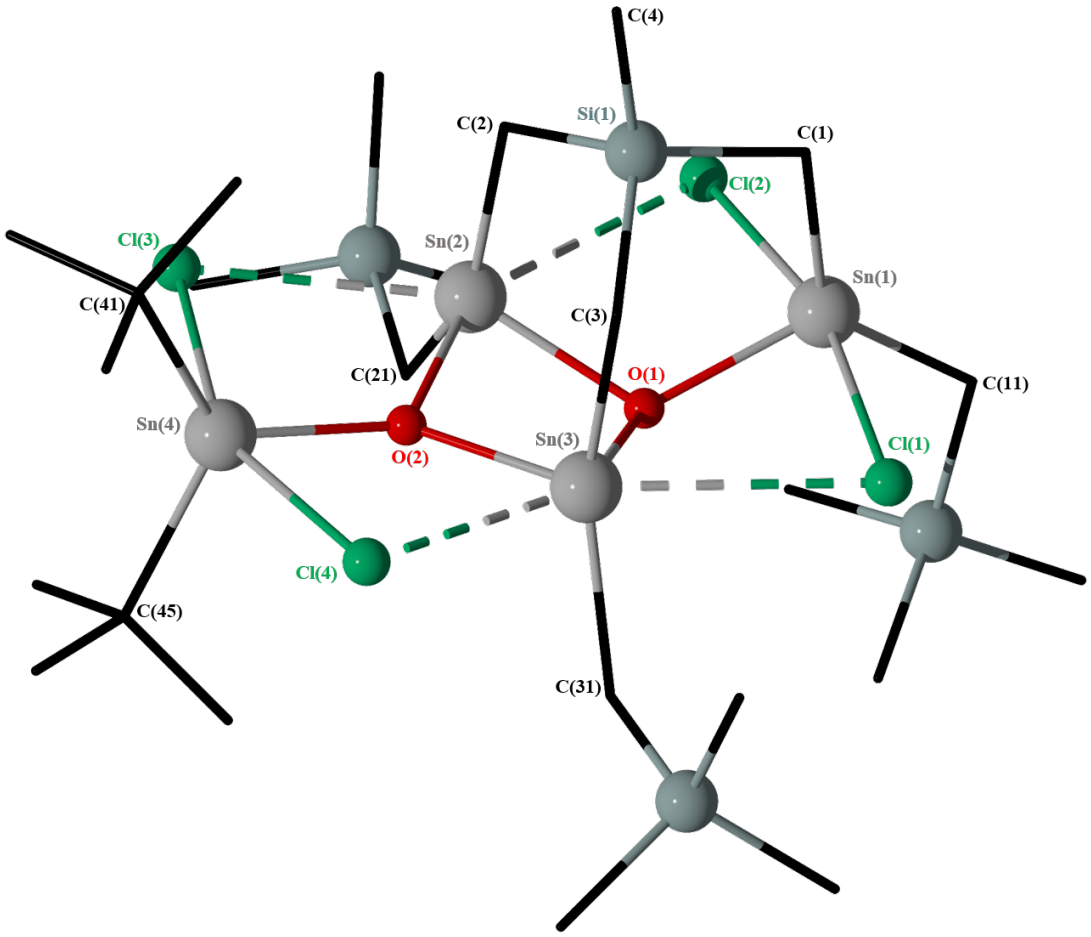

Figure 50. POV-Ray image of the molecular structure of {[MeSi(CH_2)$_3$]SnCl(CH_2SiMe_3)(μ_3-O)SnCl(CH_2SiMe_3)Sn(μ_3-O)$(Cl)_2$ (CH_2SiMe_3) Sn(*t*-Bu)$_2$}, **27**. Selected interatomic distances (Å): Sn(1)–O(1) 2.031(6), Sn(2)–Cl(2) 2.994(3), Sn(2)–Cl(3) 2.964(3), Sn(2)–O(1) 2.108(6), Sn(2)–O(2) 2.072(6), Sn(3)–Cl(1) 3.011(3), Sn(3)–Cl(4) 2.925(3), Sn(3)–O(1) 2.102(6), Sn(3)–O(2) 2.073(6), Sn(4)–O(2) 2.040(6), Sn(1)–Cl(1) 2.576(3), Sn(1)–Cl(2) 2.560(3), Sn(4)–Cl(3) 2.609(2), Sn(4)–Cl(4) 2.620(3). Selected interatomic angles (°): O(2)–Sn(2)–Cl(2) 147.24(18), O(1)–Sn(2)–Cl(3) 145.86(17), Cl(2)–Sn(2)–Cl3) 142.38(7), O(1)–Sn(2)–C(21) 104.9(3), O(2)–Sn(2)–C(21) 108.1(3), C(2)–Sn(2)–C(21) 148.8(3), O(1)–Sn(3)–Cl(4) 147.58(18), O(2)–Sn(3)–Cl(1) 146.58(17), Cl(1)–Sn(3)–Cl(4) 141.66(7), O(1)–Sn(3)–C(31) 102.2(3), O(2)–Sn(3)–C(31) 109.4(3), C(3)–Sn(3)–C(31) 149.5(4), C(1)–Sn(1)–C(11) 136.2(4), Cl(2)–Sn(1)–C(11) 92.9(3), Cl(2)–Sn(1)–C(1) 92.5(3), C(45)–Sn(4)–C(41) 126.5(4), O(2)–Sn(4)–Cl(3) 78.62(18), C(45)–Sn(4)–Cl(3) 101.4(3), Si(1)–C(1)–Sn(1) 111.6(5), Si(1)–C(3)–Sn(3) 115.1(5).

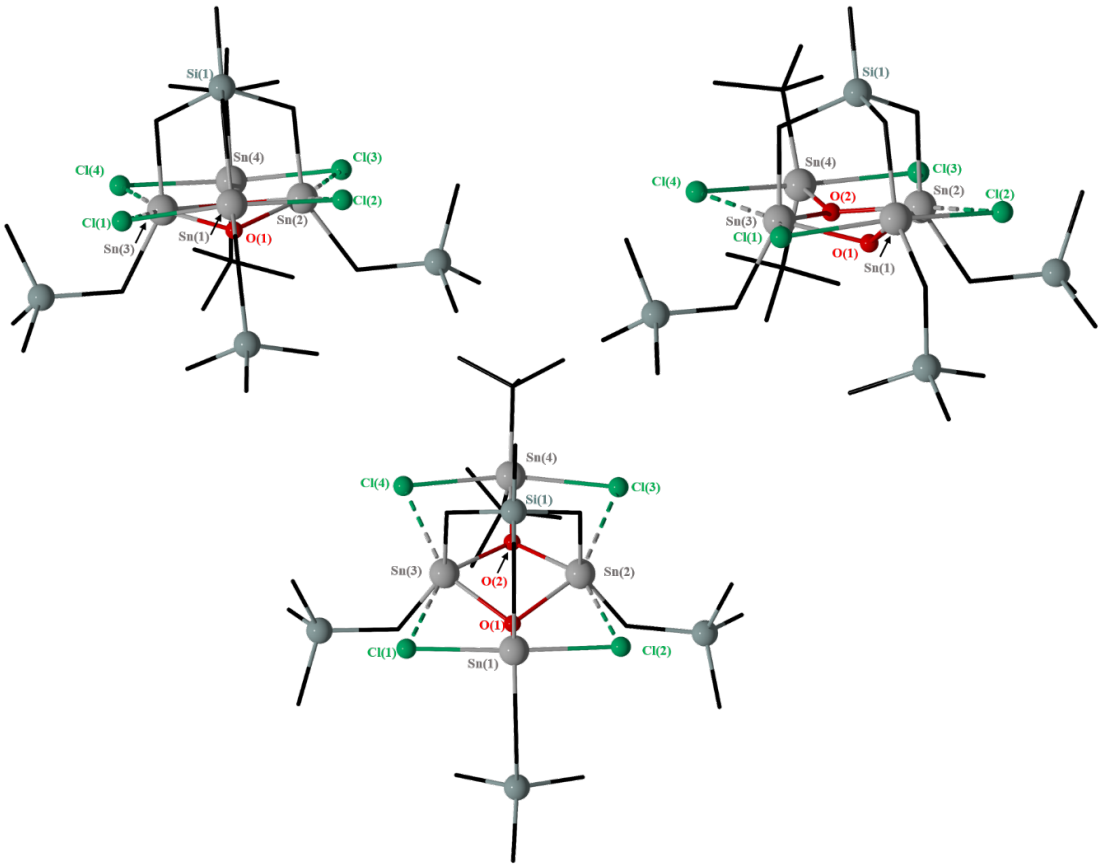

Figure 51. Different perspectives of the adamantine-like structure [MeSi($CH_2SnCH_2SiMe_3$)$_3$(O)Cl_2] coordinated with μ_3-O and a *t*-Bu_2SnCl_2 molecule.

Sn(2) and Sn(3) are incorporated in the central four-membered Sn_2O_2-ring as for Sn(1) and Sn(4) are bonded exocyclic to this ring. The endo-cyclic Sn atoms are hexa-coordinated and exhibit each a distorted octahedral all-trans $SnC_2Cl_2O_2$ environment at Sn(2) and Sn(3) with angles of (O2–Sn2–Cl2) 147.24(18)°, (O1–Sn2–Cl3) 145.86(17)°, (Cl2–Sn2–Cl3) 142.38(7)°, (O1–Sn2–C21) 104.9(3)°, (O2–Sn2–C21) 108.1(3)°, (C2–Sn2–C21) 148.8(3)°, (O1–Sn3–Cl4) 147.58(18)°, (O2–Sn3–Cl1) 146.58(17)°, (Cl1–Sn3–Cl4) 141.66(7)°, (O1–Sn3–C31) 102.2(3)°, (O2–Sn3–C31) 109.4(3)°, ($C_3--Sn_3--C_{31}$) 149.5(4)°. The chlorido– and the oxido– bridges; Cl–Sn_{endo}–Cl and O–Sn_{endo}–O are unsymmetrical at Sn(2) and Sn(3) with Sn(2)–Cl(2), Sn(2)–Cl(3), Sn(2)–O(1), Sn(2)–O(2), Sn(3)–Cl(1), Sn(3)–Cl(4), Sn(3)–O(1), Sn(3)–O(2), distances of 2.994(3), 2.964(3), 2.108(6), 2.072(6), 3.011(3), 2.925(3), 2.102(6), and 2.073(6) Å, respectively. These distances prove, however, that the Sn_{endo}-μ3-O-Sn_{endo} bridges are approximately equal. This affirmation is typical for such ladder-like compounds.[20,22,23] The exo-cyclic tin atoms Sn(1) and Sn(4) exhibit a distorted trigonal bipyramidal environments, in which Sn(1) is coordinated to two CH_2SiMe-groups, two chlorine and one oxygen atoms, as to Sn(4) is coordinated to two *t*-Bu- groups, two chlorine and one oxygen atoms, with the equatorial

positions being occupied by two carbon atoms and one oxygen atom (C(1), C(11), O(1) for Sn(1)), (C(41), C(45), O(2) for Sn(4)).

As to the axial positions, are being occupied by two oxygen atoms (Cl(1), Cl(2) for Sn(1)), (Cl(3), Cl(4) for Sn(4)), (O(3A),O(4A) for Sn(3A)). The geometrical goodnesses $\Delta\Sigma(\theta)$[22] are equal to 92.1° for Sn(1) and 87.9° for Sn(4). Notably, $\Delta\Sigma(\theta)$ of Sn1 is higher than 90°, this is probably due to the distortion of the angles (C1–Sn1–C11) 136.2(4)°, (Cl2–Sn1–C11) 92.9(3)°, and (Cl2–Sn1–C1) 92.5(3)° from the ideal geometry, respectively, 120 and 90°. This distortion from the ideal geometry is mainly the result of the Cl(1) and Cl(2) atoms intramolecularly approaching Sn(2) and Sn(3).

The Sn–O interatomic distances range between 2.031(6) and 2.108(6) Å, as to the Sn–Cl interatomic distances range between 2.560(3) and 3.011(3). The Sn_{endo}-(μ3-O)-Sn_{exo} bridges are unsymmetrical with distances of Sn(1)–O(1) 2.031(6) Å, Sn(2)–O(1) 2.108(6) Å, Sn(3)–O(1) 2.102(6) Å, Sn(2)–O(2) 2.072(6) Å, Sn(4)–O(2) 2.040(6) Å, Sn(3)–O(2) 2.073(6) Å. As to the Sn_{endo}-Cl-Sn_{exo} bridges are unsymmetrical with distances of Sn(1)–Cl(1) 2.576(3) Å, Sn(3)–Cl(1) 3.011(3) Å, Sn(1)–Cl(2) 2.560(3) Å, Sn(2)–Cl(2) 2.994(3) Å, Sn(2)–Cl(3) 2.964(3) Å, Sn(4)–Cl(3) 2.609(2) Å, Sn(3)–Cl(4) 2.925(3) Å, Sn(4)–Cl(4) 2.620(3) Å.

Bond distances and angles around the silicon methylene-bridged organotin arms Si(1)–C(1)–Sn(1), Si(1)–C(2)–Sn(2) and Si(1)–C(3)–Sn(3) are almost equal. The corresponding angles vary between 111.6(5)° (Si1–C1–Sn1), 115.1(5)° (Si1–C3–Sn3). This statement refers to the tripod geometry characteristic of these novel organotin precursors.

A close inspection of the interatomic distances support the interpretation of the solid state structure as it is schematically shown in Scheme 22. The central Sn_2O_2 four-membered ring is coordinated by one *t*-Bu_2SnCl_2 and the remaining CH_2SnCl_2R (R = CH_2SiMe_3) substituent attached to the bridgehead MeSi silicon atom. The situation resembles that reported for the unsymmetrical tetraorganodistannoxane (*t*-$Bu_2ClSnOSnClMe_2)_2$.[51]

Scheme 22. Schematic drawing of the solid-state structure of compound **27**.

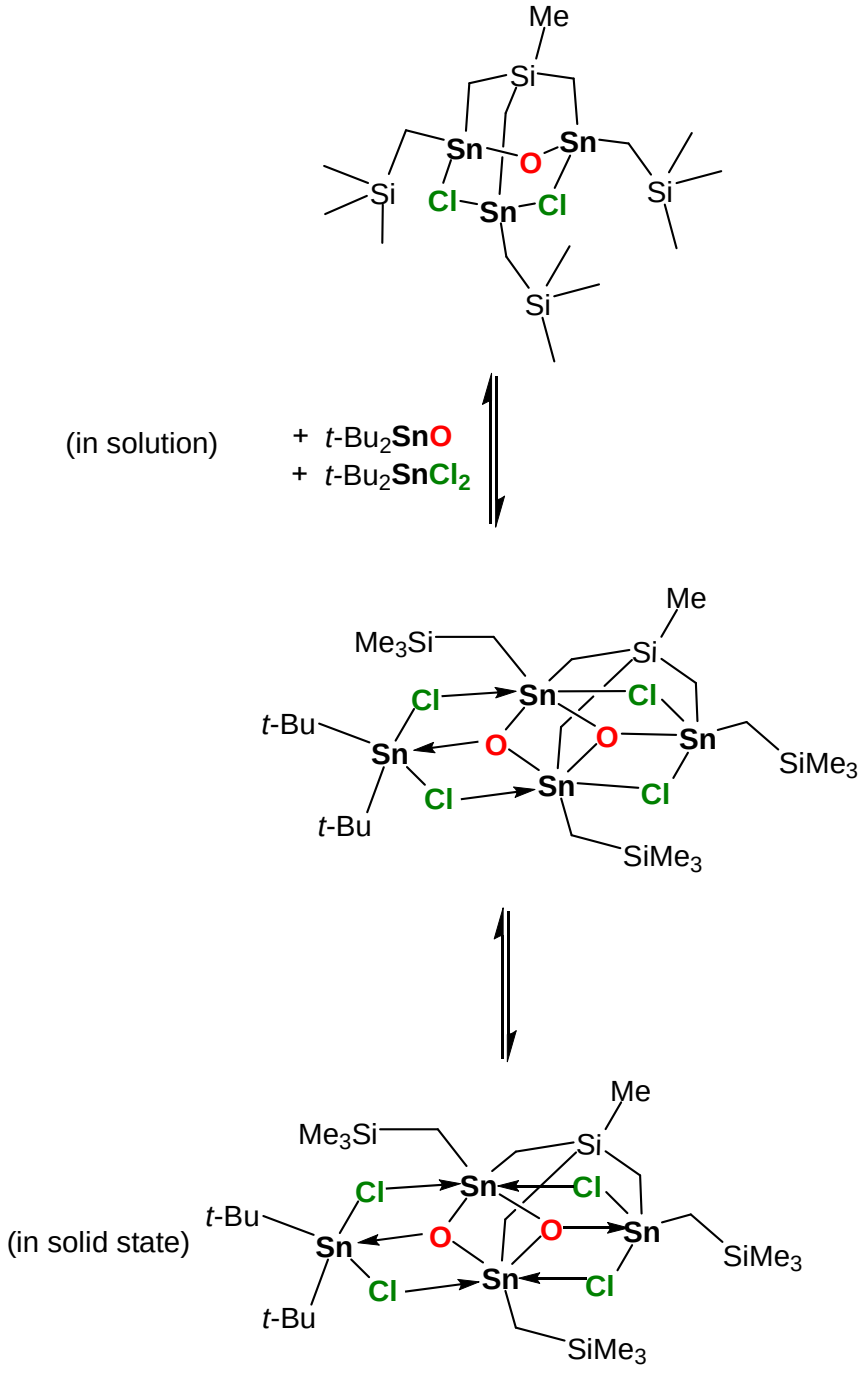

The solid state structure of **27** is retained in solution. Thus, a ^{119}Sn NMR spectrum of a solution in C_6D_6 of a crystalline sample of **27** (See Supporting Information, Chapter 4, Figure S19) shows four signal resonances with equal ratio; 1:1:1:1 at δ –218 referring to the exocyclic Sn(4) atom ($^2J(^{119}Sn_4 - {}^{117/119}Sn_{endo})$ = 208 Hz), -149 ppm referring most probably to the second exocyclic Sn(1) atom ($^2J(^{119}Sn_1 - {}^{117/119}Sn_{endo})$) = 214 Hz), given the almost equal $^2J(^{119}Sn_{exo} - {}^{117/119}Sn_{endo})$ coupling constants, and two resonance signals referring to the endocyclic Sn atoms Sn(2)/Sn(3) at δ –158 ppm

($^2J(^{119}Sn_{endo} - ^{117}Sn_{endo})$ = 125 Hz) and δ –132 ppm. These four signal resonances correspond to four non-equivalent tin atoms which matches perfectly with the molecular structure found in the solid state. This is the same case as the resembling dimeric compound $\{[(R(Cl)Sn(CH_2)_3Sn(Cl)(CH_2)_2SiMe_2]O_2\}_2$, R = CH_2SiMe_3.[20] A ^{29}Si NMR spectrum (See Supporting Information, Chapter 4, Figure S17) of this sample matches perfectly with the previous statement. There are three resonance signals at 0.81, 1.3, and 1.5 ppm referring to the CH_2SiMe_3 silicon atoms bound to three non-equivalent Sn atoms. The resonance for the SiMe appears at -21 ppm. This also underlines the stability of **27** in solution, which is rather rare for such organotin oxo clusters.[22,50]

A ^1H NMR spectrum (C_6D_6 solution, see Supporting Information, Chapter 4, Figure S16) confirms, as well the retention of the solid-state structure of **27** in solution. It shows two resonances referring to two *t*-Bu_2 groups at δ 1.38 and 1.41 (integral 18H). The resonance signals corresponding to $SiCH_3$ protons of the head SiMe and the CH_2SiMe_3 groups appear as a complex pattern at δ 1.24–1.36 ppm (integral 30H). The $SiCH_2$ protons appear as three resonance signals at δ 0.21, 0.26, and 0.27 ppm with integration of 12H. The coupling constants are difficult to identify due to the quality of the NMR spectrum. No further measurements could be done within the time frame of this PhD.

An ESI-MS spectrum (positive mode, see Supporting Information, Chapter 4, Figure S20- 22) of **27** shows two intense mass clusters centred at m/z 793.1270, and 807.1418 corresponding, respectively, to the cation $[C_{16}H_{45}Cl_2OSi_4Sn_3]^+\{[MeSi(CH_2SnCH_2SiMe_3)_3(O)Cl_2] + H^+\}^+$ and $[C_{16}H_{44}Cl_2O_2Si_4Sn_3]^+\{[MeSi(CH_2SnCH_2SiMe_3)_3(O)Cl_2] + (\mu_3\text{-}O)\}^+$. These two mass clusters refer to the formation of adamantane-like structure in solution, suggested in Scheme 22 and support, with caution, the ring-opening mechanism as a formation path of **27**.

The reaction of the hexaiodido derivative $MeSi(CH_2SnCH_2SiMe_3I_2)_3$, **11**, with one molar equiv cyclo-(*t*-$Bu_2SnO)_3$ in $CHCl_3$ gives a white solid material soluble in almost all halogenated organic solvents. A ^{119}Sn NMR spectrum in $CDCl_3$ solution of this material, , shows one resonance signal at δ 62 ppm (51 %), corresponding to the by-product *t*-Bu_2SnI_2, and three resonances at -183.8, -156, and -150 ppm with a sum integration of 49 % (See Supporting Information, Chapter 4, Figure S27). After several washings of this white solid material with *iso*-hexane, recrystallization from dichloromethane/*iso*-hexane gives compound **28**, $\{[MeSi(CH_2)_3]SnI(CH_2SiMe_3)(\mu_2\text{-}OH)[SnO(CH_2SiMe_3)]_2Sn(\mu_2\text{-}OH)ISn(t\text{-}Bu)_2\}$, (Scheme 23) as colourless single crystals suitable for X-Ray diffractometer study.

Scheme 23. Synthesis of the tetranuclear ladder-like diorganotin oxocluster **28**.

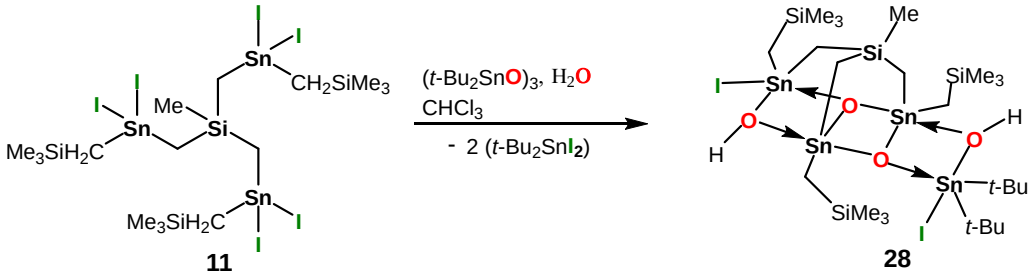

Figures 52 and 53 show the molecular structure of **28** and the figure caption contains selected interatomic distances and angles.

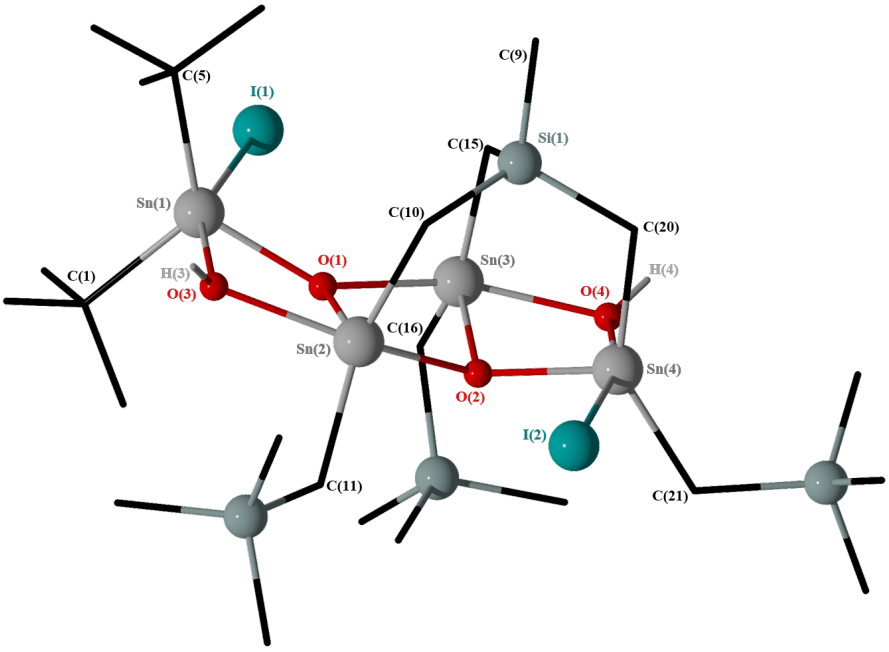

Figure 52. POV-Ray image of the molecular structure of $\{[MeSi(CH_2)_3]SnI(CH_2SiMe_3)(\mu_2\text{-}OH)[SnO(CH_2SiMe_3)]_2Sn(\mu_2\text{-}OH)I\ Sn(t\text{-}Bu)_2\}$, **28**. Selected interatomic distances (Å): Sn(1)–O(1) 2.036(2), Sn(2)–O(1) 2.048(2), Sn(3)–O(1) 2.157(2), Sn(1)–O(3) 2.175(3), Sn(2)–O(3) 2.195(3), Sn(2)–O(2) 2.138(2), Sn(4)–O(2) 2.033(2), Sn(4)–O(4) 2.196(3), Sn(3)–O(4) 2.176(3), Sn(1)–I(1) 2.9508(3), Sn(4)–I(2) 2.9173(4). Selected interatomic angles (°): (C1–Sn1–C5) 122.82(14), (O3–Sn1–I1) 157.55(7), (O3–Sn1–O1) 73.30(9), O(1)–Sn(2)–O(2) 76.03(9), O(1)–Sn(2)–C(10) 101.75(12), O(2)–Sn(2)–O(3) 148.46(9), (O2–Sn3–C16) 115.05(12), (O2–Sn3–O1) 75.39(9), (O1–Sn2–O4) 149.06(9), C(20)–Sn(4)–C(21) 142.82(14), O(4)–Sn(4)–I(2) 164.16(7), O(2)–Sn(4)–I(2) 89.98(7).

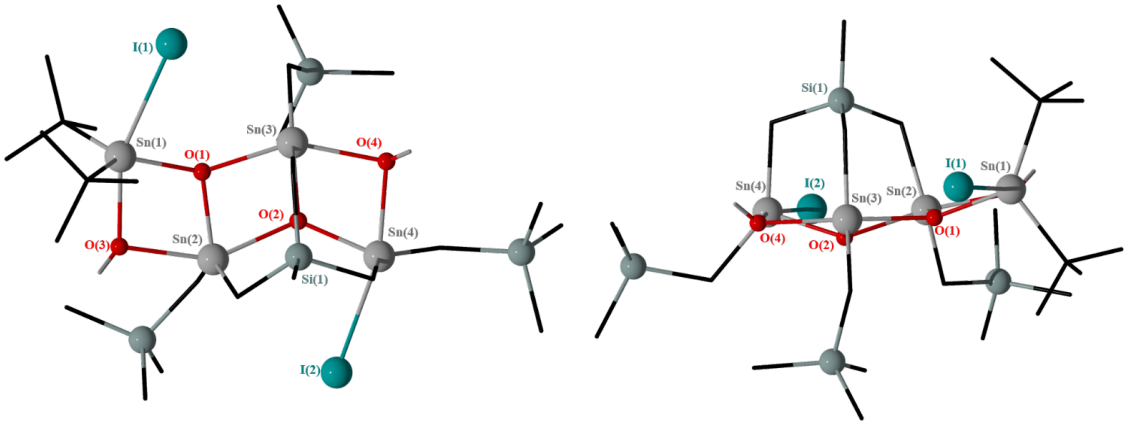

Figure 53. Different perspectives of the the adamantine-like structure [MeSi($CH_2SnOCH_2SiMe_3$)$_3$] coordinated with one H_2O and a *t*-Bu_2SnI_2 molecules.

Compound **28** crystallizes in the monoclinic space group P21/n. It contains four crystallographically independent tin atoms (Sn1, Sn2, Sn3 and Sn4) (Figure 52) and shows a typical $Sn_4O_2X_2Y_2$-structural motif, (X, Y = OH, I), characteristic for tetraorganodistannoxanes.[23][48] This is due to O→Sn and I→Sn intramolecular coordinations. In analogy to **27**, the structure can formally be interpreted as containing a four-membered Sn_2O_2 ring that is coordinated by one $CH_2Sn(OH)ICH_2SiMe_3$ moiety and one *t*-$Bu_2Sn(OH)I$ (Scheme 24).

Scheme 24. Formal interpretation of the solid-state structure of compound **28**.

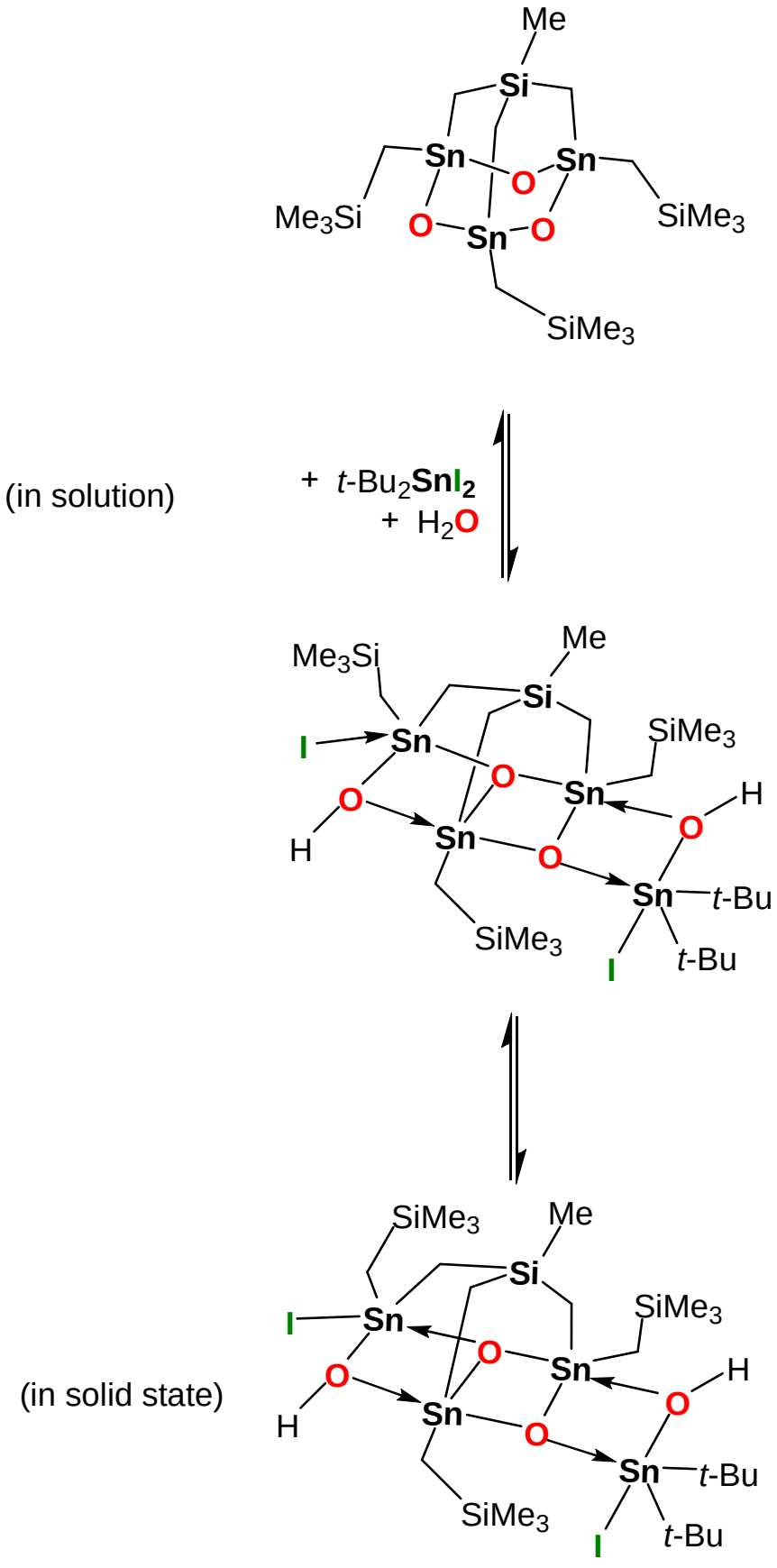

Both the endo-cyclic and exo-cyclic tin atoms exhibit a distorted trigonal bipyramidal environments with the equatorial positions being occupied for the endocyclic Sn atoms Sn2 and Sn3 by two carbon atoms and one oxygen atom (C(10), C(11), O(1) for Sn(2)), (C(15), C(16), O(2) for Sn(3)). As to the axial positions, are being occupied for the endo-cyclic tin atoms by two oxygen atoms (μ_2–O(2), μ_2–O(3) for Sn(2)), (μ_2-O(1), μ_2-O(4) for Sn(3)). Also, for the exocyclic tin atom Sn(1) and Sn(4), respectively, the equatorial positions are occupied by two carbon atoms and one oxygen atom (C(1), C(5), O(1) for Sn(1)), (C(20), O(21), O(2) for Sn(4)), the axial position is occupied by two donor atoms μ_2–O(3) and I(1) for Sn(1) and μ_2–O(4) and I(2) for Sn(4) (Figure 52). The geometrical goodness[22] is $\Delta\Sigma(\theta)$ =82.7° for Sn(1) , 82.6° for Sn(4), 95.0° for Sn(2), and 95.4° for Sn(3). Notably, $\Delta\Sigma(\theta)$ of Sn(2) and Sn(3) are higher than 90°, this is probably due to the distortion of the angles (C11–Sn2–C10) 142.53(14)°, (C16-Sn3-C15) 143.21(14)°, (C11–Sn2–O2) 95.08(12)°, and (C16-Sn2-O1) 99.04(12)° from the ideal geometry, respectively, 120 and 90°. The Sn–O interatomic distances range between 2.033(2) and 2.196(3) Å. The Sn_{endo}–μ_2–OH–Sn_{exo} bridges are almost symmetric with Sn(1)–O(3) 2.175(3) Å, Sn(2)–O(3) 2.195(3) Å, Sn(4)–O(4) 2.196(3) Å, and Sn(3)–O(4) 2.176(3) Å .

The Sn-I interatomic distances are 2.9173(4) Å for Sn(4)–I(2) and 2.9508(3) Å for Sn(1)–I(1). As to the Sn_{endo}-μ_2-O-Sn_{endo} bridges are comparable taking as example Sn(2)–O(1) 2.048(2) Å and Sn(3)–O(1) 2.157(2) Å. This data is typical for such ladder-like compounds.[20,22,23] Also the bond distances and angles around the silicon methylene-bridged organotin arms C(9)–Si(1)–C(20), C(10)–Si(1)–C(20), C(15)–Si(1)–C(20), and C(10)–Si(1)–C(15) are almost equal. The corresponding angles are, respectively, equal to 109.8(17), 110.38(17), 108.19(16), and 114.06(16)°. This refers to the tripod geometry characteristic the novel organotin precursors.

The solid state structure of **28** is retained in solution. Thus, a ^{119}Sn NMR spectrum of a solution in $CDCl_3$ of crystalline sample of **28** (Figure 54) shows four signal resonances with equal ratio; 1:1:1:1. Two resonance signals at δ –183.5 and -183.2 ppm (2J($^{119}Sn_{exo}$-^{117}/$^{119}Sn_{endo}$) = 248 Hz) refer to the exocyclic Sn(1) and Sn(4) atoms. The other two resonance signals appear at -156 ppm ($^2J(^{119}Sn_{endo}-{}^{117}Sn_{endo})$ = 167 Hz) and -150 ppm (2J($^{119}Sn_{exo}$-^{117}/$^{119}Sn_{endo}$) = 242 Hz). These resonance shifts resemble to those corresponding in [t-$Bu_2(\mu_2-OH)Sn(\mu_3-O)SnCl(CH_2Si(Me)_3)_2$].[23] These four signal resonances correspond to four non-equivalent tin atoms, which matches perfectly with the molecular structure found in solid state. This is the same case as the resembling compounds presenting similar structural motifs [t-$Bu_2(\mu_2-OH)Sn(\mu_3-O)SnCl(CH_2Si(Me)_3)_2$],[23] [$t-Bu_2(\mu_2-OH)Sn(\mu_3-O)SnPh(CH_2(Me)_2SiO)Sn-t-Bu_2(\mu_3-O)$],[22] and $\{[(R(Cl)Sn(CH_2)_3Sn(Cl)(CH_2)_2SiMe_2]O_2\}_2$, R = CH_2SiMe_3.[20] The ^{29}Si NMR spectrum (see Supporting Information, Chapter 4, Figure S25) of this sample matches also with the solid state structure of 28, there are three resonance signals at 0.72, 1.42,

and 1.58 ppm referring to the silicon atoms in the CH_2SiMe_3 groups bound to three non-equivalent Sn atoms. The head SiMe resonance signal appears at -21 ppm. An ESI-MS spectrum (positive mode, see Supporting Information Chapter 4, Figure S28-30) of 28 shows one intense mass cluster centred at m/z 796.93 and one less intense mass cluster at 750.93 corresponding, respectively, to the cations of $[C_{16}H_{43}O_3Si_4Sn_3]^+ + \frac{1}{2}CH_2Cl_2$: $\{[MeSi(CH_2SnOCH_2SiMe_3)_3] + H^+ + \frac{1}{2}CH_2Cl_2\}^+$ and $[C_{16}H_{43}O_3Si_4Sn_3]^+$: $\{[MeSi(CH_2SnOCH_2SiMe_3)_3] + H^+\}^+$.These two mass clusters support the formation of the adamantane-like structure $[MeSi(CH_2SnOCH_2SiMe_3)_3$ in solution, and, with caution, the ring-opening mechanism for the formation path of **28**, suggested in Scheme 24. Also the 1H and ^{13}C NMR spectra ($CDCl_3$ solution, see Supporting Information, Chapter 4, Figure S24, S25) confirm as well the retention of the solid-state structure of 28 in solution. Finally, in IR spectroscopy, we notice the presence of the absorption band at ν 3656-3493 cm^{-1} and ν 2950-2850 cm^{-1}, corresponding to OH groups (See Supporting Information, Chapter 4, Figure S32).

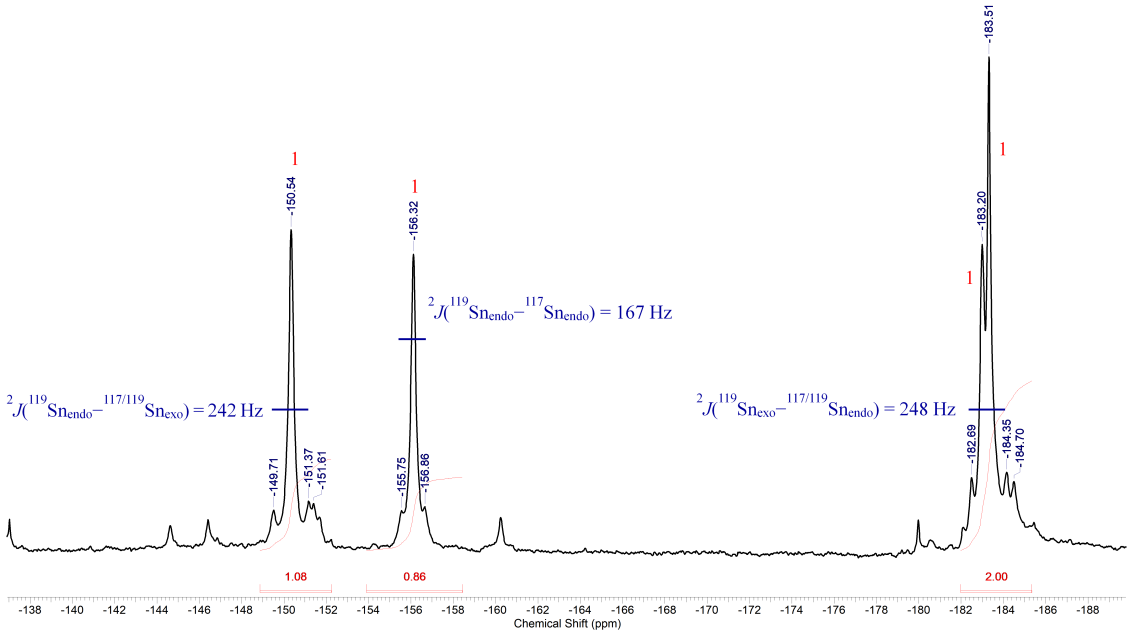

Figure 54. ^{119}Sn NMR spectrum (149.26 MHz, $CDCl_3$) of crystals sample of **28**.

Treatment in CH_2Cl_2 of the organotin iodide **3** with $(t\text{-}Bu_2SnO)_3$ gave a reaction mixture a ^{119}Sn NMR spectrum of which displayed four resonances at δ 61 ($t\text{-}Bu_2SnI_2$), -203 (29), -225 (29), and -228 ppm (29), respectively (See Supporting Information, Chapter 4, Figure S38). The spectrum indicates complete oxygen transfer from $(t\text{-}Bu_2SnO)_3$ to the organotin iodide **5** and formation of $t\text{-}Bu_2SnI_2$ and the oktokaideka-nuclear (18-nuclear) organotin oxide $[MeSi(CH_2SnPhO)_3]_6$, **29** (Figure 55). The latter compound was isolated from the reaction mixture as colourless crystalline material. It crystallized as a solvate from dichloromethane solution. (Scheme 25)[45]

Scheme 25. Synthesis of the macrocycle **29**.

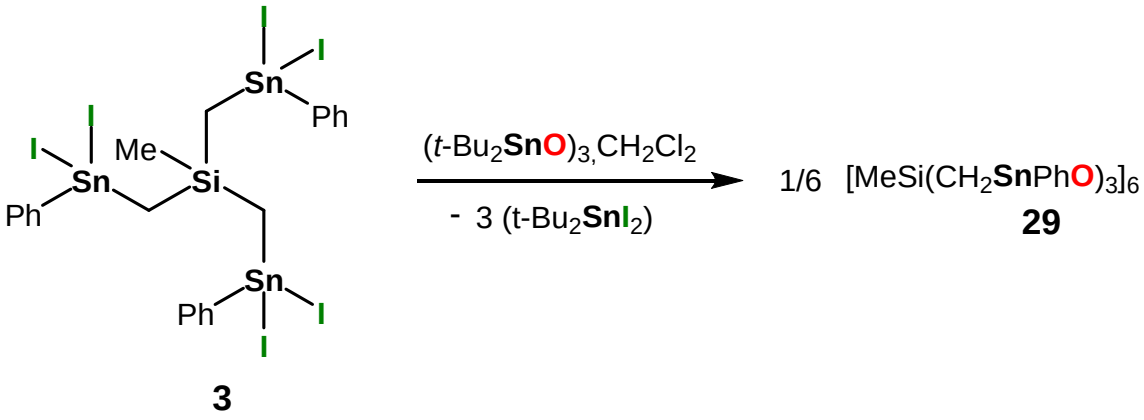

Figure 52 shows its molecular structure. The figure caption contains selected interatomic distances and angles. Complete interatomic distances and angles are presented in Supporting Information, Chapter 4, Figure S54.[45]

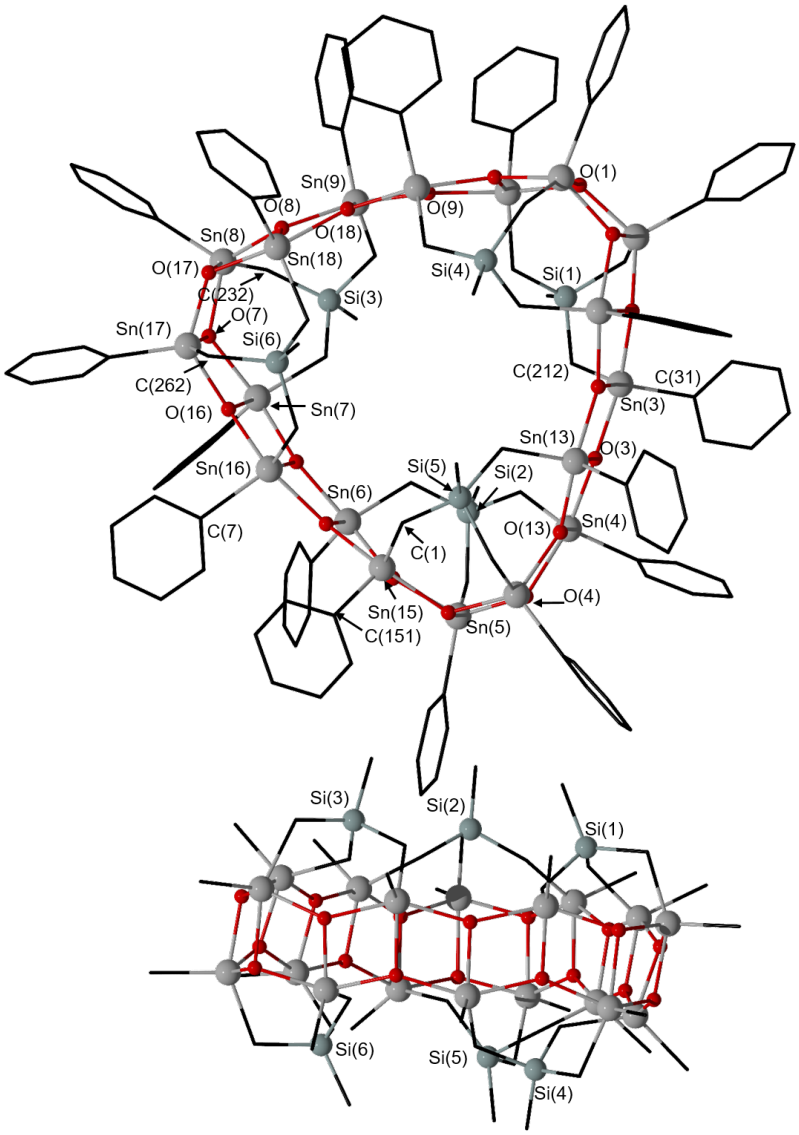

Figure 55. Top: General view (ball and stick) of a molecule of the organotin oxide **29** containing the numbering of the atoms that appear below in the listing of distances and angles. Only the C_i carbon atoms of the phenyl substituents, are shown. The hydrogen atoms are omitted for clarity. Bottom: Side view of a molecule of **29** including the numbering for the silicon atoms. Selected interatomic distances (Å): Sn–C 2.05(2) (Sn6–C707) – 2.256(17) (Sn16–C265), Sn–O_{ax} 2.074(8) (Sn13–O13) – 2.158(7) (Sn4–O4), Sn–O_{equ} 2.009(9) (Sn7–O16) – 2.055(8) (Sn9–O18). Selected interatomic angles (°): C_{equ}–Sn–C_{equ} 111.6(4) (C31–Sn3–C212) – 138.1(7) (C1–Sn15–C151), O_{ax}–Sn–O_{ax} 147.8(3) (O3–Sn4–O4) – 150.8(3) (O17–Sn18–O18), C_{ax}–Sn–O_{ax} 150.0(4) (C262–Sn17–O7) – 153.4(4) (C232–Sn8–O17).[45]

Compound **29** crystallizes in the monoclinic space group P21/n with four crystallographic equivalent molecules in the unit cell. Each of these contains six MeSi($CH_2SnPh)_3$ moieties in which the tin atoms are connected by a total of 18 oxygen atoms giving a triangular

shaped, belt-like macromolecule with diameters ranging between 20.06(1) (H44···H94) and 23.00(1) (H84···H144) and a thickness ranging between 10.47(1) (H55···H145) and 10.97(1) Å (H5···H154) (Figure 56). Three MeSi moieties (containing Si1 – Si3) are located above and three such moieties (containing Si4 – Si6) are located below the belt formed by the 18 tin and 18 oxygen centres (Figure 56, Figure 57).[45]

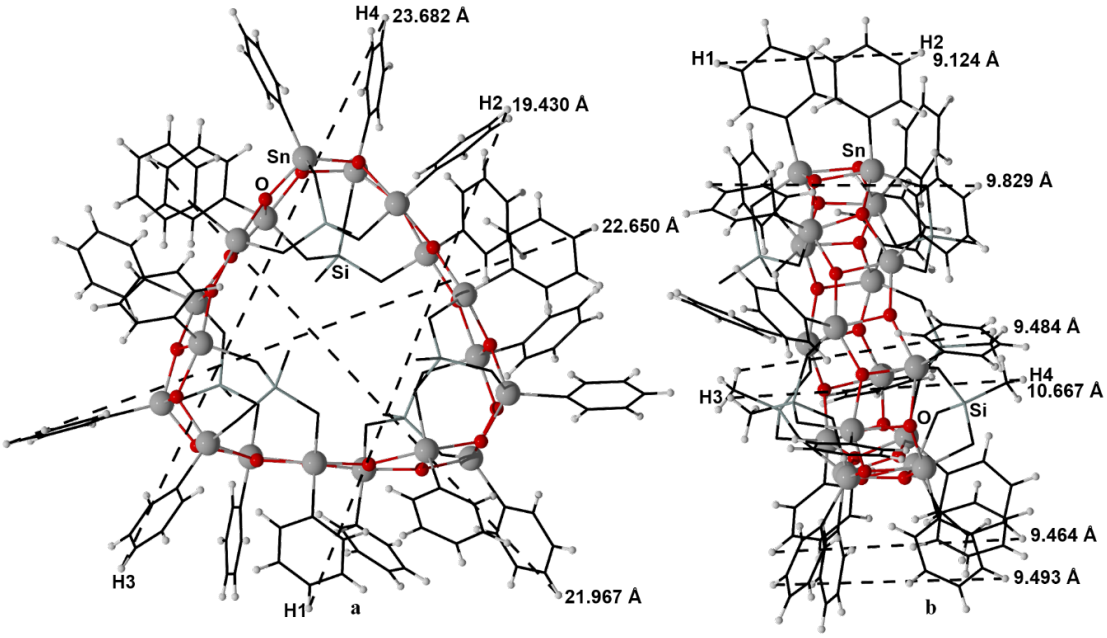

Figure 56. Front view a) and side view b) (POV-Ray) of **29** including the H44···H94 (20.06(1) Å) and H84···H144 (23.00(1) Å) distances and the distances indicative for the thickness (H55···H155 10.47(1) Å, H5···H154 10.97(1) Å).[45]

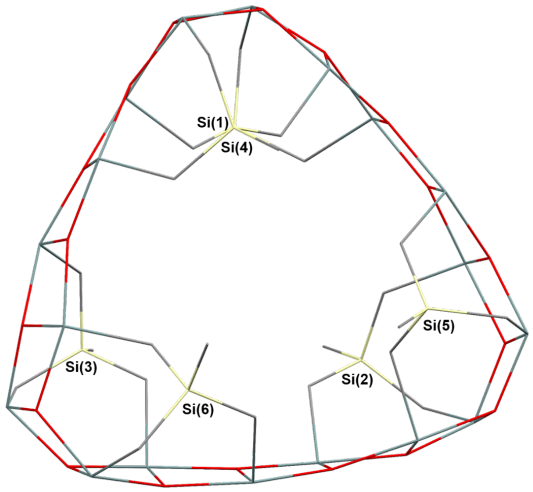

Figure 57. Simplified structure of **29** showing the non-equivalence of the $SiCH_3$ moieties.[45]

Each of the 18 crystallographic independent tin atoms is penta-coordinated and shows a distorted trigonal bipyramidal environment. For each of the Sn(1), Sn(3), Sn(4), Sn(6), Sn(7), Sn(9), Sn(10), Sn(12), Sn(13), Sn(15), Sn(16), and Sn(18) atoms, the two carbon atoms (C_i atom from the phenyl substituent and the methylene carbon atom) and one oxygen atom occupy the equatorial positions. The corresponding C_{equ}–Sn–C_{equ} angles vary between 111.6(4) (C31–Sn3–C212) and 138.1(7)° (C1–Sn15–C151). Two oxygen atoms take the axial positions with the O_{ax}–Sn–O_{ax} angles varying between 147.8(3)° (O3–Sn4–O4) and 150.8(3)° (O17–Sn18–O18). The corresponding Sn–O_{ax} distances vary between 2.074(8) (Sn13–O13) and 2.158(7) Å (Sn4–O4). The Sn–O_{equ} distances involving oxygen atoms in equatorial positions are slightly shorter and vary between 2.009(9) (Sn7–O16) and 2.055(8) Å (Sn9–O18).

Notably, for the Sn(2), Sn(5), Sn(8), Sn(11), Sn(14), and Sn(17) atoms for each case the corresponding methylene carbon atom and one out of the adjacent three oxygen atoms take the axial positions whereas the C_i and the two remaining oxygen atoms occupy the equatorial positions. This is in contrast to a situation as expected from the polarity rule according to which the electronegative substituents occupy the axial positions in a trigonal bipyramidal structure. The C_{ax}–Sn–O_{ax} angles vary between 150.0(4) (C262–Sn17–O7) and 153.4(4)° (C232–Sn8–O17). The crystal packing of **29** (Figure 58) is characterized by C–H$\cdots\pi$ interactions (Figure 59) at a H(144)-centroid (C171–C176) centroid distance of 2.89(1) Å.[45]

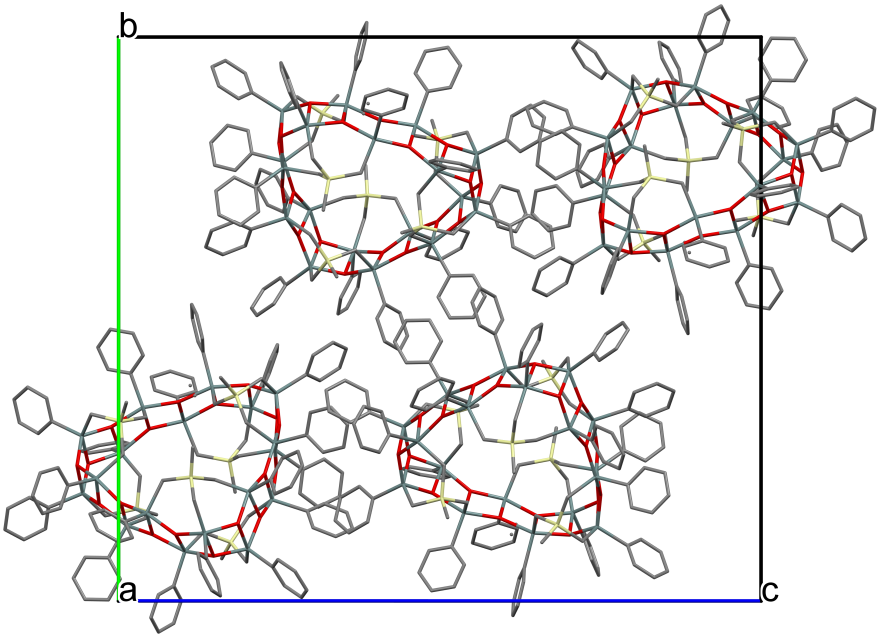

Figure 58. Crystal packing of **29**. The hydrogen atoms are omitted for clarity.[45]

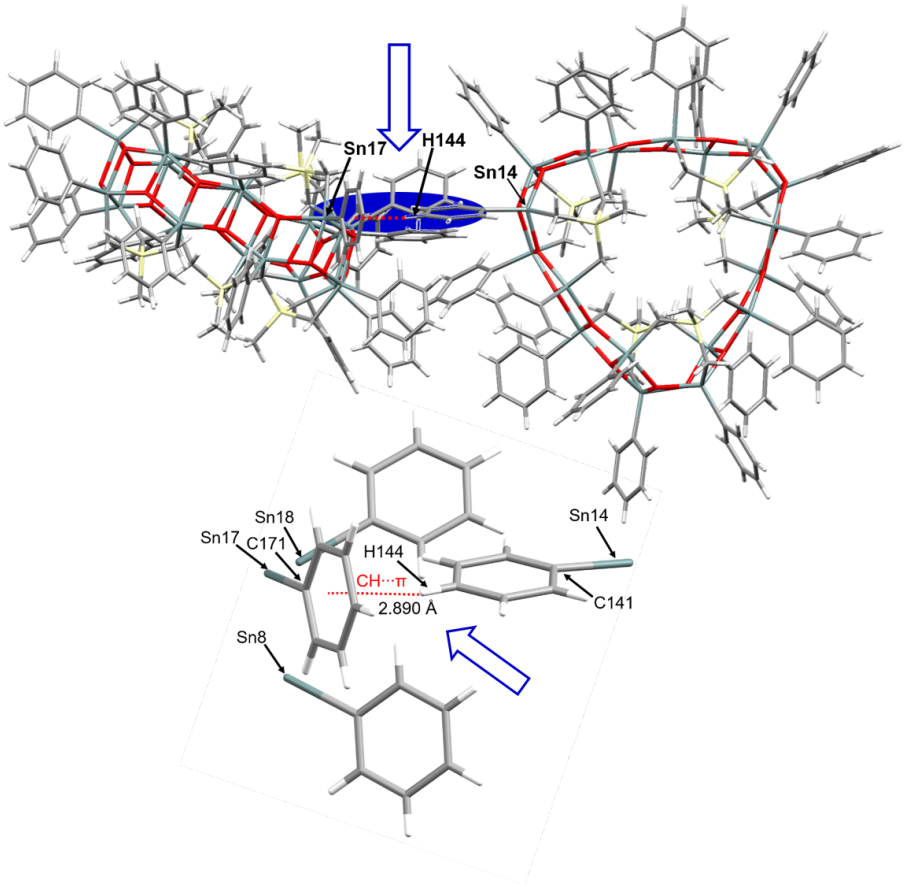

Figure 59. Illustration of the C–H···π interactions at a H(144)-centroid (C171–C176) centroid distance of 2.89(1) Å.[45]

The identity of compound **29** is retained in solution. The compound is kinetically inert on the 1H, and ^{119}Sn NMR time scales. Thus, a ^{1}H NMR spectrum ($CDCl_3$ solution, Figures 60, 61) shows two resonances at δ 0.30 (integral 2) and 1.42 (integral 1) ppm, respectively, that are assigned to non-equivalent $SiCH_3$ protons. The non-equivalence of the $SiCH_3$ protons (ratio 2:1) becomes visible when looking perpendicular through the plane defined by the belt (Figure 57). The $SiCH_2$ protons appear as three equally intense AX-type resonances at δ 0.06 ($^2J(^1H-^{117/119}Sn)$ 50 Hz, $^2J(^1H-^1H)$ 10 Hz)/0.48 ($^2J(^1H-^{117/119}Sn)$ 70 Hz, $^2J(^1H-^1H)$ 10 Hz), 0.88 ($^2J(^1H-^{117/119}Sn)$ 85 Hz, $^2J(^1H-^1H)$ 15 Hz)/1.20 ($^2J(^1H-^{117/119}Sn)$ not measured, $^2J(^1H-^1H)$ 15 Hz), and 1.28 ppm ($^2J(^1H-^{117/119}Sn)$ not measured, $^2J(^1H-^1H)$ 10 Hz)/1.91 ($^2J(^1H-^{117/119}Sn)$ 120 Hz, $^2J(^1H-^1H)$ 10 Hz), respectively. 2D NMR spectra unambiguously support the assignment of the 1H resonances (see Supporting Information Chapter 4, Figures S40- 43). A ^{119}Sn NMR spectrum of a solution of single crystalline 29 in $CDCl_3$ shows three equally intense resonances at δ 204 ppm ($^2J(^{119}Sn-^{117/119}Sn)$ 180, 315 Hz; $^2J(^{119}Sn-^{29}Si)$ 59 Hz), δ 225 ppm ($^2J(^{119}Sn-^{117/119}Sn)$ 315 Hz), and δ 228 ppm ($^2J(^{119}Sn-^{117/119}Sn)$ 180 Hz). (See Supporting Information Chapter 4, Figures S39). The chemical shift is in agreement with pentacoordinated tin atoms showing a SnC_2O_3 substituent pattern.[14,22,23] A ^{1}H

DOSY NMR spectrum ($CDCl_3$ solution, room temperature, Figure 62) provided a diffusion coefficient of $3.9(1) \times 10^{-10}$ m^2 s^{-1}. This, by using the Einstein-Stokes equation, gave a calculated hydrodynamic diameter of 20.8 Å and a sphere volume of 4813 $Å^3$. These values fit reasonably well with the single crystal X-ray diffraction data.[45]

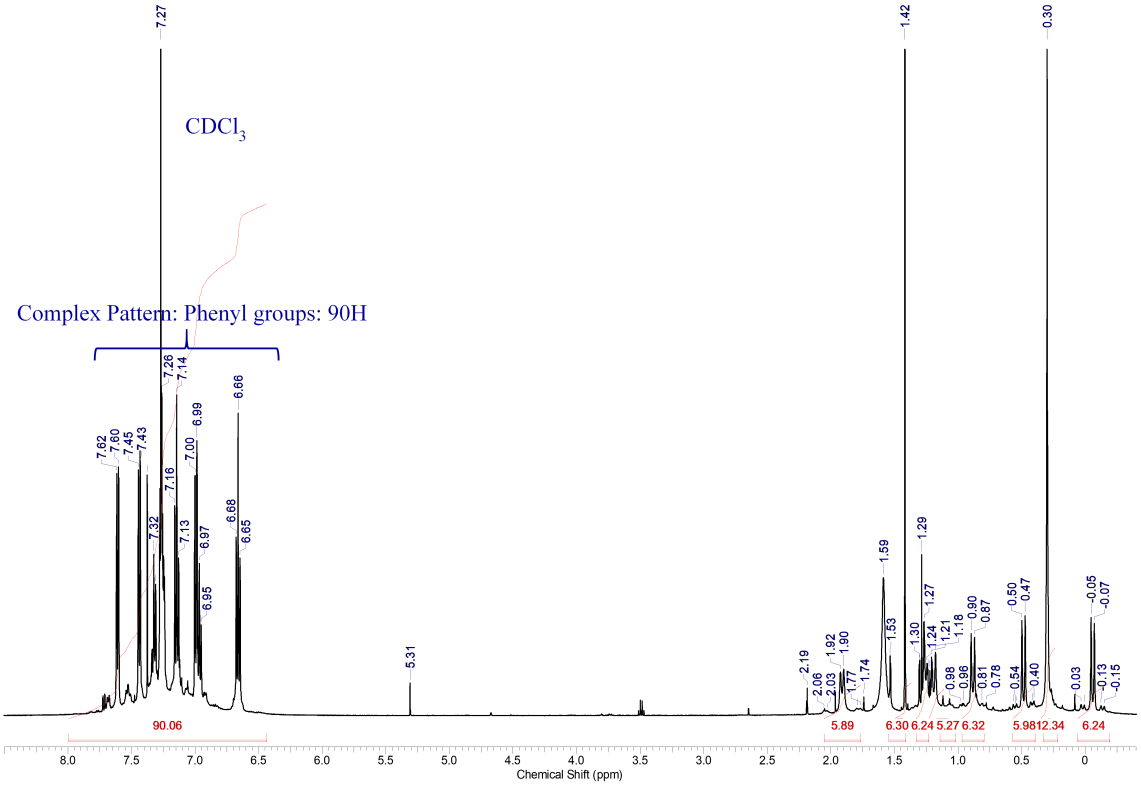

Figure 60. ^1H NMR spectrum (500.08 MHz, $CDCl_3$) of compound **29**.[45]

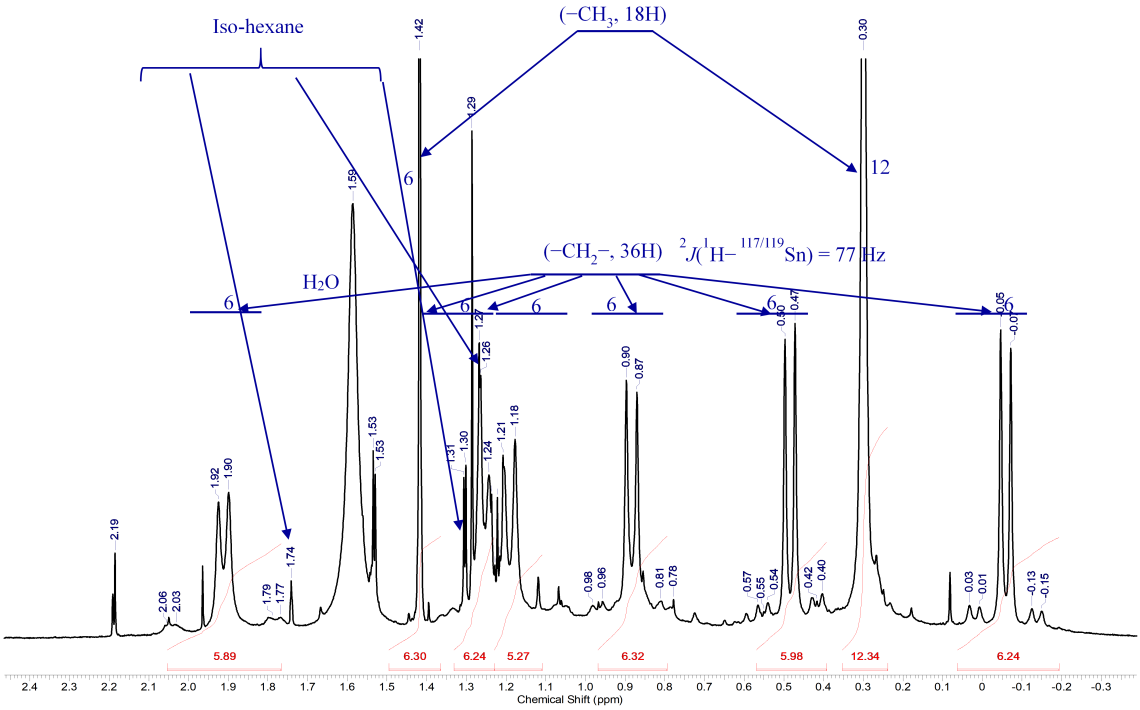

Figure 61. ^{1}H NMR spectrum (500.08 MHz, $CDCl_3$) of compound **29** (aliphatic part).[45]

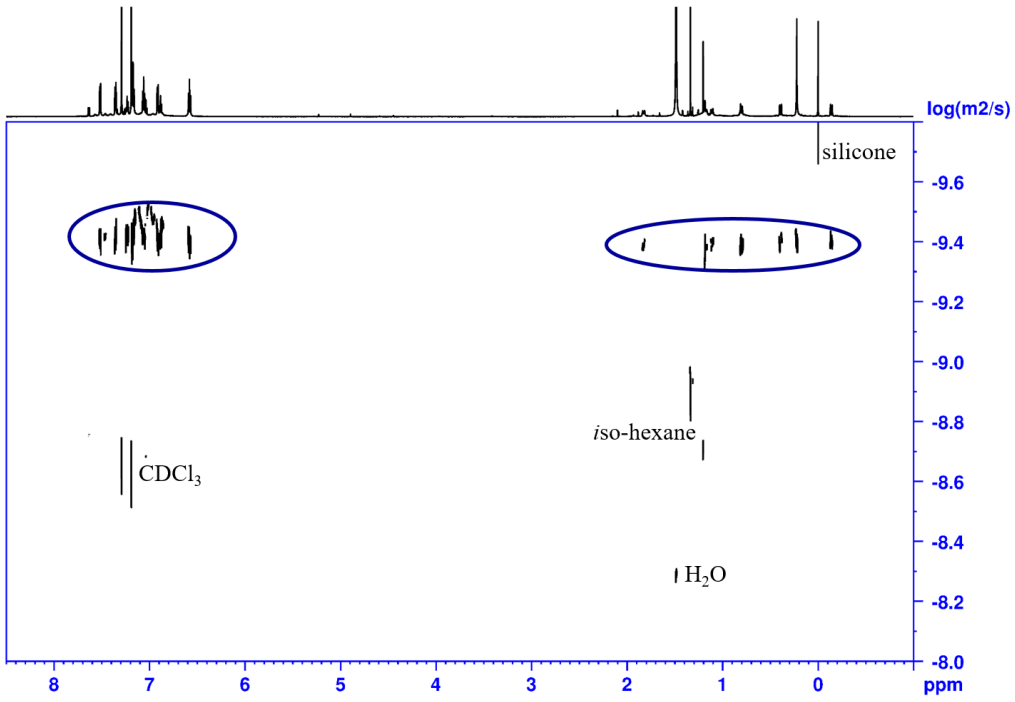

Figure 62. 2D ^{1}H DOSY NMR spectrum of $[MeSi(CH_2SnPhO)_3]_6$, **29**, in $CDCl_3$.[45]

Finally, an electrospray ionization mass spectrum (ESI MS; Supporting Information Chapter 4, Figures S45- 52) revealed a mass cluster centred at m/z = 4324.1823 that corresponds to $\{[MeSi(CH_2SnPhO)_3]_6 + H^+\}$, $[29 + H]^+$. In addition, there are mass clusters centred at m/z 1442.7312, m/z 2161.5910, 2884.4515, and m/z 3636.3600 that are assigned to $\{[MeSi(CH_2SnPhO)_3]_2 + H^+\}$, $\{[MeSi(CH_2SnPhO)_3]_3 + H^+\}$, $\{[MeSi(CH_2SnPhO)_3]_4 + H^+\}$, and $\{[MeSi(CH_2SnPhO)_3]_5 + MeOH + H^+\}$, respectively.

The reaction of the diorganotin diiodide derivative **11** with sodium hydroxide, NaOH, in a mixture of dichloromethane, methanol, and water (Scheme 26) gave a crude reaction mixture a ^{119}Sn NMR spectrum of which was rather complex and showed both broad and sharp resonances between 125 and 170 ppm (see Supporting Information, Figure S58). After the work-up procedure, a microcrystalline material was obtained. From this, a crystal was identified by single crystal X-ray diffraction analysis as the molecular diorganotin oxide solvate **30**. Figure 63 shows its simplified molecular structure and the figure caption contains selected interatomic distances and angles. Complete interatomic distances and angles are presented in Supporting Information Chapter 4, Figure S72.

The compound crystallizes in the triclinic space group $P-1$ with two molecules in the unit cell.

Scheme 26. Synthesis of the macrocycle **30**.

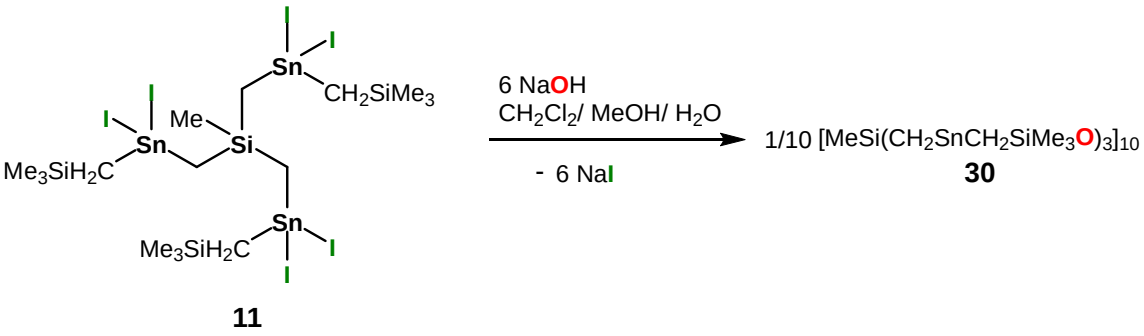

Compound **30** is a trikonta-nuclear (30-nuclear) molecular diorganotin oxide $[MeSi(CH_2SnRO)_3]_{10}$ (R = Me_3SiCH_2) in which ten $MeSi(CH_2SnRO)_3$ moieties are connected giving a belt-like ladder-type heart-shaped macrocycle (Figure 63). In this, the three methyl groups attached to Si(14), Si(30), and Si(44), respectively, are above and the three methyl groups attached to Si(17), Si(32), and Si(43), respectively, are below the ring plane. The two methyl groups attached to Si(22) and Si(26), respectively, point into the ring cavity and the two methyl groups attached to Si(10) and Si(38), respectively, point outside the ring (Figure 64, left). The methylene carbon atoms C(111), C(121), C(371), C(391), C(401), and C(491) which are attached to Sn(1), Sn(30), Sn(11), Sn(10), Sn(9), and Sn(2), respectively and which belong to the trimethylsilylmethyl substituents point also inside the ring while the remaining substituents point outside (Figure 64, right). The overall structure

is rather complex. A closer inspection reveals it formally being composed of different subunits, i. e., the corner units a (with Sn3–Sn8), b (with Sn24–Sn29), and c (with Sn12–Sn17), the double spacer d (with Sn18–Sn23), and the single spacers e (with Sn1, Sn2, Sn30) and f (with Sn9–Sn11) (Figure 63). Like in the oktokaideka-nuclear diorganotin oxide 29, all tin centres in 30 are five-coordinated and, except Sn(1), show distorted trigonal bipyramidal environments. For the Sn(2)–Sn(4), Sn(7)–Sn(13), Sn(16)–Sn(25), Sn(29), and Sn(30) atoms, for each case two carbon atoms (the Me_3SiCH_2 and the $MeSiCH_2$ methylene carbon atoms) and one oxygen atom occupy the equatorial positions. The other two oxygen atoms take the axial positions. The corresponding C_{eq}–Sn–C_{eq} angles vary between 119.0(10) (C311–Sn16–C321) and 139.8(15)° (C151-Sn28-C173). The O_{ax}–Sn–O_{ax} angles vary between 145.2(9) (O1–Sn2–O3) and 153.8(7)° (O10-Sn11-O12). The Sn(1) atom exhibits a distorted square pyramidal environment with the O(2), O(30), C(101), and C(111) atoms occupying the equatorial positions with O(2)–Sn(1)–O(30) and C(101)–Sn(1)–C(111) angles of 150.5(8) and 154(2)°, respectively. The O(1) atom occupies the apical position. The geometry about the Sn(28) atom is a borderline case between trigonal bipyramidal and square pyramidal with the O(27)–Sn(28)–O(29) and C(151)–Sn(28)–C(173) angles being 149.7(8) and 139.8(15)°. In analogy to 29, there are again six tin centres (Sn5, Sn6, Sn26, Sn27, Sn14, Sn15) belonging to the corner units (a), (b), and (c), respectively, that violate in their coordination environment the polarity rule.[52] For each of these tin centres, the corresponding $MeSiCH_2$ methylene carbon atom and one out of the adjacent three oxygen atoms take the axial positions whereas the Me_3SiCH_2 methylene carbon and the two remaining oxygen atoms occupy the equatorial positions. The C_{ax}-Sn–O_{ax} angles vary between 146.2(11) (O6–Sn6–C432, in a) and 150.9(10)° (O14–Sn14–C322, in c). Figure 65 shows with diameters ranging between H24F···H46F (27.51(1) Å) and H16K···H34K (33.98(1) Å) and a thickness ranging between H34D···H35D 9.71(1) Å and H11F···H49C 11.96(1) Å. Figure 66 shows the packing of 30 in the crystal. The $Sn_{30}O_{30}$ belt is located in the (2, -2, 0) plane.[45]

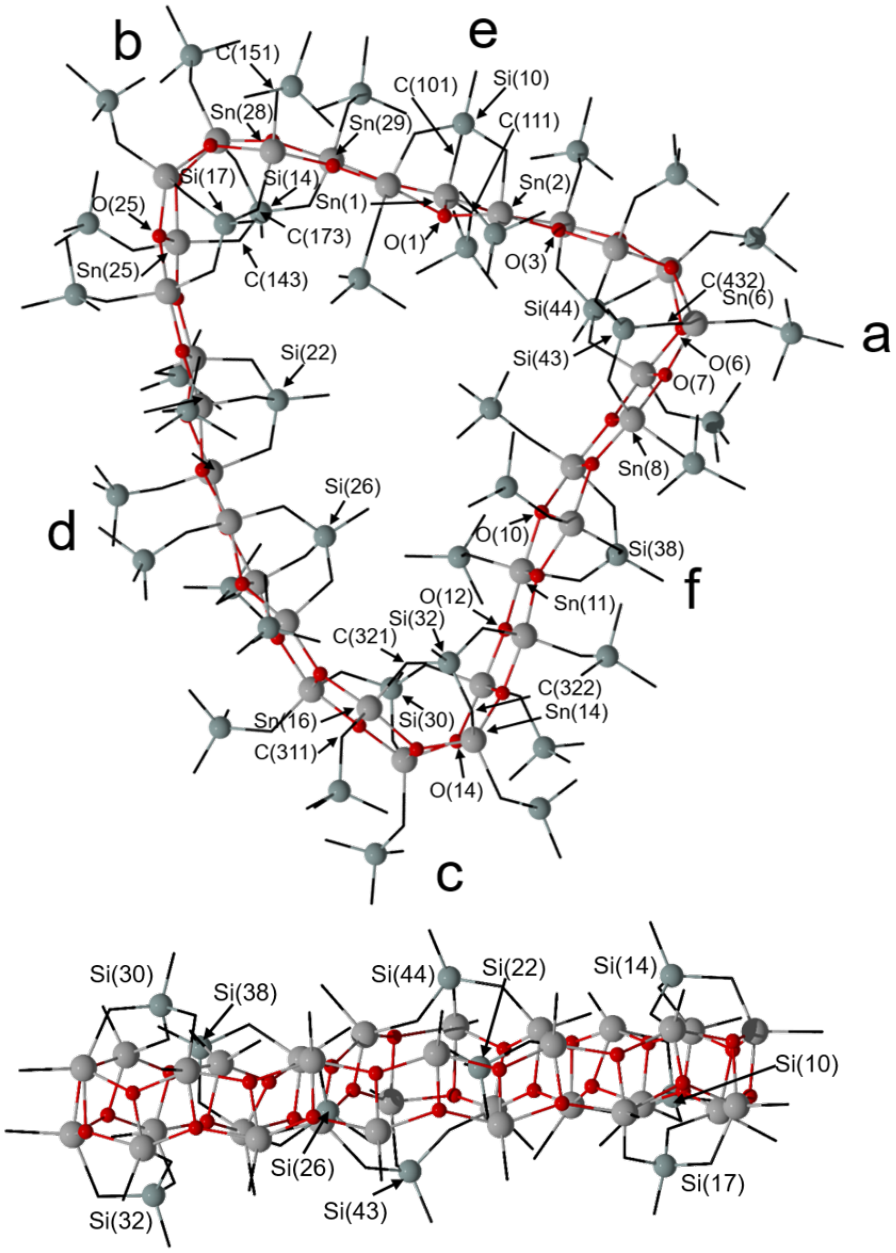

Figure 63. Top: General view (ball and stick) of a molecule of the organotin oxide **30** containing the numbering of the atoms that appear below in the listing of distances and angles. The hydrogen atoms are omitted for clarity. Bottom: Side view of a molecule of **30** including the numbering for the silicon atoms. The labels a–f refer to the different building blocks the belt-type structure is composed of. Selected interatomic distances (Å). Sn–O: 1.95(2) (Sn25–O25, in b) - 2.23(2) (Sn8–O7, in a), Sn–C: 2.01(8) (Sn1–C111, in e) – 2.38(4) (Sn28–C151, in b). Selected interatomic angles (°). O_{ax}–Sn–O_{ax}: 145.2(9) (O1–Sn2–O3, in e) – 153.8(7) (O10–Sn11–O12, in f), C_{eq}–Sn–C_{eq}: 119.0(10) (C311–Sn16–C321, in c) - 139.8(15) (C151–Sn28–C173, in b), C_{ax}–Sn–O_{ax}: 146.2(11) (O6–Sn6–C432, in a) - 150.9(10) (O14–Sn14–C322, in c).[45]

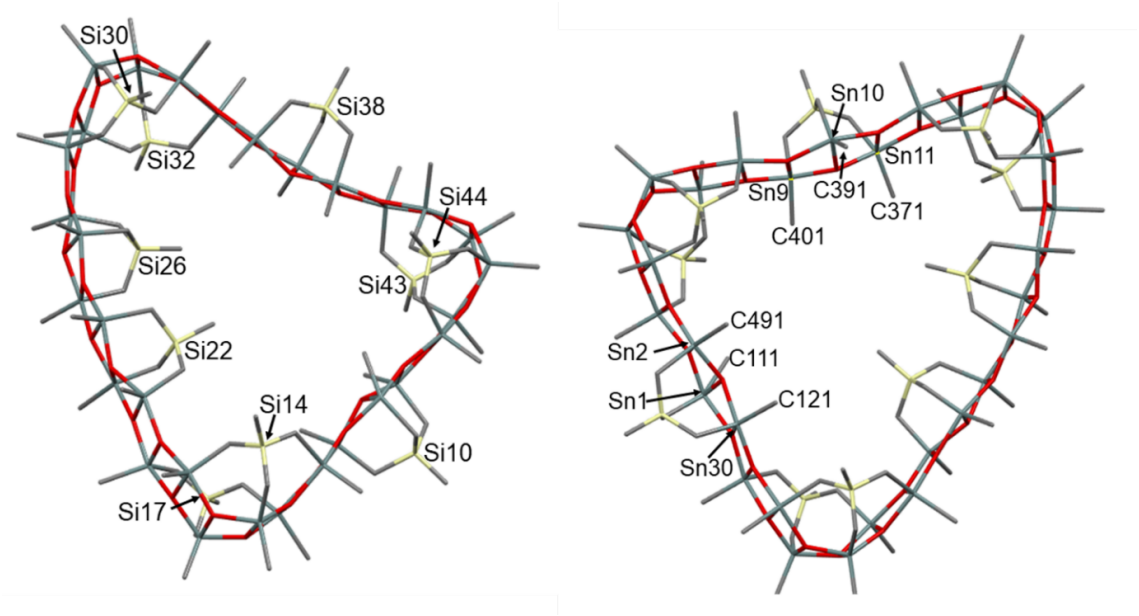

Figure 64. Simplified molecular structure of **30** illustrating the positions of the $SiCH_3$ moieties and the substituents at the tin atoms pointing inside the cavity.[45]

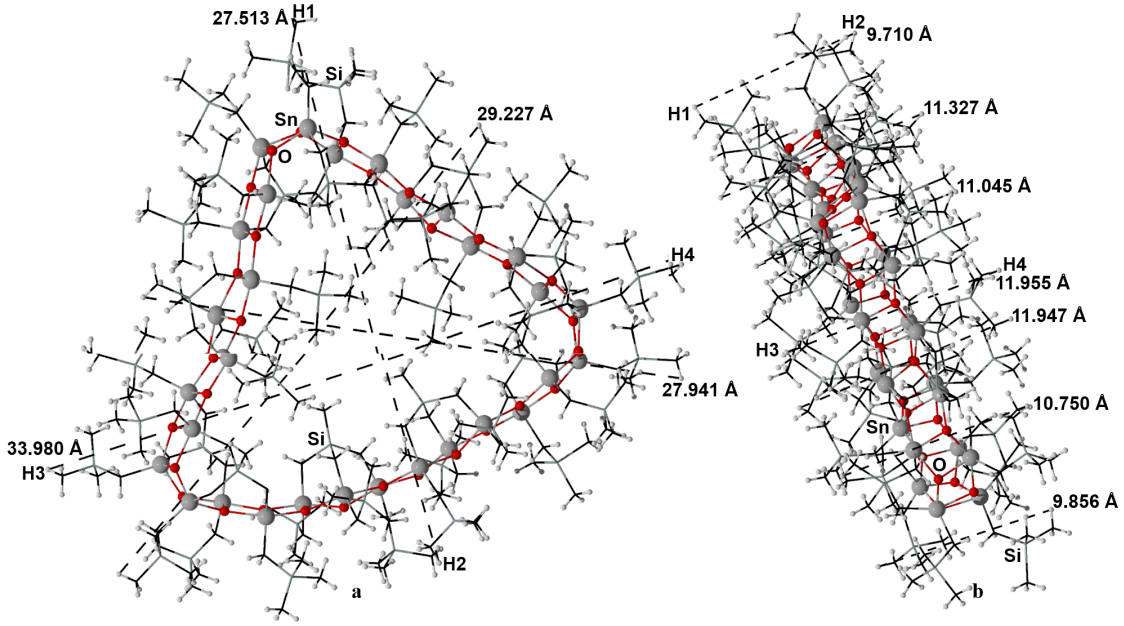

Figure 65. Front view a) and side view b) (POV-Ray) of **30** including the H24F···H46F (27.51(1) Å) and H16K···H34K (33.98(1) Å) distances and the distances indicative for the thickness (H34D···H35D 9.71(1) Å, H11F···H49C 11.96(1) Å).[45]

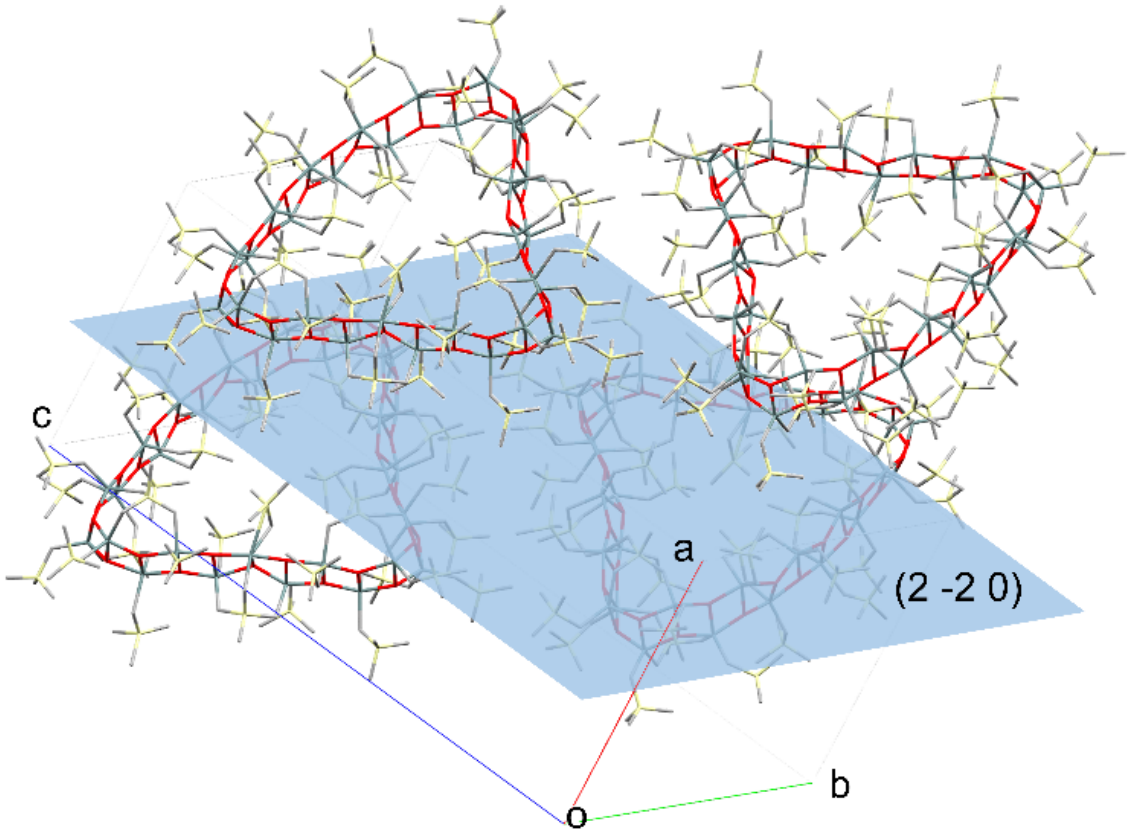

Figure 66. Crystal structure of **30**. The hydrogen atoms are omitted for clarity.[45]

Although the elemental analysis of the bulk crystalline material, obtained from the reaction between **11** and NaOH (Scheme 26), perfectly matches with the empirical formula $[MeSi(CH_2SnCH_2SiMe_3O)_3]_n$, one cannot be sure whether it exclusively consists of the trikonta-nuclear species **30** (n = 10). Given the insufficient amount of material, no powder X-ray diffraction analysis of the bulk material was performed.[45]

A ^{119}Sn NMR spectrum of a $CDCl_3$ solution of the crystalline bulk material the single crystal was taken from, (Supporting Information Chapter 4, Figure S59) in $CDCl_3$ revealed three, within the experimental error almost equally intense, resonances at δ –148 ($^2J(^{119}Sn-^{117/119}Sn)$ = 230 Hz), δ –159 ($^2J(^{119}Sn-^{117/119}Sn)$ = 257 Hz), and δ –164 ppm ($^2J(^{119}Sn-^{117/119}Sn)$ = 219 Hz). In addition, there are hub-like, partially structured broad resonances between δ –126 and δ –146 ppm. A ^{29}Si NMR spectrum (Supporting Information Chapter 4, Figure S57) of the same sample showed a major intense broad unsymmetrically shaped signal at δ 0.9 ppm and a sharp resonance at δ –21.9 ppm. A ^1H NMR spectrum (Supporting Information Chapter 4, Figure S55) revealed signals for the $SiCH_3$, $SiCH_2Sn$, $SnCH_2SiMe_3$, and $Si(CH_3)_3$ protons with correct integral ratio of 3:6:6:27. Attempts at obtaining ^1H DOSY NMR spectrum failed as the sample became gel-like over time. From the NMR data at hand, we conclude that the identity of **30** is not retained in solution. Apparently, the solution contains a mixture of different species.

With caution and in analogy to **29**, we assign the three sharp ^{119}Sn resonances (vide supra) to the oktokaideka-nuclear diorganotin oxide $[MeSi(CH_2SnCH_2SiMe_3O)_3]_6$. Either, the latter is present right from the beginning in the isolated bulk crystalline material or it forms upon dissolution of this material.[45]

An ESI MS (Supporting Information Chapter 4, Figure S61- 70) of a solution of the microcrystalline bulk material in CH3CN/CH_2Cl_2 revealed mass clusters centred at m/z 750.9293, 768.8946, 788.9056, 1646.8168, 1669.6017, 2254.7523, 3077.6608, and 4506.3980. These are assigned to $[MeSi(CH_2SnCH_2SiMe_3O)_3 + H^+]^+$, $[MeSi(CH_2SnCH_2SiMe_3O)_3 + H_2O + H^+]^+$, $[MeSi(CH_2SnCH_2SiMe_3O)_3 + K^+]^+$, $\{[MeSi(CH_2Sn(OH)_2CH_2SiMe_3)_3]_2 + 2H_2O + H^+\}^+$, $\{[MeSi(CH_2Sn(OH)_2CH_2SiMe_3)_3]_2 + CH_3CN + H_2O + H^+\}^+$. $\{[MeSi(CH_2SnCH_2SiMe_3O)_3]_6 + 2H^+\}_2^+$, $\{[MeSi(CH_2SnCH_2SiMe_3O)_3]_4 + H^+\}^+$, and $\{[MeSi(CH_2SnCH_2SiMe_3O)_3]_6 + H^+\}^+$, respectively.[45]

Although no detailed mechanistic studies have been performed, the formation of **29** and **30** can formally be seen as a stepwise process as shown in Scheme 27. Molecular diorganotin oxides **A** with adamantane-type structure undergo ring-opening dimerization via the intermediate **B** giving the hexanuclear product **C**. In case of R = Ph, three **C**-moieties assemble giving the oktokaideka-nuclear diorganotin oxide **29**. In case of R = Me_3SiCH_2, however, **C**-moieties combine with **A**- and **B**-type moieties giving, as one product out of probably several, the trikonta-nuclear molecular diorganotin oxide **30**. This view gets support from the ESI mass spectrometric studies revealing mass clusters that are in line with the presence of **A**- and **C**-type moieties (vide supra).[45]

Scheme 27. Association of two adamantane-type diorganotin oxide moieties **A** undergoing subsequent ring-opening dimerization giving **C**. The existence in solution of these moieties gets support from electrospray ionization mass spectrometry.[45]

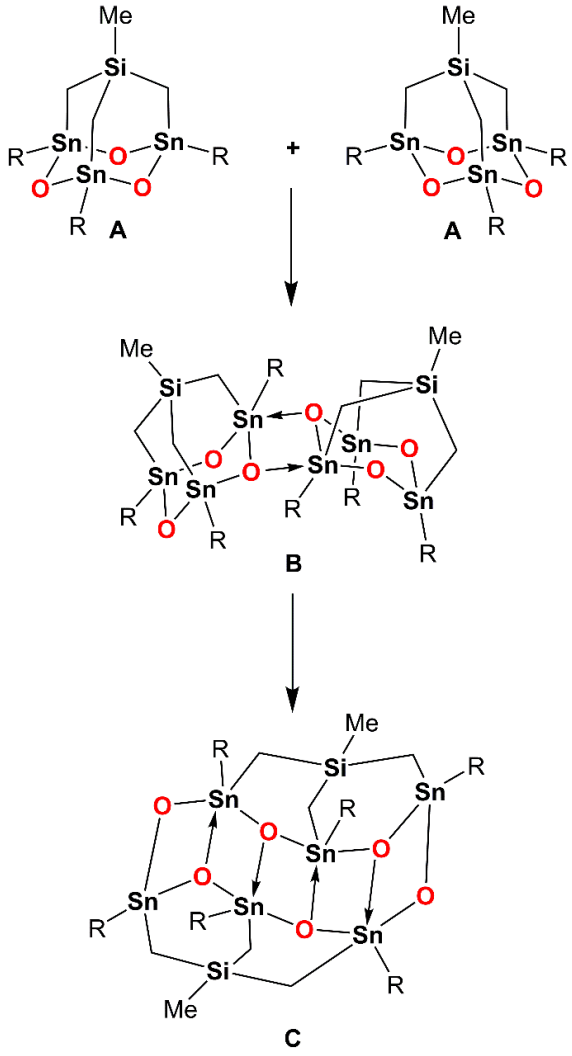

Finally, attempts failed at obtaining host-guest complexes by recrystallizing compound **7** in the presence of elemental sulphur, CCl_4, C_2Cl_4, and PPh_4I, respectively. This statement is in coherence with the fact that compounds **29** and **30** present tiny "cavities" with volume of about 8 $Å^3$, which is even too small to host a water molecule.[45]

A ^{119}Sn NMR spectrum of the crude mixture (Figure 67) in $CDCl_3$ obtained from the reaction between the organotin iodide 3 and $(t\text{-}Bu_2SnO)_3$ shows signal resonances referring to compound **29** at δ –204 , -225 , and -228 ppm with a total integral of 67 %, the by-product $t\text{-}Bu_2SnI_2$ at δ 63, and four further equally intense resonances at δ –233, -230, -196, and -173 ppm, with an integration of 20 %, referring to a Sn-containing unknown product. From this reaction mixture a crystalline material of $[(MeSi(CH_2)_3)Sn(\mu_3\text{-}O)_3(Ph)Sn(I)(Ph)Sn(\mu_2\text{-}OH)(Ph)Sn(t-Bu)_2]_2$, **31**, was isolated suitable for X-ray diffraction study.

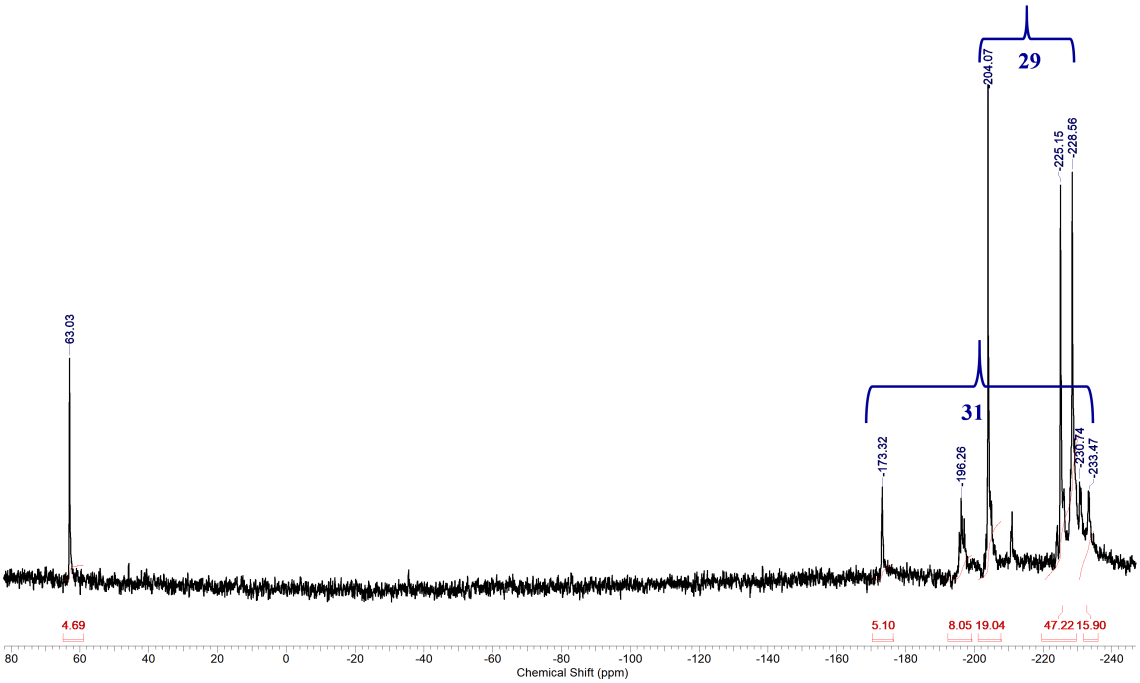

Figure 67. ^{119}Sn NMR spectrum of the crude mixture (149.26 MHz, $CDCl_3$) giving compound **29** and **31**.

The molecular structure of **31** is shown at Figure 68, selected interatomic distances and angles are listed in the figure caption. It crystallizes in the monoclinic space group $P2_1/n$ as **31**·5 DMF solvate. It shows an octanucluear ladder-like dimeric structure resembling to Compound **26** with iodine instead of chlorine substituents in the skeleton. Compound **31** is presenting a middle-stage of formation of the 18-Sn containing oxo-cluster **29**. We can consider it formed from a one-third moiety of **29** composed of $[MeSi(CH_2SnOPh)_3]_2$ with coordination with two *t*-Bu_2SnIOH molecules (Figure 69); these latter are resulted from reaction of two *t*-Bu_2SnI_2 and two H_2O molecules.

This structure is like that of **26**, composed of four 6-membred-rings (Si – C – Sn – O – Sn – C) and seven 4-membred Sn_2O_2-rings. (Figure 68).

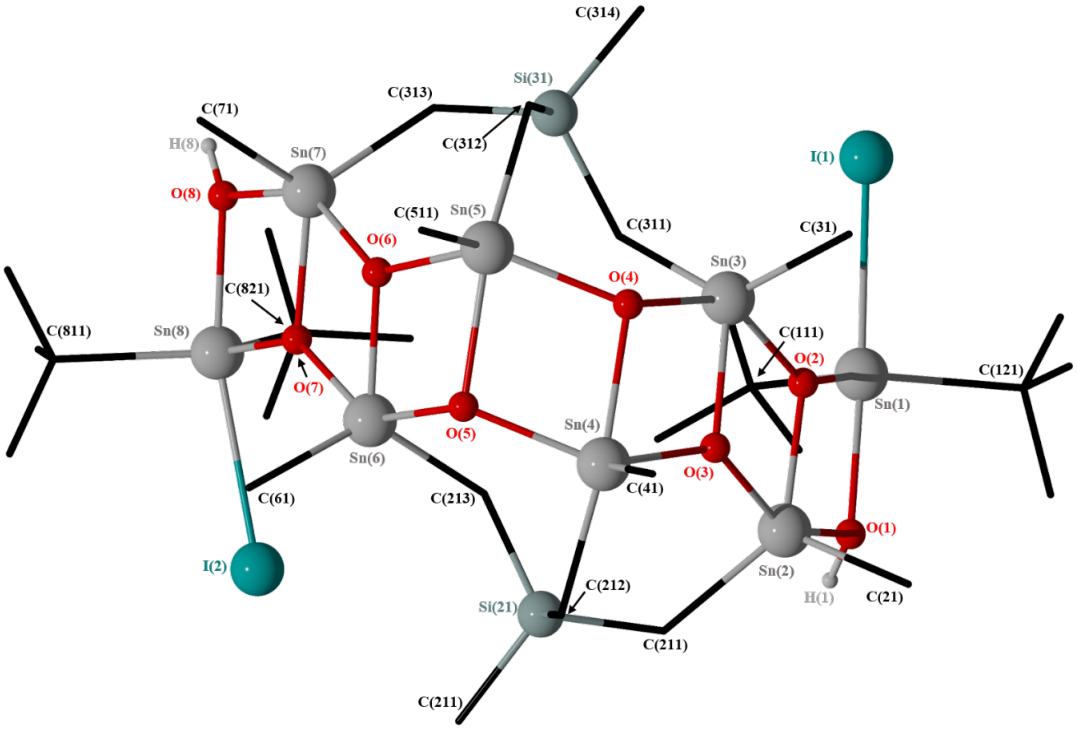

Figure 68. POV-Ray image presented in balls and sticks of the molecular structure of $[(MeSi(CH_2)_3)Sn(\mu_3\text{-}O)_3(Ph)Sn(I)(Ph)Sn(\mu_2\text{-}OH)(Ph)Sn(t\text{-}Bu)_2]_2$, **31**. Only C_i of the phenyl groups are shown for clarity. The DMF solvate molecules are omitted for clarity. Selected interatomic distances (Å): Sn(2)–O(3) 2.094(8), Sn(3)–O(2) 2.183(8), Sn(5)–O(6) 2.073(8), Sn(6)–O(5) 2.155(8), Sn(7)–O(6) 2.098(8), Sn(1)–O(1) 2.187(8), Sn(4)–O(3) 2.064(8), Sn(1)–I(1) 2.9020(14), and Sn(8)–I(2) 2.9395(13), O(1)–H(1) 0.868 , O(8)–H(8) 0.865. Selected interatomic angles (°): O(1)–Sn(1)–O(2) 73.0(3), O(1)–Sn(2)–O(3) 149.0(3), O(2)–Sn(3)–O(3) 72.8(3), O(4)–Sn(3)–O(2) 146.3(3), C(41)–Sn(4)–O(3) 115.7(4), O(4)–Sn(4)–C(212) 154.0(4), O(5)–Sn(5)–C(312) 151.5(4), O(6)–Sn(5)–O(5) 72.5(3), O(5)–Sn(6)–O(6) 73.3(3), C(71)–Sn(7)–O(6) 95.7(4), O(7)–Sn(8)–C(821) 117.5(4), O(1)–Sn(1)–I(1) 160.8(2), O(8)–Sn(8)–I(2) 157.72(19), Si(21)–C(212)–Sn(4) 111.1(5), and Si(21)–C(213)–Sn(6) 121.7(6).

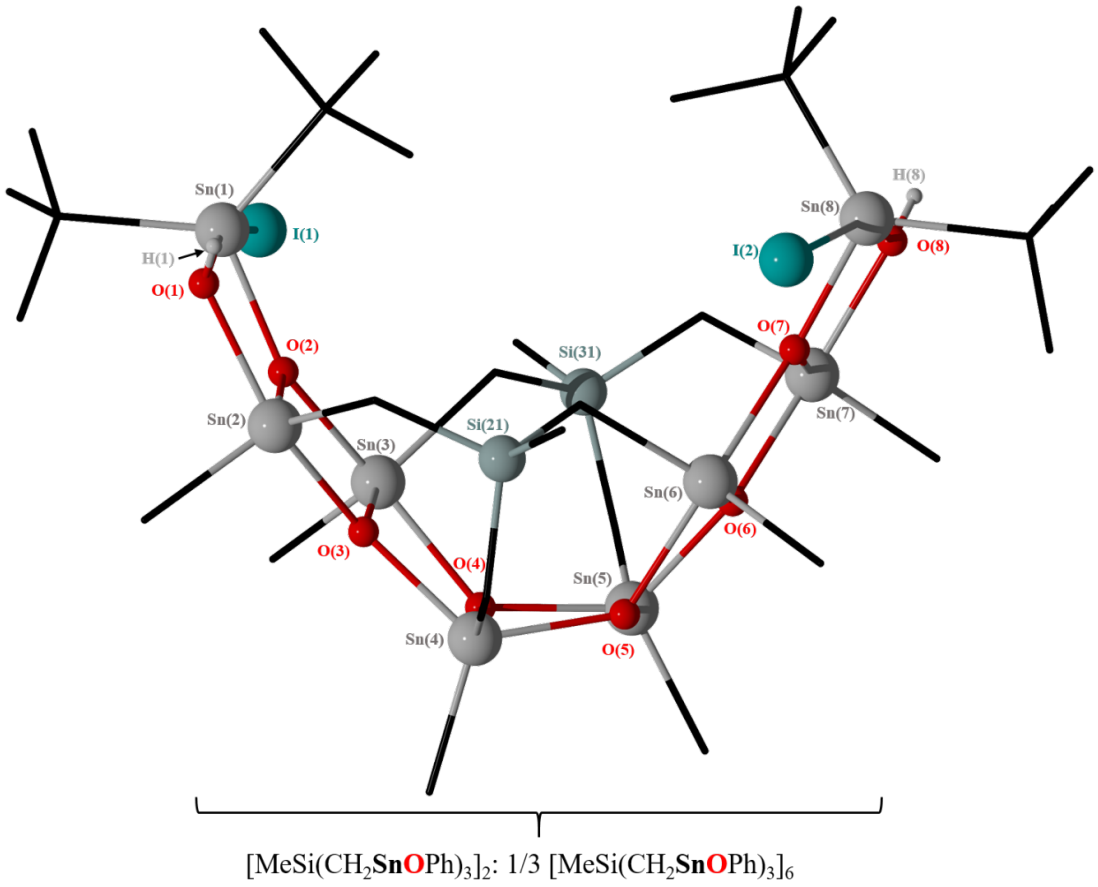

Figure 69. Presentation of **31** as one-third moiety of **29**; $[MeSi(CH_2SnOPh)_3]_2$ with coordination with two *t*-Bu_2SnIOH molecules.

The endo-cyclic- (Sn2, Sn3, Sn4, Sn5, Sn6, and Sn7) and exo-cyclic- (Sn1 and Sn8) tin atoms exhibit distorted trigonal bipyramidal environments.

For each of the Sn(2), Sn(3), Sn(6), and Sn(7) atoms, the two carbon atoms (C_i atom from the phenyl substituent and the methylene carbon atom) and one oxygen atom occupy the equatorial positions. The corresponding C_{equ}-Sn-C_{equ} angles vary between 119.0(5)° (C21–Sn2–C211) and 132.8(4)° (C31–Sn3–C311). Two oxygen atoms take the axial positions with the O_{ax}–Sn–O_{ax} angles varying between 145.5(3) (O5–Sn6–O7) and 149.0(3)° (O1–Sn2–O3). As for the exo-cyclic Sn(1) and Sn(8) atoms, the two carbon atoms (C atoms from the two t-Bu substituents) and one oxygen atom occupy the equatorial positions. The corresponding C_{equ}–Sn–C_{equ} angles are almost equal with values of 125.9(5)° (C111–Sn1–C121) and 126.8(5)° (C812–Sn8–C821). One oxygen and one iodine atom take the axial positions with the O_{ax}–Sn–I_{ax} angles varying between 157.72(19)° (O8–Sn8–I2) and 160.8(2)° (O1–Sn1–I1).

The corresponding Sn–O_{ax} distances vary between 2.031(8) (Sn4–O5) and 2.183(8) Å (Sn3–O2). The Sn-I distances are 2.9020(14) (Sn1-I1) and 2.9395(13) Å (Sn8–I2). The

$Sn–O_{equ}$ distances involving oxygen atoms in equatorial positions are slightly shorter and vary between 2.018(8) (Sn6–O6) and 2.073(8) Å (Sn5–O6).

Notably, like for the tinoxo-cluster **29**, for the tin atoms Sn(4) and Sn(5) for each case the corresponding methylene carbon atom and one out of the adjacent three oxygen atoms take the axial positions whereas the C_i and the two remaining oxygen atoms occupy the equatorial positions. This is in contrast to a situation as expected from the polarity rule according to which the electronegative substituents occupy the axial positions in a trigonal bipyramidal structure. The $C_{ax}–Sn–O_{ax}$ angles vary between 151.5(4)° (O5–Sn5–C312) and 154.0(4)° (O4–Sn4–C212). The geometrical goodness[22] $\Delta\Sigma(\theta)$ is 76.7° for Sn(1), 89.7° for Sn(2), 95.3° for Sn(3), 56° for Sn(4), 54.4° for Sn(5), 85.2° for Sn(6) , 90.2° for Sn(7), and 80.2° for Sn(8). Notably, $\Delta\Sigma(\theta)$ of Sn(3) is higher than 90°, this is probably due to the distortion of the angles (C31–Sn3–C311) 132.8(4)° from the ideal geometry of 120°.

Angles around the silicon methylene-bridged organotin arms are almost equal, varying between 111.1(5)° (Si21–C212–Sn4) and 121.7(6)° (Si21–C213–Sn6). As the matter of fact, we observe in Compound **31**, same the case for **26** the $Sn_4O_2X_2Y_2$-structural motif, (X, Y = OH, I), characteristic for di-organostannoxanes.[23,47,48] This motif is presented as $Sn_4O_6OH_2I_2$, exhibiting an asymmetric combination, in which the hydroxyl groups are located in the bridging positions and the iodine atoms are bonded to the exo-cyclic tin atoms.

Given the lack of sufficient amount of material, no further investigations in solution could be realized. However, the ^{119}Sn NMR resonance shifts of **31** (Figure 67) resembles the corresponding signals observed for 26 at δ –230, -228, -209, and -196 ppm. They are all equally intense, which matches with the solid state structure of **31**. We can with caution presume that the solid state structure is also retained in solution like the case for compound **26**.

An attempt of recrystallization the nonabromido-organotin compound **9** under non-inert condition from dichloromethane/ethanol solution gives a product of partial hydrolysis as brownish needles suitable for X-ray diffraction study (Scheme 28). The compound **32** crystallized as its ethanol solvate $[MeSi(CH_2SnBr)_3(\mu_2\text{-}OH)_2(\mu_4\text{-}O)(\mu_3\text{-}OEt)_2]_2 \cdot 2\,EtOH$. It is almost insoluble in all organic solvents.

Scheme 28. Synthesis of the hexanuclear organotin oxo-cluster ladder-like compound **32**.

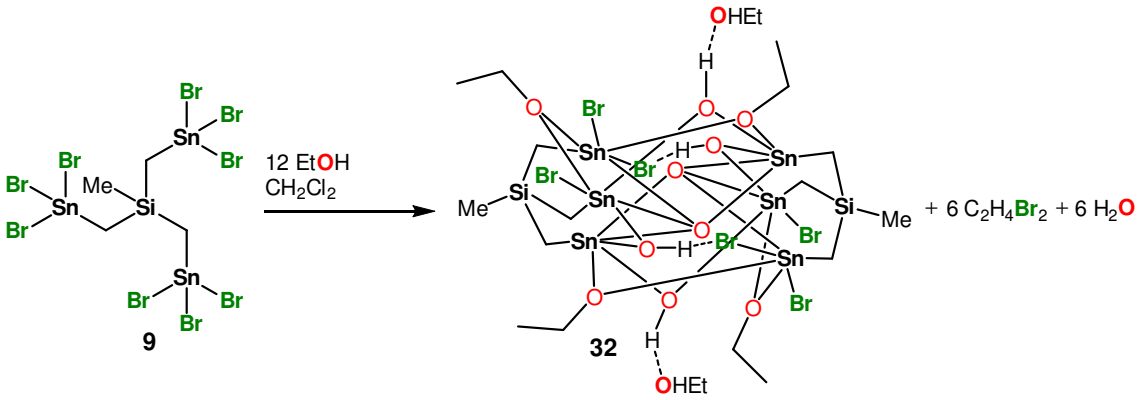

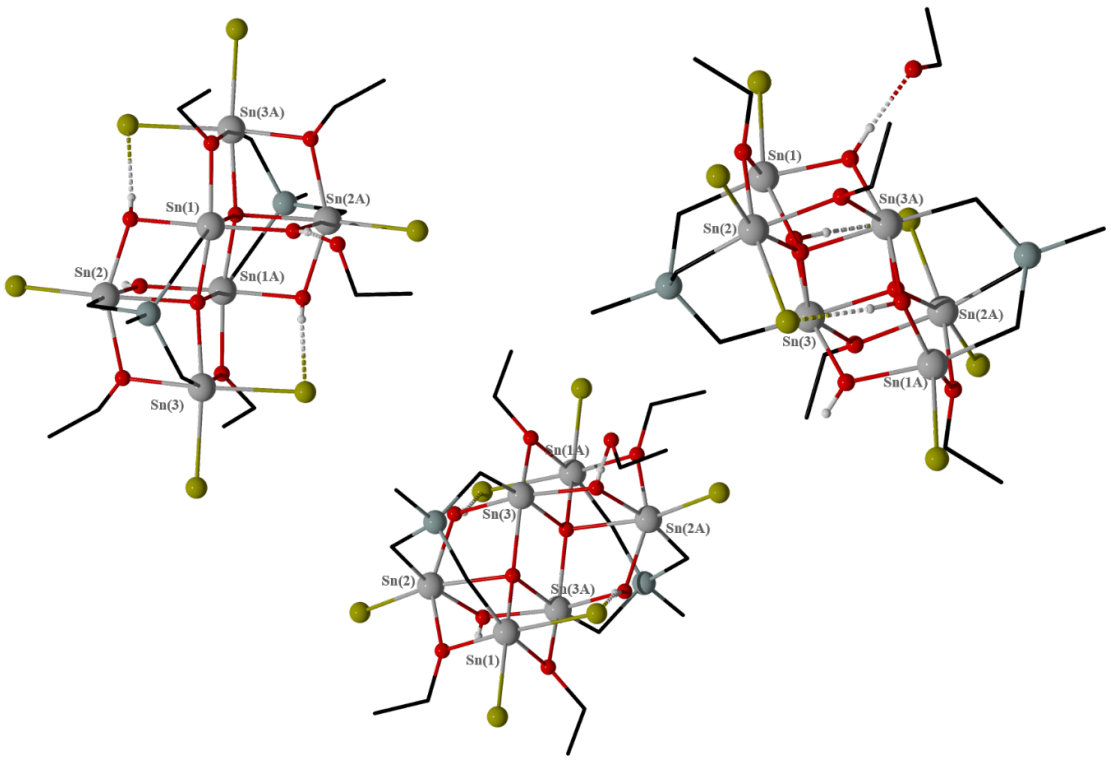

Figure 70. Different perspectives of the three ladder-like structures connected via nine Sn_2O_2 rings in the skeleton of **32**.

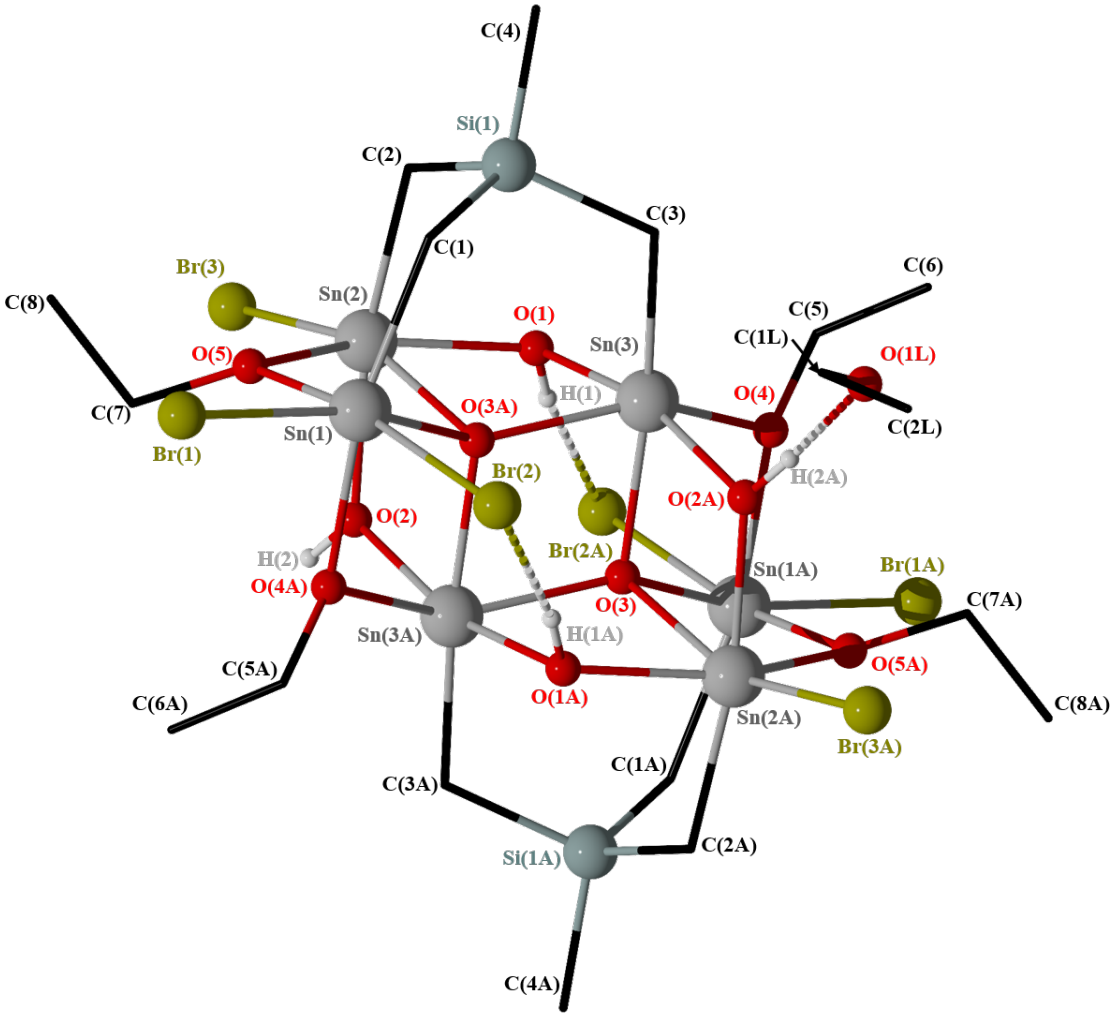

Figure 71. POV-Ray image of the molecular structure of $[MeSi(CH_2SnBr)_3(\mu_2\text{-}OH)_2(\mu_4\text{-}O)(\mu_3\text{-}OEt)_2]_2 \cdot 2EtOH$, **32**. The protons of the solvate groups between O(1L) and O(2A), and O(1LA) and O(2) cannot be found on the electron density map. Only one solvate group is shown. Selected interatomic distances (Å): Sn(1)–Br(1) 2.5555(13), Sn(1)–Br(2) 2.6610(12), Sn(1)–O(3A) 2.177(6), Sn(1)–O(4A) 2.158(7), Sn(1)–O(5) 2.147(6), Sn(2)–O(1) 2.097(7), Sn(2)–O(2) 2.068(7), Sn(2)–O(3A) 2.332(6), Sn(3)–O(5) 2.113(6), Sn(3)–O(1) 2.140(6), Sn(3)–O(3A) 2.144(6), Sn(3)–O(3) 2.097(6), Sn(3)–O(2A) 2.098(7), Sn(3)–O(4) 2.107(6), O(1)H(1)···Br(2A) 1.747, and O(2)–H(2)···O(1LA) 2.378. Selected interatomic angles (°):C(1)–Sn(1)–O(4A) 164.0(3), O(5)–Sn(1)–O(3A) 77.8(2), Br(1)–Sn(1)–O(3A) 162.41(17), Br(2)–Sn(1)–O(5) 169.23(18), Br(1)–Sn(1)– Br(2) 91.83(4), C(2)–Sn(2)–O(2) 167.2(3), O(1)–Sn(2)–O(5) 150.0(2), Br(3)–Sn(1)–O(5) 104.15(17), Br(3)–Sn(1)–O(3A) 159.88(16), O(1)–Sn(1)–Br(3) 105.33(18), C(3)–Sn(3)–O(3) 168.9(3), O(1)–Sn(3)–O(4) 83.6(2), O(3A)–Sn(3)–O(4) 147.0(3), O(1)–Sn(3)–O(2A) 164.7(3), and O(2A)–Sn(1)–O(3A) 97.2(2).

Figure 71 shows the molecular structure of compound **32**. The figure caption contains selected interatomic distances and angles. Compound **32** crystallizes in the monoclinic space group $P2_1/n$. It shows a centro-symmetric hexanuclear organotin oxo-cluster, presented as a dimer in the solid state, via bridging Sn–Br and Sn–O intramolecular interactions. There are three ladder-like structures connected with each other via nine Sn_2O_2 rings (Figure 70). Figure 70 shows the molecular structure of **32** from different perspectives. This dimer is formed via two (μ_4–O); O(3) and O(3A), two hydrogen bonds (μ_2–OH$\cdots$Br); O(1)H(1)$\cdots$Br(2A) and O(1A)H(1A)$\cdots$Br(2), two hydrogen bonds via coordination with the solvent molecules (μ_2–O–H$\cdots$OEt); O(2)–H(2)$\cdots$O(1LA)Et, and O(2A)–H(2A)$\cdots$O(1L)Et and four ethoxy- substituents; O(4)Et, O(4A)Et, O(5)Et and O(5A)Et.

All six tin centres are hexa-coordinated, and exhibit each a distorted octahedral all-trans environment, with three different types of coordinations on each two symmetrical Sn centres. For Sn(1) and Sn(1A), there is a $SnCBr_2O_3$ environment with angles of (C1–Sn1–O4A) 164.0(3)°, (O5–Sn1–O3A) 77.8(2)°, (Br1–Sn1–O3A) 162.41(17)°, (Br2–Sn1–O5) 169.23(18)°, and (Br1–Sn1–Br2) 91.83(4)°. For Sn(2) and Sn(2A), there is a SnCBrO4 environment with angles of (C2–Sn2–O2) 167.2(3)°, (O1–Sn2–O5) 150.0(2)°, (Br3–Sn1–O5) 104.15(17)°, (Br3–Sn1–O3A) 159.88(16)°, and (O1-Sn1- Br3) 105.33(18)°. For Sn(3) and Sn(3A), there is a $SnCO_5$ environment with angles of (C3–Sn3–O3) 168.9(3)°, (O1–Sn3–O4) 83.6(2)°, (O3A–Sn3–O4) 147.0(3)°, (O1–Sn3–O2A) 164.7(3)°, and (O2A–Sn1–O3A) 97.2(2)°.

There is an overall symmetry characterising this structure. The Br-Sn-Br bridge is approximately symmetric with Sn(1)–Br(1) and Sn(1)–Br(2) distances of 2.5555(13) and 2.6610(12) Å, respectively. Sn2–Br3 is also nearly equal with distance of 2.5255(12) Å. The O–Sn–O bridges are almost symmetric with distances for Sn1 of Sn(1)–O(3A), Sn(1)–O(4A), and Sn(1)–O(5), respectively, equal to 2.177(6), 2.158(7), and 2.147(6) Å. For Sn(2) the distances of Sn(2)–O(1), Sn(2)–O(2), Sn(2)–O(3A), and Sn(3)–O(5) are equal to 2.097(7), 2.068(7), 2.332(6), and 2.113(6) Å, respectively. For Sn(3), the distances of Sn(3)–O(1), Sn(3)–O(3A), Sn(3)–O(3), Sn(3)–O(2A), and Sn(3)–O(4), are equal to 2.140(6), 2.144(6), 2.097(6), 2.098(7), and 2.107(6) Å, respectively.

The hydrogen bonds O(1)H(1)$\cdots$Br(2A) and O(2)–H(2)$\cdots$O(1LA)Et are equal to 1.747 and 2.378 Å, respectively.

This reaction is reproducible. The study of **32** in solution is not realizable, given the insolubility of this compound in almost all organic solvents. However an ESI-MS spectrum of this crystalline material (negative mode, see Supporting Information, Chapter 4, Figures S73, 74) shows one mass cluster with minor intensity centred at m/z 1610.3 corresponding, respectively, to the anions of $[C_{20}H_{57}Br_4O_{14}Si_2Sn_6]^-$: $[M - Br_2 + OH^- + H_2O]^-$. In IR spectroscopy, we notice the presence of the absorption band at ν 3501-3318 cm^{-1} and ν

2969-2893 cm^{-1}, corresponding to OH groups (See Supporting Information, Chapter 4, Figure S75).

4.3 Novel S-, Se- containing silastannaadamantanes: syntheses, structures, and redistribution reactions

The ^{119}Sn NMR spectrum in $CDCl_3$ of a white residue, obtained from a reaction between one molar equiv of the diorganotin diiodide derivative **3** and 3.2 molar equiv of Na2S in acetone/methanol/water solution (Scheme 30) shows one singlet resonance at 98 ppm with a coupling constant $^2J(^{119}Sn-^{117}Sn)$ = 187 Hz (Figure 72). A crystalline material of 7-Methyl-1,3,5-tris(triphenyl-2,4,9-trithio-7-sila-1,3,5-tristannaadamantane, MeSi($CH_2SnPhS)_3$, **33**, was isolated from a diethyl-ether/dichloromethane solution as transparent needles suitable for X-ray diffraction study. Compound **33** is soluble in both polar and non-polar organic solvents.

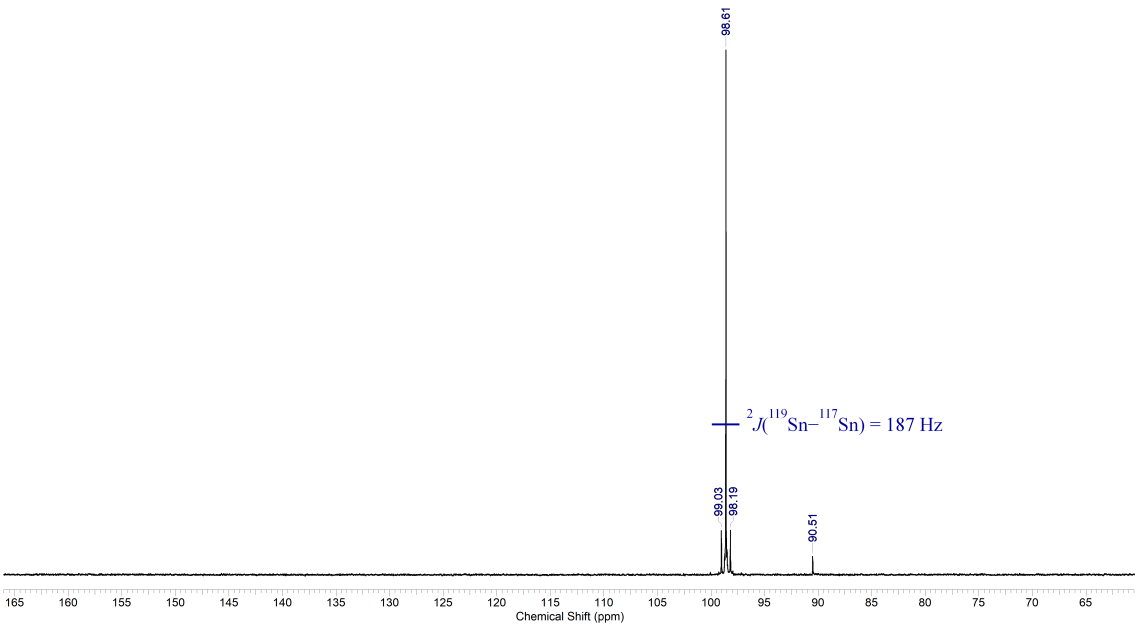

Figure 72. ^{119}Sn NMR spectrum (223.85 MHz, $CDCl_3$) of the crude mixture of the reaction of formation of of **33**.

Scheme 29. Synthesis of the silastannaadamantane compound **33**.

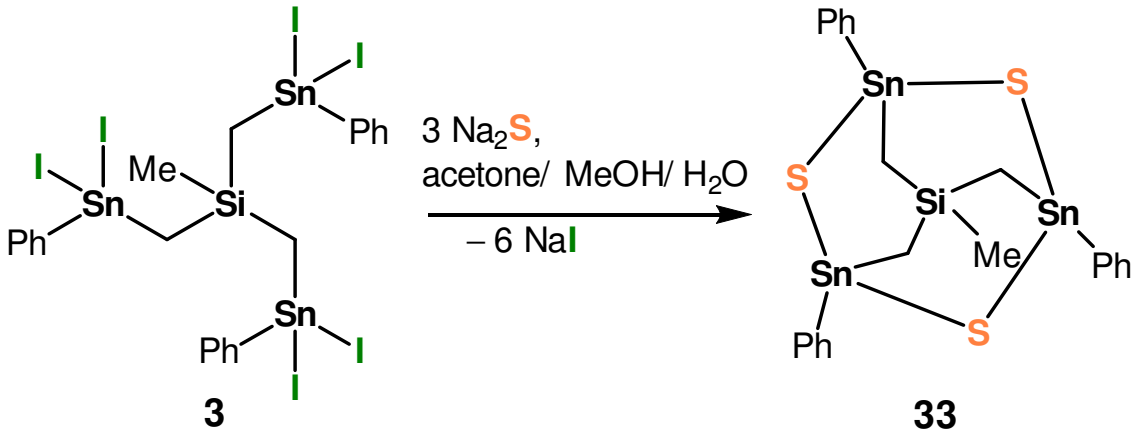

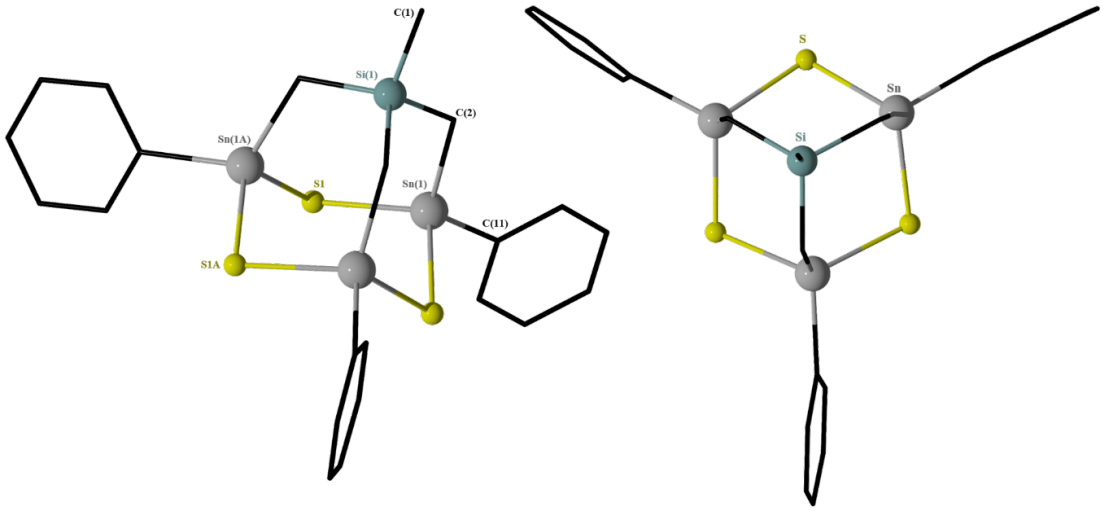

Figure 73. Left: POV-Ray image of the molecular structure of MeSi($CH_2SnPhS)_3$, **33**. Protons are omitted for clarity. Right: Overall symmetry of **33**. Selected interatomic distances (Å): Sn1–S1 2.4097(12), Sn1A–S1 2.4162(12), Si(1)–C(2) 1.870(5), Sn(1)–C(2) 2.131(5). Selected interatomic angles (°): C(2)–Sn(1)–S(1) 107.44(13), C(11)–Sn(1)–S(1) 103.30(12), S(1A)–Sn(1)–S(1) 109.37(6), C(2)–Sn(1)–C(11) 119.84(18), C(2)–Sn(1)–S(1A) 111.91(13), C(11)–Sn(1)–S(1A) 104.40(13), Sn(1A)–S(1)–Sn(1) 99.16(5), S(1)–Sn(1A)–(S1A) 109.37(6), Si(1)–C(2)–Sn(1) 117.8(2).

Figure 73 shows the molecular structure of compound **33** and the figure caption contains selected interatomic distances and angles. Compound **33** crystallizes in the trigonal space group R_{3C}. It shows an almost perfectly symmetric adamantane structure composed of

three six-membred rings (Si – C – Sn – S – Sn – C). It represents the first adamantane containing carbon, silicon and tin atoms in the skeleton.[10,50,53]

The environments about the tin atoms are distorted tetrahedral, with angles of C(2) – Sn(1) – S(1), C(2) – Sn(1) – S(1), S(1 A) – Sn(1) – S(1), S(1 A) – Sn(1) – S(1), S(1 A) – Sn(1) – S(1), S(1 A) – Sn(1) – S(1), respectively, equal to 107.44(13), 103.30(12), 109.37(6), 119.84(18), 111.91(13), and 104.40(13)°. The distortions from the ideal tetrahedral geometry are not significant.

This adamantane structure consists of three bridging S atoms in which all Sn – S – Sn angles are equal to (Sn1A–S1–Sn1) 99.16(5)°. This angle is similar to that corresponding in $[(PhSSn)_2(CH_2)_3]_2$ (Sn1-S1-Sn2) (99.62(4)°)[53] and smaller than those corresponding in $[(PhSSn)_2CH_2]_2$, varying between 102.2(1) and 104.0(1)°.[10] As well, all S-Sn-S angles are equal to 109.37(6)°, these latter are similar to those in $[(PhSSn)_2(CH_2)_3]_2$ (S1–Sn1–S2) (108.26(4)°) and (S1–Sn2–S2) (109.47(4)°) and in $[(PhSSn)_2CH_2]_2$ (S1–Sn2–S3) (109.4(4)°)[10] and larger than those reported for [PhSn(S2CNEt2)]2(S)(CH2)3 (S1–Sn1–S2) (95.54(5)°) and (S2–Sn1–S3) (65.41(5)°).[53]

The overall symmetrical characteristic of the molecular structure of 33 is also proved by the evenness of the angles at the silicon methylene-bridged organotin arms, which are all equal to (Si1–C2–Sn1) 117.8(2)°. This statement refers to the tripod geometry characteristic of these novel organotin precursors. The Sn–S bond distances are symmetrical and equal to 2.4097(12) Å (Sn1–S1) and 2.4162(12) Å (Sn1A–S1), these bond distances are very similar to those corresponding in $[(PhSSn)_2(CH_2)_3]_2$ varying between (Sn1–S2) 2.397(1) Å and (Sn1–S1) 2.407(1) Å ,[53] and $[(PhSSn)_2CH_2]_2$ varying between (Sn1–S2) 2.388(2) Å and (Sn1–S1) 2.425(1) Å .[10] Also the Si-C-Sn bridges are all similar with distances of 1.870(5) and 2.131(5) Å, respectively corresponding to Si(1)–C(2) and Sn(1)–C(2).

The identity of compound **33** is retained in solution. The compound is kinetically inert on the 1H, 13C, 29Si and ^{119}Sn NMR time scales. Thus, a ^{1}H NMR spectrum ($CDCl_3$ solution, see Supporting Information, Chapter 4, Figure S77) shows the resonance signal of $SiCH_3$ protons appearing at δ 0.43 ppm ($^4J(^1H-^{117/119}Sn)$ = 11 Hz). The $SiCH_2$ protons, with integration of 6H, appear at δ 0.80 ppm ($^2J(^1H-^{117/119}Sn)$ = 72 Hz). The complex pattern referring to the protons of the phenyl groups appears at δ 7.42-7.77 ppm with integration of 15H. In a ^{13}C NMR spectrum ($CDCl_3$ solution, see Supporting Information, Chapter 4, Figure S78), the resonances corresponding to the $SiCH_2Sn$ carbon atoms appear at δ 5.41 ppm ($^1J(^{13}C-^{29}Si)$ = 47 Hz, $^1J(^{13}C-^{117/119}Sn)$ = 279/292 Hz), and those of $SiCH_3$ at δ 8.4 ppm ($^3J(^{13}C-^{117/119}Sn)$ = 44 Hz, $^1J(^{13}C-^{29}Si)$ = 85 Hz). In the aromatic part, the C_m resonance appears at δ 128.9 ppm ($^3J(^{13}C-^{117/119}Sn)$ = 70 Hz), the C_p at δ 130.1 ppm ($^4J(^{13}C-^{117/119}Sn)$ = 10 Hz), the C_o at δ 134.4 ppm ($^2J(^{13}C-^{117/119}Sn)$ = 57 Hz), and the C_i at δ 141.4 ppm ($^1J(^{13}C-^{117/119}Sn)$ = 615/645 Hz). A ^{29}Si NMR spectrum ($CDCl_3$ solution, see Supporting Information Chapter 4, Figure S79) shows a resonance referring to the MeSi silicon atom at δ 13.4 ppm ($^2J(^{29}Si-^{117/119}Sn)$ = 50 Hz, $^1J(^{29}Si-^{13}C)$ =

94 Hz). The ^{119}Sn NMR spectrum of a crystalline material of **33** in $CDCl_3$ (Figure 74) shows a resonance at δ 98 ppm ($^2J(^{119}Sn-^{117}Sn)$ = 190 Hz) referring to three equivalent tin atoms which matches perfectly with the molecular structure found for the solid state. This signal is similar to that reported for the stannaadamantane $[(PhSSn)_2CH_2]_2$ at δ 106 ppm ($^2J(^{119}Sn-^{117}Sn)$ = 195 Hz),[10] and high-frequency-shifted comparing to the corresponding Sn atoms in $[(PhSSn)_2(CH_2)_3]_2$ at δ 53 ppm ($^2J(^{119}Sn-^{117}Sn)$ = 183 Hz).[53] An ESI-MS spectrum (positive mode) of 33 shows one mass cluster centred at m/z 793.0 corresponding to the cation $[C_{22}H_{24}NaS_3SiSn_3]^+$ ($[M + Na^+]^+$), which confirms that the cluster remains intact in solution even under harsh ESI-MS conditions (See Supporting Information, Chapter 4, Figures S82, S83).

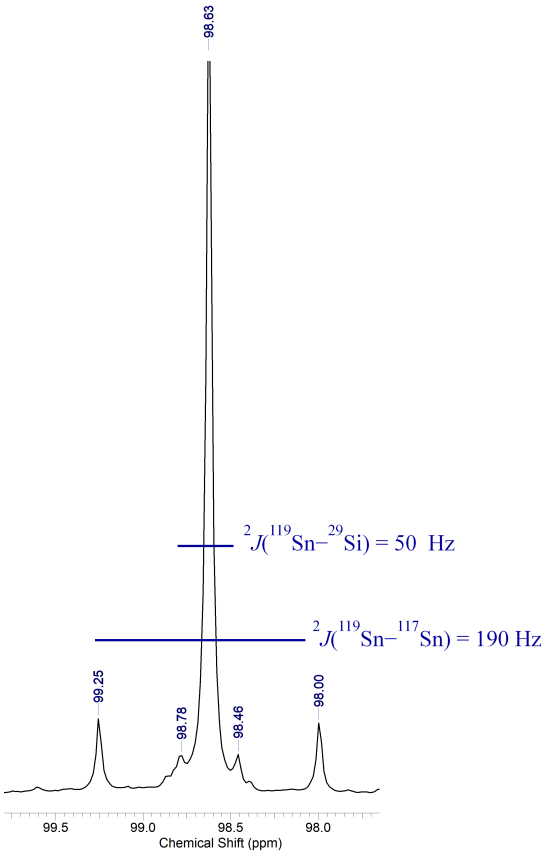

Figure 74. ^{119}Sn NMR spectrum (149.26 MHz, $CDCl_3$) of compound **33**.

We wanted to investigate the stability of **33** in solution, and the possibility to form further structural isomers in solution, which is known for such stannadamantane compounds.[50] Upon addition of one molar equiv of F^- as $NEt_4F_2 \cdot 2H_2O$ to one molar equiv of **33** in $CDCl_3$, the ^{119}Sn NMR spectrum shows the same resonance as the silastannaadamantane **33** (see supporting Information, Chapter 4, Figure S85), which is opposite to the affirmation saying that of addition of Lewis base may catalyze the formation of other structural isomers in solution.[53] To study the possibility of exchange reaction between a structurally alike organotin oxide compound **29**, $[MeSi(CH_2SnPhO)_3]_6$ and the silastannaadamantane **33**,

$MeSi(CH_2SnPhS)_3$. Upon addition of one molar equiv of **29** to six molar equiv of **33** in C_6D_6, the ^{119}Sn NMR spectrum shows the three resonances referring to **29** at δ –228, -225, and -204 ppm and the signal referring to **33** at δ 98 ppm (See supporting Information, Chapter 4, Figure S86).

The ^{119}Sn NMR spectrum in $CDCl_3$ of a white residue, obtained from a reaction of one molar equiv of the dichlorido-derivative **4** with 3.2 molar equiv of Na_2Se in acetone/methanol-water solution shows one singlet resonance at 3.7 ppm with coupling constants $^2J(^{119}Sn-^{117}Sn) = 220$ Hz and $^1J(^{119}Sn-^{77}Se) = 1221$ Hz (Figure 75). From a solution of dichloromethane/diethylether, a crystalline material was isolated from this reaction mixture as transparent needles suitable for X-ray diffraction study. It proved to be 7-Methyl-1,3,5-tris(triphenyl-2,4,9-triselena-7-sila-1,3,5-tristannaadamantane $MeSi(CH_2SnPhSe)_3$, **34** (Scheme 30). Compound **34** shows very good solubility in organic solvents.

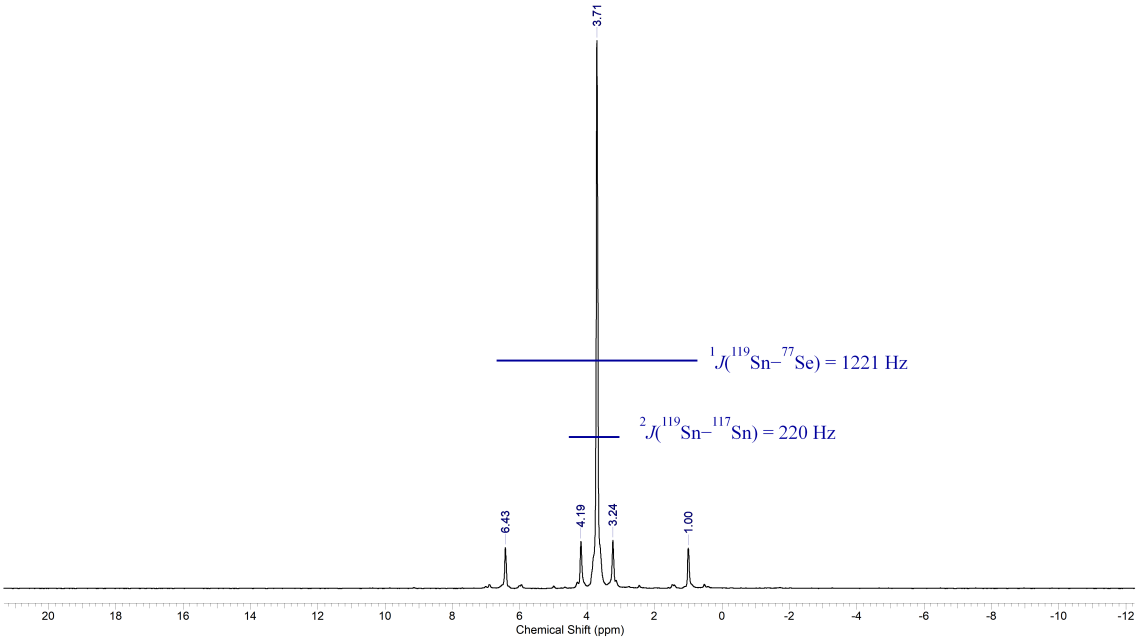

Figure 75. ^{119}Sn NMR spectrum (223.85 MHz, $CDCl_3$) of the crude mixture of the reaction of formation of **34**.

Scheme 30. Synthesis of the Se-silastannaadamantane compound **34**.

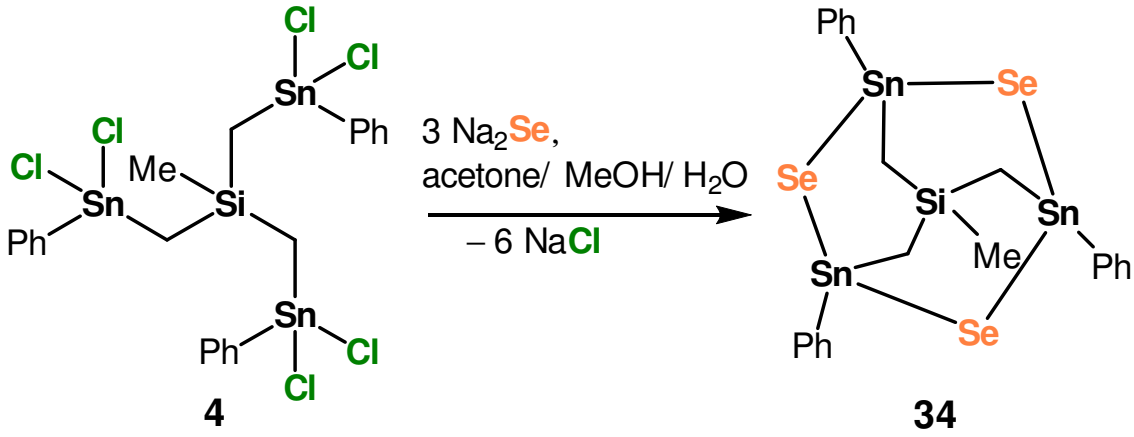

Figure 76 shows the molecular structure of compound **34**. The figure caption contains selected interatomic distances and angles. Compound **34** crystallizes in the monoclinic space group $P2_1/c$. It shows an almost symmetrical adamantane structure. The structure of **34** is similar to a first approximation to that of **33**. Figure 76 (right) shows the overall symmetry characteristic of the new Se-containing silastannaadamantane structure **34**.

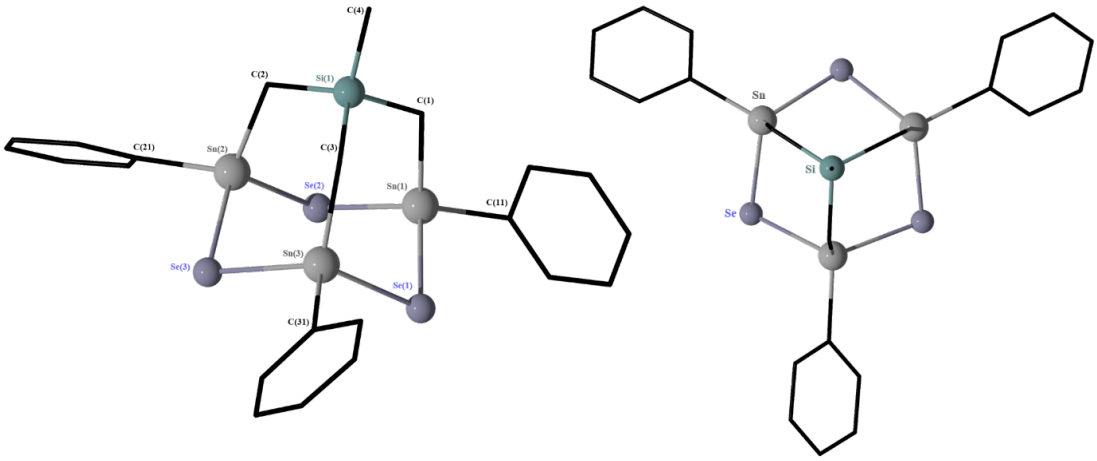

Figure 76. Left: POV-Ray image of the molecular structure of $MeSi(CH_2SnPhSe)_3$, **34**. Right: Overall symmetry characteristic of **34**. Protons are omitted for clarity. Selected interatomic distances (Å): Si(1)–C(1) 1.858(3), Si(1)–C(2) 1.870(3), Si(1)–C(3) 1.868(3), Sn(1)–C(1) 2.124(3), Sn(1)–C(2) 2.134(3), Sn(1)–C(3)2.135(3), Sn(1)–Se(1) 2.5354(3), Sn(1)–Se(2) 2.5353(3), Sn(2)–Se(2) 2.5208(3), Sn(2)–Se(3) 2.5473(3), Sn(3)–Se(1) 2.5323(3), Sn(3)–Se(2) 2.5209(3). Selected interatomic angles (°): C(11)–Sn(1)–Se(1) 105.24(7), Se(2)–Sn(1)–Se(1) 111.868(11), C(21)–Sn(2)–Se(3) 102.61(7), C(21)–Sn(2)–C(2) 114.66(10), C(31)–Sn(3)–Se(3) 106.65(7), Se(3)–Sn(3)–Se(1) 112.718(12), Sn(1)–Se(1)–Sn(3) 94.531(10), Sn(1)–Se(2)–Sn(2) 94.795(11), Sn(2)–Se(3)–Sn(3) 94.928(10), Se(2)–Sn(1)–Se(1) 111.868(11), Se(2)–Sn(2)–Se(3) 110.224(11), Se(3)–Sn(3)–Se(1) 112.718(12), Si(1)–C(1)–Sn(1) 120.29(13), Si(1)–C(2)–Sn(2) 118.53(12), Si(1)–C(3)–Sn(3) 119.35(14).

The environments about the tin atoms are distorted tetrahedral, with angles at Sn(1) varying between 105.24(7) and 111.868(11)°, corresponding, respectively to, C(11)–Sn(1)–Se(1) and Se(2)–Sn(1)–Se(1), at Sn(2) varying between 102.61(7) and 114.66(10)°, corresponding, respectively to, C(21)–Sn(2)–Se(3) and C(21)–Sn(2)–C(2), and at Sn(3) varying between 106.65(7) and 112.718(12)°, corresponding, respectively to, C(31)–Sn(3)–Se(3) and Se(3)–Sn(3)–Se(1). The distortions from the ideal tetrahedral geometry are not significant. This adamantane structure consists of three bridging Se atoms in which the Sn–Se–Sn angles are very similar, equal to Sn(1)-Se(1)–Sn(3) 94.531(10)°, Sn(1)–Se(2)–Sn(2) 94.795(11)°, and Sn(2)–Se(3)–Sn(3) 94.928(10)°. These angles are slightly smaller than those corresponding in $[(MeSeSn)_2CMe_2]_2$, with angles of (Sn1–Se1–Sn2) 99.18(7)° and (Sn1–Se2–Sn2) 99.24(7)°[10] and larger than those corresponding in $[(SnR_1)_2Se_2Cl_2]$, $[(SnR_1)_3Se_4Cl]$, and $[(SnR_1)_4Se_6]$ (R1 = $CMe_2CH_2C(O)Me$), with angles respectively of 84.52(3), 81.50(2)–83.26(2), and 85.55(1)–85.73(1)°.[54] All Se–Sn–Se angles are similar equal to (Se2–Sn1–Se1) 111.868(11)°, (Se2–Sn2–Se3) 110.224(11)°, Se(3)–Sn(3)–Se(1) 112.718(12)°. These latter angles are comparable to those in $[(MeSeSn)_2CMe_2]_2$, with

angles of (Se1–Sn1–Se2) 109.89(8)° and (Se1–Sn2–Se2) 111.31(9)°[10] and larger than those in $[(SnR_1)_2Se_2Cl_2]$, $[(SnR_1)_3Se_4Cl]$, and $[(SnR_1)_4Se_6]$ (R1 = $CMe_2CH_2C(O)Me$), with angles respectively of 95.48(3), 93.78(2)–94.14(2), and 94.03(1)–94.68(1)°.[54]

The overall symmetrical characteristic of the molecular structure of 34 is confirmed by the similarity of the angles at the silicon methylene tin bridges, equal to Si(1)–C(1)–Sn(1) 120.29(13)°, Si(1)–C(2)–Sn(2) 118.53(12)°, and Si(1)–C(3)–Sn(3) 119.35(14)°. This refers to the tripod geometry characteristic of these novel organotin precursors, in which the Si-C-Sn bridges are all similar with distances of 1.858(3), 1.870(3), 1.868(3), 2.124(3), 2.134(3), and 2.135(3) Å, respectively corresponding to Si(1)–C(1), Si(1)–C(2), Si(1)–C(3), Sn(1)–C(1), Sn(1)–C(2), Sn(1)–C(3). The S–Sn–S bridges are almost symmetrical with bond distances equal to 2.5354(3) Å (Sn1–Se1), 2.5353(3) Å (Sn1–Se2), 2.5208(3) Å (Sn2–Se2), 2.5473(3) Å (Sn2–Se3), 2.5323(3) Å (Sn3–Se1), and 2.5209(3) Å (Sn3–Se2). These bond distances are similar to those corresponding in $[(MeSeSn)_2CMe_2]_2$ equal to (Sn1–Se1) 2.496(2) Å and (Sn1–Se2) 2.506(2) Å,[51] and comparable to those in $[(SnR_1)_4Se_6]$ (R1 = $CMe_2CH_2C(O)Me$), with distances varying between 2.5156(3)-2.5954(3) Å.[54]

The identity of compound **34** is retained in solution. The compound is kinetically inert on the ^1H, ^{13}C, ^{29}Si and ^{119}Sn NMR time scales. Thus, a ^1H NMR spectrum ($CDCl_3$ solution, see Supporting Information, Chapter 4, Figure S87) shows the resonance signal of $SiCH_3$ protons appearing at δ 0.36 ppm ($^4J(^1H-^{117/119}Sn)$ = 10 Hz, $^2J(^1H-^{29}Si)$ = 20 Hz. The $SiCH_2$ protons, with integration of 6H, appear at δ 0.90 ppm ($^2J(^1H-^{117/119}Sn)$ = 72 Hz, $^3J(^1H-^{77}Se)$ = 122 Hz). The complex pattern referring to the protons of the phenyl groups appears at δ 7.42-7.72 ppm with integration of 15H. In a ^{13}C NMR spectrum ($CDCl_3$ solution, see Supporting Information, Chapter 4, Figures S88), the resonances corresponding to the $SiCH_2Sn$ carbon atoms appear at δ 5.23 ppm ($^1J(^{13}C-^{29}Si)$ = 52 Hz, $^1J(^{13}C-^{117/119}Sn)$ = 245/256 Hz) and those of the $SiCH_3$ at δ 9.37 ppm ($^3J(^{13}C-^{117/119}Sn)$ = 43 Hz, $^1J(^{13}C-^{29}Si)$ = 85 Hz). In the aromatic part, the C_m resonance appears at δ 128.9 ppm ($^3J(^{13}C-^{117/119}Sn)$ = 61 Hz), the C_p at δ 130.07 ppm (13C-117/119Sn) = 15 Hz, $^5J(^{13}C-^{77}Se)$ = 56 Hz), the C_o at δ 134.4 ppm ($^2J(^{13}C-^{117/119}Sn)$ = 57 Hz), and the C_i at δ 140.67 ppm ($^3J(^{13}C-^{117}Sn)$ = 10 Hz, $^3J(^{13}C-^{77}Se)$ = 52 Hz, $^1J(^{13}C-^{117/119}Sn)$ = 547/571 Hz). A ^{29}Si NMR spectrum ($CDCl_3$ solution, see Supporting Information, Chapter 4, Figure S89) shows a resonance referring to the MeSi silicon atom at δ 13.8 ppm ($^2J(^{29}Si-^{117/119}Sn)$ = 41 Hz, $^1J(^{29}Si-^{13}C)$ = 87 Hz). The ^{119}Sn NMR spectrum of a crystalline material of 34 in $CDCl_3$ solution (Figure 77) shows a resonance at δ 2.44 ppm ($^1J(^{119}Sn-^{77}Se)$ = 1231 Hz, $^1J(^{119}Sn-^{13}C_i)$ = 573 Hz, $^2J(^{119}Sn-^{117}Sn)$ = 217 Hz) referring to three equivalent tin atoms which matches perfectly with the molecular structure proposed for the solid state (Figure 76). This signal is similar to that at δ 3.1 ppm ($^2J(^{119}Sn-^{117}Sn)$ = 220 Hz),[10] reported for the stannaadamantane $[(PhSeSn)_2CH_2]_2$ and

low-frequency-shifted compared to the corresponding Sn atoms in $[(MeSeSn)_2CMe_2]$ at δ 42.9 ppm ($^2J(^{119}Sn-^{117}Sn)$ = 195 Hz).[10]

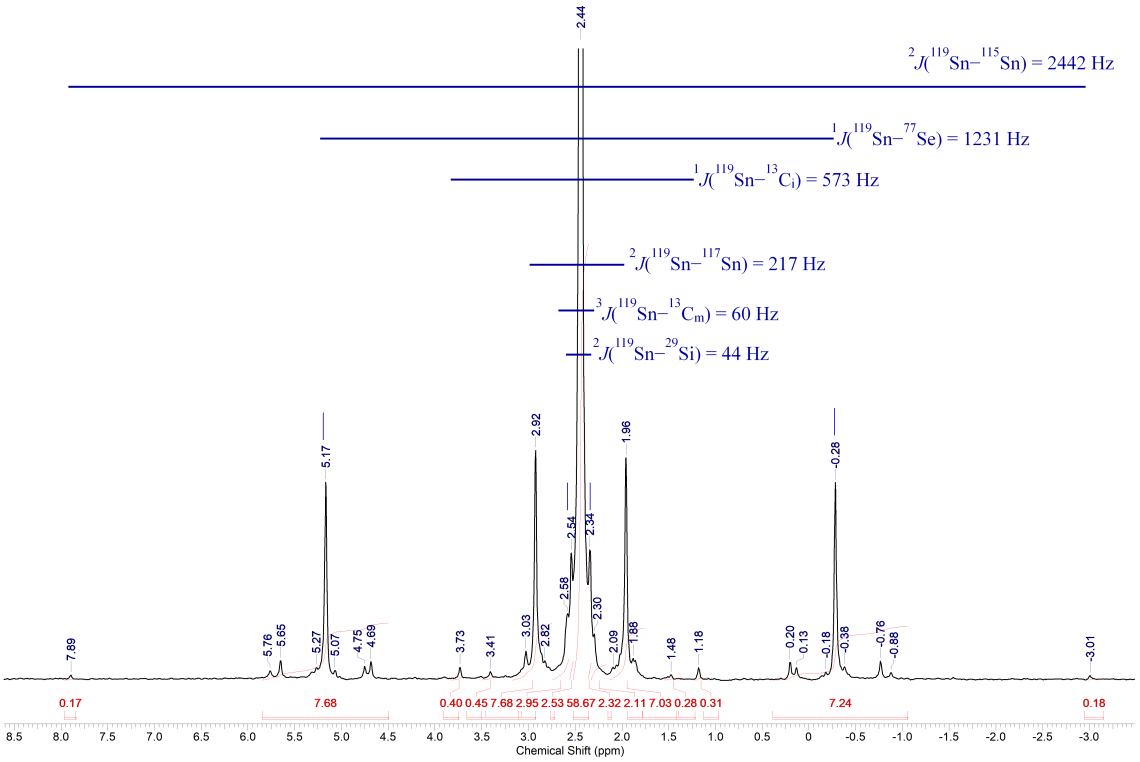

Figure 77. ^{119}Sn NMR spectrum (149.26 MHz, $CDCl_3$) of compound **34**.

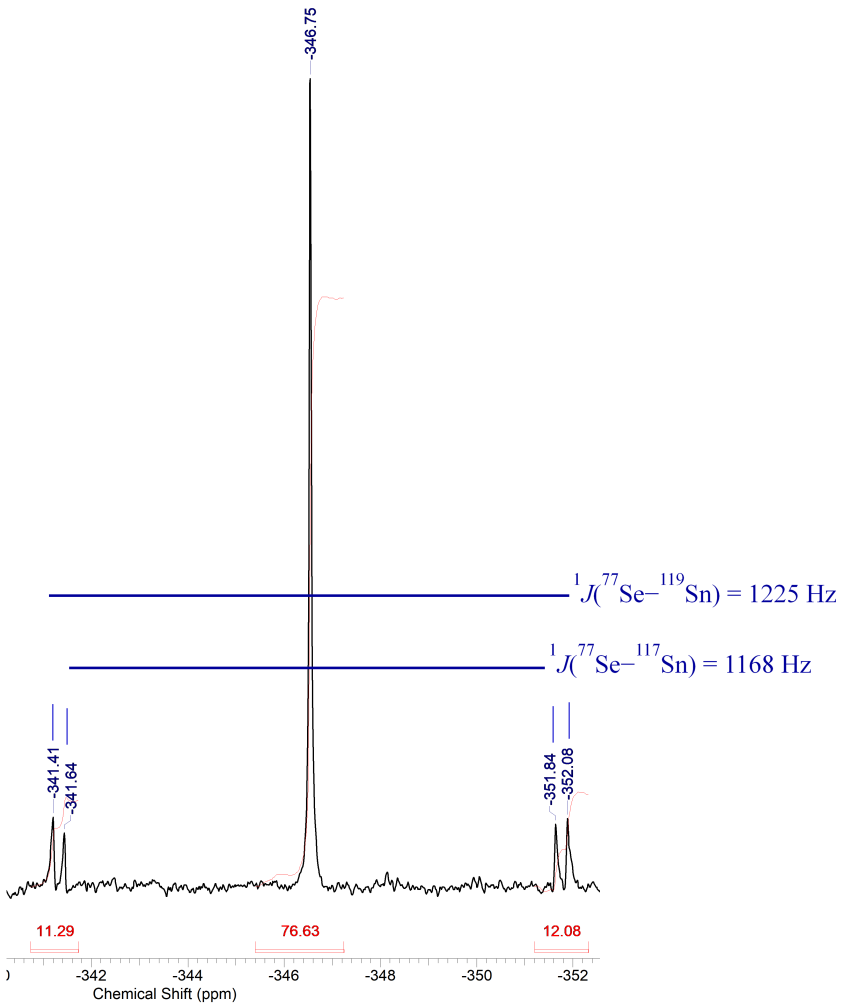

Figure 78. ^{77}Se NMR spectrum (223.85 MHz, $CDCl_3$) of compound **34**.

The ^{77}Se NMR spectrum of the same sample in $CDCl_3$ (Figure 78) shows a resonance at δ –346.75 ppm ($^1J(^{77}Se-^{117/119}Sn)$ = 1168/1225 Hz). This resonance is similar to that reported for the stannaadamantane $[(MeSeSn)_2CMe_2]$ at δ –362 ppm ($^1J(^{77}Se-^{119}Sn)$ = 1255 Hz),[10] and low-frequency-shifted comparing to the corresponding Se atoms in $[(PhSeSn)_2CH_2]_2$ at δ –323 ppm ($^1J(^{77}Se-^{119}Sn)$ = 1274 Hz).[10] An ESI-MS spectrum (positive mode) of 34 shows one mass cluster centred at m/z 2163.07 corresponding to the cations $[C_{66}H_{74}O_9Si_3Sn_9]_2^+$ $\{[MeSi(CH_2SnPhO)_3]_3 + 2H^+\}_2^+$. This refers to the polymerization process in solution via formation of the monomer-oxido-stannaadamantane in solution. This is in relation with the formation mechanism suggested for the oxo clusters **29** and **30** (See Supporting Information, Chapter 4, Figures S93- S95).

The ^{119}Sn NMR spectrum in $CDCl_3$ of a white residue, obtained from a reaction between one molar equiv of the diorganotin diiodido derivative 11 and 3.2 molar equiv of Na_2S in acetone/methanol/water solution shows one singlet resonance at 152 ppm with a coupling constant $^2J(^{119}Sn-^{117}Sn)$ = 200 Hz (Figure 79). A crystalline material is isolated from diethylether/dichlormethane solution as transparent needles suitable for X-ray diffraction

study. The compound **35**, 7-methyl-1,3,5-tris((trimethylsilyl)methyl)-2,4,9-trithia-7-sila-1,3,5-tristannaadamantane, $MeSi[CH_2Sn(CH_2SiMe_3)S]_3$ (Scheme 31) is isolated. This latter shows good solubility in organic solvents.

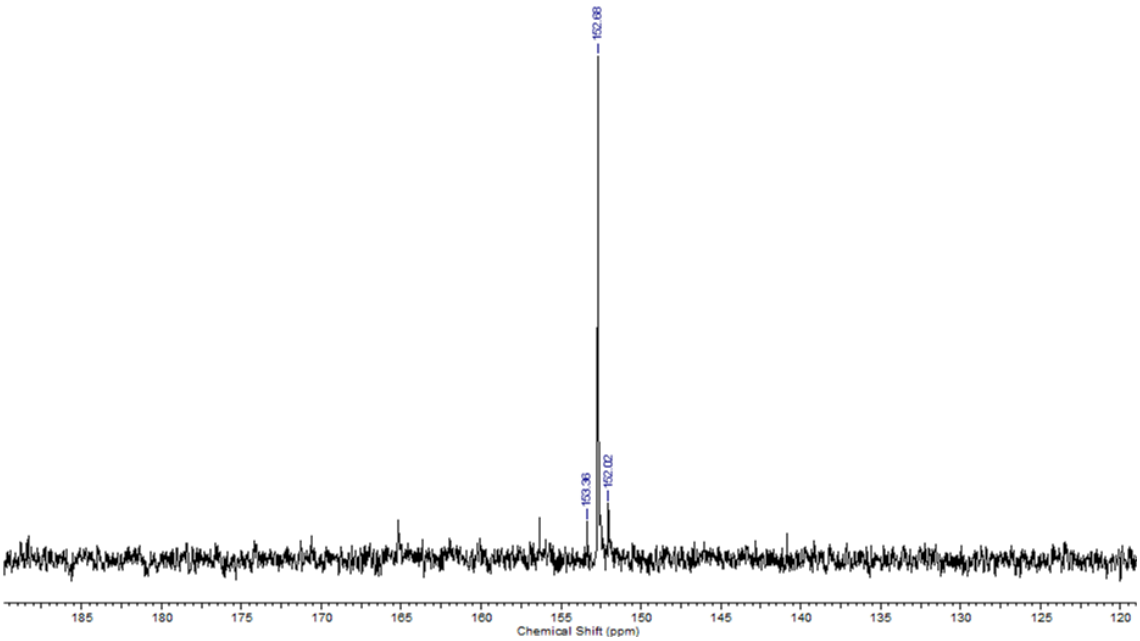

Figure 79. ^{119}Sn NMR spectrum (149.26 MHz, $CDCl_3$) of the crude mixture of the reaction of formation of **35**.

Scheme 31. Synthesis of the S-silastannaadamantane $MeSi(CH_2SnCH_2SiMe_3S)_3$, **35**.

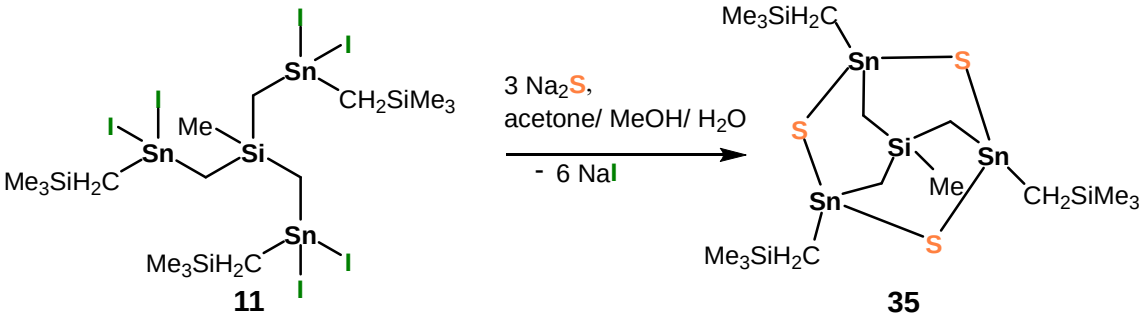

Figure 80 shows the molecular structure of compound **35**. The figure caption contains selected interatomic distances and angles. Compound **35** crystallizes in the monoclinic space group $P2_1/c$, with two molecules in the unit cell. It shows an almost perfect symmetric adamantane-type structure rather similar to that of its phenyl-substituted analogue, compound **33**.

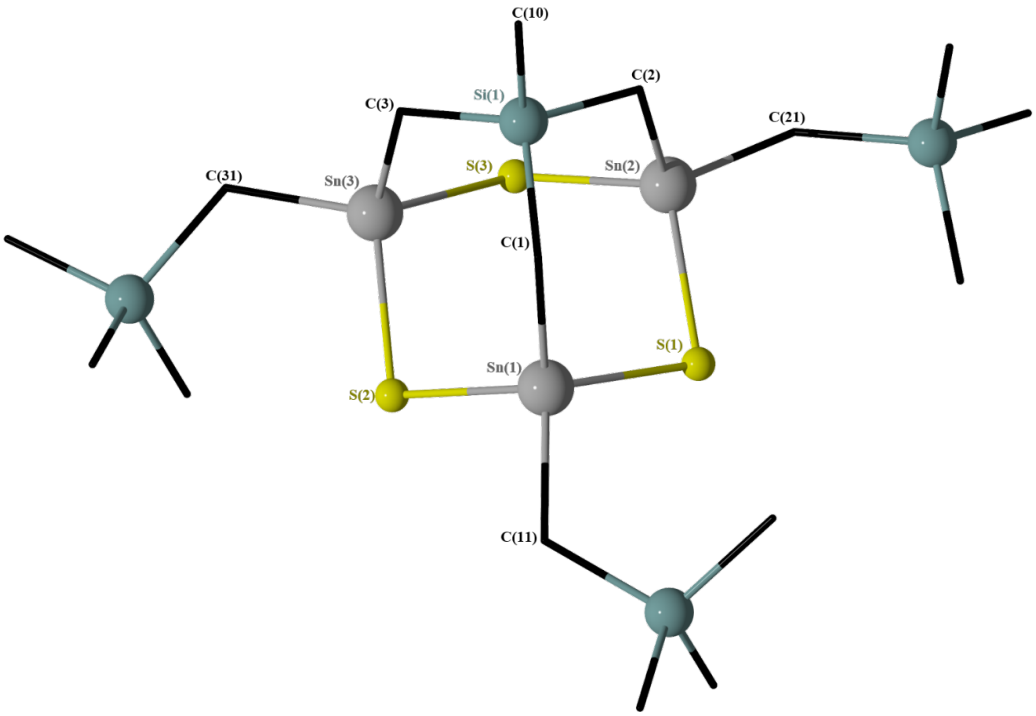

Figure 80. POV-Ray image of the molecular structure of MeSi[$CH_2Sn(CH_2SiMe_3)S]_3$, **35**. Protons are omitted for clarity. Selected interatomic distances (Å): Sn(1)–S(1) 2.417(3), Sn(2)–S(1) 2.416(2), Sn(1)–S(2) 2.416(2), Sn(3)–S(2) 2.394(2), Sn(2)–S(3) 2.425(2), Sn(3)–S(3) 2.428(2). Selected interatomic angles (°): C(11)–Sn(1)–S(2) 101.9(3), C(11)–Sn(1)–C(1) 115.6(4), Sn(1)–S(1)–Sn(2) 100.00(9), Sn(1)–S(2)–Sn(3) 100.61(9), Sn(2)–S(3)–Sn(3) 100.45(9), S(1)–Sn(1)–S(2) 107.47(9), S(1)–Sn(2)–S(3) 110.91(8), S(2)–Sn(3)–S(3) 106.51(9), Si(1)–C(1)–Sn(1) 117.9(5), Si(1)–C(2)–Sn(2) 118.5(4), Si(1)–C(3)–Sn(3) 120.2(5).

The environments about the tin atoms are distorted tetrahedral, with angles, varying from 101.9(3) and 115.6(4)°, corresponding, respectively to, C(11)–Sn(1)–S(2) and C(11)–Sn(1)–C(1). The distortions from the ideal tetrahedral geometry are not significant.
Like compound **33**, this adamantane structure consists of three bridging S atoms in which the Sn – S – Sn angles are very similar, equal to Sn(1)–S(1)–Sn(2) 100.00(9)°, Sn(1)–S(2)–Sn(3) 100.61(9)°, and Sn(2)–S(3)–Sn(3) 100.45(9)°. All S–Sn–S angles are similar equal to (S1–Sn1–S2) 107.47(9)°, (S1–Sn2–S3) 110.91(8)°, S(2)–Sn(3)–S(3) 106.51(9)°. The overall symmetrical characteristic of the molecular structure of 35 is confirmed by the similarity of the angles at the silicon methylene tin bridges, equal to Si(1) – C(1) – Sn(1) 117.9(5)°, Si(1) – C(2) – Sn(2) 118.5(4)°, and Si(1) – C(3) – Sn(3) 120.2(5)°. The Sn – S – Sn bridges are almost symmetrical with bond distances equal to 2.417(3) Å (Sn1–S1), 2.416(2) Å (Sn2–S1), 2.416(2) Å (Sn1–S2), 2.394(2) Å (Sn3–S2), 2.425(2) Å (Sn2–S3), and 2.428(2) Å (Sn3–S3).

As well, the molecular structure of **35** suggested in solid state is retained in solution. Compound **35** is kinetically inert on the ^{1}H, ^{13}C, ^{29}Si and ^{119}Sn NMR time scales (See Supporting Information, Chapter 4, Figures S98- S102). The ^{119}Sn NMR spectrum of a crystalline material of 35 in $CDCl_3$ solution (Figure 81) shows a resonance at δ 152 ppm ($^{2}J(^{119}Sn-^{117}Sn)$ = 212 Hz, $^{4}J(^{119}Sn-^{117}Sn)$ = 3614 Hz) referring to three equivalent tin atoms which matches perfectly with the molecular structure proposed in solid state. This signal is similar to that corresponding in the stannaadamantane $[(CH_2SiMe_3SSn)_2CH_2]_2$ at δ 159.4 ppm ($^{2}J(^{119}Sn-^{117}Sn)$ = 195 Hz).[10] A ^{29}Si NMR spectrum ($CDCl_3$ solution, see Supporting Information, Chapter 4, Figure S102) shows two resonances referring to the MeSi and the CH_2SiMe_3 silicon atoms, respectively, at δ 11.3 ppm ($^{2}J(^{29}Si-^{117/119}Sn)$ = 52 Hz), and δ 2.2 ppm ($^{2}J(^{29}Si-^{117/119}Sn)$ = 30 Hz, $^{1}J(^{29}Si-^{13}C)$ = 56 Hz).

An ESI-MS spectrum (positive mode, see Supporting Information, Chapter 4, Figures S103, S104) of 35 shows one intense mass clusters centred at m/z 798.8659 corresponding to the cation $[C_{16}H_{43}S_3Si_4Sn_3]^+$ $MeSi[CH_2Sn(CH_2SiMe_3)S]_3$ + H++ which confirms that the cluster remains intact in solution even under harsh ESI-MS conditions.

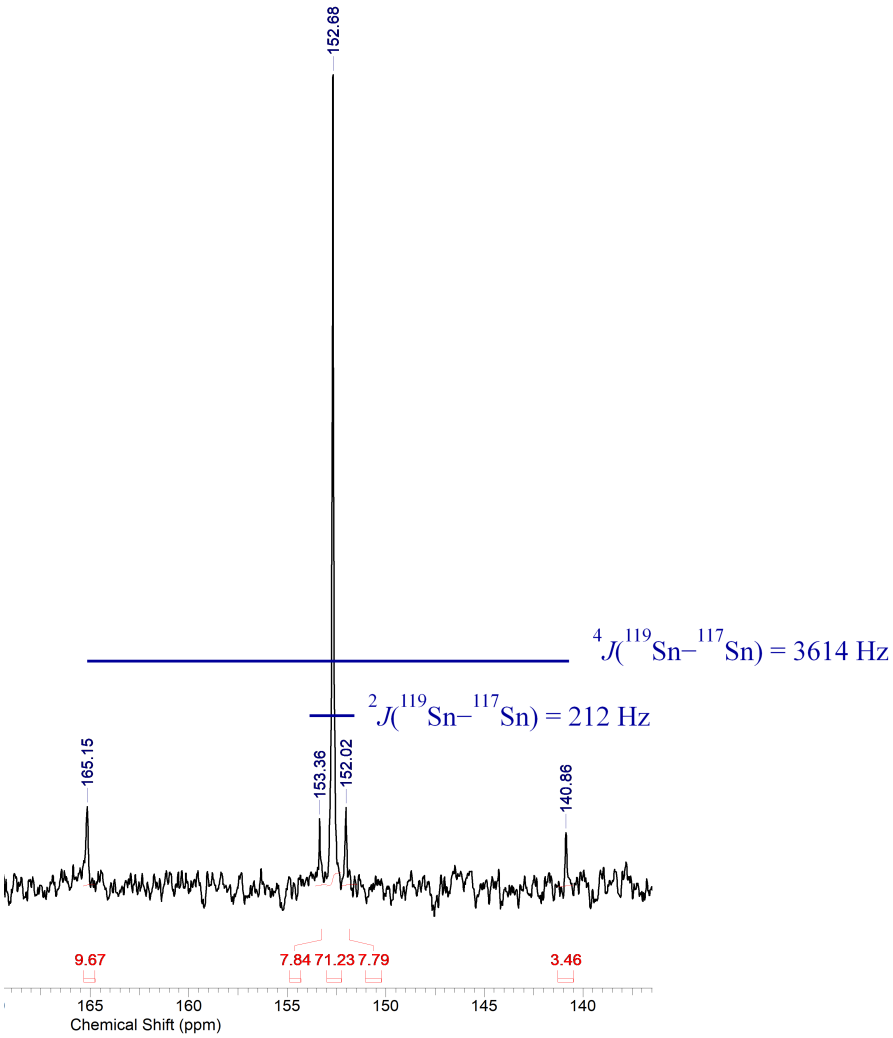

Figure 81. ^{119}Sn NMR spectrum (149.26 MHz, $CDCl_3$) of compound **35**.

We wanted to investigate whether there is an exchange reaction undergoing in solution between the compounds MeSi($CH_2SnPhS)_3$, **33**, and MeSi($CH_2SnPhSe)_3$, **34**, in $CDCl_3$ and C_6D_6. Furthermore, we studied the reaction of the Se-containing adamantane, **34**, with elemental sulphur, S_8, in $CDCl_3$. Such redistribution reactions have not been fairly investigated for stannaadamantane compounds.[53]

A ^{119}Sn NMR spectrum measured 24h after equimolar quantities of of **33** and **34** had been mixed in $CDCl_3$-solution shows the following signals (assigned to according to Scheme 32): δ 2.9 ppm (**A**), δ 98.9 ppm (**B**), at δ 0.3 and 52.6 ppm with integral ratio of 1:2 (**C**), and δ 100.4 and 50.5 ppm with integral ratio of 1:2 (**D**).

Scheme 32. Different intermediate species (**A**, **B**, **C**, and **D**) formed in course of the redistribution reaction between **33** and **34** in $CDCl_3$.

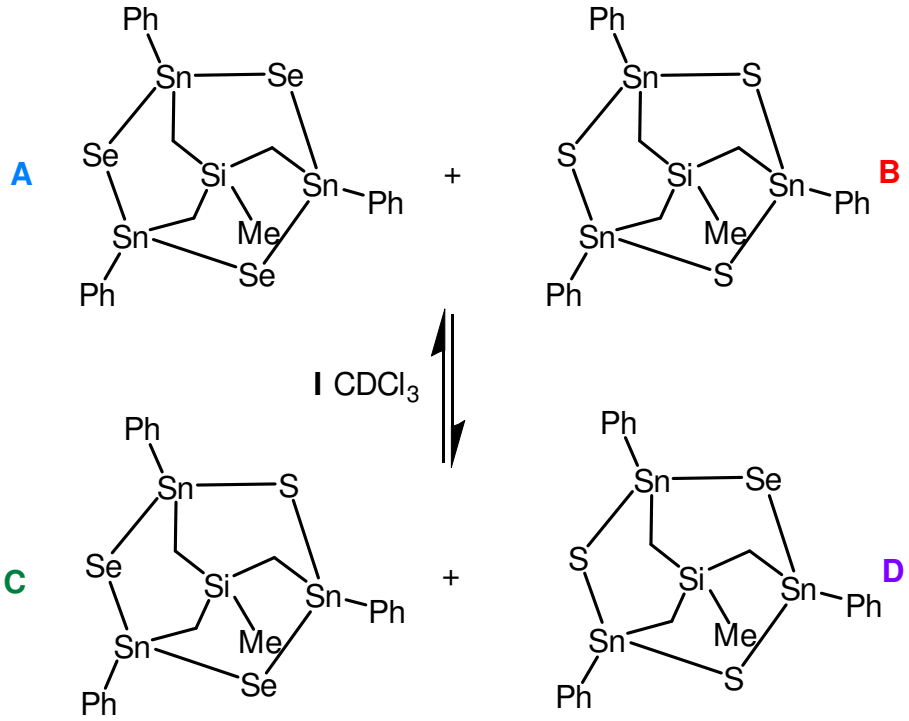

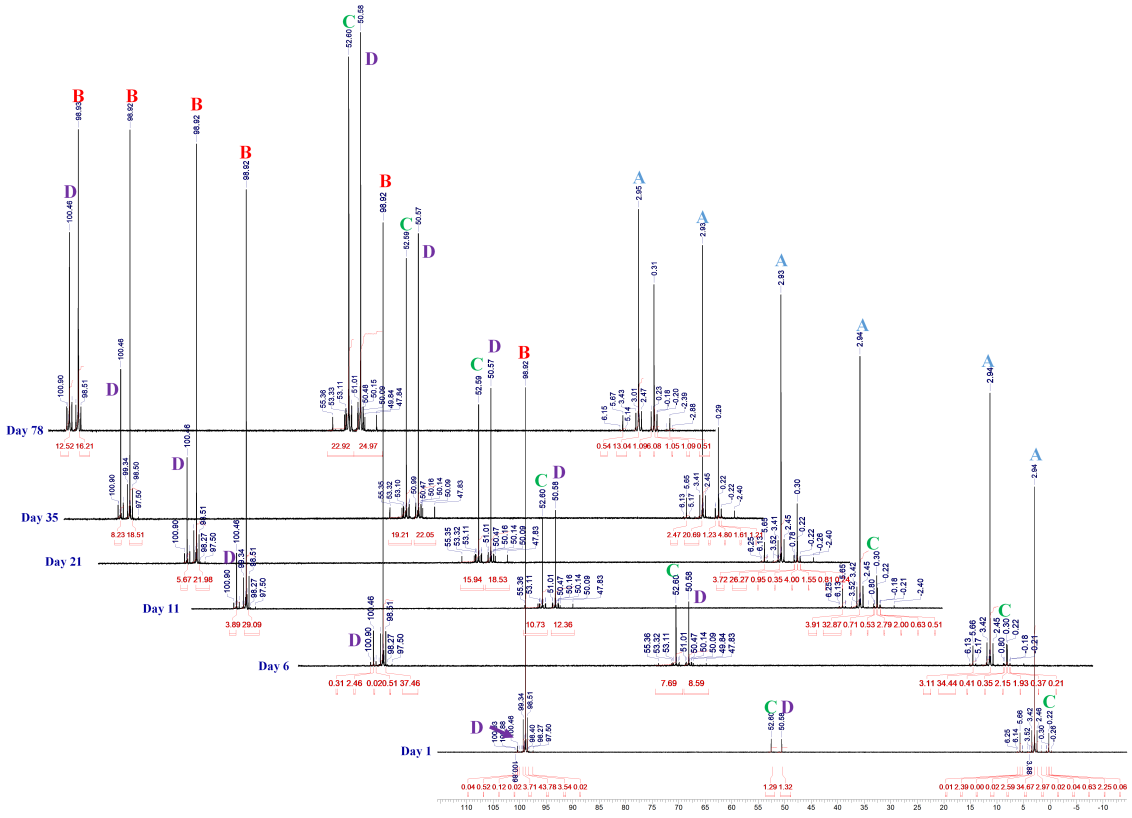

Figure 82. ^{119}Sn NMR spectra (223.85 MHz, $CDCl_3$) of redistribution reactions of **33** and **34**.

We performed ^{119}Sn NMR measurements over a period of 78 days. Figure 82 represents the corresponding ^{119}Sn NMR spectra measured over this period of time. The diagram shown in Figure 83, presenting the integration of each species over this period of time. It shows approximately a consumtion of **A** (14.5 %) and **B** (16.2 %) at day 78, in favour for the formation of **C** and **D** with a slight domination of species **D** (37.5 %) in comparison to that of species **C** (31.3 %).

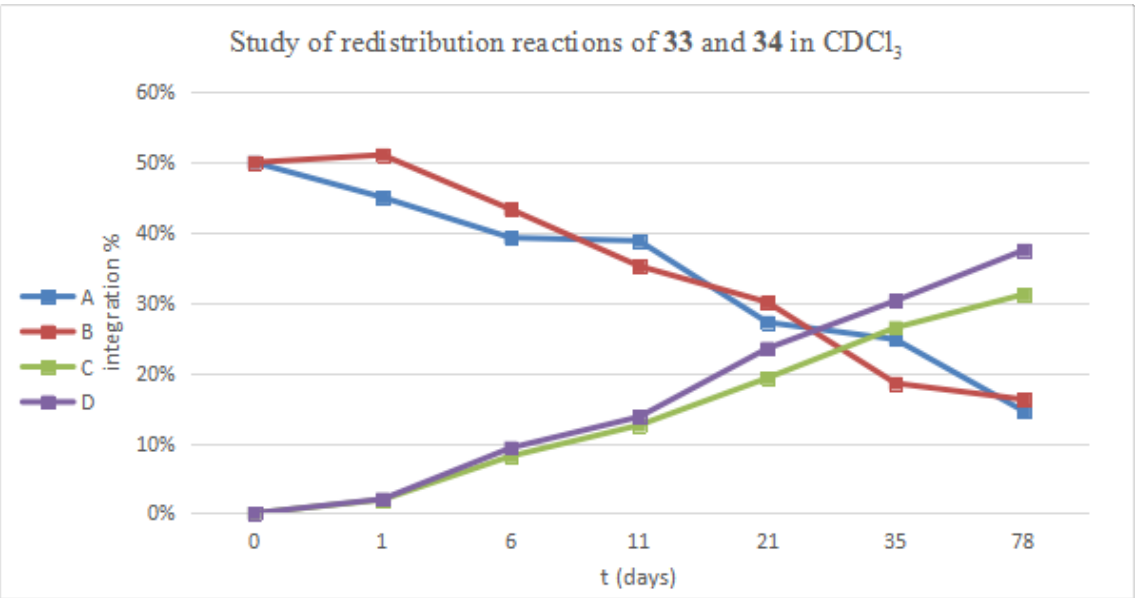

Figure 83. Kinetic study of redistribution reactions of **33** and **34** in $CDCl_3$ (Integration % = f(t)).

The ^{119}Sn NMR spectrum recorded at day 21 (Figure 84), taken as example, shows the two signals corresponding to species **C** at δ 0.3 ppm ($^1J(^{119}Sn-^{77}Se)$ = 1209 Hz, $^2J(^{119}Sn-^{117/119}Sn)$ = 217/227 Hz, $^2J(^{119}Sn-^{29}Si)$ = 48 Hz) (Figure 85) , which refers to the one $SnSe_2$ atom in (**C**), and at δ 52.6 ppm ($^1J(^{119}Sn-^{77}Se)$ = 1683 Hz, $^2J(^{119}Sn-^{117}Sn)$ = 185 Hz, $^2J(^{119}Sn-^{117/119}Sn)$ = 218/229 Hz, $^1J(^{119}Sn-^{13}C_i)$ = 781 Hz, $^3J(^{119}Sn-^{13}C_m)$ = 69 Hz, $^2J(^{119}Sn-^{29}Si)$ = 48 Hz) (Figure 86), which refers to the two Se*Sn*S atoms in (**C**). The two resonance signals corresponding to species **D** appear at δ 100.4 ppm ($^2J(^{119}Sn-^{117/119}Sn)$ = 185/195 Hz, $^2J(^{119}Sn-^{29}Si)$ = 48 Hz), the $^3J(^{119}Sn-^{77}Se)$ is not detected (Figure 87), which refers to the one SnS_2 atom in (**D**) , and at δ 50.5 ppm ($^1J(^{119}Sn-^{77}Se)$ = 1683 Hz, $^2J(^{119}Sn-^{117}Sn)$ = 218 Hz, $^2J(^{119}Sn-^{117/119}Sn)$ = 186/195 Hz, $^1J(^{119}Sn-^{13}C_i)$ = 781 Hz, $^3J(^{119}Sn-^{13}C_m)$ = 69 Hz, $^2J(^{119}Sn-^{29}Si)$ = 48 Hz) (Figure 86), which refers, as well, to the two *Sn*SSe atoms in (**D**). These earlier mentioned NMR shifts and coupling constants are very near to the corresponding shifts in the species resulting from the redistribution reaction between $[CH_2(SnSPh)_2]_2$ and $[CH_2(SnSePh)_2]_2$.[10]

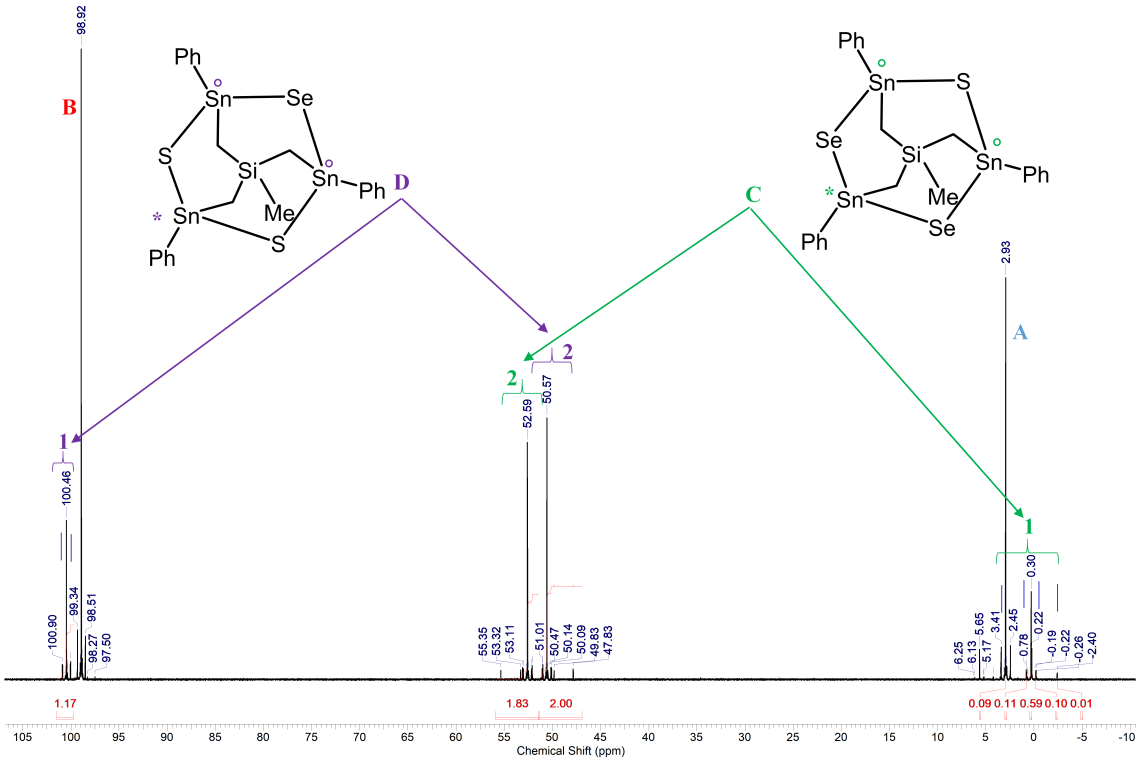

Figure 84. A ^{119}Sn NMR spectrum (223.85 MHz, $CDCl_3$) of a solution containing equimolar amounts of **33** and **34** at day 21.

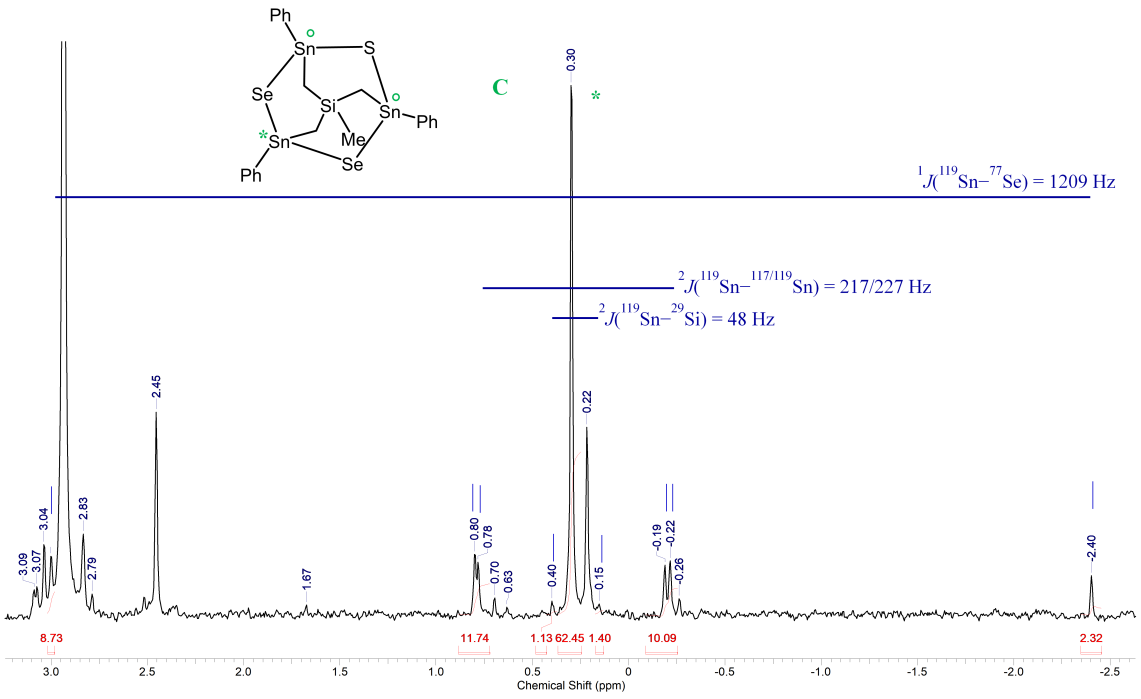

Figure 85. Cut-out of an ^{119}Sn NMR spectrum (223.85 MHz, $CDCl_3$) showing the signal for the $SnSe_2$ atom in (**C**).

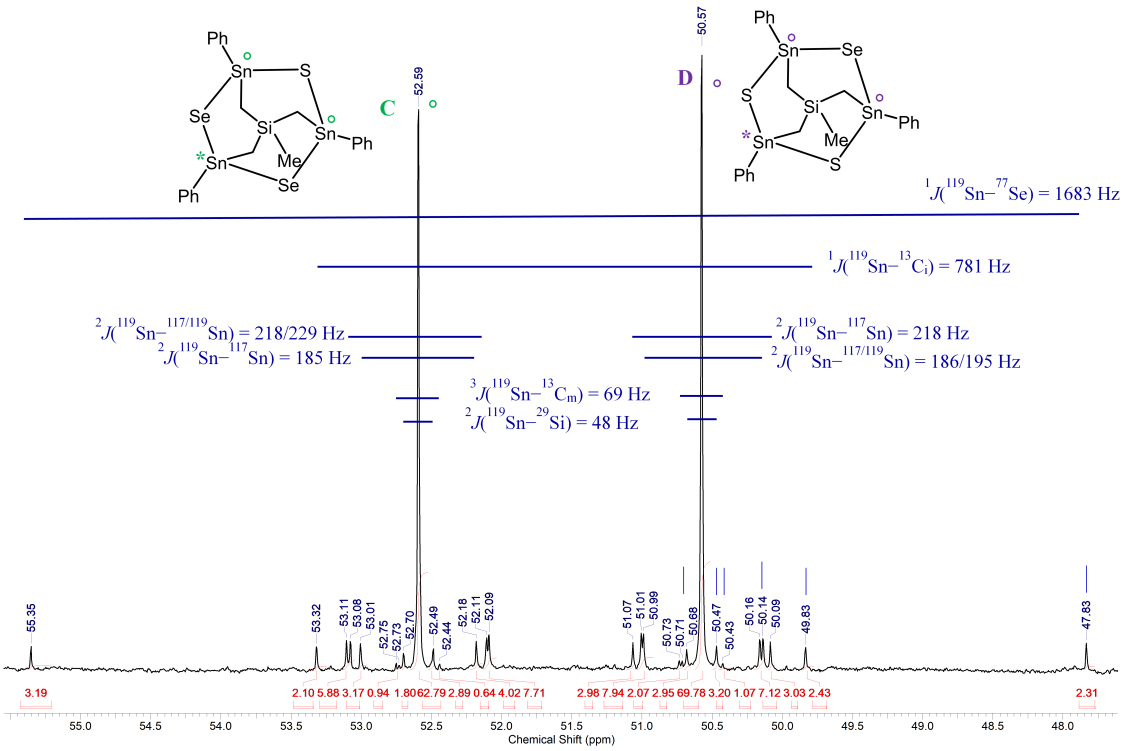

Figure 86. Cut-out of an ^{119}Sn NMR spectrum (223.85 MHz, $CDCl_3$) showing the signals for species **C**+**D**.

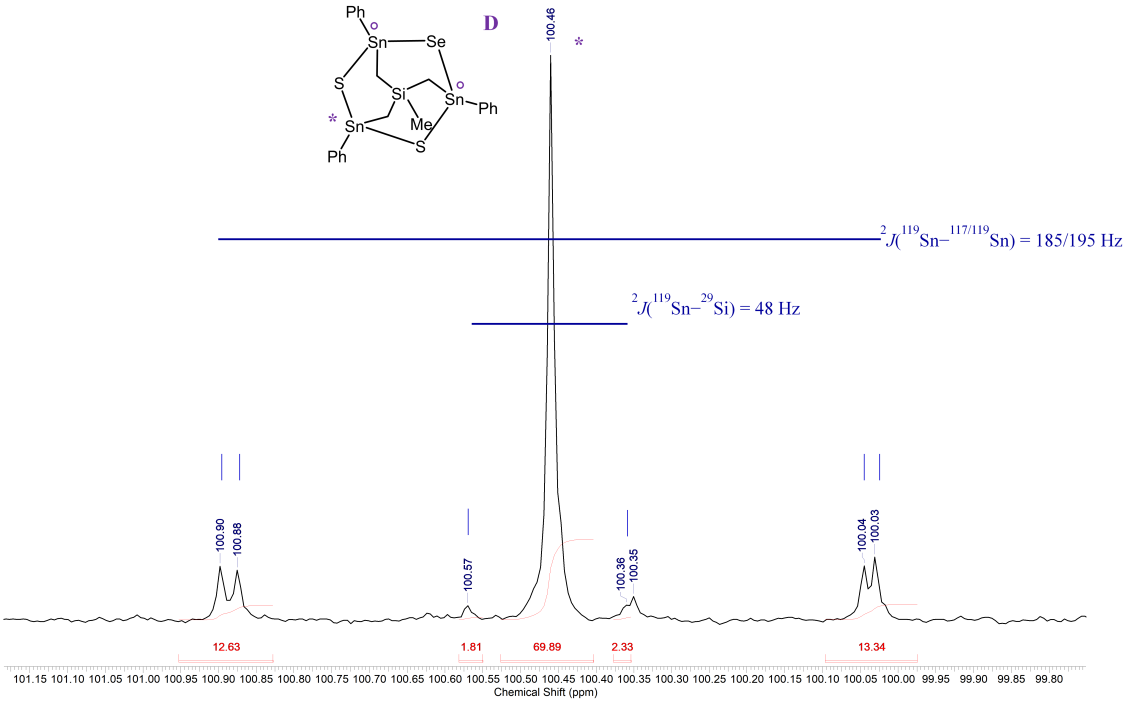

Figure 87. Cut-out of an ^{119}Sn NMR spectrum (223.85 MHz, $CDCl_3$) showing the signal for the *Sn*S_2 atom in (**D**).

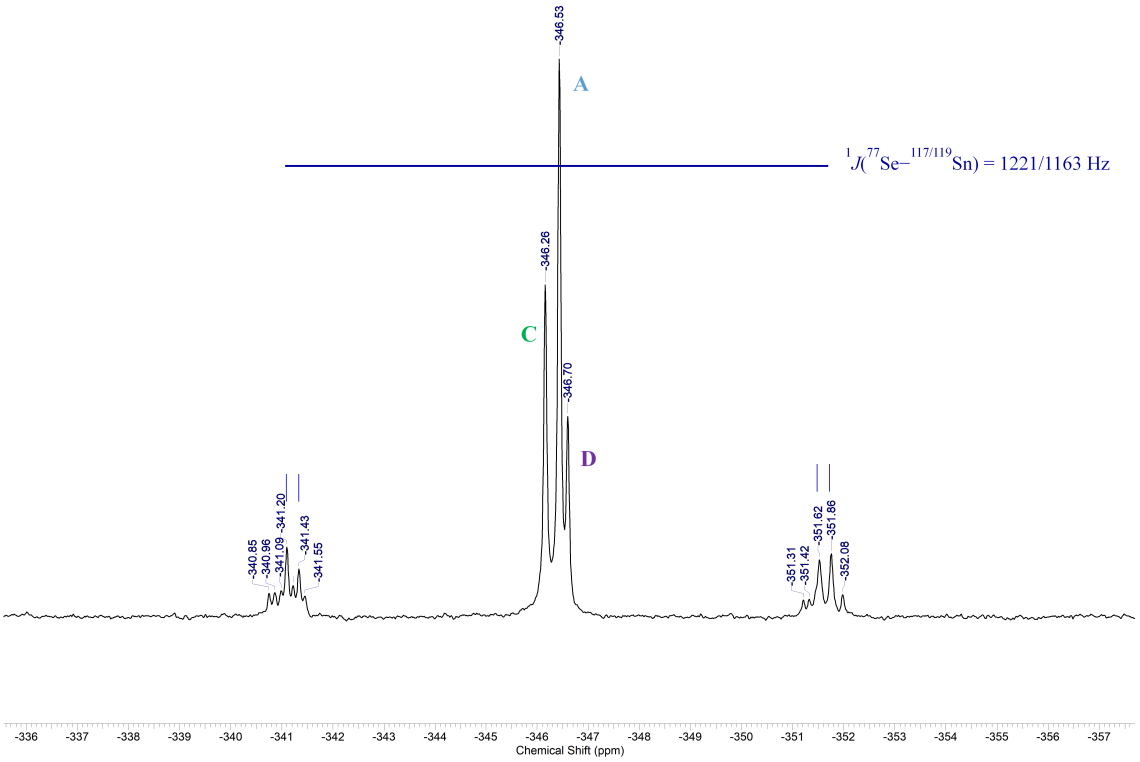

Figure 88. ^{77}Se NMR spectrum (114.48 MHz, $CDCl_3$) of a solution containing equimolar amounts of **33** and **34** (day 21).

The resonance shift corresponding to the species **A** [$MeSi(CH_2SnSe)_3$] appears at δ 2.9 ppm ($^1J(^{119}Sn-^{77}Se)$ = 1217 Hz, $^1J(^{119}Sn-^{13}C_i)$ = 571 Hz, $^2J(^{119}Sn-^{117}Sn)$ = 214 Hz, $^3J(^{119}Sn-^{13}C_m)$ = 68 Hz, $^2J(^{119}Sn-^{29}Si)$ = 48 Hz) (Supporting Information Chapter 4, Figure S106). As to the resonance shift corresponding to the specie **B** [$MeSi(CH_2SnS)_3$] appear at δ 98.9 ppm ($^4J(^{119}Sn-^{115}Sn)$ = 291 Hz, $^2J(^{119}Sn-^{117}Sn)$ = 187 Hz, $^1J(^{119}Sn-^{13}C_i)$ = 639 Hz, $^3J(^{119}Sn-^{13}C_m)$ = 71 Hz, $^2J(^{119}Sn-^{29}Si)$ = 50 Hz) (See Supporting Information, Chapter 4, Figure S107). The ^{77}Se NMR spectrum of the same sample (Figure 88) shows three signals at δ –346.7, –346.5 ($^1J(^{77}Se-^{117/119}Sn)$ = 1221/1163 Hz), and –346.2 ppm, referring to, respectively, the one *Se*Sn atom in (**D**), the three *Se*Sn atoms in (**A**), and the two *Se*Sn atoms in (**C**). The $^1J(^{77}Se-^{117/119}Sn)$ coupling constants for species **C** and **D** were not determined. Table 9 summarizes the ^{119}Sn and ^{77}Se NMR data of species **A**, **B**, **C**, and **D** resulting from the redistribution reactions between **33** and **34** in $CDCl_3$.

Table 9. Summary of ^{119}Sn and ^{77}Se NMR Data and coupling constants for Species **A**, **B**, **C**, and **D** presented in the exchange reaction between **33** and **34** in $CDCl_3$.

Species	δ (^{119}Sn) ppm	δ (^{77}Se) ppm	$^1J(^{119}Sn–^{77}Se)$ Hz	$^2J(^{119}Sn–^{117}Sn)$ Hz
A	2.9	–346.5	1217	214
B	98.9	—	—	187
C	0.3, 52.6	–346.2	1209, 1683	185
D	50.5, 100.4	–346.7	1683	218
Species	$^2J(^{119}Sn–^{117/119}Sn)$ Hz	$^2J(^{119}Sn–^{29}Si)$ Hz	$^1J(^{119}Sn–^{13}C)$ C_i, $-(CH_2)-$ Hz	$^3J(^{119}Sn–^{13}C_m)$ Hz
A	—	47	570	68
B	—	50	639, 291	71
C	218/229	48	781	69
D	186/195	48	781	69

A ^{119}Sn NMR spectrum measured 24 h after equimolar amounts of **33** and **34** had been dissolved in C_6D_6, shows rather similar signals as observed for the corresponding mixture in $CDCl_3$ (δ 2.59 ppm, species **A**; δ 100.1 ppm, species **B**; δ 0.23 and 53.06 ppm with integral 1:2, species **C**; δ 101.7 and 50.95 ppm with integral 1:2, species **D**), (Scheme 33). These signals have the same coupling constants mentioned for the intermediate species **A**, **B**, **C**, and **D** in the previous redistribution reaction in $CDCl_3$. This is also valid for the ^{77}Se NMR spectrum of this reaction mixture.

Scheme 33. Different intermediate species (**A**, **B**, **C**, and **D**) formed during the exchange reaction between **33** and **34** in C_6D_6.

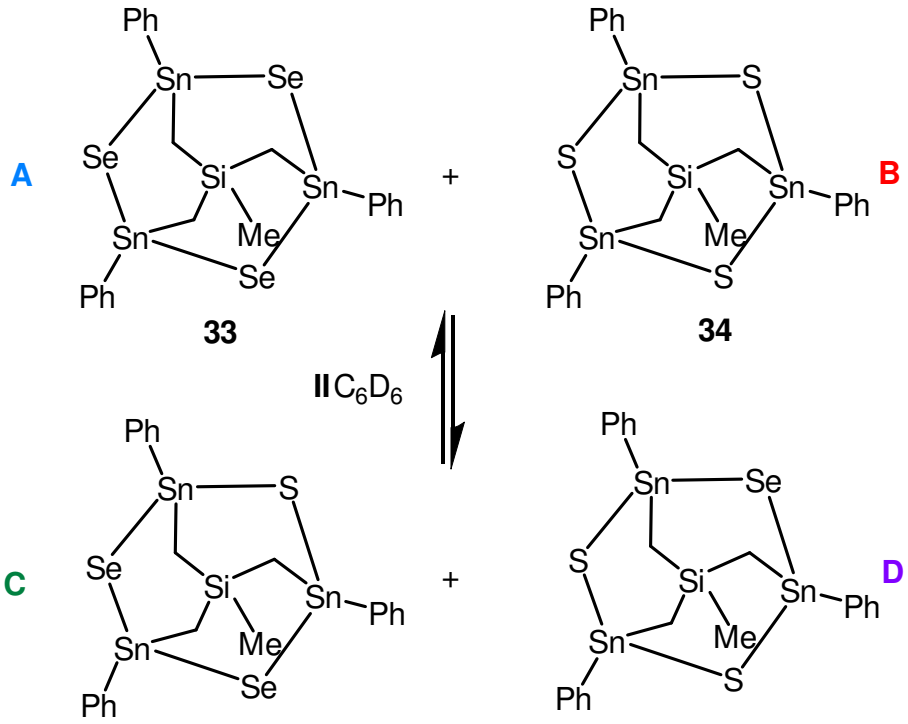

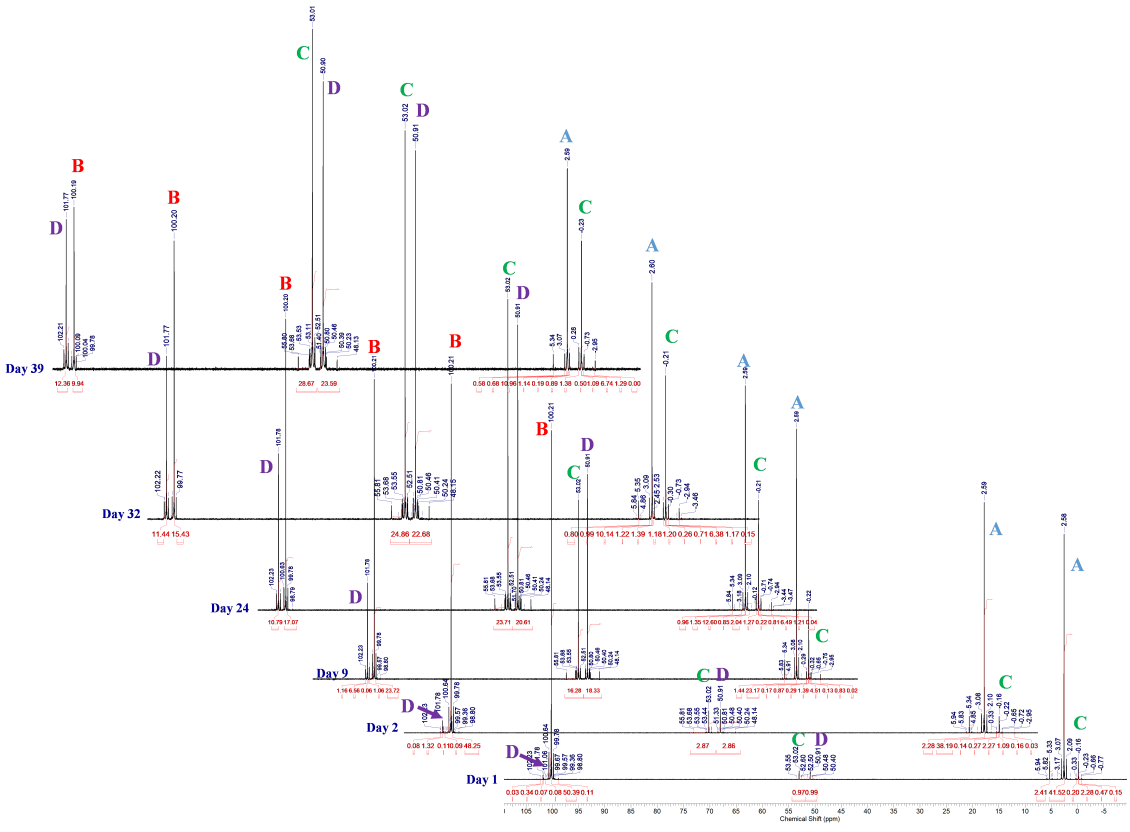

Figure 89. ^{119}Sn NMR spectra (223.85 MHz, C_6D_6) of redistribution reactions of **33** and **34**.

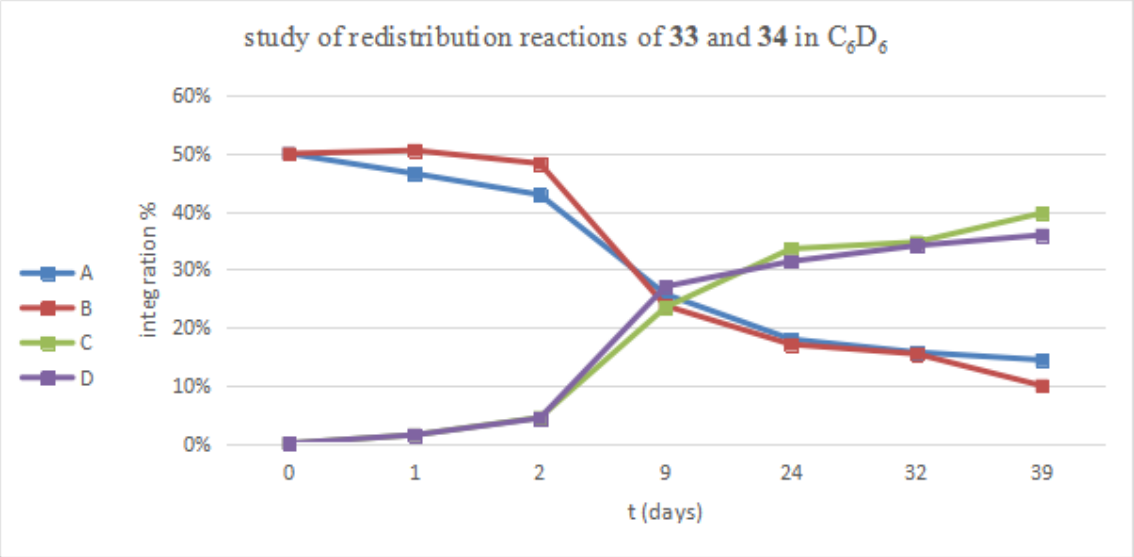

Figure 90. Kinetic study of redistribution reactions of **33** and **34** in C_6D_6: (Integration % = f(t)).

The ^{119}Sn NMR measurements were performed over a period of 39 days. Figure 89 represents the corresponding ^{119}Sn NMR spectra measured over this period of time. Figure 90 shows the kinetic study of the redistribution reaction between **33** and **34** in C_6D_6: (Integration % = f(t)).

We notice that the reaction is kinetically much faster than that in $CDCl_3$ and there is a slight domination of the selenide-species in comparison to those of sulfide. At day 39 the integration of each specie is equal to 15 % for (**A**), 10 % for (**B**), 40 % for (**C**), and 35 % for (**D**).

Scheme 34 shows the redox reaction in $CDCl_3$ between compound **34** and elemental sulfur, S8, in the molar ratio 1:1. A ^{119}Sn NMR spectrum measured after 24 h shows three signals at 2.46, -0.26, and 52.2 ppm, respectively, referring to species **A** and **C**. After one week, the same species **B**, **C**, and **D** appear, as in the redistribution reaction shown in Scheme 33. The Se-containing stannaadamantane **34** almost completely disappeared and elemental selenium precipitated. The ^{119}Sn NMR spectrum shows almost the same NMR shifts resonances at δ 2.46 ppm (specie A), δ 98.6 ppm (specie **B**), δ 0.26, 52.1 ppm (species **C**; [$MeSi(CH_2Sn)_3Se_2S$]), with integration of 1:2, and δ 100.7, 50.09 ppm (species **D**; [$MeSi(CH_2Sn)_3SeS_2$]), with integration of 1:2. These signals have the same coupling constants mentioned for the intermediate species **A**, **B**, **C**, and **D** in the previous redistribution reactions. This is also valid for the ^{77}Se NMR spectrum of this reaction mixture.

Scheme 34. Different intermediate species (**A**, **B**, **C**, and **D**) formed during the redox reaction between **34** with $\mathbf{S_8}$ in $CDCl_3$.

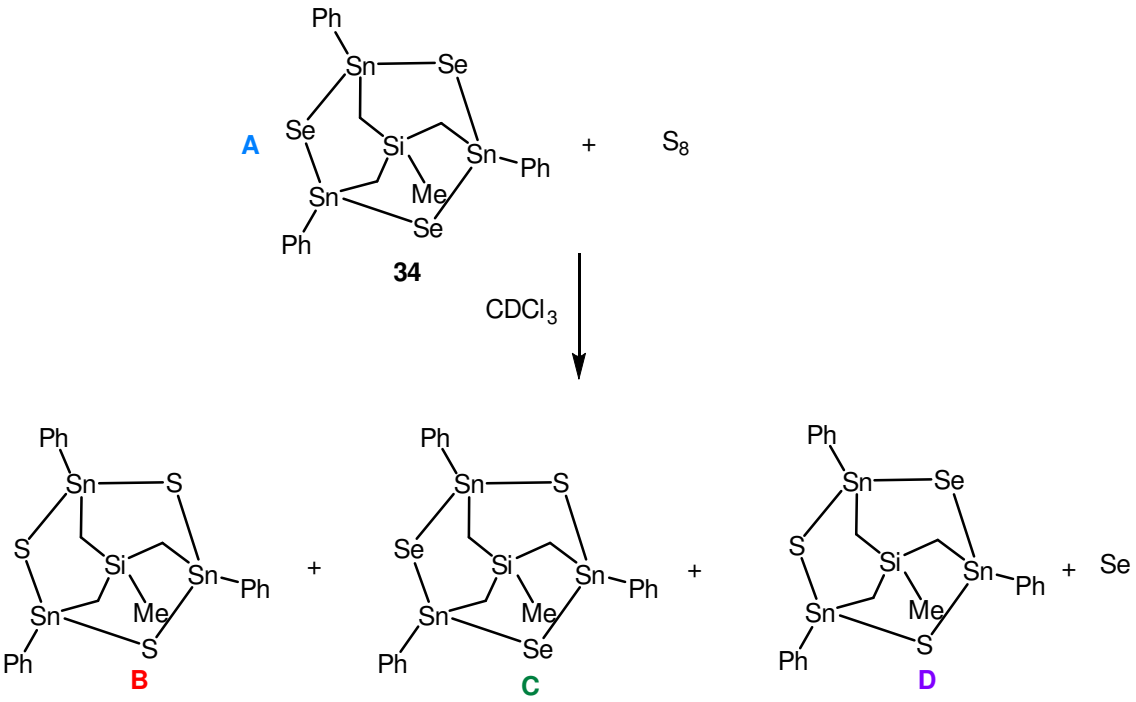

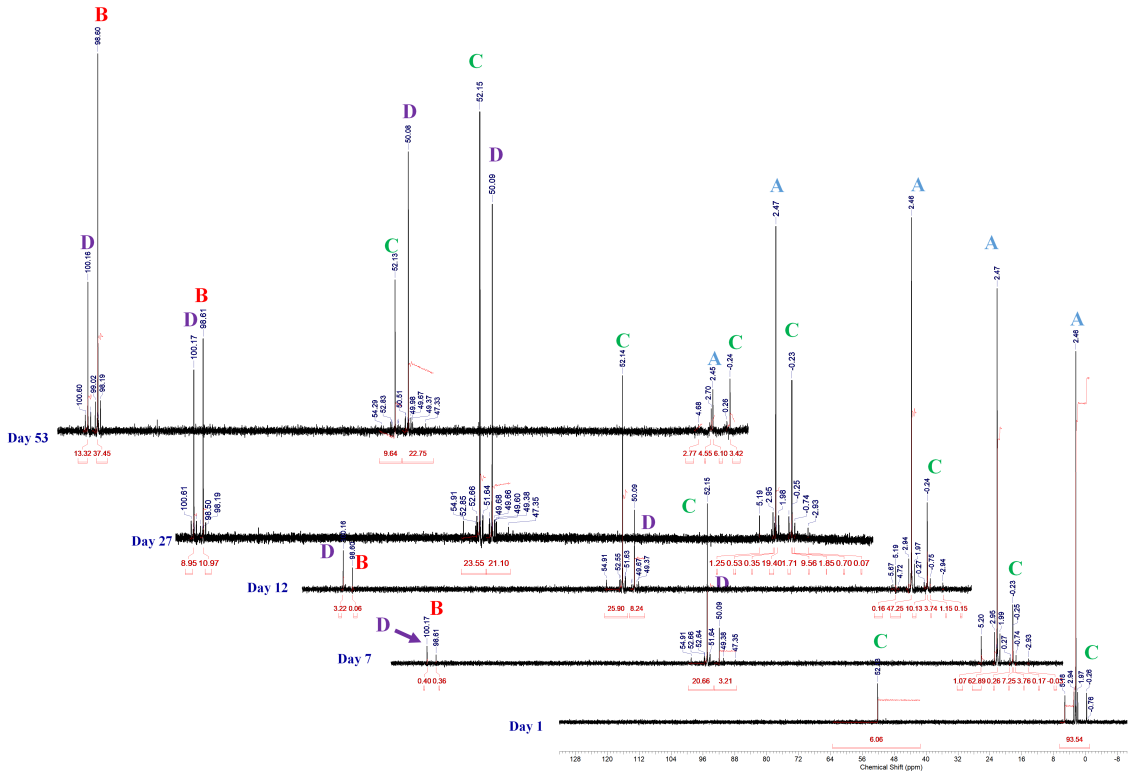

Figure 91. ^{119}Sn NMR spectra (223.85 MHz, $CDCl_3$) of redox reactions of **34** with S_8 in 1:1 ratio.

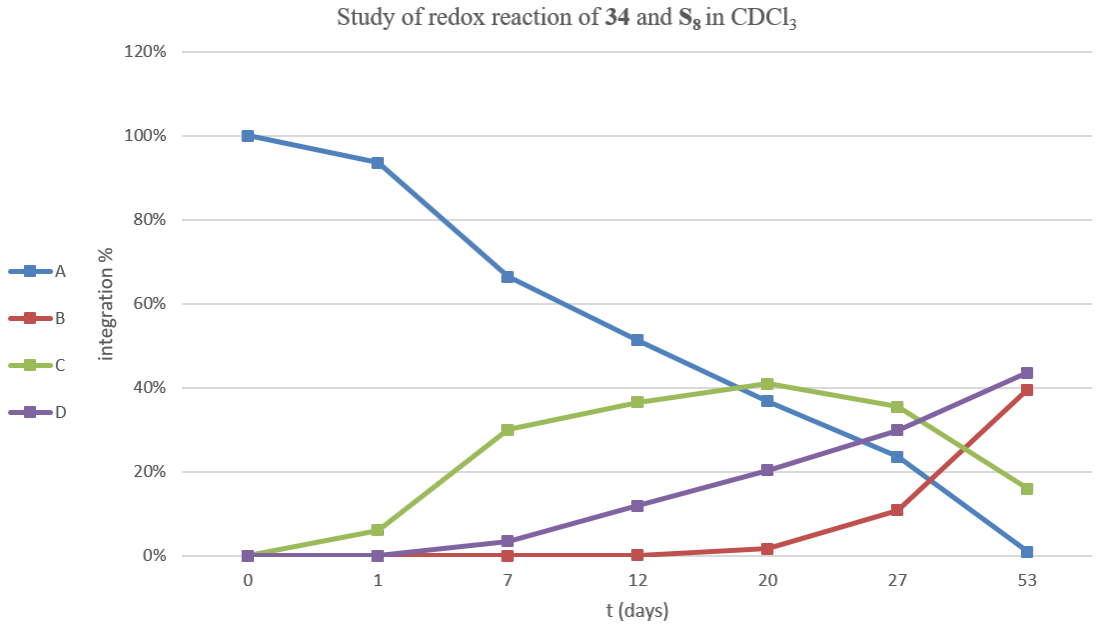

Figure 92. Kinetic study of redox reactions of **34** with S_8 in $CDCl_3$: (Integration % = f(t)).

The ^{119}Sn NMR measurements was realized over a period of 53 days. Figure 91 represents the corresponding ^{119}Sn NMR spectra measured over this period of time. Figure 92 shows the kinetic study of the redox reaction of **34** with S_8 in $CDCl_3$: (Integration % = f(t)). We notice that the reaction is slower than the redistribution reactions. However, it ends with a total consumption of species (**A**) Se-containing silastannaadamantane. There is a clear domination of the sulfur-containing-species in comparison to those of selenium-containing species. At Day 53, the integration of each specie is equal to 0 % for (**A**), 40 % for (**B**), 18 % for (**C**), and 42 % for (**D**).

No detailed studies have been performed concerning the mechanisms that account for the redistribution and redox-type reactions shown in Schemes 32, 33, and 34, respectively. The fact that the redistribution reaction between **33** and **34** is, with caution, apparently faster in C_6D_6 than in $CDCl_3$ makes protons less likely being involved in the mechanism. Chloroform usually contains trace amounts of protons. One hypothesis is that a bimolecular mechanism accounts for the redistribution reaction.[55] Compounds **33** and **34** form a Lewis base – Lewis acid adduct via intermolecular S→Sn and Se→Sn interactions as shown in Scheme 35.

Scheme 35. Possible intermediate (or transition state) involved in the redistribution reaction between **33** and **34**.

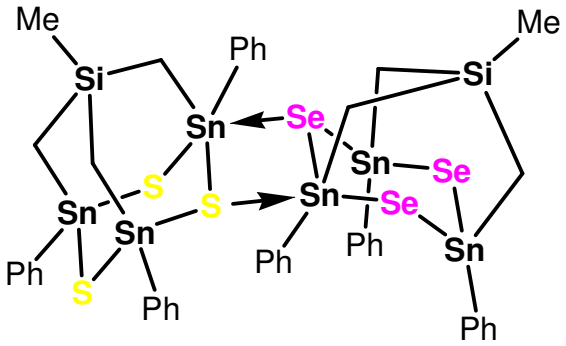

One way to check this hypothesis is recording variable time ^{119}Sn NMR spectra at different concentrations. In addition, DFT calculation could be performed to check whether the adduct shown in Scheme 35 is in a thermodynamic minimum or not. However, this could not be done in course of the work done for this PhD thesis.
A similar intermediate can be assumed being involved in course of the redox reaction between compound **34** and elemental sulfur. The S_8 molecule coordinates to a tin centre of **34** followed by a single electron transfer (Scheme 36).

Scheme 36. Possible intermediate (or transition state) involved in the redox reaction between compound **34** and elemental sulfur, S_8.[56]

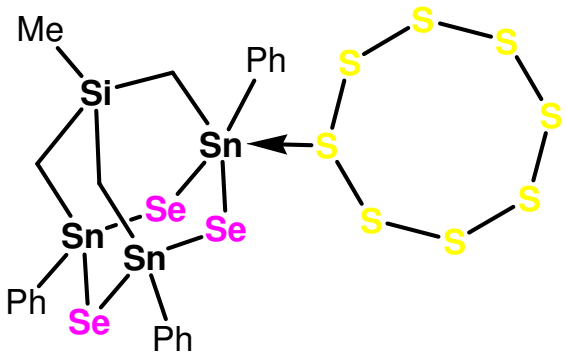

One characteristic of compounds **33**–**35** is UV-Vis emission. Figure 93 represents the calculated emission for UV as a function of the fundamental electronic transition energy. It shows that the intermediate species **C** and **D** have more potential for UV emission than that of **A** (compound **34**) and **B** (compound **33**). In addition, the trimethylsilylmethyl-substituted silastannadamantane intermediates, theoretically have weak UV emission capacity (Figure 93).

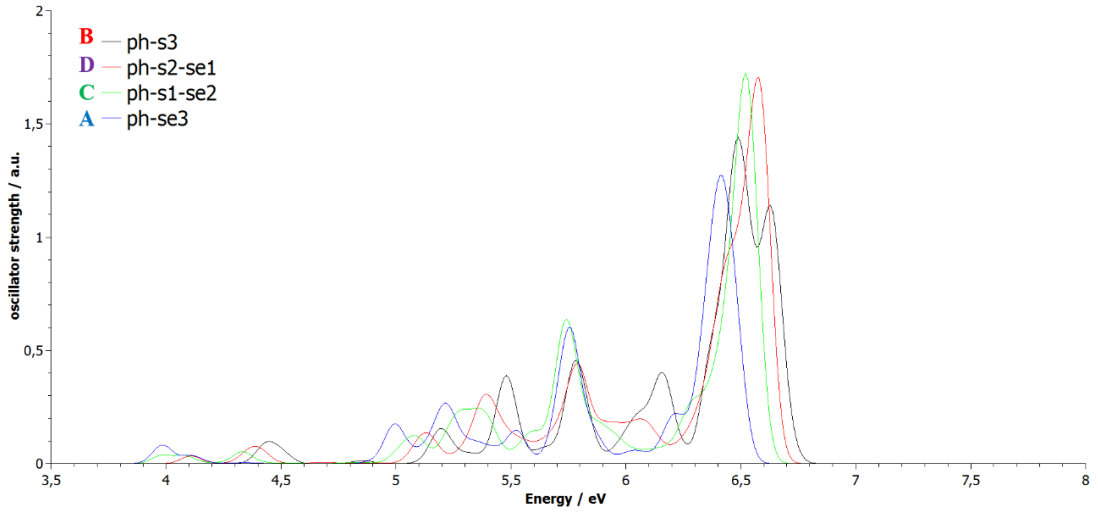

Figure 93. Calculated Spectral emission characteristics of **33** (**B**), **34** (**A**) and the intermediates (**C**) and (**D**): UV (a.u) = f(Energy).

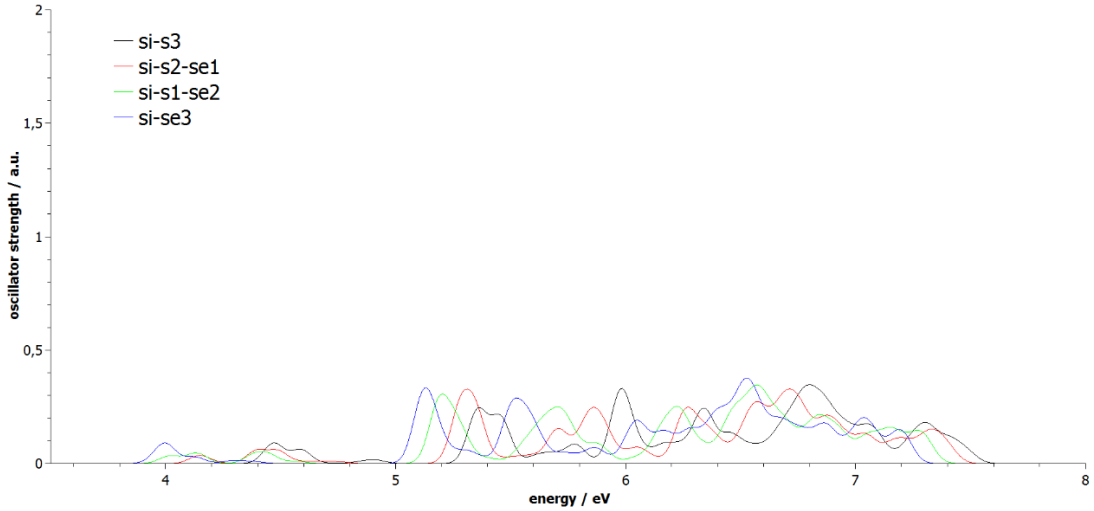

Figure 94. Calculated Spectral emission characteristics of the CH_2SiMe_3-substituted silastannadamantane theoretical intermediates: UV (a.u) = f(Energy).

4.4 Conclusion

In conclusion we have shown that simple tripod-type diorganotin halides MeSi($CH_2SnR_{(3-n)}X_n)_3$ (n = 0– 3; X = I, Cl, Br; R = Ph, CH_2SiMe_3) serve as precursors for unprecedented ladder-like containing diorganotin oxo clusters. Among these, the novel belt-shaped molecular diorganotin oxides [MeSi(CH2SnRO)3]n of unprecedented oktokaideka (n = 18) and trikonta (n = 30) nuclearity are striking. The results obtained fit well into the ongoing interest in large-sized metaloxo clusters in

general[57] and tinoxo clusters of high nuclearity in particular.[58] The concept shown herein holds great potential for future work. Just to mention a few options out of many, variation of the substituents R and/or replacing the CH_3 group with other substituents, variation of the spacing between the silicon and tin centres as well as replacement of the MeSi bridgehead moiety with MeGe or with isoelectronic P, P=E (E=O, S, Se) or PM (M = transition metal moiety such as $W(CO)_5$ and others) might give a plethora of novel diorganotin oxides showing polynuclear structures. Moreover, replacing the organic substituent R in Roesky's $(RSn)_4O_6$ (R = $(Me_3Si)_2CH$)[59] to a R'of slightly reduced steric bulk could give well defined oligomers $[(R'Sn)_4O_6]_n$ similar to **29** and **30**.[45] As well, these same precursors hold potential to form first silicon containing Sulfur- and selenium adamantane-like structures, which have interesting exchange reactions that can be subject of future work focusing on the reactional mechanisms taking place.

4.5 Experimental section

- **Synthesis of [(MeSi(CH_2)$_3$)Sn(μ$_3$-O)$_3$(Ph)Sn(Cl)(Ph)Sn(μ$_2$-OH)(Ph)Sn(*t*-Bu)$_2$]$_2$ (26)**

To a solution of 4 (263.00 mg, 0.279 mmol) in 30 mL of $CHCl_3$ was added to three equiv molar of freshly synthesized *t*-Bu_2SnO (221.85 mg, 0.891 mmol).[51,60] The resulting mixture was stirred at room temperature overnight. Chloroform was removed in vacuo (10^{-3} mmHg) and *t*-Bu_2SnCl_2 was washed out successively with *iso*-hexane. We obtain a white residue. Recrystallization of this latter from CH_2Cl_2/ *iso*-hexane gives 142 mg (47 %) of pure **5** as transparent needles, mp 382 °C. ^{1}H NMR (C_6D_6, 600.29, 298 K): δ 0.075 ($^2J(^1H-^{117/119}Sn)$ = 81 Hz, $^2J(^1H-^1H)$ = 13 Hz, 2H, SiCH_2Sn), 0.215 ($^2J(^1H-^{117/119}Sn)$ = 68 Hz, $^2J(^1H-^1H)$ = 13 Hz, 2H, SiCH_2Sn), 0.52 ($^2J(^1H-^{117/119}Sn)$ = 80 Hz, $^2J(^1H-^1H)$ = 13 Hz, 2H, SiCH_2Sn), 0.805 ($^2J(^1H-^{117/119}Sn)$ not measured, $^2J(^1H-^1H)$ = 13 Hz, 2H, SiCH_2Sn), 2.17 ppm ($^2J(^1H-^{117/119}Sn)$ = 126 Hz, $^2J(^1H-^1H)$ = 13 Hz, 2H, SiCH_2Sn), 2.37 ($^2J(^1H-^{117/119}Sn)$ = 106 Hz, $^2J(^1H-^1H)$ = 13 Hz, 2H, SiCH_2Sn), 0.78 (s, 6H, SiCH_3), 1.07, 1.63 (s, 36H, $^3J(^1H-^{117/119}Sn)$ = 116 Hz, *t*-Bu_2SnCl), 6.98–8.27 (complex pattern, 30H, Ph). $^{13}C\{^1H\}$ NMR (C_6D_6, 150.94, 298 K): δ 5.5 ($^3J(^{13}C-^{117/119}Sn)$ = 53 Hz, $^1J(^{13}C-^{29}Si)$ = 74, SiCH_3), 7.6 ($^1J(^{13}C-^{117/119}Sn)$ = 464 Hz, SiCH_2Sn), 11.4 ($^1J(^{13}C-^{117/119}Sn)$ = 517 Hz, SiCH_2Sn) , 18.1 ($^1J(^{13}C-^{117/119}Sn)$ = 503 Hz, SiCH_2Sn), 41.4 ($^1J(^{13}C-^{117/119}Sn)$ = 568 Hz, SiCH_2Sn), 42.0 ($^1J(^{13}C-^{117/119}Sn)$ = 576 Hz, SiCH_2Sn), 30.5, 31.6 (t-Bu2SnCl), 128.7, 128.8, 128.9 (C_m), 130.23, 130.26, 130.4 ($^4J(^{13}C-^{117/119}Sn)$ = 14 Hz, C_p), 136.2, 136.7, 137.1 ($^2J(^{13}C-^{117/119}Sn)$ = 59 Hz, C_o), 143.9, 144.61, 144.67 ($^1J(^{13}C-^{117/119}Sn)$ = 759/805 Hz, C_i). ^{29}Si NMR (C_6D_6, 119.26, 298 K): δ 3.32 ($^2J(^{29}Si-^{117/119}Sn)$ = 63 Hz, *Si*CH_3). ^{119}Sn NMR ($CDCl_3$, 223.85, 298 K): δ –195 ($^2J(^{119}Sn_3A-^{117/119}Sn_{exo})$ = 298 Hz, $^2J(^{119}Sn_3A-^{117}Sn_{endo})$ = 180 Hz, $^2J(^{119}Sn_3A-^{29}Si)$ = 62 Hz), Sn(3A)), -208 ($^2J(^{119}Sn_2-^{117/119}Sn_{endo})$ =

243 Hz, $^2J(^{119}Sn_2-{}^{117}Sn_{endo})$ = 90 Hz), Sn(2)), -228 ($^2J(^{119}Sn_1-{}^{117}Sn_{endo})$ = 99 Hz, $^2J(^{119}Sn_1-{}^{117/119}Sn_{exo})$ = 285 Hz, $^2J(^{119}Sn_2-{}^{117/119}Sn_{endo})$ = 209 Hz, Sn(1)), -230 Sn(4A). Anal. Calcd (%) for $C_{60}H_{86}Cl_2Si_2Sn_8$: C 35.82 H 4.31 Found: C 35.9, H 4.3. Electrospray MS: m/z (%) positive mode: 2012.7 (100, $[M + H^+]^+$). IR (cm^{-1}): ν(Sn–O–Sn) 695-726; ν(Sn–C) 539-562, and ν(OH) 2924- 2849.

- **Synthesis of {[MeSi(CH$_2$)$_3$]SnCl(CH$_2$SiMe$_3$)(μ$_3$-O)SnCl(CH$_2$SiMe$_3$)Sn(μ$_3$-O)(Cl)$_2$(CH$_2$SiMe$_3$)Sn(*t*-Bu)$_2$} (27)**

To a solution of **12** (58.00 mg, 0.062 mmol) in 30 mL of $CHCl_3$ was added to three equiv molar of freshly synthesized *t*-Bu_2SnO (139.59 mg, 0.186 mmol).[51,60] The resulting mixture was stirred at room temperature overnight. Chloroform was removed in vacuo (10^{-3} mmHg) and (*t*-$Bu_2SnOHCl)_2$ was washed out successively with *iso*-hexane. We obtain a white residue. Recrystallization of this latter from CH_2Cl_2/ *iso*-hexane gives 30 mg (42 %) of pure 27 as transparent needles, mp 160 °C. ^{1}H NMR (C_6D_6, 600.29, 298 K): δ 0.21, 0.26, 0.27 (12H, SiC*H*$_2$Sn), 1.24–1.36 (complex pattern, 30H, SiC*H*$_3$), 1.38, 1.41 (18H, *t*-Bu_2Sn). ^{29}Si NMR (C_6D_6, 119.26, 298 K): δ –21.8 (*Si*CH_3), 0.81, 1.3, 1.5 (CH_2*Si*Me_3). ^{119}Sn NMR (C_6D_6, 223.85, 298 K): δ –218 ($^2J(^{119}Sn_4-{}^{117/119}Sn_{endo})$ = 208 Hz, *Sn*(4)), -158 ($^2J(^{119}Sn_{endo}-{}^{117}Sn_{endo})$ = 125 Hz, Sn_{endo}), -149 ($^2J(^{119}Sn_1-{}^{117/119}Sn_{endo})$) = 214 Hz), *Sn*(1)), -132 (Sn_{endo}). Anal. Calcd (%) for $C_{24}H_{64}Cl_4O_2Si_4Sn_4$ + 3 (*t*-$Bu_2SnO)_3$: C 34.38, H 6.7. Found: C 34.4, H 6.4. Electrospray MS: m/z (%) positive mode: 793.1270 $[C_{16}H_{45}Cl_2OSi_4Sn_3]^+\{[MeSi(CH_2SnCH_2SiMe_3)_3(O)Cl_2] + H^+\}^+$, 807.1418 $[C_{16}H_{44}Cl_2O_2Si_4Sn_3]^+$ $\{[MeSi(CH_2SnCH_2SiMe_3)_3(O)Cl_2] + (\mu_3\text{-}O)\}^+$.

- **Synthesis of {[MeSi(CH$_2$)$_3$]SnI(CH$_2$SiMe$_3$)(μ$_2$-OH)[SnO(CH$_2$SiMe$_3$)]$_2$Sn(μ$_2$-OH)ISn(*t*-Bu)$_2$} (28)**

To a solution of **11** (863 mg, 0.589 mmol) in 50 mL of $CHCl_3$ was added to one equiv molar of freshly synthesized *t*-Bu_2SnO (440 mg, 0.589 mmol).[51,60] The resulting mixture was stirred at room temperature overnight. Chloroform was removed in vacuo (10^{-3} mmHg) and (*t*-$Bu_2SnOHCl)_2$ was washed out successively with *iso*-hexane. We obtain a white residue. Recrystallization of this latter from CH_2Cl_2/ *iso*-hexane gives 444 mg (60 %) of pure 28 as transparent needles, mp 156-165 °C. ^{1}H NMR ($CDCl_3$, 600.29, 298 K): δ 0.12, 0.27 (12H, SiC*H*$_2$Sn), 0.17, 0.20, 0.20 (30H, SiC*H*$_3$), 1.36, 1.42, 1.42 (18H, *t*-Bu_2Sn). ^{13}C{^{1}H} NMR ($CDCl_3$, 150.94, 298 K): δ 1.58, 2.2, 2.51 (Si*C*H_3), 1.44 (Si*C*H_2Sn), 29.1, 30.3, 30.5 (*t*-Bu_2Sn). No coupling constants are determined given the quality of the NMR spectra for such compounds. No further measurements could be realized within the tine frame of this PhD: ^{29}Si NMR ($CDCl_3$, 79.26, 298 K): δ –21 (*Si*CH_3), 0.72, 1.42, 1.58 (CH2*Si*Me3). ^{119}Sn NMR ($CDCl_3$, 149.26, 298 K): δ –183.5, -183.2 (2J(119Sn_{exo}-117/119Sn_{endo}) = 248 Hz, *Sn*(1), *Sn*(4)), -156 ($^2J(^{119}Sn_{endo}-{}^{117}Sn_{endo})$ = 167 Hz, Sn_{endo}), -150 (2J(119Sn_{exo}-117/119Sn_{endo}) = 242 Hz, Sn_{endo}). Anal. Calcd (%) for $C_{24}H_{62}I_2O_4Si_4Sn_4$: C 29.96, H 4.98. Found: C 22.9, H 5.0. Electrospray MS: m/z (%) positive mode: 750.93 {10, $[C_{16}H_{43}O_3Si_4Sn_3]^+\}^+$: {[MeSi(CH$_2$SnOCH$_2$SiMe$_3$)$_3$] +

$H^+\}^+$, 796.93 {100, $[C_{16}H_{43}O_3Si_4Sn_3]^+ + \frac{1}{2}CH_2Cl_2\}^+$: $\{[MeSi(CH_2SnOCH_2SiMe_3)_3] + H^+ + \frac{1}{2}CH_2Cl_2\}^+$. IR ($cm^{-1}$): ν(OH) 3656-3493, 2950-2850 cm^{-1}.

- **Synthesis of $[MeSi(CH_2SnPhO)_3]_6$ (29)**

To a solution of **3** (888.00 mg, 0.581 mmol, 1 equiv) in 30 mL of $CHCl_3$ was added freshly synthesized *t*-Bu_2SnO (434.45 mg, 1.75 mmol, 3 equiv).[51,60] The resulting mixture was stirred at room temperature overnight. Chloroform was removed in vacuo (10^{-3} mmHg) and *t*-Bu_2SnI_2 was washed out successively with *iso*-hexane. A white residue was obtained (433.54 mg, 98 %). Recrystallization of this latter from CH_2Cl_2/ diethyl ether gave transparent crystals suitable for X-ray diffraction analysis, mp over 400 °C. ^1H NMR ($CDCl_3$, 500.08, 298 K): δ 0.06 ($^2J(^1H-^{117/119}Sn)$ 50 Hz, $^2J(^1H-^1H)$ 10 Hz)/0.48 ($^2J(^1H-^{117/119}Sn)$ 70 Hz, $^2J(^1H-^1H)$ 10 Hz), 0.88 ($^2J(^1H-^{117/119}Sn)$ 85 Hz, $^2J(^1H-^1H)$ 15 Hz)/1.20 ($^2J(^1H-^{117/119}Sn)$ not measured, $^2J(^1H-^1H)$ 14.7 Hz), and 1.28 ppm ($^2J(^1H-^{117/119}Sn)$ not measured, $^2J(^1H-^1H)$ 10 Hz)/1.91 ($^2J(^1H-^{117/119}Sn)$ 120 Hz, $^2J(^1H-^1H)$ 10 Hz), 0.3, 1.42 (s, 18H, $SiCH_3$), 6.65–7.72 (complex pattern, 90H, Ph). $^{13}C\{^1H\}$ NMR ($CDCl_3$, 125.75, 298 K): δ 5.3, 29.1 ($SiCH_3$), 7.5 ($^1J(^{13}C-^{29}Si)$ = 80 Hz), 13.6, 14.6 ($SiCH_2Sn$)), 127.5, 128.1, 128.4 (C_m), 129.4, 129.5 (we didn't recognized the third signal) (C_p), 135.3, 135.4, 135.7 (C_o), 143.1, 143.9, 144.3 (C_i) we didn't recognized the $^{117/119}Sn$ satellites fault of bad resolution of the spectrum. ^{29}Si NMR no signal could be detected even with long measurement. ^{119}Sn NMR ($CDCl_3$, 149.26, 298 K): δ –204 $^2J(^{117/119}Sn-^{29}Si)$ = 59 Hz), ($^2J(^{119}Sn-^{117}Sn)$ = 180 Hz, $^2J(^{119}Sn-^{117/119}Sn)$ = 315 Hz, -225 ($^2J(^{119}Sn-^{117/119}Sn)$ = 315 Hz), -228 ($^2J(^{119}Sn-^{117}Sn)$ = 180 Hz) (*Sn*Ph). Anal. Calcd (%) for $C_{132}H_{144}O_{18}Si_6Sn_{18}$: C 36.67 H 3.36 Found: C 35.9, H 4.4. Electrospray MS: m/z (%) positive mode:1442.7312 $C_{44}H_{49}O_6Si_2Sn_6^+$ (100, $[MeSi(CH_2SnPhO)_3]_2+H^+)^+$, 2161.5910 $C_{66}H_{73}O_9Si_3Sn_9^+$ (0.7, $[MeSi(CH_2SnPhO)_3]_3+H^+)^+$, 3636.3600 $C_{11}H_{125}O_{16}Si_5Sn_{15}^+$ (2, $[MeSi(CH_2SnPhO)_3]_3$ + MeOH + $H^+)^+$, 4324.1823 $C_{132}H_{145}O_{18}Si_6Sn_{18}^+$ ($[MeSi(CH_2SnPhO)_3]_6+H^+)^+$. IR ($cm^{-1}$): ν(Sn–O-Sn) 695–726; ν(Sn-C) 494–559.

- **Synthesis of $[MeSi(CH_2SnCH_2SiMe_3O)_3]_{10}$ (30)**

Over a period of 1h, a solution of NaOH in water (20mL) (83.25mg, 2.08 mmol, 6 equiv) was added to a solution of **11** (508.00 mg, 346.90 µmol, 1 equiv) in 50 mL of acetone at 0 °C. The resulting mixture was stirred at room temperature overnight. All solvents were removed in vacuo (10^{-3} mmHg) and NaI was washed out successively with water. An oily residue (255.29 mg, 98 %) was obtained showing good solubility in $CHCl_3$ and CH_2Cl_2. Crystallization from CH_2Cl_2/ diethyl ether gave transparent crystals suitable for X-ray diffraction analysis, mp 347 °C. ^1H NMR ($CDCl_3$, 600.29, 298 K): δ 0.04–0.33 (complex pattern, 270H, $CH_2Si(CH_3)_3$), 0.85-0.89 (complex pattern, 30H, $SiCH_3$), 1.26 (s, 60H, $SiCH_2Me_3$), 1.59 (s, 60H, $SiCH_2Sn$). $^{13}C\{^1H\}$ NMR ($CDCl_3$, 150.94, 298 K): δ 1.02-2.67 ($SiCH_3$), 14.12, 22.69, 29.36, 31,12 ($SiCH_2Sn$), 29.69 (CH_2SiMe_3). Even with long data acquisition, no $^{117/119}Sn$ satellites were obtained .^{29}Si

NMR ($CDCl_3$, 119.26, 298 K): δ –21 (SiMe), -0.8-1.6 (CH_2SiMe_3). ^{119}Sn NMR ($CDCl_3$, 223.85, 298 K): δ –163-126 ($SnCH_2SiMe_3$). Anal. Calcd (%) for $C_{160}H_{420}O_{30}Si_{40}Sn_{30}$: C 25.59 H 5.64 Found: C 25.6, H 5.7. Electrospray MS: m/z (%) positive mode: 750.9293 $C_{16}H_{43}O_3Si_4Sn_3^+$ (2.5, $[MeSi(CH_2SnCH_2SiMe_3O)_3] + H^+)^+$, 768.8946 $[MeSi(CH_2SnCH_2SiMe_3O)_3 + H_2O + H^+]^+$, 788.9056 $[MeSi(CH_2SnCH_2SiMe_3O)_3 + K^+]^+$, 1646.8168 $\{[MeSi(CH_2Sn(OH)_2CH_2SiMe_3)_3]_2 + 2H_2O + H^+\}^+$, 1669.6017 $\{[MeSi(CH_2Sn(OH)_2CH_2SiMe_3)_3]_2 + CH_3CN + H_2O + H^+\}^+$, 2254.7532 $\{[MeSi(CH_2SnCH_2SiMe_3O)_3]_6 + 2H^+\}_2^+$, 3077.6608 $\{[MeSi(CH_2SnCH_2SiMe_3O)_3]_4 + H^+\}^+$, 4506.3980 $C_{96}H_{253}O_{18}Si_{24}Sn_{18}^+$ (4, $[MeSi(CH_2SnCH_2SiMe_3O)_3]_6 + H^+)^+$. IR ($cm^{-1}$): ν(Sn–O-Sn) 652–713; ν(Sn–C) 423–550.

- **Synthesis of $[MeSi(CH_2SnBr)_3(\mu_2\text{-}OH)_2(\mu_4\text{-}O)(\mu_3\text{-}OEt)_2]_2 \cdot 2EtOH$ (32)**

A recrystallization attempt of the nonabromido-organotin compound **9**, in an excess of EtOH in presence of dichloromethane gives $[MeSi(CH_2SnBr)_3(\mu_2\text{-}OH)_2(\mu_4\text{-}O)(\mu_3\text{-}OEt)_2]_2 \cdot 2EtOH$, **32** as brownish needles crystals. This crystalline material is insoluble in organic solvents and water. Anal. Calcd (%) for $C_{38}H_{106}Br_{12}O_{25}Si_4Sn_{12}$: ($2C_{20}H_{54}Br_6O_{12}Si_2Sn_6 + 2H_2O$ – EtOH: C 13.2 H 3.09. Found: C 13.2, H 3.1. Electrospray MS: m/z (%) negative mode: 1610.3 $[C_{20}H_{57}Br_4O_{14}Si_2Sn_6]^-$: (2.5, $[M - Br_2 + OH^- + H_2O]^-$). IR ($cm^{-1}$): ν(OH) 3501–3318, 2969-2893 cm^{-1}.

- **Synthesis of 7-Methyl-1,3,5-tris(triphenyl-2,4,9-trithio-7-sila-1,3,5-tristannaadamantane: $MeSi(CH_2SnPhS)_3$ (33)**

A (2.18 g, 1.52 mmol, 1 equiv) sample of **3** was dissolved in 100 mL acetone and added dropwise to a magnetically stirred ice-cooled solution of $Na_2S \cdot 9H_2O$ (1.17 g, 4.87 mmol, 3.2 equiv) in water. The reaction mixture was stirred over night at room temperature, and the precipitate was filtered off, dried in vacuo, giving **1** as amorphous white solid (1.17 g, 768.83 mmol, 98 % yield). Further purification was achieved by recrystallization from dichloromethane - diethyl ether to give transparent needles.

^1H NMR ($CDCl_3$, 400.25, 298 K): δ 0.43 (s, 3H, $^4J(^1H-^{117/119}Sn)$ = 11 Hz, $^2J(^1H-^{29}Si)$ = 20 Hz, SiMe), 0.80 (s, 6H, $^2J(^1H-^{117/119}Sn)$ = 72 Hz, $SiCH_2Sn$), 7.42–7.77 (complex pattern, 15H, Ph). $^{13}C\{^1H\}$ NMR ($CDCl_3$, 100.46, 298 K): δ 5.41 ($^1J(^{13}C-^{117/119}Sn)$ =275/294 Hz, $SiCH_2Sn$), 8.45 ($^1J(^{13}C-^{29}Si)$ = Hz, SiMe), 128.96 ($^3J(^{13}C-^{117/119}Sn)$ = 70 Hz, C_m), 130.19 ($^4J(^{13}C-^{117/119}Sn)$ = 10 Hz, C_p), 134.47 ($^2J(^{13}C-^{117/119}Sn)$ = 57 Hz, C_o), 141.49 ($^1J(^{13}C-^{117/119}Sn)$ =615/645 Hz, C_i). ^{29}Si NMR ($CDCl_3$, 119.26, 298 K): δ 13.4 ($^2J(^{29}Si-^{117/119}Sn)$ = 50 Hz, $^1J(^{29}Si-^{13}C)$ = 94 Hz, CH_2SiMe). ^{119}Sn NMR ($CDCl_3$, 149.26, 298 K): δ 98 ($^2J(^{119}Sn-^{117}Sn)$ = 190 Hz, *Sn*PhS). Anal. Calcd (%) for $C_{22}H_{24}S_3SiSn_3$: C 34.37, H 3.15. Found: C 34.3, H 3.3. Electrospray MS: m/z (%) positive mode 793.5 (65, $[M + Na^+]^+$).

- **Synthesis of 7-Methyl-1,3,5-tris(triphenyl-2,4,9-triselen-7-sila-1,3,5-tristannaadamantane: $MeSi(CH_2SnPhSe)_3$ (34)**

A (0.511 mg, 4.03 mmol, 3 equiv) sample of Na_2Se was added in to a magnetically stirred ice-cooled solution of **4** (1.19 g, 1.34 mmol, 1 equiv) in 50 mL acetone. The reaction mixture was stirred over night at room temperature, and the precipitate was filtered off, dried in vacuo, giving **2** as amorphous white solid (0.854 g, 0.938 mmol, 70 % yield). Due to the sensibility of **2**, a part of the product was oxidized to elemental Se under air). Further purification was achieved by recrystallization from dichloromethane - diethyl ether to give transparent needles with a mp of 280-286°.

^1H NMR ($CDCl_3$, 600.29, 298 K): δ 0.36 (s, 3H, $^4J(^1H-^{117/119}Sn)$ = 10 Hz, $^2J(^1H-^{29}Si)$ = 20 Hz, $^5J(^1H-^{77}Se)$ = 120 Hz, $SiCH_3$), 0.90 (s, 6H, $^2J(^1H-^{117/119}Sn)$ = 72 Hz, $^3J(^1H-^{77}Se)$ = 122 Hz, $SiCH_2Sn$), 7.42-7.72 (complex pattern, 15H, Ph). $^{13}C\{^1H\}$ NMR ($CDCl_3$, 150.94, 298 K): δ 5.23 ($^1J(^{13}C-^{29}Si)$ = 52 Hz, $^1J(^{13}C-^{117/119}Sn)$ = 245/256 Hz, $SiCH_2Sn$), 9.37 ($^3J(^{13}C-^{117/119}Sn)$ = 43 Hz, $^1J(^{13}C-^{29}Si)$ = 85 Hz, $SiCH_3$), 128.91 ($^3J(^{13}C-^{117/119}Sn)$ = 61 Hz, C_m), 130.07 ($^4J(^{13}C-^{117/119}Sn)$ = 15 Hz, $^5J(^{13}C-^{77}Se)$ = 56 Hz, C_p), 134.50 ($^2J(^{13}C-^{117/119}Sn)$ = 54 Hz, C_o), 140.67 ($^3J(^{13}C-^{117}Sn)$ = 10 Hz, $^3J(^{13}C-^{77}Se)$ = 52 Hz, $^1J(^{13}C-^{117/119}Sn)$ = 547/571 Hz, C_i). ^{29}Si NMR ($CDCl_3$, 119.26, 298 K): δ 13.88 ($^2J(^{29}Si-^{117/119}Sn)$ = 41 Hz, $^1J(^{29}Si-^{13}C)$ = 87 Hz, CH_2SiMe). ^{119}Sn NMR ($CDCl_3$, 149.26, 298 K): δ 2.44 (2J(119Sn-115Sn) = 2442 Hz, $^1J(^{119}Sn-^{77}Se)$ = 1231 Hz, $^1J(^{119}Sn-^{13}C_i)$ = 573 Hz, $^2J(^{119}Sn-^{117}Sn)$ = 217 Hz, *Sn*PhSe). ^{77}Se NMR ($CDCl_3$, 114.48, 298 K): δ –346.75 ($^1J(^{77}Se-^{117/119}Sn)$ = 1168/1225 Hz, *Se*SnPh). Anal. Calcd (%) for $C_{22}H_{24}Se_3SiSn_3$ + MeOH + 2 H_2O: C 28.26, H 3.3. Found: C 28.3, H 3.3. Electrospray MS: (positive mode) m/z (%) 2163.07 {30, $[MeSi(CH_2SnPhO)_3]_3 + 2H^+\}^{2+}$.

- **Synthesis of 7-Methyl-1,3,5-tris((trimethylsilyl)methyl)-2,4,9-trithio-7-sila-1,3,5-tristannaadamantane: $MeSi[CH_2Sn(CH_2SiMe_3)S]_3$ (35)**

A (0.643 g, 439.09 µmol, 1 equiv) sample of **11** was dissolved in 30 mL acetone and added dropwise to a magnetically stirred ice-cooled solution of Na2S.9H2O (0.340 g, 1.41 mmol, 3.2 equiv) in water. The reaction mixture was stirred over night at room temperature, and the precipitate was filtered off, dried in vacuo, giving **7a** as amorphous white solid (0.343 g, 430.3 µmol, 98 % yield). Further purification was achieved by recrystallization from acetone to give transparent needles with a mp of 190-196 °C.

^1H NMR ($CDCl_3$, 400.25, 298 K): δ 0.30 (s, 3H, $^4J(^1H-^{117/119}Sn)$ = 10 Hz, $SiCH_3$), 0.15-0.17 (s, 27H, $SiMe_3$), 0.55 (s, 6H, $^2J(^1H-^{117/119}Sn)$ = 87/92 Hz, $SiCH_2Sn$), 0.47 (s, 6H, CH_2SiMe_3). $^{13}C\{^1H\}$ NMR ($CDCl_3$, 150.94, 298 K): δ 1.39 ($^1J(^{13}C-^{29}Si)$ = 54 Hz, $^3J(^{13}C-^{117/119}Sn)$ = 23 Hz, $SiMe_3$), 7.62 ($^1J(^{13}C-^{117/119}Sn)$ = 260/273 Hz, $^1J(^{13}C-^{29}Si)$ = 50 Hz, $SnCH_2SiMe_3$), 9.03 ($^3J(^{13}C-^{117/119}Sn)$ = 38 Hz, SiMe), 10.62 ($^1J(^{13}C-^{117/119}Sn)$ = 287/300 Hz, $^1J(^{13}C-^{29}Si)$ = 42 Hz, $SiCH_2Sn$). ^{29}Si NMR ($CDCl_3$, 119.26, 298 K): δ 2.26 ($^2J(^{29}Si-^{117/119}Sn)$ = 30 Hz, $^1J(^{29}Si-^{13}C)$ = 56 Hz, (CH_2SiMe_3), 11.33 ($^2J(^{29}Si-^{117/119}Sn)$ = 52 Hz, $SnCH_2SiMe$). ^{119}Sn NMR ($CDCl_3$, 149.26, 298 K): δ 152.7 ($^2J(^{119}Sn-^{117}Sn)$ = 202 Hz, 2J(119Sn-115Sn) = 3625 Hz, $SnCH_2SiMe_3S$). Anal.

Calcd (%) for $C_{16}H_{42}S_3Si_4Sn_3$: C 24.05, H 5.3. Found: C 24.2, H 5.3. Electrospray MS: m/z (%) positive mode 798.8659 (100, $[M + H^+]^+$) $[C_{16}H_{43}S_3Si_4Sn_3]^+$).

- **Redistribution reaction of 33 and 34 in $CDCl_3$**

A (0.0186 g, 24.19 µmol, 1 equiv) sample of pure **33** was dissolved in 5 mL $CDCl_3$ and added to (0.022 g, 24.19 µmol, 1 equiv) sample of pure **34**. The reaction mixture was stirred for 30 min and send to ^{119}Sn NMR measurement. Series of ^{119}Sn NMR measurements were realized over a period of 78 Days to study the redistribution reactions taking place in this reaction mixture.

^{119}Sn NMR ($CDCl_3$, 223.85, 298 K, Day 21): δ 2.9 ppm (*Sn*Se_2, **A**, **34**), 0.3 ppm (*Sn*Se_2, **C**, 1*Sn*), 52.6 ppm (S*Sn*Se, **C**, 2*Sn*), 100.4 (*Sn*S_2, **D**, 1*Sn*), 50.5 (S*Sn*Se, **D**, 2*Sn*), 98.9 ppm (*Sn*S_2, **B**, **33**). ^{77}Se NMR ($CDCl_3$, 114.48, 298 K): δ –346.7 ppm (*Se*Sn, **D**, 1*Se*), -346.5 ppm ($^1J(^{77}Se-^{117/119}Sn)$ = 1221/1163 Hz, *Se*Sn, **A**, 3*Se*), -346.2 ppm (*Se*Sn, **C**, 2*Se*).

- **Redistribution reaction of 33 and 34 in C_6D_6**

A (0.0186 g, 24.19 µmol, 1 equiv) sample of pure **33** was dissolved in 5 mL C_6D_6 and added to (0.022 g, 24.19 µmol, 1 equiv) sample of pure **34**. The reaction mixture was stirred for 30 min and send to ^{119}Sn NMR measurement. Series of ^{119}Sn NMR measurements were realized over a period of 39 Days to study the redistribution reactions taking place in this reaction mixture.

^{119}Sn NMR ($CDCl_3$, 223.85, 298 K, Day 39): δ 2.59 ppm (*Sn*Se_2, **A**, **34**), 0.23 ppm (*Sn*Se_2, **C**, 1*Sn*), 53.06 ppm (S*Sn*Se, **C**, 2*Sn*), 101.7 (*Sn*S_2, **D**, 1*Sn*), 50.95 (S*Sn*Se, **D**, 2*Sn*), 100.1 ppm (*Sn*S_2, **B**, **33**).

- **Redistribution reaction of 34 and S_8 in $CDCl_3$**

A (0.057 g, 62.67 µmol, 1 equiv) sample of pure **34** was dissolved in 5 mL $CDCl_3$ and added to (0.016 g, 62.67 µmol, 1 equiv) sample of S_8. The reaction mixture was stirred for 30 min and send to ^{119}Sn NMR measurement. Series of ^{119}Sn NMR measurements were realized over a period of 53 Days to study the redistribution reactions taking place in this reaction mixture.

^{119}Sn NMR ($CDCl_3$, 149.26, 298 K, Day 7): δ 2.47 ppm (*Sn*Se_2, **A**, **34**), 0.23 ppm (*Sn*Se_2, **C**, 1*Sn*), 52.1 ppm (S*Sn*Se, **C**, 2*Sn*), 100.17 (*Sn*S_2, **D**, 1*Sn*), 50.09 (S*Sn*Se, **D**, 2*Sn*), 98.6 ppm (*Sn*S_2, **B**, **33**).

5. The Unprecedented Octanuclear Organotin Oxo Cluster $\{[MeSi(MeSnCl)(CH_2)_3(\mu_3-O)(MeSnCl)(CH_2)_3]_2O\}_2$

5.1 Introduction

Controlled hydrolysis of diorganotin dichlorides gives dimeric tetraorganodistannoxanes $[R_2XSnOSnXR'_2]_2$ (X = Cl, OH) of type A (Scheme 37). There is an increased interest of such compounds, given their applications as catalysts in organic chemistry and their capacity to present a variety of molecular structures depending on the substituents bound to the tin centres.[20] A special class of tetraorganodistannoxanes are compounds derived from spacer-bridged ditin derivatives. These tetraorganodistannoxanes exhibit so-called double ladder structures.
This chapter reports a novel such compound the central part of which contains a siloxane moiety.

Scheme 37. Base hydrolysis as a Synthesis method for obtaining ladder-like tetraorgandistannoxanes.

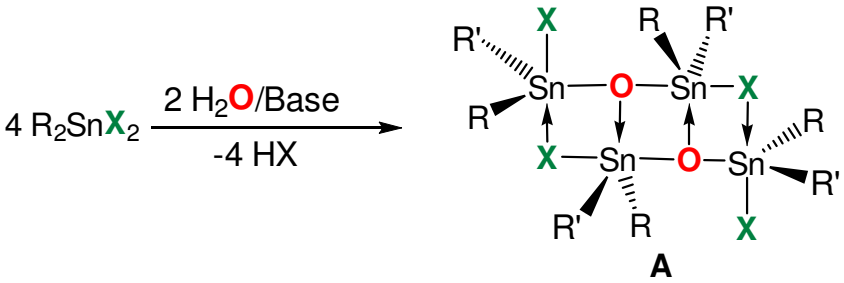

R, R' = Alkyl, Aryl; X = Halogen, OH, OC(O)R', OR', OSiR'$_3$, NR'$_2$, NCO, NCS,

5.2 Synthesis and structure

The reaction under non-inert conditions of the organochlorosilane $MeClSi((CH_2)_3SnMeCl_2)_2$, **1**, with an excess of pyridine in CH_3CN solution gives a slightly yellow oily material that is soluble in CH_3CN. Compound **1** was supplied from the stock in the laboratory. No procedure for its synthesis was avialable. A ^{119}Sn NMR of this crude mixture, in $CDCl_3$, (See Supporting Information, Chapter 5, Figure S1), shows two major broad signals at δ –43 ppm (38 %) and 48 ppm (43 %), referring to the the

distannoxane derivative **2**, four lower-intense signals at -132, -127, -84, and -76 ppm, with a whole integration of 10 % to which no assignments are made, and one signal referring to the remaining compound **1** at δ 162 ppm (4 %).

A crystalline material is isolated from this reaction mixture suitable for X-ray diffraction study, corresponding to compound **2**, $\{[MeSi(MeSnCl)(CH_2)_3(\mu_3-O)(MeSnCl)(CH_2)_3]_2O\}_2$, (Scheme 38) as colourless crystals suitable for X-ray diffraction study.

Scheme 38. Synthesis of the distannoxane derivative **2**.

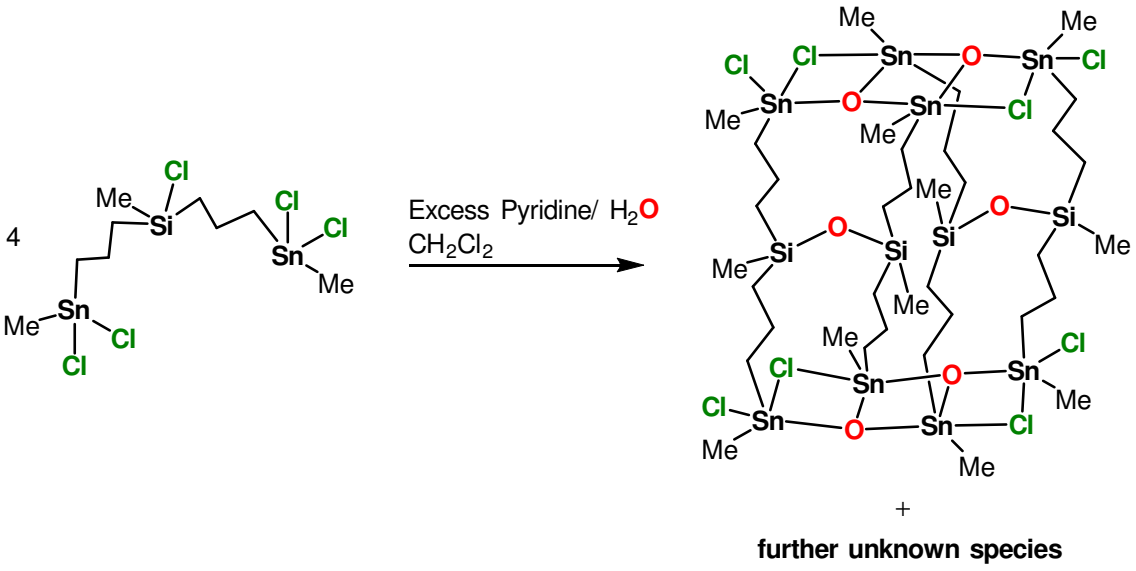

Figure 95 shows the molecular structure of **2**. The figure caption contains selected interatomic distances and angles. Compound **2** shows a centrosymmetric head-to-tail dimer presenting a double ladder structure in which two planar $Sn_4Cl_4O_2$ layers are linked by eight silicon-containing trimethylene chains. The four silicon atoms form two siloxanes bridges. This makes the structure unique given that it is the first octanuclear double ladder organotin oxocluster containing siloxane moieties linked to the bridging alkyl chains, referring to the Cambridge Structural Data Base.[60] This structure shows a similarity to the monomeric ladder-like compound **27**, $\{[MeSi(CH_2)_3]SnCl(CH_2SiMe_3)(\mu_3-O)SnCl(CH_2SiMe_3)Sn(\mu_3-O)(Cl)_2(CH_2SiMe_3)Sn(t\text{-}Bu)_2\}$ of Chapter 4 presenting a similar layer moiety. The exocyclic Sn atoms in this latter are unsymmetrically substituted.

Compound 2 contains four crystallographical independent tin atoms (Sn1, Sn2, Sn3 and Sn4) (Figure 94). The Sn(1) and Sn(2) atoms are incorporated in the central four-membered Sn2O2-ring as for Sn(3) and Sn(4) are bonded exocyclic to this ring. The endocyclic Sn atoms Sn(1) and Sn(2) are hexa-coordinated and exhibit each a distorted octahedral all-trans $SnC_2Cl_2O_2$ environment at with angles of (O1–Sn1–Cl1) 150.525(4)°, (O2–Sn1–Cl4) 138.64(5)°, (Cl1–Sn1–Cl4) 143.496(3)°, (O1–Sn1–C11) 96.497(6)°, (O2–Sn1–C11)

123.003(7)°, (C1–Sn1–C11) 129.872(13)°, (O1–Sn2–Cl3) 136.386(5)°, (O2–Sn2–Cl2) 150.871(4)°, (Cl2–Sn2–Cl3) 144.507(3)°, (O1–Sn2–C21) 109.794(7)°, (O2–Sn2–C21) 100.474(7)°, and (C2–Sn2–C21) 136.559(15)°. The chlorido- and the oxido- bridges Cl–Sn_{endo}–Cl and O–Sn_{endo}–O are unsymmetrical at Sn(2) and Sn(3) with Sn(1)–Cl(1), Sn(1)–Cl(4), Sn(1)–O(1), Sn(1)–O(2), Sn(2)–Cl(2), Sn(2)–Cl(3), Sn(2)–O(1), Sn(2)–O(2), distances equal to 2.6699(5), 3.4646(5), 2.0387(3), 2.052(4), 2.7176(5), 3.3512(5), 2.027(4), and 2.116(3) Å, respectively. The chlorine atoms Cl(3) and Cl(4) are approaching, respectively, Sn(2) and Sn(1), and making the environment hexaccordinated, given that bond distances (Sn1–Cl4) 3.4646(5) Å and (Sn2–Cl3) 3.3512(5) Å, are shorter than the sum of van der Waals radii of tin (2.17 Å) and chlorine (1.75 Å).[30]

The exo-cyclic tin atoms Sn(3) and Sn(4) exhibit a distorted trigonal bipyramidal environments, with the equatorial positions being occupied by two carbon atoms and one oxygen atom (C(3), C(31), O(2) for Sn(3)), (C(4), C(41), O(1) for Sn(4)).

As to the axial positions, are being occupied by two chlorine atoms (Cl1, Cl3 for Sn3, and Cl2 and Cl4 for Sn4). The geometrical goodnes $\Delta\Sigma(\theta)$[22] is 62.6° for Sn(3) and 82.6° for Sn(4). The Sn_{exo}–O interatomic distances range between 2.0361(3) and 2.1192(4) Å, corresponding to Sn(3)–O(2) and Sn(4)–O(1), respectively, which are longer than the Sn_{endo}–O bond distances. The Cl–Sn_{exo}–Cl bridges are unsymmetrical with distances of Sn(3)–Cl(1) 2.817(5) Å, Sn(3)–Cl(3) 2.4553(4) Å, Sn(4)–Cl(2) 2.7349(5) Å, and Sn(4)–Cl(4) 2.492(4) Å.

Bond distances and angles around the siloxane-bridges are similar to the corresponding bridges in siloxane-containing compounds reported in the literature.[22] The Si–O intramolecular distances are equal to 1.5966(3) and 1.6736(3) Å, corresponding, respectively, to Si(1)–O(3) and Si(2)–O(3). The corresponding angle is equal to 151.168(8)° (Si1–O3–Si2).

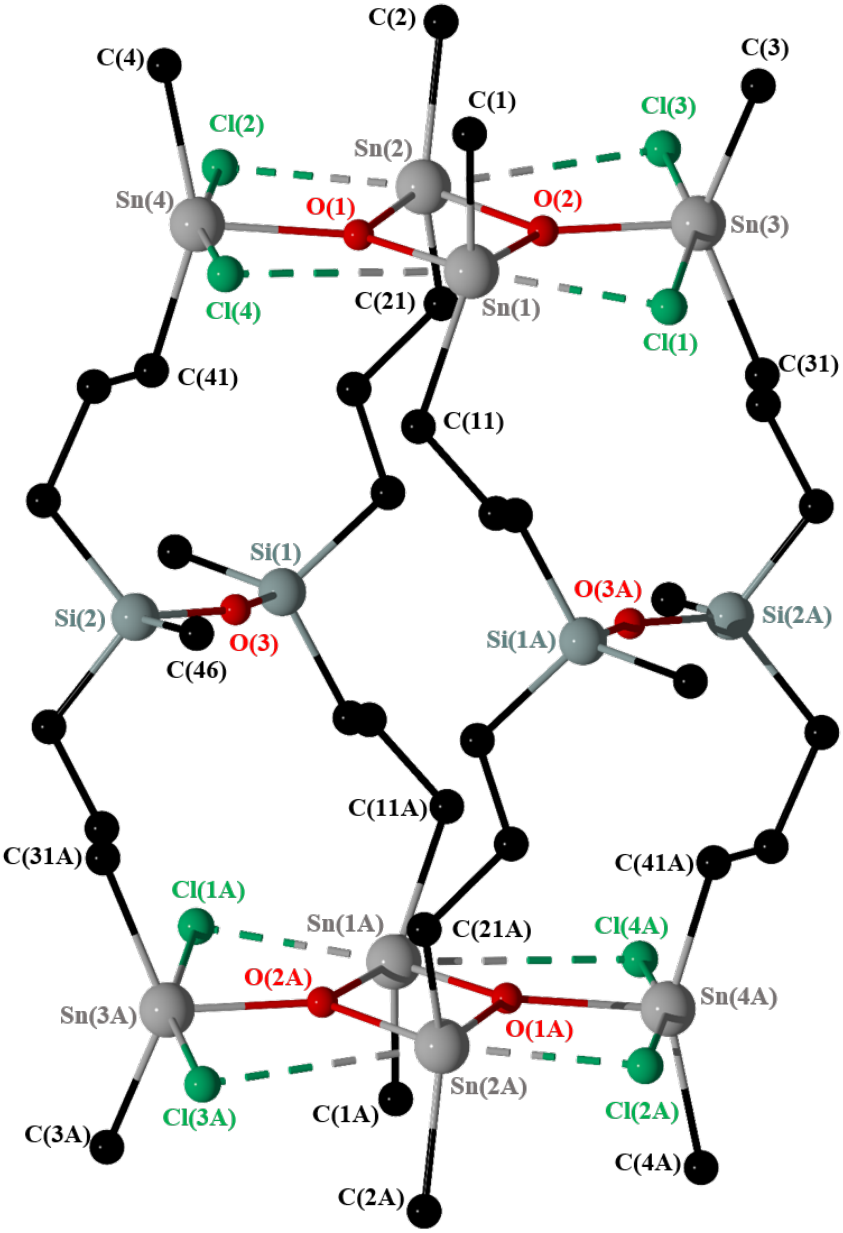
C(2)
C(4)
C(3)
C(1)
Cl(2)
Cl(3)
Sn(2)
Sn(4)
O(1)
O(2)
Sn(3)
Cl(4)
C(21)
Sn(1)
Cl(1)
C(41)
C(31)
C(11)
Si(1)
O(3A)
Si(2)
Si(1A)
Si(2A)
O(3)
C(46)
C(11A)
C(31A)
C(41A)
Cl(1A)
Sn(1A)
C(21A)
Cl(4A)
O(2A)
Sn(3A)
Sn(4A)
O(1A)
Sn(2A)
Cl(3A)
C(1A)
Cl(2A)
C(3A)
C(4A)
C(2A)

Figure 95. POV-Ray image of the molecular structure of $\{[MeSi(CH_2)_3]SnCl(CH_2SiMe_3)(\mu_3\text{-}O)SnCl(CH_2SiMe_3)Sn(\mu_3\text{-}O)(Cl)_2$ $(CH_2SiMe_3)Sn(Me)_2\}$, **2**. Selected interatomic distances (Å): Sn(1)–Cl(1) 2.6699(5), Sn(1)–Cl(4) 3.4646(5), Sn(1)–O(1) 2.0387(3), Sn(1)–O(2) 2.052(4), Sn(2)–Cl(2) 2.7176(5), Sn(2)–Cl(3) 3.3512(5), Sn(2)–O(1) 2.027(4), Sn(2)–O(2) 2.116(3), Sn(1)–Cl(4) 3.4646(5), Sn(2)–Cl(3) 3.3512(5), Si(1)–O(3) 1.5966(3), Si(2)–O(3) 1.6736(3) Selected interatomic angles (°): O(1)–Sn(1)–Cl(1) 150.525(4), O(2)–Sn(1)–Cl(4) 138.64(5), Cl(1)–Sn(1)–Cl(4) 143.496(3), O(1)–Sn(1)–C(11) 96.497(6), O(2)–Sn(1)–C1(1) 123.003(7), C(1)–Sn(1)–C(11) 129.872(13), O(1)–Sn(2)–Cl(3) 136.386(5), O(2)–Sn(2)–Cl(2) 150.871(4), Cl(2)–Sn(2)–Cl(3) 144.507(3), O(1)–Sn(2)–C(21) 109.794(7), O(2)–Sn(2)–C(21) 100.474(7), C(2)–Sn(2)–C(21) 136.559(15), O(2)–Sn(3)–C(3) 109.535(5), Cl(1)–Sn(3)–Cl(3) 161.41(5), O(1)–Sn(4)–C(4) 106.725(6), Cl(2)–Sn(4)–Cl(4) 165.356(5), Si(1)–O(3)–Si(2) 151.168(8).
Giving the lack of material, no further investigation in solution was done. An ESI-MS spectrum (positive mode) of **2** shows low intense mass clusters centred at m/z 1228.7775 and 1923.5218 corresponding, respectively, to the cations $[C_{26}H_{68}ClOSi_3Sn_6]^+$ and $[C_{35}H_{94}Cl_8O_3Si_4Sn_8]^+$ (See Supporting Information, Chapter 5, Figures S2-S5).

5.3 Conclusion

Compound **2** presents a new type of double ladder-like structure, preserving the structural moeity characteristic of tetraoganodistannoxanes and presenting siloxanes bridging in the skeleton. Within the time frame of this PhD, no further studies of its behaviour in solution, could be performed. However, such compound holds potential for novel generation of its own.

5.4 Experimental section

- **Synthesis of $\{[MeSi(MeSnCl)(CH_2)_3(\mu_3-O)(MeSnCl)(CH_2)_3]_2O\}_2$ (2)**

To a solution of $MeClSi((CH_2)_3SnMeCl_2)_2$, **1**, (109.00 mg, 0.19 mmol) in 15 mL of CH_3CN was added three molar equiv of pyridine (45.2 mg, 0.57 mmol). The resulting mixture was stirred at room temperature overnight. A crystalline material of **2** is isolated as colourless crystals from this reaction mixture (10 mg, 11 % yield).
Anal. Calcd (%) for $C_{36}H_{88}Cl_8O_6Si_4Sn_8$ + 2 pyridine + CH_3CN: C 26.7, H 4.7, N 1.94. Found: C 26.0, H 4.5, N 2.2. Electrospray MS: m/z (%) positive mode: 1228.7775 $[C_{26}H_{68}ClOSi_3Sn_6]^+$ and 1923.5218 $[C_{35}H_{94}Cl_8O_3Si_4Sn_8]^+$.

6. Novel Triorganotin-functionalized Aminoalcohol Derivatives as Potential Precursors for the Synthesis of Organtin-containing Azidocryptands

6.1 Introduction

Since the innovative works from Pedersen, Lehn, and Cram work[61,62] on crown-ethers, cryptands, and related species, host-guest supramolecular chemistry became the focus of research,[62] The concept got new momentum when by combining crown ethers with Lewis acids thus creating so-called ditopic receptors that bind cations and anions simultaneously. One representative is the complex A (Scheme 39) in which sodium fluoride, NaF, is ditopically complexed by such a host.

Scheme 39. Ditopic complex of sodium fluoride, NaF.[63]

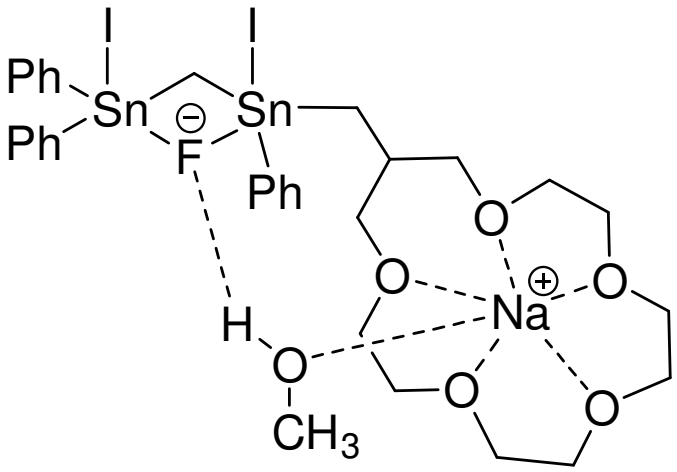

A challenge for future work is to synthesize a host combined of a cryptand and a Lewis acid, as it is shown in Scheme 40. This short chapter reports preliminary results on the way to achieve this goal.

Scheme 40. Concept of synthesis of organotin-functionalized cryptand.

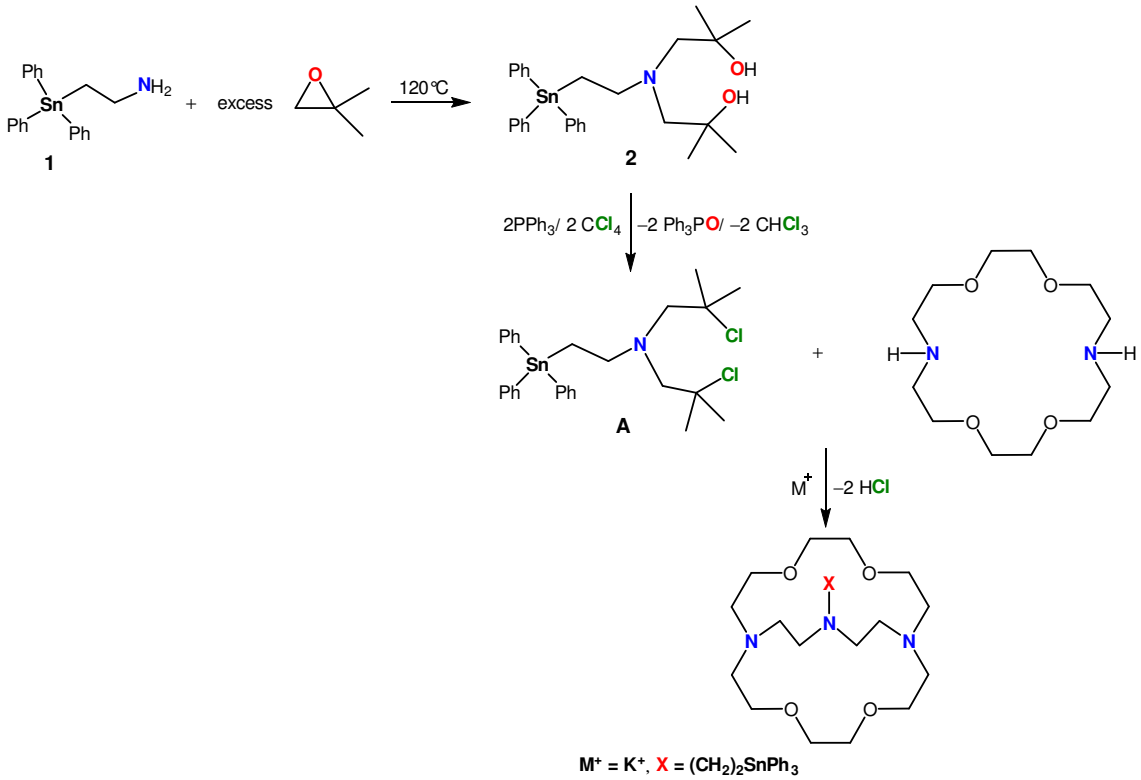

6.2 Synthesis of $Ph_3Sn(CH_2)_2N[CH_2C(CH_3)_2OH]_2$ and its reaction with tetra-tert-butoxystannane

The reaction of a slight excess of 2-chloroethyl amine, obtained via reaction between equimolar amounts of trimethylamine and 2-chloroethylamine hydrochloride,[64] with one molar equiv of sodium triphenylstannide, $NaSnPh_3$, in THF affords a white solid material that is soluble in almost all organic solvent. A ^{119}Sn NMR spectrum of a solution of this material, in C_6D_6, (Figure 96), shows one resonance at δ -100 ppm. Recrystallization from diethyl-ether/ dichloromethane affords 1-triphenylstannyl-2-aminoethane, $Ph_3Sn(CH_2)_2NH_2$, **1**, as colourless crystals suitable for X-ray diffraction analysis (Scheme 41).

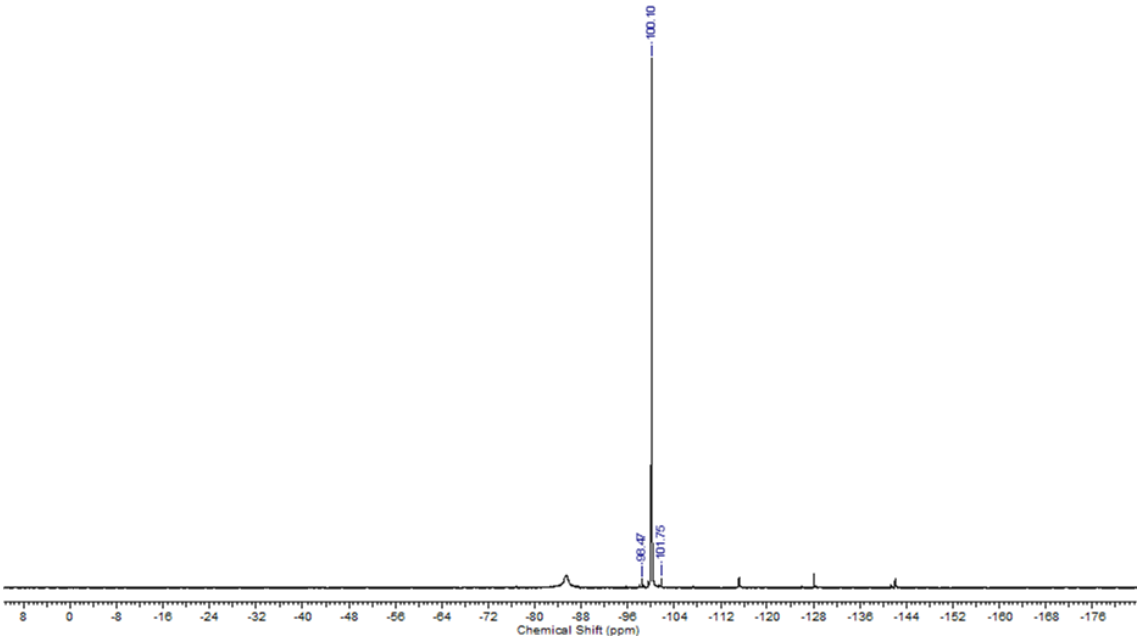

Figure 96. ^{119}Sn NMR spectrum (149.26 MHz, C_6D_6) of crude mixture reaction of compound **1**.

Scheme 41. Synthesis of $Ph_3Sn(CH_2)_2NH_2$, **1**.

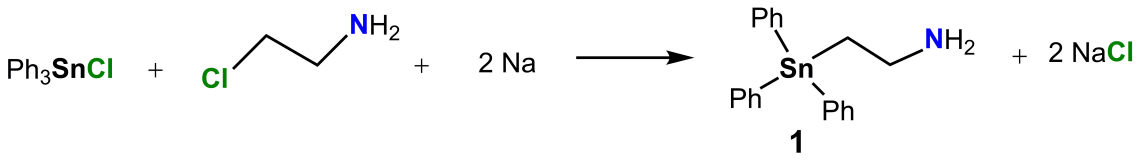

Compound **1** crystallizes in the monoclinic space group $P2_1/n$, with two molecules in the unit cell.

Figure 97 shows the molecular structure of **1**, and the figure caption contains selected interatomic distances and angles.

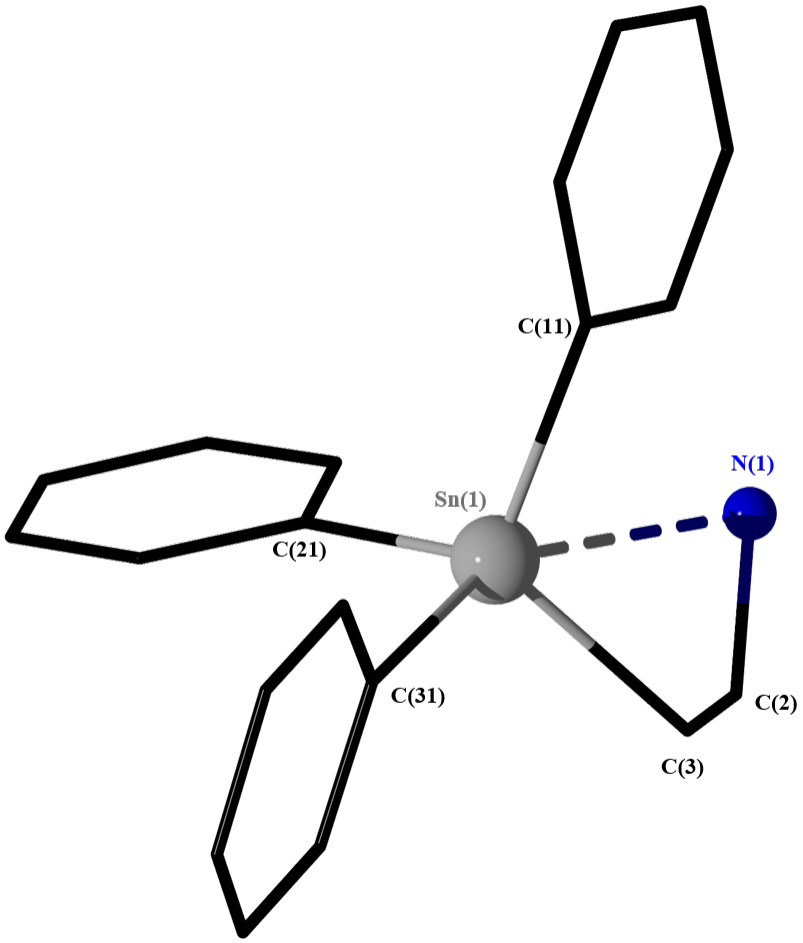

Figure 97. POV-Ray image of the molecular structure of $Ph_3Sn(CH_2)_2NH_2$, **1**. Hydrogens are omitted for clarity. Selected interatomic distances (Å): Sn(1)–N(1) 3.049(3), Sn(1)–C(21) 2.136(3), Sn(1)–C(31) 2.159(3). Selected interatomic angles (°): C(3)–Sn(1)–N(1) 52.08(10), C(11)–Sn(1)–N(1) 83.93(9), C(21)–Sn(1)–N(1) 87.78(9), C(31)–Sn(1)–N(1) 157.13(9), C(11)–Sn(1)–C(3) 114.19(11), C(21)–Sn(1)–C(3) 113.74(11), C(31)–Sn(1)–C(3) 105.07(10), C(11)–Sn(1)–C(21) 109.63(10), C(11)–Sn(1)–C(31) 108.50(10), C(21)–Sn(1)–C(31) 105.09(10).

The Sn(1) atom is pentacoordinated and exhibits a distorted trigonal bipyramidal environment, with N(1), and C(31) occupying the axial, and C(3), C(11), and C(21) occupying the equatorial positions. The geometrical goodness $\Delta\Sigma(\theta)$[22] is equal to 18.9°. There is a rapprochement of N(1) to the Sn centre via N →Sn intramolecular coordination equal to 3.049(3) Å (Sn1–N1), which is shorter than the sum of van der Waals radii of Sn (2.27 Å) and N (1.55 Å). This bond distance is longer than those corresponding in comparable compounds such as $\{Me_2N(CH_2)_3\}Ph_3SnCH_2$,[29] in which Sn–N is equal to 2.433(3) Å and in $[Me_2NCH_2N(CH_2CH_2O)_2]_2Sn$, in which Sn–N is equal to 2.524(2) Å.[65] The Sn–C vary between 2.136(3) Å (Sn1–C21) and 2.159(3) Å (Sn1–C31).

A ^{119}Sn NMR spectrum of a crystalline material of compound **1** dissolved in in $CDCl_3$ shows one singlet resonance at -102 ppm ($^1J(^{119}Sn-^{13}C_i)$ = 490 Hz). A ^{1}H NMR spectrum shows the singlet corresponding to the NH_2 protons at δ 1.81 ppm and the triplet resonances assigned to the (CH_2Sn) protons at δ 1.92 ppm ($^2J(^1H-^{117/119}Sn)$ = 60 Hz) and to the (CH_2N) protons at δ 3.26 ppm ($^3J(^1H-^{117/119}Sn)$ = 40 Hz). The complex pattern referring to the protons of the phenyl groups appears at δ 7.32– 8.01 ppm with integration of 15H. In a ^{13}C NMR spectrum (C_6D_6 solution), the chemical shift at δ 17.41 ppm ($^1J(^{13}C-^{117/119}Sn)$ = 385/404 Hz) is assigned to the (CH_2Sn) carbon atom (C3) and at δ 38.8 ppm is assigned to the (CH_2N) carbon atom (C2). (Figure 97)

An electrospray ionization mass spectrum (ESI MS positive mode) shows an intense mass cluster centred at m/z 344.04 corresponding to the anion $[C_{14}H_{16}NaSn]^+$. An IR spectrum shows an absorption band at ν 3100 cm^{-1}, corresponding to the NH_2 group (See Supporting Information, Chapter 6, Figures S1- S6).

Heating of an excess of isobutylene oxide with one molar equiv of **1** in a pressure Young-vessel during three days, affords a yellow oily substance soluble in almost all organic solvent. After removal of volatiles at reduced pressure and recrystallization from diethyl-ether/dichloromethane affords bis-triphenylstannylethylenamine(2-methyl-2-propanol), $Ph_3Sn(CH_2)_2NH_2(CH_2CMe_2OH)_2$, **2**, as colourless crystals suitable for X-ray diffraction analysis (Scheme 42).

Scheme 42. Synthesis of $Ph_3Sn(CH_2)_2NH_2(CH_2CMe_2OH)_2$, **2**.

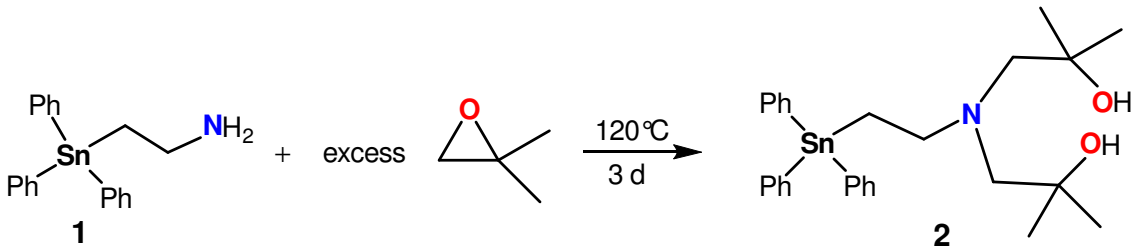

Compound **2** crystallizes in the monoclinic space group $P2_1/n$ with two molecules in the unit cell. Figure 98 shows the molecular structure of **2** and the figure caption contains selected interatomic distances and angles.

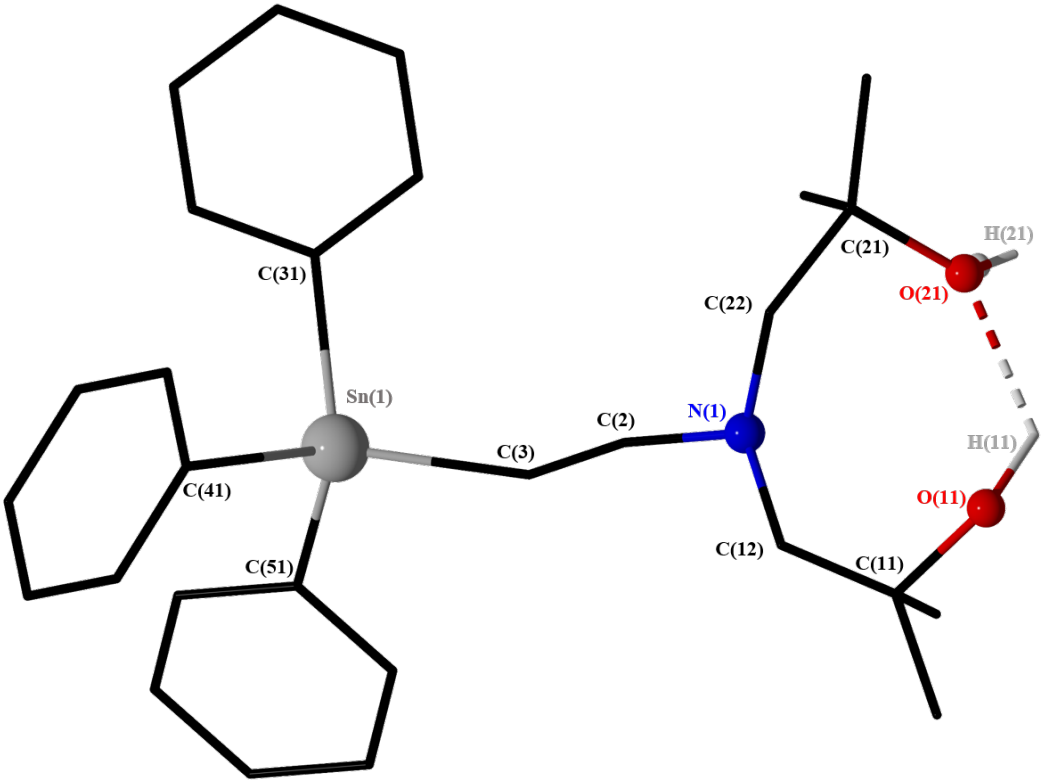

Figure 98. POV-Ray image of the molecular structure of $Ph_3Sn(CH_2)_2NH_2(CH_2CMe_2OH)_2$, **2**. Hydrogens are omitted for clarity. Selected interatomic distances (Å): H(11)–O(21) 1.984, Sn(1)–C(41) 1.990(3), Sn(1)–C(51) 2.342(4). Selected interatomic angles (°): C(3)–Sn(1)–C(31) 109.8(4), C(3)–Sn(1)–C(41) 110.6(4), C(3)–Sn(1)–C(51) 115.3(4), C(31)–Sn(1)–C(51) 104.07(18), C(31)–Sn(1)–C(41) 110.6(2), C(41)–Sn(1)–C(51) 106.31(19), C(2)–N(1)–C(12) 112.3(11), C(2)–N(1)–C(22) 112.0(12), C(12)–N(1)–C(22) 113.2(14).

The Sn(1) atom exhibits a tetrahedral environment, with angles varying between 104.07(18)° (C31–Sn1–C51) and 109.8(4)° (C3–Sn1–C31). The Sn–C distances vary between 1.990(3) Å (Sn1–C41) and 2.342(4) Å (Sn1–C51). The C–N–C angles are almost equal, varying between 112.0(12)° (C22–N1–C2) and 113.2(14)° (C22–N1–C12). There is a hydrogen bond O(11) –H(11) ··· O(21) at a O(11)–O(21) distance of 1.984 Å.
A ^{119}Sn NMR spectrum of a crystalline material of compound **2** in $CDCl_3$ shows one singlet resonance at –129 ppm. A ^{1}H NMR spectrum shows the singlet corresponding to the CH3 protons at 1.18 ppm. The signal for the OH protons appears at δ 1.36 ppm, the multiplet resonances assigned to the (CH_2Sn) protons appear at δ 1.71 and to the (CH_2N) protons at 2.98 ppm. As to the resonance corresponding to the CCH_2 protons appears at 2.63 ppm. The complex pattern referring to the phenyl protons appears at δ 7.39- 7.70 ppm with integration of 15H. In a ^{13}C NMR spectrum ($CDCl_3$ solution), the chemical

shifts at δ 8.31 and 56.3 ppm are assigned to the (CH_2Sn) carbon atom (C3) and the (CH_2N) carbon atom (C2), respectively (Figure 98). In the aromatic part, the chemical shifts corresponding to the carbon atoms C_m) at δ 128.56 ppm ($^3J(^{13}C-^{117/119}Sn)$ = 46 Hz) ppm, C_p) at δ 129.01 ppm ($^4J(^{13}C-^{117/119}Sn)$ = 15 Hz), C_o at δ 136.0 ppm, and C_i at δ 138.03 ppm ($^1J(^{13}C-^{117/119}Sn)$ = 500 Hz). An electrospray ionization mass spectrum (ESI MS positive mode) shows mass clusters centred at m/z 540.2 corresponding to the cation [M + H^+]$^+$). An IR spectrum reveals an absorption band at ν 3500-2966 cm^{-1}, corresponding to OH groups (See Supporting Information, Chapter 6, Figures S9- S15).
The reaction mixture of two molar equiv of **2** with one molar equiv of $(t-BuO)_4Sn$ in toluene is heated at reflux over night to afford a slightly yellow oily substance soluble in almost all organic solvent. Recrystallization from toluene affords the *spiro*-type compound *spiro*-$[Ph_3Sn(CH_2)_2NH_2(CH_2CMe_2O)_2]_2Sn$, **3**, as colourless crystals suitable for X-ray diffraction analysis (Scheme 43).

Scheme 43. Synthesis of $[Ph_3Sn(CH_2)_2NH_2(CH_2CMe_2O)_2]_2Sn$, **3**.

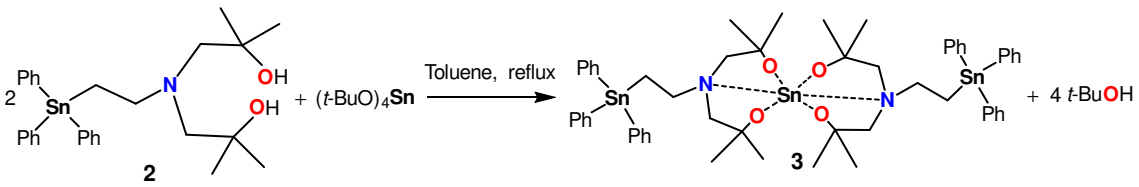

Compound **3** crystallizes in the triclinic space group *P*–1 group with two molecules in the unit cell.
Figure 99 shows the molecular structure of **3** and the figure caption contains selected interatomic distances and angles.

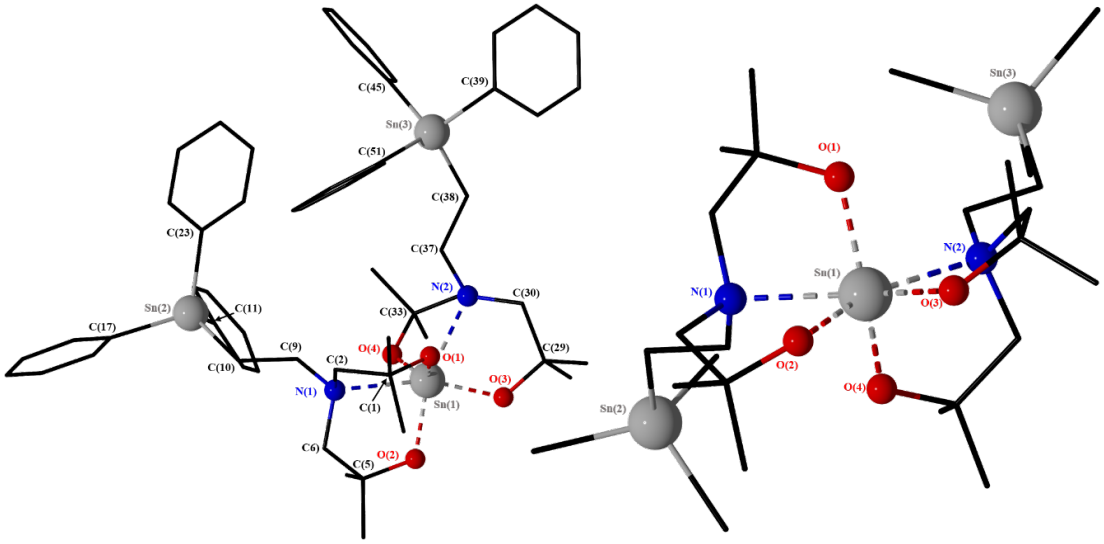

Figure 99. POV-Ray images of the molecular structure of $[Ph_3Sn(CH_2)_2NH_2(CH_2CMe_2O)_2]_2Sn$, **3**; left: complete presentation of the molecular structure of **3** (only hydrogens are omitted for clarity), right: Simplified presentation with only C_i of the phenyl groups are presented and hydrogens are omitted for clarity. Selected interatomic distances (Å): Sn(1)–O(1) 2.0051(14), Sn(1)–O(2) 1.9969(14), Sn(1)–O(3) 1.9941(15), Sn(1)–O(4) 1.9936(15), Sn(1)–N(1) 2.4439(17), Sn(1)–N(2) 2.3699(17). Selected interatomic angles (°): O(1)–Sn(1)–O(2) 110.32(6), O(1)–Sn(1)–O(3) 102.41(6), O(1)–Sn(1)–O(4) 135.65(7), O(2)–Sn(1)–O(3) 85.75(6), O(2)–Sn(1)–O(4) 102.16(6), O(3)–Sn(1)–O(4) 109.46(6), O(1)–Sn(1)–N(1) 77.45(6), O(1)–Sn(1)–N(2) 82.38(6), O(2)–Sn(1)–N(1) 76.67(6), O(2)–Sn(1)–N(2) 159.53(6), N(2)–Sn(1)–N(1) 122.79(6), O(3)–Sn(1)–N(1) 160.97(6), O(3)–Sn(1)–N(2) 75.62(6), C(11)–Sn(2)–C(23) 105.60(9), C(39)–Sn(3)–C(51) 112.83(9), C(2)–N(1)–C(9) 110.86(16), C(34)–N(2)–C(37) 114.23(17).

The Sn(1) atom is hexa-coordinated and exhibits a distorted octahedral SnO4N2 environment. The N(1) and N(2) atoms coordinate the Sn(1) centre in cis position at distances of 2.4439(17) Å (Sn1–N1) and 2.3699(17) Å (Sn1–N2), respectively. These distances are shorter than the sum of van der Waals radii of Sn (2.27 Å) and N (1.55 Å).[29] These bond distances are comparable to the corresponding in $[MeN(CH_2CH_2CH_2O)_2]_2Sn$,[66] with Sn–N ranging between 2.285(3) and 2.381(3) Å, and shorter than those corresponding in comparable compounds such as in $[Me_2NCH_2N(CH_2CH_2O)_2]_2Sn$, in which Sn–N is equal to 2.524(2) Å[66] and in $[MeOCH_2N(CH_2CH_2O)_2]_2Sn$ with the corresponding Sn–N bond is equal to 2.526(2) Å,[65] and the resembling stannylene compound $RN(CH_2CR'2O)_2Sn$; R = CH_2CMe_2OH, R' = H,[66] in which Sn–N is equal to 2.561(3) Å. There are four O→Sn intramolecular coordination with bond distances of 2.0051(14), 1.9969(14), 1.9941(15), and 1.9936(15), corresponding to Sn(1)–O(1), Sn(1)–O(2), Sn(1)–O(3), and Sn(1)–O(4),

respectively. These later are all shorter than the corresponding Sn-O bond distances in the spiro-type compounds $[Me_2NCH_2N(CH_2CH_2O)_2]_2Sn$ and $[MeOCH_2N(CH_2CH_2O)_2]_2Sn$, with Sn–O, respectively, of 2.130(2)/ 2.253(2), and 2.128(2)/ 2.250(2) Å.[65] The O–Sn–O angles O(1)–Sn(1)–O(2), O(1)–Sn(1)–O(3), O(1)–Sn(1)–O(4), O(2)–Sn(1)–O(3), O(2)–Sn(1)–O(4), and O(3)–Sn(1)–O(4) are equal to 110.32(6), 102.41(6), 135.65(7), 85.75(6), 102.16(6), and 109.46(6)°, respectively. These angles are comparable to those corresponding in $[Me_2NCH_2N(CH_2CH_2O)_2]_2Sn$,[65] varying between 69.09(7)°and 100.50(7)°, $[MeOCH_2N(CH_2CH_2O)_2]_2Sn$,[65] varying between 68.50(7)°and 101.69(8)° and smaller than those corresponding in $[MeN(CH_2CH_2CH_2O)_2]_2Sn$,[66] varying between 92.33(10)°and 154.12(10)°. The O–Sn–N angles vary between 75.62(6)° (O3–Sn1–N2) and 160.97(6)° (O3–Sn1–N1). These values are comparable to those corresponding in $[MeN(CH_2CH_2CH_2O)_2]_2Sn$,[66] varying between 77.76(10)°and 165.89(10)°.

The Sn(2) and Sn(3) atoms exhibit tetrahedral environment, with angles varying between 105.60(9)° (C23–Sn2–C11) and 112.83(9)° (C39–Sn3–C51). The C–N–C angles are comparable, varying between 110.86(16)° (C2–N1–C9) and 114.23(17)° (C34–N2–C37).

A ^{119}Sn NMR spectrum of compound **3** in C_6D_6 shows two singlet resonances at δ –99 ppm ($^4J(^{119}Sn-^{117/119}Sn)$ = 17 Hz) and δ –435 ppm ($^4J(^{119}Sn-^{117/119}Sn)$ = 17 Hz) with an integration of 2:1 respectively. The latter chemical shift is very close to the corresponding Sn atom in $[MeN(CH_2CH_2CH_2O)_2]_2Sn$,[66] at δ –449 ppm.

The ^{1}H NMR spectrum shows the multiplet resonances assigned to the (CH_2Sn) protons at δ 0.75 ppm and (CH_2N) protons at δ 3.26 ppm. The CH_3 protons of the alkanol groups appear at δ 1.17– 1.27 ppm. The resonance corresponding to (CH_2N) protons of the alkanol groups appear at 2.61 ppm ($^3J(^1H-^{117/119}Sn_1)$ = 233 Hz).

The complex pattern referring to the protons of the phenyl groups appears at δ 7.33–7.58 ppm with integration of 30H. An electrospray ionization mass spectrum (ESI MS positive mode) shows two mass clusters centred at m/z 538.4 and 562.4 corresponding, respectively, to the cations $[C_{28}H_{37}NO_2Sn]^+$ and $[C_{28}H_{37}NaNO_2Sn]^+$ (See Supporting Information, Chapter 6, Figures S16- S21).

6.3 Conclusion

Within the time frame of this PhD, further work could not be realized. However, there is a promising start to achieve the main goal of this work which is functionalization of the triorganotin-functionalized cryptand, based on the synthesized alkanol amine organotin compound **2**, bis-triphenylstannylethylenamine(2-methyl-2-propanol), $Ph_3Sn(CH_2)_2NH_2(CH_2CMe_2OH)_2$. This result is motivating in context with previous work in our research group on of aminoalkanol derivatives of tin. It holds potential to obtain polyfunctional ligands, applied for the synthesis of a new generation of functional material in fields of catalysts and metal-organic frameworks...[65,66]

6.4 Experimental section

- **Synthesis of $Ph_3Sn(CH_2)_2NH_2$ (1)**

To a solution of $SnPh_3Cl$ (10 g, 25.64 mmol) in THF (250 mL) were added a slight excess of metallic sodium (1.25 g, 54.22 mmol) and a catalytic amount of naphthalene. The mixture was stirred at room temperature for 3 days, during which its colour changed to deep black. After the solution had been separated from non-reacted sodium, 2-chloroethylamine[65] (2.94 g, 36.97 mmol) was added dropwise at −70 °C under magnetic stirring. Overnight, the reaction mixture was warmed to room temperature and the solvent was evaporated in vacuo. The residue obtained was extracted with 300 mL diethyl ether followed by washing with 150 mL distilled water in order to remove the sodium chloride. The organic phase was dried over anhydrous $MgSO_4$ and filtrated. The solvent was removed from the filtrate under reduced pressure, giving **1** as amorphous white solid (9.22 g, 23.39 mmol, 95 % yield). Further purification was achieved by recrystallization from diethyl-ether/ dichloromethane to give transparent needles with a mp of 76 °C.
^{1}H NMR ($CDCl_3$, 400.25, 298 K): δ 1.81 ppm (s, 2H, NH_2), 1.92 ppm (t, 2H, $^2J(^1H-^{117/119}Sn)$ = 60 Hz, CH_2Sn), 3.26 ppm (t, 2H, $^3J(^1H-^{117/119}Sn)$ = 40 Hz, CH_2N), 7.32- 8.01 ppm (complex pattern, 15H, Ph). ^{13}C $\{^1H\}$ NMR (C_6D_6, 100.64, 298 K): δ 17.41 ppm ($^1J(^{13}C-^{117/119}Sn)$ = 385/404 Hz, CH$_2$Sn), 38.8 ppm (CH$_2$N), 128.35 ppm (C_m), 129.09 ppm ($^4J(^{13}C-^{117/119}Sn)$ = 11 Hz, C_p), 137.93 ppm (C_o), 140.1 ppm (C_i). ^{119}Sn NMR (C_6D_6, 149.26, 298 K): δ –102 ppm ($^1J(^{119}Sn-^{13}C)$ = 490 Hz, SnPh$_3$). Anal. Calcd (%) for $C_{20}H_{21}NSn$: C 60.95, H 5.37, N 3.55. Found: C 60.0, H 5.4, N 3.5. Electrospray MS: m/z (%) positive mode: 344.04 [100, $C_{14}H_{16}NaSn^+]^+$. IR (cm-1): $\nu(NH_2)$ 3100 cm^{-1}.

- **Synthesis of $Ph_3Sn(CH_2)_2NH_2(CH_2CMe_2OH)_2$ (2)**

2-amino-ethyltriphenylstannane (**1**) (0.596 g, 1.51 mmol) and excess of isobutylene oxide (1.09 g, 15.12 mmol) were placed in a glass vessel with a Young® valve, the mixture was heated at 120 °C for three days, and the excess of isobutylene oxide was removed in vacuum. Compound **2** was obtained as a yellow oily substance with a quantitative yield (0.773 g, 1.43 mmol, 95 %). Recrystallization from diethyl-ether/ dichloromethane gave **2** as transparent needles.
^{1}H NMR ($CDCl_3$, 400.25, 298 K): δ 1.18 ppm (s, 12H, CH_3), 1.36 ppm (s, 2H, OH), 1.71 ppm (m, 2H, CH_2Sn), 2.63 (s, 4H, CH_2CMe$_2$), 2.98 ppm (m, 2H, , CH_2N), 7.39- 7.70 ppm (complex pattern, 15H, Ph). ^{13}C $\{^1H\}$ NMR ($CDCl_3$, 100.64, 298 K): δ 8.31 ppm (CH$_2$Sn), 56.3 ppm (CH$_2$N), 67.1 (CMe$_2C$H$_2$N), 71.21 (CMe$_2$), 128.56 ppm ($^3J(^{13}C-^{117/119}Sn)$ = 46 Hz, C_m), 129.01 ppm ($^4J(^{13}C-^{117/119}Sn)$ = 15 Hz, C_p), 136.0 ppm (C_o), 138.03ppm ($^1J(^{13}C-^{117/119}Sn)$ = 500 Hz, C_i). ^{119}Sn NMR ($CDCl_3$, 149.26, 298 K): δ –129 ppm (SnPh$_3$). Anal. Calcd (%) for $C_{28}H_{37}NO_2Sn$: C 62.47, H 6.93, N 2.6. Found: C 62.5, H

6.9, N 2.4. Electrospray MS: m/z (%) positive mode: 540.2 $[C_{28}H_{38}NO_2Sn]^+$: $[M + H^+]^+$. IR (cm^{-1}): ν(OH) 3500-2966 cm^{-1}.

- **Synthesis of $[Ph_3Sn(CH_2)_2NH_2(CH_2CMe_2O)_2]_2Sn$ (3)**

A solution of **2** (1.02, 1.89 mmol) in toluene (50 mL) was added to tetra-(tert-butyl oxide)stannane (0.446 g, 0.947 mmol), and heated to reflux overnight. Solvent was removed in vacuum. Compound **3** was obtained as white solid with very good yield (1.096 g, 0.916 mmol, 97 %). Recrystallization from toluene gave 3 colourless crystals with mp of 192.8-194.4 °C.

^{1}H NMR ($CDCl_3$, 600.29, 298 K): δ 0.75 (m, 4H, CH_2Sn), 1.17- 1.27 ppm (s, 24H, CH_3), 2.61 ppm (s, $^3J(^1H - ^{117/119}Sn_1)$ = 233 Hz, 8H, CH_2CMe_2), 3.26 ppm (m, 4H, CH_2N), 7.33-7.58 ppm (complex pattern, 30H, Ph). ^{119}Sn NMR (C_6D_6, 149.26, 298 K): δ –99 ppm ($^4J(^{119}Sn - ^{117/119}Sn)$ = 17 Hz, 2Sn, *Sn*Ph_3), -435 ppm ($^4J(^{119}Sn - ^{117/119}Sn)$ = 17 Hz, 1Sn, *Sn*O_4). Anal. Calcd (%) for $C_{56}H_{74}N_2O_4Sn_3$: C 56.27, H 6.24, N 2.34. Found: C 55.8, H 6.0, N 2.2. Electrospray MS: m/z (%) positive mode: 538.4 $[C_{28}H_{37}NO_2Sn]^+$, 562.4 $[C_{28}H_{37}NaNO_2Sn]^+$.

7. Summary

The principal axes of this thesis project are the synthesis of tripodal tris(organostannylmethyl)silanes of the type $MeSi(CH_2SnR_{(3-n)}X_n)_3$ (n = 0– 3; X = I, F, Cl, Br; R = Ph, CH_2SiMe_3) , as building blocks for the synthesis of novel organostannate complexes and umprecedented organotin chlacogeno-clusters among which novel triangular belt-shaped diorganotin oxo clusters $[MeSi(CH_2SnRO)_3]_n$, R = Ph, CH_2SiMe_3 with gigantic nuclearity; oktokaideka (n = 18) and trikonta (n = 30). Furthermore, formation of new spacer-bridged tetrastannanes $R'Sn(CH_2SnR_{(3-n)}X_n)_3$, (n = 0– 2; X = I, Cl; R = Ph, R'= R, X) and their attempts for complexation are reported. Moreover, there is synthesis of an unusual silicon-trimethylen-bridged double ladder organotin oxo cluster. Finally, new aminoalkanol-triorganostannane derivatives as precursors to build future tin-functionalized azidocryptands are reported. The numbering of compounds are only related in chapters 2 and 4, and independent in chapters 3 and 5- 6. The DVD contains Supporting Information of chapters 2- 6.

In the second chapter, there is report of a series of novel silicon-bridged organotin compounds $MeSi(CH_2SnR_{(3-n)}X_n)_3$ (n = 0– 3; X = I, F, Cl, Br; R = Ph, CH_2SiMe_3), **2**–**12**, their syntheses and characterization (Chart 3), in addition to the study of complexation behaviour of compounds **4**-**7**, **9**, and **12** with neutral and charged Lewis-base; Cl^-, CH_3COO^-, F^-, Br^-, and HMPA (Chart 4. a, b).

Chart 3. The organotin compounds $MeSi(CH_2SnR_{(3-n)}X_n)_3$, **2– 12**.

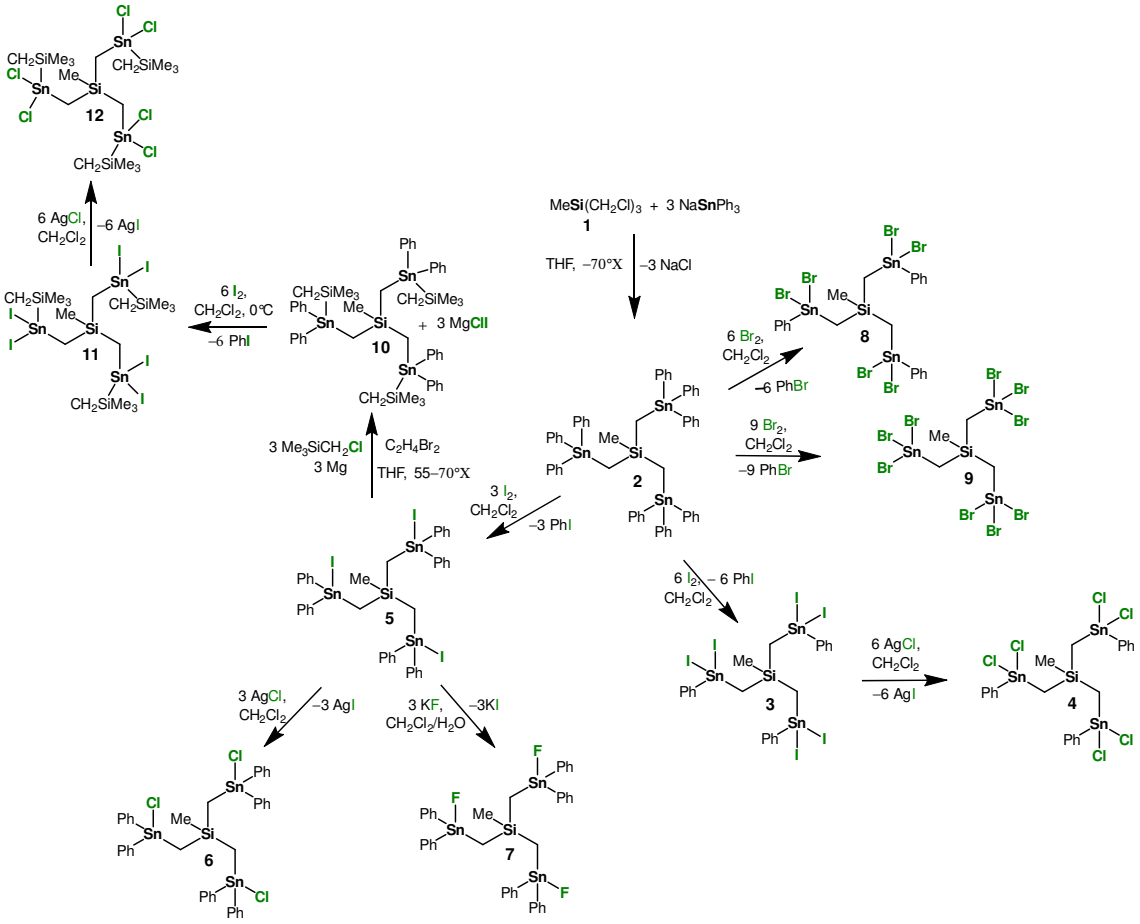

Chart 4 a). The organostannate complexes **13**– **19**.

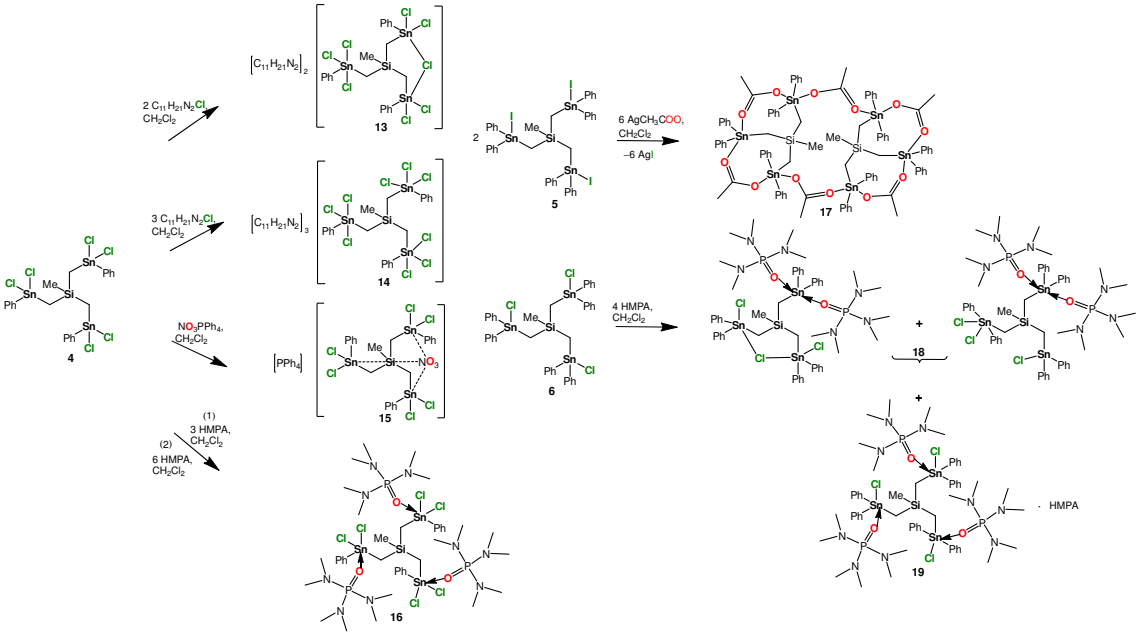

Chart 4 b). The organostannate complexes **20**– **25**.

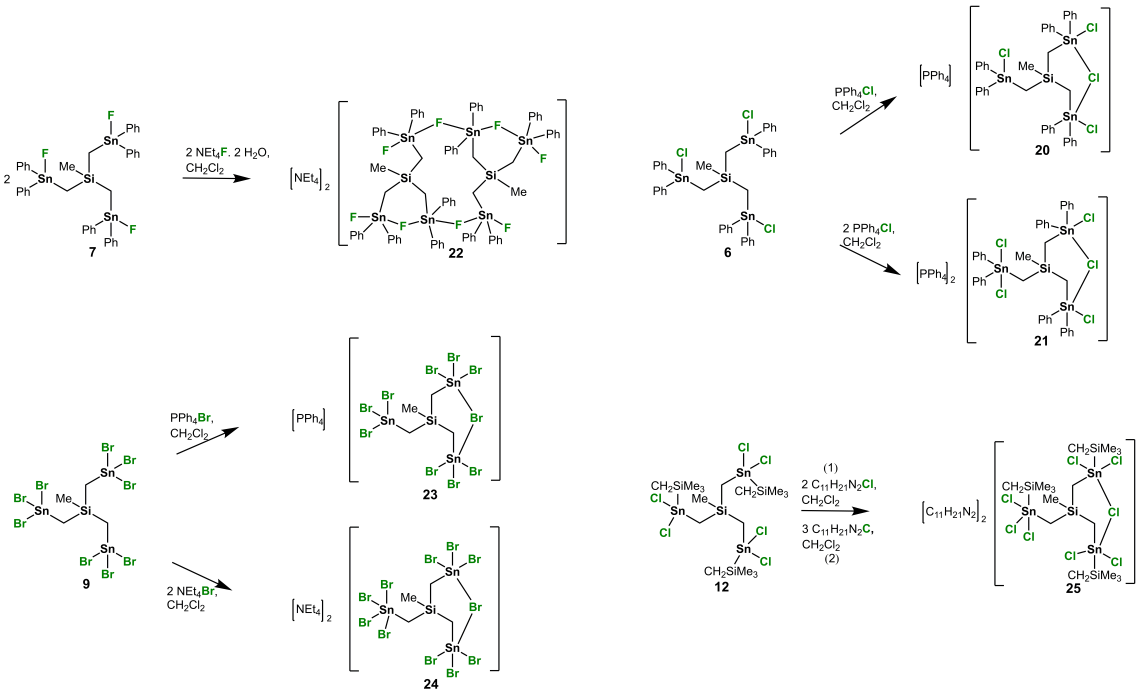

In the third chapter, synthesis and characterization of $R'Sn(CH_2SnR_{(3-n)}X_n)_3$, (n = 0–2; X = I, Cl; R = Ph, R'= R, X) derivatives are reported, and complexation attempts of derivative $ClSn(CH_2SnPhCl_2)_3$, **3**, with chloride anion give interesting binuclear and trinuclear organostannates **6**– **9** (Chart 5).

Chart 5. R'Sn($CH_2SnR_{(3-n)}X_n)_3$ derivatives **2**– **5** and organostannate complexes **6**– **9**.

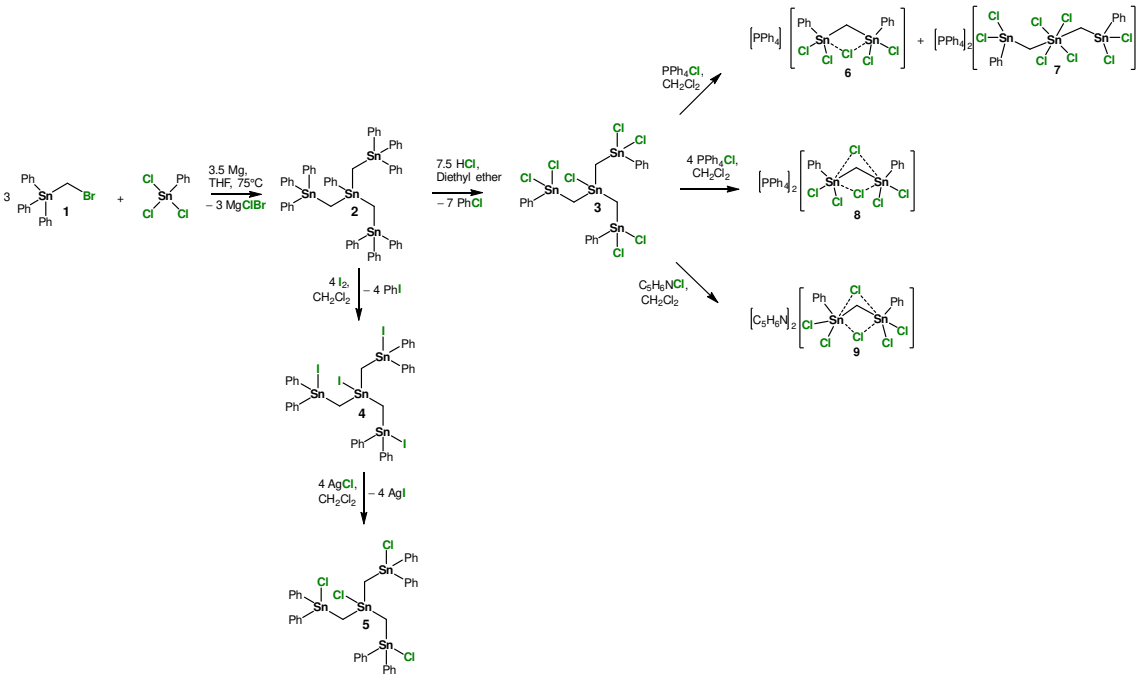

In the fourth chapter, new ladder-type containing diorganotin oxo-clusters **26**– **32**, and first examples of organotin chalcogenides S, Se-adamantane-type structures, **33**– **35**, containing both organosilicon and organotin moieties and their exchange reactions are reported. These chalcogeno organotin clusters are resulted from reactions of the halogenated precursors $MeSi(CH_2SnR_{(3-n)}X_n)_3$ (n = 0– 3; X = I, Cl, Br; R = Ph, CH_2SiMe_3) with t-Bu_2SnO, NaOH, EtOH, Na_2S and Na_2Se (Chart 6. a, b; Chart 7).

Chart 6 a). Organotin oxo clusters **26**– **27**.

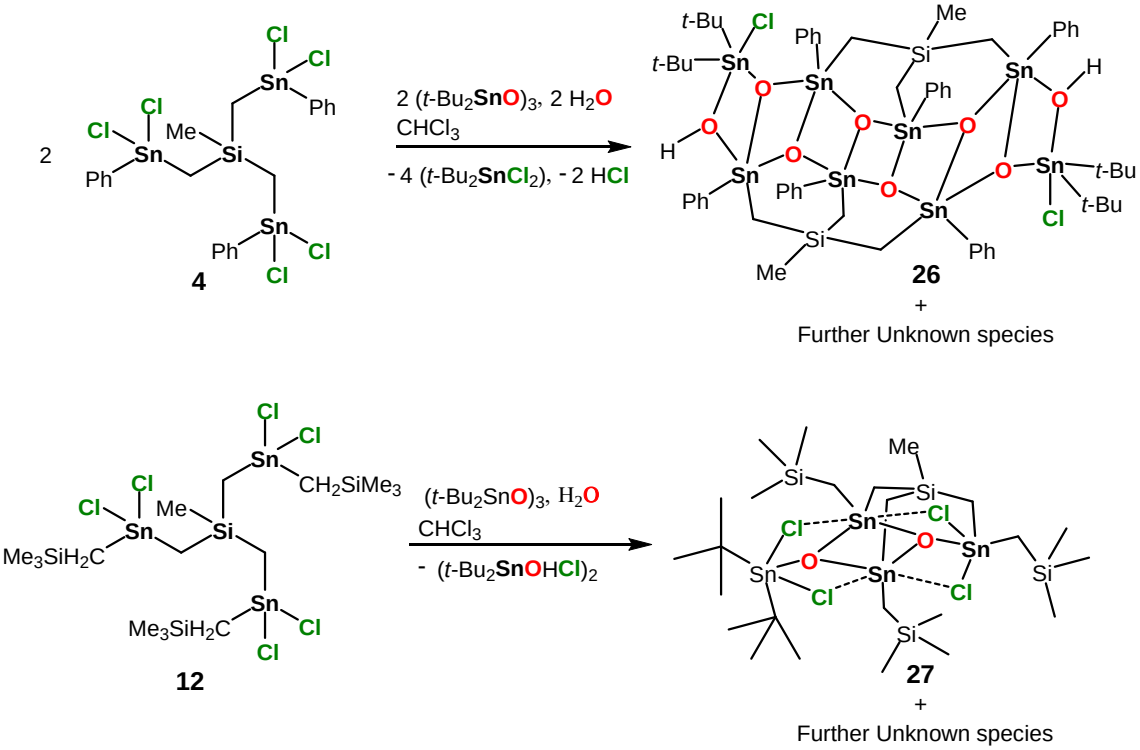

Chart 6 b). Organotin oxo clusters **26**– **27**.

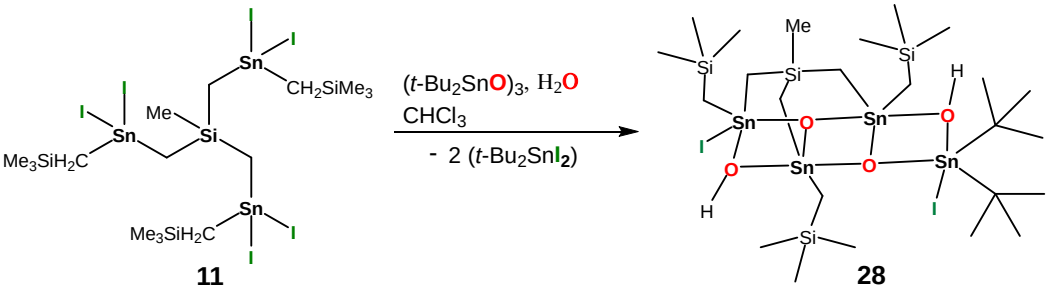

11 **28**

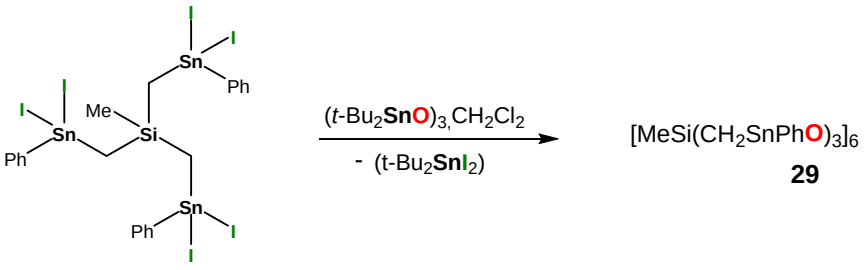

3 **29**

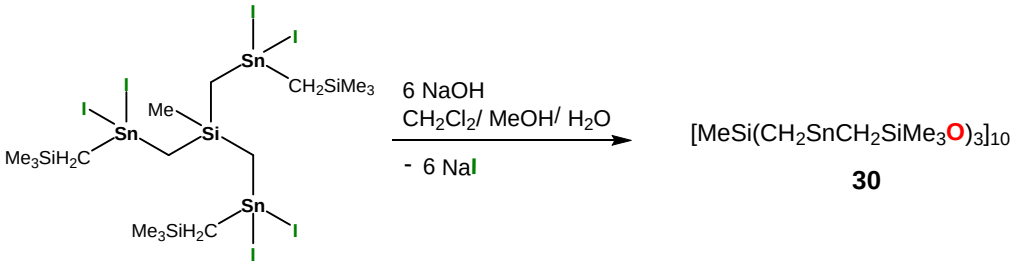

11 **30**

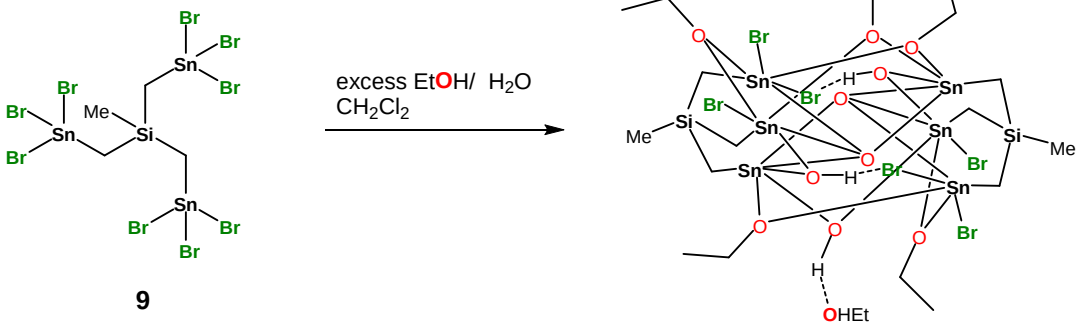

9 **32**

Chart 7. Sila-stanna-adamantane **33**– **35**.

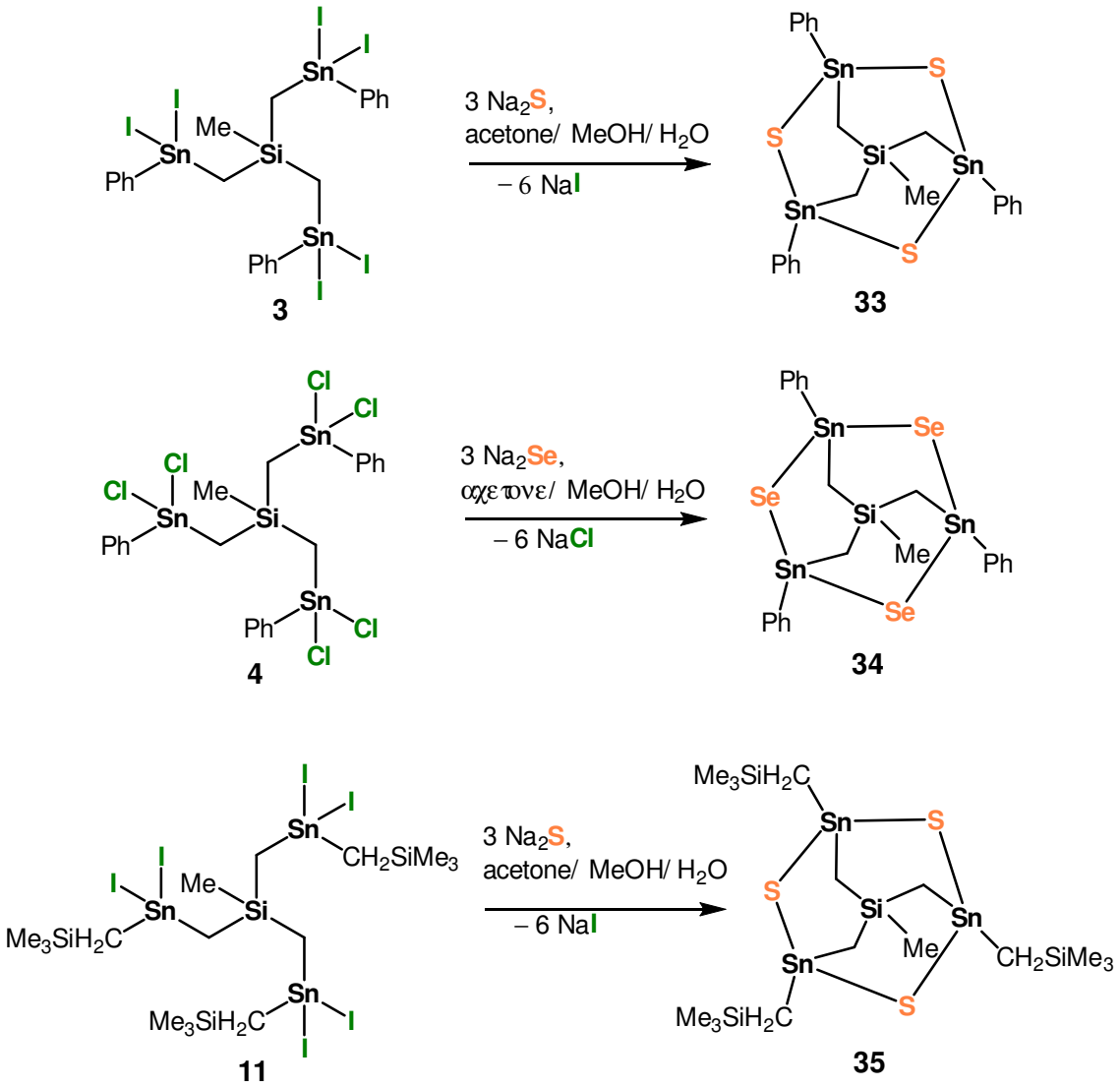

In the fifth chapter, reaction of $MeClSi((CH_2)_3SnMeCl_2)_2$, **1**, with pyridine gives the new double- ladder $\{[MeSi(MeSnCl)(CH_2)_3(\mu_3-O)(MeSnCl)(CH_2)_3]_2O\}_2$, **2** in which, layers are linked by eight silicon-containing trimethylene chains and four silicon atoms are forming two siloxanes bridges (Chart 8).

Chart 8. Double-ladder $\{[MeSi(MeSnCl)(CH_2)_3(\mu_3\text{-}O)(MeSnCl)(CH_2)_3]_2O\}_2$, **2**.

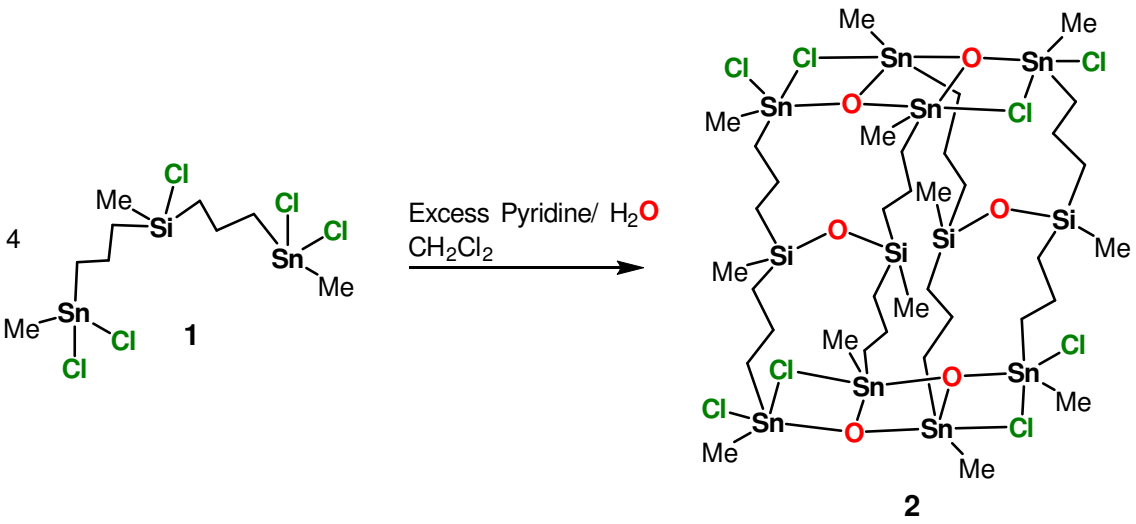

The final chapter reports synthesis and characterization of amino-stannane $Ph_3Sn(CH_2)_2NH_2$, **1**, aminoalkanol organotin $Ph_3Sn(CH_2)_2NH_2(CH_2CMe_2OH)_2$, **2** and spiro-type compound $[Ph_3Sn(CH_2)_2NH_2(CH_2CMe_2O)_2]_2Sn$, **3** as potential precursors to synthesize future tin functionalized azido-cryptands (Chart 9).

Chart 9. Aminoalkanol organostannane compounds **1**– **3**.

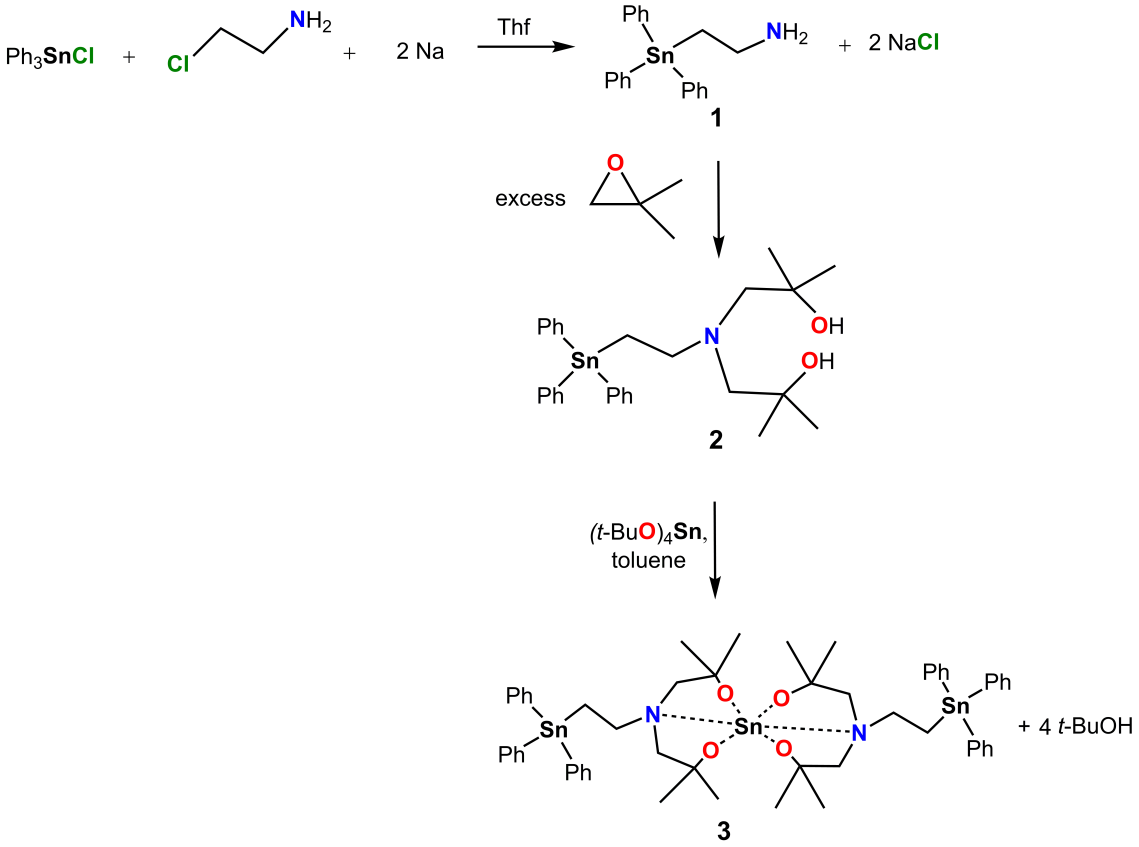

8. Zusammenfassung

Das Hauptziel dieser Arbeit waren die Synthese und Charakterisierung von tripodalen Tris-(organostannylmethyl) silanen vom Type $MeSi(CH_2SnR_{(3-n)}X_n)_3$ (n = 0– 3; X = I, F, Cl, Br; R = Ph, CH_2SiMe_3) als Bausteine für die Synthese neuartiger Organostannatkomplexe und beispielloser Organozinn-Chlacogeno-Clustern, darunter neuartige dreieckige gürtelförmige Diorganotin-Oxo-Clustern $[MeSi(CH_2SnRO)_3]_n$, R = Ph, CH_2SiMe_3 mit gigantischer Nuklearität; Okt okaideka (n = 18) und Trikonta (n = 30). Weiterhin Bildung neuer spacer-verbrückter Tetrastannane $R'Sn(CH_2SnR_{(3-n)}X_n)_3$, (n = 0– 2; X = I, Cl; R = Ph, R'= R, X) und deren Versuche zur Komplexierung werden berichtet. Darüber hinaus wird ein ungewöhnlicher Silizium-Trimethylen-verbrückter Doppelleiter-Organozinn-Oxo-Cluster synthetisiert. Schließlich werden neue Aminoalkanoltriorganostannan-Derivate als Vorläufer für den Aufbau zukünftiger zinnfunktionalisierter Azidocryptanden beschrieben. Die Nummerierung der Verbindungen ist nur in den Kapiteln 2 und 4 verwandt, und in den Kapiteln 3 und 5- 6 unabhängig. Das DVD enthält Supporting Information von Kapiteln 2- 6.

In Kapitel 2 wurde über eine Reihe neuer Silizium-verbrückter Organozinnverbindungen $MeSi(CH_2SnR_{(3-n)}X_n)_3$ (n = 0– 3; X = I, F, Cl, Br; R = Ph, CH_2SiMe_3), **2**-**12**, ihre Synthese und Charakterisierung, zusätzlich zur Untersuchung des Komplexierungsverhaltens der Verbindungen **4**– **7**, **9** und **12** mit neutraler und geladener Lewis-Base; Cl^-, CH_3COO^-, F^-, Br^- und HMPA berichtet (Abbildung 1, 2. a, b).

Abbildung 1. Organozinnverbindungen $MeSi(CH_2SnR_{(3-n)}X_n)_3$, **1**– **12**.

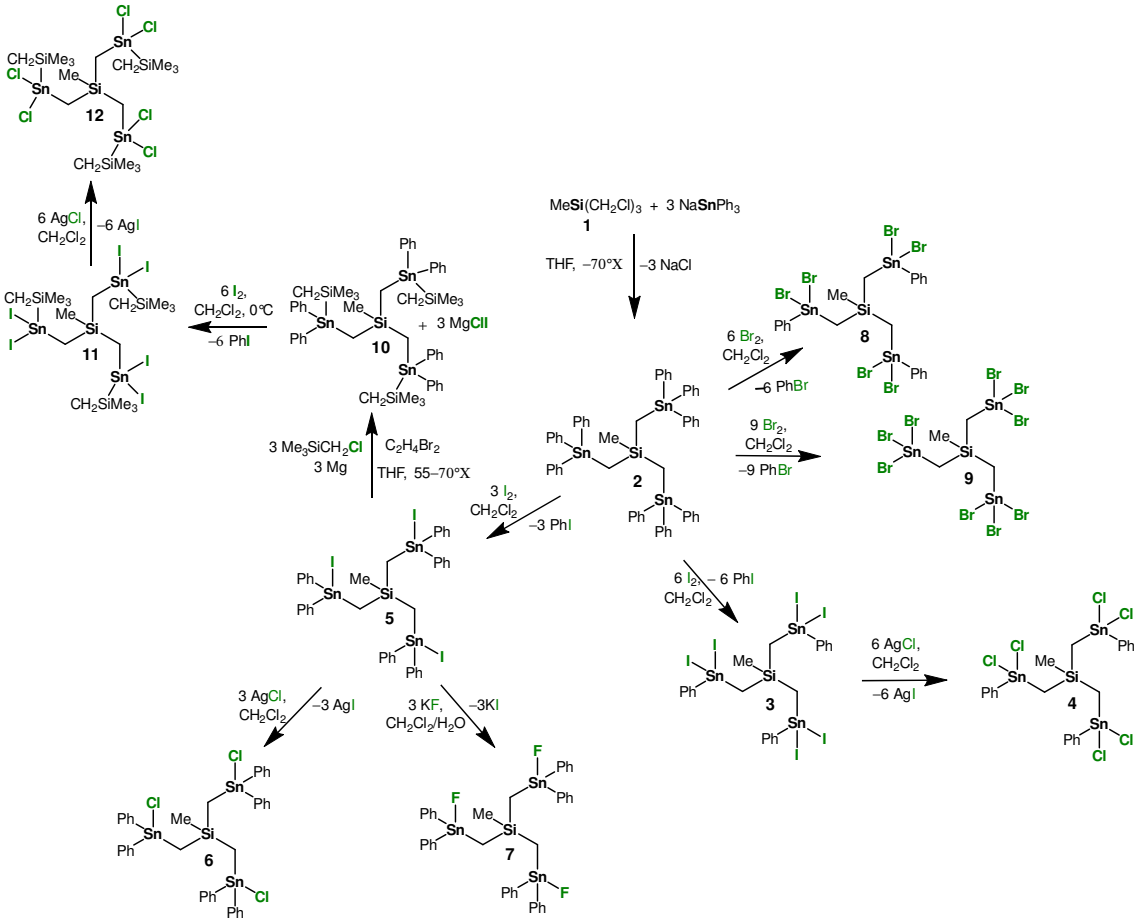

Abbildung 2 a). Die Organostannatskomplexe **13**– **19**.

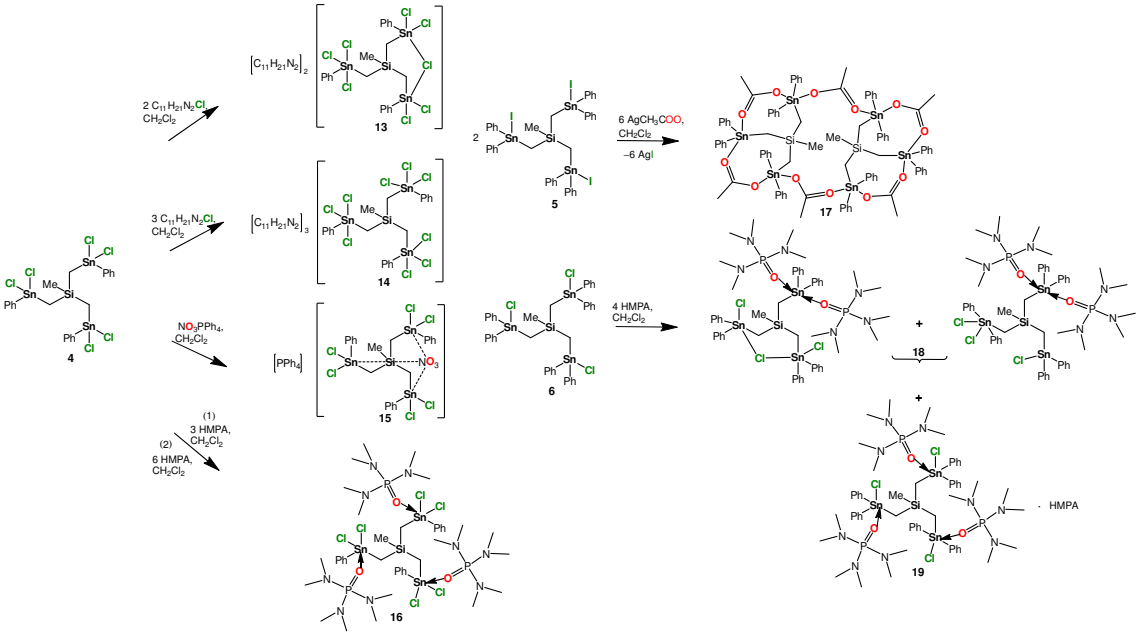

Abbildung 2 b). Die Organostannatskomplexe **20**– **25**.

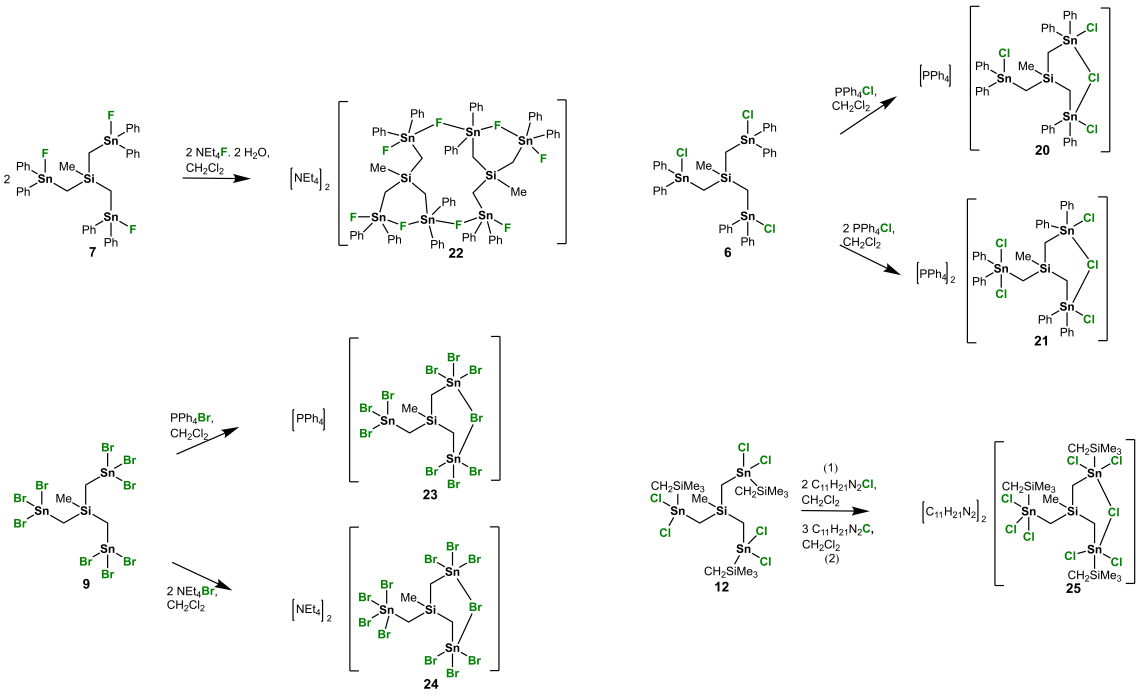

In Kapitel 3, wurde über die Synthese und Charakterisierung von R'Sn($CH_2SnR_{(3-n)}X_n$)$_3$, (n = 0– 2; X = I, Cl; R = Ph, R'= R, X) Derivaten berichtet. Komplexierungsversuche des Derivats ClSn($CH_2SnPhCl_2$)$_3$, **3** mit Cl^- Anionen ergaben interessante zweikernige und dreikernige Organostannate **6**– **9** (Abbildung 3).

Abbildung 3. R'Sn($CH_2SnR_{(3-n)}X_n)_3$ Derivate **2**– **5** und Organostannatskomplexe **6**– **9**.

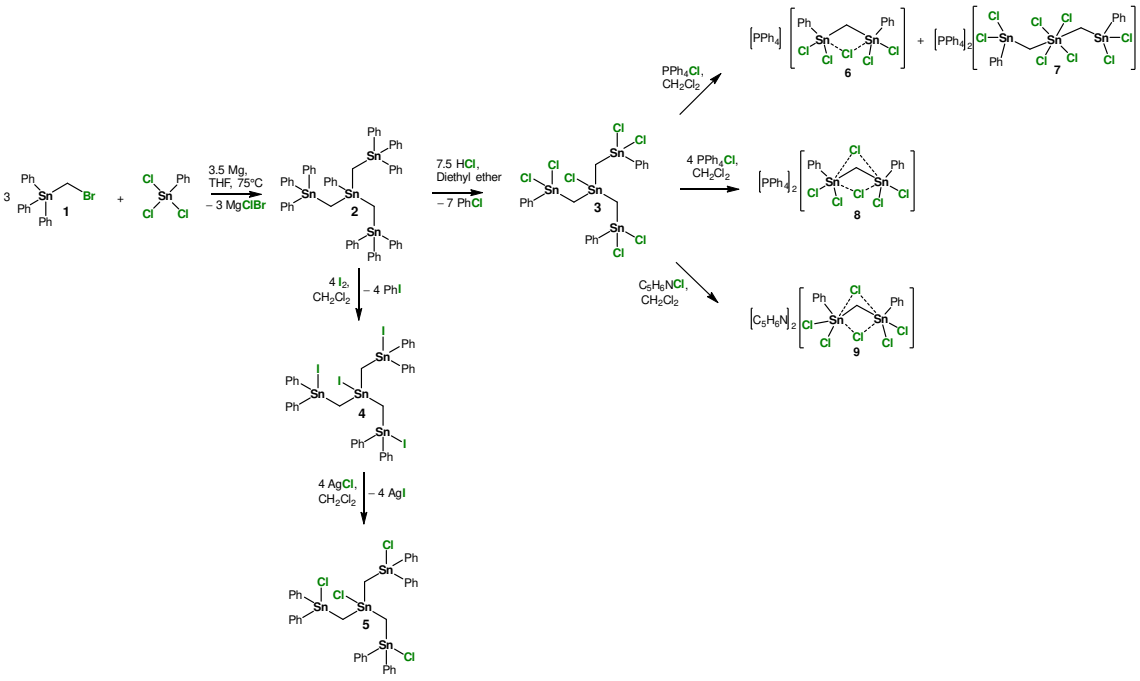

In Kapitel 4, wurden neue Leitertypen Diorganotin-Oxo-Clustern **26**– **32** berichtet. Die erste Beispiele von neuen Organozinn-Chalkogenide Adamantansverbindungen **33**– **35**, die sowohl Organosilizium- als auch Organozinn-Einheiten enthalten, und ihre Austauschreaktionen wurden beschrieben. Diese Chalkogen-Organozinn-Cluster resultieren aus Reaktionen der halogenierten Vorläufer $MeSi(CH_2SnR_{(3-n)}X_n)_3$ (n = 0– 3; X = I, F, Cl, Br; R = Ph, CH_2SiMe_3) mit *t*-Bu_2SnO, NaOH, EtOH, Na_2S und Na_2Se (Abbildung 4. a, b; Abbildung 5).

Abbildung 4 a). Organozinn-Oxo-Clustern **26**– **27**.

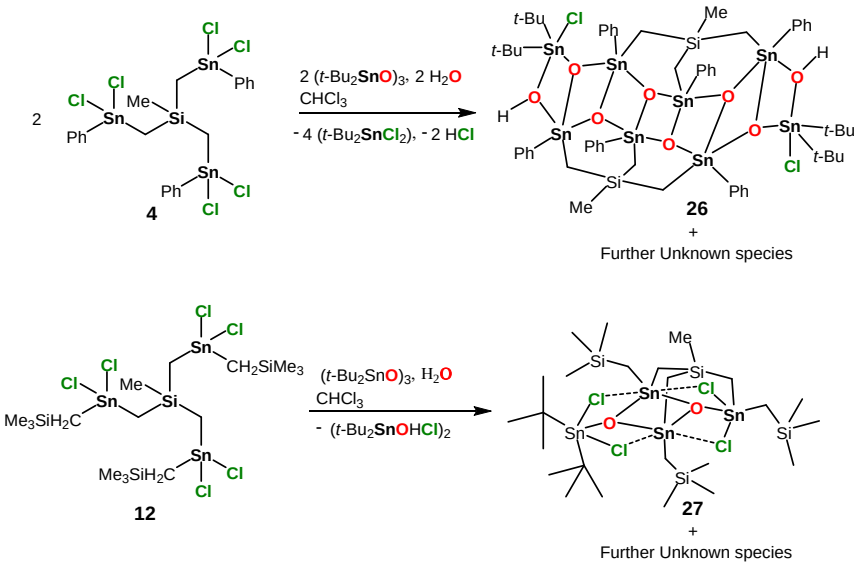

Abbildung 4 b). Organozinn-Oxo-Clustern **28**– **32**.

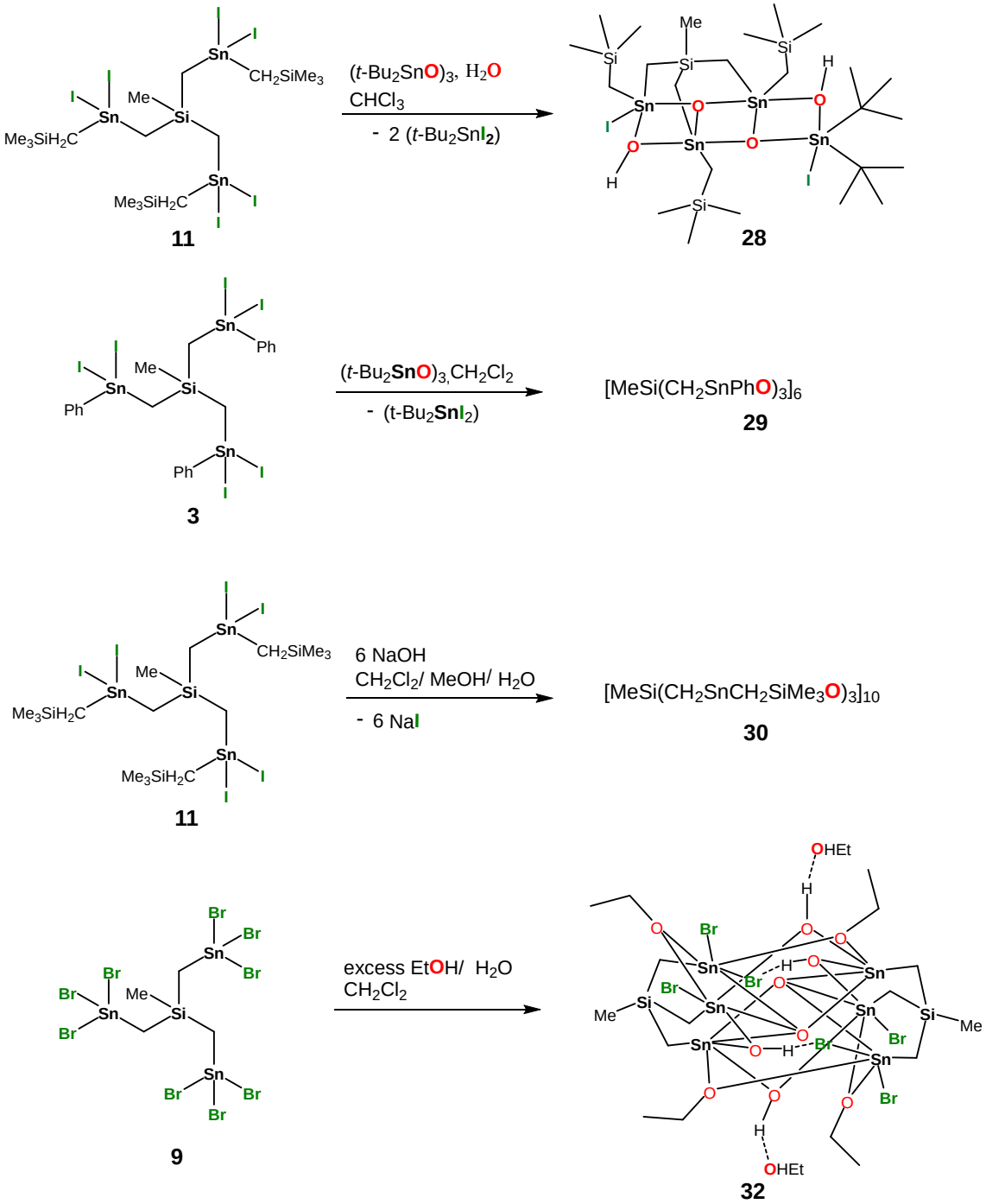

Abbildung 5. Silastannaadamantane **33**– **35**.

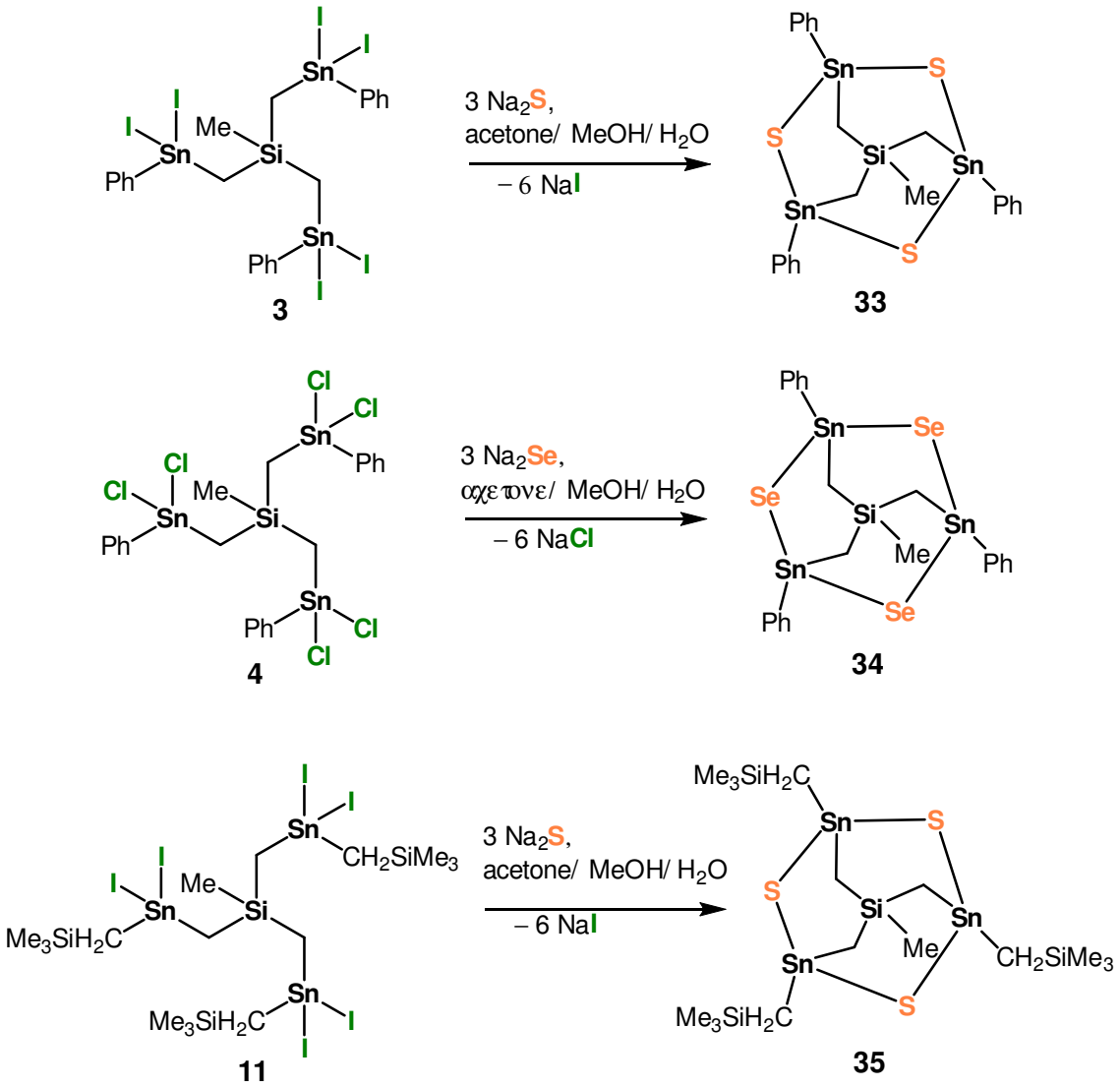

In Kapitel 5, die Reaktion von$MeClSi((CH_2)_3SnMeCl_2)_2$, **1** mit Pyridin gab die neue Doppelleiter $\{[MeSi(MeSnCl)(CH_2)_3(\mu_3-O)(MeSnCl)(CH_2)_3]_2O\}_2$, **2**, in der die zwei Leitern durch acht siliziumhaltige Trimethylenketten verbunden sind. Vier Silizium Atome bilden zwei Siloxanbrücken (Abbildung 6).

Abbildung 6. Doppelleiter $\{[MeSi(MeSnCl)(CH_2)_3(\mu_3-O)(MeSnCl)(CH_2)_3]_2O\}_2$, **2**.

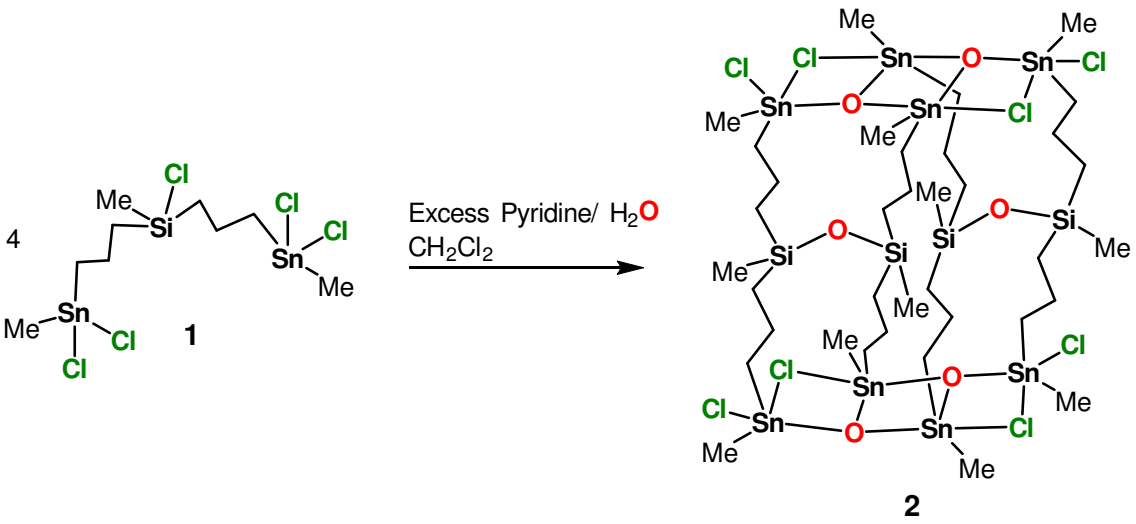

Das letzte Kapitel berichtete über die Synthese und Charakterisierung von Aminostannane $Ph_3Sn(CH_2)_2NH_2$, **1**, Aminoalkanolorganostannane $Ph_3Sn(CH_2)_2NH_2(CH_2CMe_2OH)_2$, **2** und *Spiro*-Verbindung $[Ph_3Sn(CH_2)_2NH_2(CH_2CMe_2O)_2]_2Sn$, **3** als potenzielle Vorläufer für die Synthese zukünftiger zinnfunktionalisierter Azido-Kryptanden (Abbildung 7).

Abbildung 7. Aminoalkanolorganostannane-Verbindungen **1**– **3**.

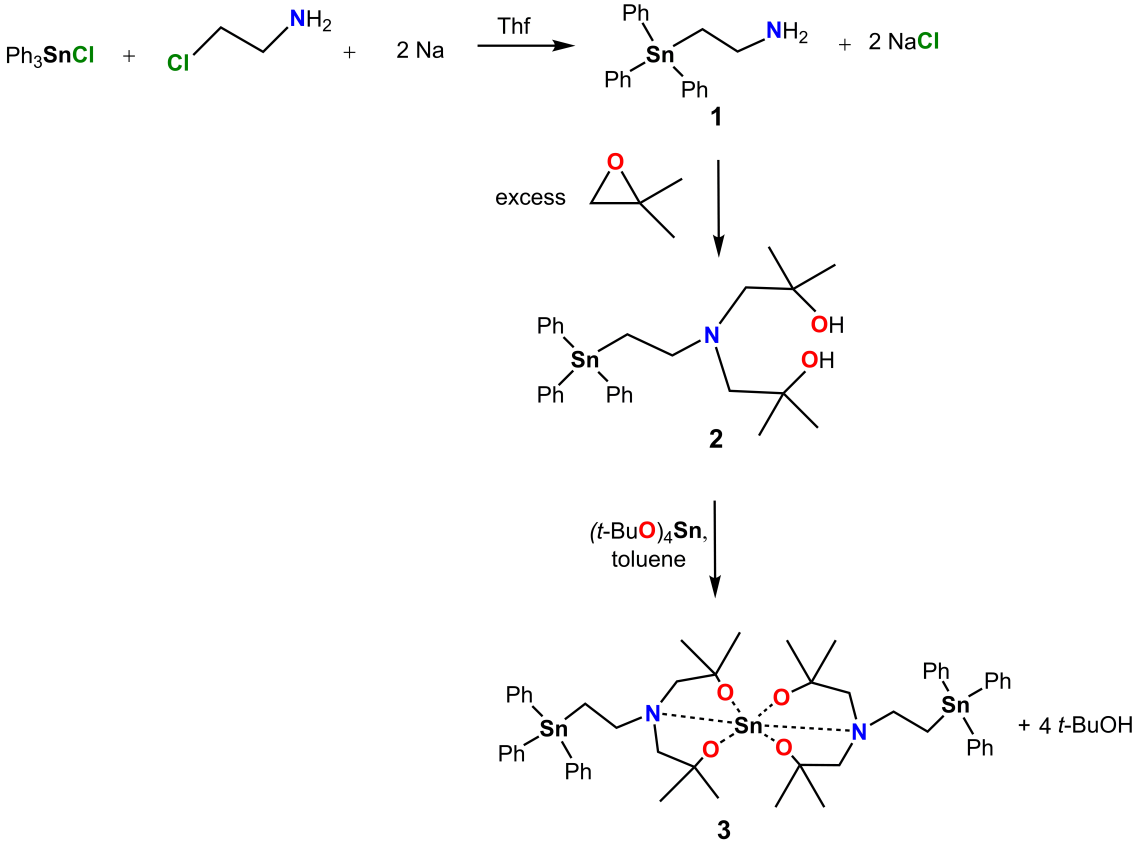

9. References

[1] J.-M. Lehn, *Polym. Int.* **2002**, *51*, 825.

[2] Host-Guest Chemistry, `http://ccb.rutgers.edu/sites/default/files/coursefiles/Courses_f09/310/Host-Guest-Chemistry_I_Part_1.pdf`.

[3] M. M. Naseer, K. Jurkschat, *Chem. Commun.* **2017**, *53*, 8122.

[4] P. D. Beer, A. R. Cowley, J. C. Jeffery, R. L. Paul, W. W. H. Wong, *Polyhedron* **2003**, *22*, 795.

[5] H. Miyake, T. Yamashita, Y. Kojima, H. Tsukube, *Tetrahedron Lett.* **1995**, *36*, 7669.

[6] A. Lawrence, PhD thesis, University of Manchester, Manchester, **2011**.

[7] J. W. Steed, *Chem. Soc. Rev.* **2009**, *38*, 506.

[8] R. Altmann, K. Jurkschat, M. Schürmann, D. Dakternieks, A. Duthie, *Organometallics* **1998**, *17*, 5858.

[9] A. S. Wendji, C. Dietz, S. Kühn, M. Lutter, D. Schollmeyer, W. Hiller, K. Jurkschat, *Chem. Eur. J* **2015**, *22*, 404.

[10] D. Dakternieks, K. Jurkschat, H. Wu, E. R. T. Tiekink, *Organometallics* **1993**, *12*, 2788.

[11] R. Altmann, O. Gausset, D. Horn, K. Jurkschat, M. Schürmann, M. Fontani, P. Zanello, *Organometallics* **2000**, *19*, 430.

[12] A. S. Wendji, M. Lutter, L. M. Stratmann, K. Jurkschat, *ChemistryOpen* **2016**, *5*, 554.

[13] R. R. Holmes, *Acc. Chem. Res.* **1989**, *22*, 190.

[14] M. Mehring, M. Schürmann, I. Paulus, D. Horn, K. Jurkschat, A. Orita, J. Otera, D. Dakternieks, A. Duthie, *J. Organomet. Chem.* **1999**, *574*, 176.

[15] V. Chandrasekhar, R. O. Day, R. R. Holmes, *Inorg. Chem.* **1985**, *24*, 1970.

[16] V. Chandrasekhar, C. G. Schmid, S. D. Burton, J. M. Holmes, R. O. Day, R. R. Holmes, *Inorg. Chem.* **1987**, *26*, 1050.

[17] R. R. Holmes, C. G. Schmid, V. Chandrasekhar, R. O. Day, J. M. Holmes, *J. Am. Chem. Soc.* **1987**, *109*, 1408.

[18] D. Dakternieks, K. Jurkschat, D. Schollmeyer, H. Wu, *Organometallics* **1994**, *13*, 4121.

[19] B. Zobel, M. Schürmann, K. Jurkschat, D. Dakternieks, A. Duthie, *Organometallics* **1998**, *17*, 4096.

[20] M. Mehring, M. Schürmann, H. Reuter, D. Dakternieks, K. Jurkschat, *Angew. Chem. Int. Ed. Engl.* **1997**, *36*, 1112.

[21] M. Mehring, G. Gabriele, S. Hadjikakou, M. Schürmann, D. Dakternieks, K. Jurkschat, *Chem. Commun.* **2002**, 834.

[22] S. B. Haj, C. Dietz, M. Lutter, K. Jurkschat, *Organometallics* **2015**, *34*, 5555.

[23] J. Beckmann, K. Jurkschat, S. Rabe, M. Schürmann, D. Dakternieks, *Z. Anorg. Allg. Chem* **2001**, *627*, 458.

[24] U.-P. Apfel, D. Troegel, Y. Halpin, S. Tschierlei, U. Uhlemann, H. Görls, M. Schmitt, J. Popp, P. Dunne, M. Venkatesan, M. Coey, M. Rudolph, J. G. Vos, R. Tacke, W. Weigand, *Inorg. Chem.* **2010**, *49*, 10117.

[25] R. Altmann, K. Jurkschat, M. Schürmann, D. Dakternieks, A. Duthie, *Organometallics* **1997**, *16*, 5716.

[26] M. Gielen, K. Jurkschat, *J. Organomet. Chem.* **1984**, *273*, 303.

[27] B. Wrackmeyer in Annual Reports on NMR Spectroscopy, (Ed.: G. A. Webb), Elsevier, **1985**, pp. 73–186.

[28] N. Alashkar, PhD thesis, **2016**.

[29] N. Alashkar, C. Dietz, S. B. Haj, W. Hiller, K. Jurkschat, *Organometallics* **2016**, *35*, 2738.

[30] A. Bondi, *J. Phys. Chem.* **1964**, *68*, 441.

[31] D. Dakternieks, F. S. Kuan, A. Duthie, E. R. T. Tiekink, *Appl. Organomet. Chem.* **2003**, *17*, 73.

[32] A. C. T. Kuate, G. Reeske, M. Schürmann, B. Costisella, K. Jurkschat, *Organometallics* **2008**, *27*, 5577.

[33] K. I. Tugashov, D. A. Gribanyov, F. M. Dolgushin, A. F. Smol'yakov, A. S. Peregudov, M. K. Minacheva, B. N. Strunin, I. A. Tikhonova, V. B. Shur, *J. Organomet. Chem.* **2013**, *747*, 167.

[34] K. Jurkschat, F. Hesselbarth, M. Dargatz, J. Lehmann, E. Kleinpeter, A. Tzschach, J. Meunier-Piret, *J. Organomet. Chem.* **1990**, *388*, 259.

[35] D. Dakternieks, K. Jurkschat, H. Zhu, E. R. T. Tiekink, *Organometallics* **1995**, *14*, 2512.

[36] T. P. Lockhart, W. F. Manders, E. M. Holt, *J. Am. Chem. Soc.* **1986**, *108*, 6611.

[37] E. R. T. Tiekink, *Appl. Organomet. Chem.* **1991**, *5*, 1.

[38] T. Kobayashi, K. H. Pannell, *Organometallics* **1991**, *10*, 1960.

[39] M. A. Edelman, P. B. Hitchcock, M. F. Lappert, *J. Chem. Soc. Chem. Commun.* **1990**, 1116.

[40] M. Gielen, (Eds.: A. G. Davies, K. Pannell, E. Tiekink), Wiley, Chichester, **2008**, 729 pp.

[41] (a) R. K. Ingham, S. D. Rosenberg, H. Gilman, *Chem. Rev.* **1960**, *60*, 459; (b) A. G. Davies, *Organotin Chemistry*, 2nd ed., Wiley, Chichester, **2004**.

[42] (a) V. K. Belsky, N. N. Zemlyansky, I. V. Borisova, N. D. Kolosova, I. P. Beletskaya, *J. Organomet. Chem.* **1983**, *254*, 189; (b) J. F. V. der Maelen Uría, M. Belay, F. T. Edelmann, G. M. Sheldrick, *Acta Crystallogr. C* **1994**, *50*, 403; (c) H. Puff, W. Schuh, R. Sievers, W. Wald, R. Zimmer, *J. Organomet. Chem.* **1984**, *260*, 271; (d) H.

Puff, W. Schuh, R. Sievers, R. Zimmer, *Angew. Chem. Int. Ed. Engl.* **1981**, *20*, 591; (e) H. W. Roesky, R. Emmert, W. Clegg, W. Isenberg, G. M. Sheldrick, *Angew. Chem. Int. Ed. Engl.* **1981**, *20*, 591; (f) M. Satoru, R. S. Lawrence, J. W. David, *J. Am. Chem. Soc.* **1983**, *105*, 630.

[43] D. Dakternieks, B. Zobel, K. Jurkschat, M. Schürmann, E. R. T. Tiekink, *Organometallics* **2003**, *22*, 1343.

[44] B. Mairychová, L. Dostál, A. Růžička, L. Beneš, R. Jambor, *J. Organomet. Chem.* **2012**, *699*, 1.

[45] J. Ayari, C. R. Göb, I. M. Oppel, M. Lutter, W. Hiller, K. Jurkschat, *Angew. Chem. Int. Ed.* **2020**, DOI 10.1002/anie.202012248.

[46] C. Ma, Q. Jiang, R. Zhang, D. Wang, *Dalton Trans.* **2003**, 2975.

[47] M. Schulte, M. Mehring, I. Paulus, M. Schurmann, K. Jurkschat, D. Dakternieks, A. Duthie, A. Orita, J. Otera, *Phosphorus Sulfur Silicon Relat. Elem.* **1999**, *150*, 201.

[48] J. Beckmann, K. Jurkschat, U. Kaltenbrunner, S. Rabe, M. Schürmann, D. Dakternieks, A. Duthie, D. Müller, *Organometallics* **2000**, *19*, 4887.

[49] (a) Q. Li, F. Wang, R. Zhang, J. Cui, C. Ma, *Polyhedron* **2015**, *85*, 361; (b) N. W. Alcock, S. M. Roe, *J. Chem. Soc. Dalton Trans.* **1989**, 1589; (c) M. Hill, M. F. Mahon, K. C. Molloy, *Main Group Chem.* **1996**, *1*, 309; (d) N. W. Mitzel, C. Lustig, S. Scharfe, *Z. Naturforsch.* **2001**, *56b*, 440; (e) K. C. K. Swamy, M. A. Said, S. Nagabrahmanandachari, D. M. Poojary, A. Clearfield, *J. Chem. Soc. Dalton Trans.* **1998**, 1645; (f) M. Veith, O. Recktenwald, *Z. Anorg. Allg. Chem.* **1979**, *459*, 208.

[50] Z. H. Fard, M. R. Halvagar, S. Dehnen, *J. Am. Chem. Soc.* **2010**, *132*, 2848.

[51] D. Dakternieks, K. Jurkschat, S. van Dreumel, E. R. T. Tiekink, *Inorg. Chem.* **1997**, *36*, 2023.

[52] H. A. Bent in *Inorganic and Analytical Chemistry*, Springer, Berlin, **1970**, pp. 1–48.

[53] D. Dakternieks, K. Jurkschat, D. Schollmeyer, H. Wu, *J. Organomet. Chem.* **1995**, *492*, 145.

[54] N. Rinn, J. P. Eußner, W. Kaschuba, X. Xie, S. Dehnen, *Chem. Eur. J.* **2016**, *22*, 3094.

[55] D. Steinmann, T. Nauser, W. H. Koppenol, *J. Org. Chem.* **2010**, *75*, 6696.

[56] R. Steudel, *Chem. Rev.* **2002**, *102*, 3905.

[57] L. Vilà-Nadal, L. Cronin, *Nat. Rev. Mater.* **2017**, *2*, DOI 10.1038/natrevmats.2017.54.

[58] (a) Y.-B. Dong, H.-Y. Shi, J. Yang, Y.-Y. Liu, J.-F. Ma, *Cryst. Growth Des.* **2015**, *3*, 1546; (b) P. V. Solntsev, D. R. Anderson, H. M. Rhoda, R. V. Belosludov, M. F. Rasekh, E. Maligaspe, N. N. Gerasimchuk, V. N. Nemykin, *Cryst. Growth Des.* **2016**, *2*; (c) Y. Zhu, L. Zhang, J. Zhang, *Chem. Sci.* **2019**, 9125; (d) Y. Zhu, L. Zhang, J. Zhang, *Chem. Commun.* **2020**, 1433; (e) B. Glowacki, M. Lutter, D. Schollmeyer, K. Jurkschat, *Inorg. Chem.* **2016**, *20*, 10218.

[59] K. Wraage, T. Pape, R. Herbst-Irmer, M. Noltemeyer, H.-G. Schmidt, H. W. Roesky, *Eur. J. Inorg. Chem.* **1999**, *1999*, 869.

[60] C. R. Groom, I. J. Bruno, M. P. Lightfoot, S. C. Ward, *Acta Crystallogr. B* **2016**, *72*, 171.

[61] C. J. Pedersen, *J. Am. Chem. Soc.* **1967**, *89*, 7017.

[62] C. Tönshoff, K. Merz, G. Bucher, *Org. Biomol. Chem.* **2005**, *3*, 303.

[63] G. Reeske, M. Schürmann, K. Jurkschat, *Dalton Trans.* **2008**, 3398.

[64] A. R. Khokhar, Q. Xu, R. A. Newman, Y. Kido, Z. H. Siddik, *J. Inorg. Biochem.* **1992**, *45*, 211.

[65] L. Iovkova-Berends, T. Berends, T. Zöller, G. Bradtmöller, S. Herres-Pawlis, K. Jurkschat, *Eur. J. Inorg. Chem.* **2012**, *2012*, 3191.

[66] T. Zöller, L. Iovkova-Berends, C. Dietz, T. Berends, K. Jurkschat, *Chem. Eur. J.* **2011**, *17*, 2361.

[67] (a) A. Jerschow, N. Mueller, *J. Magn. Reson. A* **1996**, *123*, 222; (b) A. Jerschow, N. Mueller, *J. Magn. Reson. A* **1997**, *125*, 372.

List of New Compounds

Chapter 2

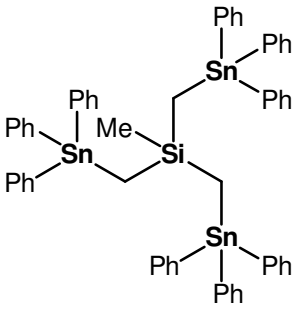

2

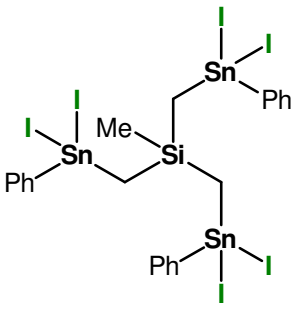

3

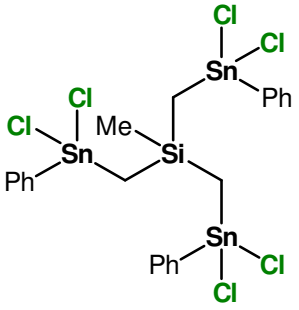

4

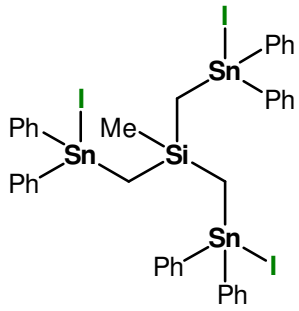

5

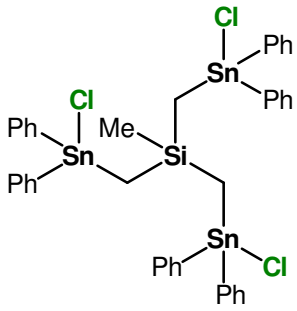

6

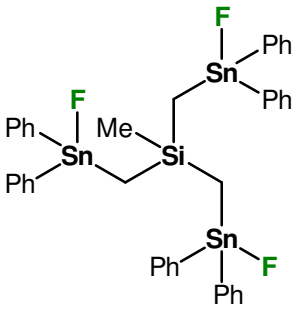

7

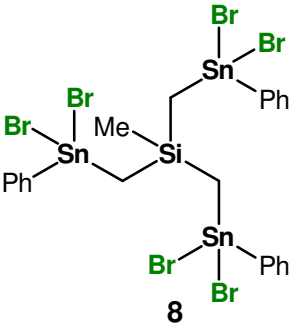

8

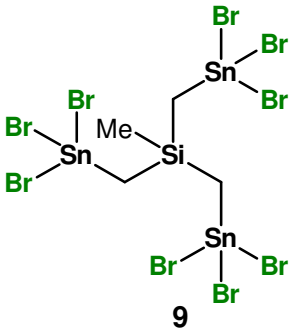

9

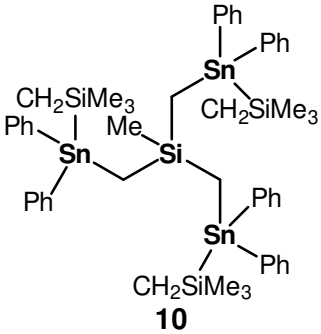

10

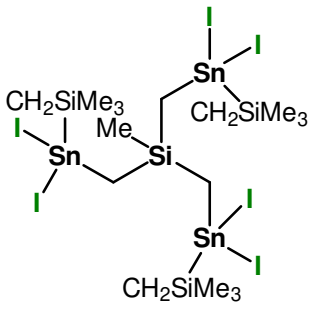

11

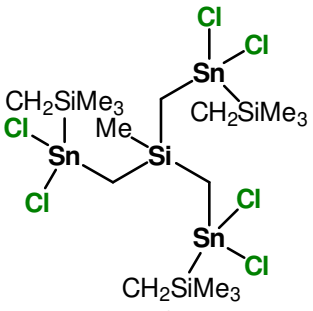

12

$[C_{11}H_{21}N_2]_2$

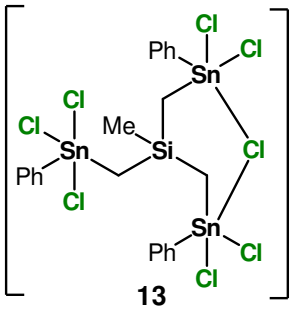

13

$[C_{11}H_{21}N_2]_3$

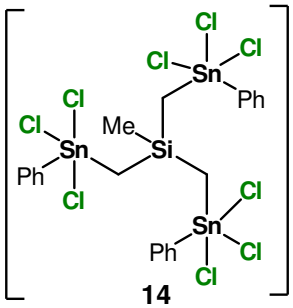

14

$[PPh_4]$

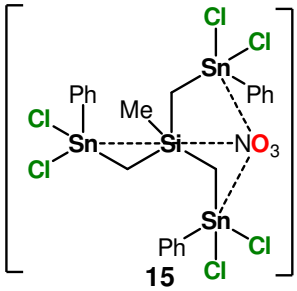

15

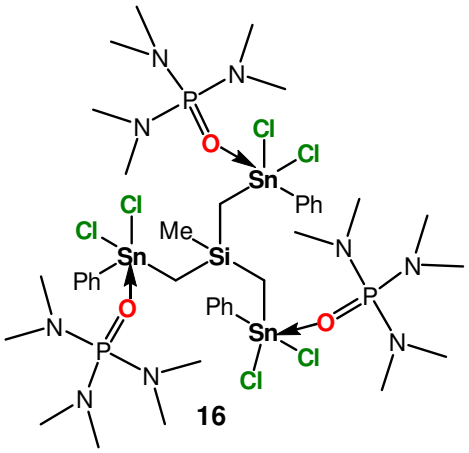

16

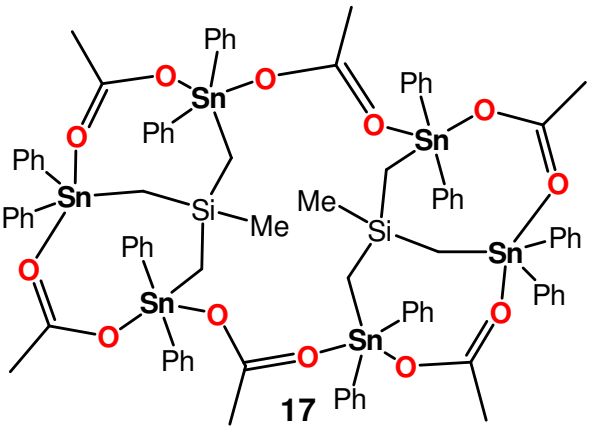

17

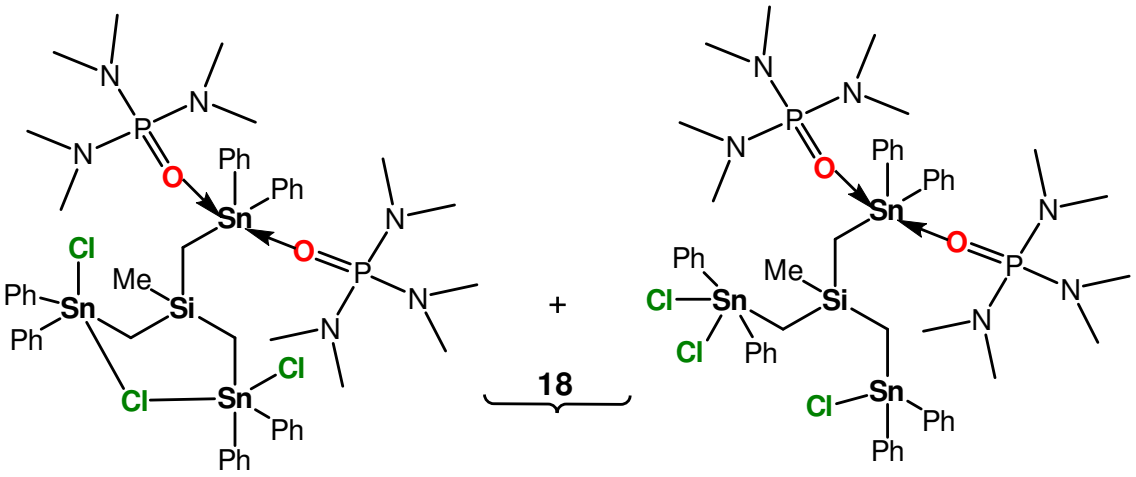

18

+

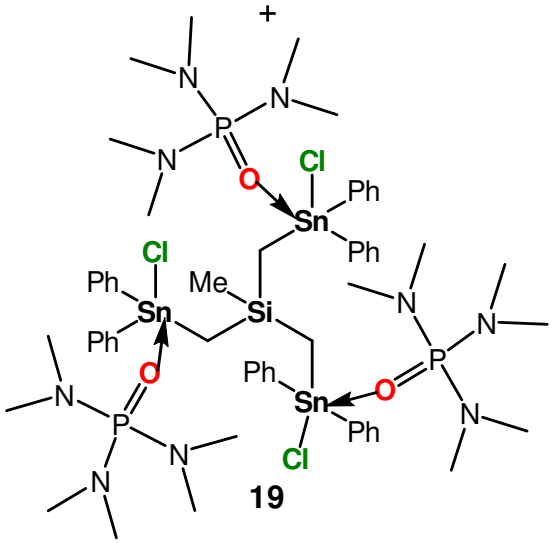

19

· HMPA

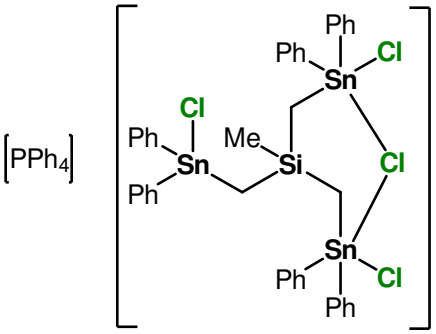

20

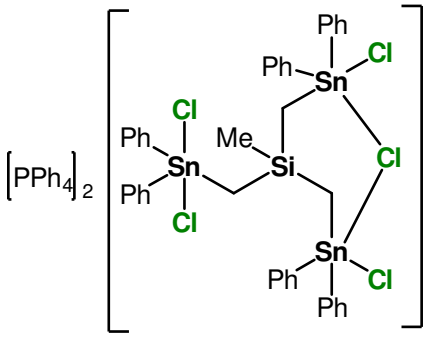

21

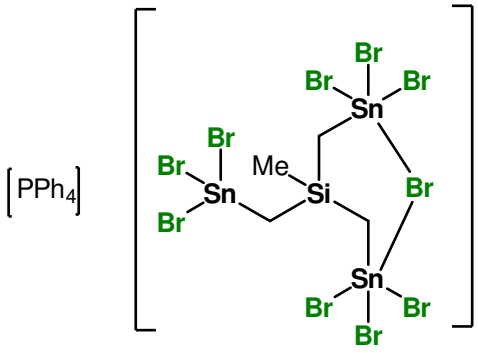

23

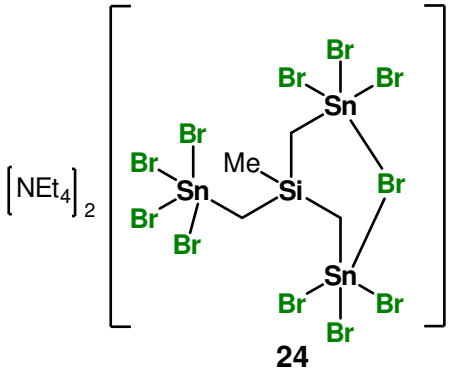

24

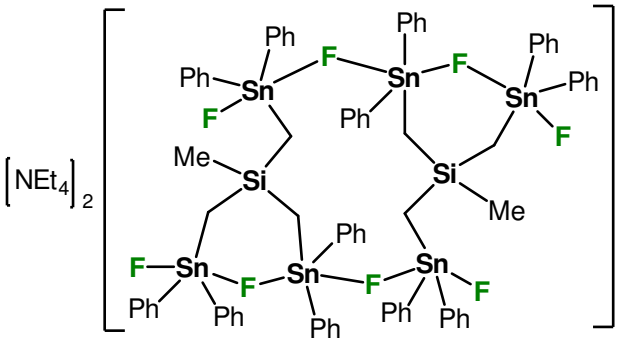

22

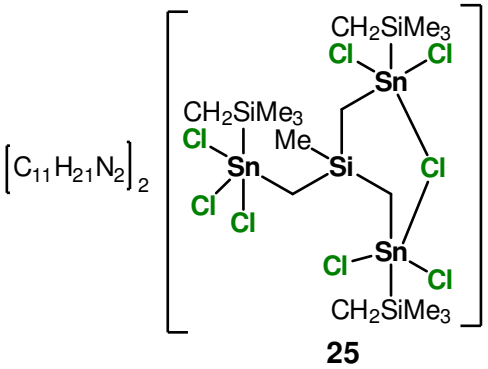

25

Chapter 3

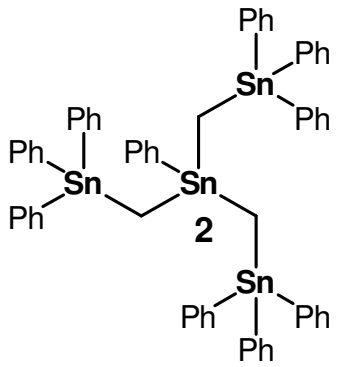

2

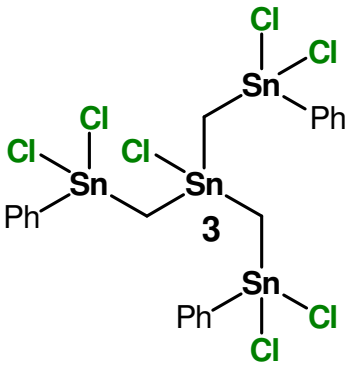

3

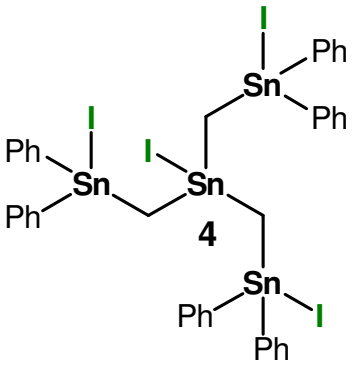

4

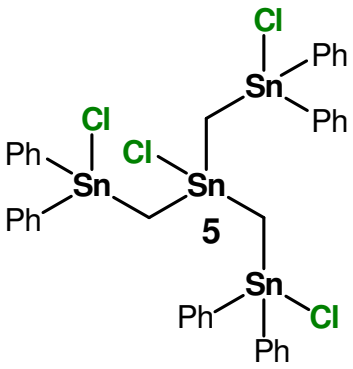

5

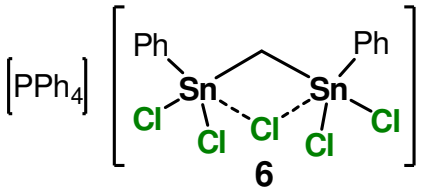

6

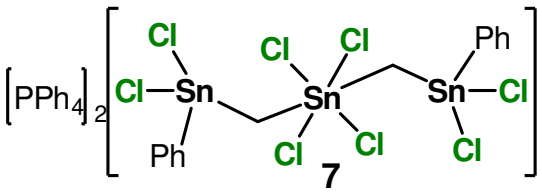

7

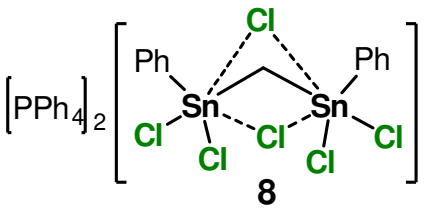

8

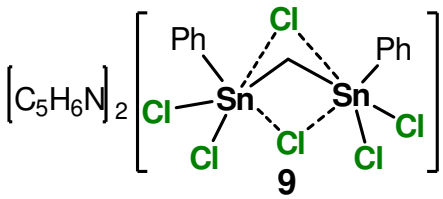

9

Chapter 4

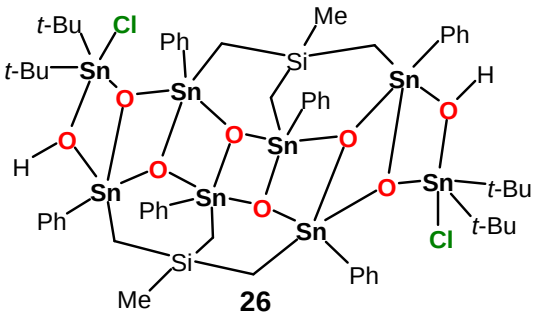

26

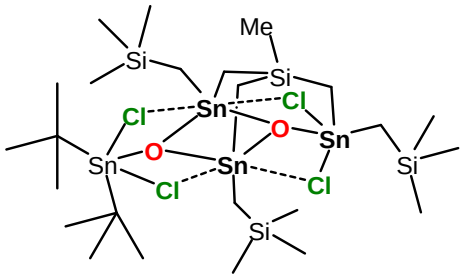

27

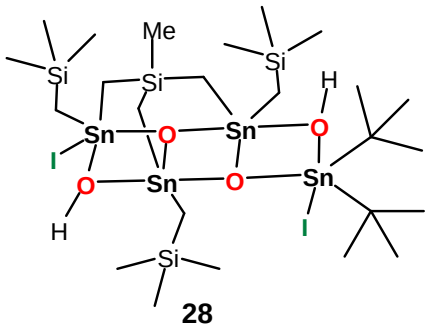

28

$[MeSi(CH_2SnPhO)_3]_6$

29

$[MeSi(CH_2SnCH_2SiMe_3O)_3]_{10}$

30

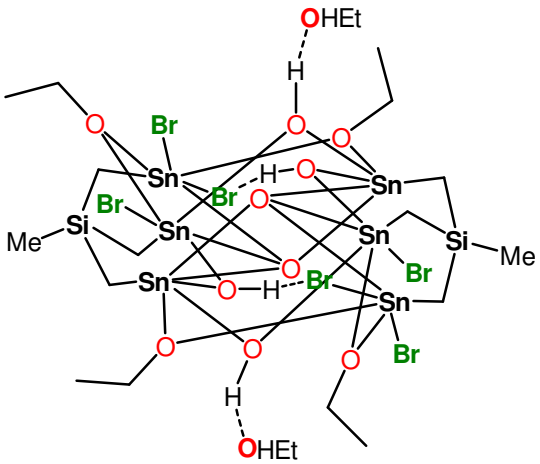

32

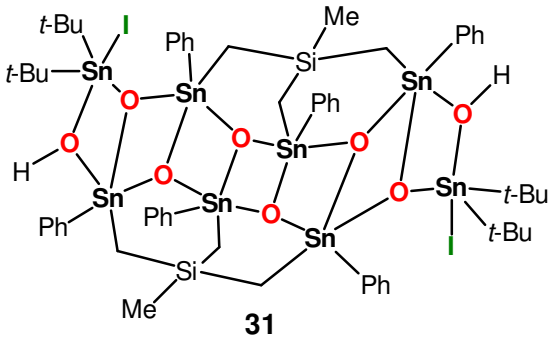

31

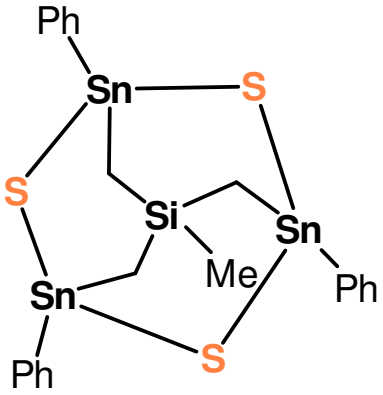

33

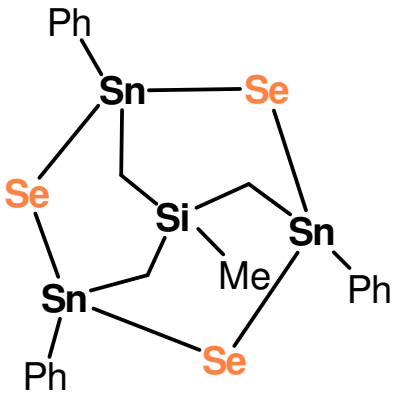

34

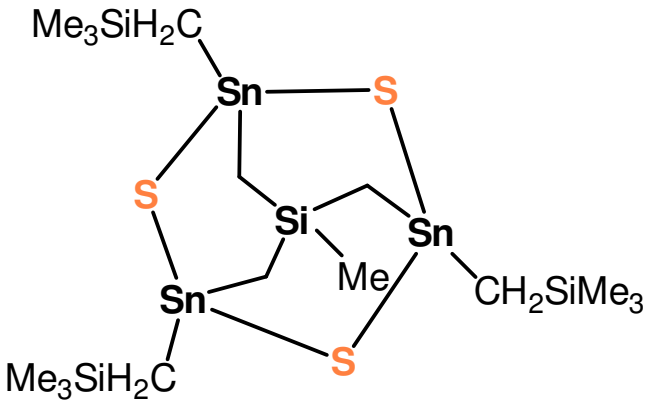

35

Chapter 5

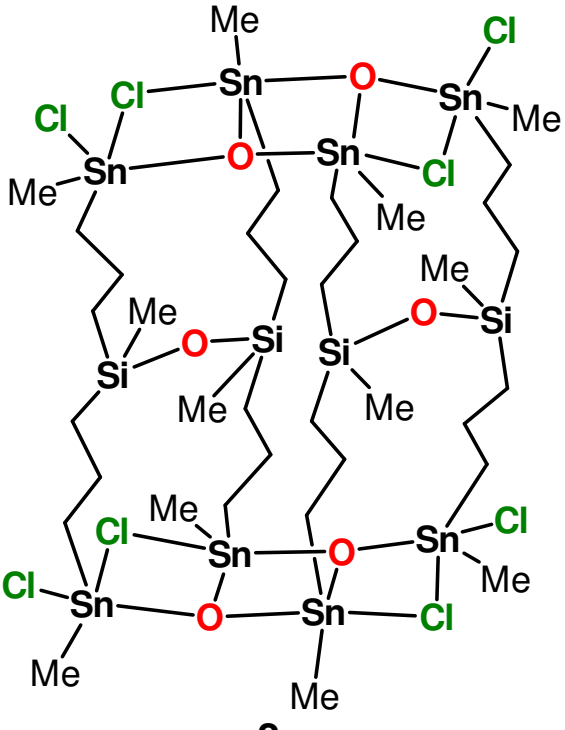

2

Chapter 6

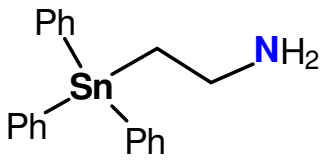

1

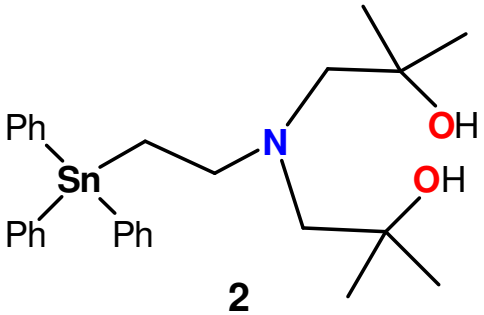

2

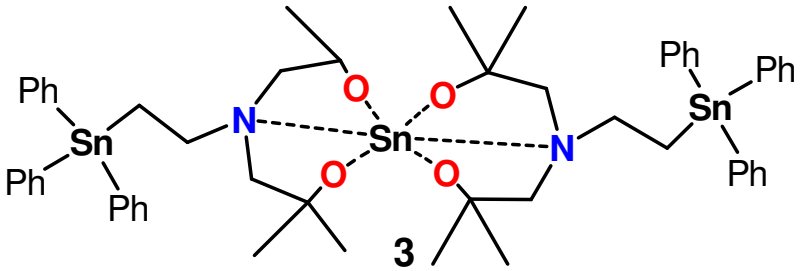

3

Appendix

Experimental Procedures

All solvents were dried and purified according to standard procedures and freshly distilled prior to use. $MeSi(CH_2Cl)_3$,[24] $NaSnPh_3$,[12] and $(t\text{-}Bu_2SnO)_3$[22] were synthesized according to the literature. Ph_3SnCl, $MeSiCl_3$, elemental iodine, and silver chloride were commercially available. They were used without further purification. The ^{1}H, ^{13}C, ^{29}Si and ^{119}Sn NMR spectra were recorded on Bruker DPX-400, DRX-600, and AVIII-600 spectrometers. Solution ^{1}H, ^{13}C, ^{29}Si and ^{119}Sn NMR chemical shifts δ are given in ppm and were referenced to Me_4Si (^{1}H, ^{13}C, ^{29}Si), and Me_4Sn (^{119}Sn). Elemental analyses were performed on a LECO-CHNS-932 analyzer. The electrospray mass spectra were recorded with a Thermoquest-Finnigan instrument. The samples were introduced as solution in CH_3CN or CH_2Cl_2 through a syringe pump operating at 0.5 µL min^{-1}. The capillary voltage was 4.5 kV, whereas the cone skimmer voltage was varied between 50 and 250 kV. Identification of the expected ions was assisted by comparison of experimental and calculated isotope distribution patterns. The m/z values reported correspond to those of the most intense peak in the corresponding isotope pattern. Melting points were determined using a Büchi Melting Point M-560. IR spectra (ATR) were recorded on a PerkinElmer FTIR spectrometer.The DOSY (diffusion-ordered spectroscopy) measurement was performed with a pulse sequence using double stimulated echo for convection compensation and LED and bipolar gradient pulses for diffusion.[67] The measurements were executed with an AVANCE-III HD 600 MHz NMR spectrometer equipped with a 5 mm heliumcooled BBFO probe from Bruker BioSpin GmbH (Rheinstetten,Germany). Thirty-two different gradient strengths varying between 3% and 95% of the maximum strength of 53 G/cm were used. Thirty-two scans per gradient strength were acquired with 16 kB data points of the FID (acquisition time of 0.97 s) and a relaxation delay of 1.5 s. According to the DOSY figure, the expansion indicates one conformational rearrangement of the compound in solution with diffusion coefficient of $3.89 \times 10^{-10} (\pm\ 1 \times 10^{-11})$ $m^2\ s^{-1}$. Single crystal X-ray diffraction data was collected with either an Oxford Diffraction Xcalibur, equipped with a Saphire3 CCD detector and an Enhance fine focus sealed tube (Mo-Kα), or a Stoe StadiVari, equipped with a Pilatus 200K HPC detector and a GeniX 3D microfocus sealed tube (Cu-Kα, Xenocs), by using ω-scans. Data collection, integration, absorption correction and space group determination were performed with the respective software packages CrysAlisPro (2014 and 2019) or X-Area (2018). Structure solutions were obtained with ShelXS (2008 and 2013) using the direct method. The structure models were refined by

using ShelXL (2018) with a least squares procedure against F^2. Unresolved electron density was subtracted from the structure factor by applying a solvent mask in the software package OLEX2.

Crystallographic data

Chapter 2

	2	**6**	**9**
CCDC number	1995881		
Chemical formula	$C_{58}H_{54}SiSn_3$	$C_{40}H_{39}Cl_3SiSn_3$	$C_4H_9Br_9SiSn_3$
M_r ($g \cdot mol^{-1}$)	1135.17	1010.22	
Crystal system	Monoclinic	Orthorhombic	Orthorhombic
Space group	*P21/c*	*Pna21*	*Pna21*
Temperature (K)	173	105	173(2)
a, b, c (Å)	18.2220(5), 10.8715(3), 26.1335(7)	23.0159(8), 23.161(5), 16.1580(5)	13.014(2), 12.1225(8), 14.2155(9)
α, β, γ (°)	90, 98.067(3), 90	90, 90, 90	90, 90, 90
V ($Å^3$)	5125.8 (2)	3998.7(2)	2242.7(4)
Z	4	4	4
Radiation type	Mo Kα	Mo Kα (λ = 0.71073)	–
μ (mm^{-1})	1.51	2.117	19.386
Crystal size (mm^3)	0.21 × 0.19 × 0.19	0.2 × 0.15 × 0.01	0.250 x 0.050 x 0.040
R_{int}	0.037	2	0.0435
θ_{max} (°)Range	30.6	4.182 to 59.594	2.208 to 25.491
$(\sin \theta/\lambda)_{max}$ ($Å^{-1}$)	0.725	0.556	
$R[F^2 > 2s(F^2)]$, $wR(F^2), S$	0.032, 0.073, 1.030	R_1 = 0.0290, wR_2 = 0.0700	R_1 = 0.0374, wR_2 = 0.0708
No. of reflections	54829	26955	6116
No. of reflections independent	14937		3754
No. of reflections observed	11515		
No. of parameters	536		
No. of restraints	72		
ρ_{max}, ρ_{min} (e $Å^{-3}$)	0.63, -0.51		0.808, -0.985

	13.2 C_7H_8	**14**	**16**
Chemical formula	$C_{58}H_{82}Cl_8N_4SiSn_3 \cdot 2C_7H_8$	$C_{55}H_{87}Cl_9N_6SiSn_3$	$C_{40}H_{78}Cl_6N_9O_3P_3SiSn_3$
M_r (g·mol^{-1})	1503.03	1535.51	1422.89
Crystal system	Monoclinic	Orthorhombic	Trigonal
Space group	$P2_1/n$	*Pna21*	R_{int}
Temperature (K)	173(2)	173(2)	110(2)
*a, b, c (*Å*)*	11.8366(12), 19.4910(13), 29.6994(19)	26.5310(16), 23.518(3), 11.5221(8)	24.9951(6), 24.9951(6), 16.6505(5)
α, β, γ (°)	90, 98.085(7), 90	90, 90, 90	90, 90, 120
V (Å^3)	6851.9(9	7189.4(11)	15444 (6)
Z	4	4	2
μ (mm^{-1})	1.451	1.421	20.73
Crystal size (mm^3)	0.119 x 0.087 x 0.046	0.200 x 0.075 x 0.042	0.48 x 0.35 x 0.25
R_{int}	0.1655	0.1125	0.0354
θ_{max} (°) Range	2.126 to 27.500	2.314 to 25.499	5.548 to 61.428
$R[F^2 > 2s(F^2)]$, $wR(F^2), S$	R_1 = 0.0650, wR_2 = 0.1006	R_1 = 0.0698, wR_2 = 0.1584	R_1 = 0.0205, wR_2 = 0.0478
No. of reflections	58734	37793	49081
No. of reflections independent	15750	12994	5883
ρ_{max}, ρ_{min} (e Å^{-3})	0.712, -0.776	2.448, -0.932	0.67, -0.41

	17	**18**	**19**
Chemical formula	$C_{92}H_{96}O_{12}Si_2Sn_6$	$C_{52}H_{75}Cl_3N_6O_2P_2SiSn_3$	$C_{64}H_{111}Cl_3N_{12}O_4P_4SiSn_3$
M_r ($g \cdot mol^{-1}$)	2162	1368.63	1727.03
Crystal system	Triclinic	Triclinic	Monoclinic
Space group	*P-1*	*P-1*	*P21/n*
Temperature (K)	173(2)	100(1)	99.98(17)
*a, b, c (*Å*)*	12.2110(18), 14.678(2), 14.917(2)	10.2180(7), 22.1006(15), 28.628(2)	15.2069(6), 18.7712(7), 15.4720(7)
α, β, γ (°)	64.521(13), 85.400(11), 69.401(13)	79.834(2), 87.530(2), 76.903(2)	90, 116.993(5), 90
V (Å^3)	2251.3(6)	6197.8(7)	3935.4(3)
Z	2	4	2
μ (mm^{-1})	1.723	1.441	1.194
Crystal size (mm^3)	0.306 x 0.169 x 0.029	0.15 x 0.135 x 0.06	0.79 x 0.47 x 0.24
R_{int}	0.0752	0.1628	0.0445
θ_{max} (°) Range	2.441 to 25.500	3.866 to 55	5.082 to 60.976
$R[F^2 > 2s(F^2)]$, $wR(F^2), S$	R_1 = 0.1293, wR_2 = 0.3790	R_1 = 0.0737, wR_2 = 0.1526	R_1 = 0.0431, wR_2 = 0.1039
No. of reflections	19675	198935	49902
No. of reflections independent	8382	28460	20736
ρ_{max}, ρ_{min} (e Å^{-3})	3.77, -1.804	1.69, -1.25	1.62, -0.78

	22	**23.0.5 CH_2Cl_2**
Chemical formula	$C_{96}H_{118}F_8N_2Si_2Sn_6$	$C_{20}H_{49}Br_{11}N_2SiSn_3$
M_r ($g \cdot mol^{-1}$)	2220.24	1622.2
Crystal system	Monoclinic	Triclinic
Space group	*P21/n*	*P-1*
Temperature (K)	173(2)	173(2)
*a, b, c (*Å*)*	16.6900(8), 10.9201(5), 26.0626(11)	7.1210(2), 17.0419(6), 18.8069(6)
α, β, γ (°)	90, 91.970(4), 90	103.058(3), 99.286(3), 91.524(3)
V (Å^3)	4747.3(4)	2189.44(12)
Z	4	2
μ (mm^{-1})	1.639	10.969
Crystal size (mm^3)	0.190 x 0.051 x 0.040	0.349 x 0.106 x 0.035
R_{int}	0.0513	0.0463
θ_{max} (°) Range	2.229 to 30.500	2.257 to 25.499
$R[F^2 > 2s(F^2)]$, $wR(F^2), S$	R_1 = 0.0707, wR_2 = 0.1934	R_1 = 0.0360, wR_2 = 0.0915
No. of reflections	45664	26948
No. of reflections independent	14488	8169
ρ_{max}, ρ_{min} (e Å^{-3})	3.295, -1.185	1.118 and -1.052

	25.0.5 CH_2Cl_2	**24**
Chemical formula	$C_{38.50}H_{85}Cl_9N_4Si_4Sn_3$	$C_{28.5}H_{30}Br_{10}ClPSiSn_3$
M_r ($g \cdot mol^{-1}$)	1391.58	1422.89
Crystal system	Triclinic	Orthorhombic
Space group	*P-1*	*Pba2*
Temperature (K)	173(2)	173(2)
a, b, c (Å)	11.8657(4), 14.9245(5), 20.4810(6)	13.8538(4), 44.2038(15), 7.0299(2)
α, β, γ (°)	84.913(3), 88.409(3), 82.289(3)	90, 90, 90
V ($Å^3$)	3579.6(2)	4305.0(2)
Z	2	4
μ (mm^{-1})	1.466	11.980
Crystal size (mm^3)	0.299 x 0.170 x 0.022	0.500 x 0.149 x 0.126
R_{int}	0.0580	0.0559
θ_{max} (°) Range	2.232 to 29.000	2.357 to 25.498
$R[F^2 > 2s(F^2)]$, $wR(F^2), S$	R_1 = 0.0520, wR_2 = 0.1572	R_1 = 0.0670, wR_2 = 0.1606
No. of reflections	69525	31806
No. of reflections independent	19013	8010
ρ_{max}, ρ_{min} (e $Å^{-3}$)	2.512, -0.770	2.570 and -1.526

Chapter 3

	2	**4**	**6**
Chemical formula	$C_{63}H_{56}Sn_4$	$C_{39}H_{36}I_4Sn_4$	$C_{37}H_{32}Cl_5PSn_2$
M_r ($g \cdot mol^{-1}$)	1287.83	1487.04	922.22
Crystal system	Triclinic	Triclinic	Triclinic
Space group	*P-1*	*P-1*	*P-1*
Temperature (K)	173(2)	173(2)	173(2)
a, b, c (Å)	9.8140(5), 15.1499(9), 19.0164(9)	10.1840(3), 13.3604(4), 17.8331(5)	11.5330(5), 11.7687(7), 14.5287(10)
α, β, γ (°)	102.424(5), 98.750(4), 98.610(5)	69.866(2), 76.357(2), 82.041(2)	68.339(6), 87.365(5), 80.461(4)
V ($Å^3$)	2679.8(3)	2209.49(12)	1807.1(2)
Z	2	2	2
μ (mm^{-1})	1.881	5.054	1.822
Crystal size (mm^3)	0.18 x 0.10 x 0.05	0.30 x 0.19 x 0.12	0.210 x 0.170 x 0.140
R_{int}	0.0483	0.0333	0.0244
θ_{max} (°) Range	2.138 to 25.500	2.181 to 25.499	2.322 to 25.500
$R[F^2 > 2s(F^2)]$, $wR(F^2), S$	R_1 = 0.0432, wR_2 = 0.0975	R_1 = 0.0260, wR_2 = 0.0571	R_1 = 0.0395, wR_2 = 0.1159
No. of reflections	26160	42994	13587
No. of reflections independent	9972	8222	6724
ρ_{max}, ρ_{min} (e $Å^{-3}$)	0.773, -0.844	1.248, -1.240	2.999, -1.124

	7	**8.0.5 H_2O**	**9**
Chemical formula	$C_{62}H_{54}Cl_8P_2Sn_3$	$C_{122}H_{111}O_{0.5}Cl_{12}P_4Sn_4$	$C_{23}H_{24}Cl_6N_2Sn_2$
M_r ($g \cdot mol^{-1}$)	1500.66	2600.36	778.52
Crystal system	Triclinic	Monoclinic	Monoclinic
Space group	*P-1*	*P21/n*	*P21/c*
Temperature (K)	173(2)	173(2)	173(2)
*a, b, c (*Å*)*	9.9526(4), 12.5607(5), 13.4456(6)	17.6121(5), 15.0792(4), 44.4098(16)	12.9246(13), 15.7566(9), 15.1585(13)
α, β, γ (°)	69.583(4), 75.496(4), 75.580(4)	90, 92.667(3), 90	90, 115.060(10), 90
V (Å^3)	1500.66(12)	11781.4(6)	2796.4(5)
Z	1	2	4
μ (mm^{-1})	1.687	1.282	2.375
Crystal size (mm^3)	0.100 x 0.080 x 0.070	0.380 x 0.310 x 0.250	0.280 x 0.120 x 0.110
R_{int}	0.0296	0.0543	0.0315
θ_{max} (°) Range	2.454 to 25.499	2.216 to 25.500	2.731 to 25.499
$R[F^2 > 2s(F^2)]$, $wR(F^2), S$	R_1 = 0.0391, wR_2 = 0.1249	R_1 = 0.0482, wR_2 = 0.0938	R_1 = 0.0293, wR_2 = 0.0639
No. of reflections	17230	68966	5856
No. of reflections independent	5584	21918	3640
ρ_{max}, ρ_{min} (e Å^{-3})	1.268, -1.094	0.600, -1.535	0.401, -0.468

Chapter 4

	26	**27**	**28**
Chemical formula	$C_{60}H_{88}Cl_2O_8Si_2Sn_8$	$C_{24}H_{60}Cl_4O_2Si_4Sn_4$	$C_{24}H_{62}I_2O_4Si_4Sn_4$
M_r ($g \cdot mol^{-1}$)	1005.94	1109.64	1255.65
Crystal system	Monoclinic	Monoclinic	monoclinic
Space group	*C2/c*	*P21/c*	*P21/c*
Temperature (K)	173(2)	173(2)	105(1)
*a, b, c (*Å*)*	26.5865(15), 22.6357(13), 15.1998(10)	15.0807(18), 11.8774(12), 23.6920(19)	14.7561(4), 22.9312(8), 12.9476(5)
α, β, γ (°)	90, 101.705(6), 90	90, 94.086(9), 90	90, 98.205(3), 90
V (Å^3)	8957.1(10)	4232.9(7)	4336.3(2)
Z	8	4	4
μ (mm^{-1})	2.316	2.719	3.836
Crystal size (mm^3)	0.265 x 0.038 x 0.026	0.082 x 0.073 x 0.046	0.6 x 0.38 x 0.18
R_{int}	0.1039	0.1544	0.236
θ_{max} (°) Range	2.514 to 27.499	2.115 to 28.997	2.777 to 30.0240
$R[F^2 > 2s(F^2)]$, $wR(F^2), S$	R_1 = 0.0505, wR_2 = 0.1049	R_1 = 0.0706, wR_2 = 0.1325	R_1 = 0.0374, wR_2 = 0.999
No. of reflections	38491	34347	22164
No. of reflections independent	10295	11261	8276
ρ_{max}, ρ_{min} (e Å^{-3})	0.957, -0.951	1.134, -1.484	Max 0.906

	29	**30**	**31.5 DMF**
CCDC number	1995233	1953399	
Chemical formula	$C_{132}H_{144}O_{18}Si_6Sn_{18}$ · $6CH_2Cl_2$	$C_{160}H_{414}O_{30}Si_{40}Sn_{30}$ · $8CH_2Cl_2$	$C_{75}H_{121}I_2N_5O_{13}Si_2Sn_8$
M_r ($g \cdot mol^{-1}$)	4323.42	7503.19	2560.26
Crystal system	Monoclinic	Triclinic	Monoclinic
Space group	*P21/n*	*P-1*	*P21/n*
Temperature (K)	173	100	100
*a, b, c (*Å*)*	14.0911 (5), 32.306 (2), 37.0724 (12)	16.822 (3), 23.161 (5), 41.207 (8)	22.831(5), 16.825(3), 24.945(5)
α, β, γ (°)	90, 97.086 (4), 90	88.47 (3), 86.28 (3),74.59 (3)	90, 101.53(3), 90
V (Å^3)	16747.4 (13)	15444 (6)	9389(3)
Z	4	2	4
Radiation type	Mo Kα	Cu Kα	–
μ (mm^{-1})	2.72	20.73	2.830
Crystal size (mm)	0.19 × 0.13 × 0.04	0.14 × 0.08 × 0.02	0.19 × 0.123 × 0.030
R_{int}	0.077	0.090	0.0690
θ_{max} (°)	23.3	60.1	25.123
$(\sin\theta / lambda)_{max}$ (Å-1)	0.556	0.562	–
$R[F^2 > 2s(F^2)]$, $wR(F^2), S$	0.065, 0.131, 0.920	0.128, 0.350, 0.840	wR_2 = 0.1904, S = 0.939
No. of reflections	52875	57472	16758
No. of reflections independent	24054	33542	16672
No. of reflections observed	13695	11350	10485
No. of parameters	1511	1183	–
No. of restraints	417	31	–
ρ_{max}, ρ_{min} (e Å^{-3})	1.03, -0.80	1.26, -1.42	–

	32	**33**
Chemical formula	$C_{20}H_{54}Br_6O_{12}Si_2Sn_6$	$C_{22}H_{24}S_3SiSn_3$
M_r (g · mol^{-1})	1734.41	765.73
Crystal system	Monoclinic	Trigonal
Space group	*P21/n*	*R3c*
Temperature (K)	173(2)	100(2)
*a, b, c (*Å*)*	9.5284(9), 17.1420(15), 14.7373(15)	12.4403(3), 12.4403(3), 29.1857(16)
α, β, γ (°)	90, 108.393(11), 90	90, 90, 120
V (Å^3)	2284.2(4)	3911.7(3)
Z	2	6
μ (mm^{-1})	8.575	2.719
Crystal size (mm^3)	0.350 x 0.030 x 0.020	0.185 x 0.100 x 0.088
R_{int}	0.1272	0.0226
θ_{max} (°) Range	2.264 to 25.499	3.275 to 25.446
$R[F^2 > 2s(F^2)]$, $wR(F^2), S$	R_1 = 0.0523, wR_2 = 0.1203	R_1 = 0.0166, wR_2 = 0.0363
No. of reflections	30171	6706
No. of reflections independent	4252	1487
ρ_{max}, ρ_{min} (e Å^{-3})	1.394, -1.311	0.398, -0.359

	35	**34**
Chemical formula	$C_{16}H_{42}S_3Si_4Sn_3$	$C_{22}H_{24}Se_3SiSn_3$
M_r (g · mol^{-1})	799.10	909.45
Crystal system	Monoclinic	Monoclinic
Space group	$P121/c$	$P21/c$
Temperature (K)	173.15	173(2)
*a, b, c (*Å*)*	12.6438(4), 11.7267(5), 42.4292(17)	12.1798(3), 13.9112(4), 16.1275(5)
α, β, γ (°)	90, 97.246(3), 90	90, 98.468(2), 90
V (Å^3)	6240.7(4)	2702.78(13)
Z	8	4
μ (mm^{-1})	2.740	6.843
Crystal size (mm^3)	0.081 x 0.073 x 0.054	0.301 x 0.242 x 0.213
R_{int}	0.0804	0.0495
θ_{max} (°) Range	2.264 to 25.499	2.236 to 28.996
$R[F^2 > 2s(F^2)]$, $wR(F^2), S$	R_1 = 0.0706, wR_2 = 0.1075	R_1 = 0.0231, wR_2 = 0.0490
No. of reflections	47531	37776
No. of reflections independent	11615	6661
ρ_{max}, ρ_{min} (e Å^{-3})	1.944, -1.917	1.050 and -0.673

Chapter 5

	2
Chemical formula	$C_{72}O_{12}Cl_{16}Si_8Sn_{16}$
M_r ($g \cdot mol^{-1}$)	3748.07
Crystal system	Monoclinic
Space group	*P21/n*
Temperature (K)	173.15
*a, b, c (*Å*)*	8.7441(17), 18.6157(37), 22.0047(44)
α, β, γ (°)	90, 92.618(30), 90
V (Å^3)	3578.13(123)
Z	4
μ (mm^{-1})	–
Crystal site (mm^3)	–
R_{int}	–
θ_{max} (°) Range	–
$R[F^2 > 2s(F^2), wR(F^2), S]$	–
No. of reflections	–
No. of reflections independent	–
ρ_{max}, ρ_{min} (e Å^{-3})	–

Chapter 6

	1	**2**	**3.C_7H_8**
Chemical formula	$C_{20}H_{21}NSn$	$C_{28}H_{37}NO_2Sn$	$C_{56}H_{70}N_2O_4Sn_3 \cdot C_7H_8$, $C_3 \cdot 5$; $C_{66.50}H_{78}N_2O_4Sn_3$
M_r ($g \cdot mol^{-1}$)	394.07	538.27	1325.37
Crystal system	Monoclinic	Monoclinic	triclinic
Space group	*P21/n*	*P21/c*	*P-1*
Temperature (K)	173(2)	173(2)	105
*a, b, c (*Å*)*	9.7902(3), 11.5823(3), 31.0993(9)	23.092(2), 6.4775(5), 19.2207(12)	9.5316(2), 15.9036(4), 21.5036(6)
α, β, γ (°)	90, 92.621(2), 90	90, 112.224(8), 90	76.996(2), 77.796(2), 75.614(2)
V (Å^3)	3522.75(17)	2661.4(4)	3034.43(15)
Z	8	4	2
μ (mm^{-1})	1.447	0.983	1.451
Crystal size (mm^3)	0.213 x 0.199 x 0.058	0.228 x 0.089 x 0.065	0.15 x 0.15 x 0.05
R_{int}	0.0288	0.0664	0.0332
θ_{max} (°) Range	2.193 to 29.500	2.289 to 30.500	2.6350 to 29.4410
$R[F^2 > 2s(F^2)]$, $wR(F^2), S$	R_1 = 0.0344, wR_2 = 0.0712	R_1 = 0.0730, wR_2 = 0.1852	R_1 = 0.0335
No. of reflections	20249	24152	20722
No. of reflections independent	9799	8111	–
ρ_{max}, ρ_{min} (e Å^{-3})	1.156, -0.658	1.455, -1.066	Max 0.905

Eidesstattliche Versicherung (Affidavit)

_____ _____

Name, Vorname
(Surname, first name)

Matrikel-Nr.
(Enrolment number)

Belehrung:

Wer vorsätzlich gegen eine die Täuschung über Prüfungsleistungen betreffende Regelung einer Hochschulprüfungsordnung verstößt, handelt ordnungswidrig. Die Ordnungswidrigkeit kann mit einer Geldbuße von bis zu 50.000,00 € geahndet werden. Zuständige Verwaltungsbehörde für die Verfolgung und Ahndung von Ordnungswidrigkeiten ist der Kanzler/die Kanzlerin der Technischen Universität Dortmund. Im Falle eines mehrfachen oder sonstigen schwerwiegenden Täuschungsversuches kann der Prüfling zudem exmatrikuliert werden, § 63 Abs. 5 Hochschulgesetz NRW.

Die Abgabe einer falschen Versicherung an Eides statt ist strafbar.

Wer vorsätzlich eine falsche Versicherung an Eides statt abgibt, kann mit einer Freiheitsstrafe bis zu drei Jahren oder mit Geldstrafe bestraft werden, § 156 StGB. Die fahrlässige Abgabe einer falschen Versicherung an Eides statt kann mit einer Freiheitsstrafe bis zu einem Jahr oder Geldstrafe bestraft werden, § 161 StGB.

Die oben stehende Belehrung habe ich zur Kenntnis genommen:

Official notification:

Any person who intentionally breaches any regulation of university examination regulations relating to deception in examination performance is acting improperly. This offence can be punished with a fine of up to EUR 50,000.00. The competent administrative authority for the pursuit and prosecution of offences of this type is the chancellor of the TU Dortmund University. In the case of multiple or other serious attempts at deception, the candidate can also be unenrolled, Section 63, paragraph 5 of the Universities Act of North Rhine-Westphalia.

The submission of a false affidavit is punishable.

Any person who intentionally submits a false affidavit can be punished with a prison sentence of up to three years or a fine, Section 156 of the Criminal Code. The negligent submission of a false affidavit can be punished with a prison sentence of up to one year or a fine, Section 161 of the Criminal Code.

I have taken note of the above official notification.

_____ _____

Ort, Datum
(Place, date)

Unterschrift
(Signature)

Titel der Dissertation:
(Title of the thesis):

_____

_____

_____

Ich versichere hiermit an Eides statt, dass ich die vorliegende Dissertation mit dem Titel selbstständig und ohne unzulässige fremde Hilfe angefertigt habe. Ich habe keine anderen als die angegebenen Quellen und Hilfsmittel benutzt sowie wörtliche und sinngemäße Zitate kenntlich gemacht.
Die Arbeit hat in gegenwärtiger oder in einer anderen Fassung weder der TU Dortmund noch einer anderen Hochschule im Zusammenhang mit einer staatlichen oder akademischen Prüfung vorgelegen.

I hereby swear that I have completed the present dissertation independently and without inadmissible external support. I have not used any sources or tools other than those indicated and have identified literal and analogous quotations.

The thesis in its current version or another version has not been presented to the TU Dortmund University or another university in connection with a state or academic examination.*

*Please be aware that solely the German version of the affidavit ("Eidesstattliche Versicherung") for the PhD thesis is the official and legally binding version.

_____ _____

Ort, Datum
(Place, date)

Unterschrift
(Signature)